# GREEN SYNTHESIS OF MEDICINE AND DEVELOPMENT OF INHIBITORS FOR DRUGGABLE PROTEINS OF SARS-COV-2

**CHEN QISHU**

**PhD**

**The Hong Kong Polytechnic University**

**2024**

# The Hong Kong Polytechnic University
# Department of Applied Biology and Chemical Technology


## GREEN SYNTHESIS OF MEDICINE AND DEVELOPMENT OF INHIBITORS FOR DRUGGABLE PROTEINS OF SARS-COV-2


**CHEN Qishu**


**A thesis submitted in partial fulfillment of**

**the requirements for the degree of**

**Doctor of Philosophy**

**08 2023**

# *CERTIFICATION OF ORIGINALITY*

I hereby declare that this thesis is my own work and that, to the best of my knowledge and belief, it reproduces no material previously published or written, nor material that has been accepted for the award of any other degree or diploma, except where due acknowledgement has been made in the text.

**CHEN Qishu**

# *ABSTRACT*

Abstract of the thesis entitled

## GREEN SYNTHESIS OF MEDICINE AND DEVELOPMENT OF INHIBITORS FOR DRUGGABLE PROTEINS OF SARS-COV-2

Submitted by CHEN Qishu

for the degree of Doctor of Philosophy

at The Hong Kong Polytechnic University in 08 2023

As human activity continuously develops, especially after the impact of SARS-CoV-2, medicine-related manufacturing and development of new druggable targets for obscure diseases have become a noteworthy segment of the society. Green synthetic methods, especially step and atom economical methodologies towards sustainable and environmentally friendly medicine synthesis have long been the focus of scientists. Among the mainstream topics, one of them is methodology towards selective C–N bond formation. Nitrogen containing molecules serve as a fundamental part of peptide backbone, and amino groups serve as pervasive constructing element of pharmaceutical agents or synthetic intermediates. Thus, introducing amine structure motif into organic molecules with accurate selectivity plays an important role in modern chemistry, especially in medicine synthesis. While classical C($sp^3$)–H activation provided us many choices in regioselectivity, most of the developed reactions target at activated C–H bonds, possibly due to the reason that unactivated C–H bond own similar C–H activation energy. Also, there are still reactivity beyond the reach of classical C–H activation. Alkenes, as abundant organic resources in reserve, have been standing under

the spotlight for its functionalization recently. The concept "metal-walk", which represents the migration of metal through reversible *β*-hydride elimination / migratory insertion, provides another pathway towards unactivated C($sp^3$)–N formation. In Chapter 2, we report a selective C($sp^3$)–H amidation of alkenes directed by thioether group, with dioxazolones as the amide source, and Ni–H as the catalyst. Due to the preference for five-membered nickelacycle, the Ni–H migration would be terminated at *γ*-site, selectively and remote from the alkene group. The reaction can be achieved at ideal yields (up to 90% yield) and remarkable selectivity (*γ*-product : other isomers up to 24:1), with a wide substrate scope (>40 examples reported).

As SARS-CoV-2 emerged in human population in 2019, COVID-19 and its therapeutic treatment quickly dominated human debate in recent years. The disease rapidly spread around the world, with quick generation of new variants. Despite the grievous harm it caused, medication towards SARS-CoV-2 remained largely unexplored. SARS-CoV-2 encodes 16 non-structural proteins (nsps) in total, which serve as the key enzymes in the replication of the virus. Among the enzymes encoded, nsp12, which is RNA dependent RNA polymerase (RdRp) for SARS-CoV-2, attracted the attention of scientists. RdRp is highly conservative, among all the variants and even among other members of coronavirus family. Even "drug repurposing" strategy brought us with several candidate, the proposed RdRp inhibitors still hold some disadvantages such as possibility of mutations, or poor pharmacokinetic (PK) properties, etc. We thus hope to seek for more ideal inhibitors of nsp12 towards more effective oral anti-SARS-CoV-2 candidates. In Chapter 3, we report a series of GS-441524 ester prodrug derivatives as COVID-19 oral drug candidate. We tested their inhibition reactivities towards SARS-CoV-2 RdRp, and their pharmacokinetic properties were also briefly examined. Compound **3-1**, the cyclohexyl carboxylic ester prodrug examined, displayed the best inhibition ability, pharmacokinetic property, and oral bioavailability. The $EC_{50}$ value of **3-1** is 0.26 μM, lower than that of GS-441524 ($EC_{50}$ = 1.644 μM). F value of **3-1** also reached 53.4±3.4%, displaying an ideal oral bioavailability. $C_{max}$ of **3-1** through oral intake was close to that through intravenous injection, demonstrating the

potential of **3-1** as oral medicine against COVID-19. We further renamed the compound as SHEN 26, and we went on to optimize its synthetic route and analyzed the quality y of industrial produced batch. We achieved a protection-esterification-deprotection 3-step route towards SHEN 26, without protecting the free amine group. We also determined and synthesized potential impurities and analyzed the purity of SHEN 26 from industrial kilogram batch. The purity of SHEN 26 reached 98.8%, with nearly all impurities meeting the acceptance criteria, demonstrating the feasibility of this route in industrial production of SHEN 26.

Apart from RdRp, nsp14 is also a recently heated area. In the replication of SARS-CoV-2, nsp14 is responsible for the methylation (capping) progress of the single-strand RNA. The methylated RNA cap serves as a pivotal instrument, assisting the single-strand RNA with immune escape and further translation. *S*-Adenosyl methionine (SAM) serves as methyl source, which would give out a methyl group and turns into *S*-Adenosylhomocysteine (SAH) during methylation of single-strand RNA molecule. Thus, SAH analogues are considered as potential inhibitors for methyl transferases. Despite its great potential, few examples of SAH analogues as SARS-CoV-2 nsp14 inhibitors were reported, and room for improvements still exists, especially for their selectivity and cellular intake. To further pursue a better inhibitor, meanwhile being highly selective towards SARS-CoV-2 nsp14, we designed and synthesized a series of different SAH analogues in Chapter 3. Their inhibition ability against the SARS-CoV-2 nsp14 was tested with three different testing assays, at fixed concentration and in a dose-response manner. Among all inhibitors synthesized, ester **MTI-ZC-007** and amide **MTI-ZC-014** displayed the best inhibition ability against SARS-CoV-2 nsp14 ( 100% inhibition of both compounds at 10 μM and 50 μM; $IC_{50}$ = 1.57 μM and 1.70 μM respectively, $IC_{50\text{-}LCMS}$ = 2.26 μM and 1.65 μM respectively), and we were also glad to see cellular inhibition of both **MTI-ZC-007** and **MTI-ZC-014** against SARS-CoV-2 virus ($EC_{50}$ = 21.84 μM and 14.88 μM respectively) A brief docking study was conducted, and structure-activity relationship (SAR) regarding to this series of structure was also briefly discussed.

# *PUBLICATIONS AND CONFERENCES*

1. Du, B.; Ouyang, Y.; Chen, Q.; Yu, W.-Y., Thioether-Directed NiH-Catalyzed Remote $\gamma$-C(sp3)–H Hydroamidation of Alkenes by 1,4,2-Dioxazol-5-ones. *J. Am. Chem. Soc.* **2021,** *143* (37), 14962-14968.

2. Zhou, Q.; Luo, Y.; Zhu, Y.; Chen, Q.; Qiu, J.; Cong, F.; Li, Y.; Zhang, X., Nonsteroidal anti-inflammatory drugs (NSAIDs) and nucleotide analog GS-441524 conjugates with potent in vivo efficacy against coronaviruses. *Eur. J. Med. Chem.* **2023,** *249*, 115113.

3. Chen, Q.; Zhou, Q.; Li, G.; Li, S.; Li, Y.; Zhang, X., Optimized kilogram-scale synthesis and impurity identification of SHEN26 (ATV014) for treating COVID-19, *Org. Process Res. Dev.* 2023, Article ASAP. https://doi.org/10.1021/acs.oprd.3c00248.

# ACKNOWLEDGEMENT

I would like to express my heartfelt gratitude to my chief supervisor: Prof. Xumu Zhang. All the way through my undergraduate and postgraduate study, Prof. Zhang offered me inspiring encouragement and illuminating guidance, which guided me through the lasting journey of postgraduate study and led me to the deeper insight of medicinal chemistry. It is my great honor to study in his research group and benefit from his dedicated guidance.

Also, I would like to thank my co-supervisor Prof. Wing-yiu Yu, Michael, for his kind encouragement, enlightening suggestions and professional instructions. Prof. Yu has a great patience towards academic research and educational undertaking. During my study period in Prof. Yu's group he spent a lot of time talking with students in lab about our academic progress. He was always able to offer precise suggestion, which supported me to break through all the obstacles. I felt honestly grateful to be offered this opportunity to study in Prof. Yu's group.

I would like to thank Dr. Yingjun Li, she gave me detailed instructions with my projects and she helped me with biological aspects, which I had little insight into. I would like to thank all the colleagues, especially Dr. Bingnan Du and Dr. Qifan Zhou, for offering me with patient help and kind guidance with my postgraduate project. I would like to thank all the technical staff who provided me with all their technical advice.

I would like to thank Miss. Chao Wu, Miss. Yao Zhang, Miss. Jingxin Wang and Miss Yuanjun Zhang, for all their companion throughout my postgraduate study. Through the long and winding road in pursue of our academic goals, we were lucky to have firm support from each other. They truly made my postgraduate study glow in my long life journey. Most importantly, I would like to thank my father and mother, for their support and patience.

# TABLE OF CONTENTS

# ABBREVIATIONS AND SYMBOLS

| | |
|---|---|
| Ac | acetyl/acetate |
| acac | acetylacetonate |
| ATP / ADP | adenosine triphosphate / adenosine diphosphate |
| BDE | bond dissociation energy |
| BHT | butylated hydroxytoluene |
| CARM1 | coactivator associated arginine methyltransferase 1 |
| CCD | charge couple device |
| CDI | *N*,*N*'-carbonyldiimidazole |
| COD | cyclooctadiene |
| CoV | coronavirus |
| COVID-19 | Corona Virus Disease 2019 |
| DBpin | deuterated pinacolborane |
| DCC | *N*,*N*'-dicyclohexylcarbodiimide |
| DIC | *N*,*N*'-diisopropylcarbodiimide |
| DIU | *N*,*N*'-diisopropylurea |
| DCE | 1,2-dichloroethane |
| DCM | dichloromethane |
| DMA | dimethylacetamide |
| DMAP | 4-dimethylaminopyridine |
| DMEM | Dulbecco's modified eagle medium |
| DMF | dimethylformamide |
| DMSO | dimethyl sulfoxide |
| DMV | double-membrane vesicles |
| DOT1L | DOT1-like histone lysine methyltransferase |
| dppp | 1,3-bis(diphenylphosphino)propane |
| dr | diastereomeric ratio |
| EA | ethyl acetate |

| | |
|---|---|
| $EC_{50}$ | concentration for 50% maximal effect |
| eIF4E | eukaryotic translation initiation factor 4E |
| E protein | envelope protein |
| equiv. | equivalence |
| ERK | extracellular regulated protein kinases |
| ESI | electrospray ionization |
| EZH2 | enhancer of zeste 2 polycomb repressive complex 2 subunit |
| FDA | food and drug administration |
| FT | Fourier transform |
| hACE2 | human angiotensin-converting enzyme 2 |
| HBpin | pinacolborane |
| HCoV | human coronavirus |
| HCV | hepatitis C virus |
| HEK293T | human embryonic kidney 293T (cell line) |
| HIV | human immunodeficiency virus |
| HPLC | high-performance liquid chromatography |
| HR | heptad repeat |
| HRMS | high resolution mass spectra |
| ICTV | International Committee on Taxonomy of Viruses |
| ICR | ion cyclotron resonance |
| $IC_{50}$ | concentration for 50% maximal inhibition |
| IFN | interferon |
| IFN-α | interferon-α |
| IFN-β | interferon-β |
| kb | kilobase |
| logP | octanol-water partition coefficient |
| MAPK | mitogen-activated protein kinase |
| MeCN | acetonitrile |
| MeOH | methanol |
| MERS | Middle East respiratory syndrome |

| | |
|---|---|
| MERS-CoV | Middle East respiratory syndrome coronavirus |
| Mpro | main protease |
| M protein | membrane protein |
| Ms | mass spectrometry |
| MTase | methyltransferase |
| NANC | nucleic acid negative conversion |
| NMR | nuclear magnetic resonance |
| N protein | nucleocapsid protein |
| NHC | β-D-$N^4$-hydroxycytidine |
| NiRAN | nidovirus RdRp-associated nucleotidyltransferase |
| Nsp | non-structural protein |
| NTP | nucleoside triphosphate |
| ORF | open reading frame |
| pBAC | plasmid bacterial artificial chromosome |
| PE | petroleum ether |
| PK | pharmacokinetic |
| PLB | passive lysis buffer |
| PLpro | papain-like protease |
| PRMT1 | protein arginine methyltransferase 1 |
| Q-TOF | quadrupole time-of-flight |
| RBD | receptor-binding domain |
| RdRp | RNA dependent RNA polymerase |
| RL | renilla luciferase |
| rpm | revolutions per minute |
| RTC | replicase-transcriptase complex |
| SAM | *S*-Adenosyl methionine |
| SAH | *S*-Adenosyl-L-homocysteine |
| SAR | structure-activity relationship |
| SARS-CoV | severe acute respiratory syndrome coronavirus |
| SARS-CoV-2 | severe acute respiratory syndrome coronavirus 2 |

| | |
|---|---|
| SD | Sprague Dawley |
| SD | standard deviation |
| S protein | spike protein |
| TEMPO | 2,2,6,6-tetramethylpiperidin-1-oxyl |
| Tf | trifluoromethanesulfonate |
| THF | tetrahydrofuran |
| TK | thymidine kinase |
| TLC | thin layer chromatography |
| TMPRSS2 | transmembrane protease, serine 2 |
| UV | ultraviolet |
| VOC | variants of concern |
| WHO | World Health Organization |
| 3CL pro | 3C-like protease |

# LIST OF FIGURES

## Chapter 1



## Chapter 2



## Chapter 3



## Chapter 4

# LIST OF TABLES

## Chapter 2



## Chapter 3



## Chapter 4

# LIST OF SCHEMES

## Chapter 1



## Chapter 2

## *Chapter 3*



## *Chapter 4*

# *Chapter 1 Introduction*

## 1.1 General Background

Science and technology developed rapidly in the current society. Chemistry, especially organic synthesis, constructed a crucial part of human activity. However, due to the reason that human activity produces waste faster than the environment degrades, natural environment is facing great pressure. Also, the amount of available natural resources is continuously decreasing. Classical industrial synthesis produces by-product as waste, which largely decreases the efficiency of chemical synthesis and meanwhile increases the natural degradation pressure. Thus, green synthesis, especially atom- and step-economical synthesis become a crucial part of modern chemistry. Construction of C–N bond is a important part of synthetic chemistry, for its abundance in bioactive and pharmaceutical molecules. Despite the great effectiveness of synthetic approaches such as cross coupling in C – N bond construction, site-selective construction of $C(sp^3) – N$ bond is still challenging. Discussion on the current development of $C(sp^3)$–N bond construction will be included in later section (Chapter 1.2).

Also, under the sudden strike of COVID-19, effective antivirus reagents towards SARS-CoV-2 virus quickly dominated human debate in recent years. Continuous emergence of variants significantly reduced the function of vaccines and antibodies, while currently proposed clinical medication towards COVID-19 still need improvements. SARS-CoV-2 has a large genome which encodes 4 structural proteins, several accessory proteins, and 16 nonstructural proteins (nsp1−16). The encoded proteins play a crucial part in the replication cycle, and by targeting at the inhibition of conservative proteins in the replication cycle, efficient drug candidate that withstands the effect of emergence of SARS-CoV-2 variants would be achievable. Here, our discussion mainly focuses on two target proteins: nsp12 (RNA dependent RNA

polymerase, RdRp) and nsp14 (Methyltransferase, MTase). Nsp12 is the RNA dependent RNA polymerase (RdRp) of SARS-CoV-2, responsible for the replication of +ssRNA. Nsp14 assists synthesis of +ssRNA methylated cap structure, which helps SARS-CoV-2 virus with translation and immune escape. Discussion on the current development of inhibitors for SARS-CoV-2 nsp12 and nsp14 will be included in later sections (Chapter 1.3 and Chapter 1.4).

## 1.2 Directed Catalytic C($sp^3$)–H Amination/Amidation

### 1.2.1 Current Scenario of C–N Bond Formation

Nitrogen-containing molecules construct the cornerstone of biological macromolecules and pharmaceutical intermediates, serving as a fundamental part of modern synthetic chemistry. Facing the large industrial demand, the development of methodology for more efficient C–N bond construction is continuously required. Classical industrial chemistry builds C–N bond in harsh conditions with stoichiometric by-products, raising the cost of industrial production and reducing atom economy. In modern chemistry, catalytic C–H amination/amidation[1] provided scientists with methodologies towards atom- and step-economical amine synthesis.

**Scheme 1 Transition metal catalyzed C($sp^2$)-N coupling reactions**

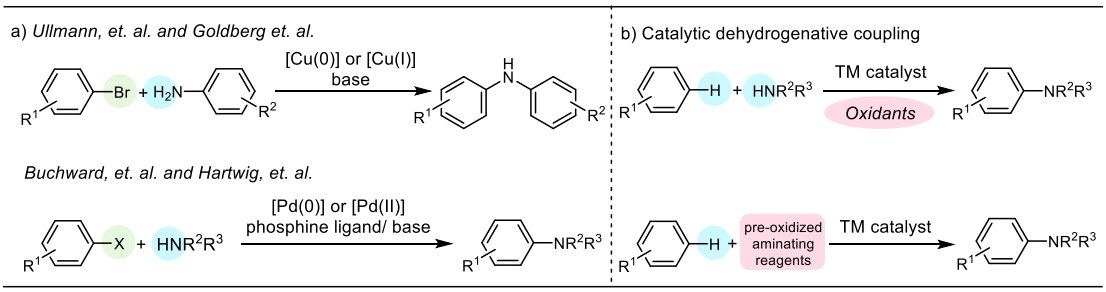


Metal-catalyzed direct C–N bond formation through cross coupling reactions was pioneered by Ullmann[2] and Goldberg[3]'s work on Cu-catalyzed amination of aryl halides in 1903 and 1906 accordingly. Buchwald[4] and Hartwig[5] later on reported Pd-catalyzed cross-coupling reactions of aryl halides with $Bu_3SnNRR'$ as nitrogen source independently (Scheme 1a). This protocol is continuously explored and widely used in the construction of C($sp^2$)–N bond[6, 7]. However, cross coupling reactions use pre-functionalized starting materials and generates stoichiometric by-products, while at the same time require addition of base or other reagents to promote the reaction. To elevate the atom economy, direct reactions between arenes that are not prefuctionalized and amino sources has been continuously pursued by scientists. Under mild oxidative environment or with pre-oxidized aminating reagents (electrophilic aminating reagents, azides, etc.), direct C–N bond formation between unactivated arenes and amine sources

can be achieved (Scheme 1b)[8, 9]. Transition metal catalyzed C−N coupling reactions provides a new path in organic synthesis, and is widely adopted in synthesis of nitrogen-containing organic motifs.

**Scheme 2 Transition Metal Catalyzed C(sp$^2$)–H Amination**

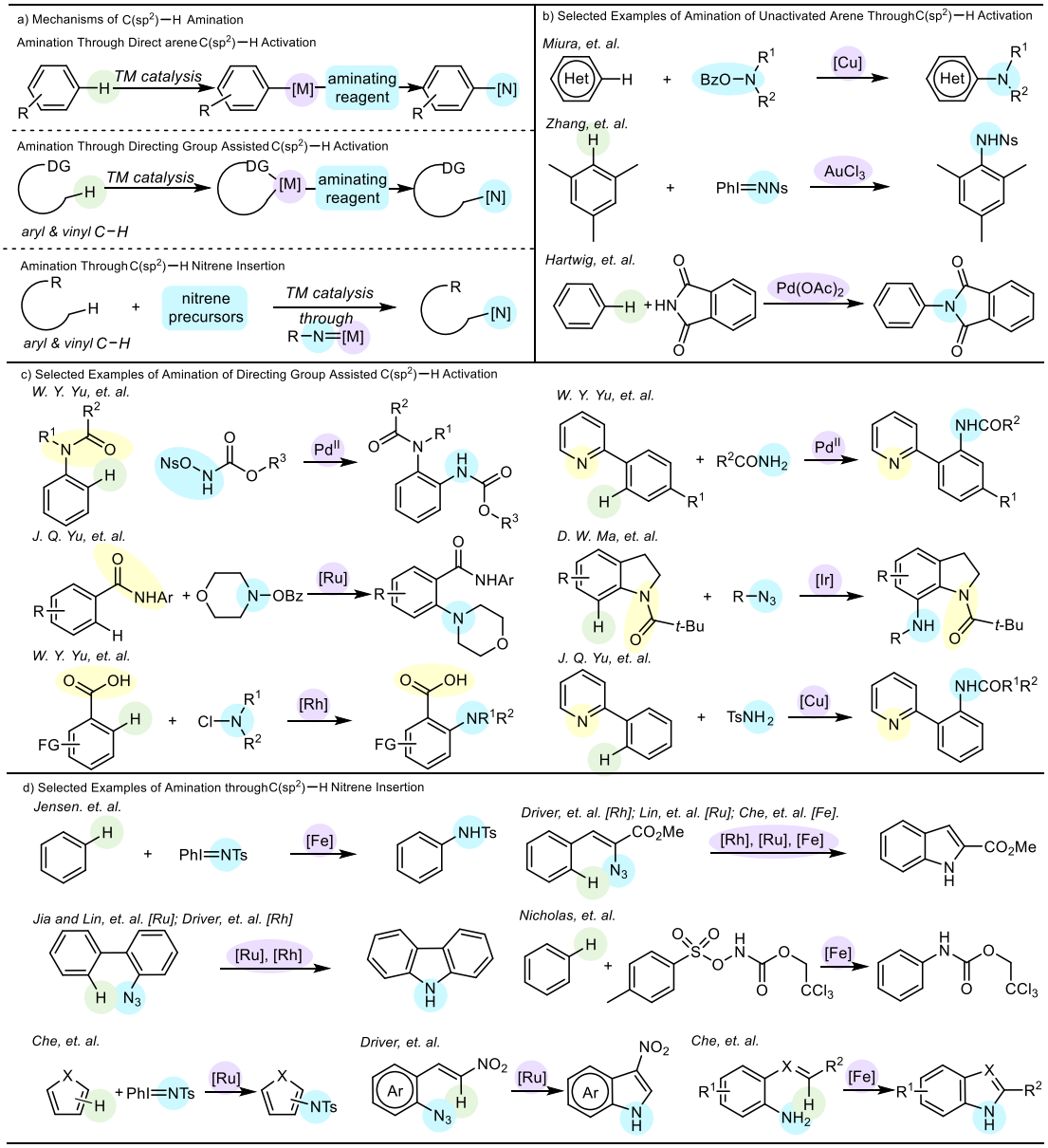


Apart from C−N coupling reactions, examples of C(sp$^2$)–N bond formation through C(sp$^2$)–H amination/amidation are also reported. One of the pathways for C(sp$^2$)–H amination/amidation include direct amination/amidation through inner-sphere C(sp$^2$)–H activation, where the metal first breaks the aryl C(sp$^2$)–H bond, forming metal-arene complex. Then aminating reagents engage with the metal-arene complex to form the

aminated/amidated product (Scheme 2a). Several amination/amidation reactions of unactivated arenes through this pathway were reported[10-14] (Scheme 2b). Through the spatial proximity from directing group coordination, breaking of the aryl C($sp^2$)–H bond is more facilitated (Scheme 2a). Various works are reported (Scheme 2c), including examples of transition metals such as Pd[15-23], Ru[24-31], Rh[32-59], Ir[60-81], Co&Fe[82-89], Ni[90], Cu[91-96] etc. Also, transition metals (Rh[97-101], Ru[102-104], Fe[105-107], Cu[108], etc.) form metal-nitrene intermediates with nitrene precursors (Scheme 2a), and then insert into the aryl C($sp^2$)–H bond, achieving amination/amidation reactions of C($sp^2$)–H bond through outer-sphere pathway. Several examples are listed in Scheme 2d.

Transition-metal-catalyzed C($sp^3$)–N formation was pioneered by Breslow and Gellman's work in 1983, where a series of transition metals including $Fe^{III}$, $Mn^{III}$ and $Rh^{II}$ was explored on their capability for catalyzing the intramolecular amidation of 2,5-diisopropylbenzenesulfonamide towards cyclic sultam[109] (Scheme 2a). By identifying the key intermediate involved, the mechanism for C($sp^3$)–N bond formation catalyzed by transition metal can be generally divided into two categories: C–H insertion pathway (outer-sphere) and C–H activation (inner-sphere) pathway.

The first pathway (outer-sphere pathway, Scheme 3a) includes C–H insertion through metal-nitrenoid species generated from nitrene precursors (azide, dioxazolone, etc.). By using Rh[110-126], Ru[127-130], Fe[131-137], Mn[138, 139], Cu[140-145], Co[146], Au[147], Ir[148-151], Ag[152-154] etc. as catalyst, both intramolecular and intermolecular C($sp^3$)–N bond formation can be achieved[155-159]. Despite great advances in this methodology, selectivity, especially regioselectivity in C–H amination/amidation through nitrene insertion is an important feature to address. Classical C–H amination/amidation reaction through metal-nitrenoid intermediate successfully targets at either benzylic C–H bonds (White[132], Du Bois & Sigman[119]) or tertiary C–H bonds (Dauban[160]) , for their relatively lower bond dissociation energies (BDEs) and distinctive steric environment (Scheme 3b). C($sp^3$)–H amination/amidation reactions through C–H insertion are widely adopted in total synthesis of natural product[161-167]. Selected works of nitrene C–H insertion are listed in Scheme 3c.

## Scheme 3 Transition Metal Catalyzed C(sp³)–H Amination

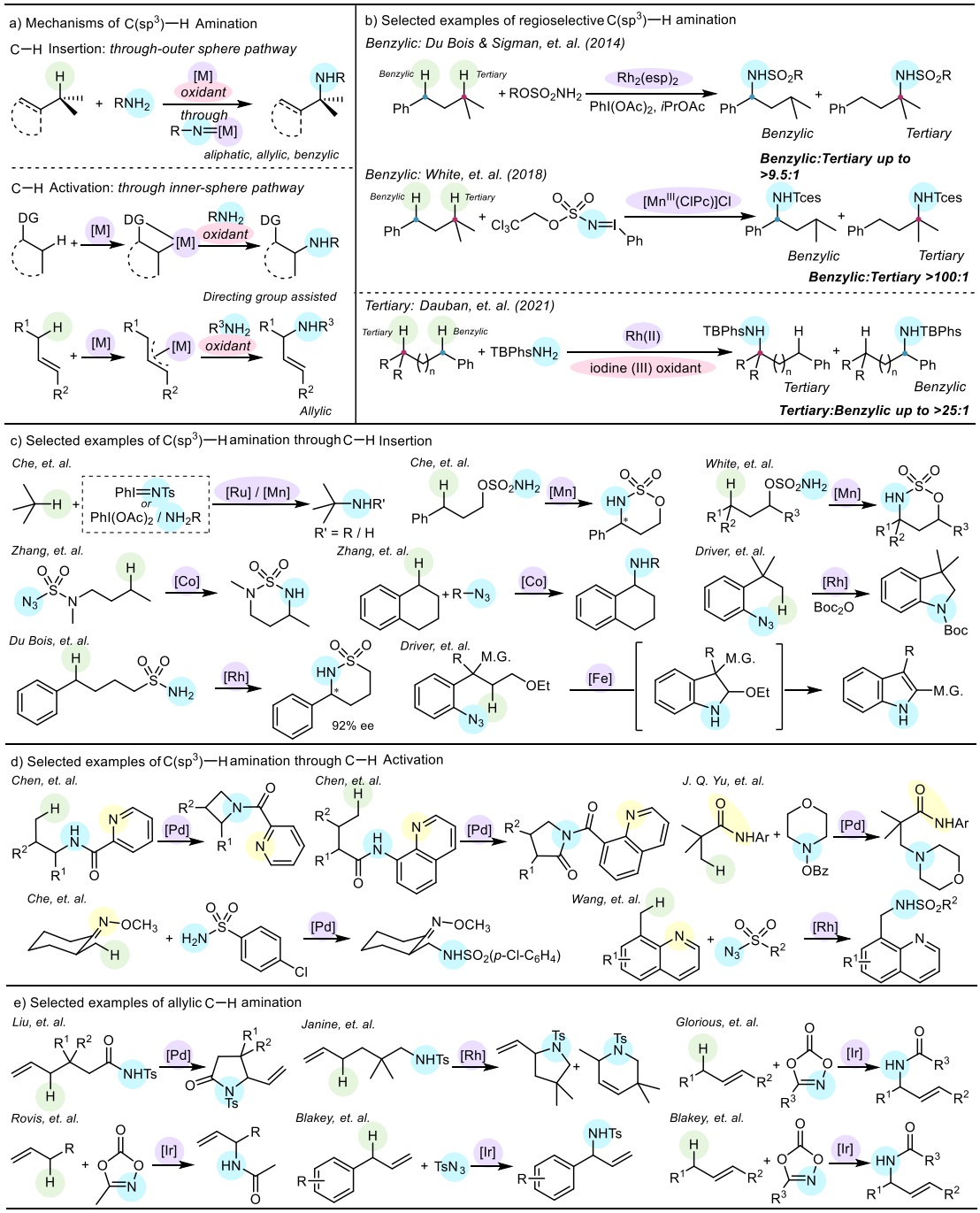


The second pathway (inner-sphere pathway, Scheme 3a) includes C–H activation as the key step. C–H activation generates an organometallic intermediate, where the transition metal breaks the C–H bond to form a metallacyclic or metal-allyl intermediate[168]. While this pathway has been found to work well in the functionalization of C(sp²)−H bonds, the cleavage of C(sp³)−H bonds is more difficult since aliphatic system own high activation energies, low acidity and relatively unreactive molecular orbital profile. Through directing group chelation, a spatially

close interaction between transition metal catalyst and C($sp^3$)−H bonds occurs, forming metallacycle intermediates. With a nitrogen source an aminated/amidated product can be generated (Scheme 3d), catalyzed by late transition metals such as Pd[14, 169-176], Cu[177], Ir[178, 179], Rh[180-184], Ru[185], Co[186], etc. Amination/amidation reactions at allylic site (Scheme 3e) were also reported due to the relatively high activity from stabilized allyl intermediate, under catalysis of Rh[187-193], Ir[194-200], Pd[201-208], Mn[209], etc.

### 1.2.2 Current Scenario of Unactivated Methylene C($sp^3$)–N Bond Construction

Although C($sp^3$)–N formation underwent its great advances in the past decade, examples of unactivated methylene C($sp^3$)–N bond formation are still relatively scarce[210-214], especially with high regioselectivity.

**Scheme 4** Regioselective unactivated methylene C–H activation

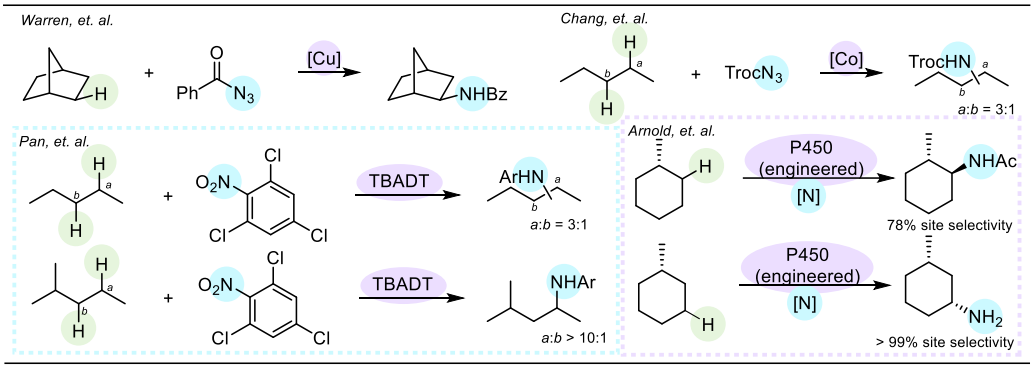


Warren, et. al. reported a regioselective methylene C–H amidation of norbornane with Cu catalyst, where an *exo* regioisomer is generated with relatively high enantioselectivity (dr = 13:1, 63% yield)[215]. Through Co catalysis, Chang and his co-workers reported a regioselective methylene C–H amidation of *n*-pentane, where a 3:1 regioselectivity is achieved between methylene sites[216]. Pan group reported a regioselective methylene C–H amination of *n*-pentane with 3:1 regioselectivity, and of 2-methylpentane with >10:1 regioselectivity[217]. Arnold, et. al. reported a series of regioselective methylene C–H amination/amidation catalyzed by engineered enzyme P450, where a maximum regioselectivity of >99% between methylene sites was achieved[135]. The above-mentioned works are listed in Scheme 4.

Despite the above-mentioned progress in methylene C–H amination/amidation, site

selectivity remains a great challenge. To further develop methodology for effective and selective C($sp^3$)–N bond formation, in Chapter 2, a regioselective alkene hydroamidation reaction will be reported.

## 1.3 Design and Synthesis of SARS-CoV-2 Nsp12 (RdRp) Inhibitors

### 1.3.1 Current Scenario of COVID-19 and Clinical Treatment

Coronaviruses are positive, single-stranded, non-segmented RNA viruses with a sequence size of about 26~32 kb, owning a methylated cap at the 5' end and a polyadenylate tail at the 3' end[218]. The orthocoronavirinae subfamily contains 4 genera (Alphacoronavirus, Betacoronavirus, Gammacoronavirus, and Deltacoronavirus), and SARS-CoV and SARS-CoV-2 belong to genus betacoronavirus. They tend to cross the species barrier and can cause human and animal diseases. Currently reported human-infecting coronaviruses mainly include human coronavirus NL63 (HCoV-NL63), human coronavirus 229E (HCoV-229E), human coronavirus OC43 (HCoV-OC43), human coronavirus HKU1 (HCoV-HKUl), severe acute respiratory syndrome coronavirus (SARS-CoV), Middle East respiratory syndrome coronavirus (MERS-CoV), and the novel severe acute respiratory syndrome coronavirus 2 (SARS-CoV-2), with SARS-CoV, MERS-CoV and SARS-CoV-2 leading to spreading transmission in human population[218]. In the past years, SARS-CoV, MERS-CoV and SARS-CoV-2 caused severe respiratory symptoms, all reporting fatal patients.

COVID-19, caused by severe acute respiratory syndrome coronavirus 2 (SARS-CoV-2), rapidly spread around the global society. Over 6 million deaths are reported until now by WHO, and the number of infections is still climbing. The new coronavirus epidemic gravitates towards long-term coexistence with human beings, and has a high degree of mutability, leading to continuous rise of new variants. The variants of concern (VOCs) include the following ones: B.1.1.7 (Alpha), detected in the UK in December 2020; B.1.351 (Beta) detected in South Africa in December 2020; P.1 (Gamma), detected in Brazil in January 2021; B.1.617.2 (Delta), first outbroke in India in April 2021 and B.1.1.529 (Omicron), detected in November 2021[219]. Omicron is currently the dominant variant, owing to its powerful ability to evade vaccine protection and to decline the efficiency of antibodies. From Alpha to Omicron, emerging and evolving

variants showed a tendency to bring the virus enhanced immune escaping ability and transmissibility[220].

The infection of virus begins with recognizing surface receptor of the cell, and then the virus membrane fuses with the cell membrane with the help of S protein, injecting RNA into the cytoplasm to begin viral replication, transcription and translation[221]. The genomic RNA of SARS-CoV-2 consists of 14 open reading frames (ORFs). There are two main ORFs, ORF1a and ORF1b, that comprises two-thirds of the genome. Translation of ORFla relies on cap structure to produce the polymer pp1a, and translation of ORF1b yields polyprotein pp1ab. Processed by SARS-CoV-2 proteases (PLpro and 3CLpro), pp1a and pp1ab form non-structural proteins (nsps) 1 to 16 with different functions[222]. The digested non-structural proteins gather on vesicles with a double-membrane structure (DMV) and assemble into replicase-transcriptase complex (RTC). The RTCs are the central machinery responsible for the transcription, replication, assembly and other steps of the genome during viral replication[222]. The remaining one-third of the genome encodes four major structural proteins: spike (S), Membrane (M), Envelope (E) and Nucleocapsid (N), and some accessory proteins[222].

Among the nsps encoded, several druggable targets of SARS-CoV-2 has been continuously explored by scientists. Nsp 12, RNA dependent RNA polymerase (RdRp) of SARS-CoV-2, is responsible for replication of its +ssRNA[223]. RdRp has been continuously explored for its potential as a druggable target against coronaviruses, due to its high conservativity among the coronavirus family. Detailed discussion on function of SARS-CoV-2 nsp12 and development of its inhibitors will be included in later section (Chapter 1.3.2). 3CLpro, also known as Mpro and nsp5 in SARS-CoV-2, is responsible for cleaving the ORF1ab protein at 11 fixed cleavage sites, and the generated peptides further folds to form 16 nsps[224]. Lopinavir is a 3CLpro inhibitor, approved for the clinical treatment for HIV. Reports also show that Lopinavir can be effective for MERS-CoV, SARS-CoV in animal and COVID-19 clinical treatment, but its effectiveness and safety still require further experiments[225]. Pfizer also developed an effective 3CLpro inhibitor named Paxlovid [active ingredients include Nirmatrelvir (PF-07321332) and Ritonavir][226]. Nirmatrelvir is the effective 3CLpro inhibiting

ingredient, and Ritonavir is adopted to slow down the metabolism of Nirmatrelvir. Paxlovid was reported to lower the death and hospitalization risk by 89% in Phase III clinical experiment[227] and is now approved by FDA as clinical treatment to COVID-19. Ensitrelvir [S-217622] is another 3CLpro inhibitor developed by Shionogi Pharmaceutical Company from Japan. It is reported to be effective in reducing the viral load, while at the same time showing minor side effects. Ensitrelvir received emergency approval for the clinical treatment of COVID-19 from the Japanese Ministry of Health and Welfare in December 2022[228]. In 2023, Zhong and his group also reported a potent 3CLpro inhibitor Leritrelvir [RAY1216]. RAY1216 displayed potent inhibitory efficacy, with $EC_{50}$ in nM scale concentration scale against a series of different SARS-CoV-2 variants. Leritrelvir is now approved for the clinical treatment of SARS-CoV-2 in China[229]. PLpro enzyme of coronavirus mainly conducts the functions of hydrolyzing proteins, deglycosylating and several other functions. It is an indispensable enzyme in the replication cycle of SARS-CoV-2. Many PLpro enzyme inhibitors are reported, but the inhibitors displayed poor performance in in vivo experiments[230]. Structures of the above-mentioned inhibitors are enclosed in Figure 1.

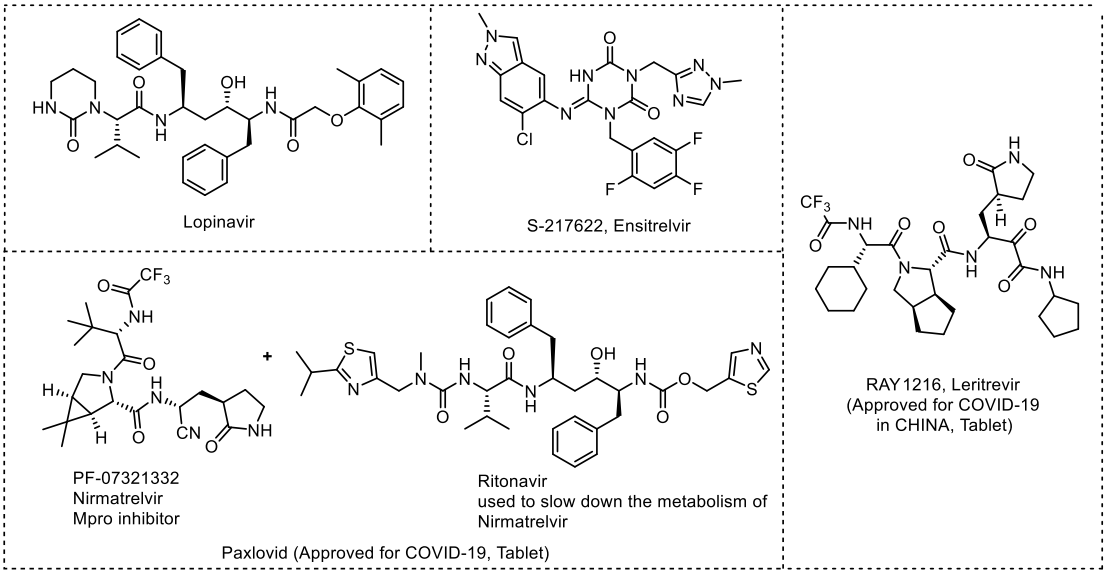


**Figure 1** Structure of Lopinavir, Ensitrelvir and Paxlovid

S protein is another hit target in the development of anti-coronavirus drugs[231]. S protein inhibitors are mainly neutralizing inhibitors and peptides. S protein contains

two domains: $S_1$ region is the receptor-binding domain (RBD), responsible for the regulation of recognition between virus and receptor on the host cell surface. $S_2$ is responsible for assisting the fusion of viral and host cell membrane[222]. S protein has been the major target for vaccine development. The serum of convalescent patients has also been proved to be efficient in the clinical treatment of diseases caused by SARS-CoV, MERS-CoV, and SARS-CoV-2[232]. Obtained by cloning the corresponding antibody sequence and expressing it in vitro, neutralizing antibodies can reduce the risk of immune response caused by antiserum[233]. Peptide fusion inhibitors is also reported to be effective to block the virus from entering the host cells, even in in vivo experiments. The heptad repeat (HR) regions were reported to conduct the function to induce the fusion of virus with cell membrane, and peptides of the conserved fractions displayed a broad-spectrum anti-coronavirus activity[234].

Interferons produced by the natural immune response is another important barrier in preventing viral expansion. By using supplemental interferon or interferon inducers, the level of interferon in the body of the host can be uplifted. Recombinant interferon α (IFN-α) and interferon β (IFN-β) in combination with the antiviral drug Ribavirin inhibited SARS-CoV and MERS-CoV replication in animal tests[235]. Nitazoxanide is another type I interferon inducer, and it was reported to inhibit a wide range of viruses[236]. In addition to directly upregulate the expression of interferons, modulating other signal molecules can also efficiently block the replication of SARS-CoV-2 in host cells. Chloroquine is an initiator of the p38/MAPK/ERK pathway, having a broad-spectrum anti-coronavirus ability to some extent. By acting on proteases on cell surface, some small molecule compounds, such as camostat mesylate (a TMPRSS2 inhibitor), also exhibits inhibition ability towards the replication of coronaviruses in host, but side effects are important factors to consider for these inhibitors to be clinical treatments[237]. Some traditional Chinese medicine pharmaceutics, such as Lianhua Qingwen capsules (granules), lung cleansing and detoxification soup, cold and wet epidemic formula, Xuanfei Baidu formula, Q-14 (Huashi Baidu formula), and Xuebijing injection etc., was also used in clinical treatment of COVID-19, mainly through enhancing the immune system to better identify and purge the viruses.

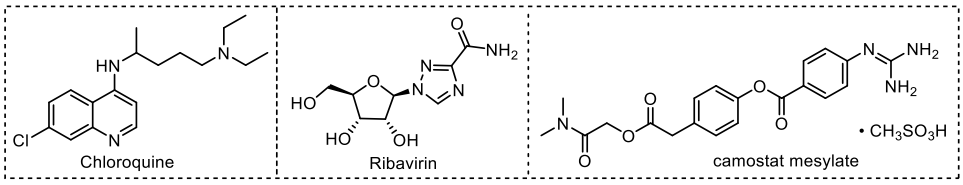


**Figure 2** Structure of Chloroquine, Ribavirin and camostat mesylate

Considering the tragic harm COVID-19 brought to our society, effective treatments, especially anti-SARS-CoV-2 drugs are in immediate need. Even though monoclonal antibodies and neutralizing antibodies display good antiviral reactivity, S protein is still not conserved enough to overlook the influence of drug resistance caused by mutations. Interferons when combined with organ supporting drugs can rescue critically severe patients, but due to its high cost and inconvenience usage, it is not suitable for clinical treatment for patients with mild infections. Traditional Chinese medicine preparations mainly deal with the symptoms caused by SARS-CoV-2 infection, and the job of viral clearance is all dependent on the immune system of the patient. Also, the effective component of Chinese medicine is still on a far way to isolation. Facing repeated and accelerated emergence of highly pathogenic coronaviruses, we urgently need to develop oral anti-coronavirus drugs for clinical treatment of COVID-19 and for preparation of potential upcoming epidemic caused by coronaviruses.

### 1.3.2 Functional Insights into SARS-CoV-2 RNA Dependent RNA Polymerase (RdRp) and Development of Nsp12 Inhibitors for SARS-CoV-2

RNA dependent RNA polymerase (RdRp), responsible for SARS-CoV-2 +ssRNA replication, is considered as the typical characteristic of coronaviruses. RdRp in SARS-CoV-2 is a complex formed by nsp7, nsp8 and nsp12. The structure of RdRp is ~97% homology with SARS-CoV, highly conservative along the coronavirus family[238]. Nsp12 includes a right-hand RdRp domain (including a palm domain, a finger domain and a thumb domain) and a nidovirus-specific N terminal extension domain that adopts a nidovirus RdRp-associated nucleotidyl-transferase (NiRAN) structure. The nsp7-nsp8 pair binds to the thumb domain, and an additional copy of nsp8 binds to the finger

domain. Except from the conserved regions of the polymerase family, nsp12 contains another new $\beta$-hairpin domain at N terminus. The $\beta$-hairpin domain inserts to the groove between the NiRAN domain and the palm subdomain, stabilizing the total architecture of RdRp[239]. Nsp12 is the active center of RdRp, and its catalytic site contains 7 conserved motifs (A to G), with motifs A B C D located in the palm domain and FG located on the finger domain. Nsp12 itself cannot carry the function of RNA replication; only when nsp12 is complexed with nsp7 and nsp8 can nsp12 carry out the function of RNA replication. During RNA replication, the RNA template enters the active site built by motifs A and C through a groove clipped by motifs F and G. Motif E and the thumb domain supports the nascent RNA string during replication, and the product RNA exits the active site through the exit channel at the front of RdRp[239, 240]. Due to its conserved structure along the coronavirus family and indispensability in the viral replication cycle, scientists have been regarding nsp12 as an important target in development of anti-SARS-CoV-2 drugs. Drug repurposing strategies and rational design offered us with choices of anti-SARS-CoV-2 drug candidates such as Molnupiravir[241], Remdesivir[242], Azvudine[243], etc.

Molnupiravir is a prodrug of the ribonucleoside analog β-D-$N^4$-hydroxycytidine (NHC). Upon uptake, molnupiravir is converted to NHC in plasma, and then converted to the active triphosphate form in the host cell[244]. The active triphosphate form serves as a competitive substrate for the viral replication, and once incorporated, molnupiravir would induce mutations of the viral RNA that gradually accumulate in the replication cycles, achieving its antiviral effect[241]. Molnupiravir showed more active (with 14 days to total viral clearance in 800 mg molnupiravir group and 15 days to total viral clearance in placebo group) and more effective (with up to 92.5% total viral clearance in 800 mg molnupiravir group and 80.3% in placebo group) viral clearance compared to placebo in clinical study. It also displayed a broad-spectrum antiviral activity against the coronavirus family[245]. However, risk for adopting molnupiravir in general clinical treatment is that it can also serve as competitive substrate for human RNA replication. Subsequent studies revealed that the parent drug EIDD-1931 of Molnupiravir could also be utilized by mitochondrial DNA dependent RNA polymerase in vitro,

incorporating into human RNA and leading to mutation in mammalian cells[244]. Molnupiravir was approved by FDA as an oral anti-SARS-CoV-2 drug in clinical treatment in March 2020.

Remdesivir, also named as GS-5734, is a previously reported prodrug of an adenosine analogue against Ebola virus[246]. Remdesivir is a monophosphoramidate prodrug, and is quickly converted to the active nucleoside triphosphate form (NTP), which is a competitive substrate for +ssRNA synthesis. The triphosphate form of remdesivir is highly preferred over ATP in RNA synthetic incorporation, raising its inhibition activity. Once incorporated into the nascent RNA, the RNA replication process would generally be terminated at three nucleosides after incorporation[247]. Remdesivir also displayed a broad-spectrum antiviral activity against the coronavirus family in animal study[242]. However, due to its poor oral bioavailability, clinical delivery of remdesivir is limited to intravenous injection, largely restricting its application. Remdesivir was approved by FDA as clinical treatment for COVID-19, but later WHO issued a conditional recommendation against the use of remdesivir in hospitalized patients regardless of severity, due to the lack of evidence for improvement towards survival rate and other clinical outcomes in these patients.

Sofosbuvir, reported by Gilead Inc., has been approved for the clinical treatment of hepatitis C virus (HCV) infection[248]. Drug repurposing strategy suggested that sofosbuvir is also a potential nsp12 inhibitor[249]. Galidesivir (BCX4430) is another repurposed anti-SARS-CoV-2 drug[250, 251]. Similar repurposed drugs include favipiravir[252, 253], ribavirin[254], etc. Unfortunately, the clinical progresses of the above-mentioned candidates remained not ideal.

Roche and Atea Pharmaceuticals worked together on the development of AT-527. AT-527 is a guanosine analog, functioning in its triphosphate form AT-9010. First molecule of AT-9010 incorporates into the nascent RNA string, preventing correct alignment of the second AT-9010. Then the third AT-9010 binds to the NiRAN domain, leading to immediate chain termination[255, 256]. However, AT-527 did not reach its expected primary clinical endpoint at global clinical phase II trial, failing to lower the viral load in patients with low risk and mild to moderate symptoms[257]. Azvudine,

developed by Genuine Biotech, also incorporates into the RNA string, leading to chain termination. Azvudine was approved for the treatment of HIV infection in China on July 2021, and was repurposed for the treatment of mild to moderate COVID-19 patients. Azvudine displayed an average nucleic acid negative conversion (NANC) period of 4.5 days[258]. Researchers also discovered that oral administration of Azvudine would concentrate the active form of drug in thymus, preventing thymus immune functions. They concluded that Azvudine would shorten the NANC time compared to standard antiviral treatment (including interferon alpha, lopinavir/ritonavir, and ribavirin, according to the Diagnosis and treatment program trial version 5 guidelines) and would also support lung function and vital signs of patients[243]. Azvudine have now been approved for the treatment of COVID-19 in China. VV-116, first synthesized by Jingshan Shen's group at Shanghai Institute of Materia Medica, is a triisobutyrate ester prodrug of 7-deuterated GS-441524, which is the active nucleoside of Remdesivir. The prodrug is rapidly converted into its parent nucleoside in the body, displaying strong antiviral activity with an $EC_{50}$ value of $0.39 \pm 0.08$ μM[259]. VV-116 is now under phase III clinical study.

The above-mentioned studies proved the potential of nsp12 as an anti-SARS-CoV-2 drug target. Considering the continuous mutation of the virus, further explorations in RdRp inhibitors are still under urgent requirement. In Chapter 2, we report a series of nucleoside ester prodrugs, and optimization on industrial synthesis of nucleoside 5'-ester prodrugs were conducted.

## 1.4 RNA Capping Procedure and Biological Insights into SARS-CoV-2 Nsp14

Cap structure is essential for the biological function of coronaviruses. RNA caps assist export of mRNA from the host nucleus, direct mRNA splicing and support RNA recognition by eukaryotic translation initiation factor (eIF4E) to assure successful translation[260]. Uncapped viral RNAs may suffer from issues such as being detected by host cell as "nonself"[261]. The viral RNA cap structure can either be stolen from the host mRNA or be synthesized by either its own synthetic machinery or apparatus from the host cell. SARS-CoV-2 owns a set of capping synthetic apparatus itself, and it adopts a "cap-1" structure[262]. The capping procedure was proposed to proceed first by 5'-triphosphatase site of helicase (nsp13) to remove the $\gamma$-phosphate and then nsp12 NiRAN domain to transfer GTP onto the RNA string. Next, nsp14 methylate the N7 position of guanine to form the "cap-0" structure, and the nsp10/nsp16 complex methylate the 2'-OH ribose group of the first nucleotide to form "cap-1" structure, concluding the capping procedure[262]. Cap-0 introduces a methyl group at 7-N position of the terminal guanine, and cap-1 structure is methylated at 2'-O position of the first nucleotide of the mRNA[262]. The structure of RNA cap and procedure of RNA capping are enclosed in Figure 3a and Figure 3b.

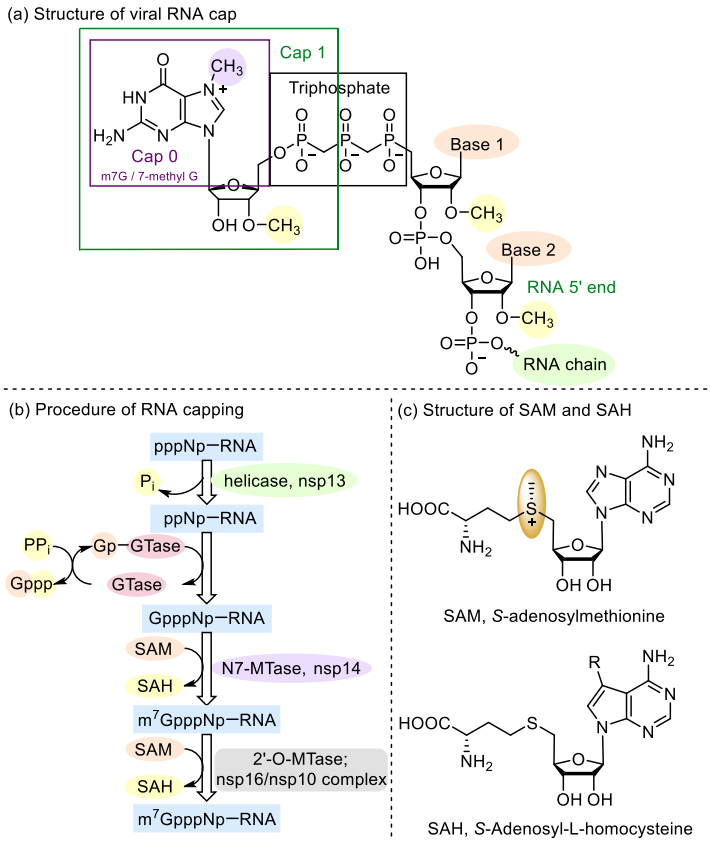


**Figure 3** Structure of SARS-CoV-2 cap and procedure of RNA capping

Nsp14 is a bifunctional enzyme, with N7-MTase activity located at its C-terminal and 3'-5' exoribonuclease located at its N-terminal[262]. The MTase domain and ExoN domain were reported to be separated domains, with their functions independent from the presence of the other. In between the N7-MTase domain and the ExoN domain is a hinge region highly conserved along the coronavirus family, which is a distinguish structure character of nsp14[263]. Structural analysis of SARS-CoV-2 nsp14 bound to GpppA and SAM revealed the binding pockets: RNA binding pocket and SAM binding pocket. During methylation procedure on N7 position, nsp14 first stabilizes GpppA with RNA-binding pocket, and then SAM-binding pocket grabs SAM and transfers the *S*-methyl to GpppA. The enzyme then releases SAH and methylated RNA, finishing the N7-methylation procedure[263].

SAH, the by-product of N7-methylation from SAM, was reported to exhibit certain inhibition effect on SARS-CoV-2 nsp14[264]. Except from RNA methylation by SARS-CoV-2 nsp14, SAM is also a methyl source widely adopted in many other methylation

procedures, and thus SAH analogues demonstrate broad-spectrum inhibition in many different targets[265], including DOT1L[266], EZH2[267], PRMT1[268] and CARM1[268] for the treatment of cancer, etc.

Exploration on SAH analogues as inhibitors has been attracting scientists' attention ever since the unravelling of the protein as a druggable target, but despite its great potential, successful reports on SAH analogues as SARS-CoV-2 nsp14 inhibitors remain scarce. In Chapter 4, we report design and synthesis of a series of SAH analogues, also biological test on their inhibition efficacy against SARS-CoV-2 nsp14.

# *Chapter 2 Thioether-Directed NiH-Catalyzed γ-selective Remote Hydroamidation of Alkenes by 1,4,2-Dioxazol-5-ones*

## 2.1 Introduction

Alkenes are a group of synthetic building block abundantly reserved in nature, and functionalization of alkenes through transition metal intermediate have been widely explored by scientists[269-272]. During this procedure, scientists revealed a migration process where transition metal move along different methylene C($sp^3$)–H sites through a reversible *β*-hydride elimination/migratory insertion cascade process to form stabilized metal-alkyl species. The migration process is named as chain-walking, providing access for activation of methylene C–H sites remote from the original position of the alkene group. Among the transition metals triggering chain-walking process, Ni attracted the interest of scientists for its effectiveness in remote C–H functionalization[273-275] and its earth abundance. Through addition of NiH species to alkenes Ni-alkyl complexes are generated, which then undergoes chain-walking to form stabilized Ni-alkyl complexes (Scheme 5). The migration of metal commonly ends at primary positions or benzylic positions, due to the lack of steric hindrance (primary position[276-281], Scheme 5a) or resonance stability (benzylic positions[282-288], Scheme 5b). Termination at *α*-positions of the heteroatoms are also reported in several works[289, 290] (Scheme 5c).

**Scheme 5** Ni-catalyzed site-selective hydrofunctionalization of alkenes

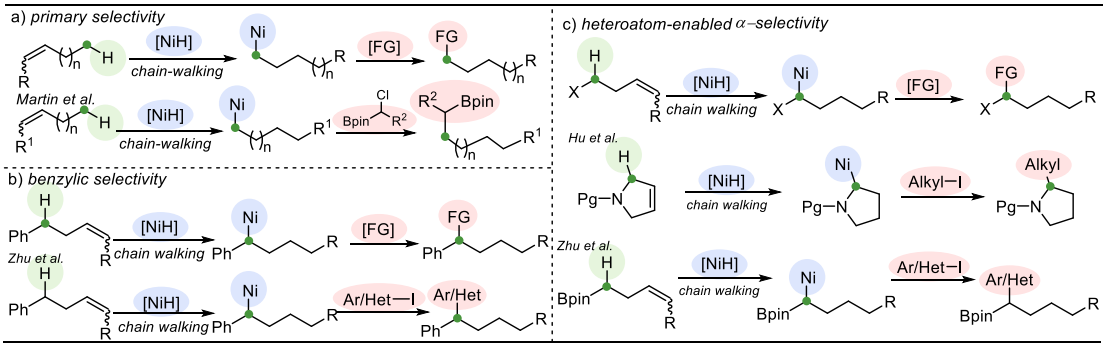

Despite great advances in Ni-catalyzed remote functionalization of alkenes, site-selectivity beyond primary, benzylic and $\alpha$-positions remained as terra incognita. C–H bonds beyond these positions own similar bond dissociation energies, resulting in similar stability in corresponding Ni-alkyl species. In difunctionalization of alkenes, Zhao's group[291] and Giri's group[292] independently discovered that 1,3-difunctionalization happens at alkenes bearing directing groups with coordinating ability (Scheme 6b), achieving selective installation of functional groups at beyond primary, benzylic and $\alpha$-positions. The selectivity can be attributed to formation of a thermodynamically favored five-membered metallacycle during metal migration.

**Scheme 6** Directing-group-enabled remote functionalization

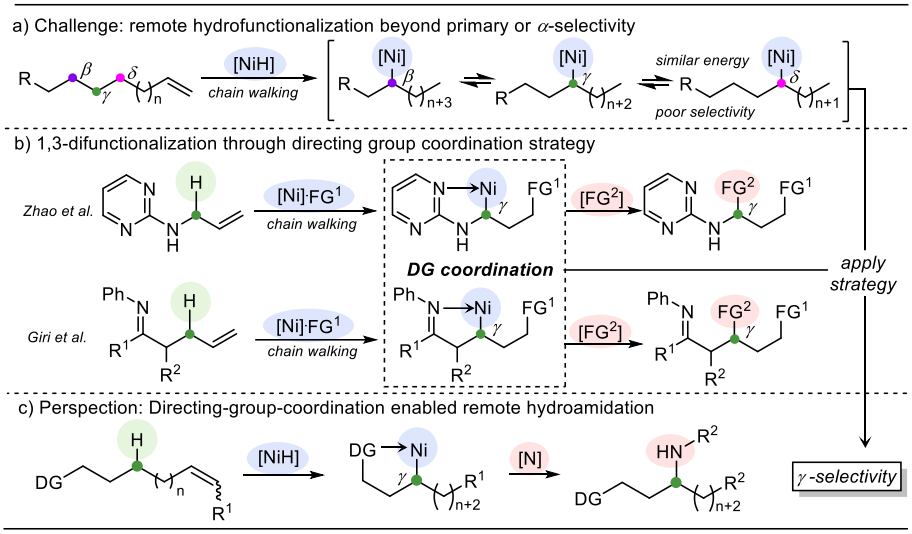


To solve the challenge in differentiation between methylene C–H sites, we wish to adopt this coordination strategy into hydrofunctionalization of alkenes (Scheme 6c) towards site-selective hydroamination of alkenes. By adopting suitable coordinating group into Ni-catalyzed remote hydrofunctionalization reactions, we wish to direct walking of Ni through 5-membered metallacycle, achieving selective installation of amide group at $\gamma$-position. We also wish to adopt dioxazolones as amide source for its versatility and facility in synthesis.

# 2.2. Methodology

## 2.2.1 Directing Group Screening[a]

First a series of synthetically useful directing groups were screened (Scheme 7). Thioether group gave the most ideal reaction outcoming among all screened directing groups, yielding 95% *γ*- and 4% Markovnikov product. With piperidine, a strong coordinating group as directing group, no hydroamidation product is detected.

**Scheme 7** Directing group screening[b]

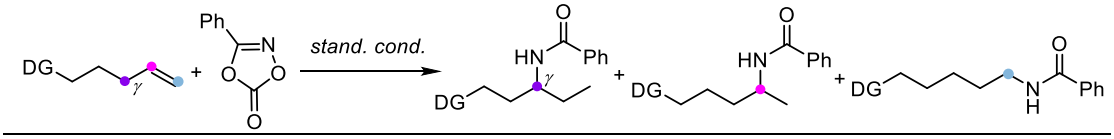


| Different DGs | *γ*%[a] | Markovnikov%[a] | Anti-Markovnikov%[a] |
|---|---|---|---|
| 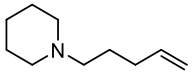 | n.d.[c] | n.d.[c] | n.d.[c] |
| 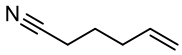 | n.d.[c] | n.d.[c] | 42 |
| 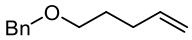 | n.d.[c] | 15 | 70 |
| 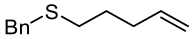 | 95 | 4 | n.d.[c] |

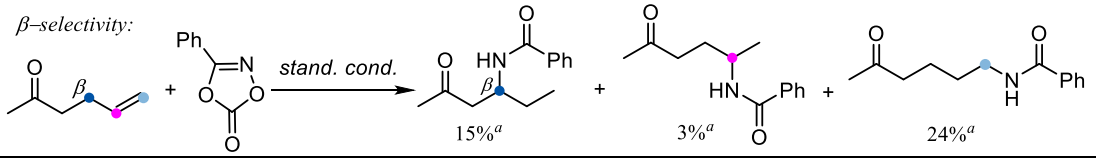


[a]Yields determined by crude NMR, $CH_2Br_2$ as internal standard. [b]Standard conditions: alkenes (0.2 mmol), dioxazolones (0.24 mmol), $[Ni(ClO_4)_2]\cdot 6H_2O$ (10 mol%), L4 (12 mol%), HBpin (2.0 equiv.), THF (2.0 mL) in $N_2$ at room temperature for 3 h unless otherwise specified. [c]not detected.

Cyanide group displayed almost no directing ability, with only anti-Markovnikov furnished in 42% yield. 70% anti-Markovnikov products and 15% Markovnikov product was obtained with ether as directing group. No *γ*-product was detected when adopting cyanide and ether group as directing group. Ni-walking was directed towards *β*-position by ketone, yielding 15% *β*-aminated product. However, differentiation between *β*- (15%), Markovnikov (3%) and anti-Markovnikov (24%) amination were not ideal under the direction of ketone. Considering the above-mentioned results

(Scheme 7), we choose to adopt thioether as directing group to achieve remote amidation at $\gamma$-position.

### 2.2.2 Reaction Optimization-Hydroamidation at Remote Site

After determining basic working principle and choosing the most ideal directing group, we went on to further explore detailed reaction conditions for remote hydroamidation. Ni precatalyst was first explored. Among all Ni precatalysts studied, $Ni(ClO_4)_2 \cdot 6H_2O$ gave the most ideal reaction outcoming, (95% NMR yield, >20:1 regioselectivity; Table 1, Entry 1). $NiX_2$ (X = Cl, Br, I), $Ni(OAc)_2 \cdot 4H_2O$ and $Ni(OTf)_2$ displayed almost no reactivity (Table 1, Entry 2-6). $Ni(acac)_2 \cdot 2H_2O$ showed certain reactivity, but with poor selectivity (Table 1, Entry 7). Except from above-mentioned Ni(II) centers, $Ni(COD)_2$ with a Ni(0) center was also able to catalyze the reaction, but the yield and regioselectivity obtained was not ideal (Table 1, Entry 8).

**Table 1** Optimization of Ni precatalyst

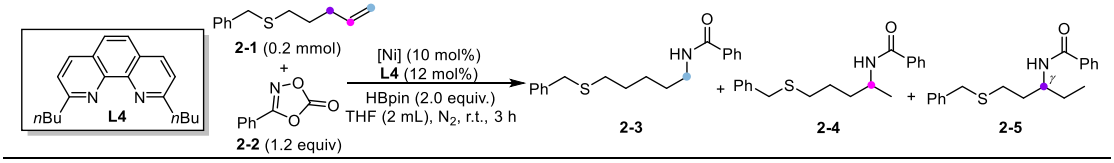


| Entry | [Ni] | **2-3**%[a] | **2-4**%[a] | **2-5**%[a] |
|---|---|---|---|---|
| 1 | $Ni(ClO_4)_2 \cdot 6H_2O$ | 4 | n.d.[b] | 95 |
| 2 | $NiCl_2$ | trace | n.d.[b] | n.d.[b] |
| 3 | $NiBr_2$ | trace | n.d.[b] | n.d.[b] |
| 4 | $NiI_2$ | trace | n.d.[b] | n.d.[b] |
| 5 | $Ni(OAc)_2 \cdot 4H_2O$ | trace | n.d.[b] | n.d.[b] |
| 6 | $Ni(OTf)_2$ | 5 | n.d.[b] | 36 |
| 7 | $Ni(acac)_2 \cdot 2H_2O$ | 7 | 6 | 4 |
| 8 | $Ni(COD)_2$ | 1 | 10 | 4 |

[a]Yields determined by crude NMR, $CH_2Br_2$ as internal standard. [b]not detected.

Next, we screened a series of solvents for their effect on the reaction. Among all the solvents explored, THF performed best (95% yield, >20:1 regioselectivity; Table 2,

Entry 1), followed by acetone (91% yield, >20:1 regioselectivity; Table 1, Entry 6) and DCE (86% yield, >20:1 regioselectivity; Table 2, Entry 7). With a structure similar to THF, dioxane also gave a fair reaction outcome (78% yield, ~16:1 regioselectivity; Table 1, Entry 2). Middling yields were given by DMF (60% yield) and DMA (63% yield), with unsatisfactory selectivities (<10:1) (Table 2, Entry 4 and 5). Exceeding our expect, MeCN gave a poor reaction outcoming (30% yield, ~6:1 regioselectivity) (Table 2, Entry 3). Nonpolar solvents such as toluene and diethyl ether also showed a poor performance (<20% yield) (Table 2, Entry 8 and 9).

**Table 2** Optimization of solvents[a]

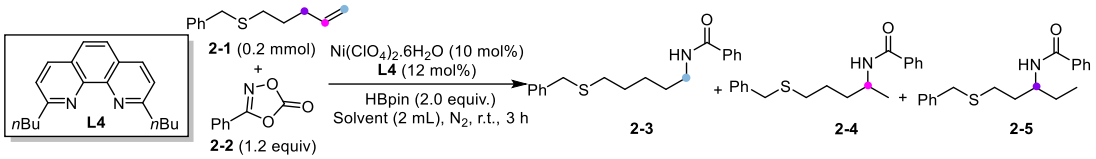


| Entry | Solvent | **2-3**%[a] | **2-4**%[a] | **2-5**%[a] |
|---|---|---|---|---|
| 1 | THF | 4 | n.d.[b] | 95 |
| 2 | dioxane | 5 | n.d.[b] | 78 |
| 3 | MeCN | 5 | 3 | 30 |
| 4 | DMF | 12 | trace | 60 |
| 5 | DMA | 7 | n.d.[b] | 63 |
| 6 | Acetone | 2 | n.d.[b] | 91 |
| 7 | DCE | n.d.[b] | n.d.[b] | 86 |
| 8 | toluene | 2 | n.d.[b] | 15 |
| 9 | diethyl ether | n.d.[b] | n.d.[b] | 4 |

[a]Yields determined by crude NMR, $CH_2Br_2$ as internal standard. [b]not detected.

After deciding the combination of $Ni(ClO_4)_2 \cdot 6H_2O$ and THF, the effect of ligand on the reaction was studied. 2,9-Dibutyl-1,10-phenanthroline (**L4**) favored chain-walking to give remote hydroamidation product most, giving 95% *γ*-product **2-5**; no Markovnikov product **2-4** and only 4% anti-Markovnikov product **2-3** was detected. When no ligand was present, the reaction proceeded with an unfavorable total yield (57%) and poor regioselectivity (~1:1.5) (Table 3, Entry 2). Among all phenanthroline ligands, 1,10-phenanthroline with no substituent on 2,9-positions (**L1**) gave a relatively

low yield (Table 3, Entry 3), while **L2** ~ **L4** with one or two substituents on 2,9-positions gave fair to high yields (Table 3, Entry 1, 4-6). These results together indicate that having at least one substituent on 2,9-positions is crucial for the reaction. 2-Methylphenanthroline (**L2**) favored Markovnikov product **2-4** with a 71% yield (Table 3, Entry 4), while **L3** and **L4** both favored *γ*-product **2-5**, with yields of 74% and 95%, respectively (Table 3, Entry 5 and 1). Between the chain-walking-favoring ligands **L3** and **L4**, the selectivity of **L3** (~3.5:1; chain-walking product to all side products) was not comparable to **L4** (>20:1). Considering that **L4** is much bulkier than **L3**, we reasoned that a more hindered environment would lead to a higher preference towards chain-walking products. Also, several other ligands were examined, such as bipyridine (Table 3, Entry 7), 6,6'-dimethyl-2,2'-bipyridine (Table 3, Entry 8), diamine (Table 3, Entry 9), pyridine (Table 3, Entry 10), terpyridine (Table 3, Entry 11) and dppm (Table 3, Entry 12). These ligands all gave unfavorable yields and selectivity.

**Table 3** Optimization of ligands[a]

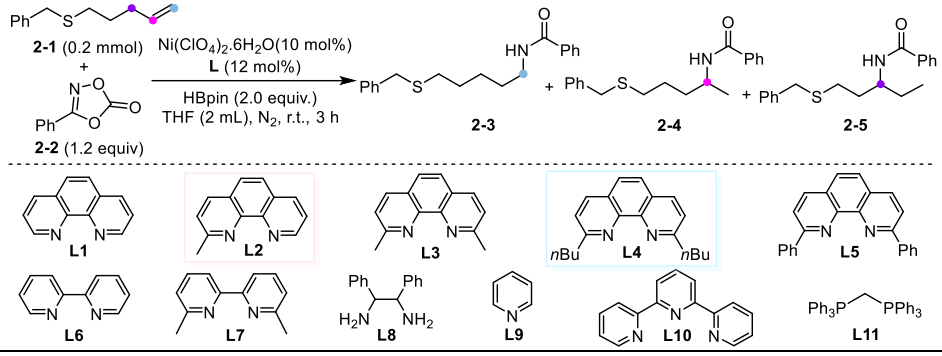


| Entry | ligand | **2-3**%[a] | **2-4**%[a] | **2-5**%[a] |
|---|---|---|---|---|
| 1 | **L4** | 4 | n.d.[b] | 95 |
| 2 | /[c] | n.d.[b] | 35 | 22 |
| 3 | **L1** | n.d.[b] | 30 | 12 |
| 4 | **L2** | 3 | 71 | 14 |
| 5 | **L3** | 6 | 16 | 74 |
| 6 | **L5** | n.d.[b] | 20 | 20 |
| 7 | **L6** | n.d.[b] | 8 | 21 |
| 8 | **L7** | 13 | 6 | 73 |
| 9 | **L8** | n.d.[b] | 18 | 7 |
| 10 | **L9** | n.d.[b] | 28 | 13 |
| 11 | **L10** | n.d.[b] | 25 | 8 |
| 12 | **L11** | n.d.[b] | 27 | 26 |

[a]Yields determined by crude NMR, $CH_2Br_2$ as internal standard. [b]not detected. [c]no ligand added

Further exploration was done on the selection of hydride source. HBpin is an effective hydride source at room temperature, under which both MeOH and $(EtO)_2MeSiH$ showed almost no reactivity (Table 4, Entry 1-3). Notably, by raising the temperature to 70℃, remote hydroamidation product **2-5** and linear amidation product **2-3** was furnished in 20% yield and 4% yield accordingly with $(EtO)_2MeSiH$ as hydride source (Table 4, Entry 4).

**Table 4** Optimization of hydride sources[a]

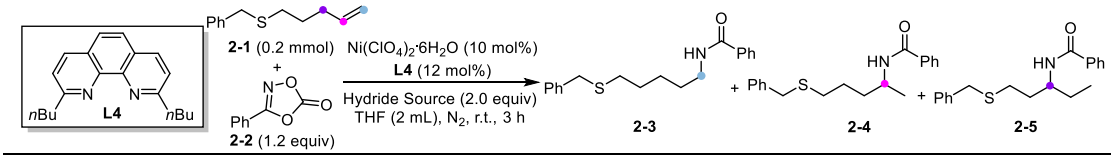


| Entry | Hydride Source | **2-3**%[a] | **2-4**%[a] | **2-5**%[a] |
|---|---|---|---|---|
| 1 | HBpin | 4 | n.d.[b] | 95 |
| 2 | MeOH | n.d.[b] | n.d.[b] | n.d.[b] |
| 3 | $(EtO)_2MeSiH$, r.t. | 1 | n.d.[b] | n.d.[b] |
| 4 | $(EtO)_2MeSiH$, 70℃ | 4 | n.d.[b] | 20 |

[a]Yields determined by crude NMR, $CH_2Br_2$ as internal standard. [b]not detected.

Associating all the optimization results above, we defined the combination of most powerful conditions as standard conditions: 10 mol% $Ni(ClO_4)_2·6H_2O$, 12 mol% 2,9-dibutyl-1,10-phenanthroline, THF as solvent, HBpin (2.0 equiv.) as hydride source, running under $N_2$ at room temperature for 3h.

**Table 5** Other deviations from standard conditions[a]

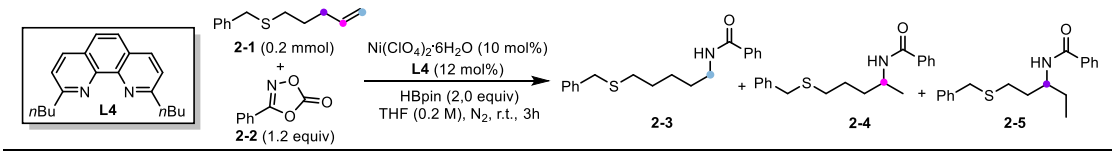


| Entry | Deviation from standard conditions | **2-3**%[a] | **2-4**%[a] | **2-5**%[a] |
|---|---|---|---|---|
| 1 | None | 4 | n.d.[b] | 95 |
| 2 | without $Ni(ClO_4)_2·6H_2O$ | n.d.[b] | n.d.[b] | n.d.[b] |
| 3 | 5 mol% $Ni(ClO_4)_2·6H_2O$ | trace | n.d.[b] | 60 |
| 4 | 2 mol% $Ni(ClO_4)_2·6H_2O$ | trace | n.d.[b] | 38 |
| 5 | 1 mol% $Ni(ClO_4)_2·6H_2O$ | trace | n.d.[b] | 42 |
| 6 | 1.5 equiv. **2-2** | 4 | n.d.[b] | 97 |
| 7 | 2.0 equiv. **2-2** | 3 | n.d.[b] | 95 |

[a]Yields determined by crude NMR, $CH_2Br_2$ as internal standard. [b]not detected.

Some deviations were further made from the standard conditions to probe the minimum equivalence of $Ni(ClO_4)_2·6H_2O$ and dioxazolone. Reducing the amount of $Ni(ClO_4)_2·6H_2O$ led to an notable reduce in yield: 60% product were furnished with 5%

$Ni(ClO_4)_2·6H_2O$ (Table 5, Entry 3), and reducing the amount of $Ni(ClO_4)_2·6H_2O$ to 2 mol% and 1 mol% led to further reduced yields of around 40% (Table 5, Entry 4 and 5). No product was obtained without $Ni(ClO_4)_2·6H_2O$ (Table 5, Entry 2).The reaction showed no better performance towards lifting the amount of dioxazolone (Table 5, Entry 6 and 7). No further lowering in the amount of dioxazolone were conducted since 1.2 equiv. is already a satisfying equivalence.

### 2.2.3 Reaction Optimization-Hydroamidation at Original Site

Noticing the special Markovnikov selectivity of **L2** (Table 6, Entry 4), we further optimized several solvents to switch the selectivity to Markovnikov product by hydroamidation at the original double bond. By elevating the amount of dioxazolone to 2 equiv., a better selectivity towards Markovnikov product was given by several common organic solvents.

**Table 6** Optimization of solvents (original site)[a]

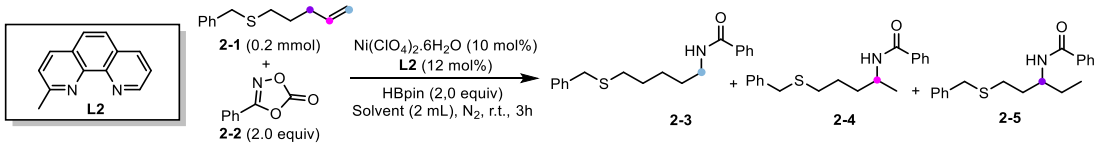


| Entry | Solvent | **2-3**%[a] | **2-4**%[a] | **2-5**%[a] |
|---|---|---|---|---|
| 1 | THF | 3 | 71 | 14 |
| 2 | dioxane | 4 | 64 | 18 |
| 3 | DMF | 3 | 50 | 4 |
| 4 | MeCN | 2 | 77 | 6 |
| 5 | acetone | 3 | 55 | 6 |
| 6 | DCE | 3 | 59 | 17 |
| 7 | DMA | 3 | 64 | 5 |

[a]Yields determined by crude NMR, $CH_2Br_2$ as internal standard.

MeCN gave the best performance among all solvents screened, furnishing Markovnikov product in 77% yield with >10:1 selectivity (Table 6, Entry 4). Similar in structure, THF and dioxane (Table 6, Entry 1 and 2) gave moderate yields (both >60%),

but with unfavorable selectivity (THF around 4:1; dioxane <3:1). DMF and DMA also gave a pair of similar result, with fair selectivity (>7:1) but relatively low yields of Markovnikov products (64% and 50%, respectively) (Table 6, Entry 4 and 8). Other solvents such as DCE and acetone were also proved to be less efficient than MeCN for this transformation (Table 6, Entry 5 and 6).

## 2.3. Results and Discussions

### 2.3.1 Substrate Scope-Hydroamidation at Remote Site

After settling the standard reaction conditions, we went on to examine the synthetic versatility of the reaction (Scheme 8). Around 30 structurally diverse dioxazolones were first selected and subjected to react with 5-(benzylthio)-1-pentene **2-1** under standard conditions.

**Scheme 8** Dioxazolone scope (remote site hydroamidation)

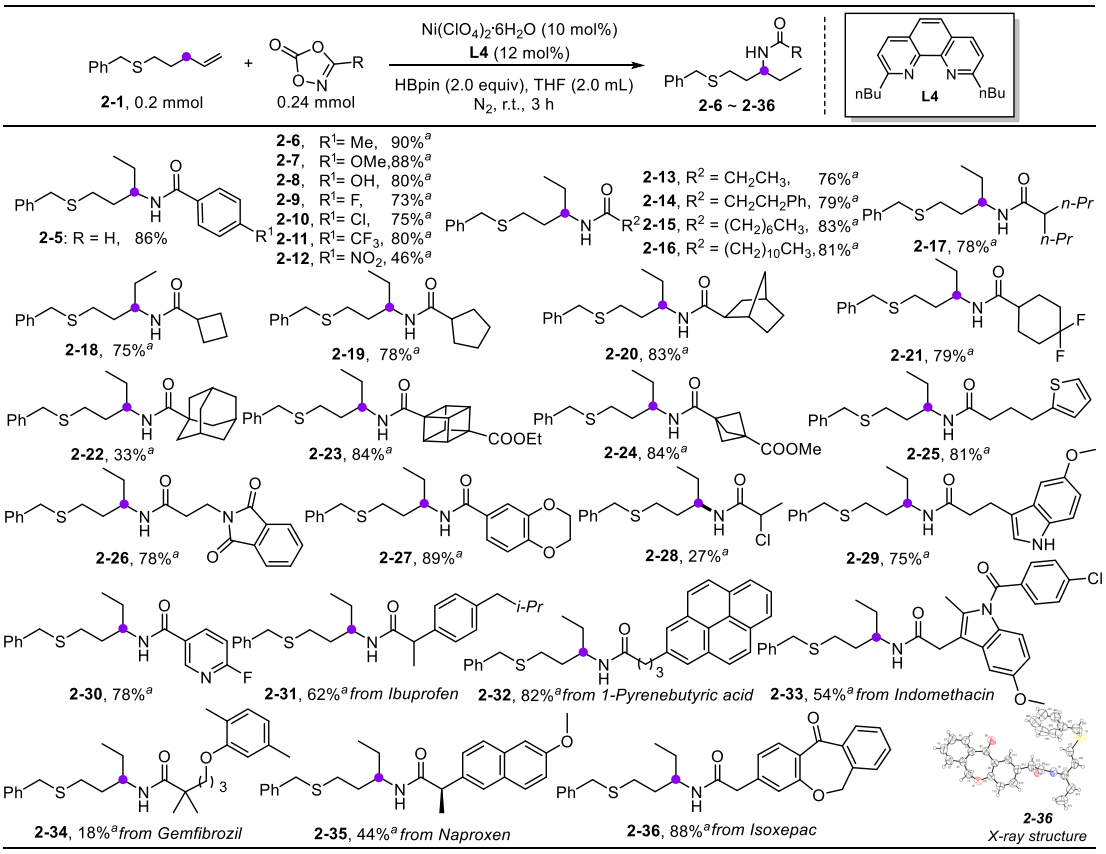


[a]Isolated yields.

Aryl dioxazolones reacted efficiently to furnish corresponding amides, with isolated yields up to 90% (**2-5** ~ **2-12**, **2-27**, **2-30**). For 4-substituted aryl dioxazolones, bearing electron donating groups (EDG) would lead to higher yields (>80%) than electron withdrawing groups (EWG) (<80%). Dioxazolones linked to primary alkyl groups and saturated carbocycles (including strained carbocycles) were also proved to be powerful reaction counterparts, giving targeted amides in ~80% yields (**2-13** ~ **2-21**, **2-25**, **2-26**). However, when rising the steric hindrance by installing tertiary alkyl group, yields are largely reduced (**2-22**, 33%; **2-34**, 18%). Even so, stringed rings showed successful coupling to give **2-23** and **2-24** in >80% yields. Luckily, dioxazolone derived from 2-chloropropanoic acid also coupled with **2-1** successfully to give **2-28** in 27% yield, showing a secondary halide group tolerance. However, yield to **2-28** is low, presumably due to the influence of high acidity of hydrogen atom on carbon next to the chloride group. Dioxazolones derived from biological active molecules and natural products, such as Ibuprofen (**2-31**, 62%), 1-Pyrenebutyric acid (**2-32**, 82%), Indomethacine (**2-33**, 54%), Gemfibrozil (**2-34**, 18%), Naproxen (**2-35**, 44%) and Isoxepac (**2-36**, 88%) also gave corresponding products in satisfactory yields. Unfortunately, for all products bearing two chiral centers, dr value was close to 1:1.

**Scheme 9** Alkene scope (remote site hydroamidation)[a]

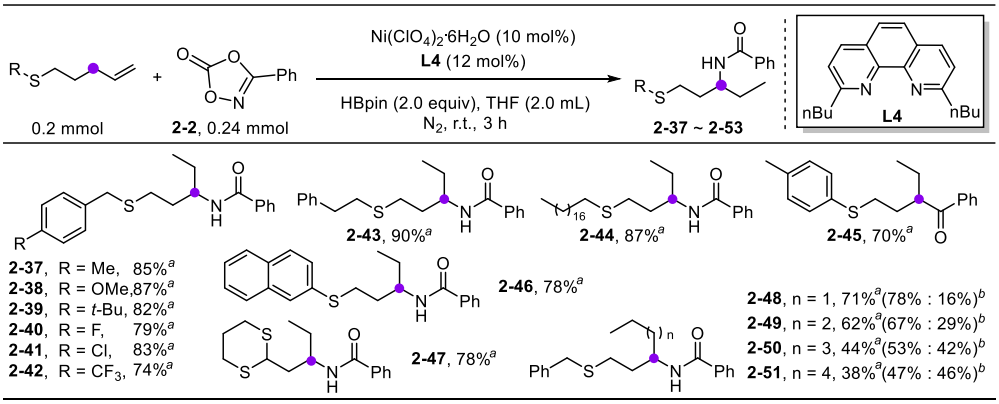


[a]Isolated yields. [b]Yields of main product:yields of all other isomers; Yields determined by crude NMR, $CH_2Br_2$ as internal standard.

Next, a series of alkenes were subjected to react with 3-phenyl-1,4,2-dioxazol-5-one **2-2** under standard conditions to further explore the substrate scope of the reaction (Scheme 9). Derivations made by substitution on benzene ring of **2-1** led to almost no

change in the yield of amide products (**2-37** ~ **2-42**). Also, adding carbon between benzene ring and sulfur atom (**2-43**) and replacing benzene ring with alkyl group (**2-44**) caused negligible influence to the product yield. Replacing alkyl sulfides with aryl sulfides caused a slight decrease in product yields (**2-45** ~ **2-46**), presumably due to increase in steric hindrance during coordination of sulfur atom to Ni. Alkenes with two sulfur atoms also coupled successfully with **2-2** to give **2-47** in 78% yield. Longer distance between double bond and sulfur atom was allowed, but the yield toward targeted chain-walking product decreases as more carbon is adopted between sulfur atom and double bond (**2-48** ~ **2-51**).

### 2.3.2 Substrate Scope-Hydroamidation at Original Site

Having studied the synthetic versatility of remote hydroamidation, we further examined the substrate scope of hydroamidation at original site enabled by **L2** (Scheme 10).

**Scheme 10** Substrate scope (original site hydroamidation)[a]

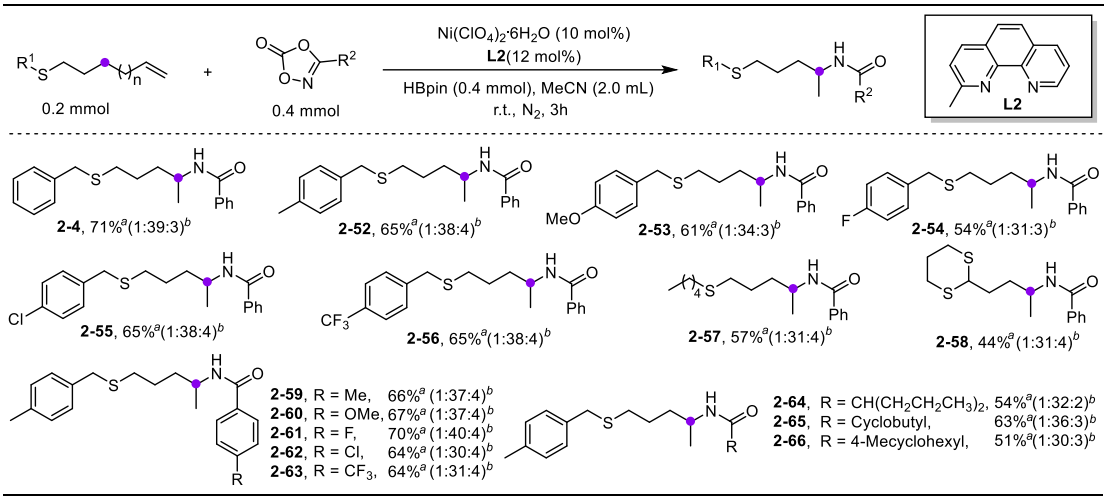


[a]Isolated yields. [b]Yields of main product:yields of all other isomers; Yields determined by crude NMR, $CH_2Br_2$ as internal standard.

Similar to remote hydroamidation, substitution on benzene ring led to trivial changes (**2-4**, **2-52** ~ **2-56**), with satisfactory yields and high selectivity (up to 10:1, NMR yield of Markovnikov product:NMR yield of all side products). Alkenes bearing aliphatic group next to sulfur atom and two sulfur atoms also reacted smoothly to give targeted

products **2-57** and **2-58**. A series of structurally diverse dioxazolones also showed reactivity towards Markovnikov products in satisfying yields and selectivity (**2-59** ~ **2-66**).

### 2.3.2 Mechanistic Studies

After examining the substrate scope of our methodology, we went on to seek for the underlying mechanism of the reaction. First of all, to verify the binding ability of sulfur in forming stabilized metallacycle, we synthesized 2-((pent-4-en-1-ylthio)methyl)pyridine **2-67**. **2-67** has a strong binding ability, and is able to form stable complex **2-68** when treated with 0.5 equiv. $NiCl_2$. X-ray structure of **2-68** clearly displays a six-coordinated Ni center, bound to two molecules of **2-67** in a *N*,*S*-bidentate manner and two Cl anions (Scheme 11a). As 6-membered ring would be more stable than 5-membered ring when fused with a 5-membered ring, considering the two possible intermediate when **2-67** was subjected to react, 5,6-fused ring **A** would be more stable than 5,5-fused ring **B**. Thus, we predicted that if sulfur atom is responsible for directing the selectivity by forming stabilized metallacycles, in this situation the selectivity should be guided towards Markovnikov product **2-70** instead of $\gamma$-amidation product **2-71**. The observed overpowering selectivity towards **2-70** (20% yield, no **2-71** detected) largely supports our conjecture that sulfur atom helps differentiate challenging methylene positions by binding to Ni (Scheme 11b).

**Scheme 11** Role of sulfur atom[a]

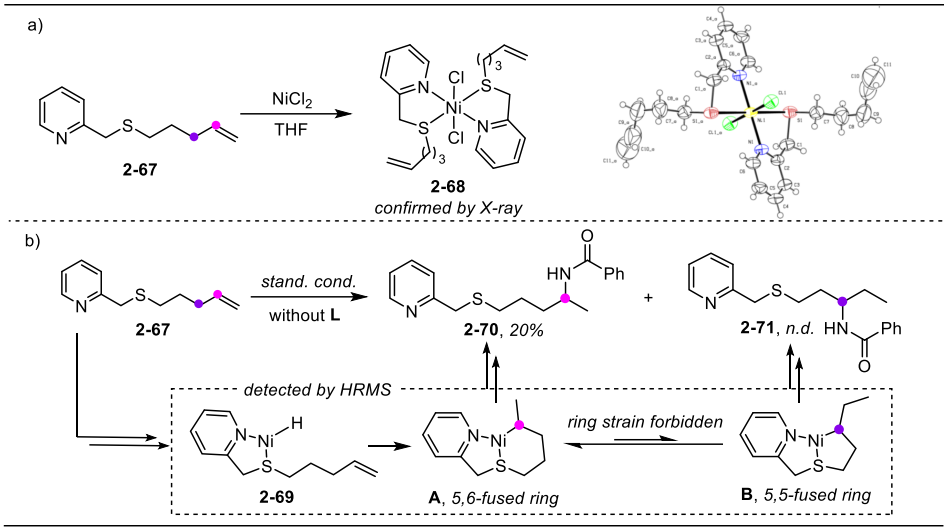


[a]Standard conditions: alkenes (0.2 mmol), dioxazolones (0.24 mmol), $[Ni(ClO_4)_2]\cdot 6H_2O$ (10 mol%), **L4** (12 mol%), HBpin (2.0 equiv.), THF (2.0 mL) in $N_2$ at room temperature for 3 h unless otherwise specified.

To further explore the preference of directing ability of sulfur-directed *γ*-selectivity over benzylic and primary selectivity, we constructed substrate **2-74** and **2-75**, where the metal will undergo one-carbon migrations to both *γ*-position and linear/benzylic position (Scheme 12). When subjecting **2-72** to standard reaction conditions, a powerful preference towards *γ*-position over linear position was shown with a high regioisomeric ratio. Reaction done with **2-73** gave a result where *γ*-position was slightly preferred over benzylic position, producing a 2:1 mixed product.

**Scheme 12** Competition with other preferred positions[a]

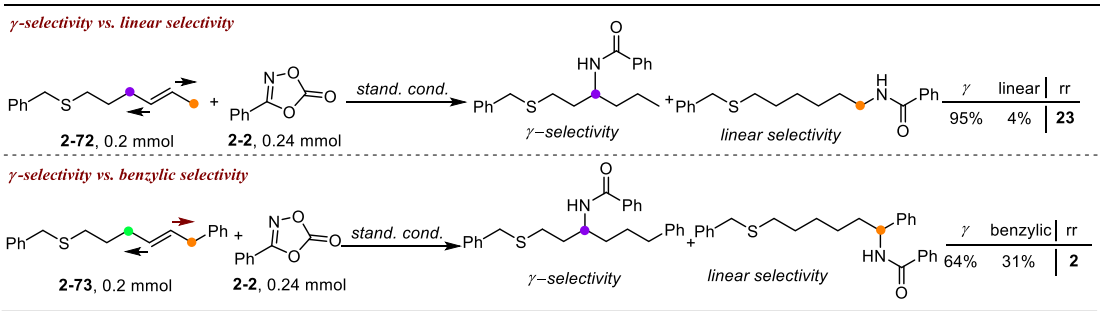


[a]Standard conditions: alkenes (0.2 mmol), dioxazolones (0.24 mmol), $[Ni(ClO_4)_2]\cdot 6H_2O$ (10 mol%), **L4** (12 mol%), HBpin (2.0 equiv.), THF (2.0 mL) in $N_2$ at room temperature for 3 h unless otherwise specified.

Next, to probe the underlying process of Ni walking on the hydrocarbon chain, a deuterium labelling study was conducted (Scheme 13). Substrate **2-76** was subjected to

react with **2-2** under standard reaction condition but with DBpin as hydride source. From terminal position to *γ*-position, D incorporation can be found all positions in between along the chain. This scrambling of deuterium suggests that metal migrates along the chain by 1,2-hydride shift mechanism, through a cascade *β*-hydride elimination/migratory insertion process.

**Scheme 13** Deuterium labelling experiment[a]

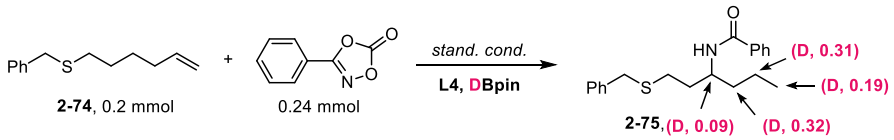


[a]Standard conditions: alkenes (0.2 mmol), dioxazolones (0.24 mmol), $[Ni(ClO_4)_2]\cdot 6H_2O$ (10 mol%), **L4** (12 mol%), HBpin (2.0 equiv.), THF (2.0 mL) in $N_2$ at room temperature for 3 h unless otherwise specified.

To examine whether or not the reaction involves radical intermediates, three parallel experiments were done by reacting under standard conditions with radical scavengers such as TEMPO, BHT and α-cyclopropylstyrene (Scheme 14). Compared to reaction without a radical scavenger, introducing BHT and α-cyclopropylstyrene caused nearly no influence to the reaction, suggesting that the reaction is not likely to occur through radical intermediates. However, introducing TEMPO reduced the yield to 63%, and we reasoned that part of the low valence intermediates were oxidized by TEMPO, causing a deactivation in part of the catalyst.

**Scheme 14** Radical trapping experiments[a]

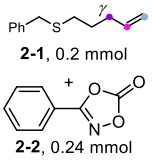


*stand. cond.*

| radical scavenger (0.4 mmol) | *γ* | Markovnikov | anti-Markovnikov | (total yield) |
|---|---|---|---|---|
| TEMPO | 63% | n.d. | n.d. | (63%) |
| BHT | 87% | n.d. | 6% | (93%) |
| *α*-cyclopropylstyrene | 81% | n.d. | 4% | (85%) |

[a]Standard conditions: alkenes (0.2 mmol), dioxazolones (0.24 mmol), $[Ni(ClO_4)_2]\cdot 6H_2O$ (10 mol%), **L4** (12 mol%), HBpin (2.0 equiv.), THF (2.0 mL) in $N_2$ at room temperature for 3 h unless otherwise specified.

To uncover the rate determining step of the reaction, competing reactions were done by using a series of aryl dioxazolones (**2-77** ~ **2-83**) differing only in *para*-substituents to compete with **2-2** under standard reaction conditions (Scheme 15). 6 parallel reactions were conducted as [**2-2**+**2-77**], [**2-2**+**2-78**], [**2-2**+**2-79**], [**2-2**+**2-80**], [**2-2**+**2-**

**81**], [**2-2**+**2-82**] and [**2-2**+**2-83**], and the yields were determined by $^1$H NMR with $CH_2Br_2$ as internal standard.

**Scheme 15** Competing reactions[a]

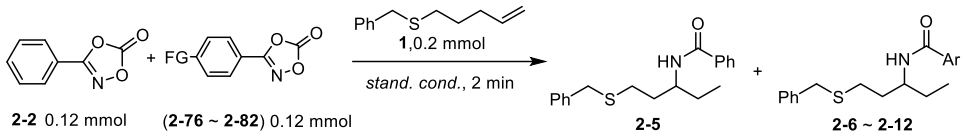


[a]Standard conditions: alkenes (0.2 mmol), dioxazolones (0.24 mmol), $[Ni(ClO_4)_2]\cdot 6H_2O$ (10 mol%), **L4** (12 mol%), HBpin (2.0 equiv.), THF (2.0 mL) in $N_2$ at room temperature for 3 h unless otherwise specified.

A Hammett plot was drawn by applying σ(para)as horizontal axis and $\log(k_{FG}/k_H)$ as vertical axis (Figure 4). The plot showed a good linear relationship, with a slope of -0.483 and $R^2$ of 0.975. These findings suggest that the rate determining step is related to dioxazolones, and during rate determining step, partial positive charge would be built up.

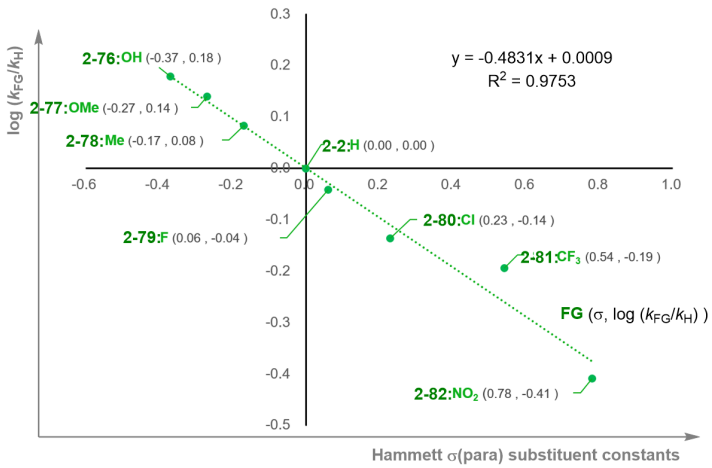


**Figure 4** Hammett Plot

Combining all previous experimental results, A possible reaction mechanism can be proposed (Figure 5).

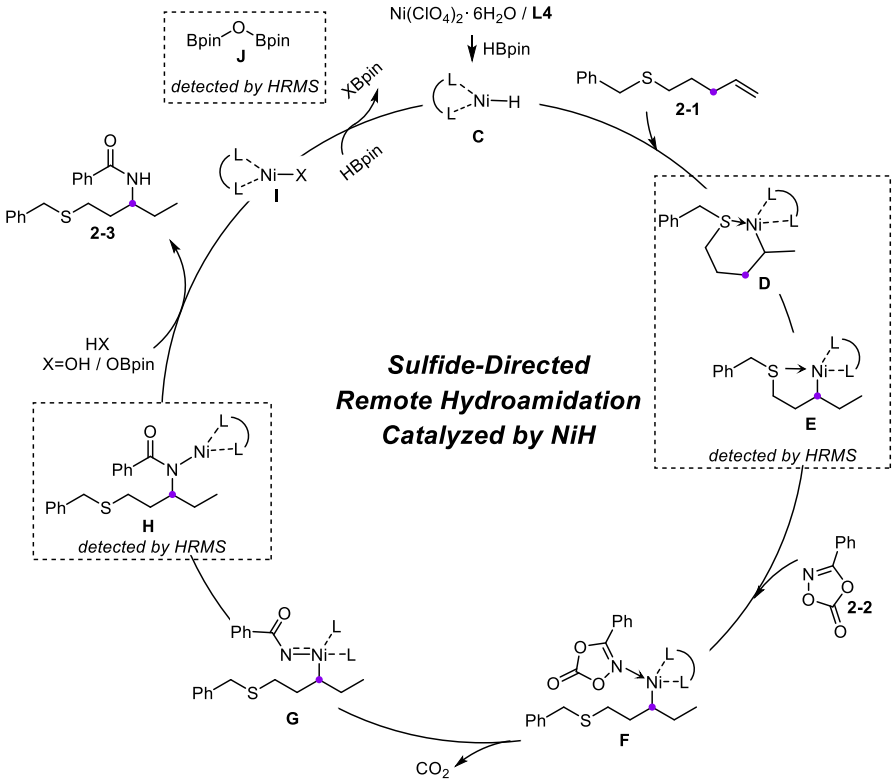


**Figure 5** Proposed Reaction Mechanism

Starting from $Ni(ClO_4)_2·6H_2O$ and **L4**, a [NiH] species **C** is likely to be generated by addition of HBpin. Alkene **2-1** then would undergo hydrometalation with **C** to generate Ni-alkyl species **D**, which would then rapidly go through a reversible *β*-H elimination/migratory insertion process to give a thermodynamically stabled intermediate **E**. **E** then coordinates with dioxazolone to form **F**. Through releasing a molecule of $CO_2$, metal-nitrenoid complex **G** would be generated from **E**. **G** then goes through nitrene insertion to generate **H**, which was then protonated to give the product **5** and a [NiX] species **I**. [NiH] species **C** was then regenerated from **I** by HBpin, and the catalytical cycle was completed.

**Scheme 16** Variation of two conjectures

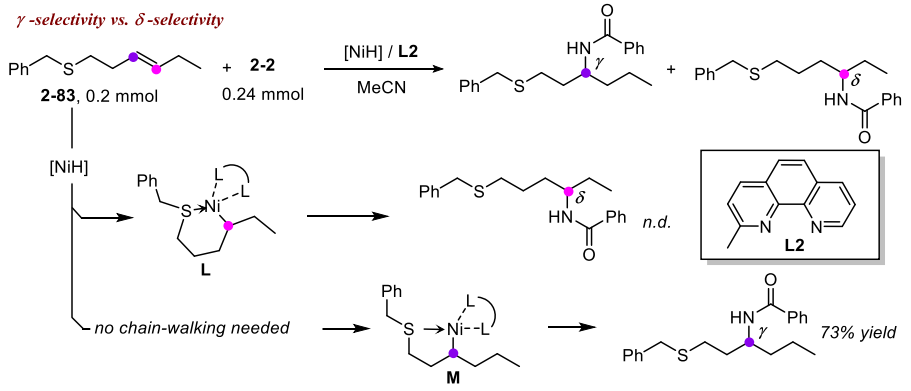


After settling the mechanism study for remote hydroamidation, we then turned to discuss why switching to **L2** would lead to hydroamidation at original double bond. Two possible reasons were proposed: the first being that using **L2** lead to a change in thermodynamic stability of 5- and 6- membered rings, and the second being that using **L2** lead to difference in relative speed of chain-walking and coupling, completing the reaction before chain-walking to *γ*-position was achieved. To decide which one of the conjectures is correct, we synthesized internal alkene **2-83**, where no chain-walking is required to both *γ*-position and *δ*-position (Scheme 16). A high *γ*-selectivity was observed by treating **2-83** to react with **2-2** by using **L2**, suggesting that instead of a reversal in stability of metallacycles, an insufficient chain-walking lead to the original site selectivity of **L2**.

**Scheme 17** Relative speed of metal migration and cross coupling

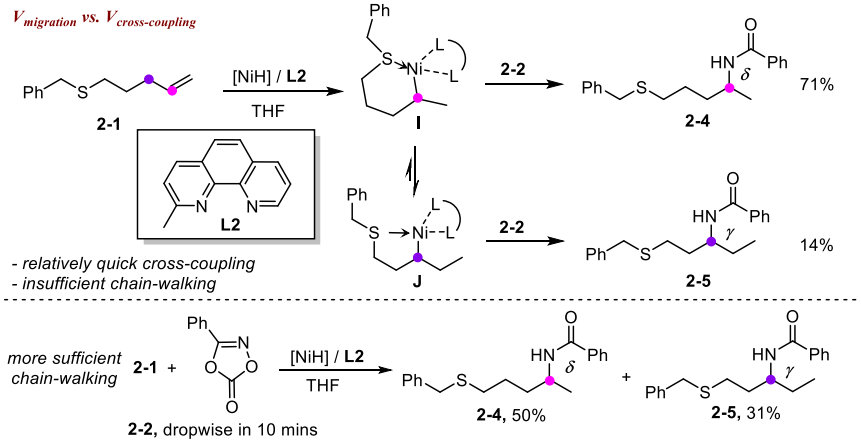


To further verify the conjecture that the original site selectivity is caused by the change in relative speed of metal migration and cross-coupling, we performed an experiment where **2-1** was subject to react with **2-2** by using **L2** as ligand, under the

condition where **2-2** was added dropwise over 10 minutes (Scheme 17). By adding **2-2** in a dropwise pattern, we manually provided more time for metal to walk along the chain, leading to more sufficient chain-walking than adding **2-2** in one portion. A lifted selectivity towards *γ*-position was observed, proving that the high original site selectivity was caused by insufficient chain-walking, which can be attributed to a relative quicker cross-coupling resulted from adopting **L2** as ligand.

## 2.4. Conclusion

In conclusion, we developed a thioether-directed Ni-catalyzed hydroamidation reaction of alkenes. By applying 2,9-dibutyl-1,10-phenanthroline as ligand, hydroamidation product was formed at *γ*-position in high regioselectivity. During this process, forming thermodynamically favored metallacycle fixed metal at *γ*-position during migration process, which helped to differentiate sites besides primary and α-positions. Switching ligand to **L2** shifted the selectivity towards Markovnikov products in ideal yields. A wide substrate scope can be applied to both synthetic protocols, with >40 examples with up to 90% yield and up to >20:1 rr reported. Natural product derivatives and biological active elements can also be introduced to the substrate scope. Some mechanistic studies were conducted, and a possible reaction mechanism was proposed based on all the mechanistic studies.

## 2.5 Experimental Section

### 2.5.1 General Information

All solvents (including superdry solvents) and reagents are used as received from commercial sources without any purification. All glassware were dried at 150 °C overnight before use. All Ni-catalyzed hydroamidation were carried out in a glovebox. Monitoring of reaction was done with TLC by using UV light (254 nm) or $KMnO_4$ stain. Purification on flash column chromatography was done with silica gel (Merck, 230-400 mesh) column. $^{1}H$ and $^{13}C$ NMR spectra were recorded on a Brüker DPX-400 MHz

spectrometer, with chemical shift (δ) values given in ppm and referenced to solvent residual peaks. Coupling constants (*J*) were reported in hertz (Hz). NMR yields were calculated and reported with $CH_2Br_2$ as internal standard, giving a singlet signal at $\delta_H$ 4.9 ppm in $CDCl_3$. Unless stated as NMR yields, all isolated yields refer to chromatographically and spectroscopically pure product isolated. High-resolution mass spectra (HRMS) were collected on a VG MICROMASS Fison VG platform, a Finnigan Model Mat 95 ST instrument, or a Brüker APEX 47e FT-ICR mass spectrometer. X-ray crystallographic study was performed by a Brüker CCD area detector diffractometer.

## 2.5.2 Substrate Preparation

### *Preparation of Alkenes*

*General Method A*

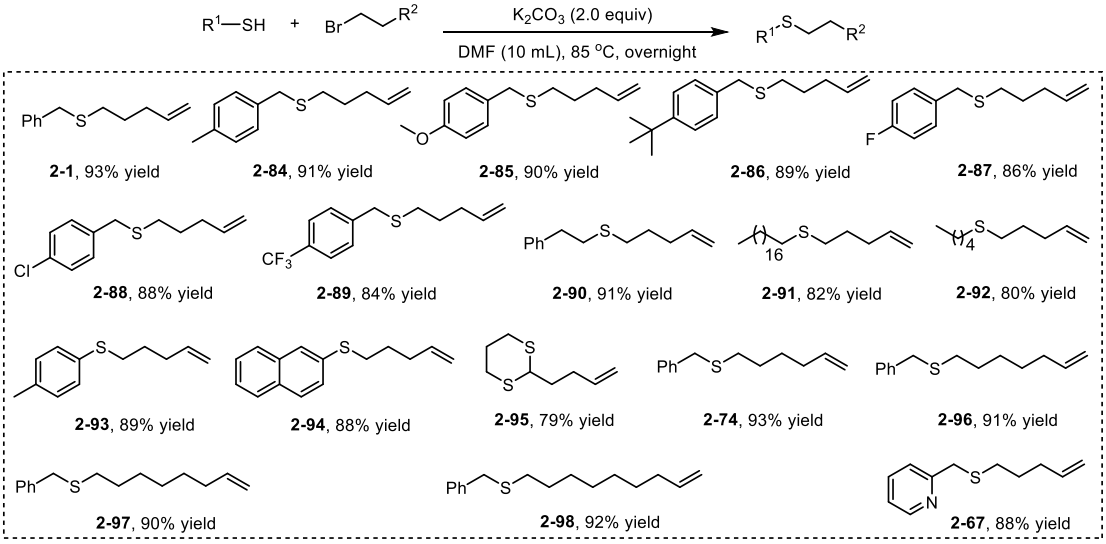


A 50 mL sealed tube was charged with a magnetic stir bar. Benzyl mercaptan (5.0 mmol), 5-bromopent-1-ene (7.5 mmol, 1.5 equiv.), $K_2CO_3$ (15.0 mmol, 3.0 equiv.) and DMF (10 mL) was then added to the tube. The tube was then charged to 85 ºC heating and the reaction mixture was allowed to go overnight under vigorous stirring. Upon finishing, the reaction mixture was cooled to room temperature, poured into water (50 mL) and then extracted with DCM (20 mL × 3). The organic layer was combined, dried over $Mg_2SO_4$ and concentrated in vacuo. The residue was purified by flash column chromatography (*n*-hexane:EA = 100:1) to give the corresponding products.

*General Method B*

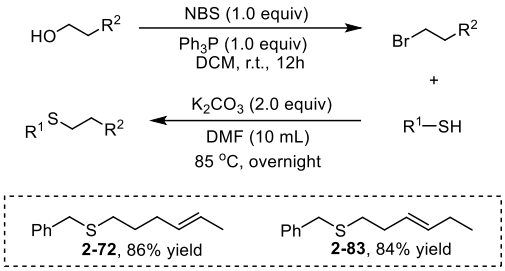


Corresponding alcohol (10.0 mmol) was dissolved in DCM (20 mL) in a 50 mL round bottom flask charged with a magnetic stir bar. To the solution was then added $PPh_3$ (10.5 mmol, 1.05 equiv.). *N*-bromosuccinimide (10.5 mmol, 1.05 equiv.) was added to the mixture in portions over 40 minutes. The reaction mixture was then stirred at room temperature overnight. The resulting $Ph_3PO$ precipitate was removed through filtration. The filtrate was concentrated in vacuo, and the crude product obtained was used directly for the next step as General Method B without any purification. Through General Method B, compound **2-72** and **2-83** was obtained.

*General Method C*

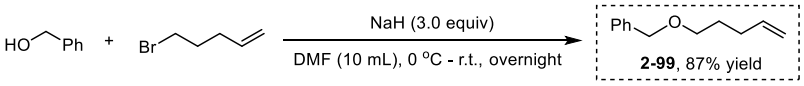


To a 50 mL round bottom flask with a magnetic stir bar was added benzyl alcohol (5.0 mmol), NaH (15.0 mmol, 3.0 equiv.) and DMF (10 mL). The flask was then cooled to 0 ºC, and 5-bromopent-1-ene (7.5 mmol, 1.5 equiv.) was added dropwise via syringe. Upon completing addition, the reaction mixture was slowly brought back to room temperature and stirred overnight. The reaction was then quenched with saturated aqueous $NH_4Cl$ solution and extracted with DCM (20 mL × 3). The combined organic extract was then dried over $Mg_2SO_4$ and concentrated in vacuo. The resulting crude mixture was purified by flash column chromatography (*n*-hexane:EA = 100:1) to give the corresponding product **2-99**.

*General Method D*

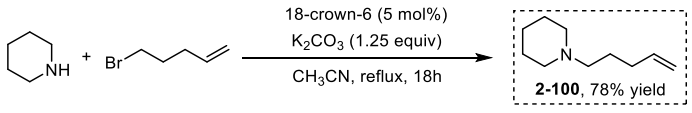


18-crown-6 (0.360 g, 1.36 mmol), $K_2CO_3$ (4.83 g, 35.0 mmol) and piperidine (2.39 mL, 28.1 mmol) was added to a 100 mL sealed tube with a magnetic stir bar. 5-bromo-

1-butene (5.00 g, 33.6 mmol) and $CH_3CN$ (20 mL) was then added to the mixture. The reaction mixture was then refluxed overnight. Upon finishing, the reaction mixture was slowly cooled to room temperature, poured into water and extracted with DCM (20 mL × 3). The combined organic phase was then dried over $MgSO_4$ and solvent is removed in vacuo. The crude product obtained was then purified by flash column chromatography (*n*-hexane:EA = 100 : 1) to give **2-100** as colorless oil.

*General Method E*

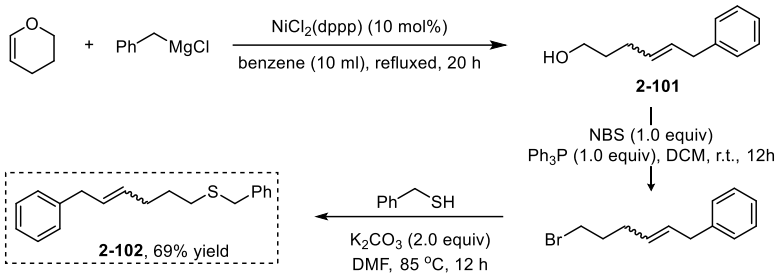


In a nitrogen-filled glovebox, $NiCl_2$(dppp) (1.0 mmol, 10 mol%) and benzylmagnesium bromide (2.0 mmol, 20 mol%) was added to a 50 mL round bottom flask with a magnetic stir bar. To the flask was then added 15 mL dry benzene. The flask was sealed with a rubber septum, taken out of glovebox, and the resulting mixture was stirred at room temperature for 15 minutes. Next, another portion of benzylmagnesium bromide (10.0 mmol, 1 equiv.) and 3,4-dihydro-2*H*-pyran (10.0 mmol, 1 equiv.) was added. The reaction mixture was stirred at room temperature for another 15 minutes, and then subjected to reflux for 20 h. Upon finishing, the reaction was quenched with saturated aqueous $NH_4Cl$ solution, poured into water (50 mL) and then extracted with DCM (20 mL × 3). The combined organic extract was dried over $Mg_2SO_4$, and concentrated in vacuo. The residue was purified by flash column chromatography (*n*-hexane:EA = 4 : 1) to give pure **2-101**. **2-101** was then converted to alkene substrate **2-102** through General Method C.

## *Preparation of Dioxazolones*

*General Method F*

*Step A*

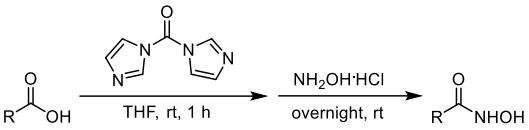


A 50 mL round bottom flask was charged with a magnetic stir bar. To the flask was added carboxylic acid (10.0 mmol, 1.0 equiv.) and THF (20 mL). Then at room temperature, to the solution was added CDI (1,1'-carbonyldiimidazole) (15.0 mmol, 1.5 equiv.). The resulting mixture was allowed to stir at room temperature for 1 h. $NH_2OH·HCl$ (20.0 mmol, 2.0 equiv.) was then added to the mixture, stirred overnight, quenched with 20 mL 5% $KHSO_4$ aq. and extracted with EA (20 mL × 3). The combined organic phase was dried over $Na_2SO_4$. Solvent was removed under vacuo. The crude hydroxamic acid was used directly for the next step without further purification.

*Step B*

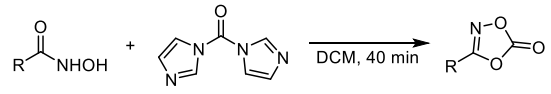


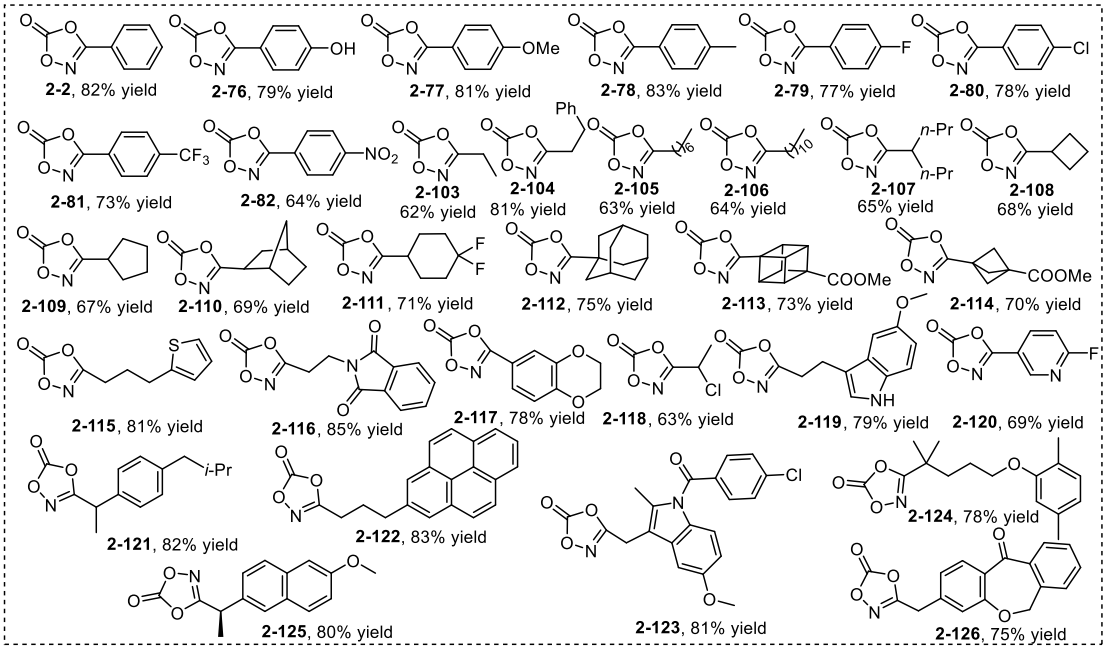


To the crude hydroxamic acid obtained above in a round bottom flask, magnetic stirrer and CDI (10.0 mmol, 1.0 equiv.) was added. DCM (30 mL) was then added to the flask, and the mixture was then stirred at room temperature for 30 min. The reaction

was quenched with 1 M HCl (20 mL) and extracted with DCM (20 mL × 3). The combined organic phase was dried over $Na_2SO_4$ and solvent was removed in vacuo. The crude product obtained were purified by flash chromatography (*n*-hexane:EA = 100:1 to 4:1) to afford pure dioxazolones.

### *Preparation of DBpin*

*General Method G*

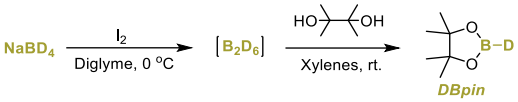


To a three-neck 100 mL round bottom flask equipped with a magnetic stir bar were added $NaBD_4$ (0.5 g, 12.0 mmol) and diethylene glycol dimethyl ether (10 mL) in a nitrogen-filled glovebox. To one neck of the flask was then fitted a dropping funnel, and the other two necks were sealed with a septum. To the funnel was then added iodine (1.6 g, 6.3 mmol) and diethylene glycol dimethyl ether (10 mL). To another 50 mL round flask with a magnetic stir bar were added pinacol (0.48 g, 4.0 mmol) and anhydrous xylenes (3 mL), and the flask was then sealed with rubber septum. With a double-tipped needle, the two flasks were connected and removed from glovebox. A nitrogen balloon was connected to the 50 mL round flask, and the three-neck flask were then charged to ice water bath and cooled to 0℃. The iodine solution was added dropwise over 1 h to the $NaBD_4$ solution in the three-neck flask from the dropping funnel. The resulting gas ($B_2D_6$) was vented to the pinacol solution (50 mL flask connected to balloon) through the double-tipped needle. After complete addition of the iodine solution, the whole reaction unit was allowed to stir at room temperature for another 1 h until no bubble could be observed. The double tipped needle and the nitrogen balloon was then removed from the round bottom flask, and DBpin was given in xylenes solution.

### 2.4.3 General Procedure for Ni-catalyzed Amidation

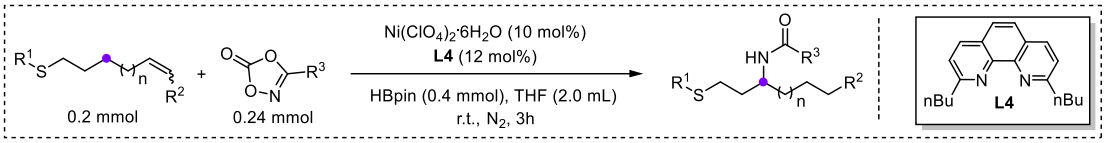


To an 8 mL vial was added a magnetic stir bar, $Ni(ClO_4)_2.6H_2O$ (7.3 mg, 10 mol%) and 2,9-dibutyl-1,10-phenanthroline (7.0 mg, 12 mol%) in a nitrogen-filled glovebox. Anhydrous THF (2.0 mL) were then added to the mixture via a syringe. The vial was then capped and stirred for 10 min at room temperature, resulting in a green solution. A separated 8 mL vial was prepared parallelly with a magnetic stir bar. To the vial were then added alkene (0.20 mmol, 1.0 equiv.) and 1,4,2-dioxazol-5-one (0.24 mmol, 1.2 equiv.). The green [Ni + L] solution obtained above was transferred to the vial and vigorously stirred with the alkene-dioxazolone mixture. 4,4,5,5-Tetramethyl-1,3,2-dioxaborolane [HBpin, (0.40 mmol, 2.0 equiv.)] was then added dropwise to the mixture through a syringe. Upon addition, the color of the solution would be changed from green to dark or dark green. The vial was then capped, taken out of the glovebox and stirred at room temperature for 3h. The reaction was monitored with TLC, visualized by using UV light (254 nm) and $KMnO_4$ stain. The reaction mixture was then transferred to a 25mL round bottom flask, quenched with silica gel and subjected to filtration through a short-packed silica gel column (EA as eluent). The resulting solution was again concentrated in vacuo. The crude product obtained was purified by column chromatography (*n*-hexane:EA = 5 : 1 to 2 : 1) to afford the desired amide product.

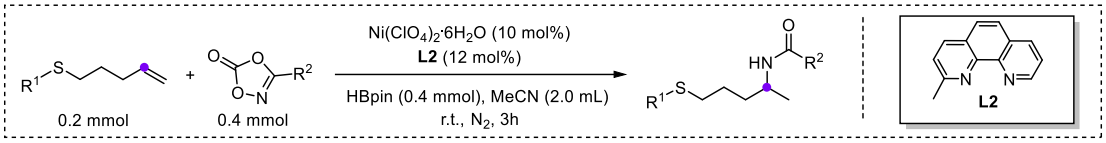


Similar to above-described procedure, an 8 mL vial with a magnetic stir bar was charged with $Ni(ClO_4)_2.6H_2O$ (7.3 mg, 10 mol%) and 2-methyl-1,10-phenanthroline (4.7 mg, 12 mol%) in a nitrogen-filled glovebox. Anhydrous MeCN (2.0 mL) were then added to the mixture via a syringe. The vial was then capped and stirred for 10 min at

room temperature, yielding a colorless solution. Alkene (0.20 mmol, 1.0 equiv.) and 1,4,2-dioxazol-5-one (0.40 mmol, 2.0 equiv.) were added to another 8 mL vial with a magnetic stir bar. The colorless [Ni + L] solution obtained above was transferred to the vial and vigorously stirred with the alkene-dioxazolone mixture. The following steps are same as the above-mentioned procedure, including the addition of HBpin, workup and purification procedures.

### 2.4.4 General Procedure for Other Experiments

***Synthesis of Complex 68 and Hydroamidation of 67***

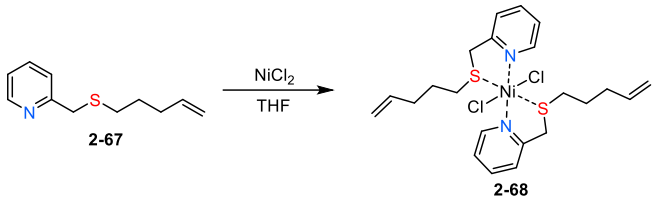


To an 8 mL vial charged with a magnetic stir bar were added 2-((pent-4-en-1-ylthio)methyl)pyridine **2-67** (0.20 mmol, 2.0 equiv.) and $NiCl_2$ (0.10 mmol, 1.0 equiv.) in a nitrogen filled glovebox. To the mixture was then added 2mL THF, and the vial was then screw-capped and removed from the glovebox. The mixture was allowed to go overnight at room temperature under vigorous stirring. The resulting mixture was collected, concentrated in vacuo and recrystallized with hexane and DCM to yield **2-68** as a green solid.

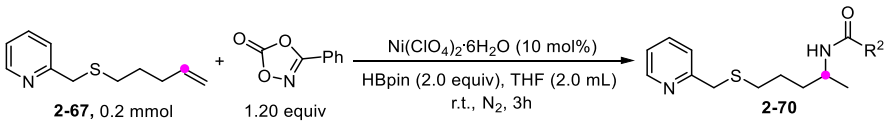


To an 8 mL vial charged with a magnetic stir bar, $Ni(ClO_4)_2·6H_2O$ (7.3 mg, 10 mol%), 2-((pent-4-en-1-ylthio)methyl)pyridine (0.20 mmol, 1.0 equiv.) and 1,4,2-dioxazol-5-one (0.24 mmol, 1.2 equiv.) was added in one portion in a nitrogen-filled glovebox. 2.0 mL anhydrous THF were then added to the vial through syringe. 4,4,5,5-Tetramethyl-1,3,2-dioxaborolane [HBpin, (0.40 mmol, 2.0 equiv.)] was then added dropwise to the mixture through another syringe. The vial was screw-capped, removed from the glovebox and stirred at room temperature for 3h, monitored by TLC. The reaction

mixture was transferred to a 25 mL round bottom flask, quenched with silica gel and concentrated in vacuo upon finishing, and the mixture obtained was filtered through a short-packed column with silica gel (ethyl acetate as eluent). The crude product obtained was purified by column chromatography (gradient eluent *n*-hexane:EA = 4:1) to afford the desired amide product **2-70**.

***Hammett Plot***

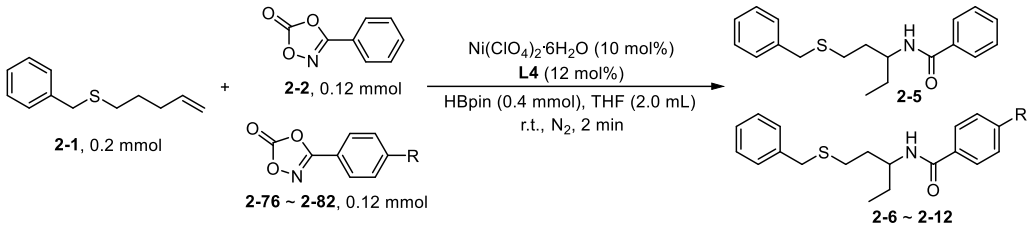


Seven 8 mL vials with a magnetic stir bar were charged with $Ni(ClO_4)_2·6H_2O$ (7.3 mg, 10 mol%) and 2,9-dibutyl-1,10-phenanthroline (7.0 mg, 12 mol%) parallelly in a glovebox filled with nitrogen. Anhydrous THF (2.0 mL) were then added to the mixture via a syringe. The vial was then screw-capped and stirred for 10 minutes at room temperature. To another seven parallel 8 mL vials with a magnetic stir bars were added **2-1** (0.20 mmol, 1.0 equiv.), **2-2** (0.12 mmol, 0.6 equiv.) and dioxazolone **2-76** ~ **2-82** accordingly (0.12 mmol, 0.6 equiv.). The [Ni + L] standard solution was then transferred to the mixtures, and then to the solution was added 4,4,5,5-Tetramethyl-1,3,2-dioxaborolane [HBpin, (0.40 mmol, 2.0 equiv.)] dropwise through a syringe. The reaction mixture was then allowed to stir for 2 minutes, immediately quenched with silica gel, concentrated in vacuo and subjected to a short-packed column with silica gel (ethyl acetate as eluent) to give a crude mixture. The yields of amide products were then examined by $^1H$ NMR, with $CH_2Br_2$ as internal standard. Then Hammett Plot was drawn with $\sigma_p$ as horizontal axis and $\log(k_R/k_H)$ as vertical axis.

### *Radical Trapping Experiment*

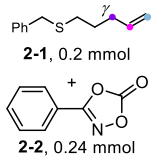


*stand. cond.*

| radical scavenger (0.4 mmol) | γ | Markovnikov | anti-Markovnikov | (total yield) |
|---|---|---|---|---|
| TEMPO | 63% | n.d. | n.d. | (63%) |
| BHT | 87% | n.d. | 6% | (93%) |
| α-cyclopropylstyrene | 81% | n.d. | 4% | (85%) |

Three parallel 8 mL vials charged with magnetic stir bars was charged with $Ni(ClO_4)_2{\cdot}6H_2O$ (7.3 mg, 10 mol%) and 2,9-dibutyl-1,10-phenanthroline (7.0 mg, 12 mol%) in a nitrogen-filled glovebox. Anhydrous THF (2.0 mL) were then added to the vials. The mixtures were allowed stirred for 10 min at room temperature to give a green solution. **2-1** (0.20 mmol, 1.0 equiv.), **2-2** (0.24 mmol, 1.2 equiv.) and radical scavengers were added to another three 8 mL vials. The [Ni + L] standard solution was then transferred to the alkene-dioxazolone-radical scavenger mixture with vigorous stirring. 4,4,5,5-Tetramethyl-1,3,2-dioxaborolane [HBpin, (0.40 mmol, 2.0 equiv.)] was then added dropwise to the mixtures through a syringe. The vial was then capped and removed from the glovebox, and the reaction mixture was then stirred at room temperature for 3 h, monitored by TLC. Upon finishing, the reaction mixtures were separately transferred to three 25 mL round bottom flasks, quenched with silica gel, concentrated in vacuo and filtered through a short-packed column with silica gel (EA as eluent). The resulting solutions was again concentrated in vacuo. The yields of amide products **2-3**, **2-4** and **2-5** were then examined by $^1H$ NMR, with $CH_2Br_2$ as internal standard.

### *Deuterated Experiment*

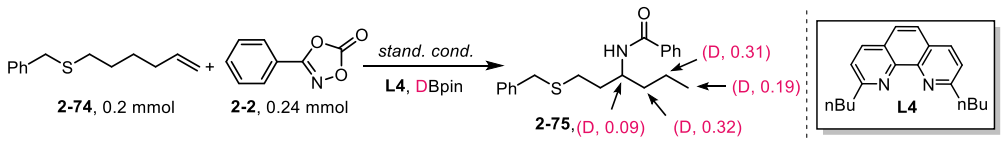


In a nitrogen-filled glovebox, an 8 mL vial with magnetic stir bar was charged with $[Ni(ClO_4)_2]{\cdot}6H_2O$ (7.3 mg, 10 mol%) and 2,9-dibutyl-1,10-phenanthroline (7.0 mg, 12 mol%) separately. Anhydrous THF (2.0 mL) were then added via a syringe. The vials were then screw-capped and stirred for 10 minutes at room temperature to give a green solution. **2-74** (0.2 mmol, 1.0 equiv.) and **2-2** (0.24 mmol, 1.2 equiv.) were added to

another 8 mL vial with magnetic stir bar. The [Ni + L] standard solution was then transferred to the alkene-dioxazolone mixture with vigorous stirring. DBpin in xylenes solution (Preparation see previous, 0.4 mmol, 2.0 equiv.) was then added dropwise to the mixture through a syringe. The vial was then capped and removed from the glovebox, and the reaction mixture was then stirred at room temperature for 3 h, monitored by TLC. Upon finishing, the reaction mixtures were separately transferred to three 25 mL round bottom flasks, concentrated in vacuo and filtered through a short-packed column with silica gel (ethyl acetate as eluent). The resulting solutions was again concentrated in vacuo, purified by flash column chromatography (*n*-hexane:ethyl acetate = 4:1) to give the corresponding deuterated amide **2-75**. **2-75** was then analyzed with $^{1}$H NMR compared to non-deuterated product **2-48** to give percentage of deuteration at all positions.

### 2.4.5 Physical Charaterization of Products

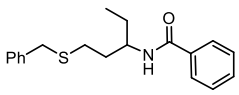

***N*-(1-(Benzylthio)pentan-3-yl)benzamide (2-5):** White solid (86%). **M.P.** 60 °C. **$^{1}$H NMR** (400 MHz, $CDCl_3$) δ 7.72 (d, *J* = 7.9 Hz, 2H), 7.53 – 7.47 (m, 1H), 7.42 (t, *J* = 7.4 Hz, 2H), 7.30 – 7.16 (m, 5H), 6.00 (d, *J* = 9.0 Hz, 1H), 4.11 (ddt, *J* = 13.7, 8.4, 4.3 Hz, 1H), 3.71 (s, 2H), 2.49 (t, *J* = 7.6 Hz, 2H), 1.87 (dtd, *J* = 16.1, 8.0, 4.5 Hz, 1H), 1.76 – 1.64 (m, 2H), 1.64 – 1.55 (m, 1H), 1.50 (dt, *J* = 14.2, 7.4 Hz, 1H), 0.93 (t, *J* = 7.4 Hz, 3H) ppm. **$^{13}$C NMR** (101 MHz, $CDCl_3$) δ 167.28, 138.24, 134.83, 131.41, 128.88, 128.59, 128.52, 127.01, 126.87, 50.83, 36.35, 34.16, 27.85, 27.69, 10.37 ppm. **HRMS** (ESI): calcd. for $C_{19}H_{24}NOS^{+}$: 314.1579. found: 314.1586.

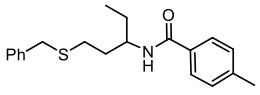

***N*-(1-(Benzylthio)pentan-3-yl)-4-methylbenzamide (2-6):** White solid (90%). **M.P.** 93 °C. **$^{1}$H NMR** (400 MHz, $CDCl_3$) δ 7.63 (d, *J* = 8.1 Hz, 2H), 7.31 – 7.15 (m, 7H), 5.97 (d, *J* = 9.0 Hz, 1H), 4.10 (tq, *J* = 8.5, 4.9, 4.3 Hz, 1H), 3.70 (s, 2H), 2.48 (t, *J* = 7.7 Hz, 2H), 2.40 (s, 3H), 1.86 (dtd, *J* = 16.1, 8.0, 4.5 Hz, 1H), 1.69 (dp, *J* = 15.1, 7.7, 7.3 Hz, 1H), 1.59 (dt, *J* = 13.4, 6.6 Hz, 1H), 1.49 (dt, *J* = 14.2, 7.4 Hz, 1H), 0.92 (t, *J* = 7.4 Hz, 3H) ppm. **$^{13}$C NMR** (101 MHz, $CDCl_3$) δ 167.19, 141.78, 138.28, 131.96, 129.22, 128.88, 128.51, 127.00, 126.88, 50.73, 36.35, 34.23, 27.88, 27.73, 21.47, 10.37 ppm. **HRMS** (ESI): calcd. for $C_{20}H_{26}NOS^{+}$: 328.1735. found: 328.1742.

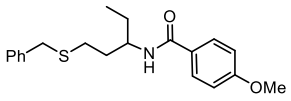

***N*-(1-(Benzylthio)pentan-3-yl)-4-methoxybenzamide (2-7):** White solid (88%). **M.P.** 100 °C. **$^{1}$H NMR** (400 MHz, $CDCl_3$) δ 7.70 (d, *J* = 8.8 Hz, 2H), 7.33 – 7.15 (m, 5H), 6.90 (d, *J* = 8.8 Hz, 2H), 6.00 (d, *J* = 9.0 Hz, 1H), 4.18 – 4.03 (m, 1H), 3.84 (s, 3H), 3.70 (s, 2H), 2.48 (t, *J* = 7.7 Hz, 2H), 1.91 – 1.80 (m, 1H), 1.69 (dq, *J* = 14.9, 7.5 Hz, 1H), 1.58 (dt, *J* = 13.9, 6.6 Hz, 1H), 1.49 (dt, *J*

= 14.2, 7.5 Hz, 1H), 0.91 (t, *J* = 7.4 Hz, 3H) ppm. **$^{13}$C NMR** (101 MHz, $CDCl_3$) δ 166.77, 162.10, 138.28, 128.88, 128.69, 128.51, 127.08, 126.99, 55.44, 50.73, 36.34, 34.21, 27.89, 27.75, 10.40 ppm. **HRMS** (ESI): calcd. for $C_{20}H_{26}NO_2S^+$: 344.1684. found: 344.1683.

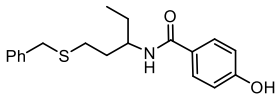

***N*-(1-(Benzylthio)pentan-3-yl)-4-methoxybenzamide (2-8):** Yellow oil (80%). **$^{1}$H NMR** (400 MHz, $CDCl_3$) δ 8.20 (s, 1H), 7.58 (d, *J* = 8.5 Hz, 2H), 7.28 – 7.21 (m, 4H), 7.21 – 7.15 (m, 1H), 6.86 (d, *J* = 8.5 Hz, 2H), 6.01 (d, *J* = 9.0 Hz, 1H), 4.10 (qt, *J* = 8.7, 5.0 Hz, 1H), 3.69 (s, 2H), 2.47 (t, *J* = 7.6 Hz, 2H), 1.93 – 1.75 (m, 2H), 1.74 – 1.63 (m, 1H), 1.58 (ddd, *J* = 13.6, 7.7, 6.0 Hz, 1H), 1.48 (dt, *J* = 14.2, 7.4 Hz, 1H), 1.25 (s, 3H), 0.91 (t, *J* = 7.4 Hz, 3H) ppm. **$^{13}$C NMR** (101 MHz, $CDCl_3$) δ 167.85, 160.04, 138.18, 128.86, 128.82, 128.52, 127.03, 125.72, 115.62, 77.36, 77.04, 76.72, 75.24, 51.01, 36.36, 34.07, 27.82, 27.68, 24.84, 10.35 ppm. **HRMS** (ESI): calcd. for $C_{19}H_{24}NO_2S^+$: 330.1528. found: 330.1532.

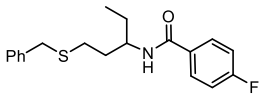

***N*-(1-(Benzylthio)pentan-3-yl)-4-fluorobenzamide (2-9):** White solid (73%). **M.P.** 88 ºC. **$^{1}$H NMR** (400 MHz, $CDCl_3$) δ 7.79 – 7.67 (m, 2H), 7.34 – 7.16 (m, 5H), 7.07 (t, *J* = 8.6 Hz, 2H), 6.12 (d, *J* = 8.9 Hz, 1H), 4.15 – 4.03 (m, 1H), 3.70 (s, 2H), 2.47 (dd, *J* = 8.4, 6.8 Hz, 2H), 1.91 – 1.81 (m, 1H), 1.71 (ddd, *J* = 13.0, 8.2, 6.5 Hz, 1H), 1.64 – 1.42 (m, 2H), 0.91 (t, *J* = 7.4 Hz, 3H) ppm. **$^{13}$C NMR** (101 MHz, $CDCl_3$) δ 166.24, 165.90, 163.40, 138.21, 131.01, 130.97, 129.27, 129.18, 128.86, 128.52, 127.03, 115.65, 115.43, 77.42, 77.10, 76.78, 50.97, 36.35, 33.98, 27.78, 27.68, 10.39, 0.02 ppm. **$^{19}$F NMR** (377 MHz, $CDCl_3$) δ -108.30, -108.32, -108.34, -108.35, -108.37. **HRMS** (ESI): calcd. for $C_{19}H_{23}FNOS^+$: 322.1484. found: 332.1497.

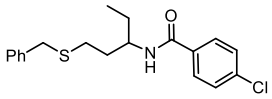

***N*-(1-(Benzylthio)pentan-3-yl)-4-chlorobenzamide (2-10):** White solid (75%). **M.P.** 110 ºC. **$^{1}$H NMR** (400 MHz, $CDCl_3$) δ 7.57 (d, *J* = 8.4 Hz, 2H), 7.28 (d, *J* = 8.2 Hz, 2H), 7.23 – 7.06 (m, 5H), 6.10 (d, *J* = 9.0 Hz, 1H), 4.00 (dtd, *J* = 13.6, 8.5, 4.9 Hz, 1H), 3.62 (s, 2H), 2.39 (t, *J* = 7.6 Hz, 2H), 1.77 (dtd, *J* = 12.5, 7.9, 4.5 Hz, 1H), 1.62 (dq, *J* = 14.8, 7.6 Hz, 1H), 1.45 (ddq, *J* = 28.7, 14.1, 7.0 Hz, 2H), 0.83 (t, *J* = 7.4 Hz, 4H) ppm. **$^{13}$C NMR** (101 MHz, $CDCl_3$) δ 166.25, 138.20, 137.55, 133.21, 128.85, 128.76, 128.52, 128.38, 127.04, 51.03, 36.37, 33.93, 27.74, 27.70, 10.39 ppm. **HRMS** (ESI): calcd. for $C_{19}H_{23}ClNOS^+$: 348.1189. found: 348.1191.

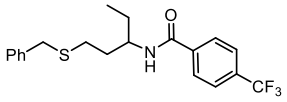

***N*-(1-(Benzylthio)pentan-3-yl)-4-nitrobenzamide (2-11):** White solid (80%). **M.P.** 130 ºC. **$^{1}$H NMR** (400 MHz, $CDCl_3$) δ 7.82 (d, *J* = 8.1 Hz, 2H), 7.68 (d, *J* = 8.2 Hz, 2H), 7.26 (d, *J* = 6.1 Hz, 4H), 7.20 (ddd, *J* = 8.3, 4.9, 2.4 Hz, 1H), 6.09 (d, *J* = 8.9 Hz, 1H), 4.13 (ddt, *J* = 13.6, 10.6, 6.6 Hz, 1H), 3.71 (s, 2H), 2.50 (td, *J* = 7.1, 6.5, 1.9 Hz, 2H), 1.89 (dtd, *J* = 14.2, 7.8, 4.4 Hz, 1H), 1.72 (dtd, *J* = 14.3, 8.1, 6.2 Hz, 1H), 1.56 (ddq, *J* = 28.7, 14.1, 7.5 Hz, 3H), 0.93 (t, *J* = 7.4 Hz, 3H) ppm. **$^{13}$C NMR** (101 MHz, $CDCl_3$) δ 165.96, 138.12, 132.98, 128.84, 128.52, 127.36, 127.07, 125.64, 125.60, 77.36, 77.04, 76.72, 51.18, 36.40, 33.75, 27.69, 27.63, 10.35 ppm. **$^{19}$F NMR** (377 MHz, $CDCl_3$) δ -62.80. **HRMS** (ESI): calcd. for $C_{11}H_{23}F_3NOS^+$: 382.1452. found: 382.1451.

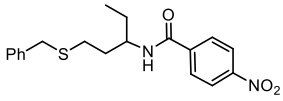

***N*-(1-(Benzylthio)pentan-3-yl)-4-nitrobenzamide (2-12):** White solid (46%). **M.P.** 118 ºC. **$^1$H NMR** (400 MHz, $CDCl_3$) δ 8.34 – 8.17 (m, 2H), 7.92 – 7.78 (m, 2H), 7.27 (d, *J* = 2.9 Hz, 4H), 7.21 (ddd, *J* = 8.0, 6.6, 3.4 Hz, 1H), 6.19 (d, *J* = 8.9 Hz, 1H), 4.13 (dtd, *J* = 15.6, 8.2, 4.8 Hz, 1H), 3.72 (s, 2H), 2.56 – 2.43 (m, 2H), 1.90 (dtd, *J* = 15.2, 7.7, 4.4 Hz, 1H), 1.73 (dtd, *J* = 14.2, 8.0, 6.1 Hz, 1H), 1.58 (dtt, *J* = 26.0, 14.1, 6.7 Hz, 2H), 0.93 (t, *J* = 7.4 Hz, 3H) ppm. **$^{13}$C NMR** (101 MHz, $CDCl_3$) δ 165.22, 149.53, 140.40, 138.08, 128.85, 128.56, 128.10, 127.12, 123.82, 77.38, 77.06, 76.74, 51.42, 36.42, 33.53, 31.60, 27.62, 27.60, 10.38 ppm. **HRMS** (ESI): calcd. for $C_{19}H_{23}N_2O_3S^+$: 359.1429. found: 359.1434.

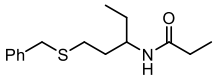

***N*-(1-(Benzylthio)pentan-3-yl)propionamide (2-13):** White solid (76%). **M.P.** 65 ºC. **$^1$H NMR** (400 MHz, $CDCl_3$) δ 7.30 (s, 4H), 7.27 – 7.20 (m, 1H), 5.40 (d, *J* = 9.2 Hz, 1H), 3.93 – 3.82 (m, 1H), 3.70 (s, 2H), 2.41 (t, *J* = 7.8 Hz, 2H), 2.15 (q, *J* = 7.6 Hz, 2H), 1.75 (dtd, *J* = 16.1, 8.0, 4.6 Hz, 1H), 1.61 – 1.42 (m, 2H), 1.42 – 1.29 (m, 1H), 1.12 (t, *J* = 7.6 Hz, 3H), 0.86 (t, *J* = 7.4 Hz, 3H) ppm. **$^{13}$C NMR** (101 MHz, $CDCl_3$) δ 173.59, 138.36, 128.87, 128.50, 127.00, 77.45, 77.14, 76.82, 50.10, 36.34, 34.38, 29.91, 27.84, 27.75, 24.86, 10.25, 10.10 ppm. **HRMS** (ESI): calcd. for $C_{15}H_{24}NOS^+$: 266.1579. found: 266.1585.

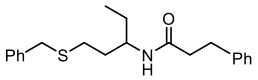

***N*-(1-(Benzylthio)pentan-3-yl)-3-phenylpropanamide (2-14):** White solid (79%). **M.P.** 58 ºC. **$^1$H NMR** (400 MHz, $CDCl_3$) δ 7.35 – 7.24 (m, 6H), 7.24 – 7.14 (m, 4H), 5.18 (d, *J* = 9.1 Hz, 1H), 3.83 (qt, *J* = 8.9, 4.9 Hz, 1H), 3.66 (s, 2H), 2.93 (t, *J* = 7.6 Hz, 2H), 2.42 (t, *J* = 7.6 Hz, 2H), 2.30 (ddd, *J* = 9.2, 6.4, 2.8 Hz, 2H), 1.67 (dddd, *J* = 13.8, 9.1, 7.1, 4.6 Hz, 1H), 1.53 – 1.34 (m, 2H), 1.27 (dp, *J* = 14.8, 7.5 Hz, 1H), 0.76 (t, *J* = 7.4 Hz, 3H) ppm. **$^{13}$C NMR** (101 MHz, $CDCl_3$) δ 171.76, 140.85, 138.38, 128.89, 128.57, 128.52, 128.41, 127.04, 126.31, 77.44, 77.12, 76.80, 50.20, 38.68, 36.35, 34.27, 31.79, 27.75, 27.71, 10.13 ppm. **HRMS** (ESI): calcd. for $C_{21}H_{28}NOS^+$: 342.1892. found: 342.1907.

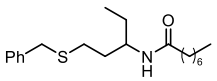

***N*-(1-(Benzylthio)pentan-3-yl)octanamide (2-15):** White solid (81%). **M.P.** 49 ºC. **$^1$H NMR** (400 MHz, $CDCl_3$) δ 7.30 (d, *J* = 4.4 Hz, 4H), 7.26 – 7.20 (m, 1H), 5.21 (d, *J* = 9.0 Hz, 1H), 3.88 (qt, *J* = 8.8, 5.0 Hz, 1H), 3.70 (s, 2H), 2.41 (t, *J* = 7.8 Hz, 2H), 2.12 (t, *J* = 7.6 Hz, 2H), 1.87 – 1.66 (m, 1H), 1.66 – 1.42 (m, 4H), 1.42 – 1.18 (m, 9H), 0.87 (q, *J* = 7.5, 7.0 Hz, 6H) ppm. **$^{13}$C NMR** (101 MHz, $CDCl_3$) δ 172.87, 138.37, 128.87, 128.50, 127.01, 77.38, 77.07, 76.75, 50.12, 37.08, 36.40, 34.42, 31.72, 29.30, 29.03, 27.87, 27.81, 25.90, 22.62, 14.08, 10.23 ppm. **HRMS** (ESI): calcd. for $C_{20}H_{34}NOS^+$: 336.2361. found: 336.2368.

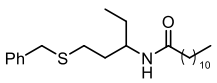

***N*-(1-(Benzylthio)pentan-3-yl)dodecanamide (2-16):** White solid (83%). **M.P.** 45 ºC. **$^1$H NMR** (400 MHz, $CDCl_3$) δ 7.30 (d, *J* = 4.4 Hz, 4H), 7.23 (dt, *J* = 8.7, 4.2 Hz, 1H), 5.19 (d, *J* = 9.1 Hz, 1H), 3.88 (qt, *J* = 8.9, 5.0 Hz, 1H), 3.70 (s, 2H), 2.41 (t, *J* = 7.8 Hz, 2H), 2.11 (t, *J* = 7.7 Hz, 2H), 1.81 – 1.69 (m, 2H), 1.65 – 1.43 (m, 4H), 1.40 – 1.17 (m, 19H), 0.87 (q, *J* = 7.3, 6.8 Hz, 6H) ppm. **$^{13}$C NMR** (101 MHz, $CDCl_3$) δ 172.87, 138.36, 128.87, 128.50, 127.01, 77.37, 77.06, 76.74, 50.12, 37.09, 36.40, 34.41, 31.92, 29.63,

29.62, 29.52, 29.38, 29.35, 27.87, 27.80, 25.90, 22.69, 14.12, 10.23 ppm. **HRMS** (ESI): calcd. for $C_{24}H_{42}NOS^+$: 392.2987. found: 392.2990.

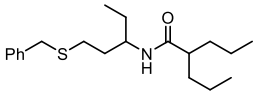

***N*-(1-(Benzylthio)pentan-3-yl)-2-propylpentanamide (2-17):** White solid (78%). **M.P.** 76 ºC. **$^1$H NMR** (400 MHz, $CDCl_3$) δ 7.30 (s, 4H), 7.26 – 7.20 (m, 1H), 5.25 (d, *J* = 9.0 Hz, 1H), 3.91 (ddt, *J* = 13.2, 8.8, 4.3 Hz, 1H), 3.71 (s, 2H), 2.42 (dd, *J* = 8.6, 7.0 Hz, 2H), 1.96 (tt, *J* = 9.5, 4.4 Hz, 1H), 1.73 (dtd, *J* = 16.1, 8.1, 7.6, 4.7 Hz, 1H), 1.67 – 1.43 (m, 4H), 1.42 – 1.16 (m, 7H), 0.88 (q, *J* = 7.2 Hz, 9H) ppm. **$^{13}$C NMR** (101 MHz, $CDCl_3$) δ 175.60, 138.39, 128.81, 128.51, 127.01, 77.39, 77.07, 76.75, 50.06, 48.00, 36.48, 35.35, 35.33, 34.42, 28.01, 27.89, 20.91, 20.86, 14.18, 14.14, 10.24 ppm. **HRMS** (ESI): calcd. for $C_{20}H_{34}NOS^+$: 336.2361. found: 336.2368.

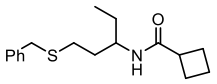

***N*-(1-(Benzylthio)pentan-3-yl)cyclobutanecarboxamide (2-18):** White solid (75%). **M.P.** 52 ºC. **$^1$H NMR** (400 MHz, $CDCl_3$) δ 7.29 (d, *J* = 5.1 Hz, 4H), 7.25 – 7.19 (m, 1H), 5.09 (d, *J* = 9.1 Hz, 1H), 3.87 (qt, *J* = 8.8, 5.0 Hz, 1H), 3.69 (s, 2H), 2.93 (pd, *J* = 8.5, 1.0 Hz, 1H), 2.39 (dd, *J* = 8.7, 6.9 Hz, 2H), 2.22 (dddd, *J* = 11.5, 8.9, 7.1, 4.4 Hz, 2H), 2.17 – 2.04 (m, 2H), 1.95 (dq, *J* = 11.1, 8.8 Hz, 1H), 1.89 – 1.78 (m, 2H), 1.78 – 1.68 (m, 1H), 1.60 – 1.41 (m, 2H), 1.34 (dt, *J* = 13.8, 7.4 Hz, 1H), 0.85 (t, *J* = 7.4 Hz, 3H) ppm. **$^{13}$C NMR** (101 MHz, $CDCl_3$) δ 174.72, 138.37, 128.86, 128.50, 127.00, 77.39, 77.07, 76.76, 50.02, 40.04, 36.38, 34.44, 27.92, 27.76, 25.42, 25.38, 18.15, 10.24 ppm. **HRMS** (ESI): calcd. for $C_{17}H_{26}NOS^+$: 292.1735. found: 292.1741.

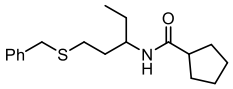

***N*-(1-(Benzylthio)pentan-3-yl)cyclopentanecarboxamide (2-19):** White solid (78%). **M.P.** 58 ºC. **$^1$H NMR** (400 MHz, $CDCl_3$) δ 7.30 (d, *J* = 4.3 Hz, 4H), 7.23 (q, *J* = 4.4 Hz, 1H), 5.19 (d, *J* = 9.2 Hz, 1H), 3.88 (qt, *J* = 8.9, 4.9 Hz, 1H), 3.70 (s, 2H), 2.43 (dt, *J* = 15.5, 7.8 Hz, 3H), 1.90 – 1.64 (m, 7H), 1.64 – 1.43 (m, 4H), 1.35 (dp, *J* = 14.9, 7.5 Hz, 1H), 0.86 (t, *J* = 7.4 Hz, 3H) ppm. **$^{13}$C NMR** (101 MHz, $CDCl_3$) δ 175.92, 138.39, 128.86, 128.50, 126.99, 77.38, 77.06, 76.74, 50.08, 46.08, 36.41, 34.52, 30.52, 30.50, 27.96, 27.82, 25.92, 10.24 ppm. **HRMS** (ESI): calcd. for $C_{18}H_{28}NOS^+$: 306.1892. found: 306.1902.

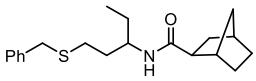

**(1S,2S,4R)-*N*-(1-(Benzylthio)pentan-3-yl)bicyclo[2.2.1]heptane-2-carboxamide (2-20):** White solid (83%). **M.P.** 92 ºC. **$^1$H NMR** (400 MHz, $CDCl_3$) δ 7.35 – 7.27 (m, 4H), 7.26 – 7.18 (m, 1H), 5.18 (dd, *J* = 9.6, 4.6 Hz, 1H), 3.86 (ddp, *J* = 17.9, 13.7, 4.8 Hz, 1H), 3.74 – 3.64 (m, 2H), 2.49 – 2.19 (m, 4H), 2.04 (dd, *J* = 9.0, 5.2 Hz, 1H), 1.90 – 1.66 (m, 2H), 1.63 – 1.45 (m, 5H), 1.45 – 1.25 (m, 4H), 1.25 – 1.07 (m, 3H), 0.93 – 0.80 (m, 3H) ppm. **$^{13}$C NMR** (101 MHz, $CDCl_3$) δ 175.45, 173.63, 138.39, 128.88, 128.87, 128.85, 128.50, 127.00, 77.41, 77.09, 76.77, 50.22, 50.09, 48.24, 47.31, 41.66, 41.15, 40.52, 37.01, 36.51, 36.38, 35.95, 34.60, 34.54, 34.40, 34.38, 31.30, 29.83, 29.23, 28.69, 28.02, 27.95, 27.84, 27.81, 24.33, 10.32, 10.30 ppm. **HRMS** (ESI): calcd. for $C_{20}H_{30}NOS^+$: 332.2048. found: 332.2055.

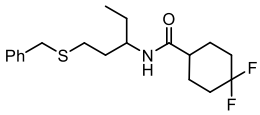

***N*-(1-(Benzylthio)pentan-3-yl)-4,4-difluorocyclohexane-1-carboxamide (2-21):** White solid (79%). **M.P.** 111 ºC. **$^1$H NMR** (400 MHz,

$CDCl_3$) δ 7.34 – 7.27 (m, 4H), 7.23 (dtd, *J* = 8.6, 4.1, 3.0 Hz, 1H), 5.30 (d, *J* = 8.5 Hz, 1H), 3.87 (dtd, *J* = 13.9, 8.8, 5.0 Hz, 1H), 3.69 (s, 2H), 2.38 (ddd, *J* = 9.0, 6.6, 2.5 Hz, 2H), 2.23 – 2.02 (m, 3H), 1.91 – 1.61 (m, 8H), 1.52 (dddd, *J* = 29.1, 13.4, 8.1, 5.8 Hz, 2H), 1.42 – 1.28 (m, 1H), 0.85 (t, *J* = 7.4 Hz, 3H) ppm. **$^{13}$C NMR** (101 MHz, $CDCl_3$) δ 173.77, 138.28, 128.86, 128.52, 127.04, 125.06, 122.66, 120.26, 77.40, 77.08, 76.77, 50.13, 43.10, 36.39, 34.20, 33.11, 32.88, 32.64, 27.86, 27.67, 26.08, 25.99, 10.27 ppm. **$^{19}$F NMR** (377 MHz, $CDCl_3$) δ -98.36, -98.99, -106.50, -107.13 ppm. **HRMS** (ESI): calcd. for $C_{19}H_{28}F_2NOS^+$: 356.1860. found: 356.1867.

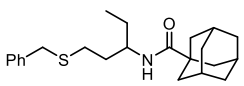

**(3R,5R,7R)-*N*-(1-(Benzylthio)pentan-3-yl)adamantane-1-carboxamide (2-22):** White solid (33%). **M.P.** 127 ºC. **$^1$H NMR** (400 MHz, $CDCl_3$) δ 7.30 (d, *J* = 4.4 Hz, 4H), 7.23 (dp, *J* = 7.5, 3.6 Hz, 1H), 5.31 (d, *J* = 9.0 Hz, 1H), 3.89 (qt, *J* = 9.0, 5.0 Hz, 1H), 3.70 (s, 2H), 2.46 – 2.32 (m, 2H), 2.03 (t, *J* = 3.4 Hz, 3H), 1.83 – 1.64 (m, 14H), 1.52 (dddd, *J* = 28.5, 14.8, 11.0, 6.7 Hz, 2H), 1.35 (dp, *J* = 14.9, 7.5 Hz, 1H), 0.85 (t, *J* = 7.4 Hz, 3H) ppm. **$^{13}$C NMR** (101 MHz, $CDCl_3$) δ 177.64, 138.37, 128.85, 128.51, 126.98, 77.38, 77.07, 76.75, 49.66, 40.64, 39.38, 36.53, 36.37, 34.47, 28.16, 27.99, 27.71, 10.25 ppm. **HRMS** (ESI): calcd. for $C_{23}H_{34}NOS^+$: 372.2361. found: 372.2368.

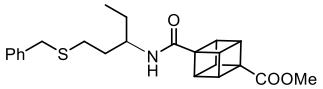

**Methyl (1R,2R,3R,4S,5S,6S,7R,8S)-4-((1-(be-nzylthio)penta-n-3-yl)carbamoyl)cubane-1-carboxylate (2-23):** White solid (84%). **M.P.** 112 ºC. **$^1$H NMR** (400 MHz, $CDCl_3$) δ 7.35 – 7.26 (m, 4H), 7.26 – 7.14 (m, 1H), 5.35 (d, J = 9.2 Hz, 1H), 4.21 (dd, *J* = 5.7, 3.9 Hz, 3H), 4.13 (dd, *J* = 5.7, 4.0 Hz, 3H), 3.92 (qt, *J* = 9.4, 5.0 Hz, 1H), 3.71 (d, *J* = 6.2 Hz, 5H), 2.41 (t, *J* = 7.7 Hz, 2H), 1.77 (dtd, *J* = 12.7, 7.9, 4.5 Hz, 1H), 1.60 (ddd, *J* = 12.7, 8.5, 6.6 Hz, 1H), 1.55 – 1.43 (m, 1H), 1.39 (dt, *J* = 14.2, 7.4 Hz, 1H), 0.87 (t, *J* = 7.4 Hz, 3H) ppm. **$^{13}$C NMR** (101 MHz, $CDCl_3$) δ 172.08, 171.00, 138.28, 128.83, 128.50, 127.04, 77.42, 77.10, 76.79, 57.82, 55.81, 51.66, 50.01, 46.97, 46.65, 36.39, 34.11, 27.81, 27.73, 10.32 ppm. **HRMS** (ESI): calcd. for $C_{23}H_{28}NO_3S^+$: 398.1790. found: 398.1793.

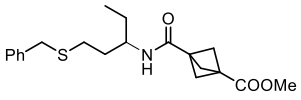

**Methyl 3-((1-(benzylthio)pentan-3-yl)carbamo-yl)bicyclo[1.1.1]pentane-1-carboxylate (2-24):** Yellow oil (84%). **$^1$H NMR** (400 MHz, $CDCl_3$) δ 7.37 – 7.16 (m, 5H), 5.36 (d, *J* = 9.2 Hz, 1H), 3.87 (qt, *J* = 8.7, 4.9 Hz, 1H), 3.70 (s, 5H), 2.43 – 2.35 (m, 2H), 2.24 (s, 6H), 1.86 – 1.67 (m, 2H), 1.59 (ddd, *J* = 11.9, 8.4, 6.1 Hz, 1H), 1.50 (ddd, *J* = 13.6, 8.5, 4.4 Hz, 1H), 1.37 (dp, *J* = 14.8, 7.5 Hz, 1H), 0.85 (t, *J* = 7.3 Hz, 3H) ppm. **$^{13}$C NMR** (101 MHz, $CDCl_3$) δ 169.87, 168.86, 138.24, 128.84, 128.55, 127.08, 77.39, 77.08, 76.76, 52.22, 51.88, 50.28, 39.39, 36.67, 36.39, 33.92, 27.67, 27.64, 24.87, 10.23 ppm. **HRMS** (ESI): calcd. for $C_{20}H_{28}NO_3S^+$: 362.1790. found: 362.1779.

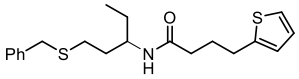

***N*-(1-(Benzylthio)pentan-3-yl)-4-(thiophen-2-yl)butanamide (2-25):** White solid (81%). **M.P.** 80 ºC. **$^1$H NMR** (400 MHz, $CDCl_3$) δ 7.27 (d, *J* = 12.7 Hz, 4H), 7.25 – 7.17 (m, 1H), 7.12 (dd, *J* = 5.1, 1.2 Hz, 1H), 6.92 (dd, *J* = 5.2, 3.4 Hz, 1H), 6.78 (dd, *J* = 3.5, 1.2 Hz, 1H), 5.25 (d, *J* = 9.1 Hz, 1H), 3.93 – 3.82 (m, 1H),

3.69 (s, 2H), 2.85 (t, *J* = 7.2 Hz, 2H), 2.40 (t, *J* = 7.7 Hz, 2H), 2.16 (t, *J* = 7.4 Hz, 2H), 1.97 (ddt, *J* = 13.2, 8.2, 6.4 Hz, 2H), 1.74 (dtd, *J* = 16.1, 8.1, 4.6 Hz, 1H), 1.59 – 1.41 (m, 2H), 1.34 (dt, *J* = 13.8, 7.5 Hz, 1H), 0.86 (t, *J* = 7.4 Hz, 3H) ppm. **$^{13}$C NMR** (101 MHz, $CDCl_3$) δ 172.15, 144.28, 138.35, 128.89, 128.53, 127.04, 126.88, 124.57, 123.24, 77.44, 77.12, 76.81, 50.22, 36.40, 35.76, 34.35, 29.19, 27.86, 27.79, 27.60, 10.31 ppm. **HRMS** (ESI): calcd. for $C_{20}H_{28}NOS_2^+$: 362.1612. found: 362.1617.

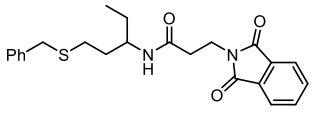

***N*-(1-(Benzylthio)pentan-3-yl)-3-(1,3-dioxoisoi-ndolin-2-yl)propanamide (2-26):** White solid (78%). **M.P.** 121 ºC. **$^1$H NMR** (400 MHz, $CDCl_3$) δ 7.85 – 7.77 (m, 2H), 7.74 – 7.65 (m, 2H), 7.32 – 7.25 (m, 4H), 7.25 – 7.18 (m, 1H), 5.71 (d, *J* = 9.0 Hz, 1H), 3.97 (td, *J* = 7.1, 1.3 Hz, 2H), 3.91 – 3.81 (m, 1H), 3.66 (s, 2H), 2.59 (t, *J* = 7.2 Hz, 2H), 2.37 (dd, *J* = 8.6, 6.9 Hz, 2H), 1.71 (dtd, *J* = 15.9, 8.1, 7.6, 4.7 Hz, 1H), 1.55 (dq, *J* = 13.9, 8.0 Hz, 1H), 1.44 (tq, *J* = 13.4, 7.8, 6.7 Hz, 1H), 1.39 – 1.30 (m, 1H), 0.80 (t, *J* = 7.4 Hz, 3H) ppm. **$^{13}$C NMR** (101 MHz, $CDCl_3$) δ 169.36, 168.15, 138.34, 134.08, 131.98, 128.87, 128.49, 126.99, 123.32, 77.47, 77.15, 76.83, 50.31, 36.29, 35.04, 34.48, 34.11, 27.75, 27.60, 10.18 ppm. **HRMS** (ESI): calcd. for $C_{23}H_{27}N_2O_3S^+$: 411.1742. found: 411.1745.

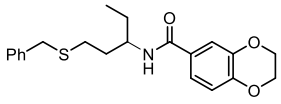

***N*-(1-(Benzylthio)pentan-3-yl)-2,3-dihydrobenzo[b] [1,4]dioxine-6-carboxamide (2-27):** White solid (89%). **M.P.** 112 ºC. **$^1$H NMR** (400 MHz, $CDCl_3$) δ 7.30 (d, *J* = 2.2 Hz, 1H), 7.28 – 7.24 (m, 3H), 7.21 (ddd, *J* = 12.2, 7.1, 2.2 Hz, 2H), 6.86 (d, *J* = 8.4 Hz, 1H), 6.00 (d, *J* = 9.0 Hz, 1H), 4.31 – 4.22 (m, 4H), 4.12 – 4.02 (m, 1H), 3.69 (s, 2H), 2.46 (t, *J* = 7.6 Hz, 2H), 1.83 (dtd, *J* = 14.1, 8.0, 4.5 Hz, 1H), 1.68 (ddd, *J* = 14.4, 8.2, 6.8 Hz, 1H), 1.61 – 1.40 (m, 2H), 0.90 (t, *J* = 7.4 Hz, 3H) ppm. **$^{13}$C NMR** (101 MHz, $CDCl_3$) δ 166.56, 146.35, 143.35, 138.29, 128.88, 128.51, 128.12, 126.99, 120.30, 117.19, 116.47, 77.45, 77.13, 76.81, 64.56, 64.23, 50.76, 36.33, 34.24, 27.86, 27.75, 10.38 ppm. **HRMS** (ESI): calcd. for $C_{21}H_{26}NO_3S^+$: 372.1633. found: 372.1642.

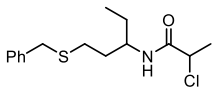

***N*-(1-(Benzylthio)pentan-3-yl)-3-(1H-indol-3-yl)propanamide (2-28):** White solid (27%). **M.P.** 47 ºC. **$^1$H NMR** (400 MHz, $CDCl_3$) δ 7.40 – 7.30 (m, 4H), 7.30 – 7.21 (m, 2H), 6.32 (d, *J* = 9.1 Hz, 1H), 4.40 (q, *J* = 7.0 Hz, 1H), 3.90 (ddq, *J* = 13.6, 8.8, 4.9 Hz, 1H), 3.78 – 3.68 (m, 2H), 2.43 (dd, *J* = 8.6, 6.8 Hz, 2H), 1.88 – 1.70 (m, 4H), 1.70 – 1.50 (m, 3H), 1.43 (dq, *J* = 14.3, 7.5 Hz, 1H), 0.90 (t, *J* = 7.4 Hz, 3H) ppm. **$^{13}$C NMR** (101 MHz, $CDCl_3$) δ 169.28, 138.29, 128.87, 128.54, 127.05, 77.36, 77.04, 76.72, 56.21, 50.76, 39.59, 36.33, 34.16, 31.90, 29.64, 29.55, 29.31, 27.66, 27.64, 27.57, 26.92, 22.93, 22.69, 14.13, 10.13, 0.01 ppm. **HRMS** (ESI): calcd. for $C_{15}H_{23}ClNOS^+$: 300.1189. found: 300.1191.

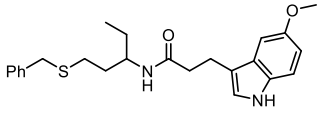

***N*-(1-(Benzylthio)pentan-3-yl)-3-(1H-indol-3-yl)propanamide (2-29):** Colorless oil (75%). **$^1$H NMR** (400 MHz, $CDCl_3$) δ 8.08 (s, 1H), 7.31 – 7.17 (m, 6H), 7.03 (d, *J* = 2.4 Hz, 1H), 6.90 (d, *J* = 2.4 Hz, 1H), 6.84 (dd, *J* = 8.8, 2.4 Hz, 1H), 5.14 (d, *J* = 9.0 Hz, 1H), 3.84 (s, 4H), 3.62 (s, 2H), 3.04 (t, *J* = 7.3 Hz, 2H), 2.51 (td, *J* = 7.3, 2.2 Hz, 2H), 2.22 (ddd, *J* = 9.1, 6.5, 2.6 Hz, 2H), 1.62 (dddd, *J* = 13.7, 9.1, 7.2, 4.5 Hz, 1H), 1.36 (ttd, *J* = 12.7, 8.0, 7.2, 5.6 Hz, 2H), 1.29 – 1.16 (m,

2H), 0.72 (t, *J* = 7.4 Hz, 3H) ppm. **$^{13}$C NMR** (101 MHz, $CDCl_3$) δ 172.45, 153.96, 138.51, 131.62, 128.88, 128.52, 127.50, 127.03, 122.74, 114.47, 112.10, 112.06, 100.71, 77.42, 77.10, 76.78, 56.03, 50.15, 37.47, 36.39, 34.26, 27.73, 27.69, 21.47, 10.05 ppm. **HRMS** (ESI): calcd. for $C_{24}H_{30}N_2NaO_2S^+$: 433.1926. found: 433.1934.

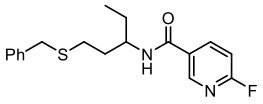

***N*-(1-(Benzylthio)pentan-3-yl)-6-fluoronicotinamide (2-30):** White solid (78%). **M.P.** 85 ºC. **$^1$H NMR** (400 MHz, $CDCl_3$) δ 8.56 (d, *J* = 2.5 Hz, 1H), 8.19 (td, *J* = 8.0, 2.5 Hz, 1H), 7.27 (d, *J* = 3.1 Hz, 4H), 7.20 (ddt, *J* = 8.6, 5.2, 2.9 Hz, 1H), 6.98 (dd, *J* = 8.5, 2.8 Hz, 1H), 6.32 (d, *J* = 8.9 Hz, 1H), 4.10 (dtd, *J* = 13.6, 8.3, 4.9 Hz, 1H), 3.71 (s, 2H), 2.56 – 2.41 (m, 2H), 1.87 (ddt, *J* = 15.5, 7.8, 4.0 Hz, 1H), 1.72 (dtd, *J* = 14.3, 8.0, 6.3 Hz, 1H), 1.56 (dtt, *J* = 25.3, 14.1, 6.6 Hz, 2H), 0.92 (t, *J* = 7.4 Hz, 3H) ppm. **$^{13}$C NMR** (101 MHz, $CDCl_3$) δ 166.14, 164.26, 163.72, 146.68, 146.52, 140.89, 140.80, 138.09, 128.84, 128.78, 128.54, 127.10, 109.86, 109.49, 77.42, 77.10, 76.79, 51.25, 36.37, 33.62, 27.64, 27.60, 10.39 ppm. **$^{19}$F NMR** (377 MHz, $CDCl_3$) δ -69.68, -69.69, -69.70, -69.71 ppm. **HRMS** (ESI): calcd. for $C_{18}H_{22}FN_2OS^+$: 333.1437. found: 333.1411.

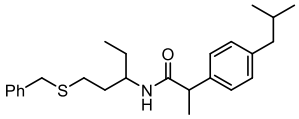

**(1-(Benzylthio)pentan-3-yl)-2-(4-isobutylphenyl) propanamide (2-31):** Orange solid (62%). **M.P.** 65 ºC. **$^1$H NMR** (400 MHz, $CDCl_3$) δ 7.35 – 7.20 (m, 5H), 7.15 (d, *J* = 8.1 Hz, 2H), 7.10 (d, *J* = 8.1 Hz, 2H), 4.99 (d, *J* = 9.1 Hz, 1H), 3.83 (ddt, *J* = 13.1, 8.8, 4.4 Hz, 1H), 3.66 (s, 2H), 3.46 (q, *J* = 7.1 Hz, 1H), 2.45 (d, *J* = 7.2 Hz, 2H), 2.34 (t, *J* = 7.7 Hz, 2H), 1.83 (dh, *J* = 13.6, 6.8 Hz, 1H), 1.72 – 1.60 (m, 2H), 1.49 (d, *J* = 7.2 Hz, 3H), 1.47 – 1.31 (m, 2H), 1.19 (dt, *J* = 13.8, 7.4 Hz, 1H), 0.89 (dd, *J* = 6.6, 1.1 Hz, 6H), 0.67 (t, *J* = 7.4 Hz, 3H) ppm. **$^{13}$C NMR** (101 MHz, $CDCl_3$) δ 174.19, 140.73, 138.73, 138.42, 129.64, 128.86, 128.50, 127.31, 127.00, 77.36, 77.05, 76.73, 50.20, 46.91, 45.01, 36.41, 34.35, 30.19, 27.81, 27.66, 22.36, 22.32, 18.32, 9.90 ppm. **HRMS** (ESI): calcd. for $C_{25}H_{36}NOS^+$: 398.2518. found: 398.2521.

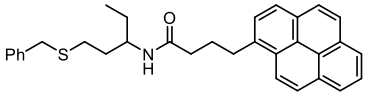

***N*-(1-(Benzylthio)pentan-3-yl)-4-(pyren-1-yl)butanamide (2-32):** White solid (82%). **M.P.** 125 ºC. **$^1$H NMR** (400 MHz, $CDCl_3$) δ 8.32 (d, *J* = 9.3 Hz, 1H), 8.19 (dd, *J* = 7.7, 2.8 Hz, 2H), 8.14 (d, *J* = 8.7 Hz, 2H), 8.04 (d, *J* = 14.4 Hz, 3H), 7.88 (d, *J* = 7.8 Hz, 1H), 7.33 – 7.21 (m, 4H), 7.21 – 7.14 (m, 1H), 5.14 (d, *J* = 9.1 Hz, 1H), 3.94 (qt, *J* = 8.7, 5.0 Hz, 1H), 3.69 (s, 2H), 3.39 (t, *J* = 7.1 Hz, 2H), 2.42 (t, *J* = 7.7 Hz, 2H), 2.30 – 2.15 (m, 4H), 1.82 – 1.66 (m, 2H), 1.60 – 1.42 (m, 2H), 1.41 – 1.28 (m, 1H), 0.88 (t, *J* = 7.4 Hz, 3H) ppm. **$^{13}$C NMR** (101 MHz, $CDCl_3$) δ 172.31, 138.31, 135.89, 131.44, 130.93, 129.99, 128.85, 128.81, 128.48, 127.51, 127.47, 127.42, 126.99, 126.77, 125.91, 125.13, 125.01, 124.97, 124.83, 124.82, 123.41, 77.40, 77.08, 76.76, 50.22, 36.38, 36.29, 34.34, 32.85, 27.86, 27.78, 27.57, 10.30 ppm. **HRMS** (ESI): calcd. for $C_{32}H_{34}NOS^+$: 480.2361. found: 480.2364.

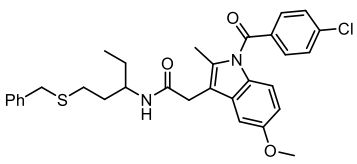

***N*-(1-(Benzylthio)pentan-3-yl)-2-(1-(4-chlorobenzoyl)-5-methoxy-2-methyl-1H-indol-3-yl)acetamide (2-33):** White solid (54%). **M.P.** 129 ºC. **$^1$H NMR** (400 MHz, $CDCl_3$) δ 7.66 – 7.56 (m, 2H), 7.51 – 7.42 (m, 2H), 7.31 – 7.15 (m, 5H), 6.88 (dd, *J* = 5.7, 3.2 Hz, 2H), 6.70 (dd, *J* = 9.1, 2.5 Hz, 1H), 5.50 (d, *J* = 9.1 Hz, 1H), 3.90 (qt, *J* =

8.6, 4.9 Hz, 1H), 3.80 (s, 3H), 3.63 (s, 2H), 3.56 (d, *J* = 1.8 Hz, 2H), 2.34 (s, 3H), 2.30 (t, *J* = 7.5 Hz, 2H), 1.64 (dtd, *J* = 12.6, 7.9, 4.6 Hz, 1H), 1.51 – 1.32 (m, 2H), 1.24 (s, 9H), 0.75 (t, *J* = 7.4 Hz, 3H) ppm. **$^{13}$C NMR** (101 MHz, $CDCl_3$) δ 169.64, 168.36, 156.34, 139.57, 138.25, 136.30, 133.59, 131.19, 130.91, 130.34, 129.24, 128.79, 128.50, 127.01, 115.21, 112.92, 112.52, 100.68, 77.41, 77.09, 76.77, 75.02, 55.74, 50.47, 36.39, 33.77, 32.39, 27.78, 27.44, 24.87, 13.31, 10.20 ppm. **HRMS** (ESI): calcd. for $C_{31}H_{34}ClN_2O_3S^+$: 549.1979. found: 549.1980.

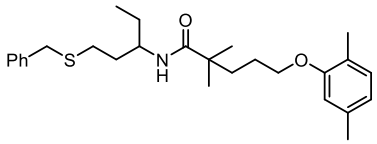

***N*-(1-(Benzylthio)pentan-3-yl)-5-(2,5-dimethylphenoxy)-2,2-dimethylpentanamide (2-34):** Colorless oil (18%). **$^{1}$H NMR** (400 MHz, $CDCl_3$) δ 7.29 (d, *J* = 4.4 Hz, 4H), 7.22 (ddd, *J* = 8.7, 5.2, 3.4 Hz, 1H), 7.00 (d, *J* = 7.5 Hz, 1H), 6.66 (d, *J* = 7.5 Hz, 1H), 6.61 (d, *J* = 1.5 Hz, 1H), 5.42 (d, *J* = 8.9 Hz, 1H), 3.96 – 3.83 (m, 3H), 3.69 (s, 2H), 2.41 (ddd, *J* = 8.5, 6.6, 1.7 Hz, 2H), 2.30 (s, 3H), 2.17 (s, 3H), 1.82 – 1.54 (m, 8H), 1.54 – 1.44 (m, 1H), 1.42 – 1.28 (m, 1H), 1.17 (s, 7H), 0.86 (t, *J* = 7.4 Hz, 3H) ppm. **$^{13}$C NMR** (101 MHz, $CDCl_3$) δ 177.08, 156.94, 138.33, 136.55, 130.32, 128.84, 128.54, 127.02, 123.53, 120.78, 112.10, 77.38, 77.06, 76.75, 68.01, 50.15, 41.94, 37.61, 36.44, 34.29, 27.85, 27.83, 25.70, 25.63, 25.19, 21.43, 15.86, 10.31 ppm. **HRMS** (ESI): calcd. for $C_{27}H_{40}NO_2S^+$: 442.2780. found: 442.2782.

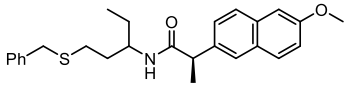

***N*-*((R)*-1-(Benzylthio)pentan-3-yl)-2-(6-methoxynaphthalen-2-yl)propanamide (2-35):** White solid (44%). **M.P.** 96 ºC. **$^{1}$H NMR** (400 MHz, $CDCl_3$) δ 7.76 – 7.59 (m, 3H), 7.28 (td, *J* = 18.8, 18.1, 6.2 Hz, 6H), 7.19 – 7.10 (m, 2H), 5.07 (d, *J* = 9.2 Hz, 1H), 3.91 (s, 4H), 3.63 (d, *J* = 7.0 Hz, 3H), 2.34 (t, *J* = 7.8 Hz, 2H), 1.64 (p, *J* = 7.9, 6.7 Hz, 1H), 1.57 (d, *J* = 7.1 Hz, 3H), 1.45 (dt, *J* = 14.6, 7.7 Hz, 1H), 1.35 (dq, *J* = 13.8, 6.9 Hz, 1H), 1.17 (dp, *J* = 14.9, 7.6 Hz, 1H), 0.67 (t, *J* = 7.4 Hz, 3H) ppm. **$^{13}$C NMR** (101 MHz, $CDCl_3$) δ 174.01, 157.80, 138.42, 136.65, 133.76, 129.22, 129.01, 128.84, 128.48, 127.56, 126.98, 126.28, 126.11, 119.18, 105.73, 77.36, 77.05, 76.73, 55.34, 50.35, 47.25, 36.43, 34.31, 27.87, 27.66, 18.48, 10.04 ppm. **HRMS** (ESI): calcd. for $C_{26}H_{32}NO_2S^+$: 422.2154. found: 422.2155.

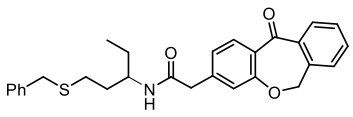

***N*-(1-(Benzylthio)pentan-3-yl)-2-(11-oxo-6,11-dihydrodibenzo[b,e]oxepin-3-yl)acetamide (2-36):** White solid (88%). **$^{1}$H NMR** (400 MHz, $CDCl_3$) δ 8.09 (d, *J* = 2.4 Hz, 1H), 7.88 (dd, *J* = 7.6, 1.4 Hz, 1H), 7.56 (td, *J* = 7.4, 1.4 Hz, 1H), 7.46 (td, *J* = 7.6, 1.2 Hz, 1H), 7.42 – 7.32 (m, 2H), 7.32 – 7.16 (m, 5H), 7.03 (d, *J* = 8.4 Hz, 1H), 5.40 (d, *J* = 9.0 Hz, 1H), 5.17 (s, 2H), 3.95 – 3.80 (m, 1H), 3.65 (s, 2H), 3.53 (s, 2H), 2.35 (t, *J* = 7.7 Hz, 2H), 1.69 (dtd, *J* = 12.8, 8.0, 4.6 Hz, 1H), 1.58 – 1.36 (m, 2H), 1.31 (dq, *J* = 14.4, 7.5 Hz, 1H), 0.80 (t, *J* = 7.4 Hz, 3H) ppm. **$^{13}$C NMR** (101 MHz, $CDCl_3$) δ 190.87, 170.43, 160.56, 140.39, 138.34, 136.32, 135.52, 132.92, 132.32, 129.50, 129.34, 128.95, 128.86, 128.51, 127.91, 127.02, 125.24, 121.53, 77.43, 77.11, 76.80, 75.02, 73.64, 50.52, 42.86, 36.40, 34.06, 27.78, 27.64, 24.87, 10.23 ppm. **HRMS** (ESI): calcd. for $C_{28}H_{30}NO_3S^+$: 460.1946. found: 460.1939.

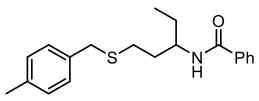

***N*-(1-((4-Methoxybenzyl)thio)pentan-3-yl)benzamide (2-37):** White solid (85%). **M.P.** 99 ºC. **$^{1}$H NMR** (400 MHz, $CDCl_3$) δ 7.78 – 7.67

(m, 2H), 7.50 (t, *J* = 7.3 Hz, 1H), 7.42 (t, *J* = 7.5 Hz, 2H), 7.15 (d, *J* = 7.9 Hz, 2H), 7.04 (d, *J* = 7.7 Hz, 2H), 6.02 (d, *J* = 9.1 Hz, 1H), 4.11 (ddt, *J* = 13.5, 8.3, 4.1 Hz, 1H), 3.67 (s, 2H), 2.48 (t, *J* = 7.7 Hz, 2H), 2.29 (s, 3H), 1.97 – 1.80 (m, 1H), 1.76 – 1.64 (m, 2H), 1.64 – 1.40 (m, 2H), 0.93 (t, *J* = 7.4 Hz, 3H) ppm. **$^{13}$C NMR** (101 MHz, $CDCl_3$) δ 167.25, 136.62, 135.10, 134.87, 131.38, 129.19, 128.76, 128.57, 126.87, 77.38, 77.06, 76.75, 50.86, 36.01, 34.11, 27.84, 27.60, 21.08, 10.35 ppm. **HRMS** (ESI): calcd. for $C_{20}H_{26}NOS^+$: 328.1735. found: 328.1737.

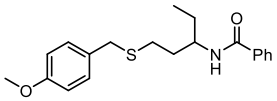

***N*-(1-((4-Methylbenzyl)thio)pentan-3-yl)benzamide (2-38):** White solid (87%). **M.P.** 84 ºC. **$^1$H NMR** (400 MHz, $CDCl_3$) δ 7.77 – 7.68 (m, 2H), 7.54 – 7.47 (m, 1H), 7.43 (dd, *J* = 8.3, 6.6 Hz, 2H), 7.23 – 7.13 (m, 2H), 6.82 – 6.73 (m, 2H), 5.98 (d, *J* = 9.0 Hz, 1H), 4.12 (qt, *J* = 8.5, 5.0 Hz, 1H), 3.75 (s, 3H), 3.67 (s, 2H), 2.48 (t, *J* = 7.7 Hz, 2H), 1.89 (dtd, *J* = 16.1, 8.1, 4.6 Hz, 1H), 1.72 (dt, *J* = 14.4, 7.5 Hz, 1H), 1.67 – 1.56 (m, 2H), 1.51 (dt, *J* = 14.1, 7.4 Hz, 1H), 0.94 (t, *J* = 7.4 Hz, 3H) ppm. **$^{13}$C NMR** (101 MHz, $CDCl_3$) δ 167.25, 158.62, 134.86, 131.39, 130.15, 129.92, 128.59, 126.85, 113.91, 77.36, 77.04, 76.72, 55.26, 50.87, 35.69, 34.11, 27.83, 27.53, 10.36 ppm. **HRMS** (ESI): calcd. for $C_{20}H_{26}NO_2S^+$: 344.1684. found: 344.1693.

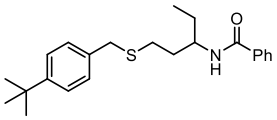

***N*-(1-((4-(*t*-Butyl)benzyl)thio)pentan-3-yl)benzamide (2-39):** White solid (82%). **M.P.** 91 ºC. **$^1$H NMR** (400 MHz, $CDCl_3$) δ 7.75 (dd, *J* = 7.2, 1.8 Hz, 2H), 7.54 – 7.46 (m, 1H), 7.42 (dd, *J* = 8.3, 6.6 Hz, 2H), 7.31 – 7.23 (m, 2H), 7.23 – 7.15 (m, 2H), 6.08 (d, *J* = 9.1 Hz, 1H), 4.12 (tq, *J* = 8.5, 4.6, 4.1 Hz, 1H), 3.68 (s, 2H), 2.51 (t, *J* = 7.7 Hz, 2H), 1.88 (dtd, *J* = 12.5, 7.9, 4.4 Hz, 1H), 1.71 (ddd, *J* = 14.6, 8.2, 7.0 Hz, 2H), 1.59 (ddd, *J* = 13.5, 7.5, 5.9 Hz, 1H), 1.50 (dt, *J* = 14.1, 7.5 Hz, 1H), 1.28 (s, 9H), 0.92 (t, *J* = 7.4 Hz, 3H) ppm. **$^{13}$C NMR** (101 MHz, $CDCl_3$) δ 167.26, 149.94, 135.18, 134.86, 131.39, 128.59, 128.52, 126.88, 125.43, 77.39, 77.07, 76.76, 50.88, 35.98, 34.46, 34.16, 31.34, 27.83, 10.36 ppm. **HRMS** (ESI): calcd. for $C_{23}H_{32}NOS^+$: 370.2205. found: 370.2204.

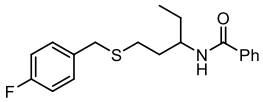

***N*-(1-((4-Fluorobenzyl)thio)pentan-3-yl)benzamide (2-40):** White solid (79%). **M.P.** 101 ºC. **$^1$H NMR** (400 MHz, $CDCl_3$) δ 7.72 (d, *J* = 7.7 Hz, 2H), 7.50 (t, *J* = 7.3 Hz, 1H), 7.43 (t, *J* = 7.5 Hz, 2H), 7.32 – 7.17 (m, 2H), 6.92 (t, *J* = 8.6 Hz, 2H), 5.99 (d, *J* = 9.1 Hz, 1H), 4.12 (qt, *J* = 8.9, 5.0 Hz, 1H), 3.68 (s, 2H), 2.48 (t, *J* = 7.7 Hz, 2H), 1.87 (dtd, *J* = 12.7, 8.0, 4.5 Hz, 1H), 1.82 – 1.66 (m, 2H), 1.61 (dt, *J* = 13.9, 6.8 Hz, 1H), 1.51 (dt, *J* = 14.1, 7.3 Hz, 1H), 0.94 (t, *J* = 7.4 Hz, 3H) ppm. **$^{13}$C NMR** (101 MHz, $CDCl_3$) δ 167.30, 163.05, 160.62, 134.77, 133.98, 133.95, 131.46, 130.40, 130.32, 128.61, 126.83, 115.44, 115.23, 77.38, 77.06, 76.74, 50.80, 35.59, 34.21, 27.85, 27.70, 10.38 ppm. **$^{19}$F NMR** (377 MHz, $CDCl_3$) δ -121.53, -121.55, -121.56, -121.57, -121.58, -121.58, -121.59, -121.61 ppm. **HRMS** (ESI): calcd. for $C_{19}H_{23}FNOS^+$: 332.1484. found: 332.1480.

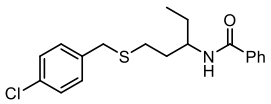

***N*-(1-((4-Chlorobenzyl)thio)pentan-3-yl)benzamide (2-41):** White solid (83%). **M.P.** 98 ºC. **$^1$H NMR** (400 MHz, $CDCl_3$) δ 7.72 (dt, *J* = 7.0, 1.4 Hz, 2H), 7.55 – 7.47 (m, 1H), 7.43 (dd, *J* = 8.3, 6.6 Hz, 2H), 7.20 (s, 4H), 6.00 (d, *J* = 9.0 Hz, 1H), 4.12 (dtd, *J* = 13.7, 8.5, 4.9 Hz, 1H), 3.66 (s, 2H), 2.47 (dd, *J* = 8.5, 6.8 Hz, 2H), 1.87 (dtd, *J* = 12.7, 7.9, 4.4 Hz, 1H), 1.76 – 1.65 (m, 1H), 1.65 – 1.55

(m, 1H), 1.51 (dq, *J* = 14.2, 7.4, 6.5 Hz, 1H), 0.94 (t, *J* = 7.4 Hz, 3H) ppm. **$^{13}$C NMR** (101 MHz, $CDCl_3$) δ 167.32, 136.81, 134.75, 132.73, 131.48, 130.20, 128.64, 126.83, 77.40, 77.08, 76.76, 50.77, 35.65, 34.20, 27.86, 27.69, 10.41 ppm. **HRMS** (ESI): calcd. for $C_{19}H_{23}ClNOS^+$: 348.1189. found: 348.1186.

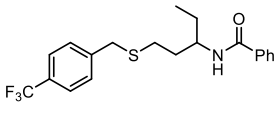

***N*-(1-((4-(Trifluoromethyl)benzyl)thio)pentan-3-yl)benzamide (2-42):** White solid (74%). **M.P.** 139 ºC. **$^1$H NMR** (400 MHz, $CDCl_3$) δ 7.72 (dd, *J* = 6.9, 1.8 Hz, 2H), 7.49 (dd, *J* = 7.9, 2.7 Hz, 3H), 7.45 – 7.34 (m, 4H), 5.98 (d, *J* = 9.0 Hz, 1H), 4.19 – 4.08 (m, 1H), 3.73 (s, 2H), 2.48 (dd, *J* = 8.4, 6.8 Hz, 2H), 1.88 (dtd, *J* = 12.7, 7.9, 4.6 Hz, 1H), 1.77 – 1.68 (m, 2H), 1.66 – 1.55 (m, 1H), 1.50 (dt, *J* = 14.2, 7.4 Hz, 1H), 0.94 (t, *J* = 7.4 Hz, 3H) ppm. **$^{13}$C NMR** (101 MHz, $CDCl_3$) δ 167.32, 142.55, 134.72, 131.50, 129.40, 129.16, 129.08, 128.62, 126.80, 125.49, 125.46, 125.42, 125.38, 122.78, 77.37, 77.06, 76.74, 50.74, 35.93, 34.25, 27.87, 27.85, 10.38 ppm. **$^{19}$F NMR** (377 MHz, $CDCl_3$) δ -68.44 ppm. **HRMS** (ESI): calcd. for $C_{20}H_{23}F_3NOS^+$: 382.1452. found: 382.1455.

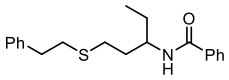

***N*-(1-(Phenethylthio)pentan-3-yl)benzamide (2-43):** White solid (90%). **M.P.** 104 ºC. **$^1$H NMR** (400 MHz, $CDCl_3$) δ 7.79 – 7.74 (m, 2H), 7.51 – 7.45 (m, 1H), 7.41 (dd, *J* = 8.2, 6.5 Hz, 2H), 7.26 (dd, *J* = 7.9, 6.6 Hz, 2H), 7.22 – 7.12 (m, 3H), 6.21 (d, *J* = 9.0 Hz, 1H), 4.15 (ddt, *J* = 13.7, 8.6, 4.3 Hz, 1H), 2.90 – 2.81 (m, 2H), 2.81 – 2.72 (m, 2H), 2.59 (dd, *J* = 8.4, 6.9 Hz, 2H), 1.90 (dtd, *J* = 12.5, 7.9, 4.5 Hz, 1H), 1.81 – 1.69 (m, 1H), 1.63 (tq, *J* = 13.0, 7.4, 6.5 Hz, 1H), 1.53 (dt, *J* = 14.2, 7.4 Hz, 1H), 0.95 (t, *J* = 7.4 Hz, 3H) ppm. **$^{13}$C NMR** (101 MHz, $CDCl_3$) δ 167.33, 140.49, 134.81, 131.43, 128.60, 128.53, 128.49, 126.93, 126.38, 77.45, 77.13, 76.81, 50.92, 36.27, 34.64, 33.85, 28.88, 27.96, 10.44 ppm. **HRMS** (ESI): calcd. for $C_{20}H_{26}NOS^+$: 328.1735. found: 328.1738.

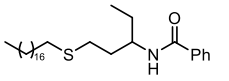

***N*-(1-(Octadecylthio)pentan-3-yl)benzamide (2-44):** White solid (87%). **M.P.** 88 ºC. **$^1$H NMR** (400 MHz, $CDCl_3$) δ 7.85 – 7.74 (m, 2H), 7.52 (dd, *J* = 8.5, 6.0 Hz, 1H), 7.45 (t, *J* = 7.5 Hz, 2H), 6.13 (d, *J* = 9.1 Hz, 1H), 4.20 (qt, *J* = 8.6, 4.9 Hz, 1H), 2.62 (t, *J* = 7.6 Hz, 2H), 2.53 (t, *J* = 7.4 Hz, 2H), 1.95 (dtd, *J* = 12.5, 7.9, 4.4 Hz, 1H), 1.78 (dq, *J* = 14.9, 7.7 Hz, 1H), 1.73 – 1.63 (m, 3H), 1.58 (pd, *J* = 7.7, 4.9 Hz, 4H), 1.27 (d, *J* = 3.8 Hz, 34H), 0.99 (t, *J* = 7.4 Hz, 3H), 0.90 (t, *J* = 6.7 Hz, 3H) ppm. **$^{13}$C NMR** (101 MHz, $CDCl_3$) δ 167.23, 134.84, 131.40, 128.59, 126.84, 77.35, 77.04, 76.72, 50.96, 34.54, 32.36, 31.94, 29.71, 29.69, 29.67, 29.62, 29.60, 29.54, 29.37, 29.26, 28.93, 28.62, 27.93, 22.70, 14.13, 10.37 ppm. **HRMS** (ESI): calcd. for $C_{30}H_{54}NOS^+$: 476.3926. found: 476.3924.

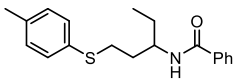

***N*-(1-(*p*-Tolylthio)pentan-3-yl)benzamide (2-45):** White solid (70%). **M.P.** 101 ºC. **$^1$H NMR** (400 MHz, $CDCl_3$) δ 7.79 – 7.70 (m, 2H), 7.48 (t, *J* = 7.3 Hz, 1H), 7.41 (t, *J* = 7.5 Hz, 2H), 7.23 (d, *J* = 7.9 Hz, 2H), 7.07 (d, *J* = 7.8 Hz, 2H), 6.11 (d, *J* = 9.0 Hz, 1H), 4.17 (qt, *J* = 9.0, 5.0 Hz, 1H), 2.94 (t, *J* = 7.7 Hz, 2H), 2.30 (s, 3H), 1.94 (dtd, *J* = 16.0, 7.9, 4.4 Hz, 1H), 1.77 (ddd, *J* = 14.6, 8.4, 6.8 Hz, 1H), 1.70 – 1.57 (m, 1H), 1.52 (dt, *J* = 14.2, 7.4 Hz, 1H), 0.93 (t, *J* = 7.4 Hz, 3H) ppm. **$^{13}$C NMR** (101 MHz, $CDCl_3$) δ 167.40, 136.30, 134.80, 132.35, 131.42, 130.17, 129.75, 128.58, 126.90, 77.41, 77.10, 76.78,

50.84, 34.59, 31.20, 28.07, 21.02, 10.37 ppm. **HRMS** (ESI): calcd. for $C_{19}H_{24}NOS^+$: 314.1579. found: 314.1576.

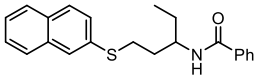

***N*-(1-(Naphthalen-2-ylthio)pentan-3-yl)benzamide (2-46):** White solid (78%). **M.P.** 118 ºC. **$^1$H NMR** (400 MHz, $CDCl_3$) δ 7.81 – 7.72 (m, 3H), 7.72 – 7.63 (m, 3H), 7.50 – 7.43 (m, 2H), 7.43 – 7.35 (m, 4H), 6.16 (d, *J* = 9.1 Hz, 1H), 4.21 (qt, *J* = 9.0, 5.0 Hz, 1H), 3.07 (t, *J* = 7.7 Hz, 2H), 1.99 (dtd, *J* = 16.1, 7.9, 4.4 Hz, 1H), 1.81 (ddt, *J* = 14.3, 8.8, 7.3 Hz, 1H), 1.69 – 1.56 (m, 1H), 1.52 (dt, *J* = 14.3, 7.5 Hz, 1H), 0.93 (t, *J* = 7.4 Hz, 3H) ppm. **$^{13}$C NMR** (101 MHz, $CDCl_3$) δ 167.50, 134.78, 133.80, 133.76, 131.79, 131.47, 128.62, 128.50, 127.74, 127.37, 127.10, 126.96, 126.94, 126.60, 125.70, 77.44, 77.12, 76.80, 50.91, 34.60, 30.37, 28.14, 10.42 ppm. **HRMS** (ESI): calcd. for $C_{22}H_{24}NOS^+$: 350.1579. found: 350.1580.

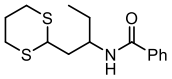

***N*-(1-(1,3-Dithian-2-yl)butan-2-yl)benzamide (2-47):** White solid (78%). **M.P.** 113 ºC. **$^1$H NMR** (400 MHz, $CDCl_3$) δ 7.80 (dd, *J* = 7.0, 1.9 Hz, 2H), 7.55 – 7.47 (m, 1H), 7.44 (dd, *J* = 8.2, 6.5 Hz, 2H), 6.13 (d, *J* = 9.1 Hz, 1H), 4.36 (qt, *J* = 8.3, 4.6 Hz, 1H), 4.13 (dd, *J* = 8.5, 5.4 Hz, 1H), 2.96 – 2.76 (m, 4H), 2.17 – 2.02 (m, 2H), 1.97 (ddd, *J* = 14.5, 8.4, 5.4 Hz, 1H), 1.88 (dddd, *J* = 17.8, 14.2, 9.0, 5.0 Hz, 1H), 1.76 – 1.55 (m, 3H), 0.98 (t, *J* = 7.4 Hz, 3H) ppm. **$^{13}$C NMR** (101 MHz, $CDCl_3$) δ 167.09, 134.80, 131.41, 128.59, 126.94, 77.35, 77.04, 76.72, 49.39, 43.95, 40.32, 30.40, 30.20, 27.95, 25.68, 10.38 ppm. **HRMS** (ESI): calcd. for $C_{15}H_{22}NOS_2^+$: 296.1143. found: 296.1148.

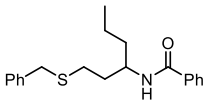

***N*-(1-(Benzylthio)hexan-3-yl)benzamide (2-48):** White solid (78%). **M.P.** 104 ºC. **$^1$H NMR** (400 MHz, $CDCl_3$) δ 7.76 – 7.67 (m, 2H), 7.52 – 7.44 (m, 1H), 7.44 – 7.36 (m, 2H), 7.30 – 7.15 (m, 5H), 6.09 (d, *J* = 9.0 Hz, 1H), 4.19 (dtd, *J* = 13.5, 8.5, 5.4 Hz, 1H), 3.69 (s, 2H), 2.48 (t, *J* = 7.6 Hz, 2H), 1.86 (dtd, *J* = 14.1, 8.0, 4.5 Hz, 1H), 1.71 (ddd, *J* = 13.1, 8.2, 6.8 Hz, 1H), 1.47 (qdd, *J* = 9.8, 6.0, 1.7 Hz, 2H), 1.41 – 1.27 (m, 2H), 0.90 (t, *J* = 7.2 Hz, 3H) ppm. **$^{13}$C NMR** (101 MHz, $CDCl_3$) δ 167.19, 138.26, 134.83, 131.38, 128.88, 128.56, 128.51, 127.00, 126.91, 77.43, 77.11, 76.80, 49.24, 37.19, 36.32, 34.62, 27.67, 19.26, 14.01 ppm. **HRMS** (ESI): calcd. for $C_{20}H_{26}NOS^+$: 328.1735. found: 328.1728.

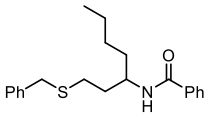

***N*-(1-(Benzylthio)heptan-3-yl)benzamide (2-49):** White solid (62%). **M.P.** 93 ºC. **$^1$H NMR** (400 MHz, $CDCl_3$) δ 7.72 (dd, *J* = 7.1, 1.8 Hz, 2H), 7.53 – 7.46 (m, 1H), 7.42 (dd, *J* = 8.2, 6.6 Hz, 2H), 7.31 – 7.15 (m, 5H), 6.00 (d, *J* = 9.0 Hz, 1H), 4.26 – 4.09 (m, 1H), 3.70 (s, 2H), 2.49 (t, *J* = 7.7 Hz, 2H), 1.93 – 1.81 (m, 1H), 1.77 – 1.64 (m, 2H), 1.58 – 1.41 (m, 2H), 1.32 (qd, *J* = 7.1, 6.6, 3.0 Hz, 4H), 0.88 (h, *J* = 3.2 Hz, 3H) ppm. **$^{13}$C NMR** (101 MHz, $CDCl_3$) δ 167.14, 138.26, 134.84, 131.39, 128.88, 128.58, 128.51, 127.00, 126.87, 77.38, 77.06, 76.75, 49.45, 36.35, 34.71, 34.59, 28.13, 27.66, 22.59, 14.01 ppm. **HRMS** (ESI): calcd. for $C_{21}H_{28}NOS^+$: 342.1892. found: 342.1898.

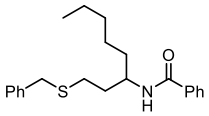

***N*-(1-(Benzylthio)octan-3-yl)benzamide (2-50):** White solid (44%). **M.P.** 75 ºC. **$^1$H NMR** (400 MHz, $CDCl_3$) δ 7.72 (dd, *J* = 7.0, 1.7 Hz, 2H), 7.53 – 7.46 (m, 1H), 7.42 (dd, *J* = 8.3, 6.6 Hz, 2H), 7.31 – 7.16 (m, 5H), 6.03 (d,

*J* = 9.0 Hz, 1H), 4.18 (dtt, *J* = 13.6, 8.3, 4.6 Hz, 1H), 3.70 (s, 2H), 2.48 (t, *J* = 7.7 Hz, 2H), 1.87 (dtd, *J* = 15.8, 8.0, 4.4 Hz, 1H), 1.71 (ddd, *J* = 14.5, 8.1, 6.7 Hz, 1H), 1.48 (dtd, *J* = 18.8, 13.4, 7.6 Hz, 2H), 1.38 – 1.19 (m, 6H), 0.95 – 0.76 (m, 3H) ppm. **$^{13}$C NMR** (101 MHz, $CDCl_3$) δ 167.16, 138.26, 134.84, 131.39, 128.88, 128.58, 128.51, 127.01, 126.88, 77.40, 77.08, 76.77, 49.48, 36.34, 34.98, 34.57, 31.71, 27.66, 25.67, 22.57, 14.05 ppm. **HRMS** (ESI): calcd. for $C_{22}H_{30}NOS^+$: 356.2048. found: 356.2053.

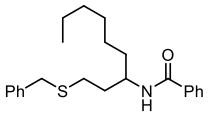

***N*-(1-(Benzylthio)nonan-3-yl)benzamide (2-51):** White solid (38%). **M.P.** 68 ºC. **$^1$H NMR** (400 MHz, $CDCl_3$) δ 7.73 (dd, *J* = 7.1, 1.8 Hz, 2H), 7.56 – 7.48 (m, 1H), 7.44 (dd, *J* = 8.2, 6.6 Hz, 2H), 7.33 – 7.17 (m, 5H), 5.97 (d, *J* = 9.0 Hz, 1H), 4.19 (dp, *J* = 13.6, 4.9, 4.2 Hz, 1H), 3.72 (s, 2H), 2.50 (t, *J* = 7.6 Hz, 2H), 1.89 (dtd, *J* = 16.0, 8.0, 4.5 Hz, 1H), 1.72 (ddd, *J* = 14.7, 8.0, 6.7 Hz, 1H), 1.50 (tdd, *J* = 13.5, 10.8, 5.7 Hz, 2H), 1.40 – 1.18 (m, 8H), 0.88 (t, *J* = 6.7 Hz, 3H) ppm. **$^{13}$C NMR** (101 MHz, $CDCl_3$) δ 167.13, 138.26, 134.86, 131.38, 128.87, 128.58, 128.50, 127.00, 126.85, 77.36, 77.04, 76.72, 49.49, 36.35, 35.02, 34.57, 31.74, 29.19, 27.65, 25.94, 22.59, 14.06 ppm. **HRMS** (ESI): calcd. for $C_{23}H_{32}NOS^+$: 370.2205. found: 370.2206.

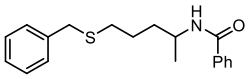

***N*-(5-(Benzylthio)pentan-2-yl)benzamide (2-4):** White solid (71%). **M.P.** 78 ºC. **$^1$H NMR** (400 MHz, $CDCl_3$) δ 7.81 – 7.69 (m, 2H), 7.54 – 7.45 (m, 1H), 7.41 (dd, *J* = 8.3, 6.6 Hz, 2H), 7.28 (d, *J* = 4.4 Hz, 4H), 7.21 (dt, *J* = 9.0, 4.3 Hz, 1H), 5.99 (d, *J* = 8.4 Hz, 1H), 4.27 – 4.06 (m, 1H), 3.68 (s, 2H), 2.57 – 2.35 (m, 2H), 1.61 (tq, *J* = 12.0, 7.1, 6.1 Hz, 4H), 1.21 (d, *J* = 6.6 Hz, 3H) ppm. **$^{13}$C NMR** (101 MHz, $CDCl_3$) δ 166.92, 138.51, 134.88, 131.38, 128.84, 128.57, 128.51, 126.97, 126.87, 77.42, 77.10, 76.78, 45.46, 36.36, 36.09, 31.32, 25.79, 21.16 ppm. **HRMS** (ESI): calcd. for $C_{19}H_{24}NOS^+$: 314.1579. found: 314.1583.

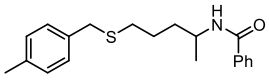

***N*-(5-((4-Methylbenzyl)thio)pentan-2-yl)benzamide (2-52):** Colorless oil (65%). **$^1$H NMR** (400 MHz, $CDCl_3$) δ 7.79 – 7.69 (m, 2H), 7.52 – 7.46 (m, 1H), 7.42 (dd, *J* = 8.2, 6.5 Hz, 2H), 7.17 (d, *J* = 7.9 Hz, 2H), 7.09 (d, *J* = 7.8 Hz, 2H), 5.93 (d, *J* = 8.4 Hz, 1H), 4.25 – 4.12 (m, 1H), 3.65 (s, 2H), 2.48 – 2.40 (m, 2H), 2.31 (s, 3H), 1.62 (ddt, *J* = 11.7, 9.2, 5.8 Hz, 4H), 1.21 (d, *J* = 6.6 Hz, 3H) ppm. **$^{13}$C NMR** (101 MHz, $CDCl_3$) δ 166.89, 136.57, 135.35, 134.91, 131.36, 129.18, 128.71, 128.57, 126.83, 77.38, 77.06, 76.75, 45.48, 36.10, 36.03, 31.26, 25.79, 21.15, 21.08 ppm. **HRMS** (ESI): calcd. for $C_{20}H_{26}NOS^+$: 328.1735. found: 328.1743.

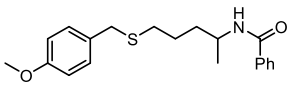

***N*-(5-((4-Methoxybenzyl)thio)pentan-2-yl)benzamide (2-53):** White solid (61%). **M.P.** 79 ºC. **$^1$H NMR** (400 MHz, $CDCl_3$) δ 7.74 (dd, *J* = 7.0, 1.9 Hz, 2H), 7.52 – 7.46 (m, 1H), 7.42 (dd, *J* = 8.2, 6.5 Hz, 2H), 7.23 – 7.16 (m, 2H), 6.85 – 6.79 (m, 2H), 5.92 (d, *J* = 8.4 Hz, 1H), 4.25 – 4.12 (m, 1H), 3.78 (s, 3H), 3.64 (s, 2H), 2.45 (t, *J* = 6.8 Hz, 2H), 1.70 – 1.55 (m, 4H), 1.22 (d, *J* = 6.6 Hz, 3H) ppm. **$^{13}$C NMR** (101 MHz, $CDCl_3$) δ 166.89, 158.60, 134.89, 131.38, 130.42, 129.88, 128.58, 126.82, 113.91, 77.37, 77.05, 76.74, 55.28, 45.48, 36.13, 35.70, 31.20, 25.80, 21.17 ppm. **HRMS** (ESI): calcd. for $C_{20}H_{26}NO_2S^+$: 344.1684. found: 344.1692.

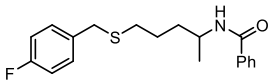

***N*-(5-((4-Fluorobenzyl)thio)pentan-2-yl)benzamide (2-54):** White solid (54%). **M.P.** 74 ºC. **$^{1}$H NMR** (400 MHz, $CDCl_3$) δ 7.79 – 7.71 (m, 2H), 7.53 – 7.46 (m, 1H), 7.42 (dd, *J* = 8.3, 6.6 Hz, 2H), 7.30 – 7.18 (m, 2H), 6.96 (t, *J* = 8.7 Hz, 2H), 5.92 (d, *J* = 8.3 Hz, 1H), 4.30 – 4.09 (m, 1H), 3.66 (s, 2H), 2.55 – 2.34 (m, 2H), 1.70 – 1.47 (m, 4H), 1.22 (d, *J* = 6.6 Hz, 3H) ppm. **$^{13}$C NMR** (101 MHz, $CDCl_3$) δ 166.89, 163.06, 160.62, 134.85, 134.18, 131.41, 130.35, 130.27, 128.59, 126.82, 115.43, 115.22, 77.37, 77.05, 76.74, 45.39, 36.14, 35.59, 31.29, 25.77, 21.17 ppm. **$^{19}$F NMR** (377 MHz, $CDCl_3$) δ -115.58, -115.59, -115.61, -115.61, -115.63. **HRMS** (ESI): calcd. for $C_{19}H_{23}FNOS^+$: 332.1484. found: 332.1489.

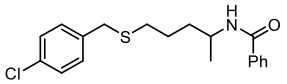

***N*-(5-((4-Chlorobenzyl)thio)pentan-2-yl)benzamide (2-55):** White solid (78%). **M.P.** 74 ºC. **$^{1}$H NMR** (400 MHz, $CDCl_3$) δ 7.77 – 7.71 (m, 2H), 7.50 (t, *J* = 7.3 Hz, 1H), 7.43 (dd, *J* = 8.3, 6.5 Hz, 2H), 7.28 – 7.17 (m, 4H), 5.88 (d, *J* = 8.5 Hz, 1H), 4.26 – 4.12 (m, 1H), 3.64 (s, 2H), 2.44 (td, *J* = 6.7, 2.3 Hz, 2H), 1.71 – 1.52 (m, 5H), 1.23 (d, *J* = 6.6 Hz, 3H) ppm. **$^{13}$C NMR** (101 MHz, $CDCl_3$) δ 166.87, 137.04, 134.85, 132.71, 131.42, 130.15, 128.63, 128.60, 126.81, 77.36, 77.04, 76.72, 45.38, 36.16, 35.67, 31.28, 25.74, 21.19 ppm. **HRMS** (ESI): calcd. for $C_{19}H_{23}ClNOS^+$: 348.1189. found: 348.1194.

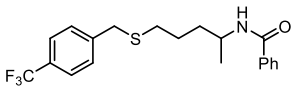

***N*-(5-((4-Hydroxybenzyl)thio)pentan-2-yl)benzamide (2-56):** White solid (57%). **M.P.** 91 ºC. **$^{1}$H NMR** (400 MHz, $CDCl_3$) δ 7.57 (d, *J* = 8.4 Hz, 2H), 7.28 (d, *J* = 8.2 Hz, 2H), 7.23 – 7.06 (m, 5H), 6.10 (d, *J* = 9.0 Hz, 1H), 4.00 (dtd, *J* = 13.6, 8.5, 4.9 Hz, 1H), 3.62 (s, 2H), 2.39 (t, *J* = 7.6 Hz, 2H), 1.77 (dtd, *J* = 12.5, 7.9, 4.5 Hz, 1H), 1.62 (dq, *J* = 14.8, 7.6 Hz, 1H), 1.45 (ddq, *J* = 28.7, 14.1, 7.0 Hz, 2H), 0.83 (t, *J* = 7.4 Hz, 4H) ppm. **$^{13}$C NMR** (101 MHz, $CDCl_3$) δ 166.25, 138.20, 137.55, 133.21, 128.85, 128.76, 128.52, 128.38, 127.04, 51.03, 36.37, 33.93, 27.74, 27.70, 10.39 ppm. **$^{19}$F NMR** (377 MHz, $CDCl_3$) δ -62.33. **HRMS** (ESI): calcd. for $C_{20}H_{23}F_3NOS^+$: 382.1452. found: 382.1459.

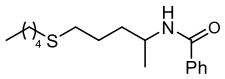

***N*-(5-((4-(Trifluoromethyl)benzyl)thio)pentan-2-yl)benzamide (2-57):** Yellow oil (57%). **$^{1}$H NMR** (400 MHz, $CDCl_3$) δ 7.76 (d, *J* = 7.6 Hz, 2H), 7.48 (t, *J* = 7.3 Hz, 1H), 7.41 (t, *J* = 7.5 Hz, 2H), 6.11 (d, *J* = 8.5 Hz, 1H), 4.22 (h, *J* = 6.6 Hz, 1H), 2.53 (q, *J* = 6.5 Hz, 2H), 2.48 (t, *J* = 7.4 Hz, 2H), 1.67 (h, *J* = 4.1, 3.5 Hz, 4H), 1.57 (q, *J* = 7.3 Hz, 2H), 1.41 – 1.15 (m, 7H), 0.88 (t, *J* = 6.9 Hz, 3H) ppm. **$^{13}$C NMR** (101 MHz, $CDCl_3$) δ 166.93, 134.89, 131.32, 128.52, 126.86, 77.41, 77.09, 76.78, 45.46, 36.06, 32.16, 31.98, 31.10, 29.37, 26.20, 22.29, 21.15, 13.98 ppm. **HRMS** (ESI): calcd. for $C_{19}H_{34}NOS^+$: 324.2361. found: 324.2366.

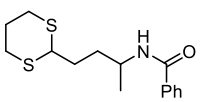

***N*-(4-(1,3-Dithian-2-yl)butan-2-yl)benzamide (2-58):** White solid (44%). **M.P.** 154 ºC. **$^{1}$H NMR** (400 MHz, $CDCl_3$) δ 7.79 – 7.72 (m, 2H), 7.49 (t, *J* = 7.2 Hz, 1H), 7.43 (dd, *J* = 8.3, 6.6 Hz, 2H), 5.97 (d, *J* = 8.4 Hz, 1H), 4.23 (dq, *J* = 13.5, 7.1, 6.6 Hz, 1H), 4.08 (t, *J* = 6.7 Hz, 1H), 2.84 (tdd, *J* = 10.5, 6.9, 4.4 Hz, 4H), 2.17 – 2.07 (m, 1H), 1.87 (qd, *J* = 7.6, 7.0, 2.6 Hz, 3H), 1.82 – 1.71 (m, 2H), 1.26 (d, *J* = 6.6 Hz, 3H) ppm. **$^{13}$C NMR** (101 MHz, $CDCl_3$) δ 166.93, 134.82, 131.39, 128.57, 126.85, 77.36,

77.05, 76.73, 47.30, 45.42, 33.83, 32.11, 30.40, 30.38, 25.93, 21.26 ppm. **HRMS** (ESI): calcd. for $C_{15}H_{22}NOS_2^+$: 296.1143. found: 296.1147.

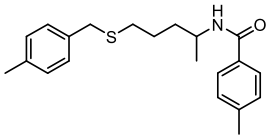

**4-Methyl-*N*-(5-((4-methylbenzyl)thio)pentan-2-yl)benzamide (2-59):** White solid (66%). **M.P.** 97 ºC. **$^1$H NMR** (400 MHz, $CDCl_3$) δ 7.64 (d, *J* = 7.9 Hz, 2H), 7.22 (d, *J* = 8.0 Hz, 2H), 7.17 (d, *J* = 7.9 Hz, 2H), 7.09 (d, *J* = 7.7 Hz, 2H), 5.87 (d, *J* = 8.5 Hz, 1H), 4.25 – 4.08 (m, 1H), 3.65 (s, 2H), 2.44 (t, *J* = 6.9 Hz, 2H), 2.39 (s, 3H), 2.31 (s, 3H), 1.67 – 1.54 (m, 4H), 1.21 (d, *J* = 6.5 Hz, 3H) ppm. **$^{13}$C NMR** (101 MHz, $CDCl_3$) δ 166.80, 141.74, 136.56, 135.36, 132.04, 129.21, 129.18, 128.71, 126.81, 77.36, 77.05, 76.73, 45.37, 36.14, 36.01, 31.26, 25.77, 21.43, 21.18, 21.08 ppm. **HRMS** (ESI): calcd. for $C_{21}H_{28}NOS^+$: 342.1892. found: 342.1900.

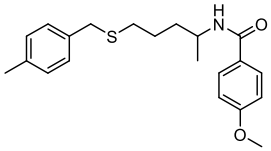

**4-Methoxy-*N*-(5-((4-methylbenzyl)thio)pentan-2-yl) benzamide (2-60):** White solid (67%). **M.P.** 101 ºC. **$^1$H NMR** (400 MHz, $CDCl_3$) δ 7.75 – 7.68 (m, 2H), 7.17 (d, *J* = 7.8 Hz, 2H), 7.09 (d, *J* = 7.8 Hz, 2H), 6.94 – 6.86 (m, 2H), 5.88 (d, *J* = 8.4 Hz, 1H), 4.16 (dq, *J* = 8.2, 6.2 Hz, 1H), 3.83 (s, 3H), 3.65 (s, 2H), 2.44 (t, *J* = 6.1 Hz, 2H), 2.31 (s, 3H), 1.68 – 1.54 (m, 4H), 1.20 (d, *J* = 6.6 Hz, 3H) ppm. **$^{13}$C NMR** (101 MHz, $CDCl_3$) δ 166.39, 162.09, 136.56, 135.36, 129.18, 128.71, 128.62, 127.17, 113.73, 77.39, 77.07, 76.75, 55.41, 45.37, 36.15, 36.01, 31.28, 25.79, 21.20, 21.08 ppm. **HRMS** (ESI): calcd. for $C_{21}H_{28}NO_2S^+$: 358.1841. found: 358.1845.

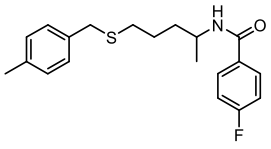

**4-Fluoro-*N*-(5-((4-methylbenzyl)thio)pentan-2-yl)benzamide (2-61):** White solid (70%). **M.P.** 103 ºC. **$^1$H NMR** (400 MHz, $CDCl_3$) δ 7.79 – 7.71 (m, 2H), 7.17 (d, *J* = 7.8 Hz, 2H), 7.09 (dt, *J* = 8.6, 4.7 Hz, 4H), 5.88 (d, *J* = 8.5 Hz, 1H), 4.16 (p, *J* = 6.4 Hz, 1H), 3.65 (s, 2H), 2.51 – 2.36 (m, 2H), 2.31 (s, 3H), 1.61 (tq, *J* = 11.8, 7.3, 6.2 Hz, 4H), 1.21 (d, *J* = 6.6 Hz, 3H) ppm. **$^{13}$C NMR** (101 MHz, $CDCl_3$) δ 165.91, 165.82, 163.41, 136.60, 135.32, 131.06, 131.03, 129.18, 129.09, 128.70, 115.68, 115.46, 77.36, 77.05, 76.73, 45.62, 36.05, 31.25, 25.77, 21.12, 21.07 ppm. **$^{19}$F NMR** (377 MHz, $CDCl_3$) δ -108.33, -108.35, -108.36, -108.38, -108.39. **HRMS** (ESI): calcd. for $C_{20}H_{25}FNOS^+$: 346.1641. found: 346.1645.

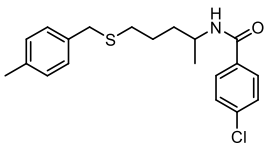

**4-Chloro-*N*-(5-((4-methylbenzyl)thio)pentan-2-yl)benzamide (2-62):** White solid (64%). **M.P.** 103 ºC. **$^1$H NMR** (400 MHz, $CDCl_3$) δ 7.72 – 7.64 (m, 2H), 7.42 – 7.35 (m, 2H), 7.16 (d, *J* = 7.7 Hz, 2H), 7.09 (d, *J* = 7.8 Hz, 2H), 5.94 (d, *J* = 8.3 Hz, 1H), 4.16 (dt, *J* = 8.6, 6.1 Hz, 1H), 3.65 (s, 2H), 2.48 – 2.38 (m, 2H), 2.31 (s, 3H), 1.66 – 1.56 (m, 4H), 1.21 (d, *J* = 6.5 Hz, 3H) ppm. **$^{13}$C NMR** (101 MHz, $CDCl_3$) δ 165.82, 137.58, 136.61, 135.31, 133.24, 129.19, 128.80, 128.70, 128.30, 77.38, 77.06, 76.74, 45.67, 36.06, 36.01, 31.25, 25.76, 21.08 ppm. **HRMS** (ESI): calcd. for $C_{20}H_{25}ClNOS^+$: 362.1345. found: 362.1349.

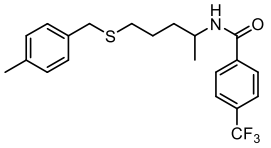

***N*-(5-((4-Methylbenzyl)thio)pentan-2-yl)-4-(trifluoro-methyl)benzamide (2-63):** White solid (64%). **M.P.** 101 ºC. **$^1$H NMR** (400 MHz, $CDCl_3$) δ 7.84 (d, *J* = 8.1 Hz, 2H), 7.68 (d, *J* = 8.2 Hz, 2H), 7.17 (d, *J*

= 8.0 Hz, 2H), 7.09 (d, *J* = 7.8 Hz, 2H), 5.94 (d, *J* = 8.5 Hz, 1H), 4.26 – 4.11 (m, 1H), 3.66 (s, 2H), 2.46 (td, *J* = 6.0, 5.2, 3.5 Hz, 2H), 2.31 (s, 3H), 1.70 – 1.56 (m, 5H), 1.23 (d, *J* = 6.6 Hz, 3H) ppm. **$^{13}$C NMR** (101 MHz, $CDCl_3$) δ 136.64, 135.28, 129.20, 128.69, 127.33, 125.65, 125.62, 77.35, 77.04, 76.72, 45.83, 36.08, 35.97, 31.23, 25.75, 21.06 ppm. **HRMS** (ESI): calcd. for $C_{21}H_{25}F_3NOS^+$: 396.1609. found: 396.1612.

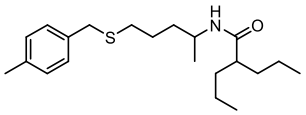

***N*-(5-((4-Methylbenzyl)thio)pentan-2-yl)-2-prop-ylpentanamide (2-64):** White solid (54%). **M.P.** 70 ºC. **$^{1}$H NMR** (400 MHz, $CDCl_3$) δ 7.20 (d, *J* = 7.8 Hz, 2H), 7.12 (d, *J* = 7.7 Hz, 2H), 5.18 (d, *J* = 8.8 Hz, 1H), 4.01 (hept, *J* = 6.8 Hz, 1H), 3.67 (s, 2H), 2.43 (tt, *J* = 8.2, 4.1 Hz, 2H), 2.34 (s, 3H), 1.95 (tt, *J* = 9.4, 4.3 Hz, 1H), 1.59 (p, *J* = 7.7, 7.0 Hz, 4H), 1.49 (hept, *J* = 6.7, 6.2 Hz, 2H), 1.31 (dtt, *J* = 27.4, 16.6, 13.3, 5.6 Hz, 7H), 1.11 (d, *J* = 6.6 Hz, 3H), 0.90 (t, *J* = 6.9 Hz, 6H) ppm. **$^{13}$C NMR** (101 MHz, $CDCl_3$) δ 175.23, 136.57, 135.39, 129.18, 128.71, 77.35, 77.03, 76.72, 47.99, 44.62, 36.04, 35.98, 35.41, 35.28, 31.21, 25.77, 21.31, 21.08, 20.89, 20.83, 14.16, 14.14 ppm. **HRMS** (ESI): calcd. for $C_{21}H_{36}NOS^+$: 350.2518. found: 350.2524.

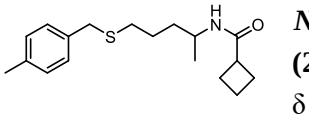

***N*-(5-((4-Methylbenzyl)thio)pentan-2-yl)cyclobutanecarboxamide (2-65):** White solid (63%). **M.P.** 83 ºC. **$^{1}$H NMR** (400 MHz, $CDCl_3$) δ 7.18 (d, *J* = 8.0 Hz, 2H), 7.11 (d, *J* = 7.7 Hz, 2H), 5.07 (d, *J* = 8.6 Hz, 1H), 4.03 – 3.90 (m, 1H), 3.66 (s, 2H), 2.93 (p, *J* = 8.5 Hz, 1H), 2.42 (td, *J* = 7.0, 1.8 Hz, 2H), 2.33 (s, 3H), 2.30 – 2.18 (m, 2H), 2.12 (dtd, *J* = 11.9, 8.5, 3.3 Hz, 2H), 1.95 (dq, *J* = 11.2, 8.8 Hz, 1H), 1.86 (tq, *J* = 9.7, 5.0, 4.5 Hz, 1H), 1.62 – 1.51 (m, 2H), 1.51 – 1.37 (m, 2H), 1.09 (d, *J* = 6.6 Hz, 3H) ppm. **$^{13}$C NMR** (101 MHz, $CDCl_3$) δ 174.24, 136.57, 135.39, 129.18, 128.70, 77.36, 77.04, 76.73, 44.64, 40.08, 36.11, 36.01, 31.25, 25.69, 25.40, 25.33, 21.12, 21.08, 18.11 ppm. **HRMS** (ESI): calcd. for $C_{18}H_{28}NOS^+$: 306.1892. found: 306.1896.

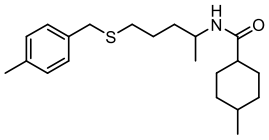

**4-Methyl-*N*-(5-((4-methylbenzyl)thio)pentan-2-yl)cy-clohexane-1-carboxamide (2-66):** White solid (51%). **M.P.** 105 ºC. **$^{1}$H NMR** (400 MHz, $CDCl_3$) δ 7.18 (d, *J* = 7.9 Hz, 2H), 7.11 (d, *J* = 7.8 Hz, 2H), 5.20 (d, *J* = 8.6 Hz, 1H), 3.97 (dq, *J* = 15.7, 6.8 Hz, 1H), 3.65 (s, 2H), 2.41 (td, *J* = 7.0, 2.2 Hz, 2H), 2.33 (s, 3H), 1.93 (tt, *J* = 12.1, 3.5 Hz, 1H), 1.88 – 1.71 (m, 5H), 1.59 – 1.51 (m, 2H), 1.51 – 1.38 (m, 4H), 1.35 (ddq, *J* = 11.7, 6.7, 3.5, 2.6 Hz, 1H), 1.09 (d, *J* = 6.6 Hz, 3H), 0.99 – 0.83 (m, 5H) ppm. **$^{13}$C NMR** (101 MHz, $CDCl_3$) δ 175.50, 136.56, 135.39, 129.18, 128.71, 77.37, 77.06, 76.74, 45.58, 44.46, 36.12, 36.01, 34.50, 34.47, 32.03, 31.25, 29.85, 29.65, 25.70, 22.53, 21.16, 21.09 ppm. **HRMS** (ESI): calcd. for $C_{21}H_{34}NOS^+$: 348.2361. found: 348.2366.

# X-ray structure of 2-68:

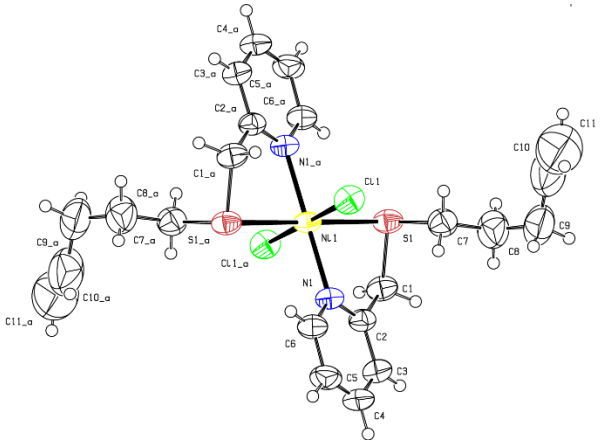


**68** (CCDC: 2079166)

**Table 2. Crystal data and structure refinement for 2-68**

| | |
|---|---|
| Empirical formula | C22 H30 Cl2 N2 Ni S2 |
| Formula weight | 516.21 |
| Temperature | 296(2) K |
| Wavelength | 0.71073 A |
| Crystal system, space group | Rhombohedral, R -3 |
| Unit cell dimensions | a = 27.8756(6) A alpha = 90 deg. |
| Volume | 5645.6(2) A^3 |
| Z, Calculated density | 9, 1.366 Mg/m^3 |
| Absorption coefficient | 1.164 mm^-1 |
| F (000) | 2430 |
| Crystal size | 0.24 x 0.18 x 0.16 mm |
| Theta range for data collection | 2.57 to 27.52 deg. |
| Limiting indices | -36<=h<=36, -36<=k<=36, -10<=l<=10 |
| Reflections collected / unique | 39039 / 2886 [R(int) = 0.0315] |
| Completeness to theta = 72.20 | 99.7 % |
| Absorption correction | Semi-empirical from equivalents |
| Max. and min. transmission | 0.8357 and 0.7675 |
| Refinement method | Full-matrix least-squares on F^2 |
| Data / restraints / parameters | 2886 / 1 / 133 |
| Goodness-of-fit on F^2 | 1.043 |
| Final R indices [I>2 sigma (I)] | R1 = 0.0277, wR2 = 0.0694 |
| R indices (all data) | R1 = 0.0341, wR2 = 0.0746 |
| Extinction coefficient | 0.0019(3) |
| Largest diff. peak and hole | 0.375 and -0.334 e.A^-3 |

# *Chapter 3*

## 3.1 GS-441524 Ester as Anti-SARS-CoV-2 Drug Candidate

### 3.1.1 Introduction

COVID-19 pandemic, breaking out in human society in 2019, quickly spread around the world with unparalleled speed and destructive influence. The disease resulted in over 700 million confirmed cases and over 6 million deaths, and the number of infections is still climbing. The pathogen of COVID-19 is a single-stranded positive-sense RNA (+ssRNA) virus, named as SARS-CoV-2. Due to the high mutation rate in the replication cycles, new variants kept emerging, with five main variants raising concerns from human society: alpha, beta, gamma, delta, and omicron. The variations of SARS-CoV-2 bring the virus with enhanced ability of immune evasion and transmissibility. Among the five variants, omicron is currently the dominant variant among the globe, due to its strong ability to evade the protection of antibodies and vaccines. Considering the trend of continuous emergence of variants, discovery of convenient and cheap anti-SARS-CoV-2 medicine is now one of the main concerns for scientists.

RNA dependent RNA polymerase (RdRp) is one of the key enzymes in the life cycle of SARS-CoV-2, responsible for replication of its +ssRNA. The catalytic domain of SARS-CoV-2 is highly conserved among the coronavirus family, making RdRp one of the most strategic target for development of broad-spectrum antiviral reagents. Also, analysis of the RdRp sequence revealed that the mutation among different variants of SARS-CoV-2 did not bring obvious change in the structure of RdRp. Drug repurposing strategy brought scientists with a series of different nucleoside analogues in the past years. Four nucleoside or nucleotide analogs, Molnupiravir (EIDD-2801), Remdesivir, Azvudine and VV-116 were approved for the clinical treatment of SARS-CoV-2 infection. Molnupiravir, developed by Merck & Co. Inc., was first launched on August,

2021. However, subsequent study revealed the risk of incorporation of Molnupiravir into mitochondrial DNA dependent RNA polymerase, leading to mammalian cell mutations. Roche and Atea Pharmaceuticals developed a guanosine analogue named as AT-527. AT-527 was originally taken as oral therapeutic medicine against HCV, and was reproposed for the treatment of SARS-CoV-2. Although AT-527 displayed effective inhibition on SARS-CoV-2 in preclinical studies, the drug failed its phase II clinical trial due to the lack of significant decrease in virus tilter. Azvudine is a thymus-homing approved anti-HIV drug reproposed as anti-SARS-CoV-2 drug targeting at RdRp. Azvudine acts in its triphosphate form, incorporating into the generated RNA string and leading to chain termination[243]. Azvudine displayed effective shortening in the nucleic acid negative conversion (NANC) time, where the mean times of the first NANC is 2.60 d for Azvudine group, and 5.60 d for the control group[293]. It is currently approved for the clinical treatment of COVID-19 in China.

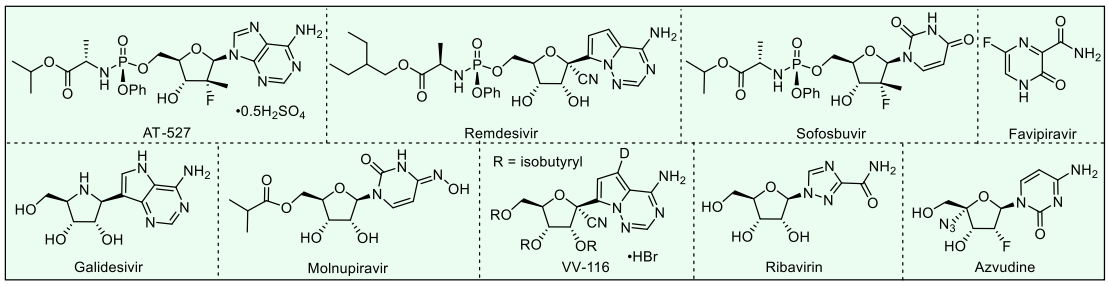


**Figure 6** Structures of reported RdRp inhibitors

Several other broad spectrum RdRp inhibitors, including Sofosbuvir, Galidesivir, Favipiravir and Ribavirin was also reported, but they unfortunately did not display satisfactory clinical results. Remdesivir, reported by Gilead Inc., is a phosphoramidate prodrug of 1′-CN-4-aza-7,9-dideazaadenosine C-nucleoside (GS-441524). Remdesivir was the first approved drug for the emergency treatment of COVID-19. Early administration of remdesivir to non-hospitalized high-risk patients was reported to reduce the risk of hospitalization or death by 87%. Also, analysis of different variants showed no obvious resistance towards remdesivir. Remdesivir further metabolizes into GS-441524, and was then transformed into the active triphosphate form. However, the clinical administration of remdesivir is restricted to intravenous injection, which largely

limited its application to outpatients of COVID-19. Despite the limited administration of remdesivir, researchers discovered that GS-441524, the parent nucleoside of remdesivir was more potent against SARS-CoV-2 than remdesivir. It was also previously found that remdesivir was highly selective towards inhibition of SARS-CoV-2 RdRp against human RNA polymerase, with up to 500-fold selectivity. However, the oral bioavailability of GS-441524 was not ideal, thus displaying no in vivo antiviral activity. Xie et. al also reported a 7'-deuterated ester prodrug (VV-116) based on GS-441524. The anti-SARS-CoV-2 activity of VV-116 was comparable to that of GS-441524 in replicator and hACE2-transduced mice model, while VV-116 own better oral bioactivity (up to 80% in rats). We consider that investigation on novel derivative of GS-441524 towards better bioavailability and anti-SARS-CoV-2 activity is necessary and our group previously reported a 5'-isopropyl ester derivative (ATV006), which presented significant anti-SARS-CoV-2 activity in mice infected with delta variant of SARS-CoV-2. In this study, we continued to explore on ester prodrug derivatives of GS-441524, where we synthesized a series of ester derivatives with cyclic or long-chain aliphatic acid, and their anti-SARS-CoV-2 efficacy, pharmacokinetic properties and oral bioavailability was examined.

### 3.1.2 GS-441524 Esters and Identification of Their Inhibition Efficacy, Pharmacokinetic Properties and Oral Bioavailability

Cyclic carboxylates were initially introduced to obtain **3-1** ~ **3-3**. Quaternary carbon, bridging skeletons and adamantyl group was assembled for increased steric effect of the ester to improve plasma stability, yielding **3-4** ~ **3-6**. Oxygen atom or substituted nitrogen atom were introduced to improve physical and chemical properties, obtaining **3-7** ~ **3-10**. Saturated aliphatic acids were adopted to obtain long-acting compounds **3-11**, **3-12**. The nicotinic acid ester compound **3-13** was also designed and synthesized (Figure 7). Synthetic route of the above-mentioned compounds is listed in Chapter 3.5.

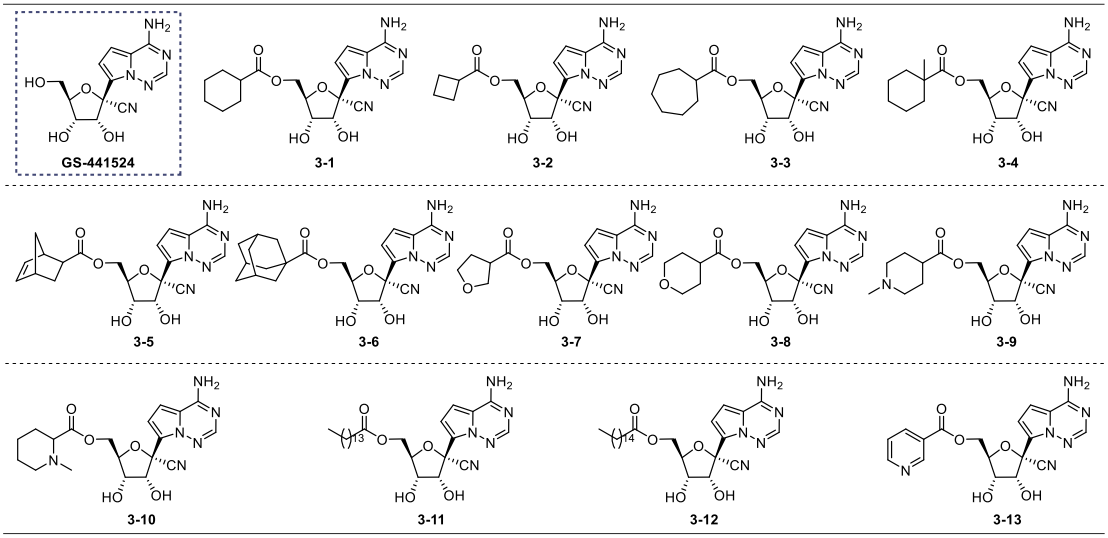


**Figure 7** Synthesized GS-441524 ester prodrugs

The synthesized compounds were evaluated for their anti-SARS-CoV-2 efficacy with a previously developed replicon system. Compounds **3-1** ~ **3-8** and **3-10** ~ **3-12** showed comparable or more potent antiviral ability against SARS-CoV-2, with $EC_{50}$ ranging from 0.26 μM to 1.61 μM. The antiviral activities of compounds **3-9** and **3-13** were not comparable to that of GS-441524, with $EC_{50}$ values of 9.37 μM and 9.12 μM, respectively. The downturn in their antiviral efficacy can be mostly attributed to difficulty in their hydrolysis to GS-441524. Noteworthy, cyclohexancarboxylate ester prodrug **3-1** displayed an inhibitory activity ($EC_{50}$ = 0.26 μM) about three times that of GS-441524 ($EC_{50}$ = 1.644 μM). We also examined the stability of synthesized compounds in human plasma. As the steric hindrance of ester motif increases, the prodrugs become less facile towards plasma hydrolysis. The lipophilicity of most synthesized compounds displayed ideal logP value, falling within a range of 0-5[294], including compound **3-1** with the most ideal replicon inhibition. Detailed information of their antiviral ability is enclosed in Table 7.

**Table 7** Inhibition efficacy and stability of synthesized GS-441524 esters

| Entry | Compound | Stability of Compounds in Human Plasma $T_{1/2}$ (min)[a] | SARS-CoV-2 replicon $EC_{50}$ (μM)[b] | ClogP[c] |
|---|---|---|---|---|
| 1 | GS-441524 | N. A. | 1.644 | -1.43 |
| 2 | **3-1** | 7.945 | 0.26 | 1.075 |
| 3 | **3-2** | 5.80 | 1.05 | 0.163 |
| 4 | **3-3** | 33.33 | 1.23 | 1.532 |
| 5 | **3-4** | 587.031 | 1.39 | 1.492 |
| 6 | **3-5** | 326.49 | 0.44 | 0.307 |
| 7 | **3-6** | 218.70 | 0.99 | 1.505 |
| 8 | **3-7** | 15.69 | 0.48 | -1.015 |
| 9 | **3-8** | 31.93 | 1.61 | -0.694 |
| 10 | **3-9** | 199.48 | 9.37 | -0.424 |
| 11 | **3-10** | 978.382 | 0.64 | 0.008 |
| 12 | **3-11** | 255.86 | 1.16 | 5.09 |
| 13 | **3-12** | 665.04 | 0.95 | 5.547 |
| 14 | **3-13** | 115.632 | 9.12 | -0.537 |

[a]The slope value, k, was determined by linear regression of the natural logarithm of the remaining percentage of the parent drug vs. incubation time curve. The *in vitro* half-life was determined from the slope value: *in vitro* $T_{1/2}$ = -0.693/k. [b]The analysis of the antiviral effect of compounds were performed through a luciferase-based SARS-CoV-2 replicon system in HEK293T cells. The EC50 values were measured with GraphPad Prism Software. [c]Octanol-water partition coefficient (logP) was calculated according to the Pharma Algorithms' AB/LogP v2.0 algorithm.

Based on the replicon inhibition data obtained, we chose **3-1**, **3-8** and **3-12** for the evaluation of single-dose PK parameters in SD rats. With an oral dose of 25 mg/kg, **3-1** showed oral bioactivity (F%) of 53.4% and $T_{1/2}$ of 3.9 h. A maximum concentration of 2463±142 ng/mL was reached 0.8h after oral intake for **3-1**, demonstrating effective blood exposure of **3-1**. Also, compound **3-1** was quickly metabolized to GS-441524, with a $T_{max}$ of 0.8±0.3 h for oral intake group. To our disappointment, compound **3-8** bearing tetrahydropyranyl motif and compound **3-12**, a long-chain aliphatic acid ester, displayed poor oral absorption, with low oral maximum concentration and fast metabolism. The corresponding PK parameters are enclosed in Table 8

**Table 8** PK parameters of **3-1**, **3-8** and **3-12**

| Comp-ound | Administra-tion Route[a] | Dose Level (mg/kg) | $T_{1/2}$ (h) | $T_{max}$ (h) | $C_{max}$ (ng/mL) | $AUC_{(0-\infty)}$ (h*ng/mL) | $MRT_{(0-\infty)}$ (h) | F (%) |
|---|---|---|---|---|---|---|---|---|
| **3-1** | p.o. | 25.0 | 3.9±0.0 | 0.8±0.3 | 2463±142 | 6081±0.00 | 2.51±0.00 | 53.4±3.4 |
| | i.v. | 5.0 | 1.3±0.2 | -- | 3030±451 | 2358±354 | 0.96±0.07 | / |
| **3-8** | p.o. | 25.0 | 1.2±0.1 | 2.2±1.8 | 822±145 | BLQ[a] | BLQ | 36.0±3.3 |
| | i.v. | 5.0 | 0.8±0.2 | -- | 2374±238 | 3064.94±389.73 | 0.03±0.00 | / |
| **3-12** | p.o. | 25.0 | 1.4±0.2 | 1.7±2.0 | 841±180 | BLQ | BLQ | 35.6±3.6 |
| | i.v. | 5.0 | 0.9±0.2 | -- | 2042.8±212.4 | 308.68±158.58 | 0.04±0.00 | / |

[a]p.o.: per os; i.v.: intravenous injection. [b]Below the lower limit of quantitation.

Considering the above-mentioned results, we believe that ester prodrug strategy by introducing ester motif at ribose 5'-position of GS-441524 could significantly improve the pharmacokinetic properties. Compound **3-1** was renamed as SHEN 26 and was further explored with its preclinical evaluation.

## 3.2 Optimization on Synthetic Route of SHEN 26

### 3.2.1 Introduction

Considering the potential industrial of SHEN 26, we further went on to optimize its synthetic route. Several examples of synthesis for nucleoside 5'-ester prodrugs were previously reported. Liu et al. presented a synthetic route (Scheme 18a) which involved a selective protection of the 5'-hydroxy with triaryl methylation reagent first, and then protection of the ribose 2'- and 3'-hydroxy and aryl amino group with allyloxycarbonylation reagent. The protection group on 5'-hydroxy is then removed under acidic conditions, and the deprotected 5'-hydroxy is then esterified. The allyloxycarbonyl protecting groups are then removed with palladium acetate, achieving regioselective esterification at 5'-position. However, this synthetic route includes several steps of protection and deprotection, resulting in a long operation route and low atom economy. Also, removing alloxycarbonyl group requires a reaction temperature of -50 ℃, bringing extra requirements on instruments and thus elevating production

cost. Sun et al. also reported a route (Scheme 18b), where they firstly used benzyl chloroformate (Cbz-Cl) to selectively protect the aryl amino group, then the 5'-hydroxy group was condensed with corresponding acid. The Cbz protection group was then removed with Pd catalyst, obtaining the 5'-esterified products. However, this route lacked protection for the hydroxy group on the ribose 2'- and 3'- position, resulting in complex condensation outcoming.

**Scheme 18** Selected routes for synthesis of 5'-ester prodrugs

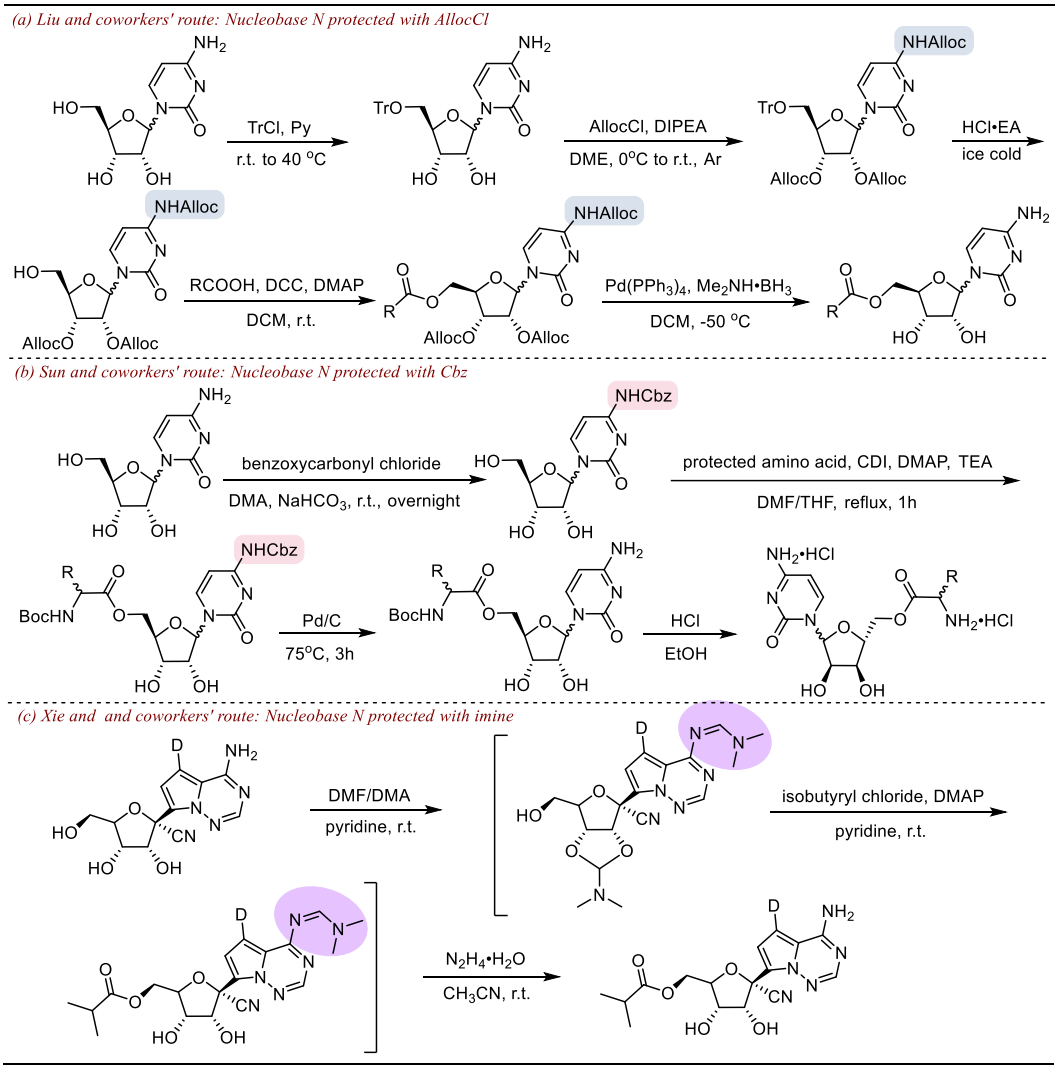


Xie and his co-workers also reported an example of synthesis for 5'-esterified prodrugs (Scheme 18c). The amino group and hydroxy groups at 2'- and 3'-position of the deuterated nucleoside was first protected with imine in one step. Esterification at 5'-position happened with isobutyryl chloride, and protection on ribose 2'- and 3'-

hydroxy groups is simultaneously removed. The imine protection on nucleobase amino group is then removed with hydrazine-hydrate, yielding the target compound. The synthetic route is short, with only three steps, and two protection groups on hydroxy groups and amino group were introduced in one step.

Still, all three mentioned routes required extra steps of protection and deprotection on the amino group of nucleobases. Also, the removal of *N*-protection group generally requires costly conditions such as transition metal catalysis, which largely increased the difficulty and cost in industrial production. Thus, synthetic route for 5'-ester prodrugs still need to be optimized. Herein, we report an optimized synthesis route for SHEN 26, with a three-step short route and simple operation process. The post-reaction treatments are column-free, bringing low environmental pollution.

### 3.2.2 Synthetic Route Optimization

Our synthesis of SHEN 26 starts with compound GS-441524 (Scheme 19). The ribose 2'- and 3'-hydroxy groups of GS-441524 can be selectively protected with ketal protection group, catalyzed by acid to obtain **3-15**. **3-15** then undergoes regioselective esterification at ribose 5'-hydroxy group to obtain **3-16**. The ketal protection on ribose 2'- and 3'-hydroxy groups can then be removed under acidic conditions to obtain our target compound SHEN 26. This provides us with a shortened technical route (3 steps) while assuring the selectivity of condensation.

**Scheme 19** Proposed synthetic route for SHEN 26

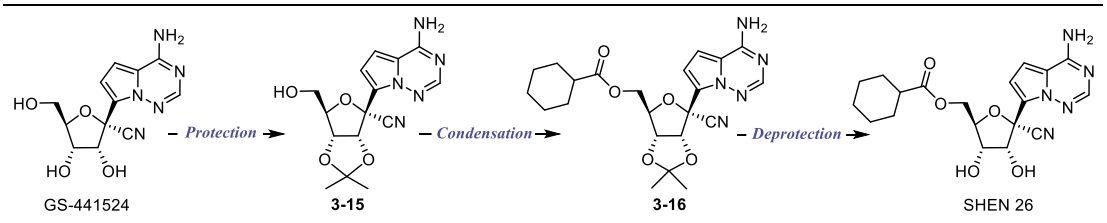


After establishing the basic principle of this route, we further refined the reaction conditions for each step. For step 1, we screened the acid catalyst/promoter.

**Table 9** Optimization of ketal protection: Step 1[a]

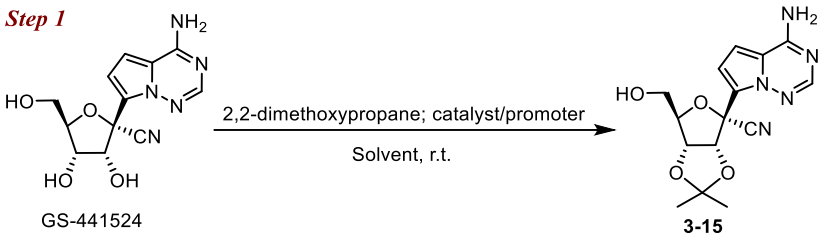


| Entry | Catalyst/promoter | Catalyst/ promoter equivalence | Solvent | DMP equivalence | Area% (GS-441524:3-15)[b] | 3-15%[d] |
|---|---|---|---|---|---|---|
| 1 | Amberlyst 15 | 20% W/W | Acetone | 4.8 equiv. | 76.3%:21.5% | 21.9% |
| 2 | conc. sulfuric acid | 1.4 equiv. | Acetone | 4.8 equiv. | 7.2%:59.6% | 89.2% |
| 3 | *p*-TsOH | 0.5 equiv. | Acetone | 4.8 equiv. | 8.5%:68.4% | 88.9% |
| 4 | *p*-TsOH | 0.5 equiv. | MeCN | 4.8 equiv. | 13.5%:84.9% | 86.2% |
| 5 | *p*-TsOH | 0.5 equiv. | DCM | 4.8 equiv. | 6.9%:61.2% | 89.8% |
| 6 | *p*-TsOH | 0.8 equiv. | DCM | 4.8 equiv. | 30.1%:69.9% | 69.9% |
| 7 | *p*-TsOH | 1.1 equiv. | DCM | 4.8 equiv. | 4.4%:95.6% | 95.6% |
| 8 | *p*-TsOH | 1.1 equiv. | DCM | 6.2 equiv. | 1.3%:98.7% | 98.7% |
| 9[c] | *p*-TsOH | 1.1 equiv. | DCM | 6.2 equiv. | 0.4%:99.1% | 99.6% |

[a]To the reaction flask were added GS-441524 (0.1 g, 1.0 eq), solvent (0.5 mL), acid promoter and 2,2-dimethoxypropane (DMP). The reaction was stirred at room temperature and monitored by HPLC (0.1% HCOOH: 0.1% ACN= 20: 80, Flow rate: 0.8 mL/min; UV detection at λ = 254 nm). [b]HPLC area% of GS-441524 and **3-15**. [c]GS-441524 (200 g, 1.0 eq), DMP (443.4 g, 6.2 eq), TsOH (143.5 g, 1.1 eq) and DCM (1 L). 209 g **3-15** obtained, 99.4% purity, 91.8% yield. [d]**3-15**% = Area% (**3-15**)/Area% (GS-441514 + **3-15**) × 100.

Conc. $H_2SO_4$, Amberlyst 15 and *p*-toluenesulfonic acid were tested for their catalytic or promotion ability, and both conc. $H_2SO_4$ and *p*-toluenesulfonic acid had a good promotion effect (Table 9, Entry 1-3). However, product **3-15** was discovered to decompose irreversibly with conc.$H_2SO_4$ as promoter, requiring a strict time control, which is not convenient in industrial operation. With *p*-toluenesulfonic acid as promoter, we went on to screen acetone, dichloromethane and acetonitrile as solvent, discovering that DCM gave the best reaction outcoming (Table 9, Entry 3-5). 1.1 equiv. *p*-toluenesulfonic acid and 6.2 equiv. dimethyl propane was discovered to be the most favored load of promoter and substrate (Table 9, Entry 5-9). The reaction occurred at room temperature for 5 h, then 5 V heptane was added to the reaction solution and further stirred for 2 h. The suspension was filtered, and the filter cake was put into 20%

$Na_2CO_3$ solution (5 V), further stirred for another 2 h. The suspension was again filtered, and the filter cake was washed with water, vacuum dried at 50°C to obtain white solid **3-15**.

We then optimized the conditions for selective esterification. Inspired by the Steglich Esterification reaction, we selected and cyclohexylcarboxylic acid as acyl source. Considering the exposed amino group, we also monitored the generation of diacylated by-product **3-14** during optimization. Condensation agents were screened (Table 10, Entry 1-3), with both *N*,*N*'-dicyclohexylcarbodiimide (DCC) and *N*,*N*'-diisopropylcarbodiimide (DIC) displaying ideal condensation efficacy and selectivity. We selected DIC as the condensing agent, considering its convenience for industrial operation as a liquid. Solvents such as acetone, dichloromethane and acetonitrile were examined (Table 10, Entry 3-5), with acetonitrile displaying best result and least **3-14** generated. The equivalence of DIC was then explored, and with 1.25 equiv. DIC the best reaction outcoming was obtained, observing complete conversion of raw materials and better selectivity (Table 10, Entry 6).

**Table 10** Optimization of acylation: Step 2

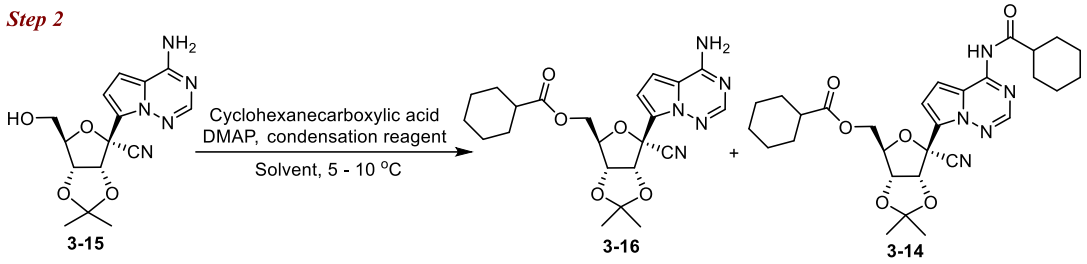


| Entry | Condensation reagent | Solvent | Area% (3-15:3-16:3-14) | 3-14%[c] |
|---|---|---|---|---|
| 1[a] | DCC (1.33 equiv.) | DMF (10 V) | 63%:36%:0% | 36.4% |
| 2[a] | EDCI (1.33 equiv.) | MeCN (10 V) | 1%:94.4%:4.7% | 94.3% |
| 3[a] | DIC (1.33 equiv.) | MeCN (10 V) | 0%:97.8%:2.2% | 97.8% |
| 4[a] | DIC (1.25 equiv.) | MeCN (10 V) | 0%:98.7%:1.4% | 98.6% |
| 5[a] | DIC (1.2 equiv.) | MeCN (10 V) | 0%:95.6%:4.4% | 95.6% |
| 6[b] | DIC (1.25 equiv.) | MeCN (5 V) | 0%:98.4%:1.6% | 98.4% |

[a]To the reaction flask were added **3-15** (0.1 g, 1.0 eq), cyclohexylcarboxylic acid (32 mg, 1.2 eq), DMAP (18.5 mg, 0.5 eq) and solvent (1 mL, 10V), and the reaction mixture was cooled to 5-10℃. Condensation reagent dissolved in solvent (1 mL) was added dropwise to the reaction mixture, and then the reaction mixture was stirred at 5-10℃ for 24 h. HPLC was then used to monitor the reaction (0.1% HCOOH:0.1% ACN= 20:80, Flow rate: 0.8 mL/min; UV detection at λ = 254 nm). [b]**3-15** (120 g, 1.0 eq), cyclohexylcarboxylic acid (38.3 g, 1.2 eq), DMAP (22.1 g, 0.5 eq) and MeCN (600 mL, 5V), DIC (57.1 g, 1.25 equiv.), 135 g III, 96.7% purity, 93.1% yield. [c]**3-16**% = Area% (**3-16**)/Area% (**3-15** + **3-16** + **3-14**) × 100.

After the reaction completes, precipitated diisopropylurea (DIU) by-product was firstly removed by filtration, and 5V EA and 1N HCl was then added to the filtrate. The organic layer was then washed with saturated $Na_2CO_3$ aqueous solution, water and saturated NaCl aqueous solution. The organic phase was then concentrated, and the crude product of **3-16** was directly used for the next step without any purification.

**Table 11** Optimization of deprotection: Step 3

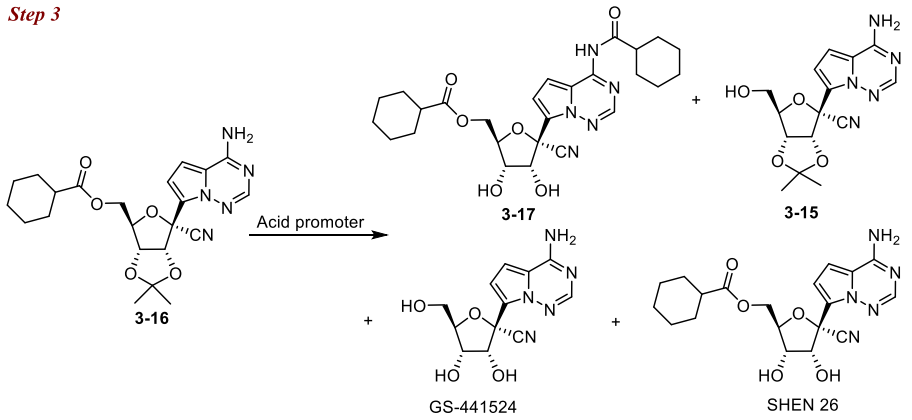


| Entry | Acid promoter | Reaction Temperature | Area% (GS-441524:3-15: 3-16:3-17:SHEN 26) | SHEN 26%[c] |
|---|---|---|---|---|
| 1[a] | 2N HCl (aq., 15 V) | 0°C | 8.9%:0%:12.2%:0%:78.9% | 78.9% |
| 2[a] | AcOH (15 V) | 0°C | 0%:0%:92%:5.1%:3% | 3.0% |
| 3[a] | TFA (15 V) | 0°C | 42.2%:0%0%:0%:50.9% | 54.6% |
| 4[a] | $HBF_4$ (15 V) | 0°C | 7.2%:6.8%:0%:0%:85.2% | 85.9% |
| 5[a] | Formic acid: $H_2O$ = 1:1 (10 V) | 0°C | 1.6%:0%:33.6%:1.4%:60.9% | 62.5% |
| 6[a] | Formic acid: $H_2O$ = 2:1 (10 V) | 25°C | 1.1%:0%:0.4%:0.8%:93.5% | 97.6% |
| 7[a] | Formic acid: $H_2O$ = 1:2 (5 V) | 25°C | 1.1%:0%:15.6%:0.9%:80.1% | 82.0% |
| 8[a] | Formic acid: $H_2O$ = 2:1 (3 V) | 25°C | 0.9%:0%:31.4%:1.1%:64.4% | 65.8% |
| 9[b] | Formic acid: $H_2O$ = 2:1 (10 V) | 25°C | 1.0%:0%:2.1%:0.9%:92.7% | 95.9% |

[a]To the reaction flask was added **3-16** (1.0 eq) and corresponding acid (0.5 mL, 10V). The reaction mixture was cooled to 0 ± 5°C and was stirred for 24 h. The reaction was then monitored by HPLC (0.1% HCOOH:0.1% ACN= 20:80, Flow rate: 0.8 mL/min; UV detection at λ = 254 nm). [b]**3-16** (93 g, 1.0 eq) and formic acid: $H_2O$ = 2:1 (930 mL, 10V). 62 g SHEN 26 obtained, 98% purity, 74% yield. [c]SHEN 26% = Area% (SHEN 26)/Area% (GS-441524 + SHEN 26 + **3-15** + **3-16** + **3-17**) × 100.

The removal of ketal protection is carried out in acidic condition (Table 3). Selectivity towards ketal deprotection over ester hydrolysis is a crucial factor to consider in this step. Thus, we herein monitor the generation of GS-441524, ketal hydrolysis product SHEN 26, ester hydrolysis product **3-15** and **3-17** (from diacylation by-product **3-14**). We first screened a series of acids as solvent, with formic acid aqueous solution and $HBF_4$ displaying ideal outcoming (Table 11, Entry 1-4). When using $HBF_4$ as solvent, area% of target product SHEN 26 reached 85.2%, while

excessive hydrolysis partly occurs towards generation of **3-15**. Although area% of SHEN 26 by using formic acid aqueous solution is lower than by using $HBF_4$ as solvent, selectivity towards SHEN 26 over **3-15** is better in formic acid aqueous solution. To increase conversion of starting materials, and for the convenience of industrial operation, we tried to conduct the reaction at 25℃. Under 25℃, 10 V 66.7 % formic acid aqueous solution (Table 11, Entry 6) exhibited the highest conversion with area% of SHEN 26 reaching 93.5%. The amount and concentration of formic acid aqueous solution is crucial to the reaction. When using 50% formic acid (Table 11, Entry 5) or with 5V (Table 11, Entry 7) and 3V (Table 11, Entry 8) formic acid solution, conversion of starting material **3-16** was low. After completion of the reaction, 2 V EA was added, and the pH was adjusted to 7-8 with 50% sodium carbonate aqueous solution under 0 °C. The suspension was filtered, and the filter cake was then stirred in methyl *t*-butyl ether at 50 °C for 10 h to obtain the target compound.

### 3.2.3 Impurity Analysis

After developing the synthetic route, we went on to identify the possible impurities in SHEN 26 production (Scheme 20). The impurities of concern include leftovers of starting materials (GS-441524, Impurity I; **3-16**, Impurity II), reaction by-products (**3-17**, Impurity V) and stereochemical diastereomers (**3-20**, Impurity VI; **3-21**, Impurity VII). Standards of reaction by-products and diastereomers were synthesized. The impurities of concern include the leftover of starting materials (GS-441524, **3-15** and **3-16**), reaction by-products (**3-14** and **3-17**). Acylation of **3-15** with cyclohexylcarboxylic acid chloride yields diacylated intermediate **3-14**, and deprotection of **3-14** yields diacylated impurity **3-17**. We also discovered formylated by-product **3-19** during the deprotection procedure, and **3-19** was obtained through concentration. The industrial production of GS-441524 involves a cyanidation procedure, where a molecule of oxonium ion intermediate **c** was generated while removing a molecule of $H_2O$ catalyzed by trifluoromethanesulfonic acid. Although steric hindrance of the benzyloxy group on the ribose blocks attack from the back to

form $\beta$ intermediate **d**, still $\beta$ intermediate **d** would be generated, and $S_N2$ cyanidation reverses the $\beta$ intermediate to form product **f** in $\alpha$ configuration. This would lead to residue of **3-20** in batches of GS-441524, which would go through the whole synthetic procedure along with GS-441524 to form **3-21**. **3-20** was synthesized with a previously described route: first enantioselectively substitute the hydroxy group with cyano group, and then remove the benzyl group using boron trichloride. The 5'-cyclohexanecarboxylic **3-21** was obtained through a 3-step of conversion same as the synthesis of SHEN 26.

**Scheme 20** Generation of impurities

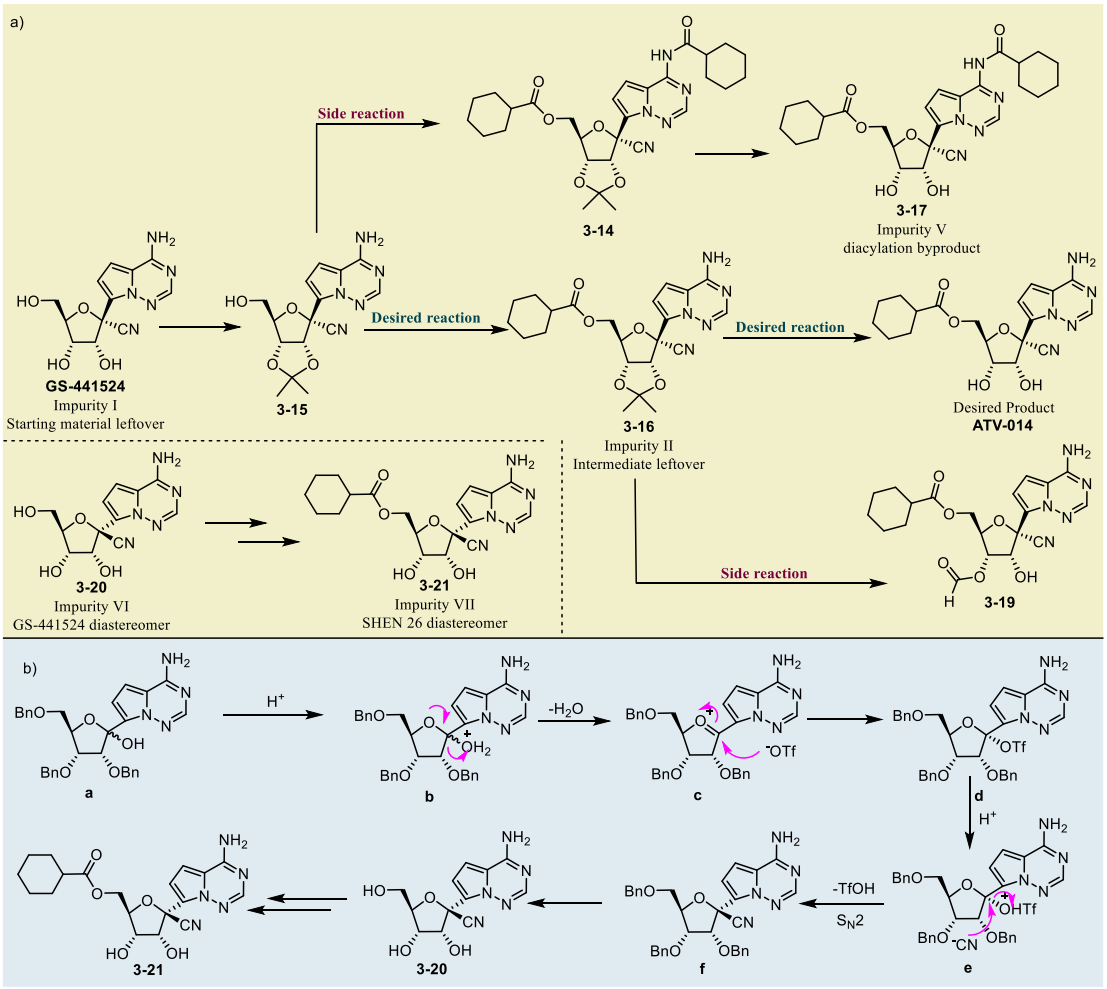


After obtaining the standard compound for potential impurities, we analyzed the purity of SHEN 26 and quantified the proportion of impurities. SHEN 26 obtained from the industrial large-scale batch is sampled, and the impurities are analyzed, quantified and compared with the corresponding acceptance criteria. the details of other mentioned

impurities are listed in Table 12. **3-15**, **3-14** and **3-21** were not detected, and the amount of GS-441524, **3-16**, **3-17**, **3-19** and **3-21** met their acceptance criteria. The purity of SHEN 26 reached 98.9% (<1.1% impurity), demonstrating the feasibility of this synthetic route in SHEN 26 production.

**Table 12** HPLC quantification of impurities

| Entry | Impurity | Acceptance criteria% | Area% |
|---|---|---|---|
| **1** | Other unknown impurities | ≤ 0.2 | 0.09442 |
| **2** | **SHEN 26** | N. A.[b] | 98.88747 |
| **3** | **3-21** | ≤ 0.15 | N. D.[a] |
| **4** | **3-19** | ≤ 0.7 | 0.63509 |
| **5** | **3-16** | ≤ 0.5 | 0.17318 |
| **6** | **3-17** | ≤ 0.2 | 0.20984 |

[a]Not detected. [b]Not applicable.

## 3.3 Conclusion

In summary, we designed and synthesized a series of ester prodrugs at the ribose 5'-position of GS-441524, the activity core of remdesivir, to improve its pharmacokinetics properties. Among these synthesized compounds, compound **3-1** (SHEN 26) with a 5'-cyclohexyl ester prodrug motif displayed the best inhibition ability against SARS-CoV-2 with an $EC_{50}$ value of 0.26 μM through the SARS-CoV-2 replicon inhibition assay and 53.4% bioavailability suggested by the PK results. Further on, we optimized the synthetic route for a potent novel RdRp inhibitor SHEN 26. This route contains 3 steps, with column-free post reaction treatments. Impurities involved in the synthetic route were synthesized and analyzed. Also, SHEN 26 obtained through the kilogram-scale synthetic batch from industrial production was sampled and qualified through HPLC. All impurities met the acceptance criteria, also illustrating the possibility of industrial adaptation of this synthetic route. This route provides simple industrial operations, with

high atom economy and low environmental influence, providing a practical example for the industrial synthesis of 5'-ester prodrugs.

## 3.4 Experimental Section

### 3.4.1 General Information

All reagents used were commercially available. Reactions were monitored by thin-layer chromatography (TLC) on glass plates coated with silica gel with a fluorescent indicator (GF254). Flash silica gel column chromatography was performed using Tsingdao silica gel (60, particle size 300-400 mesh). All the $^{1}H$ NMR and $^{13}C$ NMR spectra were recorded on a Bruker 400 MHz or 600 MHz spectrometer. Chemical shifts (δ) were expressed in parts per million using tetramethylsilane as an internal reference. High-resolution mass spectra (HRMS) were measured with an Agilent Accurate-Mass Q-TOF 6530 in ESI mode (Agilent, Santa Clara, CA, USA). HPLC analyses were performed using a Hewlett Packard Model HP 1100 Series instruments, the compounds are at least ≥ 95% pure (OD-3; eluent, *n*-hexane/isopropanol = 80/20; flow rate 0.8 mL/min; temperature 30 °C; wavelength 254 nm; HPLC analysis data are reported in relative area % and were not adjusted to weight %).

### 3.4.2 Chemistry

***Synthetic Route for 3-1 ~ 3-13***

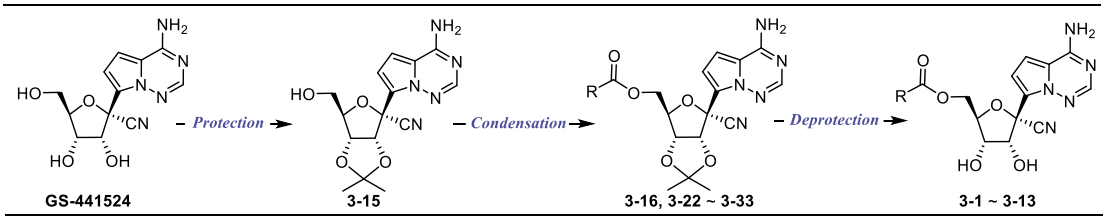


The synthetic route of **3-1** ~ **3-12** starts with GS-441524. GS-441524 was first protected with ketal protection group to give intermediate **3-15**. **3-15** was then condensed with corresponding carboxylic acid with DIC and DMAP in DCM, yielding

intermediate **3-16** and **3-24 ~ 3-36**. The ketal protection of **3-16**, **3-22 ~ 3-33** was then removed under acidic conditions to give **3-1 ~ 3-13**.

***Synthesis of 3-15***

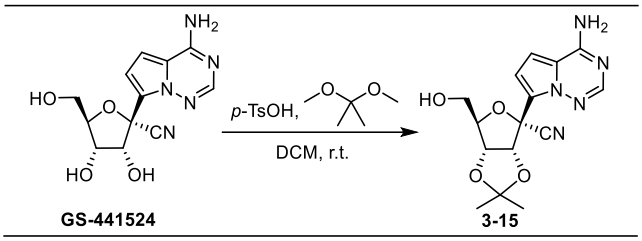


To a solution of GS-441524 (4.0 g, 13.7 mmol) in dichloromethane (20 mL) was added 2,2-dimethoxypropane (8.9 g, 85.5 mmol). Then *p*-toluenesulfonic acid (2.9 g, 16.8 mmol) was added dropwise at room temperature. The mixture was stirred at room temperature. After 8 h, the reaction was completed as monitored by TLC. The mixture was quenched with heptane (20 mL) and stirred for additional 2 h. The suspension was filtered and the filter was washed with saturated solution of sodium carbonate. After drying the product at 45 ℃ in the oven, **3-15** was obtained.

***General procedure for preparation of compounds 3-16 and 3-22 ~ 3-33.***

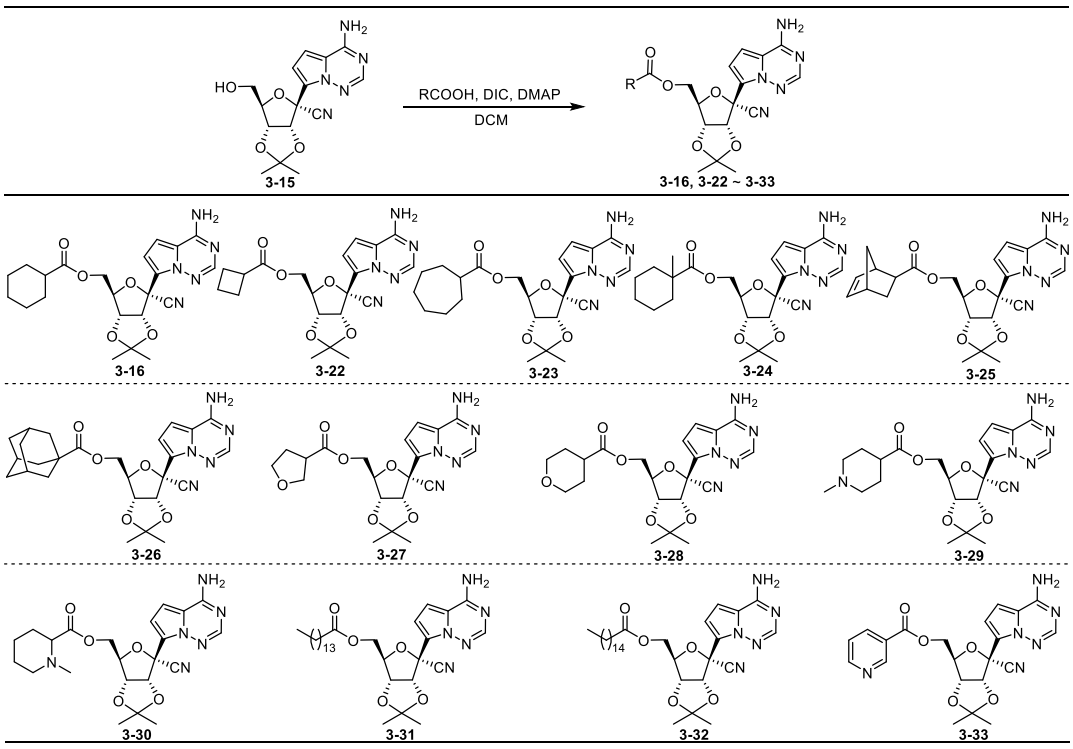

To a solution of **3-15** (1.50 g, 4.5 mmol), corresponding acid (4.5 mmol), 4-dimethylaminopyridine (DMAP, 55.40 mg, 0.45 mmol) in DCM (15 mL) was added *N*,*N*′-diisopropylcarbodiimide (DIC, 0.62 g, 4.9 mmol). The mixture was stirred at room temperature for 12 h. The suspension was filtered and the solvent was washed with 30 mL of saturated solution of $Na_2CO_3$ and then with 30 mL of an aqueous solution of citric acid (20 % w/v). The organic layer was dried over anhydrous $Na_2SO_4$. After removal of the solvent *in vacuo*, the residue was purified by column chromatography (PE/EA = 1:1).

***General procedure for preparation of compounds 3-1 ~ 3-13***

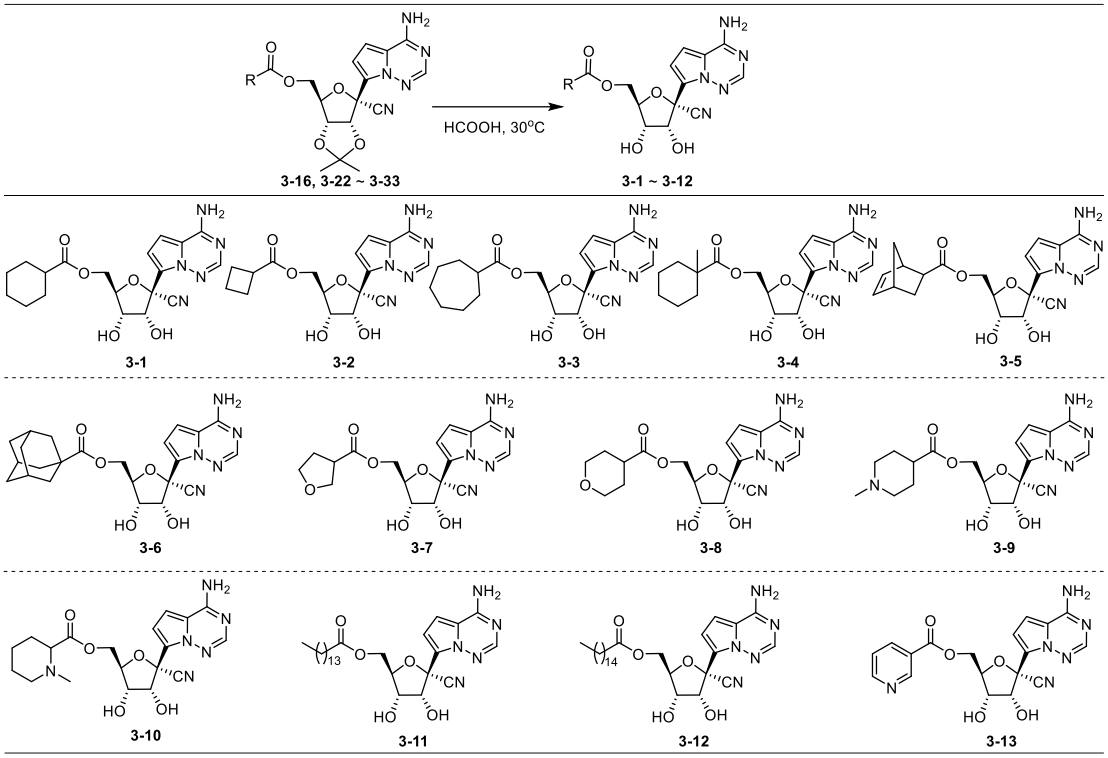


Compound **3-16** and **3-22** ~ **3-33** was added to the mixture of formic acid (6 V) and water (3 V). The reaction solution was stirred at 30ºC. After 36 h, the reaction was completed as monitored by TLC. The formic acid was removed *in vacuo*, and the resulting residue was dissolved with ethyl acetate (5 mL). Then the pH was adjusted to 7-8 with 50% $Na_2CO_3$ and stirred for at least 1 h at 0~5 ℃. The precipitate was collected by filtration and washed with ethyl acetate to furnish compound **3-1** ~ **3-13**.

## *Physical Characterization of Synthesized Compounds*

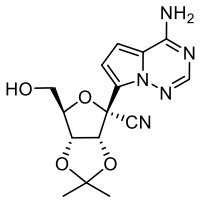

**((3*aR*,4*R*,6*R*,6*aR*)-4-(4-aminopyrrolo[2,1-*f*][1,2,4]triazin-7-yl)-6-(hydroxymethyl)-2,2-dimethyltetrahydrofuro[3,4-*d*][1,3]dioxole-4-carbonitrile (3-15):** white solid, 93.3% yield. $^1$H NMR (400 MHz, Chloroform-*d*) δ 7.93 (s, 1H), 7.08 (d, *J* = 4.6 Hz, 1H), 6.66 (d, *J* = 4.9 Hz, 1H), 5.98 (s, 2H), 5.43 (d, *J* = 6.5 Hz, 1H), 5.24 (dd, *J* = 6.6, 2.3 Hz, 1H), 4.67 (q, *J* = 1.9 Hz, 1H), 4.04 – 3.74 (m, 2H), 1.81 (s, 3H), 1.40 (s, 3H).

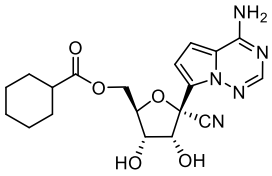

**((2*R*,3*S*,4*R*,5*R*)-5-(4-aminopyrrolo[2,1-*f*][1,2,4]triazin-7-yl)-5-cyano-3,4-dihydroxytetrahydrofuran-2-yl)methyl cyclohexanecarboxylate (3-1):** white solid, 73% yield. HPLC purity: 99.4%. $^1$H NMR (600 MHz, DMSO-$d_6$) δ 8.01 – 7.79 (m, 3H), 6.92 (d, *J* = 4.5 Hz, 1H), 6.82 (d, *J* = 4.5 Hz, 1H), 6.34 (d, *J* = 6.0 Hz, 1H), 5.38 (d, *J* = 5.9 Hz, 1H), 4.71 (t, *J* = 5.2 Hz, 1H), 4.31 (dd, *J* = 12.2, 2.9 Hz, 1H), 4.26 – 4.20 (m, 1H), 4.15 (dd, *J* = 12.2, 5.0 Hz, 1H), 3.97 (q, *J* = 5.4 Hz, 1H), 2.29 – 2.19 (m, 1H), 1.79 – 1.53 (m, 5H), 1.31 – 1.10 (m, 5H). $^{13}$C NMR (151 MHz, DMSO-$d_6$)) δ 175.2, 156.1, 148.4, 124.0, 117.4, 117.0, 110.7, 101.2, 81.7, 79.4, 74.5, 70.6, 63.0, 42.6, 29.0, 28.9, 25.7, 25.2, 25.2. ESI-HRMS: m/z $[M+H]^+$ calcd for $C_{19}H_{24}N_5O_5$: 402.1772; found: 402.1765.

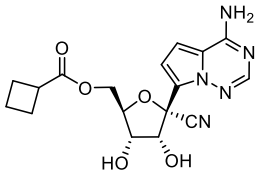

**((2*R*,3*S*,4*R*,5*R*)-5-(4-aminopyrrolo[2,1-*f*][1,2,4]triazin-7-yl)-5-cyano-3,4-dihydroxytetrahydrofuran-2-yl)methyl cyclobutanecarboxylate (3-2):** white solid, 62% yield. HPLC purity: 99.24%. $^1$H NMR (400 MHz, DMSO-$d_6$) δ 7.93 (s, 1H), 7.90 (br, 2H), 6.93 (d, *J* = 4.5 Hz, 1H), 6.80 (d, *J* = 4.5 Hz, 1H), 6.34 (d, *J* = 5.9 Hz, 1H), 5.38 (d, *J* = 5.8 Hz, 1H), 4.68 (t, *J* = 5.2 Hz, 1H), 4.35-4.31 (m, 1H), 4.25-4.15 (m, 2H), 3.96-3.92 (m, 1H), 3.19-3.11 (m, 1H), 2.15-2.09 (m, 4H), 1.97-1.73 (m, 2H). $^1$H NMR (101 MHz, DMSO-$d_6$) δ 174.7, 156.1, 148.4, 124.0, 117.4, 117.0, 110.7, 101.3, 81.6, 79.5, 74.5, 70.6, 63.3, 37.6, 25.2, 25.1, 18.2. ESI-HRMS: m/z $[M+H]^+$ calcd for $C_{17}H_{20}N_5O_5$: 374.1459; found: 374.1452.

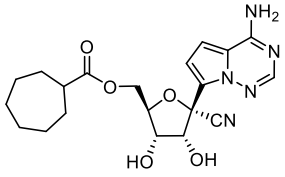

**((2*R*,3*S*,4*R*,5*R*)-5-(4-aminopyrrolo[2,1-*f*][1,2,4]triazin-7-yl)-5-cyano-3,4-dihydroxytetrahydrofuran-2-yl)methyl cycloheptanecarboxylate (3-3):** white solid, 50% yield. HPLC purity: 97.75%. $^1$H

NMR (600 MHz, DMSO-$d_6$) δ 7.93 (s, 1H), 7.90 (br, 1H), 6.92 (d, $J$ = 4.5 Hz, 1H), 6.81 (d, $J$ = 4.5 Hz, 1H), 4.70 (d, $J$ = 4.8 Hz, 1H), 4.31-4.29 (m, 1H), 4.24-4.22 (m, 1H), 4.17-4.14 (m, 1H), 3.97-3.95 (m, 1H), 2.46-2.41 (m, 1H), 1.80-1.77 (m, 2H), 1.63-1.37 (m, 10H). $^1$H NMR (151 MHz, DMSO-$d_6$) δ 176.1, 156.1, 148.4, 124.1, 117.4, 117.0, 110.6, 101.2, 81.7, 79.4, 74.6, 70.6, 63.1, 60.2, 44.4, 30.7, 30.6, 28.2, 28.1, 26.2. ESI-HRMS: m/z $[M+H]^+$ calcd for $C_{20}H_{26}N_5O_5$: 416.1928; found: 416.1920.

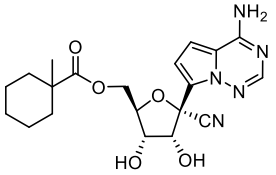

**((2*R*,3*S*,4*R*,5*R*)-5-(4-aminopyrrolo[2,1-*f*][1,2,4]triazin-7-yl)-5-cyano-3,4-dihydroxytetrahydrofuran-2-yl)methyl 1-methylcyclohexane-1-carboxylate (3-4):** white solid, 33% yield. HPLC purity: 98.59%. $^1$H NMR (400 MHz, Methanol-$d_4$) δ 7.86 (s, 1H), 6.95 – 6.80 (m, 2H), 4.90 – 4.86 (m, 1H), 4.42 – 4.32 (m, 3H), 4.17 (t, $J$ = 5.7 Hz, 1H), 2.03 – 1.88 (m, 2H), 1.55 – 1.42 (m, 3H), 1.34 – 1.13 (m, 5H), 1.09 (s, 3H). $^{13}$C NMR (101 MHz, Methanol-$d_4$) δ 177.5, 155.9, 146.9, 124.3, 116.6, 116.2, 110.7, 101.1, 82.0, 79.8, 74.3, 70.7, 62.9, 43.1, 35.2, 25.3, 22.9. ESI-HRMS: m/z $[M+H]^+$ calcd for $C_{20}H_{26}N_5O_5$: 416.1928; found: 416.1922.

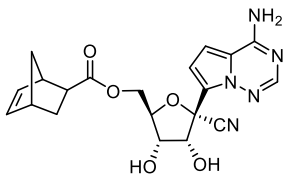

**((2*R*,3*S*,4*R*,5*R*)-5-(4-aminopyrrolo[2,1-*f*][1,2,4]triazin-7-yl)-5-cyano-3,4-dihydroxytetrahydrofuran-2-yl)methyl (1*R*,4*R*)-bicyclo[2.2.1]hept-5-ene-2-carboxylate (3-5):** white solid, 61% yield. HPLC purity: >99%. $^1$H NMR (400 MHz, DMSO-$d_6$) δ 7.93 (s, 1H), 8.0 (br, 2H), 6.93-6.91 (m, 1H), 6.85-6.82 (m, 1H), 6.35-6.32 (m, 1H), 6.17-6.11 (m, 1H), 5.85-5.78 (m, 1H), 5.40-5.37 (m, 1H), 4.73-4.69 (m, 1H), 4.25-4.09 (m, 3H), 3.99-3.93 (m, 1H), 3.07-2.84 (m, 3H), 1.87-1.75 (m, 1H), 1.35-1.16 (m, 3H). $^{13}$C NMR (101 MHz, DMSO-$d_6$) δ 174.0, 156.1, 148.4, 138.0, 136.1, 132.8, 124.0, 117.4, 117.0, 110.7, 101.3, 81.7, 79.3, 74.5, 70.6, 63.5, 49.5, 45.5, 43.0, 42.4, 29.2. ESI-HRMS: m/z $[M+H]^+$ calcd for $C_{20}H_{22}N_5O_5$: 412.1615; found: 412.1607.

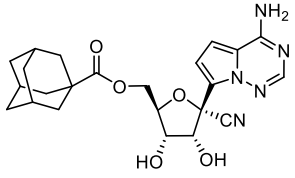

**((2*R*,3*S*,4*R*,5*R*)-5-(4-aminopyrrolo[2,1-f][1,2,4]triazin-7-yl)-5-cyano-3,4-dihydroxytetrahydrofuran-2-yl)methyl (3*R*,5*R*,7*R*)-adamantane-1-carboxylate (3-6):** white solid, 67% yield. HPLC purity: 98.30%. $^1$H NMR (600 MHz, DMSO-$d_6$) δ 7.93 (s, 1H), 7.90 (br, 2H), 6.93 (d, $J$ = 4.5 Hz, 1H), 6.83 (d, $J$ = 4.5 Hz, 1H), 6.37 (d, $J$ = 5.9 Hz, 1H), 5.37 (d, $J$ = 5.9 Hz, 1H), 4.71 (t, $J$ = 5.3 Hz, 1H), 4.29-4.23 (m, 2H), 4.16-4.13 (m, 1H), 4.01-3.98 (m,

1H), 1.94-1.91 (m, 3H), 1.71-1.60 (m, 12H). $^{13}$C NMR (151 MHz, DMSO-$d_6$) δ 176.7, 156.1, 148.4, 124.1, 117.4, 117.0, 110.5, 101.2, 81.6, 79.2, 74.7, 70.4, 62.7, 38.7, 36.3, 27.7. ESI-HRMS: m/z $[M+H]^+$ calcd for $C_{23}H_{28}N_5O_5$: 454.2085; found: 454.2077.

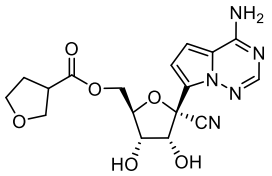

**((2*R*,3*S*,4*R*,5*R*)-5-(4-aminopyrrolo[2,1-*f*][1,2,4]triazin-7-yl)-5-cyano-3,4-dihydroxytetrahydrofuran-2-yl)methyl tetrahydrofuran-3-carboxylate (3-7):** white solid, 69% yield. HPLC purity: 99.20%. $^1$H NMR (600 MHz, DMSO-$d_6$) δ 7.94 (s, 1H), 7.90 (br, 2H), 6.93 (d, $J$ = 4.4 Hz, 1H), 6.82 (d, $J$ = 4.4 Hz, 1 H), 6.33 (t, $J$ = 5.5 Hz, 1H), 5.40 (d, $J$ = 5.8 Hz, 1H), 4.71 (t, $J$ = 5.3 Hz, 1H), 4.37-4.34 (m, 1H), 4.25-4.20 (m, 2H), 3.97-3.96 (m, 1H), 3.81-3.78 (m, 1H), 3.75-3.69 (m, 2H), 3.66-3.62 (m, 1H), 3.15-3.10 (m, 1H), 2.08-1.95 (m, 2H). $^{13}$C NMR (151 MHz, DMSO-$d_6$) δ 150.1, 148.4, 124.0, 117.4, 117.1, 110.8, 101.3, 81.6, 81.5, 79.5, 74.5, 70.7, 70.6, 69.8, 69.7, 67.8, 63.9, 63.8, 43.4, 29.5, 29.4. ESI-HRMS: m/z $[M+H]^+$ calcd for $C_{17}H_{20}N_5O_6$: 390.1408; found: 390.1401.

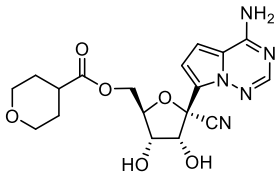

**((2*R*,3*S*,4*R*,5*R*)-5-(4-aminopyrrolo[2,1-*f*][1,2,4]triazin-7-yl)-5-cyano-3,4-dihydroxytetrahydrofuran-2-yl)methyl tetrahydro-2H-pyran-4-carboxylate (3-8):** white solid, 71% yield. HPLC purity: 99.5%. $^1$H NMR (600 MHz, DMSO-$d_6$) δ 7.93 (s, 1H), 7.90 (br, 1H), 6.92 (d, $J$ = 4.6 Hz, 1H), 6.82 (d, $J$ = 4.6 Hz, 1H), 6.35 (d, $J$ = 5.7 Hz, 1H), 5.41 (d, $J$ = 5.6 Hz, 1H), 4.71 (t, $J$ = 5.3 Hz, 1H), 4.34-4.32 (m, 1H), 4.25-4.22 (m, 1H), 4.19-4.16 (m, 1H), 3.99-3.96 (m, 1H), 3.79-3.77 (m, 2H), 3.33-3.29 (m, 2H), 2.55-2.50 (m, 1H), 1.68-1.63 (m, 2H), 1.53-1.45 (m, 2H). $^{13}$C NMR (151 MHz, DMSO-$d_6$) δ 156.2, 148.5, 124.0, 117.4, 117.1, 110.7, 101.2, 81.6, 79.4, 74.5, 70.6, 66.5, 63.3, 28.8, 28.7. ESI-HRMS: m/z $[M+H]^+$ calcd for $C_{18}H_{22}N_5O_6$: 404.1565; found: 404.1559.

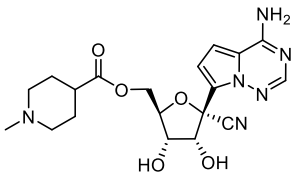

**((2*R*,3*S*,4*R*,5*R*)-5-(4-aminopyrrolo[2,1-*f*][1,2,4]triazin-7-yl)-5-cyano-3,4-dihydroxytetrahydrofuran-2-yl)methyl 1-methylpiperidine-4-carboxylate (3-9):** white solid, 30% yield. HPLC purity: 95.91%. $^1$H NMR (600 MHz, Methanol-$d_4$) δ 7.86 (s, 1H), 6.89 (q, $J$ = 4.6 Hz, 2H), 4.90 – 4.88 (m, 1H), 4.46 – 4.39 (m, 1H), 4.39 – 4.30 (m, 2H), 4.16 (t, $J$ = 5.7 Hz, 1H), 3.02 – 2.86 (m, 2H), 2.45 – 2.33 (m, 6H), 1.97 – 1.86 (m, 2H), 1.82 – 1.65 (m, 2H). $^{13}$C NMR (151 MHz, Methanol-$d_4$) δ 175.3, 157.3, 148.4, 125.6, 118.0, 117.7, 112.2, 102.6,

83.4, 81.5, 75.6, 72.2, 64.7, 55.1, 49.5, 49.3, 49.2, 49.0, 48.9, 48.8, 48.6, 45.5, 40.3, 28.1. ESI-HRMS: m/z $[M+H]^+$ calcd for $C_{19}H_{25}N_6O_5$: 417.1881; found: 417.1873.

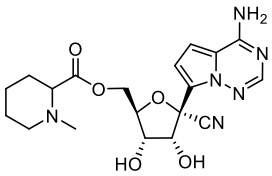

**((2*R*,3*S*,4*R*,5*R*)-5-(4-aminopyrrolo[2,1-*f*][1,2,4]triazin-7-yl)-5-cyano-3,4-dihydroxytetrahydrofuran-2-yl)methyl 1-methylpiperidine-2-carboxylate (3-10):** white solid, 37% yield. HPLC purity: 98.3%. $^1$H NMR (600 MHz, Methanol-$d_4$) δ 7.86 (s, 1H), 6.90 (d, $J$ = 2.5 Hz, 2H), 4.91 – 4.87 (m, 1H), 4.49 – 4.34 (m, 3H), 4.22 – 4.12 (m, 1H), 2.89 (dd, $J$ = 11.9, 3.3 Hz, 1H), 2.79 – 2.68 (m, 1H), 2.19 (s, 1H), 2.17 (s, 2H), 2.13 – 2.06 (m, 1H), 1.82 – 1.49 (m, 5H), 1.35 – 1.24 (m, 1H). $^{13}$C NMR (151 MHz, Methanol-$d_4$) δ 174.1, 174.0, 157.3, 148.4, 125.7, 118.0, 117.6, 112.2, 102.6, 102.5, 83.3, 81.5, 81.5, 75.6, 72.3, 72.2, 68.6, 64.7, 64.6, 55.9, 44.4, 30.7, 30.6, 26.0, 23.8. ESI-HRMS: m/z $[M+H]^+$ calcd for $C_{19}H_{25}N_6O_5$: 417.1881; found: 417.1874.

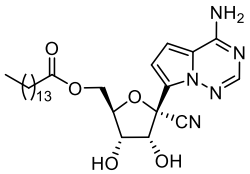

**((2*R*,3*S*,4*R*,5*R*)-5-(4-aminopyrrolo[2,1-*f*][1,2,4]triazin-7-yl)-5-cyano-3,4-dihydroxytetrahydrofuran-2-yl)methyl pentadecanoate (3-11):** white solid, 40% yield. HPLC purity: 98.91%. $^1$H NMR (600 MHz, Methanol-$d_4$) δ 7.86 (s, 1H), 6.89 (q, $J$ = 4.6 Hz, 2H), 4.42 (dd, $J$ = 12.0, 3.1 Hz, 1H), 4.37 (m, 1H), 4.31 (dd, $J$ = 11.9, 5.2 Hz, 1H), 4.17 – 4.12 (m, 1H), 2.29 (m, 2H), 1.55 (p, $J$ = 7.2 Hz, 2H), 1.39 – 1.19 (m, 24H), 0.89 (t, $J$ = 7.0 Hz, 3H). $^{13}$C NMR (151 MHz, Methanol-$d_4$) δ 175.1, 157.3, 148.3, 125.7, 118.0, 117.6, 112.1, 102.6, 83.4, 81.5, 75.7, 72.1, 64.2, 35.0, 33.1, 30.8, 30.8, 30.8, 30.7, 30.6, 30.5, 30.4, 30.2, 26.0, 23.8, 14.5. ESI-HRMS: m/z $[M+H]^+$ calcd for $C_{27}H_{42}N_5O_5$: 516.3180; found: 516.3173.

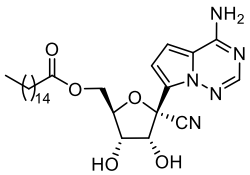

**((2*R*,3*S*,4*R*,5*R*)-5-(4-aminopyrrolo[2,1-*f*][1,2,4]triazin-7-yl)-5-cyano-3,4-dihydroxytetrahydrofuran-2-yl)methyl palmitate (3-12):** white solid, 38% yield. HPLC purity: 99.58%. $^1$H NMR (600 MHz, Methanol-$d_4$) δ 7.86 (s, 1H), 6.89 (q, $J$ = 4.6 Hz, 2H), 4.42 (dd, $J$ = 11.9, 3.1 Hz, 1H), 4.38 – 4.34 (m, 1H), 4.32 – 4.27 (m, 1H), 4.16 – 4.08 (m, 1H), 2.36 – 2.24 (m, 2H), 1.60 – 1.50 (m, 2H), 1.36 – 1.24 (m, 24H), 0.89 (t, $J$ = 7.0 Hz, 3H). $^{13}$C NMR (151 MHz, Methanol-$d_4$) δ 173.7, 155.8, 146.9, 124.3, 116.5, 116.2, 110.7, 101.1, 82.0, 80.1, 74.2, 70.7, 62.8, 33.5, 31.7, 29.4, 29.4, 29.4, 29.4, 29.3, 29.2, 29.1, 29.0, 28.7, 24.6, 22.3, 13.0. ESI-HRMS: m/z $[M+H]^+$ calcd for $C_{28}H_{44}N_5O_5$: 530.3337; found: 530.3329.

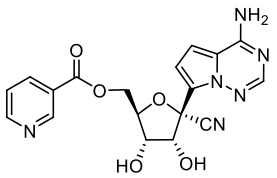

**((2*R*,3*S*,4*R*,5*R*)-5-(4-aminopyrrolo[2,1-*f*][1,2,4]triazin-7-yl)-5-cyano-3,4-dihydroxytetrahydrofuran-2-yl)methyl nicotinate (3-13):** white solid, 35% yield. HPLC purity: 97.37%. $^{1}$H NMR (600 MHz, Methanol-$d_4$) δ 9.05 (d, $J$ = 2.2 Hz, 1H), 8.73 (dd, $J$ = 5.0, 1.7 Hz, 1H), 8.35 – 8.25 (m, 1H), 7.76 (s, 1H), 7.53 (dd, $J$ = 8.0, 4.9 Hz, 1H), 6.83 (dd, $J$ = 32.8, 4.6 Hz, 2H), 4.97 (d, $J$ = 5.3 Hz, 1H), 4.82 – 4.74 (m, 1H), 4.61 – 4.45 (m, 2H), 4.39 – 4.30 (m, 1H). $^{13}$C NMR (151 MHz, Methanol-$d_4$) δ 164.5, 155.8, 152.8, 149.8, 146.9, 137.6, 126.2, 124.0, 123.8, 116.6, 116.2, 110.8, 101.1, 81.9, 80.2, 74.1, 70.6, 63.4. ESI-HRMS: m/z $[M+H]^+$ calcd for $C_{18}H_{17}N_6O_5$: 397.1255; found: 397.1250.

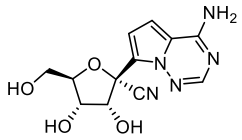

**(2*R*,3*R*,4*S*,5*R*)-2-(4-aminopyrrolo[2,1-*f*][1,2,4]triazin-7-yl)-3,4-dihydroxy-5-(hy-droxymethyl)tetrahydrofuran-2-carbonitrile (GS-441524):** $^{1}$H NMR (600 MHz, DMSO-$d_6$) δ 7.93 (s, 3H), 6.91 (q, 2H), 6.11 (d, $J$ = 6.3 Hz, 1H), 5.22 (d, $J$ = 5.2 Hz, 1H), 5.00 – 4.89 (m, 1H), 4.66 (t, $J$ = 5.7 Hz, 1H), 4.08 (q, $J$ = 4.5 Hz, 1H), 3.98 (q, $J$ = 5.3 Hz, 1H), 3.70 – 3.62 (m, 1H), 3.57 – 3.47 (m, 1H). $^{13}$C NMR (151 MHz, DMSO) δ 156.09, 148.34, 124.34, 117.82, 116.98, 111.24, 101.29, 85.89, 78.99, 74.72, 70.53, 61.40, 40.34, 40.20, 40.06, 39.92, 39.78, 39.70, 39.64, 39.51.

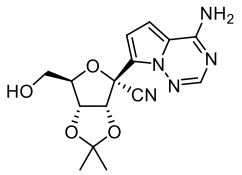

**(3a*R*,4*R*,6*R*,6a*R*)-4-(4-aminopyrrolo[2,1-*f*][1,2,4]triazin-7-yl)-6-(hydroxyme-thyl)-2,2-dimethyltetrahydrofuro[3,4-d][1,3]di-oxole-4-carbonitrile (3-16):** $^{1}$H NMR (400 MHz, Chloroform-*d*) δ 7.93 (s, 1H), 7.08 (d, $J$ = 4.6 Hz, 1H), 6.66 (d, $J$ = 4.9 Hz, 1H), 5.98 (s, 2H), 5.43 (d, $J$ = 6.5 Hz, 1H), 5.24 (dd, $J$ = 6.6, 2.3 Hz, 1H), 4.67 (q, $J$ = 1.9 Hz, 1H), 4.02 – 3.81 (m, 2H), 1.81 (s, 3H), 1.40 (s, 3H). $^{13}$C NMR (101 MHz, $CDCl_3$) δ 155.65, 147.64, 123.24, 117.02, 116.85, 113.73, 100.61, 85.45, 83.57, 82.89, 81.71, 77.37, 77.25, 77.05, 76.73, 62.74, 25.60, 25.10.

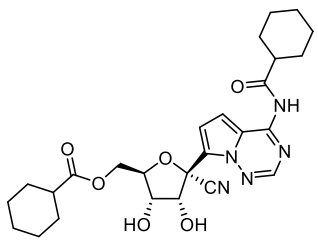

**((2*R*,3*S*,4*R*,5*R*)-5-cyano-5-(4-(cyclohexanecarboxamido)pyrrolo[2,1-*f*][1,2,4]triazin-7-yl)-3,4-dihydroxytetrahydrofuran-2-yl)methyl cyclohexanecarboxylate (3-17):** $^{1}$H NMR (400 MHz, DMSO-$d_6$) δ 10.83 (s, 1H), 8.42 (s, 1H), 7.29 (d, $J$ = 4.8 Hz, 1H), 7.09 (d, $J$ = 4.7 Hz, 1H), 6.47 (d, $J$ = 5.9 Hz, 1H), 5.46 (d, $J$ = 6.0

Hz, 1H), 4.73 (t, *J* = 5.0 Hz, 1H), 4.41 – 4.23 (m, 2H), 4.24 – 4.08 (m, 1H), 4.00 (q, *J* = 5.1 Hz, 1H), 2.96 – 2.77 (m, 1H), 2.23 (dp, *J* = 10.5, 3.8 Hz, 1H), 1.95 – 1.85 (m, 2H), 1.82 – 1.52 (m, 8H), 1.49 – 1.37 (m, 2H), 1.35 – 1.14 (m, 8H). $^{13}$C NMR (101 MHz, DMSO) δ 176.05, 175.09, 152.08, 146.86, 125.48, 117.84, 116.94, 112.32, 105.50, 81.75, 79.15, 74.66, 70.63, 62.86, 44.78, 42.57, 29.30, 28.97, 28.88, 25.82, 25.72, 25.55, 25.21, 25.19.

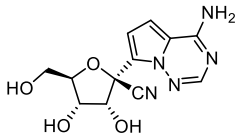

**((2*S*,3*R*,4*S*,5*R*)-2-(4-aminopyrrolo[2,1-*f*][1,2,4]triazin-7-yl)-3,4-dihydroxy-5-(hydroxymethyl)tetrahydrofuran-2-carbonitrile (3-20):** $^{1}$H NMR (400 MHz, DMSO-$d_6$) δ 8.94 (s, 1H), 8.62 (s, 1H), 8.12 (s, 1H), 7.29 (d, *J* = 4.8 Hz, 1H), 7.17 (d, *J* = 4.0 Hz, 1H), 6.77 (d, *J* = 4.0 Hz, 1H), 4.72 (d, *J* = 4.0 Hz, 1H), 4.38 (dd, *J* = 8.0 Hz, 4.0 Hz, 1H), 3.98 – 4.02 (m, 1H) , 3.77 (dd, *J* = 8.0 Hz, 4.0 Hz, 1H), 3.56 (q, *J* = 8.0 Hz, 1H). ESI-HRMS: m/z $[M+H]^+$ calcd for $C_{19}H_{24}N_5O_5$: 292.1046; found: 292.1418.

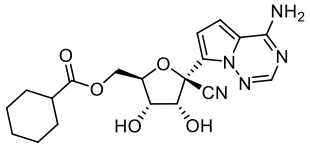

**((2*R*,3*S*,4*R*,5*S*)-5-(4-aminopyrrolo[2,1-*f*][1,2,4]triazin-7-yl)-5-cyano-3,4-dihydroxytetrahydrofuran-2-yl)methyl cyclohexane carboxylate (3-21):** $^{1}$H NMR (400 MHz, Methanol-$d_4$) δ 7.86 (s, 1H), 6.91 (d, *J* = 4.6 Hz, 1H), 6.80 (d, *J* = 4.6 Hz, 1H), 5.01 (d, *J* = 4.2 Hz, 1H), 4.71 – 4.55 (m, 2H), 4.38 – 4.12 (m, 2H), 2.56 – 2.40 (m, 1H), 2.08 – 1.93 (m, 2H), 1.84 – 1.71 (m, 2H), 1.70 – 1.61 (m, 1H), 1.59 – 1.45 (m, 2H), 1.41 – 1.27 (m, 3H). $^{13}$C NMR (151 MHz, DMSO) δ 175.35, 155.93, 148.32, 122.96, 118.46, 116.02, 110.34, 101.25, 80.26, 78.32, 75.79, 71.59, 62.36, 42.75, 31.75, 29.46, 29.01, 28.90, 25.75, 25.32, 25.26, 22.56.

### 3.4.3 Biology

#### *SARS-CoV-2 replicon assays*

The luciferase assays were carried out according to the manufacturer's instructions (Promega Corporation, Fitchburg, WI, USA). Firstly, the HEK293T cells in 24-well plate transfected with pBAC- SARS-CoV-2-Replicon-Luciferase plasmid (250 ng) and RL-TK plasmid (15 ng). After 6-8 h, the cells are transfected, the supernatant was removed and changed with fresh DMEM medium, followed by adding tested

compounds to the media with the final concentration of 10 μM, 5 μM, 2 μM, 1 μM, 0.5 μM, 0.1 μM. After 60 h, cells were lysed in 200 μL Passive Lysis Buffer (PLB). Each lysate (20 μL) was transferred into 96-well white plate and then mixed with 20 μL Luciferase Assay Reagent II, followed by 20 μL of Stop & Glo solution. The luminescence values of the two-step reaction were recorded using a luminescence detector in Synergy H1 Hybrid Multi-Mode Reader (BioTek). Data analysis was performed with GraphPad Prism 6.0 software.

***The metabolic stability determination in human plasma***

1 mM working solutions of test compounds were prepared in DMSO. 4 μL of working solutions was spiked to 796 μL of pre-incubated plasma to reach a final concentration of 5 μM. 50 μL aliquots of the spiked plasma were added into new tubes for different time points including 15, 30, 60 and 120 minutes and then incubated at 37°C water bath with shaking at 60 rpm. The assay was performed in duplicate. The reaction was stopped by adding 300 μL of room temperature quench solution acetonitrile containing internal standards (100 nM Alprazolam, 500 nM Labetalol and 2 μM Ketoprofen) to the spiked plasma samples at the appointed time points. Time 0 samples were prepared by adding 50 μL of the spiked plasma to new tubes containing 300 μL of room temperature quench solution. Vortex for 5 minutes. Samples in plate were centrifuged at 3,220 g for 30 minutes at 4°C to precipitate protein. And then 100 μL of the supernatant was transferred to a new 96-well plate with 100 μL water for LC-MS/MS analysis. Percent compounds remaining at each time point were calculated using Microsoft Excel. Peak area ratios were determined from extracted ion chromatograms.

***Pharmacokinetic study in SD rats***

Male SD rats (180-220 g, N = 3) were fasted for 12 h before drug administration. **3-1**, **3-8** and **3-12** were respectively administered intravenously at 5 mg/kg or intragastrically at 25 mg/kg. Blood samples were collected from the jugular vein into anticoagulant EDTA-K2 tubes at 0.083, 0.25, 0.5, 1, 2, 3, 4, 6, 8 and 24 h for the IV

group, and 0.25, 1, 0.5, 2, 3, 4, 6, 8 and 24 h for the IG group, respectively. All samples were centrifuged under 4000 rpm/min for 10 min at 4℃ and the plasma (supernatants) were collected and stored at -65℃ for future analysis. An aliquot of 50 μL each plasma sample was treated with 250 μL of acetonitrile. The samples were centrifuged under 4000 rpm/min for 10 min and filtered through 0.2 μm membrane filters. The concentration of analytes in each sample were analyzed by LC/MS/MS. PK parameters were determined following a noncompartmental analysis of the plasma concentration−time data by using Phoenix WinNonlin7.0. The following PK parameters are reported: clearance (CL; L/h/kg), volume of distribution at steady state (Vss; L/kg), terminal half-life ($T_{1/2}$; h), maximum concentration ($C_{max}$; μM), and area under the concentration−time curve from time 0 to infinity ($AUC_{(0-\infty)}$ (h*ng/mL)).

***Statistical analysis***

Quantitative experiments were carried out in triplicate and are indicated as the means ± standard deviations (SDs). The statistical tests utilized are two-tailed and respective details have been indicated in figure legends. A p value less than 0.05 was considered statistically significant (*, p-value of ≤ 0.05. **, p-value of ≤ 0.005. ***, p-value of ≤ 0.0005. ****, p-value of ≤ 0.0001).

# *Chapter 4*

## 4.1 Current Scenario of SARS-CoV-2 RNA N7 Methyltransferase (nsp14) Inhibitors

Known nsp14 inhibitors are mainly obtained from high-throughput virtual screening or from rational design based on SAH and its analogues. Diffley's group reported examples of prospective nsp14 inhibitors (Figure 8a). By virtual screening combined with HTRF-based assay, 4 compounds were observed to have certain inhibition activity towards SARS-CoV-2. The reported inhibitors are non-nucleosides, and have certain cellular inhibition against SARS-CoV-2. Combinational treatment of the inhibitors with remdesivir also showed improvement in $EC_{50}$ values of remdesivir. However, selectivities against human methyltransferase for the obtained inhibitors are not reported[295]. Jaudzems and co-workers also conducted high-throughput virtual screening against both nsp14 and nsp16, yielding 6 potential inhibitors (Figure 8b). Both nucleosides and non-nucleosides are included among the inhibitors identified. Nucleosides display better inhibitory activity against nsp14 in this work, with ZINC3861767 exhibiting the best inhibition (nsp14 MTase $IC_{50}$ = 1.5 μM, SI = 1.9)[295]. Vedadi and coworkers also identified two nsp14 inhibitors: DS0464 and SS148[296]. SS148 is highly potent towards nsp14, with $IC_{50}$ = 0.07 μM, but SS148 also exhibits a strong inhibition against other human MTases. While DS0464 presents an inhibition activity with $IC_{50}$ = 1.1 μM, selectivity towards other MTases is better than SS148[296]. Another virtual screening conducted over 680 million molecules identified three potential nsp14 inhibitors (Figure 8d): ZINC475239213 ($IC_{50}$ = 20 μM), ZINC730084824 ($IC_{50}$ = 50 μM), ZINC61142882 ($IC_{50}$ = 6 μM)[297].

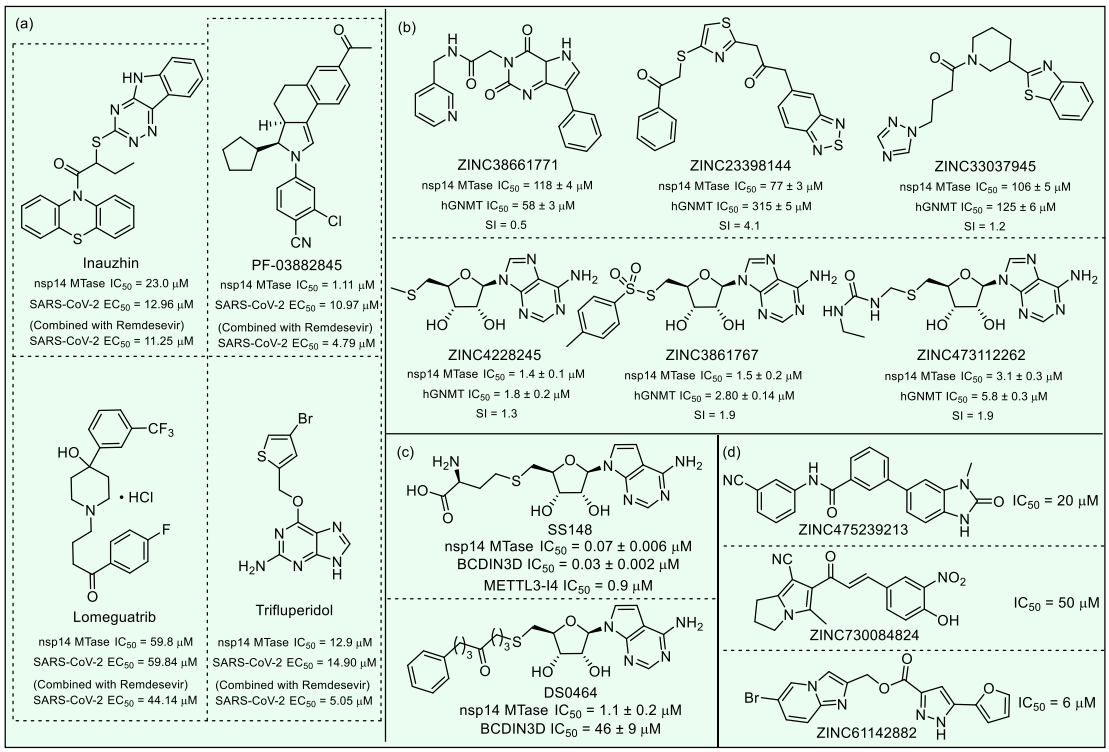


**Figure 8** Nsp14 inhibitors identified through high throughput virtual screening

Except from virtual screening, rational design is also a promising method towards effective nsp14 inhibitors. SAH is a by-product of methyl transfer yielded by SAM, and was reported to have inhibitory effect towards SARS-CoV-2 nsp14[264]. Along with SAH, an SAH analogue sinefungin was also reported to be an inhibitor of nsp14 (Figure 9a). Nencka and co-workers reported a series of nsp14 inhibitors based on rational design from SAH[298]. By analyzing the cavity of SARS-CoV nsp14, the researchers discovered a large hydrophobic cavity enclosed by Val287, Phe367, Val389, Pro429, Arg289 and Phe367 close to the 7-position of guanine group. To better fit in this cavity, the researchers introduced a large aromatic group to fit in this cavity towards design and synthesis for a series of nsp14 inhibitors. Among the synthesized nucleosides, Compound **16** (Figure 9b) presents the best inhibitory activity ($IC_{50}$ = 3 nM). However, compound **16** also significantly inhibits a series of human methyltransferase at 10 μM concentration (DNMT3A/3L $IC_{50}$ = 11 nM, DNMT3B/3L $IC_{50}$ = 29 nM, PRMT4 $IC_{50}$ = 40 nM, PRMT6 $IC_{50}$ = 75 nM)[298]. Jaudzems group also reported an example of SAH analogues as nsp14 inhibitors. Comparison along the structures of SARS-CoV Nsp14−SAM complex, SARS-CoV-2 Nsp16−SAM complex, human glycine N-

MTase−SAM complex, and human RNA guanine-N7-MTase−SAH complex was conducted. Through the comparison the researchers discovered that although the adenine-binding pocket is constrained narrowly in all structures, the amino acid binding sites for the amino acid side chain are much wider in SARS-CoV and SARS-CoV-2 MTases than in human MTases and are proposed to accommodate more sterically hindered side chains. The researchers synthesized a series of nucleosides with aromatic side chains, and along the inhibitors synthesized, Compound **2a** (Figure 9c) presented the best inhibitory ability (SARS-CoV-2 nsp14 $IC_{50}$ = 8.0 nM, SARS-CoV-2 nsp16 $IC_{50}$ = 4.0 nM, human GNMT $IC_{50}$ = 8.6 nM)[299]. Although compound **2a** is highly potent against SARS-CoV-2 nsp14 and nsp16, selectivity towards human MTases is not ideal. Debart and his co-workers also reported potent inhibitors against SARS-CoV-2 nsp14. Their group previously reported a series of dinucleoside molecules linked by sulfonamides that are effective as SARS-CoV-2 nsp14 inhibitors[300], which act as bisubstrate inhibitors with occupation at both SAM binding pocket and RNA binding pocket observed. However, none of the nucleosides exhibited molecular inhibition presumably due to a large molecular size, and the researchers thus went on to explore mononucleosides to obtain inhibitors reduced in size. The authors kept their bisubstrate strategy, introducing a phenyl ring as side chain, which was connected to adenosine by a sulfonamide linker. A series of nucleotides were designed and synthesized, and among all the molecules synthesized compound **25** (Figure 9d) displayed the best inhibition reactivity against SARS-CoV-2 nsp14 (SARS-CoV-2 nsp14 $IC_{50}$ = 0.019 μM). Compound **25** also exhibited a high selectivity towards human MTases, with >2000 fold selectivity towards hRNMT (hRNMT $IC_{50}$ = 53 μM)[301]. Unfortunately, the reported inhibitors displayed no cellular inhibition. CHEN group also reported potent nsp14 bisubstrate inhibitors. Instead of phenyl group, the author introduced larger aromatic group such as naphthalene and quinoline to fill the RNA binding pocket. The aromatic side chain is linked to the adenosine via sulfonamide. Among all the inhibitors explored, compound **3** (Figure 9e) (SARS-CoV-2 nsp14 $IC_{50}$ = 0.061 μM). To further prevent degradation, the authors replaced the C–N bond with a C–C bond, and no big changes in the inhibitory activity was caused by this change. Unexpectedly,

compound 10 (Figure 9e) with pyrrolo[2,1-*f*][1,2,4]-triazin-4-amine ring (GS-441524, the nucleobase of remdesivir) instead of adenosine displayed ideal cellular inhibitory activity ($EC_{50}$ = 0.72 μM) while having comparable inhibitory reactivity for nsp14 (SARS-CoV-2 nsp14 $IC_{50}$ = 0.093 μM)[302]. Compound **3** displayed ideal selectivity over a panel of human MTases, while the selectivity of compound **10** over human MTases were not reported.

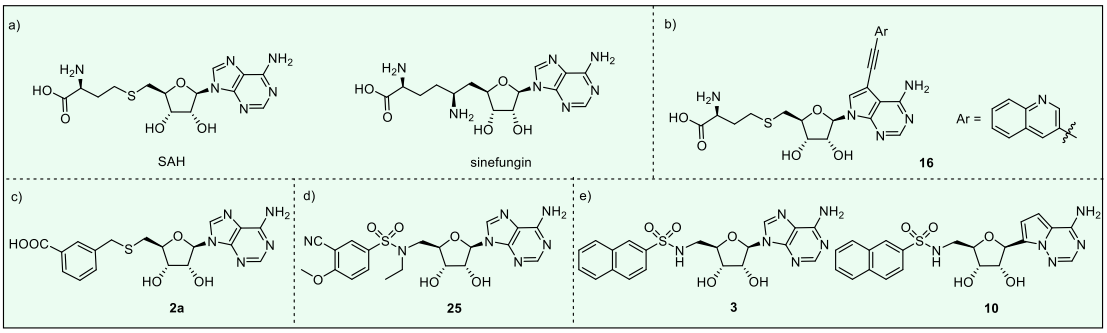


**Figure 9** SAH, sinefungin and nsp14 inhibitors identified through rational design

To tackle with continuous mutation of SARS-CoV-2, we wish to further explore the potential of nsp14 as anti-SARS-CoV-2 target. We designed and synthesized a series of different SAM analogues.

## 4.2 Design and Synthesis of Nsp14 Inhibitors

### 4.2.1 Design of SARS-CoV-2 Nsp14 Inhibitors

Based on the structure of SAH, we examined factors related to the selectivity and pharmacokinetics properties. As reported by Jaudzems et. al., the hydrophobic surface enclosed by the nsp14 residues Phe401, Tyr420, Phe426, and Phe506 would better contain an aromatic side chain than human MTases[299], and we thus choose to adopt a similar aromatic side chain for better selectivity. To improve the cellular intake of designed molecules, we introduced substitution on the exposed amino group, and used ester/amide group to mimic the carboxylic group in Jaudzems's work with better pharmacokinetic properties.

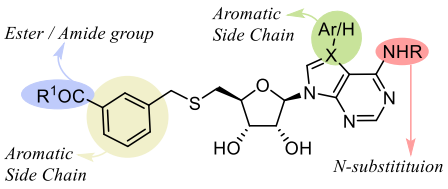


**Figure 10** Design of SAH-based nsp14 inhibitors

Nencka et. al. reported that introducing hydrophobic motifs at nucleobase 7-position would fit into a hydrophobic cavity nearby, enclosed by several hydrophobic residues (Val287, Phe367, Val389, Pro429) and Arg289[298]. We thus use a similar strategy where the nucleobase 7-*N* atom can be substituted with C atom, and then alkynes/aromatic groups can be introduced. The above-mentioned designs are enclosed in Figure 10.

### 4.2.2 Synthesis of SARS-CoV-2 Nsp14 Inhibitors

Based on the brief design in Figure 10, we synthesized a series of different potential SARS-CoV-2 nsp14 inhibitors with previously described structures, as enclosed in Figure 11.

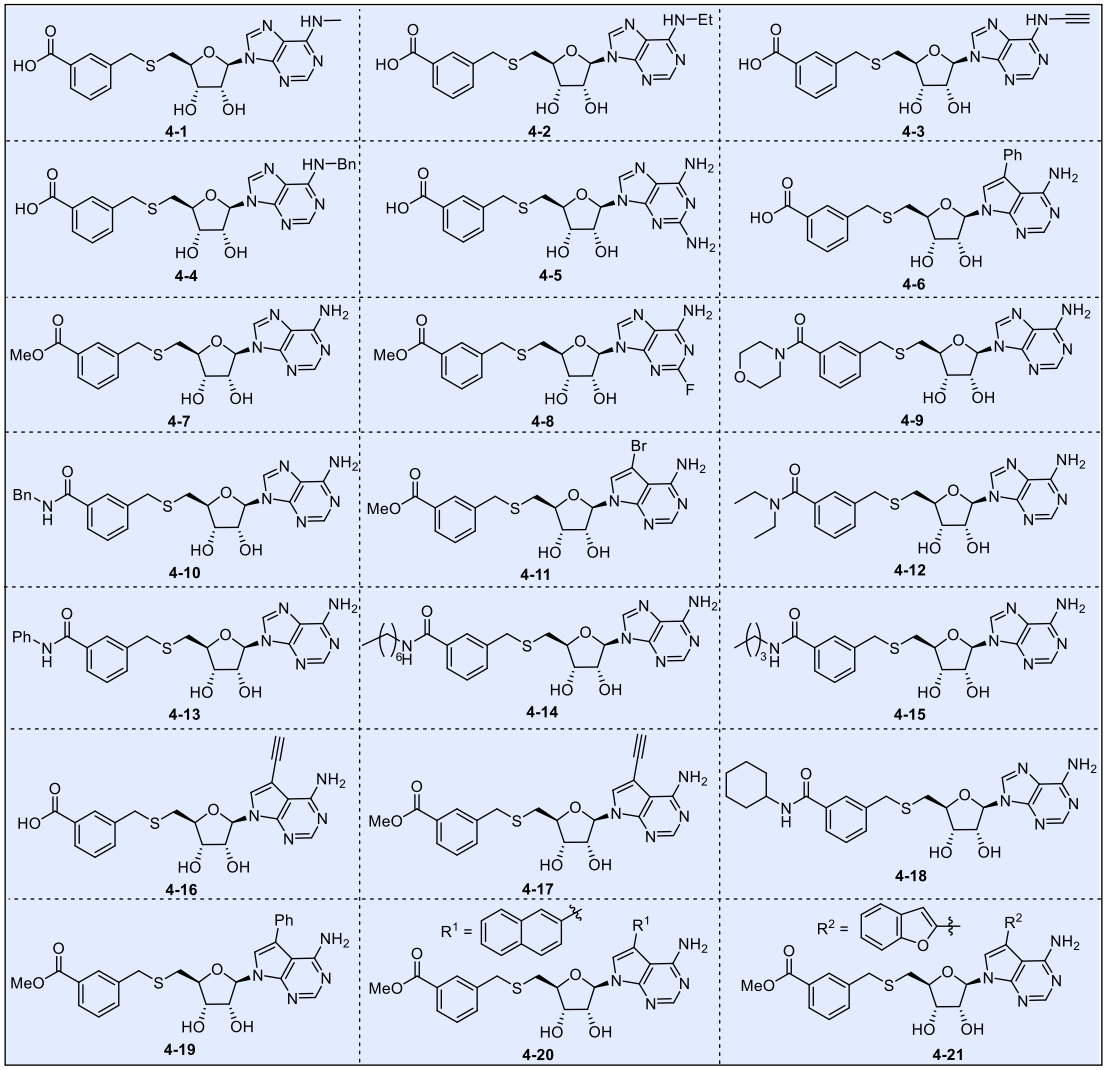


**Figure 11** Synthesized SARS-CoV-2 nsp14 inhibitors

For compounds **4-1** ~ **4-4**, **4-7** ~ **4-10**, **4-12** ~ **4-15** and **4-18**, our synthesis started with readily accessible nucleoside **4-22** (Scheme 21). Corresponding amines was attached to **1**, and then protected to yield **14-19**. **14-19** then went through condensation with thiolacetic acid, and the acetyl group was then replaced with methyl 3-(bromomethyl)benzoate, giving compounds **4-44** ~ **4-50** Compound **4-7** was obtained

through deprotection of compound **4-50** ($R^1 = R^2 = H$). The ethyl ester groups of **4-44** ~ **4-50** were hydrolyzed to generate **4-51** ~ **4-57**. Removing protection group of compounds **4-44** ~ **4-50** led to compounds **4-1** ~ **4-5** and **4-8**. Compound **4-57** ($R^1 = R^2 = H$) was then linked with a series of amines, affording compounds **4-58** ~ **4-64**. **4-58** ~ **4-64** was then deprotected to give compounds **4-9, 4-10**, **4-12** ~ **4-15** and **4-18**.

**Scheme 21** Synthetic route for **4-1** ~ **4-4**, **4-7** ~ **4-10**, **4-12** ~ **4-15** and **4-18**[a]

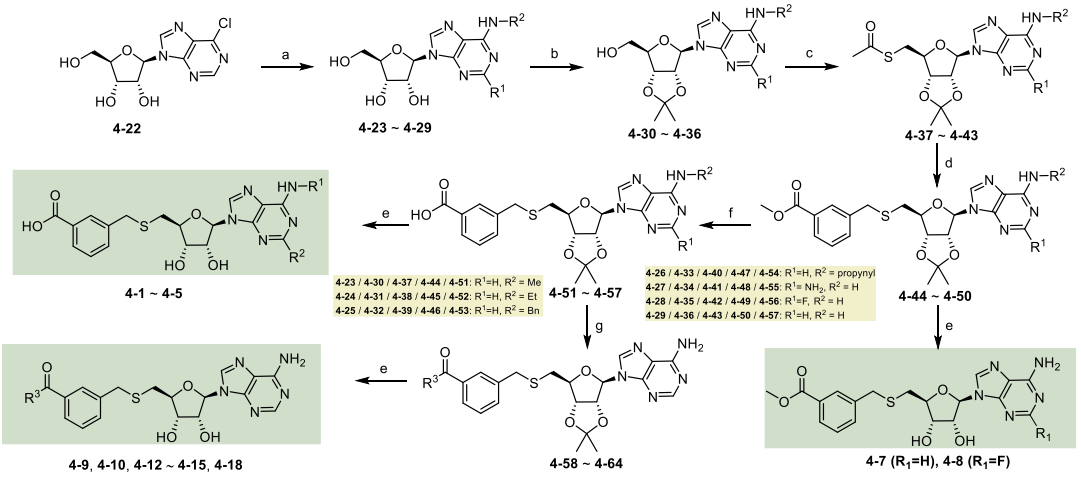


| | 4-1, 4-23 | 4-2, 4-24 | 4-3, 4-25 | 4-4, 4-26 | 4-5, 4-27 | 4-9, 4-58 | 4-10, 4-59 | 4-12, 4-60 | 4-13, 4-61 | 4-14, 4-62 | 4-15, 4-63 | 4-18, 4-64 |
|---|---|---|---|---|---|---|---|---|---|---|---|---|
| $R^1$ | Me | Et | Bn |  | $NH_2$ | H | H | H | H | H | H | H |
| $R^2$ | H | H | H | H | H | H | H | H | H | H | H | H |
| $R^3$ | OH | OH | OH | OH | OH |  | BnNH- |  | PhNH- |  |  |  |

[a]Reagents and conditions: (a) for **3** ($R^2$ = Me), **4** ($R^2$ = Et): $R^2NH_2$ in $H_2O$, 100°C, 91% to 95%; for **5** ($R^2$ = Bn), **6** ($R^2$ = 2-propynyl): $R^2NH_2$, $Et_3N$, EtOH, reflux, 82% to 91%. (b) conc. $H_2SO_4$, 2,2-dimethoxypropane, 45°C, 77% to 89%. (c) AcSH, $PPh_3$, DIAD, THF, 83% to 92%. (d) methyl 3-(bromomethyl)benzoate, MeONa, MeOH, 0°C to r.t., 79% to 86%. (e) HCOOH / $H_2O$, r.t., 82%. (f) LiOH, THF / $H_2O$. (g) corresponding amine, EDCI, HOBT, $Et_3N$, DCM, 0°C to r.t., 82% to 89% (2 steps).

Synthesis of compounds **4-6**, **4-11**, **4-16**, **4-17**, and **4-19** ~ **4-21** started with protected ribose **4-65**, which is commercially available. The ribose was then joined with 3-bromo-1*H*-indole, deprotected and protected again to give compound **4-67**. The hydroxy group was then replaced with thioacetic acid to give thioacetate **4-68**, which was transformed into **4-69** through an ester exchange-nucleophilic substitution process. Deprotection of **4-69** gives compound **4-11**. **4-69** can be coupled with various boronic acids or alkyne, then through hydrolysis and deprotection we obtained compounds **4-6**, **4-16**, **4-17**, and **4-19** ~ **4-21** (Scheme 22).

**Scheme 22** Synthetic route for **4-6**, **4-11**, **4-16**, **4-17**, and **4-19** ~ **4-21**[a]

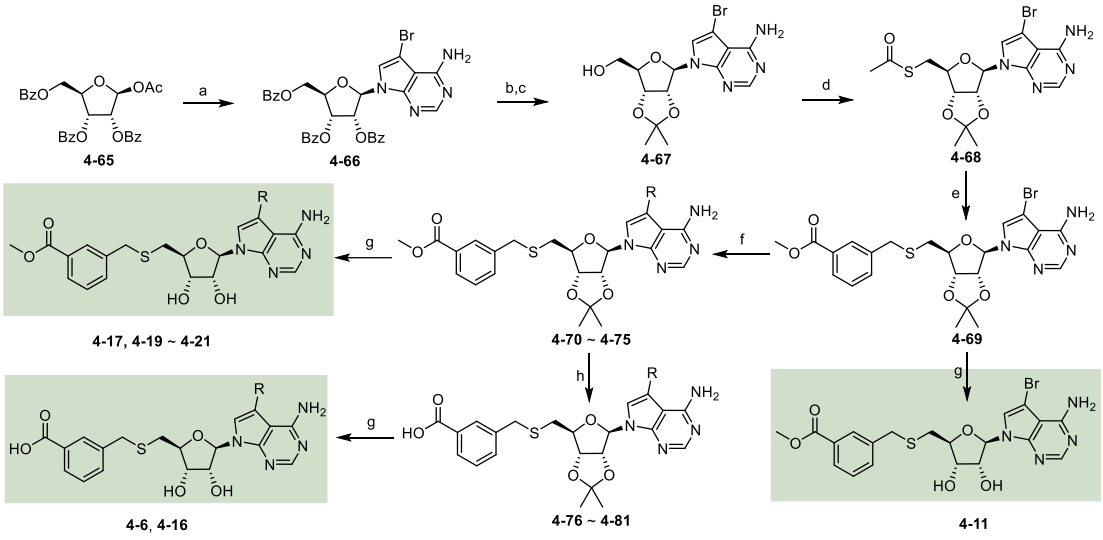


| | 4-6, 4-70, 4-76 | 4-16, 4-71, 4-77 | 4-17, 4-72, 4-78 | 4-19, 4-73, 4-79 | 4-20, 4-74, 4-80 | 4-21, 4-75, 4-81 |
|---|---|---|---|---|---|---|
| R | Ph– | – | – | Ph– | | |

[a]Reagents and conditions: (a) 3-bromo-1*H*-indole, N,O-bis(trimethylsilyl)acetamide, TMSOTf, MeCN, r.t. to 80°C. (b) $NH_3$ in $H_2O$, 130°C. (c) conc. $H_2SO_4$, 2,2-dimethoxypropane, 45°C, 60% (3 steps). (d) AcSH, $PPh_3$, DIAD, THF, 87%. (e) methyl 3-(bromomethyl)benzoate, MeONa, MeOH, 0°C to r.t., 77%. (f) for **42**-**44**: $RB(OH)_2$, $Pd(PPh_3)_4$, $K_2CO_3$, dioxane, 105°C, 66-74%; for **45** (R = alkynyl): 1) Trimethylsilylacetylene, $Pd(PPh_3)_4$, CuI, $Et_3N$, THF, 50°C; 2) TBAF, THF, r.t., 21% after 2 steps. (g) HCOOH / $H_2O$, r.t., 70% to 88%. (h) LiOH, THF / $H_2O$.

Detailed synthetic procedures can be found in Chapter 4.4.2. Chemistry.

### 4.2.3 Assessment of Inhibition Ability of Synthesized Compounds on SARS-CoV-2 Nsp14

Compounds **4-1** ~ **4-21** was tested for their inhibitory activity against SARS-CoV-2 nsp14 protein. We first screened the inhibition activity of synthesized compounds at fixed concentrations (10 μM and 50 μM). We adopted a MTase-Glo™ methyltransferase assay as testing assay (Figure 10). The assay adopts GpppA to mimic RNA substrate, and SAM is adopted as the methyl source, generating SAH by-product. The testing assay transfers the SAH by-product generated to ATP, and light energy is released when ATP is transferred to ADP. The light energy generated is measured and quantified, and with reference of background and 100% active enzyme group we can calculated inhibition percentage. For each experimental trial, wells were performed in

duplicate.

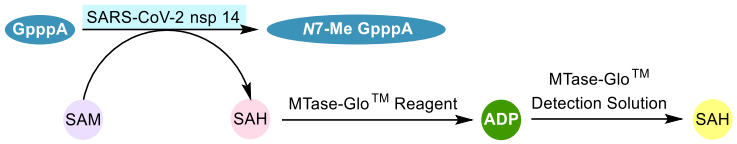


**Figure 12** Working principle of MTase-Glo™ Methyltransferase Assay

Among the synthesized inhibitors, compounds **4-1** ~ **4-5** and **4-7**, **4-8** with modifications on adenine group displayed undesirable inhibitory efficacy and negative shift in melting temperature, demonstrating the necessity of adenine group in retaining the inhibition ability and binding ability. Compounds **4-6**, **4-20** with 7-phenyl substitution, **4-11** with 7-bromo substitution and **4-16**, **4-17** with alkynyl group displayed fair inhibition reactivity, while compounds **4-19** ~ **4-21** bearing large aromatic motifs at nucleobase 7-position showed nearly no inhibition towards nsp14, and negative shifts in melting point are also observed. These results indicate that the massive 7-aromatic substituent is difficult to fit in the hydrophobic cavity near nucleobase 7-position, resulting in failure in their binding with nsp14. Compound **4-9** and **4-12** bearing secondary amide group on phenyl side chain displayed unideal inhibitory, presumably due to the steric hindrance of nitrogen atom. Compound **4-7**, **4-10**, **4-13**, **4-14** and **4-15** displayed good inhibitory efficacy against SARS-CoV-2 nsp14, with 100% inhibition at 50 μM and >70% inhibition at 10 μM. Compound **4-18** also displayed satisfactory inhibitory efficacy, with 97% inhibition at 50 μM and 89% inhibition at 10 μM. Pair **4-6**, **4-20** and **4-16**, **4-17** displayed parallel inhibition activity, displaying feasibility of substituting carboxylic group with ester motif, which may improve the pharmacokinetic properties of inhibitors.

**Table 13** Evaluation of Synthesized Potent Inhibitors

| Entry | Compound | Inhibition at 50 μM / % | Inhibition at 10 μM / % | $\Delta T_m$ at 50 μM / ℃ |
|---|---|---|---|---|
| 1 | **4-1** | 70 | 55 | /[a] |
| 2 | **4-2** | 60 | 55 | /[a] |
| 3 | **4-3** | 54 | 39 | /[a] |
| 4 | **4-4** | 40 | 31 | /[a] |
| 5 | **4-5** | 27 | 14 | /[a] |
| 6 | **4-6** | 84 | 37 | 5.8 |
| 7 | **4-7** | 100 | 92 | 4.4 |
| 8 | **4-8** | 48 | 26 | /[a] |
| 9 | **4-9** | 58 | 65 | /[a] |
| 10 | **4-10** | 31 | 71 | 3.6 |
| 11 | **4-11** | 53 | 36 | /[a] |
| 12 | **4-12** | 34 | 19 | /[a] |
| 13 | **4-13** | 100 | 86 | 3.5 |
| 14 | **4-14** | 100 | 96 | 3.8 |
| 15 | **4-15** | 74 | 87 | 3.9 |
| 16 | **4-16** | 50 | 30 | /[a] |
| 17 | **4-17** | 32 | 37 | /[a] |
| 18 | **4-18** | 97 | 89 | 3.8 |
| 19 | **4-19** | 51 | 38 | /[a] |
| 20 | **4-20** | 80 | 49 | /[a] |
| 21 | **4-21** | 39 | 27 | /[a] |

[a]Negative results obtained.

Based on the above-mentioned results at fixed concentration, we selected compound **4-7**, **4-13**, **4-14, 4-18** and **4-21** for dose-response test. $IC_{50}$ value for the tested compounds fall in an ideal range between 1 and 4 μM. To our disappointment, sinefungin displayed an $IC_{50}$ value of 0.273 μM in our testing assay, indicating that none of the synthesized inhibitors displayed reactivity better than sinefungin. Among the inhibitors analyzed, compound **4-7** with an ester motif and **4-14** with a aliphatic amide motif on phenyl *m*-position displayed the best inhibitory activity ($IC_{50}$ = 1.84 μM and 1.81 μM, respectively).

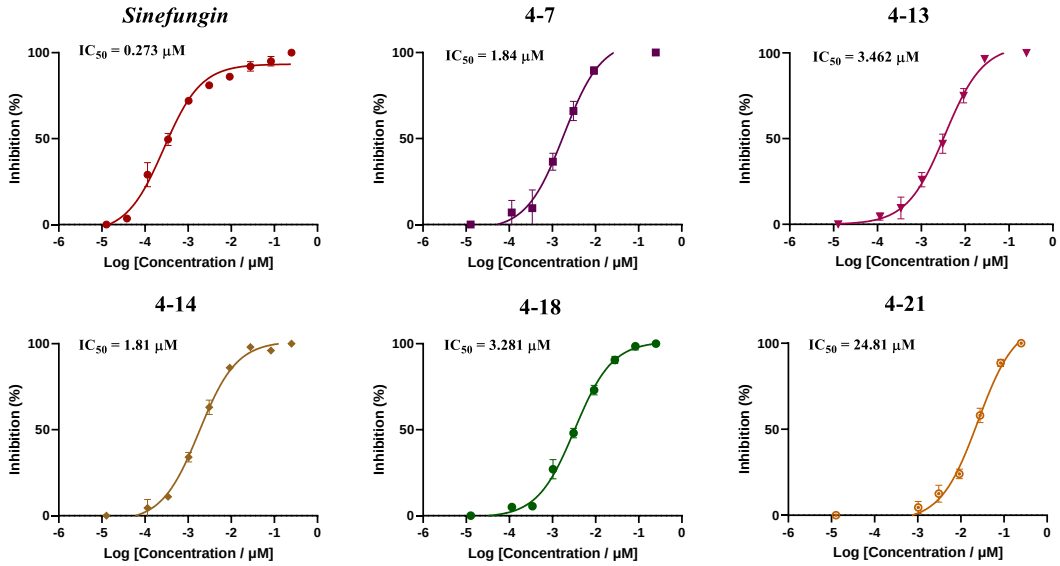


**Figure 13** $IC_{50}$ graphs of sinefungin and compounds **4-7**, **4-13**, **4-14**, **4-18** and **4-21**

Based on the results of previous biological experiments, we conclude a brief structure-activity relationship (SAR). Firstly, breaking the adenosine nucleobase largely reduces the inhibition reactivity. In our structure, introducing hydrophobic groups at 7-position did not show obvious increase to inhibitory efficacy of synthesized structures, and massive aromatic substitution at 7-position would lead to decreased inhibition activity. Substituting the carboxyl group with ester structure did not significantly change the inhibition activity, and with amide motifs we obtained ideal inhibition activity.

## 4.3 Conclusion

In this work, we synthesized a series of SAH-based SARS-CoV-2 nsp14 inhibitors, and examined their inhibition ability against SARS-CoV-2 nsp14. Among the synthesized inhibitors, **4-7** and **4-14** displayed the best inhibitory activity, with $IC_{50}$ = 1.84 μM and 1.81 μM respectively. A brief structure-activity relationship (SAR) was concluded. Future exploration of nsp14 inhibitors can be focused on the selectivity of inhibitors, on examining the selectivity against human methyltransferases, and on structures with improved selectivity against human methyltransferases. While keeping the amide/ester advantageous structure, we can seek for enlarged side chain substitution

or suitable 7-substitution to better fit in cavities specially owned by SARS-CoV-2 nsp14.

## 4.4 Experimental Section

### 4.4.1 General Information

All the solvents and reagents were obtained from commercial sources and used without purification unless stated otherwise. All glassware was dried overnight at 105 °C prior to use. Thin layer chromatography (TLC) was performed on silica gel plates. Visualization on TLC was performed by UV light (254 nm) irradiation. Flash column chromatography was performed on a silica gel (200-300 mesh) column. $^{1}H$ and $^{13}C$ NMR spectra were recorded on a Brüker DPX-400 MHz spectrometer. The chemical shift ($\delta$) values are given in ppm and are referenced to residual solvent peaks. Coupling constants ($J$) were reported in hertz (Hz). Mass spectra and high-resolution mass spectra (HRMS) were obtained on a VG MICROMASS Fison VG platform, a Finnigan Model Mat 95 ST instrument, or a Brüker APEX 47e FT-ICR mass spectrometer.

### 4.4.2 Chemistry

***Synthesis of compounds 4-1 ~ 4-21***

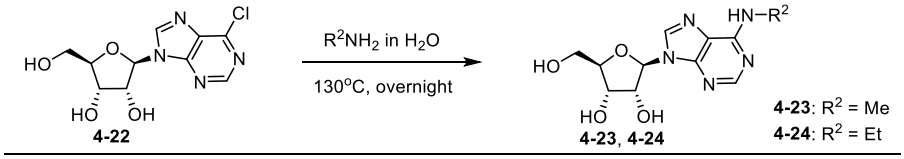


To 4g **4-22** in autoclaves were added 50mL $R^2NH_2$ in $H_2O$ (commercially available) correspondingly. Magnetic stir bars were charged to the autoclaves, then sealed and heated at 100℃ overnight. Following this the autoclaves were cooled to room temperature, and the precipitated products were filtered and washed with water. The filter residues were collected and dried with vacuum drying oven overnight. **4-23** and **4-24** were obtained in 95% yield and 91% yield, correspondingly, as white solid.

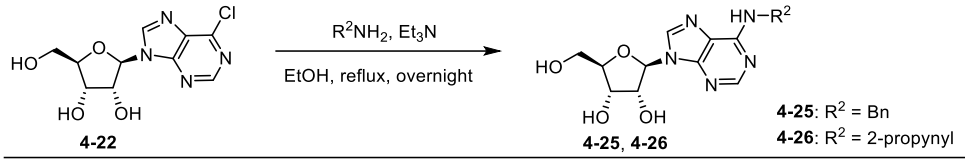


To 4g **4-22** in 250 mL round-bottom flasks were added corresponding amines (1.5 equiv.), $Et_3N$ (4.9 mL, 2.5 equiv.) and 50 mL EtOH. Magnetic stir bars were charged to the flasks. The reaction mixtures were heated at reflux overnight, then cooled to room temperature, and the reaction progress was monitored by TLC. The product was filtered from the reaction mixture and washed with dichloromethane (50 mL × 3). **4-25** was obtained as white solid with 82% yield, and **4-26** was obtained as white solid in 91% yield.

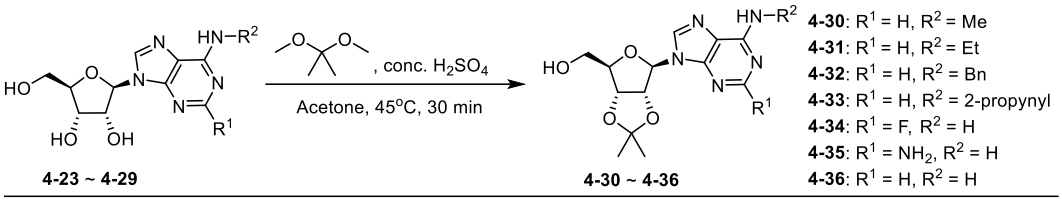


To 2g **4-23** ~ **4-29** in 100 mL round bottom flasks was added 2,2-dimethoxypropane (4.0 equiv.) and 20 mL acetone. Magnetic stir bars were charged to the flasks. The reaction mixtures were then heated to 45℃, and concentrated sulfuric acid (1.3 equiv.) was added to the reaction mixtures dropwise. After TLC indicated full conversion of the starting material, the reaction mixtures were cooled to room temperature, and their pH was adjusted to ~5 with saturated $NaHCO_3$ aqueous solution. Acetone was then removed with rotatory evaporator, and the aqueous solutions were then extracted with dichloromethane (50 mL × 3). The organic layers were then combined correspondingly, dried over $Na_2SO_4$, and **4-30** ~ **4-36** were obtained through flash column chromatography (DCM:MeOH = 40:1 to 20:1) in 77% to 89% yields.

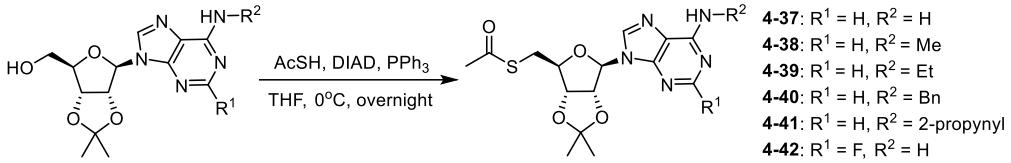


To $PPh_3$ (2.0 equiv.) in seven parallel 100 mL round-bottom flasks were charged 20 mL THF and magnetic stir bars. The reaction mixtures were cooled to 0℃, and DIAD (2.0 equiv.) was added to the mixtures dropwise. Thick suspensions formed, and were stirred for 30 minutes. 2g **4-30** ~ **4-36** were added to the suspensions accordingly, and the mixtures were stirred for another 10 minutes at 0℃. Thioacetic acid (2.0 equiv.) was added dropwise to the reaction mixtures, and the flasks were slowly warmed to room temperature. The reaction mixtures were stirred overnight and monitored with TLC. Upon completion of the reactions, THF was removed by rotatory evaporator, and the crude mixtures were purified by flash column chromatography (PE:EA = 2:1 to 1:1). **4-37** ~ **4-43** were obtained in 83% to 92% yields.

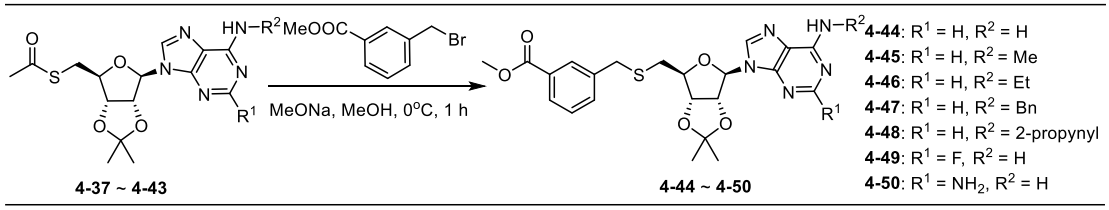


To 2g **4-37** ~ **4-43** in 100 mL round-bottom flasks under $N_2$ protection were charged with magnetic stir bars, methyl 3-(bromomethyl)benzoate (1.2 equiv.) and 20 mL dry MeOH. The flasks were cooled to 0℃, and to the reaction mixtures were added 5M MeONa in MeOH (3.0 equiv.) dropwise. The reaction solutions were stirred at 0℃ for 1 h, and TLC was adopted to monitor the reactions. Upon completion of the reaction, MeONa was quenched with saturated $NH_4Cl$ aqueous solution, and MeOH was removed by rotatory evaporator. The aqueous phases were then extracted with dichloromethane (50 mL × 3). The organic layers were combined correspondingly, dried over $Na_2SO_4$, and **4-44** ~ **4-50** were obtained in 79% to 86% yields by flash column chromatography (PE:EA = 2:1 to 1:1).

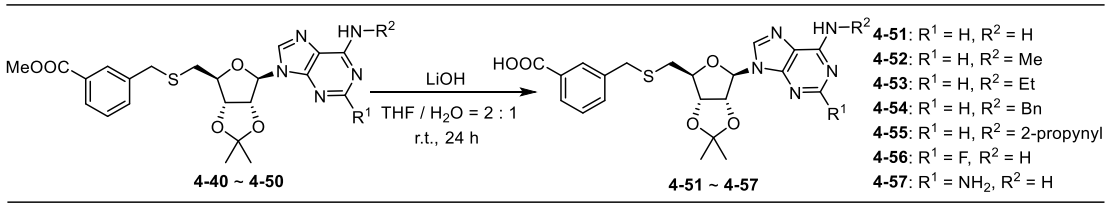


To 500 mg **4-40** ~ **4-50** in 50 mL round-bottom flasks were added LiOH (2.0 equiv.), 4 mL THF and 2 mL $H_2O$. Magnetic stir bars were charged to the flasks, and the reaction mixtures were stirred at room temperature for 24 h. Upon TLC indicated total consumption of the substrate, THF was removed by rotatory evaporator, and the aqueous phases were extracted with dichloromethane (10 mL × 3) to remove organic impurities. The aqueous phases were kept, and their pH was adjusted to ~ 5 with 1M HCl, then extracted with dichloromethane (20 mL × 3). The organic phases were combined correspondingly, dried over $Na_2SO_4$, and dichloromethane was removed by rotatory evaporator. The crude mixtures were directly used for the next step.

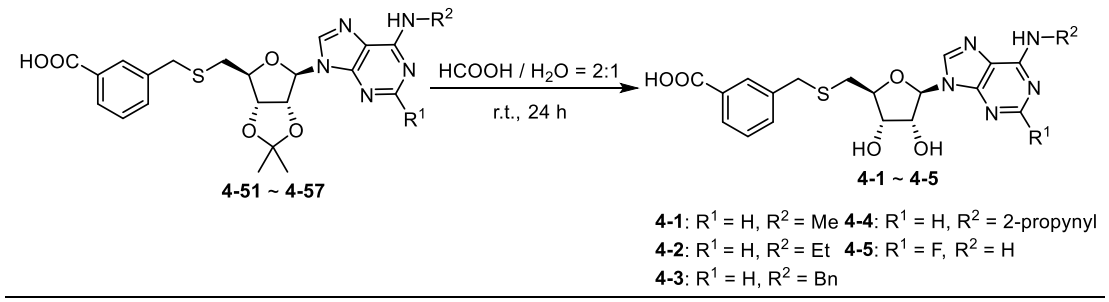


To the crude mixtures of **4-51** ~ **4-57** obtained from the above step in 25 mL round-bottom flasks were added 2 mL formic acid and 1 mL $H_2O$. Magnetic stir bars were charged to the flasks, and the reaction mixtures were stirred at room temperature for 24 h. Upon TLC indicated the completion of the reactions, solvents were removed by rotatory evaporator, and the crude mixtures were purified by flash column chromatography (DCM:MeOH = 30:1 to 10:1), or washed by hot MeOH, depending on the solubility of the crude products in MeOH. **4-1** ~ **4-5** were obtained in 60% to 75% yields (for the above 2 steps).

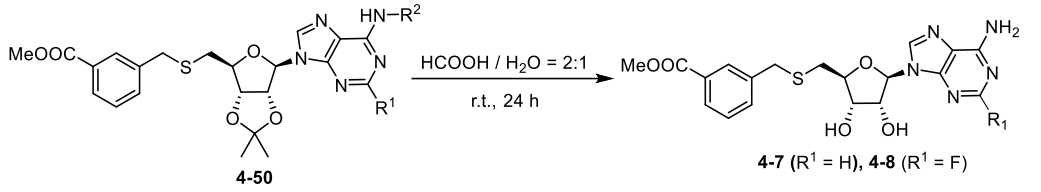


To 200 mg **4-50** in a 25 mL round-bottom flask was added 2 mL formic acid and 1 mL $H_2O$. Magnetic stir bars were charged to the flasks. The reaction mixture was stirred at room temperature for 24 h. Upon TLC indicated the completion of the reaction, solvents were removed by rotatory evaporator, and the crude mixture was purified by flash column chromatography (DCM:MeOH = 20:1). **4-7** was obtained in 82% yield.

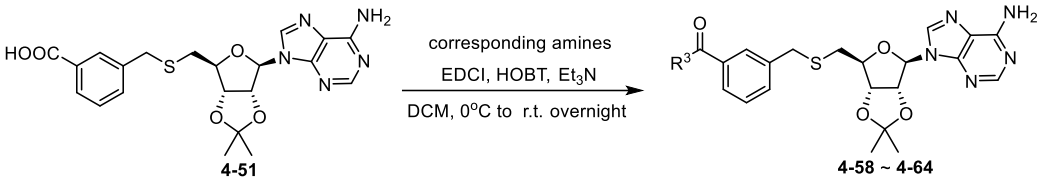


| | 4-58 | 4-59 | 4-60 | 4-61 | 4-62 | 4-63 | 4-64 |
|---|---|---|---|---|---|---|---|
| $R^3$ |  | 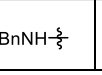 |  | 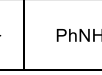 |  | 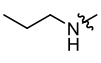 | 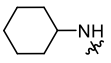 |

To 200 mg **4-51** (crude product) in 25 mL round-bottom flasks were added magnetic stir bars, EDCI (120 mg, 1.5 equiv.) and HOBT (90 mg, 1.5 equiv.). 2 mL dichloromethane were added to the solid mixtures, and the suspensions were stirred at 0℃. To the reaction mixtures were added $Et_3N$ (0.18 mL, 3.0 equiv.) dropwise, and then corresponding amines (1.5 equiv.) in 1 mL dichloromethane was added to the solutions dropwise. The reaction solutions were then moved to room temperature, and stirred overnight. Upon TLC indicated the completion of the reactions, dichloromethane were removed by rotatory evaporator, and the crude mixtures were purified by flash column chromatography (PE:EA = 2:1 to 1:1). **4-58** ~ **4-64** were obtained in 82% to 89% yields for 2 steps.

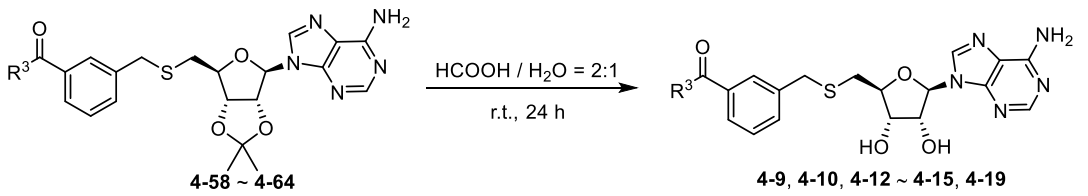


**4-58 ~ 4-64** **4-9**, **4-10**, **4-12 ~ 4-15**, **4-19**

| | 4-9 | 4-10 | 4-12 | 4-13 | 4-14 | 4-15 | 4-19 |
|---|---|---|---|---|---|---|---|
| $R^3$ | 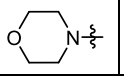 | BnNH- |  | PhNH- |  | 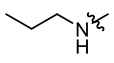 | 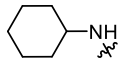 |

To 200 mg **4-58** ~ **4-64** in 25 mL round-bottom flasks were added 2 mL formic acid and 1 mL $H_2O$. Magnetic stir bars were charged to the flasks, and the reaction mixtures were stirred at room temperature for 24 h. Upon TLC indicated the completion of the reactions, solvents were removed by rotatory evaporator, and the crude mixtures was purified by flash column chromatography (DCM:MeOH = 30:1 to 10:1). **4-9,4-10, 4-12** ~ **4-15** and **4-19** were obtained in 69% to 87% yields.

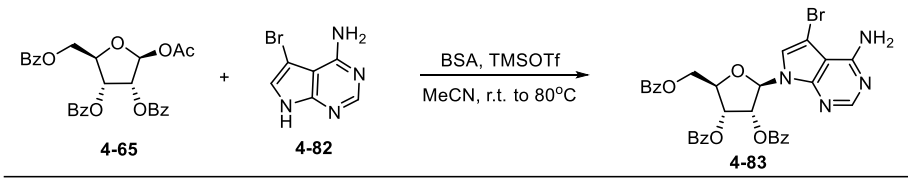


**4-65** **4-82** **4-83**

To 20 g **4-65** in a 500 mL three-necked round-bottom flask was added 200 mL acetonitrile. A magnetic stir bar was charged to the flask, and the flask was protected by $N_2$. BSA (26 mL, 1.2 equiv.) was then added to the suspension, and the mixture was stirred at room temperature for 10 minutes. **4-82** (66g, 1.5 equiv.) in 100 mL acetonitrile was added dropwise to the reaction mixture, followed by TMSOTf (26 mL, 1.6 equiv.), also in a dropwise manner. The reaction mixture was heated at 80°C for 1 h. Upon TLC indicated the completion of the reaction, the flask was cooled to room temperature, and water was added to the reaction mixture. The precipitated white solid was filtered, washed with $H_2O$, collected and then dried with vacuum drying oven overnight. **4-83** was obtained as white solid with 82% yield.

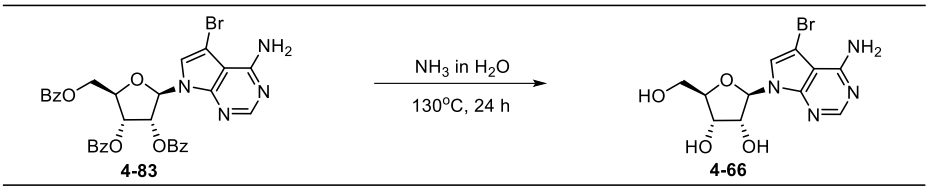


40 g **4-83**, a magnetic stir bar and 370 mL $NH_3$ in $H_2O$ (100 equiv.) were added to an autoclave. The autoclave was then fine sealed, heated to 130℃ for 24 h, and then cooled to room temperature. The reaction solution was then transformed to a 1 L eggplant shaped flask, and water was removed by rotatory evaporator. A black to purple crude solid was obtained, and the solid was washed with dichloromethane (200 mL × 3). The crude product obtained was directly used for the next step.

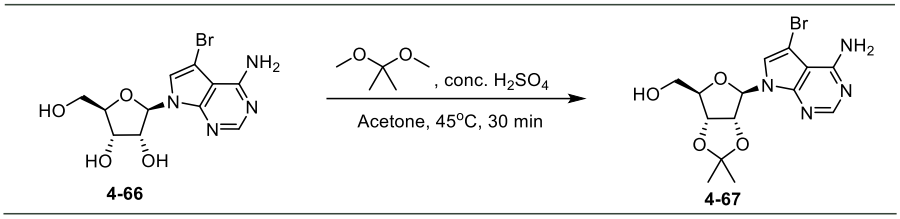


To the above-obtained crude product in a 500 mL round bottom flask was added a magnetic stir bar, 2,2-dimethoxypropane (28.5 mL, 4.0 equiv.) and 200 mL acetone. The reaction mixture was then heated to 45℃, and concentrated sulfuric acid (4 mL, 1.3 equiv.) was added dropwise. After TLC indicated full conversion of the starting material, the reaction mixture was cooled to room temperature and its pH was adjusted to ~5 with saturated $NaHCO_3$ aqueous solution. Acetone was removed with rotatory evaporator, and the aqueous solution was then extracted with dichloromethane (200 mL × 3). The organic layers were then combined, dried over $Na_2SO_4$, and **4-67** was obtained through flash column chromatography (DCM:MeOH = 20:1) in 82% yield.

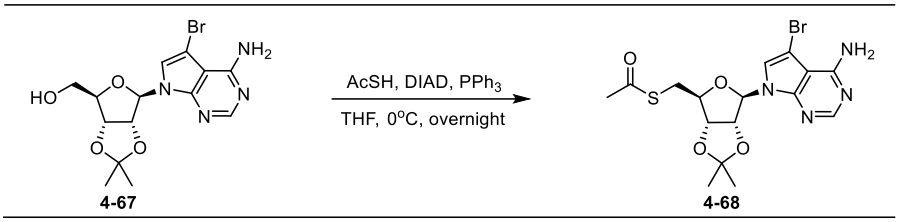


To $PPh_3$ (20 g, 2.0 equiv.) in a 500 mL round-bottom flask was charged 150 mL THF and a magnetic stir bar. The suspension was cooled to 0℃, and DIAD (13.8 mL, 2.0 equiv.) was added to it dropwise. A thick suspension was formed, and the suspension was stirred for 30 minutes. 15g **4-67** was then added to the suspension, and the mixture was stirred for another 10 minutes at 0℃. Following this, thioacetic acid (5.4 mL, 2.0 equiv.) was added dropwise to the reaction mixture. The flask was slowly warmed to room temperature and the reaction solution was stirred overnight. Upon TLC indicated the completion of the reaction, THF was removed by rotatory evaporator, and the crude mixture was purified by flash column chromatography (PE:EA = 2:1). **4-68** was obtained in 87% yield.

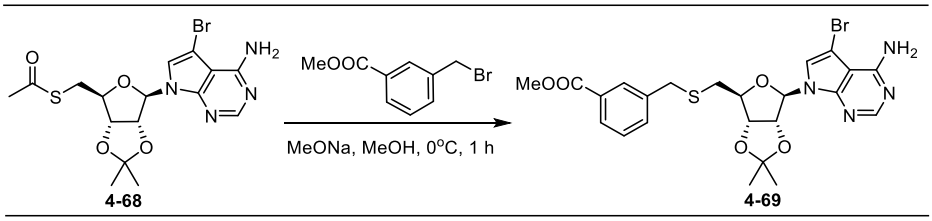


To 15g **4-68** in a 500 mL round-bottom flask under $N_2$ protection was charged with a magnetic stir bar, methyl 3-(bromomethyl)benzoate (8.5 g, 1.2 equiv.) and 150 mL dry MeOH. The reaction mixture was cooled to 0℃, and to the reaction mixture was added 5M MeONa in MeOH (20 mL, 3.0 equiv.) dropwise. The reaction mixture was stirred at 0℃ for 1 h, and TLC was adopted to monitor the reaction. Upon completion of the reaction, MeONa was quenched with saturated $NH_4Cl$ aqueous solution, and MeOH was removed by rotatory evaporator. The aqueous phase was then extracted with dichloromethane (200 mL × 3), and the organic layers were combined, dried over $Na_2SO_4$. **4-69** was obtained in 77% yield by flash column chromatography (PE:EA = 2:1).

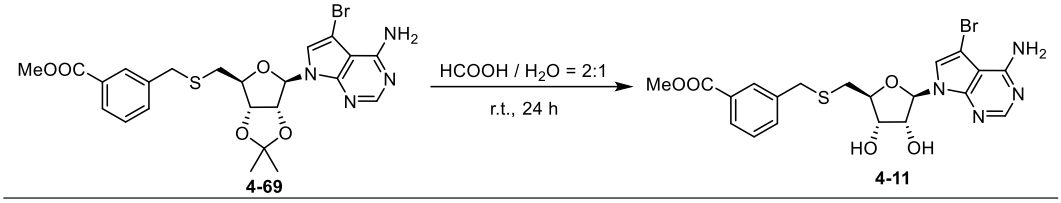


To 200 mg **4-69** and a magnetic stir bar in a 25 mL round-bottom flask were added 2 mL formic acid and 1 mL $H_2O$. The reaction mixture was stirred at room temperature for 24 h. Upon TLC indicated the completion of the reaction, solvents were removed by rotatory evaporator, and the crude mixture was purified by flash column chromatography (DCM:MeOH = 20:1 to 10:1). **4-11** was obtained in 70% yield.

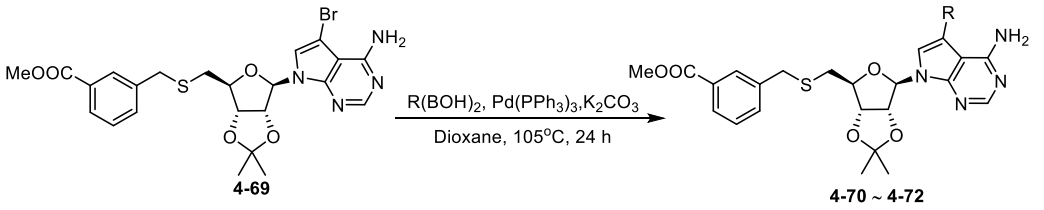


| | 4-70 | 4-71 | 4-72 |
|---|---|---|---|
| R | Ph– | | |

To 400 mg **4-69** each in three parallel 50 mL Schlenk tubes charged with magnetic stir bars was added $Pd(PPh_3)_4$ (80.1 mg, 10 mol%), corresponding boronic acids (1.5 equiv.) and $K_2CO_3$ (304 mg, 3 equiv.). The Schlenk tubes were then protected with $N_2$, and 5 mL dry and degassed dioxane was added to each of the solid mixtures. The reaction mixtures were heated to 105℃ for 24 h, and TLC was adopted to monitor the reaction process. Upon complete consumption of the starting material, the reaction mixtures were cooled to room temperature, and dioxane was removed by rotatory evaporator. **4-70** ~ **4-72** was obtained by flash column chromatography (PE:EA = 2:1), with 66% to 74% yields.

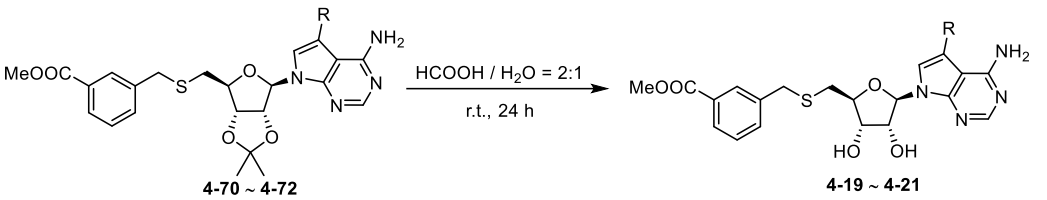


4-70 ~ 4-72 → 4-19 ~ 4-21

| | 4-19 | 4-20 | 4-21 |
|---|---|---|---|
| R | Ph– | 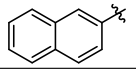 | 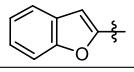 |

To 200 mg **4-70** ~ **4-72** and magnetic stir bars in three 25 mL round-bottom flasks were added 2 mL formic acid and 1 mL $H_2O$. The reaction mixtures were stirred at room temperature for 24 h. Upon TLC indicated the completion of the reactions, solvents were removed by rotatory evaporator, and the crude mixtures were purified by flash column chromatography (DCM:MeOH = 30:1 to 20:1). **4-19** ~ **4-21** were obtained in 82% to 88% yields.

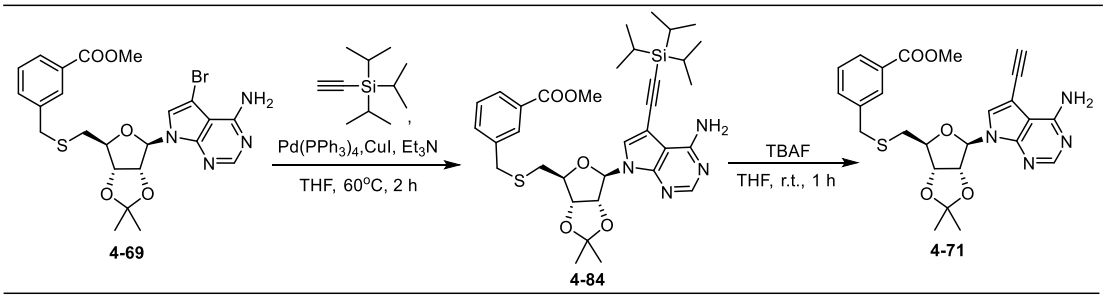


4-69 → 4-84 → 4-71

To 1 g **4-69** in a 100 mL Schlenk tube charged with a magnetic stir bar was added $Pd(PPh_3)_4$ (231.2 mg, 10 mol%) and CuI (114.2 mg, 30 mol%). The Schlenk tube was then protected with $N_2$, and 10 mL dry and degassed THF was added to the solid mixture. Ethynyltriisopropylsilane (1.2 mL, 3.0 equiv.) and $Et_3N$ (0.82 mL, 3 equiv.) were then added to the suspension. The reaction mixture was heated to 60°C for 2 h, and TLC was adopted to monitor the reaction process. The reaction mixture was cooled to room temperature, and THF was removed by rotatory evaporator. The crude mixture was filtered through a short silica gel column and washed with DCM. The filtrate was concentrated and then dissolved again in 10 mL THF. 1M TBAF (2.25 mL, 1.5 equiv.) was then added to the solution dropwise. **4-71** was obtained by flash column chromatography (PE:EA = 2:1 to 1:1) with 21% yield for 2 steps, and **4-69** was

recovered.

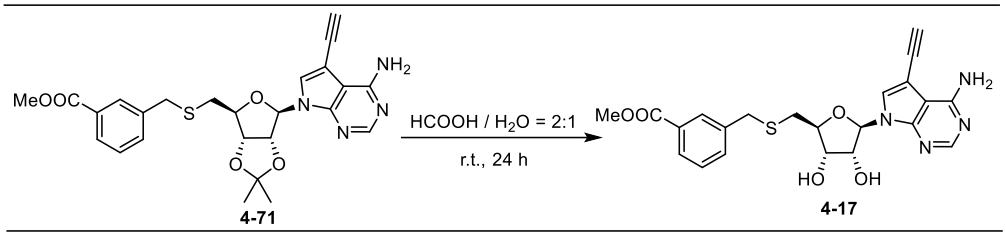


To 100 mg **4-71** and a magnetic stir bar in a 10 mL round-bottom flask were added 1 mL formic acid and 0.5 mL $H_2O$. The reaction mixture was stirred at room temperature for 24 h. Upon TLC indicated the completion of the reaction, solvents were removed by rotatory evaporator, and the crude mixture was purified by flash column chromatography (DCM:MeOH = 30:1 to 20:1). **4-17** was obtained in 83% yield.

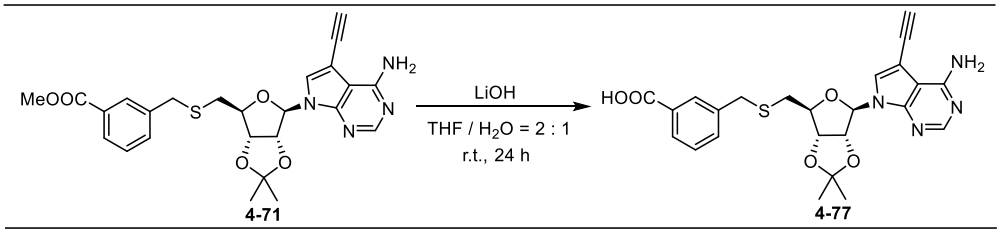


To 200 mg **4-71** in a 25 mL round-bottom flask were added LiOH (20 mg, 2.0 equiv.), 2 mL THF and 1 mL $H_2O$. A magnetic stir bar was charged to the flask. The reaction mixture was stirred at room temperature for 24 h. Upon TLC indicated the completion of the reaction, THF was removed by rotatory evaporator, and the aqueous phase was extracted with dichloromethane (5 mL × 3) to remove organic impurities. The aqueous phase was kept, and its pH was adjusted to ~ 5 with 1M HCl. Then the aqueous phase was extracted with dichloromethane (10 mL × 3). The organic phase was combined, dried over $Na_2SO_4$, and dichloromethane was removed by rotatory evaporator. The crude mixture was directly used for the next step.

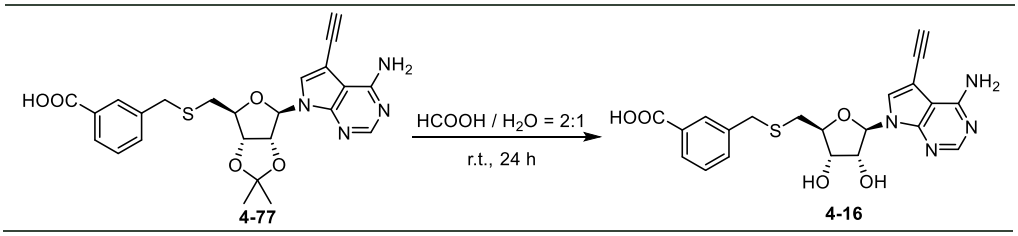


To the crude mixture from the above step in a 10 mL round-bottom flask was charged with a magnetic stir bar. 1 mL formic acid and 0.5 mL $H_2O$ was added to the flask. The reaction mixture was stirred at room temperature for 24 h. Upon TLC indicated the completion of the reaction, solvents were removed by rotatory evaporator, and the crude mixture was purified by flash column chromatography (DCM:MeOH = 10:1). **4-16** was obtained in 73% yield for 2 steps.

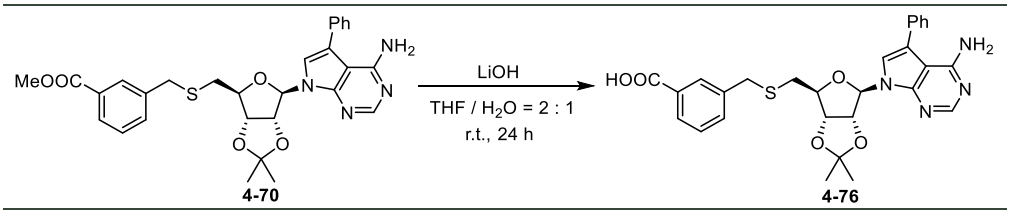


To 500 mg **4-70** in a 25 mL round-bottom flask was added LiOH (45 mg, 2.0 equiv.), 4 mL THF and 2 mL $H_2O$. A magnetic stir bar was charged to the flask. The reaction mixture was stirred at room temperature for 24 h. Upon TLC indicated the completion of the reaction, THF was removed by rotatory evaporator, and the aqueous phase was extracted with dichloromethane (10 mL × 3) to remove organic impurities. The aqueous phase was kept, and its pH was adjusted to ~ 5 with 1M HCl. The aqueous phase was then extracted with dichloromethane (25 mL × 3). The organic phases were combined, dried over $Na_2SO_4$, and dichloromethane was removed by rotatory evaporator. The crude mixture was directly used for the next step.

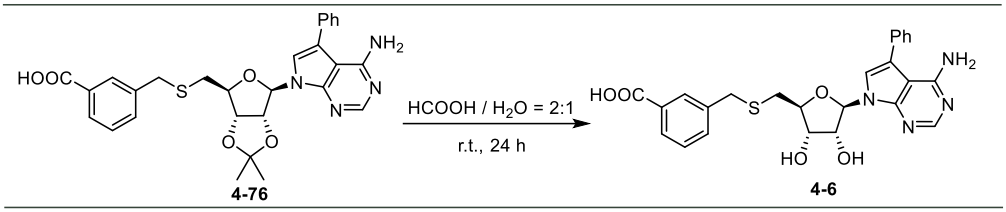


To the crude mixture from the above step in a 50 mL round-bottom flask was charged with a magnetic stir bar. 4 mL formic acid and 2 mL $H_2O$ were added to the flask. The reaction mixture was stirred at room temperature for 24 h. Upon TLC indicated the completion of the reaction, solvents were removed by rotatory evaporator, and the crude mixture was purified by flash column chromatography (DCM:MeOH = 10:1). **4-6** was obtained in 76% yield for 2 steps.

***Physical Characterization of Products***

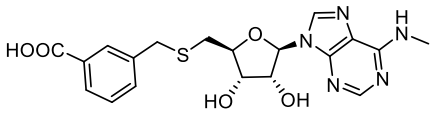

**3-(((((2*S*,3*S*,4*R*,5*R*)-3,4-dihydroxy-5-(6-(methylamino)-9*H*-purin-9-yl)tetrahydrofuran-2-yl)methyl)thio)methyl)benzoic acid (4-1)**: White solid. HPLC purity: 99.13%. $^1$H NMR (600 MHz, DMSO-$d_6$) δ 8.32 (s, 1H), 8.22 (s, 1H), 7.89 (s, 1H), 7.80 (d, $J$ = 7.7 Hz, 1H), 7.75 (s, 1H), 7.46 (d, $J$ = 7.4 Hz, 1H), 7.39 (t, $J$ = 7.6 Hz, 1H), 5.88 (d, $J$ = 5.5 Hz, 1H), 5.48 (d, $J$ = 5.8 Hz, 1H), 5.30 (s, 1H), 4.73 (d, $J$ = 5.0 Hz, 1H), 4.16 (s, 1H), 4.01 (q, $J$ = 5.8 Hz, 1H), 3.82 (s, 2H), 2.95 (s, 3H), 2.84 (dd, $J$ = 13.8, 5.9 Hz, 1H), 2.71 (dd, $J$ = 13.9, 6.9 Hz, 1H) ppm. $^{13}$C NMR (101 MHz, DMSO-$d_6$) δ 167.74, 155.50, 153.17, 149.35, 140.16, 139.56, 133.73, 131.53, 130.12, 129.07, 128.30, 120.10, 88.04, 84.07, 73.00, 35.67, 33.83, 27.44 ppm.

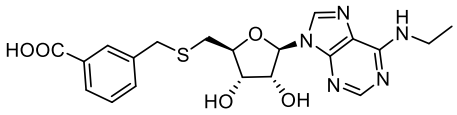

**3-(((((2*S*,3*S*,4*R*,5*R*)-5-(6-(ethylamino)-9*H*-purin-9-yl)-3,4-dihydroxytetrahydrofuran-2-yl)methyl)thio)methyl)benzoic acid (4-2)**: White solid. HPLC purity: 94.05%. $^1$H NMR (400 MHz, DMSO-$d_6$) δ 8.32 (s, 1H), 8.20 (s, 1H), 7.89 (s, 1H), 7.80 (d, $J$ = 7.6 Hz, 2H), 7.47 (d, $J$ = 7.7 Hz, 1H), 7.39 (t, $J$ = 7.6 Hz, 1H), 5.89 (d, $J$ = 5.5 Hz, 1H), 5.48 (s, 1H), 5.31 (s, 1H), 4.74 (s, 1H), 4.17 (t, $J$ = 4.4 Hz, 1H), 4.02 (q, $J$ = 6.3 Hz, 1H), 3.51 (s, 2H), 2.85 (dd, $J$ = 13.8, 5.9 Hz, 1H), 2.71 (dd, $J$ = 13.8, 6.9 Hz, 1H), 1.17 (t, $J$ = 7.1

Hz, 3H) ppm. $^{13}$C NMR (101 MHz, DMSO-$d_6$) δ 167.67, 154.95, 153.13, 148.89, 140.15, 139.61, 133.77, 131.43, 130.15, 129.04, 128.28, 120.07, 88.10, 84.09, 73.06, 73.03, 35.69, 35.01, 33.87, 15.28 ppm. HRMS (ESI): calcd. for $C_{20}H_{24}N_5O_5S^+$: 446.1498. found: 446.1507.

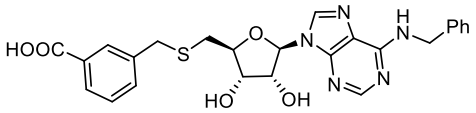

**3-(((((2*S*,3*S*,4*R*,5*R*)-5-(6-(benzylamino)-9*H*-purin-9-yl)-3,4-dihydroxytetrahydrofuran-2-yl)methyl)thio)methyl)benzoic acid (4-3)**: White solid. HPLC purity: 96.99%. $^1$H NMR (600 MHz, DMSO-$d_6$) δ 8.37 (s, 1H), 8.20 (s, 1H), 7.83 (s, 1H), 7.71 (d, $J$ = 7.0 Hz, 1H), 7.33 (d, $J$ = 7.5 Hz, 2H), 7.28 (t, $J$ = 7.6 Hz, 2H), 7.21 (dt, $J$ = 14.5, 7.8 Hz, 3H), 5.89 (d, $J$ = 5.6 Hz, 1H), 4.82 – 4.59 (m, 3H), 4.16 (t, $J$ = 4.2 Hz, 1H), 4.04 – 3.97 (m, 1H), 3.77 (s, 2H), 2.84 (dd, $J$ = 13.9, 6.0 Hz, 1H), 2.70 (dd, $J$ = 13.9, 6.7 Hz, 1H) ppm. $^{13}$C NMR (151 MHz, DMSO-$d_6$) δ 167.79, 154.90, 153.08, 149.23, 140.48, 139.50, 133.58, 131.85, 130.13, 128.98, 128.68, 128.27, 127.57, 127.09, 120.08, 88.15, 84.13, 73.06, 73.03, 43.32, 35.70, 33.87, 21.55 ppm. HRMS (ESI): calcd. for $C_{25}H_{26}N_5O_5S^+$: 508.1655. found: 508.1666.

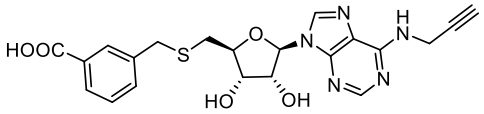

**3-(((((2*S*,3*S*,4*R*,5*R*)-3,4-dihydroxy-5-(6-(prop-2-yn-1-ylamino)-9*H*-purin-9-yl)-tetrahydrofuran-2-yl)methyl)thio)methyl)benzoic acid (4-4)**: White solid. HPLC purity: 97.02%. $^1$H NMR (600 MHz, DMSO-$d_6$) δ 8.38 (s, 1H), 8.27 (s, 1H), 8.20 (s, 1H), 7.89 (s, 1H), 7.80 (d, $J$ = 7.7 Hz, 1H), 7.45 (d, $J$ = 7.6 Hz, 1H), 7.38 (t, $J$ = 7.6 Hz, 1H), 5.90 (d, $J$ = 5.5 Hz, 1H), 5.50 (d, $J$ = 5.6 Hz, 1H), 5.31 (s, 1H), 4.74 (q, $J$ = 5.0 Hz, 1H), 4.25 (s, 2H), 4.17 (s, 1H), 4.02 (t, $J$ = 6.0 Hz, 1H), 3.82 (s, 2H), 3.03 (s, 1H), 2.85 (dd, $J$ = 13.8, 5.9 Hz, 1H), 2.71 (dd, $J$ = 13.8, 6.9 Hz, 1H) ppm. $^{13}$C NMR (151 MHz, DMSO-$d_6$) δ 167.72, 154.31, 152.93, 149.62, 140.78, 139.55, 133.73, 131.49, 130.11, 129.06, 128.29, 120.23, 88.15, 84.15, 82.30, 73.02, 72.80, 35.68, 33.82, 29.55 ppm. HRMS (ESI): calcd. for $C_{21}H_{22}N_5O_5S^+$: 456.1342. found: 456.1350.

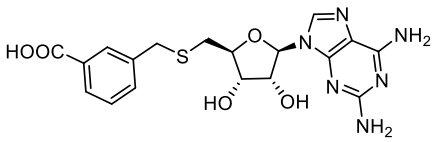

**3-(((((2*S*,3*S*,4*R*,5*R*)-5-(2,6-diamino-9*H*-purin-9-yl)-3,4-dihydroxytetrahydrofuran-2-yl)methyl)-thio)methyl)benzoic acid (4-5)**: Cream yellow solid. HPLC purity: 89.71%. $^{1}$H NMR (400 MHz, DMSO-$d_6$) δ 7.90 (s, 2H), 7.80 (d, *J* = 7.7 Hz, 1H), 7.49 (d, *J* = 7.6 Hz, 1H), 7.40 (t, *J* = 7.6 Hz, 1H), 6.70 (s, 2H), 5.80 (s, 2H), 5.72 (d, *J* = 5.8 Hz, 1H), 5.43 (d, *J* = 5.9 Hz, 1H), 5.20 (d, *J* = 5.1 Hz, 1H), 4.62 (q, *J* = 4.0 Hz, 1H), 4.07 (q, *J* = 4.9 Hz, 1H), 3.95 (q, *J* = 6.2 Hz, 1H), 3.83 (s, 2H), 2.81 (dd, *J* = 13.8, 5.9 Hz, 1H), 2.68 (dd, *J* = 13.7, 6.8 Hz, 1H) ppm. $^{13}$C NMR (101 MHz, DMSO-$d_6$) δ 167.70, 160.74, 156.59, 152.40, 139.63, 136.48, 133.81, 131.46, 130.16, 129.08, 128.27, 113.79, 87.07, 83.73, 73.09, 72.85, 35.66, 33.96 ppm. HRMS (ESI): calcd. for $C_{18}H_{21}N_6O_5S^+$: 433.1294. found: 433.1302.

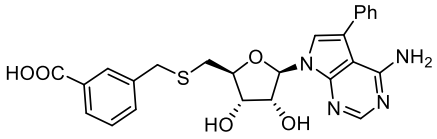

**3-(((((2*S*,3*S*,4*R*,5*R*)-5-(4-amino-5-phenyl-7*H*-pyrrolo-[2,3-*d*]pyrimidin-7-yl)-3,4-dihydro-xytetrahydrofuran-2-yl)methyl)thio)methyl)-benzoic acid (4-6)**: White solid. HPLC purity: 95.75%. $^{1}$H NMR (600 MHz, DMSO-d6) δ 8.19 (s, 1H), 8.02 (d, *J* = 8.4 Hz, 1H), 8.00 – 7.92 (m, 3H), 7.90 (d, *J* = 2.0 Hz, 1H), 7.83 – 7.71 (m, 1H), 7.67 – 7.59 (m, 2H), 7.59 – 7.48 (m, 3H), 7.37 (t, *J* = 7.7 Hz, 1H), 6.19 (d, *J* = 5.6 Hz, 2H), 5.45 (d, *J* = 6.2 Hz, 1H), 5.28 (d, *J* = 5.3 Hz, 1H), 4.55 (q, *J* = 5.7 Hz, 1H), 4.10 (q, *J* = 4.8 Hz, 1H), 4.01 (td, *J* = 6.2, 4.1 Hz, 1H), 3.85 (d, *J* = 3.6 Hz, 2H), 2.85 (dd, *J* = 13.8, 5.8 Hz, 1H), 2.69 (dd, *J* = 13.8, 6.5 Hz, 1H). $^{13}$C NMR (101 MHz, DMSO) δ 167.74, 157.69, 152.36, 151.60, 139.53, 134.70, 133.78, 131.43, 130.10, 129.51, 129.10, 128.91, 128.29, 127.52, 121.14, 117.34, 100.81, 87.22, 83.31, 73.54, 72.97, 35.77, 33.97 ppm. HRMS (ESI): calcd. for $C_{25}H_{25}N_4O_5S^+$: 493.1546. found: 493.1554.

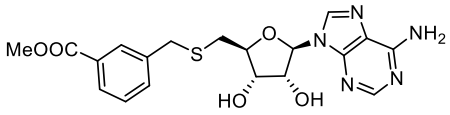

**Methyl 3-(((((2*S*,3*S*,4*R*,5*R*)-5-(6-amino-9*H*-purin-9-yl)-3,4-dihydroxytetrahydrofuran-2-yl)-methyl)thio)methyl)benzoate (4-7)**: White solid. HPLC purity: 99.72%. $^{1}$H NMR (400 MHz, DMSO-$d_6$) δ 8.33 (s, 1H), 8.13 (s, 1H), 7.90 (s, 1H), 7.82 (d, *J* = 7.7 Hz,

1H), 7.51 (d, *J* = 7.7 Hz, 1H), 7.42 (t, *J* = 7.7 Hz, 1H), 7.29 (s, 2H), 5.88 (d, *J* = 5.5 Hz, 1H), 5.49 (d, *J* = 5.9 Hz, 1H), 5.30 (d, *J* = 5.2 Hz, 1H), 4.73 (q, *J* = 5.5 Hz, 1H), 4.16 (q, *J* = 4.7 Hz, 1H), 4.05 – 3.97 (m, 1H), 3.85 (s, 3H), 3.83 (s, 2H), 2.84 (dd, *J* = 13.9, 5.8 Hz, 1H), 2.70 (dd, *J* = 13.9, 7.0 Hz, 1H) ppm. $^{13}$C NMR (101 MHz, DMSO-*d*$_6$) δ 166.56, 156.57, 153.12, 149.87, 140.43, 139.91, 134.21, 130.25, 129.94, 129.25, 128.11, 119.68, 88.08, 84.12, 73.07, 72.97, 52.63, 35.57, 33.81 ppm. HRMS (ESI): calcd. for $C_{19}H_{22}N_5O_5S^+$: 432.1342. found: 432.1347.

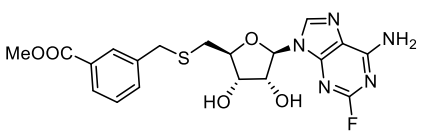


**Methyl 3-(((((2*S*,3*S*,4*R*,5*R*)-5-(6-amino-2-fluor-o-9*H*-purin-9-yl)-3,4-dihydroxytetrahydrofura-n-2-yl)methyl)thio)methyl)benzoate (4-8)**: White solid. HPLC purity: 95.02%. $^{1}$H NMR (600 MHz, DMSO-*d*$_6$) δ 8.13 (s, 1H), 7.89 (s, 1H), 7.80 (d, *J* = 7.5 Hz, 1H), 7.42 (d, *J* = 7.4 Hz, 1H), 7.36 (t, *J* = 7.5 Hz, 1H), 7.27 (s, 2H), 5.79 (d, *J* = 5.3 Hz, 1H), 4.72 (t, *J* = 5.1 Hz, 1H), 4.20 (t, *J* = 4.2 Hz, 1H), 4.03 – 3.97 (m, 1H), 3.81 (s, 2H), 3.77 (s, 3H), 2.83 (dd, *J* = 13.7, 5.6 Hz, 1H), 2.71 (dd, *J* = 13.8, 6.9 Hz, 1H) ppm. $^{13}$C NMR (151 MHz, DMSO-*d*$_6$) δ 168.02, 162.32, 157.34, 151.36, 139.45, 139.38, 133.52, 131.98, 130.12, 128.94, 128.27, 116.20, 88.21, 84.00, 73.11, 72.77, 54.45, 35.69, 33.91 ppm. $^{19}$F NMR (377 MHz, DMSO-*d*$_6$) δ -51.67. HRMS (ESI): calcd. for $C_{19}H_{21}N_5O_5^+$: 450.1247. found: 450.1255.

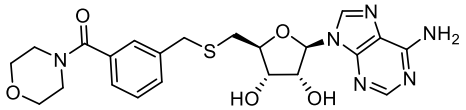


**3-(((((2*S*,3*S*,4*R*,5*R*)-5-(6-amino-9*H*-purin-9-yl)-3,4-dihydroxytetrahydrofuran-2-yl)methyl)thio)methyl)phenyl)(morpholino)methanone (4-9)**: White solid. HPLC purity: 92.34%. $^{1}$H NMR (400 MHz, Methanol-*d*$_4$) δ 8.30 (s, 1H), 8.21 (s, 1H), 7.47 – 7.21 (m, 4H), 5.99 (d, J = 4.9 Hz, 1H), 5.51 (s, 1H), 4.78 (t, J = 5.1 Hz, 1H), 4.31 (t, J = 5.1 Hz, 1H), 4.16 (q, J = 5.7 Hz, 1H), 3.94 – 3.35 (m, 11H), 2.90 (dd, J = 14.2, 5.5 Hz, 1H), 2.79 (dd, J = 14.2, 6.1 Hz, 1H) ppm. $^{13}$C NMR (151 MHz, Methanol-*d*$_4$) δ 170.95, 155.98, 152.55, 149.30, 140.10, 139.44, 135.22, 130.49, 128.52, 127.22, 125.29, 88.82, 84.26, 73.30, 72.64, 66.37, 43.56, 35.71, 32.86 ppm. HRMS (ESI): calcd. for $C_{22}H_{27}N_6O_5S^+$: 487.1764. found: 487.1771.

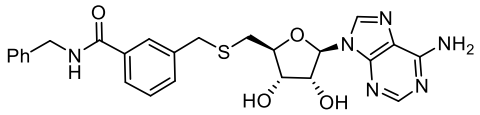

**3-(((((2*S*,3*S*,4*R*,5*R*)-5-(6-amino-9*H*-purin-9-yl)-3,4-dihydroxytetrahydrofuran-2-yl)methyl)thio)meth-yl)-*N*-benzylbenzamide (4-10)**: White solid. HPLC purity: 93.62%. $^{1}$H NMR (400 MHz, DMSO-$d_6$) δ 9.03 (t, $J$ = 5.9 Hz, 1H), 8.34 (s, 1H), 8.14 (s, 1H), 7.83 (s, 1H), 7.76 (d, $J$ = 6.9 Hz, 1H), 7.41 – 7.20 (m, 9H), 5.88 (d, $J$ = 5.5 Hz, 1H), 5.50 (d, $J$ = 6.0 Hz, 1H), 5.31 (d, $J$ = 5.2 Hz, 1H), 4.74 (q, $J$ = 5.6 Hz, 1H), 4.47 (d, $J$ = 6.0 Hz, 2H), 4.16 (q, $J$ = 5.0 Hz, 1H), 4.02 (q, $J$ = 6.3 Hz, 1H), 3.80 (s, 2H), 2.86 (dd, $J$ = 13.9, 5.9 Hz, 1H), 2.72 (dd, $J$ = 13.8, 6.9 Hz, 1H) ppm. $^{13}$C NMR (101 MHz, DMSO-$d_6$) δ 166.56, 156.53, 153.16, 149.88, 140.43, 140.09, 139.28, 134.97, 132.19, 128.81, 128.76, 128.29, 127.69, 127.22, 126.18, 119.62, 88.02, 84.06, 73.06, 72.99, 43.08, 35.92, 33.94 ppm. HRMS (ESI): calcd. for $C_{25}H_{27}N_6O_4S^+$: 507.1814. found: 507.1825.

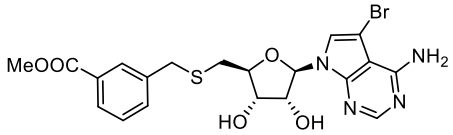

**Methyl 3-(((((2*S*,3*S*,4*R*,5*R*)-5-(4-amino-5-bromo-7*H*-pyrrolo[2,3-*d*]pyrimidin-7-yl)-3,4-dihydroxytetrahy-drofuran-2-yl)methyl)thio)methyl)benzoate (4-11)**: White solid. HPLC purity: 97.64%. $^{1}$H NMR (400 MHz, DMSO-$d_6$) δ 8.10 (s, 1H), 7.91 (s, 1H), 7.83 (d, $J$ = 7.8 Hz, 1H), 7.60 (s, 1H), 7.53 (d, $J$ = 7.8 Hz, 1H), 7.44 (t, $J$ = 7.7 Hz, 1H), 6.79 (s, 2H), 6.06 (d, $J$ = 5.8 Hz, 1H), 5.40 (d, $J$ = 6.2 Hz, 1H), 5.24 (d, $J$ = 5.2 Hz, 1H), 4.43 (q, $J$ = 5.8 Hz, 1H), 4.02 (q, $J$ = 5.2 Hz, 1H), 3.95 (q, $J$ = 4.0 Hz, 1H), 3.84 (s, 5H), 2.81 (dd, $J$ = 13.8, 6.0 Hz, 1H), 2.65 (dd, $J$ = 13.8, 6.6 Hz, 1H) ppm. $^{13}$C NMR (101 MHz, DMSO-$d_6$) δ 166.57, 157.43, 153.11, 150.40, 139.89, 134.24, 130.26, 129.95, 129.30, 128.15, 122.11, 101.47, 87.77, 87.13, 83.55, 73.45, 72.95, 52.64, 35.60, 33.91 ppm. HRMS (ESI): calcd. for $C_{20}H_{22}O_5N_4BrS$: 509.0494. found: 509.0498.

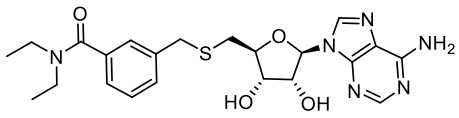

**3-(((((2*S*,3*S*,4*R*,5*R*)-5-(6-amino-9*H*-purin-9-yl)-3,4-dihydroxytetrahydrofuran-2-yl)methyl)thio)methyl)-*N*,*N*-diethylbenzamide (4-12)**: White solid. HPLC purity: 98.95%. $^{1}$H NMR (400 MHz, Methanol-$d_4$) δ 8.30 (s, 1H), 8.20 (s, 1H), 7.38 – 7.30 (m, 3H), 7.28 – 7.15 (m, 1H), 6.00 (d, $J$ = 4.8 Hz, 1H), 4.79 (t, $J$ = 5.1 Hz, 1H), 4.32 (t, $J$ = 5.1

Hz, 1H), 4.18 (q, *J* = 5.5 Hz, 1H), 3.88 – 3.74 (m, 2H), 3.54 (q, *J* = 7.4 Hz, 2H), 3.34 – 3.32 (m, 1H), 3.24 (q, *J* = 6.6 Hz, 2H), 2.90 (dd, *J* = 14.2, 5.4 Hz, 1H), 2.78 (dd, *J* = 14.2, 6.2 Hz, 1H), 1.25 (t, *J* = 6.9 Hz, 3H), 1.08 (t, *J* = 6.8 Hz, 3H) ppm. $^{13}$C NMR (101 MHz, Methanol-*d*$_4$) δ 172.02, 155.96, 152.55, 149.27, 140.10, 139.28, 136.82, 129.92, 128.43, 126.37, 124.44, 119.20, 88.81, 84.26, 73.35, 72.65, 43.55, 39.47, 35.75, 32.84, 12.98, 11.68 ppm. HRMS (ESI): calcd. for $C_{22}H_{29}N_6O_4S^+$: 473.1971. found: 473.1978.

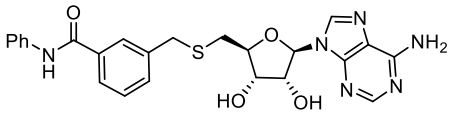

**3-(((((2*S*,3*S*,4*R*,5*R*)-5-(6-amino-9*H*-purin-9-yl)-3,4-dihydroxytetrahydrofuran-2-yl)methyl)thio)methyl)-*N*-phenylbenzamide (4-13)**: White solid. HPLC purity: 99.25%. $^1$H NMR (400 MHz, DMSO-*d*$_6$) δ 10.24 (s, 1H), 8.35 (s, 1H), 8.14 (s, 1H), 7.87 (s, 1H), 7.82 (d, *J* = 6.0 Hz, 1H), 7.75 (d, *J* = 7.8 Hz, 2H), 7.52 – 7.29 (m, 5H), 7.10 (t, *J* = 7.2 Hz, 1H), 5.89 (d, *J* = 5.3 Hz, 1H), 5.55 (d, *J* = 5.3 Hz, 1H), 5.36 (d, *J* = 4.5 Hz, 1H), 4.74 (q, *J* = 5.5 Hz, 1H), 4.18 (q, *J* = 4.6 Hz, 1H), 4.04 (q, *J* = 5.8 Hz, 1H), 3.84 (s, 2H), 2.88 (dd, *J* = 13.8, 5.5 Hz, 1H), 2.74 (dd, *J* = 13.8, 6.8 Hz, 1H), 2.51 (s, 3H) ppm. $^{13}$C NMR (101 MHz, DMSO-*d*$_6$) δ 165.86, 156.57, 153.17, 149.91, 140.43, 139.59, 139.42, 135.65, 132.47, 129.08, 128.84, 128.64, 126.61, 124.17, 120.91, 119.68, 88.08, 84.07, 73.10, 73.03, 35.94, 34.02 ppm. HRMS (ESI): calcd. for $C_{24}H_{25}N_6O_4S^+$: 493.1658. found: 493.1666.

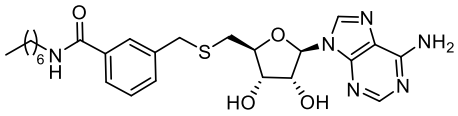

**3-(((((2*S*,3*S*,4*R*,5*R*)-5-(6-amino-9*H*-purin-9-yl)-3,4-dihydroxytetrahydrofuran-2-yl)methyl)thio)methyl)-*N*-heptylbenzamide (4-14)**: White solid. HPLC purity: 99.38%. $^1$H NMR (400 MHz, DMSO-*d*$_6$)δ 8.41 (t, *J* = 5.5 Hz, 1H), 8.35 (s, 1H), 8.15 (s, 1H), 7.78 (s, 1H), 7.69 (d, *J* = 6.8 Hz, 1H), 7.40 – 7.26 (m, 4H), 5.90 (d, *J* = 5.5 Hz, 1H), 5.51 (d, *J* = 6.0 Hz, 1H), 5.32 (d, *J* = 5.2 Hz, 1H), 4.75 (q, *J* = 5.5 Hz, 1H), 4.17 (q, *J* = 4.9 Hz, 1H), 4.03 (q, *J* = 6.2 Hz, 1H), 3.80 (s, 2H), 3.24 (q, *J* = 6.7 Hz, 2H), 2.86 (dd, *J* = 13.9, 5.8 Hz, 1H), 2.72 (dd, *J* = 13.8, 6.9 Hz, 1H), 1.57 – 1.45 (m, 2H), 1.33 – 1.21 (m, 8H), 0.85 (t, *J* = 6.8 Hz, 3H) ppm. $^{13}$C NMR (101 MHz, DMSO-*d*$_6$) δ 166.36, 156.57, 153.15, 149.90, 140.41, 139.14, 135.41, 131.89, 128.66, 128.20, 126.05, 119.67, 88.04, 84.06,

73.09, 73.01, 35.97, 33.98, 31.70, 29.57, 28.92, 26.93, 22.53, 14.42 ppm. HRMS (ESI): calcd. for $C_{25}H_{35}N_6O_4S^+$: 515.2440. found: 515.2451.

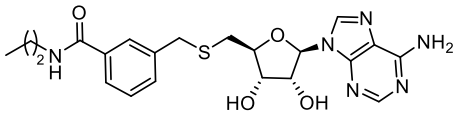

**3-(((((2*S*,3*S*,4*R*,5*R*)-5-(6-amino-9*H*-purin-9-yl)-3,4-dihydroxytetrahydrofuran-2-yl)methyl)thio)methyl)-*N*-propylbenzamide (4-15)**: White solid. HPLC purity: 96.03%. $^1$H NMR (400 MHz, Methanol-$d_4$) δ 8.30 (s, 1H), 8.20 (s, 1H), 7.78 (s, 1H), 7.67 (d, $J$ = 7.7 Hz, 1H), 7.41 (d, $J$ = 7.7 Hz, 1H), 7.35 (t, $J$ = 7.6 Hz, 1H), 6.01 (d, $J$ = 4.7 Hz, 1H), 4.77 (t, $J$ = 5.0 Hz, 1H), 4.63 (s, 2H), 4.33 (t, $J$ = 5.1 Hz, 1H), 4.21 (q, $J$ = 5.5 Hz, 1H), 3.89 – 3.77 (m, 2H), 2.92 (dd, $J$ = 14.1, 5.3 Hz, 1H), 2.81 (dd, $J$ = 14.2, 6.2 Hz, 1H), 1.64 (h, $J$ = 7.2 Hz, 2H), 0.98 (t, $J$ = 7.4 Hz, 3H) ppm. $^{13}$C NMR (101 MHz, Methanol-$d_4$) δ 168.76, 155.93, 152.50, 149.24, 140.07, 139.03, 134.79, 134.75, 131.79, 128.20, 127.48, 125.46, 119.19, 88.85, 84.22, 73.43, 72.67, 41.53, 41.40, 35.91, 32.98, 22.32, 10.38 ppm. HRMS (ESI): calcd. for $C_{21}H_{27}N_6O_4S^+$: 459.1814. found: 459.1822.

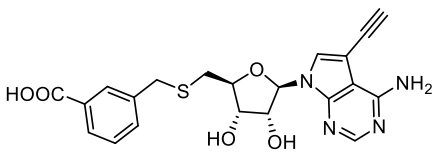

**3-(((((2*S*,3*S*,4*R*,5*R*)-5-(4-amino-5-ethynyl-7*H*-pyrrolo-[2,3-*d*]pyrimidin-7-yl)-3,4-dihydroxytetrahydrofuran-2-yl)methyl)thio)methyl)-benzoic acid (4-16)**: White solid. HPLC purity: 97.03%. $^1$H NMR (400 MHz, DMSO-$d_6$) δ 8.13 (s, 1H), 7.90 (s, 1H), 7.83 – 7.75 (m, 2H), 7.49 (d, $J$ = 7.6 Hz, 1H), 7.41 (t, $J$ = 7.6 Hz, 1H), 6.04 (d, $J$ = 5.7 Hz, 1H), 5.42 (s, 1H), 5.27 (s, 1H), 4.46 (s, 1H), 4.29 (s, 1H), 4.04 (t, $J$ = 4.4 Hz, 1H), 3.97 (t, $J$ = 5.0 Hz, 1H), 3.83 (s, 2H), 2.82 (dd, $J$ = 13.8, 6.0 Hz, 1H), 2.67 (dd, $J$ = 13.8, 6.6 Hz, 1H) ppm. $^{13}$C NMR (151 MHz, DMSO) δ 167.66, 158.01, 153.48, 150.35, 139.59, 133.77, 130.16, 129.07, 128.29, 127.76, 102.80, 94.91, 87.47, 83.68, 83.59, 77.69, 73.52, 72.98, 35.72, 33.95 ppm. HRMS (ESI): calcd. for $C_{21}H_{21}N_4O_5S^+$: 441.1233. found: 441.1231.

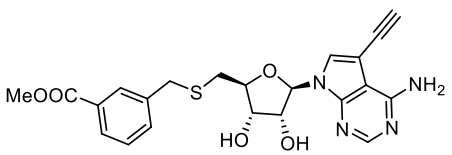

**Methyl 3-(((((2*S*,3*S*,4*R*,5*R*)-5-(4-amino-5-ethynyl-7*H*-pyrrolo[2,3-*d*]pyrimidin-7-yl)-3,4-dihydroxytetrahydrofuran-2-yl)methyl)thio)methyl)benzoate (4-17)**: Light brown solid. HPLC purity: 94.75%. $^{1}$H NMR (400 MHz, DMSO-$d_6$) δ 8.13 (s, 1H), 7.91 (s, 1H), 7.83 (d, $J$ = 7.6 Hz, 1H), 7.78 (s, 1H), 7.54 (d, $J$ = 7.6 Hz, 1H), 7.44 (t, $J$ = 7.6 Hz, 1H), 6.04 (d, $J$ = 5.6 Hz, 1H), 5.44 (d, $J$ = 6.0 Hz, 1H), 5.28 (d, $J$ = 5.0 Hz, 1H), 4.46 (q, $J$ = 5.6 Hz, 1H), 4.31 (s, 1H), 4.08 – 4.01 (m, 1H), 3.96 (q, $J$ = 6.1 Hz, 1H), 3.85 (s, 5H), 2.82 (dd, $J$ = 13.8, 5.9 Hz, 1H), 2.66 (dd, $J$ = 13.8, 6.6 Hz, 1H) ppm. $^{13}$C NMR (101 MHz, DMSO-$d_6$) δ 166.57, 158.01, 153.48, 150.33, 139.88, 134.23, 130.26, 129.95, 129.28, 128.14, 127.74, 102.79, 94.92, 87.49, 83.69, 83.62, 77.68, 73.53, 72.99, 52.63, 35.63, 33.89 ppm. HRMS (ESI): calcd. for $C_{22}H_{23}N_4O_5S^+$: 455.1389. found: 455.1397.

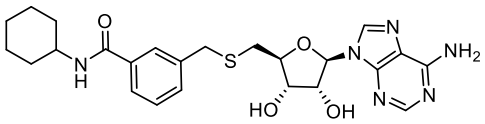

**3-(((((2*S*,3*S*,4*R*,5*R*)-5-(6-amino-9*H*-purin-9-yl)-3,4-dihydroxytetrahydrofuran-2-yl)methyl)thio)-methyl)-*N*-cyclohexylbenzamide (4-18)**: White solid. HPLC purity: 98.05%. $^{1}$H NMR (600 MHz, DMSO-$d_6$) δ 8.34 (s, 1H), 8.20 (d, $J$ = 7.9 Hz, 1H), 8.15 (s, 1H), 7.75 (s, 1H), 7.68 (d, $J$ = 6.9 Hz, 1H), 7.34 (q, $J$ = 7.8 Hz, 2H), 7.27 (s, 2H), 5.89 (d, $J$ = 5.5 Hz, 1H), 5.57 (d, $J$ = 5.9 Hz, 1H), 5.39 (d, $J$ = 5.1 Hz, 1H), 4.74 (q, $J$ = 5.5 Hz, 1H), 4.17 (q, $J$ = 4.8 Hz, 1H), 4.03 (q, $J$ = 6.0 Hz, 1H), 3.79 (s, 2H), 2.85 (dd, $J$ = 13.9, 5.7 Hz, 1H), 2.72 (dd, $J$ = 13.9, 6.9 Hz, 1H), 1.80 (m, 2H), 1.73 (m, 2H), 1.61 (d, $J$ = 12.1 Hz, 1H), 1.30 (m, 4H), 1.12 (m, 1H) ppm. $^{13}$C NMR (101 MHz, DMSO-$d_6$) δ 165.91, 156.41, 153.18, 149.81, 140.48, 139.04, 135.41, 131.93, 128.67, 128.22, 126.23, 119.52, 88.04, 84.05, 73.00, 48.89, 35.92, 33.90, 32.78, 25.64, 25.38 ppm. HRMS (ESI): calcd. for $C_{24}H_{31}N_6O_4S^+$: 499.2127. found: 499.2135.

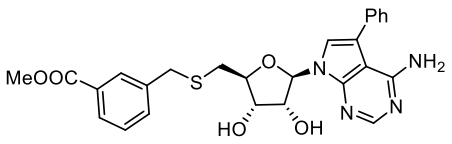


**Methyl 3-(((((2*S*,3*S*,4*R*,5*R*)-5-(4-amino-5-phenyl-7*H*-pyrrolo[2,3-*d*]pyrimidin-7-yl)-3,4-dihydroxytetrahydrofuran-2-yl)methyl)thio)methyl)benzoate (4-19)**: White solid. HPLC purity: 99.13%. $^{1}$H NMR (400 MHz, DMSO-$d_6$) δ 8.16 (s, 1H), 7.89 (s, 1H), 7.79 (d, *J* = 7.7 Hz, 1H), 7.52 – 7.44 (m, 6H), 7.37 (q, *J* = 7.7, 6.4 Hz, 2H), 6.16 (d, *J* = 5.7 Hz, 1H), 5.43 (d, *J* = 5.9 Hz, 1H), 5.28 (d, *J* = 4.2 Hz, 1H), 4.52 (q, *J* = 5.6 Hz, 1H), 4.08 (q, *J* = 4.6 Hz, 1H), 3.99 (q, *J* = 6.0 Hz, 1H), 3.83 (s, 3H), 2.84 (dd, *J* = 13.8, 5.8 Hz, 1H), 2.67 (dd, *J* = 13.8, 6.4 Hz, 1H) ppm. 13C NMR (101 MHz, DMSO-$d_6$) δ 167.69, 157.72, 152.38, 151.64, 139.57, 134.76, 133.78, 131.42, 130.12, 129.48, 129.08, 128.93, 128.28, 127.48, 121.18, 117.30, 100.82, 87.25, 83.32, 73.54, 73.00, 35.77, 33.99, 30.88 ppm. HRMS (ESI): calcd. for $C_{26}H_{27}N_4O_5S^+$: 507.1702. found: 507.1712.

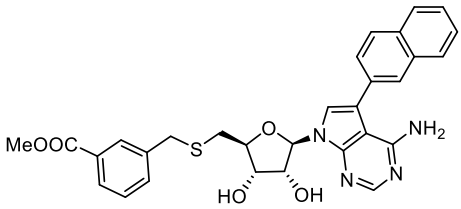


**Methyl 3-(((((2*S*,3*S*,4*R*,5*R*)-5-(4-amino-5-(naphtha-len-2-yl)-7*H*-pyrrolo[2,3-*d*]pyrimidin-7-yl)-3,4-dihydroxytetrahydrofuran-2-yl)methyl)thio)methyl)benzoate (4-20)**: White solid. HPLC purity: 98.57%. $^{1}$H NMR (400 MHz, $CDCl_3$) δ 8.26 (s, 1H), 7.98 (s, 1H), 7.95 – 7.84 (m, 5H), 7.53 (ddd, *J* = 21.7, 16.9, 8.2 Hz, 4H), 7.36 – 7.29 (m, 2H), 6.07 (d, *J* = 5.5 Hz, 1H), 5.25 (s, 2H), 4.53 (t, *J* = 5.4 Hz, 1H), 4.40 (q, *J* = 5.9 Hz, 1H), 4.33 (dd, *J* = 5.4, 3.4 Hz, 1H), 3.86 (s, 3H), 3.82 (s, 2H), 2.76 (p, *J* = 8.2 Hz, 2H) ppm. $^{13}$C NMR (101 MHz, $CDCl_3$) δ 171.33, 162.58, 157.58, 156.56, 144.61, 138.97, 138.43, 137.08, 137.00, 134.98, 134.67, 134.01, 133.72, 133.03, 132.89, 132.20, 131.89, 131.81, 131.19, 126.35, 122.13, 92.04, 88.14, 78.32, 77.79, 57.36, 40.43, 38.73 ppm. HRMS (ESI): calcd. for $C_{30}H_{29}N_4O_5^+$: 557.1859. found: 557.1860.

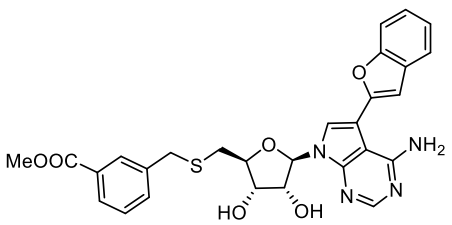

**Methyl 3-(((((2*S*,3*S*,4*R*,5*R*)-5-(4-amino-5-(benzofuran-2-yl)-7*H*-pyrrolo[2,3-*d*]pyrimidin-7-yl)-3,4-dihydroxytetrahydrofuran-2-yl)methyl)thio)methyl)benzoate (4-21)**: White solid. HPLC purity: 98.84%. $^{1}$H NMR (400 MHz, DMSO-$d_6$) δ 8.19 (s, 1H), 8.06 (s, 1H), 7.91 (s, 1H), 7.79 (d, $J$ = 7.9 Hz, 1H), 7.66 (t, $J$ = 8.1 Hz, 2H), 7.53 (d, $J$ = 7.6 Hz, 1H), 7.40 (t, $J$ = 7.7 Hz, 1H), 7.33 – 7.25 (m, 2H), 7.13 (s, 1H), 7.01 (s, 2H), 6.17 (d, $J$ = 5.4 Hz, 1H), 5.48 (d, $J$ = 6.1 Hz, 1H), 5.29 (d, $J$ = 5.2 Hz, 1H), 4.52 (q, $J$ = 5.3 Hz, 1H), 4.11 (q, $J$ = 4.8 Hz, 1H), 4.01 (q, $J$ = 6.0 Hz, 1H), 3.86 (s, 2H), 3.81 (s, 3H), 2.86 (dd, $J$ = 13.8, 5.7 Hz, 1H), 2.71 (dd, $J$ = 13.9, 6.6 Hz, 1H) ppm. $^{13}$C NMR (151 MHz, DMSO-$d_6$) δ 166.60, 157.69, 154.22, 152.96, 151.85, 151.32, 139.79, 134.21, 130.22, 129.90, 129.27, 129.19, 128.13, 124.41, 124.01, 122.77, 121.11, 111.55, 106.50, 102.22, 99.73, 87.44, 83.58, 73.66, 72.97, 52.60, 35.70, 33.91 ppm. HRMS (ESI): calcd. for $C_{28}H_{27}N_4O_6S^+$: 547.1651. found: 547.1661.

***Physical Characterization of Synthetic Intermediates***

**(2*R*,3*R*,4*S*,5*R*)-2-(hydroxymethyl)-5-(6-(methylamino)-9*H*-purin-9-yl)tetrahydrofuran-3,4-diol (4-23)**: MS (ESI): calcd. for $C_{11}H_{16}N_5O_4^+$: 282.12. found: 282.88.

**(2*R*,3*R*,4*S*,5*R*)-2-(6-(benzylamino)-9*H*-purin-9-yl)-5-(hydroxymethyl)tetrahydrofuran-3,4-diol (4-25)**: MS (ESI): calcd. for $C_{17}H_{20}N_5O_4^+$: 358.15. found: 358.66.

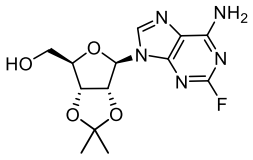

**(2*R*,3*R*,4*S*,5*R*)-2-(6-amino-2-fluoro-9*H*-purin-9-yl)-5-(hydroxymethyl) tetrahydrofuran-3,4-diol (4-28)**: White solid. $^{1}$H NMR (400 MHz, Methanol-$d_4$) δ 8.29 (s, 1H), 6.11 (d, $J$ = 3.1 Hz, 1H), 5.28 (dd, $J$ = 6.0, 3.2 Hz, 1H), 5.03 (dd, $J$ = 6.0, 2.3 Hz, 1H), 4.42 – 4.30 (m, 1H), 3.79 (dd, $J$ = 12.0, 3.7 Hz, 1H), 3.73 (dd, $J$ = 12.0, 4.4 Hz, 1H), 1.63 (s, 3H), 1.40 (s, 3H) ppm. $^{13}$C NMR (151 MHz, Methanol-$d_4$) δ 159.82, 158.44, 157.89, 157.75, 150.33, 150.20, 140.33, 117.44, 113.95, 90.97, 86.86, 83.93, 81.49, 62.02, 26.15, 24.12 ppm. MS (ESI): calcd. for $C_{13}H_{17}FN_5O_4^+$: 326.13. found: 326.55.

**((3a*R*,4*R*,6*R*,6a*R*)-6-(6-(benzylamino)-9*H*-purin-9-yl)-2,2-dimethyltetrahydrofuro[3,4-*d*][1,3]dioxol-4-yl)methanol (4-32)**: MS (ESI): calcd. for $C_{17}H_{20}N_5O_4^+$: 358.15. found: 358.29.

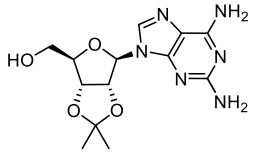

**((3a*R*,4*R*,6*R*,6a*R*)-6-(2,6-diamino-9*H*-purin-9-yl)-2,2-dimethyltetrahy-drofuro[3,4-*d*][1,3]dioxol-4-yl)methanol (4-35)**: Light yellow solid. $^1$H NMR (400 MHz, Methanol-*d*$_4$) δ 8.12 (s, 1H), 7.53 (s, 1H), 6.20 (d, J = 3.7 Hz, 1H), 5.12 (dd, J = 6.2, 3.8 Hz, 1H), 4.98 (dd, J = 6.2, 2.7 Hz, 1H), 4.29 (q, J = 3.7 Hz, 1H), 3.75 (qd, J = 12.0, 3.8 Hz, 2H), 1.62 (s, 3H), 1.38 (s, 3H) ppm. $^{13}$C NMR (151 MHz, Methanol-*d*$_4$) δ 157.34, 151.94, 148.90, 122.68, 113.99, 101.93, 90.71, 85.78, 84.06, 81.20, 62.04, 26.23, 24.19 ppm. MS (ESI): calcd. for $C_{13}H_{19}N_6O_4^+$: 323.15. found: 323.60.

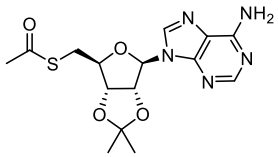

***S*-(((3a*S*,4*S*,6*R*,6a*R*)-6-(6-amino-9*H*-purin-9-yl)-2,2-dimethyltetrahydrofuro[3,4-*d*][1,3]dioxol-4-yl)methyl) ethanethioate (4-37)**: Colorless oil. $^1$H NMR (400 MHz, $CDCl_3$) δ 8.35 (s, 1H), 7.96 (s, 1H), 6.98 (s, 2H), 6.18 – 6.04 (m, 1H), 5.60 – 5.50 (m, 1H), 5.00 (dd, *J* = 6.2, 3.0 Hz, 1H), 4.35 (td, *J* = 6.9, 3.0 Hz, 1H), 3.30 (dd, *J* = 13.8, 7.3 Hz, 1H), 3.19 (dd, *J* = 13.8, 6.6 Hz, 1H), 2.34 (s, 3H), 1.60 (s, 3H), 1.39 (s, 3H) ppm. $^{13}$C NMR (101 MHz, $CDCl_3$) δ 194.64, 156.15, 153.10, 149.02, 139.85, 120.14, 114.39, 90.82, 86.10, 84.16, 83.69, 31.24, 30.55, 27.03, 25.32 ppm. MS (ESI): calcd. for $C_{15}H_{20}N_5O_4^+$: 366.12. found: 366.30.

***S*-(((3a*S*,4*S*,6*R*,6a*R*)-6-(6-(benzylamino)-9*H*-purin-9-yl)-2,2-dimethyltetrahydrofuro[3,4-*d*][1,3]dioxol-4-yl)methyl) ethanethioate (4-40)**: MS (ESI): calcd. for $C_{17}H_{20}N_5O_4^+$: 358.15. found: 358.69.

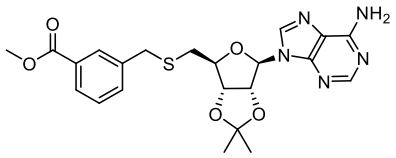

**Methyl 3-(((((3a*S*,4*S*,6*R*,6a*R*)-6-(6-amino-9*H*-purin-9-yl)-2,2-dimethyltetrahydrofuro[3,4-*d*][1,3]dioxol-4-yl)methyl)thio)methyl)benzoate (4-50)**: Colorless oil. $^{1}$H NMR (400 MHz, $CDCl_3$) δ 8.29 (s, 1H), 7.98 – 7.79 (m, 3H), 7.41 (d, *J* = 7.7 Hz, 1H), 7.33 (t, *J* = 7.6 Hz, 1H), 6.05 (d, *J* = 2.1 Hz, 1H), 5.81 (s, 2H), 5.45 (dd, *J* = 6.4, 2.2 Hz, 1H), 5.01 (dd, *J* = 6.4, 3.4 Hz, 1H), 4.45 – 4.27 (m, 1H), 3.91 (s, 3H), 3.74 (s, 2H), 2.78 (dd, *J* = 13.7, 7.0 Hz, 1H), 2.66 (dd, *J* = 13.7, 6.4 Hz, 1H), 1.61 (s, 3H), 1.38 (s, 3H) ppm. $^{13}$C NMR (151 MHz, $CDCl_3$) δ 166.85, 155.54, 153.15, 149.22, 140.00, 138.33, 133.33, 130.50, 129.94, 128.62, 128.44, 120.30, 114.60, 90.73, 86.68, 84.02, 83.80, 52.19, 36.22, 33.42, 27.12, 25.35 ppm. MS (ESI): calcd. for $C_{22}H_{25}N_5O_5S^+$: 471.16. found: 471.28.

**Methyl 3-(((((3a*S*,4*S*,6*R*,6a*R*)-6-(6-(benzylamino)-9*H*-purin-9-yl)-2,2-dimethyltetrahydrofuro[3,4-*d*][1,3]dioxol-4-yl)methyl)thio)methyl)benzoate (4-47)**: MS (ESI): calcd. for $C_{29}H_{32}N_5O_5S^+$: 562.21. found: 562.55.

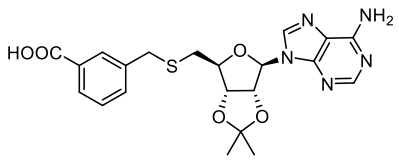

**3-(((((2*S*,3*S*,4*R*,5*R*)-5-(6-amino-9*H*-purin-9-yl)-3,4-dihydroxytetrahydrofuran-2-yl)methyl)thio)methyl)phenyl)(morpholino)methanone (4-51)**: White solid. $^{1}$H NMR (400 MHz, DMSO-$d_6$) δ 8.32 (s, 1H), 8.13 (s, 1H), 7.89 (s, 1H), 7.80 (d, *J* = 7.6 Hz, 1H), 7.50 – 7.28 (m, 4H), 6.15 (d, *J* = 2.4 Hz, 1H), 5.46 (dd, *J* = 6.3, 2.4 Hz, 1H), 4.95 (dd, *J* = 6.3, 2.9 Hz, 1H), 4.21 (td, *J* = 7.5, 2.9 Hz, 1H), 3.94 – 3.74 (m, 2H), 2.77 (dd, *J* = 13.6, 7.8 Hz, 1H), 2.62 (dd, *J* = 13.6, 6.4 Hz, 1H), 1.52 (s, 3H), 1.31 (s, 3H) ppm. $^{13}$C NMR (101 MHz, DMSO-$d_6$) δ 167.74, 156.58, 153.22, 149.17, 140.56, 139.47, 133.64, 131.53, 130.13, 129.05, 128.32, 119.59, 113.86, 89.58, 85.85, 83.76, 83.48, 55.33, 35.36, 33.55, 27.36, 25.59 ppm. MS (ESI): calcd. for $C_{21}H_{24}N_5O_5S^+$: 458.15. found: 458.82.

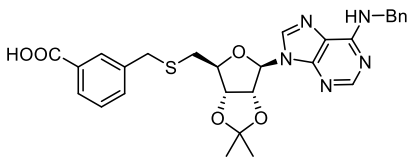

**Methyl 3-(((((2*S*,3*S*,4*R*,5*R*)-5-(6-amino-2-fluoro-9*H*-purin-9-yl)-3,4-dihydroxytetrahydrofuran-2-yl)methyl)thio)methyl)benzoate (4-54)**: White solid. $^{1}$H NMR (400 MHz, Methanol-$d_4$) δ 8.32 – 8.13 (m, 2H), 7.94 (s, 1H), 7.84 (d, $J$ = 7.7 Hz, 1H), 7.40 – 7.24 (m, 6H), 6.14 (dd, $J$ = 4.2, 2.3 Hz, 1H), 5.45 (dt, $J$ = 6.1, 3.0 Hz, 1H), 4.98 (dd, $J$ = 7.1, 3.9 Hz, 1H), 4.81 (s, 2H), 4.29 (tt, $J$ = 6.5, 3.1 Hz, 1H), 3.73 (d, $J$ = 5.8 Hz, 2H), 2.72 (qdd, $J$ = 13.8, 6.7, 4.5 Hz, 2H), 1.57 (d, $J$ = 3.3 Hz, 3H), 1.36 (d, $J$ = 3.9 Hz, 3H) ppm. $^{13}$C NMR (151 MHz, Methanol-$d_4$) δ 168.30, 152.69, 140.01, 138.89, 133.02, 130.86, 129.74, 128.16, 128.12, 127.98, 127.19, 126.85, 114.11, 90.18, 86.87, 83.77, 35.47, 33.17, 26.01, 24.14 ppm. MS (ESI): calcd. for $C_{28}H_{30}N_5O_5S^+$: 548.20. found: 548.28.

**3-(((((3a*S*,4*S*,6*R*,6a*R*)-6-(6-amino-9*H*-purin-9-yl)-2,2-dimethyltetrahydrofuro[3,4-*d*][1,3]dioxol-4-yl)methyl)thio)methyl)-*N*-heptylbenzamide (4-62)**: MS (ESI): calcd. for $C_{28}H_{39}N_6O_4S^+$: 555.28. found: 555.50.

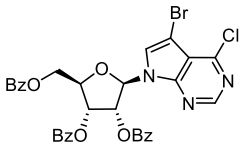

**(2*R*,3*R*,4*R*,5*R*)-2-((benzoyloxy)methyl)-5-(5-bromo-4-chloro-7*H*-pyrrolo[2,3-*d*]pyrimidin-7-yl)tetrahydrofuran-3,4-diyl dibenzoate (4-66)**: White solid. $^{1}$H NMR (400 MHz, $CDCl_3$) δ 8.58 (s, 1H), 8.11 (dd, $J$ = 8.4, 1.3 Hz, 2H), 8.00 (dd, $J$ = 8.4, 1.3 Hz, 2H), 7.92 (dd, $J$ = 8.4, 1.3 Hz, 2H), 7.65 – 7.34 (m, 11H), 6.68 (d, $J$ = 5.4 Hz, 1H), 6.15 (t, $J$ = 5.6 Hz, 1H), 6.10 (dd, $J$ = 5.8, 4.5 Hz, 1H), 4.90 (dd, $J$ = 12.3, 3.1 Hz, 1H), 4.80 (q, $J$ = 3.4 Hz, 1H), 4.68 (dd, $J$ = 12.3, 3.6 Hz, 1H) ppm. $^{13}$C NMR (101 MHz, $CDCl_3$) δ 166.15, 165.40, 165.10, 153.62, 151.63, 150.46, 133.86, 133.64, 129.87, 129.71, 129.27, 128.82, 128.67, 128.61, 128.56, 128.37, 126.46, 116.53, 90.20, 87.52, 81.33, 74.11, 71.39, 64.23 ppm. MS (ESI): calcd. for $C_{32}H_{24}BrClN_3O_7^+$: 676.05. found: 676.33.

**(2*R*,3*R*,4*S*,5*R*)-2-(4-amino-5-bromo-7*H*-pyrrolo[2,3-*d*]pyrimidin-7-yl)-5-(hydroxymethyl)tetrahydrofuran-3,4-diol (4-28)**: MS (ESI): calcd. for $C_{11}H_{14}BrN_4O_4^+$: 345.02. found: 345.80.

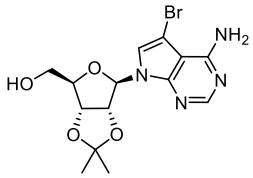

**((3a*R*,4*R*,6*R*,6a*R*)-6-(4-amino-5-bromo-7*H*-pyrrolo[2,3-*d*]pyrimidin-7-yl)-2,2-dimethyltetrahydrofuro[3,4-*d*][1,3]dioxol-4-yl)methanol (4-67)**: White solid. $^{1}$H NMR (400 MHz, Methanol-$d_4$) δ 7.83 (s, 1H), 5.88 (d, *J* = 3.7 Hz, 1H), 5.13 (dd, *J* = 6.1, 3.7 Hz, 1H), 4.94 (dd, *J* = 6.1, 2.2 Hz, 1H), 4.52 (s, 2H), 4.25 (q, *J* = 3.5 Hz, 1H), 3.71 (dd, *J* = 12.1, 3.4 Hz, 1H), 3.62 (dd, *J* = 12.1, 3.8 Hz, 1H), 1.50 (s, 3H), 1.28 (s, 3H) ppm. $^{13}$C NMR (101 MHz, Methanol-$d_4$) δ 160.17, 158.08, 150.34, 150.15, 140.34, 140.31, 113.94, 90.97, 86.85, 83.92, 81.49, 62.02, 26.15, 24.12 ppm. MS (ESI): calcd. for $C_{14}H_{18}BrN_4O_4^+$: 385.05. found: 385.21.

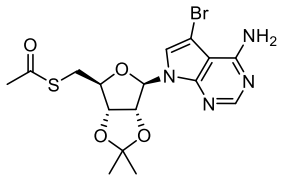

***S*-(((3a*S*,4*S*,6*R*,6a*R*)-6-(4-amino-5-bromo-7*H*-pyrrolo[2,3-*d*]pyrimidin-7-yl)-2,2-dimethyltetrahydrofuro[3,4-*d*][1,3]dioxol-4-yl)methyl) ethanethioate (4-68)**: Colorless oil. $^{1}$H NMR (600 MHz, $CDCl_3$) δ 8.28 (s, 1H), 7.09 (s, 1H), 6.11 (d, *J* = 2.3 Hz, 1H), 5.79 (s, 2H), 5.36 – 5.23 (m, 1H), 4.85 (dd, *J* = 6.4, 3.5 Hz, 1H), 4.28 (td, *J* = 6.5, 3.6 Hz, 1H), 3.28 (dd, *J* = 13.8, 7.0 Hz, 1H), 3.18 (dd, *J* = 13.8, 6.0 Hz, 1H), 2.37 (s, 3H), 1.59 (s, 3H), 1.36 (s, 3H) ppm. MS (ESI): calcd. for $C_{16}H_{20}BrN_4O_4S^+$: 443.11. found: 443.04.

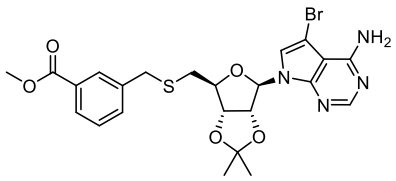

**Methyl 3-(((((3a*S*,4*S*,6*R*,6a*R*)-6-(4-amino-5-bromo-7*H*-pyrrolo[2,3-*d*]pyrimidin-7-yl)-2,2-dimethyltetrahydrofuro[3, 4-*d*][1,3]dioxol-4-yl)methyl)thio)-methyl)benzoate (4-69)**: Light yellow oil. $^{1}$H NMR (400 MHz, $CDCl_3$) δ 8.21 (s, 1H), 7.95 (s, 1H), 7.90 (d, *J* = 7.7 Hz, 1H), 7.42 (d, *J* = 7.6 Hz, 1H), 7.34 (t, *J* = 7.6 Hz, 1H), 7.11 (s, 1H), 6.25 (s, 2H), 6.14 (d, *J* = 2.4 Hz, 1H), 5.22 (dd, *J* = 6.5, 2.5 Hz, 1H), 4.89 (dd, *J* = 6.4, 3.9 Hz, 1H), 4.29 (q, *J* = 6.0 Hz, 1H), 3.90 (s, 3H), 2.76 (dd, *J* = 13.8, 6.5 Hz, 1H), 2.67 (dd, *J* = 13.8, 5.8 Hz, 1H), 1.59 (s, 3H), 1.36 (s, 3H) ppm. $^{13}$C NMR (101 MHz, $CDCl_3$) δ 166.83, 156.89, 152.34, 149.12, 138.38, 133.45, 130.44, 129.95, 128.63, 128.42, 122.24, 114.73, 102.43, 90.32, 88.33, 85.52, 84.43, 83.30, 52.20, 36.39, 33.45, 27.15, 25.37 ppm. MS (ESI): calcd. for

$C_{23}H_{26}BrN_4O_5S^+$: 549.08. found: 549.21.

**Methyl 3-(((((3a*S*,4*S*,6*R*,6a*R*)-6-(4-amino-5-phenyl-7*H*-pyrrolo[2,3-*d*]pyrimidin-7-yl)-2,2-dimethyltetrahydrofuro[3,4-*d*][1,3]dioxol-4-yl)methyl)thio)methyl)benzoate (4-70)**: MS (ESI): calcd. for $C_{29}H_{31}N_4O_5S^+$: 547.20. found: 547.68.

### 4.4.3 Biology

***Dose-response Test***

Inhibitory effect of all compounds was assessed using a luminescence-based nsp14 MTase-Glo™ methyltransferase assay. In this assay, SAH by-product generated is transferred to ATP, and generates luminescence when transferring to ADP. Drug in corresponding concentration (10 μM) and nsp14 enzyme (10 μM) was mixed on a 384 well-plate, centrifuged and incubated for 10 mins at room temperature. GpppA (7.5 μM, 10 μL) and Glo reagent (1x, 10 μL) was mixed with the incubated mixture and centrifuged, incubated again for 10 mins at room temperature. SAM (1 μM, 10 μL) was added to the mixture, centrifuged and incubated at 30°C for 60 mins. Detection buffer (10 μL, from the kit) was added to the mixture, centrifuged and incubated at 30°C for 3 h. Luminescence generated was read on a BioTek Synergy HTX automated multimode microplate reader. Background group was defined by substituting drug and protein solution with buffer, and 100% activity group was defined by substituting drug solution with buffer. All enzymatic reactions were performed in duplicate, and $IC_{50}$ values were defined as concentration displaying 50% inhibition, determined by fitting the data to Three Parameter Logistic equation using GraphPad Prism 9.3.1 software.

***Single Dose Inhibition***

Single-dose inhibition was tested with a protocol parallel to that of dose-response test, with fixed drug concentration at 50 nM and 10 nM.

### *Thermal Shift Assays*

TSA experiments were performed on a Bio-Rad C1000 thermal cycler CFX96 real-time system. Applied Biosystems™ Protein Thermal Shift™ kit was applied. Sypro Orange dye was diluted to 3.3333× with kit buffer provided by supplier, and was mixed with nsp14. The mixture was diluted to nsp14 (4 μM) and dye kit (1×), labeled as mix solution. 50 μM synthesized inhibitors (4 μL) was mixed with mixed solution (6 μL) and the mixture was incubated on ice, protect from light. Each group was replicated in triplate. TSA was performed with a melt temperature increment of 0.3 °C per 5 s from 30 °C to 80 °C. The melting temperature ($T_m$) was determined using the Boltzmann nonlinear regression formula.

# *Chapter 5 Conclusion*

Under continuous progressing of human society, especially noticing the continuous emergence of new pathogens in recent years, green synthesis and development of clinical medicine for obscure diseases continuously attracted the attention of scientists. In this thesis, we enclosed a brief methodology for site-selective synthesis of nitrogen-containing molecules and two examples of development of anti-SARS-CoV-2 medicine. Green synthetic methods towards sustainable production of medicine have long been under continuous pursue of scientists. Nitrogen containing molecules have long been the main focus for the development of synthetic methodologies, for their crucial role in peptide backbones and pharmaceutical intermediates. Classical C($sp^3$)–H activation strategies provided us with different regioselectivities such as construction for C–N bonds at benzylic primary, allylic and aromatic sites, etc., while selective construction of C–N bonds at unactivated methylene remained scarce. Alkene, as a type of organic synthetic building block abundantly reserved in nature, have been constantly receiving attention for its functionalization recently. The concept "metal-walk" represents the migration of metal along the carbon skeleton through a reversible $\beta$-hydride elimination/migratory insertion procedure, providing another pathway towards unreached selectivity in C($sp^3$)–N formation. In Chapter 2, we described a site-selective unactivated methylene C–N bond formation through coordinating group assisted and metal migration enabled alkene hydroamination. Ni migration terminated at $\gamma$-position due to preference towards five-membered metallacycle, and with following amidation with dioxazolones we were able to obtain amidation product at unactivated $\gamma$-methylene site. The reaction was achieved at up to 90% yield and remarkable selectivity ($\gamma$-product:other isomers up to 24:1).

COVID-19 rapidly spread around the world in the past three years with great harm to human society and continuous raise of variants, and effective clinical treatment for the disease have been continuously pursued by scientists. 16 non-structural proteins (nsps) encoded by SARS-CoV-2 play crucial parts in the replication of the virus,

providing potential targets for the development of anti-SARS-CoV-2 drugs. RNA dependent RNA polymerase (RdRp), responsible for the replication of SARS-CoV-2 RNA, is an enzyme highly conserved along the variants of SARS-CoV-2 and even along the coronavirus family. GS-441524, the activity core of Remdesivir, was reported to be a potent inhibitor for SARS-CoV-2 RdRp, while relative inhibitors bear poor pharmacokinetic (PK) properties and oral bioavailability. In Chapter 3, we synthesized a series of ester prodrugs of GS-441524, in pursue for improvements in PK properties. Along the compounds synthesized, the cyclohexylcarboxylic ester SHEN 26 displayed the best $EC_{50}$ (0.26 μM) and 53.4% bioavailability (suggested by PK study results). We then optimized the synthetic route of SHEN 26 for potential upcoming industrial requirement, leading to a 3-step route with column-free post-reaction treatments. SHEN 26 obtained through the kilogram-scale synthetic batch from industrial production was also qualified. Potential impurities are synthesized as standard compounds, and impurities in sampled SHEN 26 were identified and quantified. The purity of SHEN 26 synthesized reached 98.9% (< 1.1% impurity), certifying industrial adaptation of this synthetic route.

SARS-CoV-2 nsp14, responsible for the RNA methylation (capping) procedure, is another important target in suppressing SARS-CoV-2 replication. The methylated RNA cap play a vital role, as a protection against human immune system and as an assistant in RNA translation. The methylation of SARS-CoV-2 +ssRNA adopts *S*-Adenosyl methionine (SAM) as methyl source, releasing *S*-Adenosylhomocysteine (SAH) as a by-product. SAH was reported to be an inhibitor of SARS-CoV-2 nsp14, and SAH analogues are considered as potential inhibitors for SARS-CoV-2 nsp14. Despite great potential of this target, few examples of SAH analogues as SARS-CoV-2 nsp14 inhibitors were reported. In Chapter 4 we designed and synthesized a series of different SAH analogues and tested their inhibition ability against the SARS-CoV-2 nsp14. Among synthesized molecules, compounds **4-7** and **4-14** displayed the best inhibition efficacy, with $IC_{50}$ = 1.84 μM and 1.81 μM respectively. Their structure-activity relationship (SAR) were also briefly discussed, providing approach for future exploration of SAH analogues as SARS-CoV-2 nsp14 inhibitors.

# *REFERENCES*

(1) Gandeepan, P., et. al. 3d Transition Metals for C–H Activation. *Chem. Rev.* **2019**, *119* (4), 2192-2452. DOI: 10.1021/acs.chemrev.8b00507.

(2) Ullmann, F. Ueber eine neue Bildungsweise von Diphenylaminderivaten. **1903**, *36* (2), 2382-2384. DOI: https://doi.org/10.1002/cber.190303602174.

(3) Goldberg, I. Ueber Phenylirungen bei Gegenwart von Kupfer als Katalysator. *Berichte d. D. chem. Gesellschaft.* **1906**, *39* (2), 1691-1692. DOI: https://doi.org/10.1002/cber.19060390298.

(4) Guram, A. S., et. al. Palladium-Catalyzed Aromatic Aminations with in situ Generated Aminostannanes. *J. Am. Chem. Soc.* **1994**, *116* (17), 7901-7902. DOI: 10.1021/ja00096a059.

(5) Paul, F., et. al. Palladium-catalyzed formation of carbon-nitrogen bonds. Reaction intermediates and catalyst improvements in the hetero cross-coupling of aryl halides and tin amides. *J. Am. Chem. Soc.* **1994**, *116* (13), 5969-5970. DOI: 10.1021/ja00092a058.

(6) Surry, D. S., et. al. Biaryl Phosphane Ligands in Palladium-Catalyzed Amination. *Angew. Chem. Int. Ed.* **2008**, *47* (34), 6338-6361. DOI: https://doi.org/10.1002/anie.200800497.

(7) Hartwig, J. F. Evolution of a Fourth Generation Catalyst for the Amination and Thioetherification of Aryl Halides. *Acc. Chem. Res.* **2008**, *41* (11), 1534-1544. DOI: 10.1021/ar800098p.

(8) Kim, H., et. al. Transition-Metal-Mediated Direct C–H Amination of Hydrocarbons with Amine Reactants: The Most Desirable but Challenging C–N Bond-Formation Approach. *ACS Catal.* **2016**, *6* (4), 2341-2351. DOI: 10.1021/acscatal.6b00293.

(9) Wei, Y., et. al. Copper-Catalyzed Direct Alkynylation of Electron-Deficient Polyfluoroarenes with Terminal Alkynes Using O2 as an Oxidant. *J. Am. Chem. Soc.* **2010**, *132* (8), 2522-2523. DOI: 10.1021/ja910461e.

(10) Wedi, P., et. al. Arene-Limited Nondirected C-H Activation of Arenes. *Angew. Chem. Int. Ed.* **2018**, *57* (40), 13016-13027. DOI: https://doi.org/10.1002/anie.201804727.

(11) Gu, L., et. al. Gold-Catalyzed Direct Amination of Arenes with Azodicarboxylates. *Org. Lett.* **2011**, *13* (7), 1872-1874. DOI: 10.1021/ol200373q.

(12) Shrestha, R., et. al. Sterically Controlled, Palladium-Catalyzed Intermolecular Amination of Arenes. *J. Am. Chem. Soc.* **2013**, *135* (23), 8480-8483. DOI: 10.1021/ja4032677.

(13) Kuhl, N.; H., e. a. Beyond Directing Groups: Transition-Metal-Catalyzed C-H Activation of Simple Arenes. *Angew. Chem. Int. Ed.* **2012**, *51* (41), 10236-10254. DOI: https://doi.org/10.1002/anie.201203269.

(14) Thu, H., et. al. Intermolecular Amidation of Unactivated $sp^2$ and $sp^3$ C−H Bonds via Palladium-Catalyzed Cascade C−H Activation/Nitrene Insertion. *J. Am. Chem. Soc.* **2006**, *128* (28), 9048-9049. DOI: 10.1021/ja062856v.

(15) Ng, K., et. al. Pd-Catalyzed Intermolecular ortho-C-H Amidation of Anilides by *N*-Nosyloxycarbamate. *J. Am. Chem. Soc.* **2010**, *132* (37), 12862-12864. DOI: 10.1021/ja106364r.

(16) Timsina, Y. N., et. al. Palladium-Catalyzed C–H Amination of C($sp^2$) and C($sp^3$)–H Bonds: Mechanism and Scope for N-Based Molecule Synthesis. *ACS Catal.* **2018**, *8* (7), 5732-5776. DOI: 10.1021/acscatal.8b01168.

(17) Xiao, B., et. al. Palladium-Catalyzed Intermolecular Directed C-H Amidation of Aromatic Ketones. *J. Am. Chem. Soc.* **2011**, *133* (5), 1466-1474. DOI: 10.1021/ja108450m.

(18) Dick, A. R., et. al. Carbon-Nitrogen Bond-Forming Reactions of Palladacycles with Hypervalent

Iodine Reagents. *Organometallics* **2007**, *26* (6), 1365-1370. DOI: 10.1021/om061052l.

(19) Ng, K., et. al. A convenient synthesis of anthranilic acids by Pd-catalyzed direct intermolecular ortho-C–H amidation of benzoic acids. *Chem. Comm.* **2012**, *48* (95), 11680-11682, 10.1039/C2CC36502B. DOI: 10.1039/C2CC36502B.

(20) Yoo, E., et. al. Pd-Catalyzed Intermolecular C–H Amination with Alkylamines. *J. Am. Chem. Soc.* **2011**, *133* (20), 7652-7655. DOI: 10.1021/ja202563w.

(21) Anand, M., et. al. Non-innocent Additives in a Palladium(II)-Catalyzed C–H Bond Activation Reaction: Insights into Multimetallic Active Catalysts. *J. Am. Chem. Soc.* **2014**, *136* (15), 5535-5538. DOI: 10.1021/ja412770h.

(22) Anand, M., et. al. Palladium–Silver Cooperativity in an Aryl Amination Reaction through C–H Functionalization. *ACS Catal.* **2016**, *6* (2), 696-708. DOI: 10.1021/acscatal.5b02639.

(23) Zhu, D., et. al. Ligand-Promoted ortho-C-H Amination with Pd Catalysts. *Angew. Chem. Int. Ed.* **2015**, *54* (8), 2497-2500. DOI: https://doi.org/10.1002/anie.201408651.

(24) Kim, J., et. al. Ruthenium-Catalyzed Direct C-H Amidation of Arenes Including Weakly Coordinating Aromatic Ketones. *Chem. Eur. J.* **2013**, *19* (23), 7328-7333. DOI: https://doi.org/10.1002/chem.201301025.

(25) Shin, Y., et. al. Ru(II)-Catalyzed Selective C–H Amination of Xanthones and Chromones with Sulfonyl Azides: Synthesis and Anticancer Evaluation. *J. Org. Chem.* **2014**, *79* (19), 9262-9271. DOI: 10.1021/jo501709f.

(26) Thirunavukkarasu, V. S., et. al. Expedient C–H Amidations of Heteroaryl Arenes Catalyzed by Versatile Ruthenium(II) Catalysts. *Org. Lett.* **2013**, *15* (13), 3286-3289. DOI: 10.1021/ol401321q.

(27) Zhou, X., et. al. Ru-catalyzed direct C–H amidation of 2-arylbenzo[d]thiazoles with sulfonyl azides. *Tetrahedron* **2014**, *70* (38), 6742-6748. DOI: https://doi.org/10.1016/j.tet.2014.07.076.

(28) Zhang, L., et. al. Ruthenium-Catalyzed Direct C–H Amidation of Arenes: A Mechanistic Study. *Organometallics* **2014**, *33* (8), 1905-1908. DOI: 10.1021/om500080z.

(29) Pan, C., et. al. Ruthenium-Catalyzed C7 Amidation of Indoline C-H Bonds with Sulfonyl Azides. *Chem. Eur. J.* **2014**, *20* (13), 3606-3609. DOI: https://doi.org/10.1002/chem.201304236.

(30) Shin, K., et. al. Orthogonal Reactivity of Acyl Azides in C–H Activation: Dichotomy between C–C and C–N Amidations Based on Catalyst Systems. *Org. Lett.* **2014**, *16* (7), 2022-2025. DOI: 10.1021/ol500602b.

(31) Shang, M., et. al. Ru(II)-Catalyzed ortho-C–H Amination of Arenes and Heteroarenes at Room Temperature. *Org. Lett.* **2013**, *15* (20), 5286-5289. DOI: 10.1021/ol402515s.

(32) Zhao, H., et. al. Rhodium(III)-Catalyzed Intermolecular *N*-Chelator-Directed Aromatic C–H Amidation with Amides. *Org. Lett.* **2013**, *15* (19), 5106-5109. DOI: 10.1021/ol4024776.

(33) Maiden, T. M. M., et. al. A Mild and Regioselective Route to Functionalized Quinazolines. *Chem. Eur. J.* **2015**, *21* (41), 14342-14346. DOI: https://doi.org/10.1002/chem.201502891.

(34) Ng, F., et. al. [RhIII(Cp*)]-Catalyzed ortho-Selective Direct C($sp^2$)-H Bond Amidation/Amination of Benzoic Acids by *N*-Chlorocarbamates and *N*-Chloromorpholines. A Versatile Synthesis of Functionalized Anthranilic Acids. *Chem. Eur. J.* **2014**, *20* (15), 4474-4480. DOI: https://doi.org/10.1002/chem.201304855.

(35) Ng, K., et. al. [Cp*RhCl2]2-catalyzed ortho-C–H bond amination of acetophenone o-methyloximes with primary N-chloroalkylamines: convenient synthesis of N-alkyl-2-acylanilines. *Chem. Comm.* **2013**, *49* (63), 7031-7033, 10.1039/C3CC42937G. DOI: 10.1039/C3CC42937G.

(36) Grohmann, C., et. al. Rh[III]-Catalyzed C–H Amidation Using Aroyloxycarbamates To Give N-Boc

Protected Arylamines. *Org. Lett.* **2013**, *15* (12), 3014-3017. DOI: 10.1021/ol401209f.

(37) Shi, J., et. al. Rhodium(III)-catalyzed regioselective C2-amidation of indoles with *N*-(2,4,6-trichlorobenzoyloxy)amides and its synthetic application to the development of a novel potential PPARγ modulator. *Org. Biomol. Chem.* **2014**, *12* (35), 6831-6836, 10.1039/C4OB00637B. DOI: 10.1039/C4OB00637B.

(38) Wu, K., et. al. Rh(III)-Catalyzed Intermolecular C–H Amination of 1-Aryl-1H-pyrazol-5(4H)-ones with Alkylamines. *Org. Lett.* **2014**, *16* (1), 42-45. DOI: 10.1021/ol402965d.

(39) Xue, Y., et. al. $Rh^{III}$-Catalyzed Hydrazine-Directed C($sp^2$)–H Amination of Phenidones with *N*-Alkyl-*O*-benzoyl-hydroxylamines. *Eur. J. Org. Chem.* **2014**, *2014* (33), 7481-7488. DOI: https://doi.org/10.1002/ejoc.201402999.

(40) Yu, S., et. al. Rhodium(III)-Catalyzed C–H Activation and Amidation of Arenes Using *N*-Arenesulfonated Imides as Amidating Reagents. *Org. Lett.* **2013**, *15* (14), 3706-3709. DOI: 10.1021/ol401569u.

(41) Zhou, B., et. al. Rh(III)-Catalyzed C–H Amidation with *N*-Hydroxycarbamates: A New Entry to *N*-Carbamate-Protected Arylamines. *Organic Letters* **2014**, *16* (2), 592-595. DOI: 10.1021/ol403477w.

(42) Ali, M. A., et. al. [RhCp*$Cl_2$]$_2$-Catalyzed Directed *N*-Boc Amidation of Arenes "on Water". *Organic Letters* **2015**, *17* (6), 1513-1516. DOI: 10.1021/acs.orglett.5b00392.

(43) Tang, R., et. al. Rhodium(III)-Catalyzed C($sp^2$)-H Activation and Electrophilic Amidation with *N*-Fluorobenzenesulfonimide. *Adv. Synth. Catal.* **2013**, *355* (5), 869-873. DOI: https://doi.org/10.1002/adsc.201201133.

(44) Zhou, B., et. al. Rhodium-Catalyzed Direct Addition of Aryl C–H Bonds to Nitrosobenzenes at Room Temperature. *Org. Lett.* **2013**, *15* (24), 6302-6305. DOI: 10.1021/ol403187t.

(45) Du, J., et. al. Rhodium-Catalyzed Direct Amination of Arenes with Nitrosobenzenes: A New Route to Diarylamines. *Chem. Eur. J.* **2014**, *20* (19), 5727-5731. DOI: https://doi.org/10.1002/chem.201400221.

(46) Kim, J., et. al. Rhodium-Catalyzed Intermolecular Amidation of Arenes with Sulfonyl Azides via Chelation-Assisted C–H Bond Activation. *J. Am. Chem. Soc.* **2012**, *134* (22), 9110-9113. DOI: 10.1021/ja303527m.

(47) Shi, J., et. al. Rhodium-catalyzed regioselective amidation of indoles with sulfonyl azides via C–H bond activation. *Org. Biomol. Chem.* **2012**, *10* (45), 8953-8955, 10.1039/C2OB26767E. DOI: 10.1039/C2OB26767E.

(48) Yu, D., et. al. $Rh^{III}$/$Cu^{II}$-Cocatalyzed Synthesis of 1*H*-Indazoles through C–H Amidation and N–N Bond Formation. *J. Am. Chem. Soc.* **2013**, *135* (24), 8802-8805. DOI: 10.1021/ja4033555.

(49) Wang, H., et. al. Rhodium-Catalyzed Direct ortho C–N Bond Formation of Aromatic Azo Compounds with Azides. *J. Org. Chem.* **2014**, *79* (7), 3279-3288. DOI: 10.1021/jo500412w.

(50) Jia, X., et. al. Rhodium-Catalyzed Direct C–H Amidation of Azobenzenes with Sulfonyl Azides: A Synthetic Route to Sterically Hindered ortho-Substituted Aromatic Azo Compounds. *J. Org. Chem.* **2014**, *79* (9), 4180-4185. DOI: 10.1021/jo500372d.

(51) Ryu, T., et. al. Synthesis of 2-Aryl-2*H*-benzotrizoles from Azobenzenes and *N*-Sulfonyl Azides through Sequential Rhodium-Catalyzed Amidation and Oxidation in One Pot. *Org. Lett.* **2014**, *16* (11), 2810-2813. DOI: 10.1021/ol501250t.

(52) Lian, Y., et. al. Facile Synthesis of Unsymmetrical Acridines and Phenazines by a Rh(III)-Catalyzed Amination/Cyclization/Aromatization Cascade. *J. Am. Chem. Soc.* **2013**, *135* (34), 12548-12551. DOI: 10.1021/ja406131a.

(53) Yang, W., et. al. Hydroxyamination of aryl C–H bonds with *N*-hydroxycarbamate by synergistic

Rh/Cu catalysis at room temperature. *Chem. Comm.* **2014**, *50* (34), 4420-4422, 10.1039/C3CC49496A. DOI: 10.1039/C3CC49496A.

(54) Ryu, J., et. al. Rhodium-Catalyzed Direct C-H Amination of Benzamides with Aryl Azides: A Synthetic Route to Diarylamines. *Angew. Chem. Int. Ed.* **2012**, *51* (39), 9904-9908. DOI: https://doi.org/10.1002/anie.201205723.

(55) Shin, K., et. al. Direct C-H Amination of Arenes with Alkyl Azides under Rhodium Catalysis. *Angew. Chem. Int. Ed.* **2013**, *52* (31), 8031-8036. DOI: https://doi.org/10.1002/anie.201302784.

(56) Tang, C., et. al. Rh-Catalyzed Diarylamine Synthesis by Intermolecular C–H Amination of Heteroarylarenes. *Eur. J. Org. Chem.* **2013**, *2013* (33), 7480-7483. DOI: https://doi.org/10.1002/ejoc.201301430.

(57) Park, S. H., et. al. Mechanistic Studies of the Rhodium-Catalyzed Direct C–H Amination Reaction Using Azides as the Nitrogen Source. *J. Am. Chem. Soc.* **2014**, *136* (6), 2492-2502. DOI: 10.1021/ja411072a.

(58) Park, Y. e. a. Mechanistic Studies on the Rh(III)-Mediated Amido Transfer Process Leading to Robust C–H Amination with a New Type of Amidating Reagent. *J. Am. Chem. Soc.* **2015**, *137* (13), 4534-4542. DOI: 10.1021/jacs.5b01324.

(59) Park, Y., et. al. Study of Sustainability and Scalability in the Cp*Rh(III)-Catalyzed Direct C–H Amidation with 1,4,2-Dioxazol-5-ones. *Org. Process Res. Dev.* **2015**, *19* (8), 1024-1029. DOI: 10.1021/acs.oprd.5b00164.

(60) Kim, H., et. al. Iridium-Catalyzed C–H Amination with Anilines at Room Temperature: Compatibility of Iridacycles with External Oxidants. *J. Am. Chem. Soc.* **2014**, *136* (16), 5904-5907. DOI: 10.1021/ja502270y.

(61) Lee, D., et. al. Iridium-Catalyzed Direct Arene C–H Bond Amidation with Sulfonyl- and Aryl Azides. *J. Org. Chem.* **2013**, *78* (21), 11102-11109. DOI: 10.1021/jo4019683.

(62) Hermann, G. N., et. al. Mechanochemical Iridium(III)-Catalyzed C−H Bond Amidation of Benzamides with Sulfonyl Azides under Solvent-Free Conditions in a Ball Mill. *Angew. Chem. Int. Ed.* **2016**, *55* (11), 3781-3784. DOI: https://doi.org/10.1002/anie.201511689.

(63) Hwang, H., et. al. Regioselective Introduction of Heteroatoms at the C-8 Position of Quinoline N-Oxides: Remote C–H Activation Using N-Oxide as a Stepping Stone. *J. Am. Chem. Soc.* **2014**, *136* (30), 10770-10776. DOI: 10.1021/ja5053768.

(64) Liu, J. B., et. al. A Computational Mechanistic Study of Amidation of Quinoline N-Oxide: The Relative Stability of Amido Insertion Intermediates Determines the Regioselectivity. *ACS Catal.* **2016**, *6* (4), 2452-2461. DOI: 10.1021/acscatal.5b02938.

(65) Kim, J., et. al. Iridium-Catalyzed Direct C-H Amidation with Weakly Coordinating Carbonyl Directing Groups under Mild Conditions. *Angew. Chem. Int. Ed.* **2014**, *53* (8), 2203-2207. DOI: https://doi.org/10.1002/anie.201310544.

(66) Lee, D., et. al. Direct C-H Amidation of Benzoic Acids to Introduce meta- and para-Amino Groups by Tandem Decarboxylation. *Chem. Eur. J.* **2015**, *21* (14), 5364-5368. DOI: https://doi.org/10.1002/chem.201500331.

(67) Wei, M. E. Iridium-catalyzed direct ortho-CH amidation of benzoic acids with sulfonylazides. *Chinese Chemical Letters* **2015**, *26* (11), 1336-1340. DOI: https://doi.org/10.1016/j.cclet.2015.08.009.

(68) Zhu, B., et. al. Iridium(III)-Catalyzed Direct C-H Sulfonamidation of 2-Aryl-1,2,3-triazole N-Oxides with Sulfonyl Azides. *Adv. Synth. Catal.* **2016**, *358* (2), 326-332. DOI: https://doi.org/10.1002/adsc.201501036.

(69) Pi, C., et. al. Iridium-Catalyzed Direct C–H Sulfamidation of Aryl Nitrones with Sulfonyl Azides at Room Temperature. *J. Org. Chem.* **2015**, *80* (15), 7333-7339. DOI: 10.1021/acs.joc.5b01377.

(70) Chen, H., et. al. Iridium(III)-Catalyzed Benzylic Amine Directed C-H Sulfonamidation of Arenes with Sulfonyl Azides. *ChemCatChem* **2015**, *7* (5), 743-746. DOI: https://doi.org/10.1002/cctc.201402944.

(71) Gwon, D., et. al. Iridium(III)-Catalyzed C-H Amidation of Arylphosphoryls Leading to a *P*-Stereogenic Center. *Chem. Eur. J.* **2014**, *20* (39), 12421-12425. DOI: https://doi.org/10.1002/chem.201404151.

(72) Gwon, D., et. al. Dual role of carboxylic acid additive: mechanistic studies and implication for the asymmetric C–H amidation. *Tetrahedron* **2015**, *71* (26), 4504-4511. DOI: https://doi.org/10.1016/j.tet.2015.02.065.

(73) Becker, P., et. al. Acylsilanes in Iridium-Catalyzed Directed Amidation Reactions and Formation of Heterocycles via Siloxycarbenes. *Angew. Chem. Int. Ed.* **2015**, *54* (51), 15493-15496. DOI: https://doi.org/10.1002/anie.201508501.

(74) Ryu, J., et. al. Ir(III)-Catalyzed Mild C–H Amidation of Arenes and Alkenes: An Efficient Usage of Acyl Azides as the Nitrogen Source. *J. Am. Chem. Soc.* **2013**, *135* (34), 12861-12868. DOI: 10.1021/ja406383h.

(75) Kim, H., et. al. Synthesis of Phosphoramidates: A Facile Approach Based on the C–N Bond Formation via Ir-Catalyzed Direct C–H Amidation. *Org. Lett.* **2014**, *16* (20), 5466-5469. DOI: 10.1021/ol502722j.

(76) Pan, C., et. al. Iridium-Catalyzed Phosphoramidation of Arene C–H Bonds with Phosphoryl Azide. *J. Org. Chem.* **2014**, *79* (19), 9427-9432. DOI: 10.1021/jo5018052.

(77) Zhang, T., et. al. Carboxylate-Assisted Iridium-Catalyzed C−H Amination of Arenes with Biologically Relevant Alkyl Azides. *Chem. Eur. J.* **2016**, *22* (9), 2920-2924. DOI: https://doi.org/10.1002/chem.201504880.

(78) Shin, K., et. al. Iridium(III)-Catalyzed Direct C-7 Amination of Indolines with Organic Azides. *J. Org. Chem.* **2014**, *79* (24), 12197-12204. DOI: 10.1021/jo5018475.

(79) Hou, W., et. al. $Ir^{III}$-Catalyzed Direct C-7 Amidation of Indolines with Sulfonyl, Acyl, and Aryl Azides at Room Temperature. *Eur. J. Org. Chem.* **2015**, *2015* (2), 395-400. DOI: https://doi.org/10.1002/ejoc.201403355.

(80) Figg, T. M., et. al. Comparative Investigations of Cp*-Based Group 9 Metal-Catalyzed Direct C–H Amination of Benzamides. *Organometallics* **2014**, *33* (15), 4076-4085. DOI: 10.1021/om5005868.

(81) Patel, P., et. al. *N*-Substituted Hydroxylamines as Synthetically Versatile Amino Sources in the Iridium-Catalyzed Mild C–H Amidation Reaction. *Org. Lett.* **2014**, *16* (12), 3328-3331. DOI: 10.1021/ol501338h.

(82) Sun, B., et. al. Air-Stable Carbonyl(pentamethylcyclopentadienyl)cobalt Diiodide Complex as a Precursor for Cationic (Pentamethylcyclopentadienyl)cobalt(III) Catalysis: Application for Directed C-2 Selective C-H Amidation of Indoles. *Adv. Synth. Catal.* **2014**, *356* (7), 1491-1495. DOI: https://doi.org/10.1002/adsc.201301110.

(83) Patel, P., et. al. Cobalt(III)-Catalyzed C–H Amidation of Arenes using Acetoxycarbamates as Convenient Amino Sources under Mild Conditions. *ACS Catal.* **2015**, *5* (2), 853-858. DOI: 10.1021/cs501860b.

(84) Park, J., et. al. Comparative Catalytic Activity of Group 9 [$Cp^*M^{III}$] Complexes: Cobalt-Catalyzed C-H Amidation of Arenes with Dioxazolones as Amidating Reagents. *Angew. Chem. Int. Ed.* **2015**, *54*

(47), 14103-14107. DOI: https://doi.org/10.1002/anie.201505820.

(85) Liang, Y., et. al. Cationic Cobalt(III)-Catalyzed Aryl and Alkenyl C-H Amidation: A Mild Protocol for the Modification of Purine Derivatives. *Chem. Eur. J.* **2015**, *21* (46), 16395-16399. DOI: https://doi.org/10.1002/chem.201503533.

(86) Mei, R., et. al. Oxazolinyl-Assisted C–H Amidation by Cobalt(III) Catalysis. *ACS Catal.* **2016**, *6* (2), 793-797. DOI: 10.1021/acscatal.5b02661.

(87) Wang, F., et. al. Co(III)-Catalyzed Synthesis of Quinazolines via C–H Activation of N-Sulfinylimines and Benzimidates. *Org. Lett.* **2016**, *18* (6), 1306-1309. DOI: 10.1021/acs.orglett.6b00227.

(88) Matsubara, T., et. al. Synthesis of Anthranilic Acid Derivatives through Iron-Catalyzed Ortho Amination of Aromatic Carboxamides with N-Chloroamines. *J. Am. Chem. Soc.* **2014**, *136* (2), 646-649. DOI: 10.1021/ja412521k.

(89) Zhang, L. B., et. al. Cobalt(II)-Catalyzed C–H Amination of Arenes with Simple Alkylamines. *Org. Lett.* **2016**, *18* (6), 1318-1321. DOI: 10.1021/acs.orglett.6b00241.

(90) Yan, Q., et. al. Nickel-Catalyzed Direct Amination of Arenes with Alkylamines. *Org. Lett.* **2015**, *17* (10), 2482-2485. DOI: 10.1021/acs.orglett.5b00990.

(91) Peng, J., et. al. Copper-Catalyzed C(sp2)–H Amidation with Azides as Amino Sources. *Org. Lett.* **2014**, *16* (18), 4702-4705. DOI: 10.1021/ol502010g.

(92) Chen, X., et. al. Cu(II)-Catalyzed Functionalizations of Aryl C−H Bonds Using $O_2$ as an Oxidant. *J. Am. Chem. Soc.* **2006**, *128* (21), 6790-6791. DOI: 10.1021/ja061715q.

(93) John, A., et. al. Copper-Catalyzed Amidation of 2-Phenylpyridine with Oxygen as the Terminal Oxidant. *J. Org. Chem.* **2011**, *76* (10), 4158-4162. DOI: 10.1021/jo200409h.

(94) Xu, H., et. al. Cu-Catalyzed Direct Amidation of Aromatic C–H Bonds: An Access to Arylamines. *J. Org. Chem.* **2014**, *79* (10), 4414-4422. DOI: 10.1021/jo5003592.

(95) Li, G., et. al. Copper(I)-Catalyzed Dehydrogenative Amidation of Arenes Using Air as the Oxidant. *Adv. Synth. Catal.* **2015**, *357* (6), 1311-1315. DOI: https://doi.org/10.1002/adsc.201400883.

(96) Tran, L. D., et. al. . Directed Amination of Non-Acidic Arene C-H Bonds by a Copper–Silver Catalytic System. *Angew. Chem. Int. Ed.* **2013**, *52* (23), 6043-6046. DOI: https://doi.org/10.1002/anie.201300135.

(97) Pumphrey, A. L., et. al. $Rh^{II2}$-Catalyzed Synthesis of α-, β-, or δ-Carbolines from Aryl Azides. *Angew. Chem. Int. Ed.* **2012**, *51* (24), 5920-5923. DOI: https://doi.org/10.1002/anie.201201788.

(98) Stokes, B. J., et. al. $Rh_2$(II)-Catalyzed Nitro-Group Migration Reactions: Selective Synthesis of 3-Nitroindoles from β-Nitro Styryl Azides. *J. Am. Chem. Soc.* **2011**, *133* (13), 4702-4705. DOI: 10.1021/ja111060q.

(99) Stokes, B. J., et. al. $Rh_2$(II)-Catalyzed Synthesis of Carbazoles from Biaryl Azides. *J. Org. Chem.* **2009**, *74* (8), 3225-3228. DOI: 10.1021/jo9002536.

(100) Chiba, S., et. al. Rh(II)-Catalyzed Isomerization of 2-Aryl-2H-azirines to 2,3-Disubstituted Indoles. *ChemInform* **2007**, *38* (26). DOI: https://doi.org/10.1002/chin.200726104.

(101) Shen, M., et. al. Dirhodium(II)-Catalyzed Intramolecular C-H Amination of Aryl Azides. *Angew. Chem. Int. Ed.* **2008**, *47* (27), 5056-5059. DOI: https://doi.org/10.1002/anie.200800689.

(102) He, L., et. al. Ruthenium(II) Porphyrin-Catalyzed Amidation of Aromatic Heterocycles. *Org. Lett.* **2004**, *6* (14), 2405-2408. DOI: 10.1021/ol049232j.

(103) Shou, W. G., et. al. Ruthenium-Catalyzed Intramolecular Amination Reactions of Aryl- and Vinylazides. *Organometallics* **2009**, *28* (24), 6847-6854. DOI: 10.1021/om900275j.

(104) Wei, J., et. al. Ruthenium porphyrin catalyzed diimination of indoles with aryl azides as the nitrene

source. *Chem. Comm.* **2014**, *50* (25), 3373-3376, 10.1039/C3CC49052A. DOI: 10.1039/C3CC49052A.
(105) Liang, S., et. al. Half-Sandwich Scorpionates as Nitrene Transfer Catalysts. *Organometallics* **2012**, *31* (23), 8055-8058. DOI: 10.1021/om3009102.
(106) Liu, Y., et. al. [Fe($F_{20}$TPP)Cl]-Catalyzed Amination with Arylamines and {[Fe($F_{20}$TPP)(NAr)](PhI=NAr)} Intermediate Assessed by High-Resolution ESI-MS and DFT Calculations. *Chem. Asian J.* **2015**, *10* (1), 100-105. DOI: https://doi.org/10.1002/asia.201402580.
(107) Bonnamour, J., et. al. Iron(II) Triflate as a Catalyst for the Synthesis of Indoles by Intramolecular C−H Amination. *Org. Lett.* **2011**, *13* (8), 2012-2014. DOI: 10.1021/ol2004066.
(108) John, A., et. al. Copper-catalyzed C($sp^2$)-H amidation of unactivated arenes by *N*-tosyloxycarbamates. *Chem. Comm.* **2013**, *49* (93), 10965-10967. DOI: 10.1039/c3cc46412a.
(109) Breslow, R., et. al. Intramolecular nitrene carbon-hydrogen insertions mediated by transition-metal complexes as nitrogen analogs of cytochrome P-450 reactions. *J. Am. Chem. Soc.* **1983**, *105* (22), 6728-6729. DOI: 10.1021/ja00360a039.
(110) Fiori, K. W., et. al. A mechanistic analysis of the Rh-catalyzed intramolecular C–H amination reaction. *Tetrahedron* **2009**, *65* (16), 3042-3051. DOI: https://doi.org/10.1016/j.tet.2008.11.073.
(111) Du Bois, J. Rhodium-Catalyzed C–H Amination. An Enabling Method for Chemical Synthesis. *Org. Process Res. Dev.* **2011**, *15* (4), 758-762. DOI: 10.1021/op200046v.
(112) Wehn, P. M., et. al. Stereochemical Models for Rh-Catalyzed Amination Reactions of Chiral Sulfamates. *Org. Lett.* **2003**, *5* (25), 4823-4826. DOI: 10.1021/ol035776u.
(113) Espino, C. G., et. al. Expanding the Scope of C−H Amination through Catalyst Design. *J. Am. Chem. Soc.* **2004**, *126* (47), 15378-15379. DOI: 10.1021/ja0446294.
(114) Grigg, R. D., et. al. Synthesis of Propargylic and Allenic Carbamates via the C–H Amination of Alkynes. *Org. Lett.* **2012**, *14* (1), 280-283. DOI: 10.1021/ol203055v.
(115) Nguyen, Q., et. al. $Rh_2$(II)-Catalyzed Intramolecular Aliphatic C–H Bond Amination Reactions Using Aryl Azides as the N-Atom Source. *J. Am. Chem. Soc.* **2012**, *134* (17), 7262-7265. DOI: 10.1021/ja301519q.
(116) Kurokawa, T., et. al. Synthesis of 1,3-Diamines Through Rhodium-Catalyzed C-H Insertion. *Angew. Chem. Int. Ed.* **2009**, *48* (15), 2777-2779. DOI: https://doi.org/10.1002/anie.200806192.
(117) Fiori, K. W., et. al. Catalytic Intermolecular Amination of C−H Bonds: Method Development and Mechanistic Insights. *J. Am. Chem. Soc.* **2007**, *129* (3), 562-568. DOI: 10.1021/ja0650450.
(118) Roizen, J. L., et. al. Selective Intermolecular Amination of C-H Bonds at Tertiary Carbon Centers. *Angew. Chem. Int. Ed.* **2013**, *52* (43), 11343-11346. DOI: https://doi.org/10.1002/anie.201304238.
(119) Bess, E. N., et. al. Analyzing Site Selectivity in $Rh_2$(esp)$_2$-Catalyzed Intermolecular C–H Amination Reactions. *J. Am. Chem. Soc.* **2014**, *136* (15), 5783-5789. DOI: 10.1021/ja5015508.
(120) Liang, C., et. al. Efficient Diastereoselective Intermolecular Rhodium-Catalyzed C-H Amination. *Angew. Chem. Int. Ed.* **2006**, *45* (28), 4641-4644. DOI: https://doi.org/10.1002/anie.200601248.
(121) Liang, C., et. al. Toward a Synthetically Useful Stereoselective C−H Amination of Hydrocarbons. *J. Am. Chem. Soc.* **2008**, *130* (1), 343-350. DOI: 10.1021/ja076519d.
(122) Collet, F. Studies in catalytic C–H amination involving nitrene C–H insertion. *Dalton Trans.* **2010**, *39* (43), 10401-10413, 10.1039/C0DT00283F. DOI: 10.1039/C0DT00283F.
(123) Buendia, J., et. al. Tandem Catalytic C($sp^3$)-H Amination/Sila-Sonogashira–Hagihara Coupling Reactions with Iodine Reagents. *Angew. Chem. Int. Ed.* **2015**, *54* (19), 5697-5701. DOI: https://doi.org/10.1002/anie.201412364.
(124) Reddy, R. P., et. al. Dirhodium Tetracarboxylates Derived from Adamantylglycine as Chiral

Catalysts for Enantioselective C−H Aminations. *Org. Lett.* **2006**, *8* (22), 5013-5016. DOI: 10.1021/ol061742l.

(125) Zalatan, D. N., et. al. A Chiral Rhodium Carboxamidate Catalyst for Enantioselective C−H Amination. *J. Am. Chem. Soc.* **2008**, *130* (29), 9220-9221. DOI: 10.1021/ja8031955.

(126) Noda, H., et. al. *O*-Benzoylhydroxylamines as Alkyl Nitrene Precursors: Synthesis of Saturated N-Heterocycles from Primary Amines. *Org. Lett.* **2020**, *22* (22), 8769-8773. DOI: 10.1021/acs.orglett.0c02842.

(127) Yu, X.-Q., et. al. Amidation of Saturated C−H Bonds Catalyzed by Electron-Deficient Ruthenium and Manganese Porphyrins. A Highly Catalytic Nitrogen Atom Transfer Process. *Org. Lett.* **2000**, *2* (15), 2233-2236. DOI: 10.1021/ol000107r.

(128) Harvey, M. E., et. al. A Diruthenium Catalyst for Selective, Intramolecular Allylic C–H Amination: Reaction Development and Mechanistic Insight Gained through Experiment and Theory. *J. Am. Chem. Soc.* **2011**, *133* (43), 17207-17216. DOI: 10.1021/ja203576p.

(129) Milczek, E., et. al. Enantioselective C-H Amination Using Cationic Ruthenium(II)–pybox Catalysts. *Angew. Chem. Int. Ed.* **2008**, *47* (36), 6825-6828. DOI: https://doi.org/10.1002/anie.200801445.

(130) Nishioka, Y., et. al. Enantio- and Regioselective Intermolecular Benzylic and Allylic C-H Bond Amination. *Angew. Chem. Int. Ed.* **2013**, *52* (6), 1739-1742. DOI: https://doi.org/10.1002/anie.201208906.

(131) Liu, Y.; Che, C.-M. [FeIII(F20-tpp)Cl] Is an Effective Catalyst for Nitrene Transfer Reactions and Amination of Saturated Hydrocarbons with Sulfonyl and Aryl Azides as Nitrogen Source under Thermal and Microwave-Assisted Conditions. *Chemistry – A European Journal* **2010**, *16* (34), 10494-10501. DOI: https://doi.org/10.1002/chem.201000581.

(132) Paradine, S. M., et. al. Iron-Catalyzed Intramolecular Allylic C–H Amination. *J. Am. Chem. Soc.* **2012**, *134* (4), 2036-2039. DOI: 10.1021/ja211600g.

(133) King, E. R., et. al. Catalytic C−H Bond Amination from High-Spin Iron Imido Complexes. *J. Am. Chem. Soc.* **2011**, *133* (13), 4917-4923. DOI: 10.1021/ja110066j.

(134) Prier, C. K., et. al. Enantioselective, intermolecular benzylic C–H amination catalysed by an engineered iron-haem enzyme. *Nat. Chem.* **2017**, *9* (7), 629-634. DOI: 10.1038/nchem.2783.

(135) Athavale, S. V., et. al. Enzymatic Nitrogen Insertion into Unactivated C–H Bonds. *J. Am. Chem. Soc.* **2022**, *144* (41), 19097-19105. DOI: 10.1021/jacs.2c08285.

(136) Wu, L., et. al. Ligand-Free Iron-Catalyzed Intramolecular Amination of C-H Bond for the Synthesis of Imidazolinones. *Chinese Journal of Organic Chemistry* **2021**, *41* (10), 4083-4087. DOI: 10.6023/cjoc202104054.

(137) Kweon, J., et. al. Highly Robust Iron Catalyst System for Intramolecular C($sp^3$)−H Amidation Leading to γ-Lactams. *Angew. Chem. Int. Ed.* **2021**, *60* (6), 2909-2914. DOI: https://doi.org/10.1002/anie.202013499.

(138) Paradine, S. M., et. al. A manganese catalyst for highly reactive yet chemoselective intramolecular C($sp^3$)–H amination. *Nature Chem.* **2015**, *7* (12), 987-994. DOI: 10.1038/nchem.2366.

(139) Clark, J. R., et. al. Manganese-catalysed benzylic C($sp^3$)–H amination for late-stage functionalization. *Nat. Chem.* **2018**, *10* (6), 583-591. DOI: 10.1038/s41557-018-0020-0.

(140) Ni, Z., et. al. Highly Regioselective Copper-Catalyzed Benzylic C-H Amination by N-Fluorobenzenesulfonimide. *Angew. Chem. Int. Ed.* **2012**, *51* (5), 1244-1247. DOI: https://doi.org/10.1002/anie.201107427.

(141) Kohmura, Y., et. al. Benzylic and Allylic Amination. *Synlett* **1997**, *12* (12), 1456-1458. DOI: 10.1055/s-1997-1067.

(142) Gephart III, R. T., et. al. Catalytic C-H Amination with Aromatic Amines. *Angew. Chem. Int. Ed.* **2012**, *51* (26), 6488-6492. DOI: https://doi.org/10.1002/anie.201201921.

(143) Michaudel, Q., et. al. Intermolecular Ritter-Type C–H Amination of Unactivated $sp^3$ Carbons. *J. Am. Chem. Soc.* **2012**, *134* (5), 2547-2550. DOI: 10.1021/ja212020b.

(144) Tran, B. L., et. al. Copper-Catalyzed Intermolecular Amidation and Imidation of Unactivated Alkanes. *J. Am. Chem. Soc.* **2014**, *136* (6), 2555-2563. DOI: 10.1021/ja411912p.

(145) Kim, D. S., et. al. Formation of the Tertiary Sulfonamide C($sp^3$)–N Bond Using Alkyl Boronic Ester via Intramolecular and Intermolecular Copper-Catalyzed Oxidative Cross-Coupling. *J. Org. Chem.* **2021**, *86* (23), 17380-17394. DOI: 10.1021/acs.joc.1c01759.

(146) Lee, J., et. al. Versatile Cp*Co(III)(LX) Catalyst System for Selective Intramolecular C–H Amidation Reactions. *J. Am. Chem. Soc.* **2020**, *142* (28), 12324-12332. DOI: 10.1021/jacs.0c04448.

(147) Zhang, Y., et. al. Au(III)-catalyzed intermolecular amidation of benzylic C–H bonds. *Org. Biomol. Chem.* **2012**, *10* (46), 9137-9141, 10.1039/C2OB26857D. DOI: 10.1039/C2OB26857D.

(148) Sun, K., et. al. Intramolecular Ir(I)-Catalyzed Benzylic C−H Bond Amination of ortho-Substituted Aryl Azides. *Org. Lett.* **2009**, *11* (16), 3598-3601. DOI: 10.1021/ol901317j.

(149) Ichinose, M., et. al. Enantioselective Intramolecular Benzylic C-H Bond Amination: Efficient Synthesis of Optically Active Benzosultams. *Angew. Chem. Int. Ed.* **2011**, *50* (42), 9884-9887. DOI: https://doi.org/10.1002/anie.201101801.

(150) Hong, S. Y., et. al. Selective formation of $\gamma$-lactams via C-H amidation enabled by tailored iridium catalysts. *Science* **2018**, *359* (6379), 1016-1021. DOI: doi:10.1126/science.aap7503.

(151) Dydio, P., et. al. Chemoselective, Enzymatic C–H Bond Amination Catalyzed by a Cytochrome P450 Containing an Ir(Me)-PIX Cofactor. *J. Am. Chem. Soc.* **2017**, *139* (5), 1750-1753. DOI: 10.1021/jacs.6b11410.

(152) Cui, Y., et. al. A Silver-Catalyzed Intramolecular Amidation of Saturated C-H Bonds. *Angew. Chem. Int. Ed.* **2004**, *43* (32), 4210-4212. DOI: https://doi.org/10.1002/anie.200454243.

(153) Li, Z., et. al. Silver-Catalyzed Intermolecular Amination of C-H Groups. *Angew. Chem. Int. Ed.* **2007**, *46* (27), 5184-5186. DOI: https://doi.org/10.1002/anie.200700760.

(154) Alderson, J. M., et. al. Ligand-Controlled, Tunable Silver-Catalyzed C–H Amination. *J. Am. Chem. Soc.* **2014**, *136* (48), 16720-16723. DOI: 10.1021/ja5094309.

(155) Hazelard, D., et. al. Catalytic C–H amination at its limits: challenges and solutions. *Org. Chem. Front.* **2017**, *4* (12), 2500-2521, 10.1039/C7QO00547D. DOI: 10.1039/C7QO00547D.

(156) Roizen, J. L., et. al. Metal-Catalyzed Nitrogen-Atom Transfer Methods for the Oxidation of Aliphatic C–H Bonds. *Acc. Chem. Res.* **2012**, *45* (6), 911-922. DOI: 10.1021/ar200318q.

(157) Darses, B., et. al. Transition metal-catalyzed iodine(III)-mediated nitrene transfer reactions: efficient tools for challenging syntheses. *Chem. Comm.* **2017**, *53* (3), 493-508, 10.1039/C6CC07925C. DOI: 10.1039/C6CC07925C.

(158) Chiappini, N. D., et. al. Intermolecular C($sp^3$)−H Amination of Complex Molecules. *Angew. Chem. Int. Ed.* **2018**, *57* (18), 4956-4959. DOI: https://doi.org/10.1002/anie.201713225.

(159) Wang, Y.-C., et. al. Unravelling nitrene chemistry from acyclic precursors: recent advances and challenges. *Org. Chem. Front.* **2021**, *8* (7), 1677-1693, 10.1039/D0QO01360A. DOI: 10.1039/D0QO01360A.

(160) Brunard, E., et. al. Catalytic Intermolecular C($sp^3$)–H Amination: Selective Functionalization of

Tertiary C–H Bonds vs Activated Benzylic C–H Bonds. *J. Am. Chem. Soc.* **2021**, *143* (17), 6407-6412. DOI: 10.1021/jacs.1c03872.

(161) Brady, P. B., et. al. Recent Applications of Rh- and Pd-Catalyzed C($sp^3$)–H Functionalization in Natural Product Total Synthesis. *Eur. J. Org. Chem.* **2017**, *2017* (35), 5179-5190. DOI: https://doi.org/10.1002/ejoc.201700641.

(162) Abrams, D. J., et. al. Recent applications of C-H functionalization in complex natural product synthesis. *Chem. Soc. Rev.* **2018**, *47* (23), 8925-8967, 10.1039/C8CS00716K. DOI: 10.1039/C8CS00716K.

(163) Tsukano, C., et. al. Total Synthesis of Nitrogen-Containing Natural Products Based on Palladium-Catalyzed C-H Functionalization. In *Handbook of CH-Functionalization*, pp 1-49.

(164) Fleming, J. J., et. al. (+)-Saxitoxin: A First and Second Generation Stereoselective Synthesis. *J. Am. Chem. Soc.* **2007**, *129* (32), 9964-9975. DOI: 10.1021/ja071501o.

(165) Hinman, A., et. al. A Stereoselective Synthesis of (−)-Tetrodotoxin. *J. Am. Chem. Soc.* **2003**, *125* (38), 11510-11511. DOI: 10.1021/ja0368305.

(166) Lescot, C., et. al. Intermolecular C–H Amination of Complex Molecules: Insights into the Factors Governing the Selectivity. *J. Org. Chem.* **2012**, *77* (17), 7232-7240. DOI: 10.1021/jo301563j.

(167) O'Neil, L. G., et. al. Electrophilic Aminating Agents in Total Synthesis. *Angew. Chem. Int. Ed.* **2021**, *60* (49), 25640-25666. DOI: https://doi.org/10.1002/anie.202102864.

(168) Louillat, M.-L.; P., e. a. Oxidative C–H amination reactions. *Chem. Soc. Rev.* **2014**, *43* (3), 901-910, 10.1039/C3CS60318K. DOI: 10.1039/C3CS60318K.

(169) He, J., et. al. Palladium-Catalyzed Transformations of Alkyl C–H Bonds. *Chem. Rev.* **2017**, *117* (13), 8754-8786. DOI: 10.1021/acs.chemrev.6b00622.

(170) He, G., et. al. Highly Efficient Syntheses of Azetidines, Pyrrolidines, and Indolines via Palladium Catalyzed Intramolecular Amination of C(sp3)–H and C(sp2)–H Bonds at γ and δ Positions. *J. Am. Chem. Soc.* **2012**, *134* (1), 3-6. DOI: 10.1021/ja210660g.

(171) He, G., et. al. Use of a Readily Removable Auxiliary Group for the Synthesis of Pyrrolidones by the Palladium-Catalyzed Intramolecular Amination of Unactivated γ C($sp^3$)-H Bonds. *Angew. Chem. Int. Ed.* **2013**, *52* (42), 11124-11128. DOI: https://doi.org/10.1002/anie.201305615.

(172) Neumann, J. J., et. al. Palladium-Catalyzed Amidation of Unactivated C($sp^3$)-H Bonds: from Anilines to Indolines. *Angew. Chem. Int. Ed.* **2009**, *48* (37), 6892-6895. DOI: https://doi.org/10.1002/anie.200903035.

(173) McNally, A., et. al. Palladium-catalysed C–H activation of aliphatic amines to give strained nitrogen heterocycles. *Nature* **2014**, *510* (7503), 129-133. DOI: 10.1038/nature13389.

(174) He, J., et. al. Palladium(0)/PAr3-Catalyzed Intermolecular Amination of C(sp3) H Bonds: Synthesis of β-Amino Acids. *Angew. Chem. Int. Ed.* **2015**, *54* (22), 6545-6549. DOI: https://doi.org/10.1002/anie.201502075.

(175) Zhang, Q., et. al. Stereoselective Synthesis of Chiral α-Amino-β-Lactams through Palladium(II)-Catalyzed Sequential Monoarylation/Amidation of C($sp^3$)-H Bonds. *Angew. Chem. Int. Ed.* **2013**, *52* (51), 13588-13592. DOI: https://doi.org/10.1002/anie.201306625.

(176) Jin, L., et. al. Palladium-catalyzed intermolecular amination of unactivated C(sp3)–H bonds via a cleavable directing group. *Chem. Comm.* **2017**, *53* (28), 3986-3989, 10.1039/C7CC00808B. DOI: 10.1039/C7CC00808B.

(177) Wang, Z., et. al. Copper-Catalyzed Intramolecular C($sp^3$)-H and C($sp^2$)-H Amidation by Oxidative Cyclization. *Angew. Chem. Int. Ed.* **2014**, *53* (13), 3496-3499. DOI:

https://doi.org/10.1002/anie.201311105.

(178) Kang, T., et. al. Synthesis of 1,2-amino alcohols via catalytic C–H amidation of $sp^3$ methyl C–H bonds. *Chem. Comm.* **2014**, *50* (81), 12073-12075, 10.1039/C4CC05655H. DOI: 10.1039/C4CC05655H.

(179) Kang, T., et. al. Iridium-Catalyzed Intermolecular Amidation of $sp^3$ C–H Bonds: Late-Stage Functionalization of an Unactivated Methyl Group. *J. Am. Chem. Soc.* **2014**, *136* (11), 4141-4144. DOI: 10.1021/ja501014b.

(180) Wang, N., et. al. Rhodium(III)-Catalyzed Intermolecular Amidation with Azides via C(sp3)–H Functionalization. *J. Org. Chem.* **2014**, *79* (11), 5379-5385. DOI: 10.1021/jo5008515.

(181) Tang, C., et. al. Rh-Catalyzed Direct Amination of Unactivated C($sp^3$)−H bond with Anthranils Under Mild Conditions. *Chem. Eur. J.* **2016**, *22* (32), 11165-11169. DOI: https://doi.org/10.1002/chem.201602556.

(182) Huang, X., et. al. Rhodium(III)-Catalyzed Activation of C-H Bonds and Subsequent Intermolecular Amidation at Room Temperature. *Angew. Chem. Int. Ed.* **2015**, *54* (32), 9404-9408. DOI: https://doi.org/10.1002/anie.201504507.

(183) Yu, S., et. al. Anthranil: An Aminating Reagent Leading to Bifunctionality for Both C($sp^3$)−H and C($sp^2$)−H under Rhodium(III) Catalysis. *Angew. Chem. Int. Ed.* **2016**, *55* (30), 8696-8700. DOI: https://doi.org/10.1002/anie.201602224.

(184) Wang, H., et. al. Rhodium(III)-Catalyzed Amidation of Unactivated C($sp^3$)-H Bonds. *Angew. Chem. Int. Ed.* **2015**, *54* (44), 13049-13052. DOI: https://doi.org/10.1002/anie.201506323.

(185) Liu, B., et. al. Ru(II)-catalyzed amidation reactions of 8-methylquinolines with azides via C($sp^3$)–H activation. *Chem. Comm.* **2015**, *51* (91), 16334-16337, 10.1039/C5CC06230F. DOI: 10.1039/C5CC06230F.

(186) Wu, X., et. al. Cobalt-catalysed site-selective intra- and intermolecular dehydrogenative amination of unactivated sp3 carbons. *Nat. Commun.* **2015**, *6* (1), 6462. DOI: 10.1038/ncomms7462.

(187) Cochet, T., et. al. Rhodium(iii)-catalyzed allylic C–H bond amination. Synthesis of cyclic amines from ω-unsaturated N-sulfonylamines. *Chem. Comm.* **2012**, *48* (87), 10745-10747, 10.1039/C2CC36067E. DOI: 10.1039/C2CC36067E.

(188) Shibata, Y. e. a. Facile Generation and Isolation of π-Allyl Complexes from Aliphatic Alkenes and an Electron-Deficient Rh(III) Complex: Key Intermediates of Allylic C–H Functionalization. *Organometallics* **2016**, *35* (10), 1547-1552. DOI: 10.1021/acs.organomet.6b00143.

(189) Burman, J. S., et. al. Regioselective Intermolecular Allylic C−H Amination of Disubstituted Olefins via Rhodium/π-Allyl Intermediates. *Angew. Chem. Int. Ed.* **2017**, *56* (44), 13666-13669. DOI: https://doi.org/10.1002/anie.201707021.

(190) Farr, C. M. B., et. al. Designing a Planar Chiral Rhodium Indenyl Catalyst for Regio- and Enantioselective Allylic C–H Amidation. *J. Am. Chem. Soc.* **2020**, *142* (32), 13996-14004. DOI: 10.1021/jacs.0c07305.

(191) Burman, J. S., et. al. Rh(III) and Ir(III)Cp* Complexes Provide Complementary Regioselectivity Profiles in Intermolecular Allylic C–H Amidation Reactions. *ACS Catal.* **2019**, *9* (6), 5474-5479. DOI: 10.1021/acscatal.9b01338.

(192) Nelson, T. A. F., et. al. Allylic C–H functionalization via group 9 π-allyl intermediates. *Dalton Trans.* **2020**, *49* (40), 13928-13935, 10.1039/D0DT02313B. DOI: 10.1039/D0DT02313B.

(193) Sihag, P., et. al. Rh(III)-Catalyzed allylic C–H amidation of unactivated alkenes with in situ generated iminoiodinanes. *Chem. Comm.* **2021**, *57* (52), 6428-6431, 10.1039/D1CC02283K. DOI: 10.1039/D1CC02283K.

(194) Wang, F., et. al. Comprehensive Theoretical Study of Cp*Ir$^{III}$-Catalyzed Intermolecular Enantioselective Allylic C–H Amidation: Reaction Mechanism, Electronic Processes, and Regioselectivity. **2023**, *88* (4), 2493-2504. DOI: 10.1021/acs.joc.2c02951.

(195) Kazerouni, A. M., et. al. Regioselective Cp*Ir(III)-Catalyzed Allylic C–H Sulfamidation of Allylbenzene Derivatives. *J, Org. Chem* **2019**, *84* (20), 13179-13185. DOI: 10.1021/acs.joc.9b01816.

(196) Sihag, P., et. al. Iridium(III)-Catalyzed Intermolecular Allylic C–H Amidation of Internal Alkenes with Sulfonamides. *J. Org. Chem.* **2019**, *84* (20), 13053-13064. DOI: 10.1021/acs.joc.9b02047.

(197) Lei, H. e. a. A site-selective amination catalyst discriminates between nearly identical C–H bonds of unsymmetrical disubstituted alkenes. *Nat. Chem.* **2020**, *12* (8), 725-731. DOI: 10.1038/s41557-020-0470-z.

(198) Knecht, T., et. al. Intermolecular, Branch-Selective, and Redox-Neutral Cp*IrIII-Catalyzed Allylic C−H Amidation. *Angew. Chem. Int. Ed.* **2019**, *58* (21), 7117-7121. DOI: https://doi.org/10.1002/anie.201901733.

(199) Huang, F., et. al. Electrostatic repulsion-controlled regioselectivity in nitrene-mediated allylic C–H amidations. *Org. Chem. Front.* **2021**, *8* (21), 6038-6047, 10.1039/D1QO01018B. DOI: 10.1039/D1QO01018B.

(200) Lei, H., et. al. Ir-Catalyzed Intermolecular Branch-Selective Allylic C–H Amidation of Unactivated Terminal Olefins. *J. Am. Chem. Soc.* **2019**, *141* (6), 2268-2273. DOI: 10.1021/jacs.9b00237.

(201) Duarte, F. J. S., et. al. Mechanistic Study of the Direct Intramolecular Allylic Amination Reaction Catalyzed by Palladium(II). *ACS Catal.* **2016**, *6* (3), 1772-1784. DOI: 10.1021/acscatal.5b02091.

(202) Nahra, F., et. al. Striking AcOH Acceleration in Direct Intramolecular Allylic Amination Reactions. **2009**, *15* (42), 11078-11082. DOI: https://doi.org/10.1002/chem.200901946.

(203) Fraunhoffer, K. J., et. al. *syn*-1,2-Amino Alcohols via Diastereoselective Allylic C−H Amination. *Journal of the American Chemical Society* **2007**, *129* (23), 7274-7276. DOI: 10.1021/ja071905g.

(204) Rice, G. T., et. al. Allylic C−H Amination for the Preparation of syn-1,3-Amino Alcohol Motifs. *J. Am. Chem. Soc.* **2009**, *131* (33), 11707-11711. DOI: 10.1021/ja9054959.

(205) Jiang, C.; Covell, D. J.; Stepan, A. F.; Plummer, M. S.; White, M. C. Sequential Allylic C–H Amination/Vinylic C–H Arylation: A Strategy for Unnatural Amino Acid Synthesis from α-Olefins. *Organic Letters* **2012**, *14* (6), 1386-1389. DOI: 10.1021/ol300063t.

(206) Wu, L., et. al. Brønsted Base-Modulated Regioselective Pd-Catalyzed Intramolecular Aerobic Oxidative Amination of Alkenes: Formation of Seven-Membered Amides and Evidence for Allylic C−H Activation. *Org. Lett.* **2009**, *11* (12), 2707-2710. DOI: 10.1021/ol900941t.

(207) Sharma, A., et. al. Enantioselective Functionalization of Allylic C–H Bonds Following a Strategy of Functionalization and Diversification. *J. Am. Chem. Soc.* **2013**, *135* (47), 17983-17989. DOI: 10.1021/ja409995w.

(208) Pak S. C., e. a. Asymmetric intermolecular allylic C-H amination of alkenes with aliphatic amines. *Science* **2022**, *378* (6625), 1207-1213. DOI: doi:10.1126/science.abq1274.

(209) Wang, J., et. al. Theoretical studies on Mn-catalyzed intermolecular allylic C-H aminations of internal olefins: mechanism, chemo- and regioselectivity. *Molecular Catalysis* **2022**, *524*, 112278. DOI: https://doi.org/10.1016/j.mcat.2022.112278.

(210) Zhou, S., et. al. Direct intermolecular C(sp$^3$)–H amidation with dioxazolones via synergistic decatungstate anion photocatalysis and nickel catalysis: A combined experimental and computational study. *Journal of Catalysis* **2022**, *415*, 142-152. DOI: https://doi.org/10.1016/j.jcat.2022.10.003.

(211) Zheng, Y.-W., et. al. Copper(II)-Photocatalyzed N–H Alkylation with Alkanes. *ACS Catal.* **2020**,

*10* (15), 8582-8589. DOI: 10.1021/acscatal.0c01924.
(212) Wang, Q., et. al. Photoexcited Direct Amination/Amidation of Inert Csp3–H Bonds via Tungsten–Nickel Catalytic Relay. *ACS Catal.* **2022**, *12* (18), 11071-11077. DOI: 10.1021/acscatal.2c03456.
(213) Wakikawa, T., et. al. Native Amide-Directed C($sp^3$)−H Amidation Enabled by Electron-Deficient RhIII Catalyst and Electron-Deficient 2-Pyridone Ligand. *Angew. Chem. Int. Ed.* **2022**, *61* (52), e202213659. DOI: https://doi.org/10.1002/anie.202213659.
(214) Thomas, F., et. al. A new generation of terminal copper nitrenes and their application in aromatic C–H amination reactions. *Dalton Trans.* **2021**, *50* (19), 6444-6462, 10.1039/D1DT00832C. DOI: 10.1039/D1DT00832C.
(215) Bakhoda, A., et. al. Copper-Catalyzed C($sp^3$)−H Amidation: Sterically Driven Primary and Secondary C−H Site-Selectivity. *Angew. Chem. Int. Ed.* **2019**, *58* (11), 3421-3425. DOI: https://doi.org/10.1002/anie.201810556.
(216) Lee, J., et. al. Cobalt-Catalyzed Intermolecular C–H Amidation of Unactivated Alkanes. *J. Am. Chem. Soc.* **2021**, *143* (13), 5191-5200. DOI: 10.1021/jacs.1c01524.
(217) Wang, Q., et. al. Visible-light-mediated tungsten-catalyzed C-H amination of unactivated alkanes with nitroarenes. *Science China Chemistry* **2022**, *65* (4), 678-685. DOI: 10.1007/s11426-021-1170-2.
(218) Chen, B., et. al. Overview of lethal human coronaviruses. *Sig. Transduct Target Ther.* **2020**, *5* (1), 89. DOI: 10.1038/s41392-020-0190-2.
(219) Ramesh, S., et. al. Emerging SARS-CoV-2 Variants: A Review of Its Mutations, Its Implications and Vaccine Efficacy. *Vaccines* **2021**, *9* (10). DOI: 10.3390/vaccines9101195.
(220) Du, X., et. al. Omicron adopts a different strategy from Delta and other variants to adapt to host. *Sig. Transduct Target Ther.* **2022**, *7* (1), 45. DOI: 10.1038/s41392-022-00903-5.
(221) Zhang, Q., et. al. Molecular mechanism of interaction between SARS-CoV-2 and host cells and interventional therapy. *Sig. Transduct Target Ther.* **2021**, *6* (1), 233. DOI: 10.1038/s41392-021-00653-w.
(222) Arya, R., et. al. Structural insights into SARS-CoV-2 proteins. *J. Mol. Biol.* **2021**, *433* (2), 166725. DOI: 10.1016/j.jmb.2020.11.024.
(223) Gao, Y., et. al. Structure of the RNA-dependent RNA polymerase from COVID-19 virus. *Science* **2020**, *368*, 4.
(224) Bartlam, M., et. al. Structural proteomics of the SARS coronavirus: a model response to emerging infectious diseases. *J. Struct. Funct. Genomics* **2007**, *8* (2-3), 85-97. DOI: 10.1007/s10969-007-9024-5.
(225) Chu, C. M., et. al. Role of lopinavir/ritonavir in the treatment of SARS: initial virological and clinical findings. *Thorax* **2004**, *59* (3), 252-256. DOI: 10.1136/thorax.2003.012658.
(226) Yalcin, N., et. al. COVID-19 and antiepileptic drugs: an approach to guide practices when nirmatrelvir/ritonavir is co-prescribed. *Eur. J. Clin. Pharmacol.* **2022**, *78* (10), 1697-1701. DOI: 10.1007/s00228-022-03370-7.
(227) Thompson, M. G., et. al. Paxlovid Associated with Decreased Hospitalization Rate Among Adults with
COVID-19 — United States, April–September 2022. *Morb. Mortal Wkly. Rep.* **2021**, *385* (15), 1355-1371. DOI: 10.1056/NEJMoa2110362 From NLM Medline.
(228) Tyndall, J. D. A. S-217622, a 3CL Protease Inhibitor and Clinical Candidate for SARS-CoV-2. *J. Med. Chem.* **2022**, *65* (9), 6496-6498. DOI: 10.1021/acs.jmedchem.2c00624.
(229) Xiaoxin, C., et. al. Inhibition mechanism and antiviral activity of an α-ketoamide based SARS-CoV-2 main protease inhibitor. *bioRxiv* **2023**, 2023.2003.2009.531862. DOI: 10.1101/2023.03.09.531862.

(230) Báez-Santos, Y. M., et. al. The SARS-coronavirus papain-like protease: Structure, function and inhibition by designed antiviral compounds. *Antiviral Research* **2015**, *115*, 21-38. DOI: https://doi.org/10.1016/j.antiviral.2014.12.015.

(231) Walls, A. C., et. al. Structure, Function, and Antigenicity of the SARS-CoV-2 Spike Glycoprotein. *Cell* **2020**, *181* (2), 281-292.e286. DOI: https://doi.org/10.1016/j.cell.2020.02.058.

(232) Bégin, P., et. al. Convalescent plasma for hospitalized patients with COVID-19: an open-label, randomized controlled trial. *Nat. Med.* **2021**, *27* (11), 2012-2024. DOI: 10.1038/s41591-021-01488-2.

(233) Xiang, R., et. al. Neutralizing monoclonal antibodies against highly pathogenic coronaviruses. *Current Opinion in Virology* **2022**, *53*, 101199. DOI: https://doi.org/10.1016/j.coviro.2021.12.015.

(234) Xia, S., et. al. Peptide-based pan-CoV fusion inhibitors maintain high potency against SARS-CoV-2 Omicron variant. *Cell Research* **2022**, *32* (4), 404-406. DOI: 10.1038/s41422-022-00617-x.

(235) Omrani, A. S., et. al. Ribavirin and interferon alfa-2a for severe Middle East respiratory syndrome coronavirus infection: a retrospective cohort study. *The Lancet Infectious Dis.* **2014**, *14* (11), 1090-1095. DOI: https://doi.org/10.1016/S1473-3099(14)70920-X.

(236) Rossignol, J.-F. Nitazoxanide: A first-in-class broad-spectrum antiviral agent. *Antiviral Research* **2014**, *110*, 94-103. DOI: https://doi.org/10.1016/j.antiviral.2014.07.014.

(237) Lam, S., et. al. COVID-19: A review of the proposed pharmacological treatments. *European Journal of Pharmacology* **2020**, *886*, 173451. DOI: https://doi.org/10.1016/j.ejphar.2020.173451.

(238) Dong, S., et. al. A guideline for homology modeling of the proteins from newly discovered betacoronavirus, 2019 novel coronavirus (2019-nCoV). *J. Med. Virol.* **2020**, *92* (9), 1542-1548. DOI: https://doi.org/10.1002/jmv.25768.

(239) Gao, Y., et. al. Structure of the RNA-dependent RNA polymerase from COVID-19 virus. *Science* **2020**, *368* (6492), 779-782. DOI: doi:10.1126/science.abb7498.

(240) Wang, Q., et. al. Structural Basis for RNA Replication by the SARS-CoV-2 Polymerase. *Cell* **2020**, *182* (2), 417-428.e413. DOI: https://doi.org/10.1016/j.cell.2020.05.034.

(241) Gordon, C. J.; Tchesnokov, E. P.; Schinazi, R. F.; Götte, M. Molnupiravir promotes SARS-CoV-2 mutagenesis via the RNA template. *J. Biol. Chem.* **2021**, *297* (1), 100770. DOI: https://doi.org/10.1016/j.jbc.2021.100770.

(242) Eastman, R. T., et. al. Remdesivir: A Review of Its Discovery and Development Leading to Emergency Use Authorization for Treatment of COVID-19. *ACS Cent. Sci.* **2020**, *6* (5), 672-683. DOI: 10.1021/acscentsci.0c00489.

(243) Zhang, J., et. al. Azvudine is a thymus-homing anti-SARS-CoV-2 drug effective in treating COVID-19 patients. *Sig. Transduct Target. Ther.* **2021**, *6* (1), 414. DOI: 10.1038/s41392-021-00835-6.

(244) Zhou, S., et. al. β-D-$N^4$-hydroxycytidine Inhibits SARS-CoV-2 Through Lethal Mutagenesis But Is Also Mutagenic To Mammalian Cells. *The Journal of Infectious Diseases* **2021**, *224* (3), 415-419. DOI: 10.1093/infdis/jiab247 (acccessed 6/25/2023).

(245) Fischer, W. A., et. al. A phase 2a clinical trial of molnupiravir in patients with COVID-19 shows accelerated SARS-CoV-2 RNA clearance and elimination of infectious virus. *Science Translational Medicine* **2022**, *14* (628), eabl7430. DOI: doi:10.1126/scitranslmed.abl7430.

(246) Warren, T., et. al. Nucleotide Prodrug GS-5734 Is a Broad-Spectrum Filovirus Inhibitor That Provides Complete Therapeutic Protection Against the Development of Ebola Virus Disease (EVD) in Infected Non-human Primates. *Open Forum Infectious Diseases* **2015**, *2* (suppl_1). DOI: 10.1093/ofid/ofv130.02 (acccessed 5/29/2023).

(247) Tchesnokov, E. P.; Feng, J. Y.; Porter, D. P.; Götte, M. Mechanism of Inhibition of Ebola Virus

RNA-Dependent RNA Polymerase by Remdesivir. *Viruses* **2019**, *11* (4). DOI: 10.3390/v11040326 From NLM.

(248) Keating, G. M., et. al. Sofosbuvir: First Global Approval. *Drugs* **2014**, *74* (2), 273-282. DOI: 10.1007/s40265-014-0179-7.

(249) Jácome, R.; Campillo-Balderas, J. A.; Ponce de León, S.; Becerra, A.; Lazcano, A. Sofosbuvir as a potential alternative to treat the SARS-CoV-2 epidemic. *Sci. Rep.* **2020**, *10* (1), 9294. DOI: 10.1038/s41598-020-66440-9.

(250) Taylor, R., et. al. Activity of Galidesivir in a Hamster Model of SARS-CoV-2. *Viruses* **2022**, *14* (1), 8.

(251) Julander, J. G., et. al. An update on the progress of galidesivir (BCX4430), a broad-spectrum antiviral. *Antiviral Research* **2021**, *195*, 105180. DOI: https://doi.org/10.1016/j.antiviral.2021.105180.

(252) Hassanipour, S., et. al. The efficacy and safety of Favipiravir in treatment of COVID-19: a systematic review and meta-analysis of clinical trials. *Scientific Reports* **2021**, *11* (1), 11022. DOI: 10.1038/s41598-021-90551-6.

(253) Coomes, E. A., et. al. Favipiravir, an antiviral for COVID-19? *Journal of Antimicrobial Chemotherapy* **2020**, *75* (7), 2013-2014. DOI: 10.1093/jac/dkaa171 (acccessed 6/28/2023).

(254) Tong, S.; Su, Y.; Yu, Y.; Wu, C.; Chen, J.; Wang, S.; Jiang, J. Ribavirin therapy for severe COVID-19: a retrospective cohort study. *International Journal of Antimicrobial Agents* **2020**, *56* (3), 106114. DOI: https://doi.org/10.1016/j.ijantimicag.2020.106114.

(255) Steven, S. G., et. al. AT-527, a Double Prodrug of a Guanosine Nucleotide Analog, Is a Potent Inhibitor of SARS-CoV-2 *In Vitro* and a Promising Oral Antiviral for Treatment of COVID-19. *Antimicrob. Agents Chemother.* **2021**, *65* (4), 10.1128/aac.02479-02420. DOI: doi:10.1128/aac.02479-20.

(256) Shannon, A., et. al. A dual mechanism of action of AT-527 against SARS-CoV-2 polymerase. *Nat. Comm.* **2022**, *13* (1), 621. DOI: 10.1038/s41467-022-28113-1.

(257) P., V. Atea's AT-527 fails to meet primary goal of Phase II Covid-19 trial.

(258) Ren, Z., et. al. A Randomized, Open-Label, Controlled Clinical Trial of Azvudine Tablets in the Treatment of Mild and Common COVID-19, a Pilot Study. *Adv. Sci.* **2020**, *7* (19), 2001435. DOI: https://doi.org/10.1002/advs.202001435.

(259) Xie, Y., et. al. Design and development of an oral remdesivir derivative VV116 against SARS-CoV-2. *Cell Res.* **2021**, *31* (11), 1212-1214. DOI: 10.1038/s41422-021-00570-1.

(260) Filipowicz, W., et. al. A protein binding the methylated 5'-terminal sequence, m7GpppN, of eukaryotic messenger RNA. *Proc. Natl. Acad. Sci.* **1976**, *73* (5), 1559-1563. DOI: doi:10.1073/pnas.73.5.1559.

(261) Züst, R., et. al. Ribose 2′-*O*-methylation provides a molecular signature for the distinction of self and non-self mRNA dependent on the RNA sensor Mda5. *Nat. Immunol.* **2011**, *12* (2), 137-143. DOI: 10.1038/ni.1979.

(262) Decroly, E., et. al. Conventional and unconventional mechanisms for capping viral mRNA. *Nat. Rev. Microbiol.* **2012**, *10* (1), 51-65. DOI: 10.1038/nrmicro2675.

(263) Ogando, N. S., et. al. Structure-function analysis of the nsp14 N7-guanine methyltransferase reveals an essential role in *Betacoronavirus* replication. *PNAS* **2021**, *118* (49), e2108709118. DOI: doi:10.1073/pnas.2108709118.

(264) Devkota, K., et. al. Probing the SAM Binding Site of SARS-CoV-2 Nsp14 In Vitro Using SAM Competitive Inhibitors Guides Developing Selective Bisubstrate Inhibitors. *SLAS Discovery* **2021**, *26*

(9), 1200-1211. DOI: https://doi.org/10.1177/24725552211026261.
(265) Zhang, J., et. al. SAM/SAH Analogs as Versatile Tools for SAM-Dependent Methyltransferases. *ACS Chem. Biol.* **2016**, *11* (3), 583-597. DOI: 10.1021/acschembio.5b00812.
(266) Anglin, J. L., et. al. Synthesis and Structure–Activity Relationship Investigation of Adenosine-Containing Inhibitors of Histone Methyltransferase DOT1L. *J. Am. Chem. Soc.* **2012**, *55* (18), 8066-8074. DOI: 10.1021/jm300917h.
(267) Kim, K. H., et. al. Targeting EZH2 in cancer. *Nat. Med.* **2016**, *22* (2), 128-134. DOI: 10.1038/nm.4036.
(268) Dowden, J., et. al. Small molecule inhibitors that discriminate between protein arginine N-methyltransferases PRMT1 and CARM1. *Org. Biomol. Chem.* **2011**, *9* (22), 7814-7821, 10.1039/C1OB06100C. DOI: 10.1039/C1OB06100C.
(269) McDonald, R. I., et. al. Palladium(II)-Catalyzed Alkene Functionalization via Nucleopalladation: Stereochemical Pathways and Enantioselective Catalytic Applications. *Chem. Rev.* **2011**, *111* (4), 2981-3019. DOI: 10.1021/cr100371y.
(270) Lan, X.-W., et. al. Recent Advances in Radical Difunctionalization of Simple Alkenes. *Eur. J. Org. Chem.* **2017**, *2017* (39), 5821-5851. DOI: https://doi.org/10.1002/ejoc.201700678.
(271) Coombs, J. R., et. al. Catalytic Enantioselective Functionalization of Unactivated Terminal Alkenes. *Angew. Chem. Int. Ed.* **2016**, *55* (8), 2636-2649. DOI: https://doi.org/10.1002/anie.201507151.
(272) Jeon, J., et. al. Regio- and Stereoselective Functionalization Enabled by Bidentate Directing Groups. *Chem. Rec.* **2021**, *21* (12), 3613-3627. DOI: https://doi.org/10.1002/tcr.202100117.
(273) Vasseur, A., et. al. Remote functionalization through alkene isomerization. *Nature Chem.* **2016**, *8* (3), 209-219. DOI: 10.1038/nchem.2445.
(274) Sommer, H., et. al. Walking Metals for Remote Functionalization. *ACS Cent. Sci.* **2018**, *4* (2), 153-165. DOI: 10.1021/acscentsci.8b00005.
(275) Janssen-Müller, D., et. al. Tackling Remote $sp^3$ C−H Functionalization via Ni-Catalyzed "chain-walking" Reactions. *Isr. J. Chem.* **2020**, *60* (3-4), 195-206. DOI: https://doi.org/10.1002/ijch.201900072.
(276) Buslov, I., et. al. Chemoselective Alkene Hydrosilylation Catalyzed by Nickel Pincer Complexes. *Angew. Chem. Int. Ed.* **2015**, *54* (48), 14523-14526. DOI: https://doi.org/10.1002/anie.201507829.
(277) Buslov, I., et. al. An Easily Accessed Nickel Nanoparticle Catalyst for Alkene Hydrosilylation with Tertiary Silanes. *Angew. Chem. Int. Ed.* **2016**, *55* (40), 12295-12299. DOI: https://doi.org/10.1002/anie.201606832.
(278) Juliá-Hernández, F., et. al. Remote carboxylation of halogenated aliphatic hydrocarbons with carbon dioxide. *Nature* **2017**, *545* (7652), 84-88. DOI: 10.1038/nature22316.
(279) Sun, S.-Z., et. al. Site-Selective Ni-Catalyzed Reductive Coupling of α-Haloboranes with Unactivated Olefins. *J. Am. Chem. Soc.* **2018**, *140* (40), 12765-12769. DOI: 10.1021/jacs.8b09425.
(280) Sun, S.-Z., et. al. Site-Selective Catalytic Deaminative Alkylation of Unactivated Olefins. *J. Am. Chem. Soc.* **2019**, *141* (41), 16197-16201. DOI: 10.1021/jacs.9b07489.
(281) He, Y., et. al. Terminal-Selective C($sp^3$)–H Arylation: NiH-Catalyzed Remote Hydroarylation of Unactivated Internal Olefins. *Organometallics* **2021**, *40* (14), 2253-2264. DOI: 10.1021/acs.organomet.0c00819.
(282) Lee, W.-C., et. al. Tandem Isomerization and C–H Activation: Regioselective Hydroheteroarylation of Allylarenes. *Org. Lett.* **2013**, *15* (20), 5358-5361. DOI: 10.1021/ol402644y.
(283) He, Y., et. al. Mild and Regioselective Benzylic C–H Functionalization: Ni-Catalyzed Reductive Arylation of Remote and Proximal Olefins. *J. Am. Chem. Soc.* **2017**, *139* (3), 1061-1064. DOI:

10.1021/jacs.6b11962.

(284) Chen, F., et. al. Remote Migratory Cross-Electrophile Coupling and Olefin Hydroarylation Reactions Enabled by in Situ Generation of NiH. *J. Am. Chem. Soc.* **2017**, *139* (39), 13929-13935. DOI: 10.1021/jacs.7b08064.

(285) Xiao, J., et. al. Remote $sp^3$ C–H Amination of Alkenes with Nitroarenes. *Chem* **2018**, *4* (7), 1645-1657. DOI: https://doi.org/10.1016/j.chempr.2018.04.008.

(286) Zhang, Y., et. al. Nickel-catalysed selective migratory hydrothiolation of alkenes and alkynes with thiols. *Nat. Comm.* **2019**, *10* (1), 1752. DOI: 10.1038/s41467-019-09783-w.

(287) Yulong Z., e. a. Ligand-Enabled NiH-Catalyzed Migratory Hydroamination: Chain Walking as a Strategy for Regiodivergent/Regioconvergent Remote $sp^3$ C-H Amination. *CCS Chem.* **2021**, *3* (9), 2259-2268. DOI: doi:10.31635/ccschem.020.202000490.

(288) Liu, J., et. al. Nickel-Catalyzed, Regio- and Enantioselective Benzylic Alkenylation of Olefins with Alkenyl Bromide. *Angew. Chem. Int. Ed.* **2021**, *60* (8), 4060-4064. DOI: https://doi.org/10.1002/anie.202012614.

(289) Zhang, Y., et. al. Rapid Access to Highly Functionalized Alkyl Boronates by NiH-Catalyzed Remote Hydroarylation of Boron-Containing Alkenes. *Angew. Chem. Int. Ed.* **2019**, *58* (39), 13860-13864. DOI: https://doi.org/10.1002/anie.201907185.

(290) Qian, D., et. al. Ligand-Controlled Regiodivergent Hydroalkylation of Pyrrolines. *Angew. Chem. Int. Ed.* **2019**, *58* (51), 18519-18523. DOI: https://doi.org/10.1002/anie.201912629.

(291) Li, W., et. al. Nickel-catalyzed difunctionalization of allyl moieties using organoboronic acids and halides with divergent regioselectivities. *Chem. Sci.* **2018**, *9* (3), 600-607, 10.1039/C7SC03149A. DOI: 10.1039/C7SC03149A.

(292) Dhungana, R. K., et. al. Walking metals: catalytic difunctionalization of alkenes at nonclassical sites. *Chem. Sci.* **2020**, *11* (36), 9757-9774, 10.1039/D0SC03634J. DOI: 10.1039/D0SC03634J.

(293) Yu, B., et. al. Azvudine (FNC): a promising clinical candidate for COVID-19 treatment. *Sig. Transduct. Target. Ther.* **2020**, *5* (1), 236. DOI: 10.1038/s41392-020-00351-z.

(294) Lipinski, C. A., et. al. Experimental and computational approaches to estimate solubility and permeability in drug discovery and development settings. *Advanced Drug Delivery Reviews* **1997**, *23* (1), 3-25. DOI: https://doi.org/10.1016/S0169-409X(96)00423-1.

(295) Bobrovs, R., et. al. Discovery of SARS-CoV-2 Nsp14 and Nsp16 Methyltransferase Inhibitors by High-Throughput Virtual Screening. *Pharmaceuticals* **2021**, *14* (12), 1243.

(296) Otava, T.; Šála, e. a. The Structure-Based Design of SARS-CoV-2 nsp14 Methyltransferase Ligands Yields Nanomolar Inhibitors. *ACS Infect. Dis.* **2021**, *7* (8), 2214-2220. DOI: 10.1021/acsinfecdis.1c00131.

(297) Singh, I., et. al. Structure-Based Discovery of Inhibitors of the SARS-CoV-2 Nsp14 N7-Methyltransferase. *J. Med. Chem.* **2023**, *66* (12), 7785-7803. DOI: 10.1021/acs.jmedchem.2c02120.

(298) Otava, T., et. al. The Structure-Based Design of SARS-CoV-2 nsp14 Methyltransferase Ligands Yields Nanomolar Inhibitors. *ACS Infect. Dis.* **2021**, *7* (8), 2214-2220. DOI: 10.1021/acsinfecdis.1c00131.

(299) Bobiļeva, O., et. al. Potent SARS-CoV-2 mRNA Cap Methyltransferase Inhibitors by Bioisosteric Replacement of Methionine in SAM Cosubstrate. *ACS Med. Chem. Lett.* **2021**, *12* (7), 1102-1107. DOI: 10.1021/acsmedchemlett.1c00140.

(300) Ahmed-Belkacem, R., et. al. Synthesis of adenine dinucleosides SAM analogs as specific inhibitors of SARS-CoV nsp14 RNA cap guanine-N7-methyltransferase. *European Journal of Medicinal*

*Chemistry* **2020**, *201*, 112557. DOI: https://doi.org/10.1016/j.ejmech.2020.112557.

(301) Ahmed-Belkacem, R., et. al. Potent Inhibition of SARS-CoV-2 nsp14 N7-Methyltransferase by Sulfonamide-Based Bisubstrate Analogues. *J. Med. Chem.* **2022**, *65* (8), 6231-6249. DOI: 10.1021/acs.jmedchem.2c00120.

(302) Jung, E., et. al. Bisubstrate Inhibitors of Severe Acute Respiratory Syndrome Coronavirus-2 Nsp14 Methyltransferase. *ACS Med. Chem. Lett.* **2022**, *13* (9), 1477-1484. DOI: 10.1021/acsmedchemlett.2c00265.

# *APPENDICES*

### *Physical Characterization of Substrates in Chapter 2*

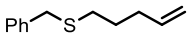

**Benzyl(pent-4-en-1-yl)sulfane (2-1):** Colorless oil. $^{1}$H NMR (400 MHz, $CDCl_3$) δ 7.38 – 7.16 (m, 5H), 5.75 (ddt, *J* = 16.9, 10.2, 6.7 Hz, 1H), 5.05 – 4.90 (m, 2H), 3.70 (s, 2H), 2.42 (dd, *J* = 8.2, 6.6 Hz, 2H), 2.15 – 2.07 (m, 2H), 1.65 (p, *J* = 7.4 Hz, 2H) ppm. $^{13}$C NMR (101 MHz, $CDCl_3$) δ 138.59, 137.82, 128.84, 128.47, 126.91, 115.14, 36.26, 32.81, 30.74, 28.41 ppm. HRMS (ESI): calcd. for $C_{12}H_{17}S^+$: 193.1045. found: 193.1044.

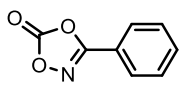

**3-Phenyl-1,4,2-dioxazol-5-one (2-2):** White solid. $^{1}$H NMR (400 MHz, $CDCl_3$) δ 7.92 – 7.80 (m, 2H), 7.69 – 7.60 (m, 1H), 7.60 – 7.47 (m, 2H) ppm. $^{13}$C NMR (101 MHz, $CDCl_3$) δ 163.56, 153.86, 133.80, 129.41, 126.63, 120.15 ppm. HRMS (ESI): calcd. for $C_7H_6NO^+$ (corresponds to the isocyanate from dioxazolone): 120.0449. found: 120.0448.

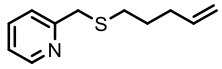

**2-((Pent-4-en-1-ylthio)methyl)pyridine (2-67):** Orange oil. $^{1}$H NMR (400 MHz, $CDCl_3$) δ 8.52 (dd, J = 4.9, 1.9 Hz, 1H), 7.65 (td, *J* = 7.6, 1.9 Hz, 1H), 7.38 (d, *J* = 7.8 Hz, 1H), 7.16 (tt, *J* = 5.5, 3.3 Hz, 1H), 5.75 (ddt, *J* = 16.9, 10.1, 6.6 Hz, 1H), 5.04 – 4.91 (m, 2H), 3.84 (d, *J* = 2.8 Hz, 2H), 2.50 (t, *J* = 7.4 Hz, 2H), 2.17 – 2.08 (m, 2H), 1.67 (q, *J* = 7.4 Hz, 2H) ppm. $^{13}$C NMR (101 MHz, $CDCl_3$) δ 159.01, 149.21, 137.76, 136.67, 123.03, 121.84, 115.13, 77.38, 77.06, 76.74, 38.18, 32.73, 31.07, 28.39 ppm. HRMS (EI): calcd. for $C_{11}H_{15}NS$: 193.0925. found: 193.0920.

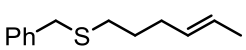

**(*Z*)-Benzyl(hex-4-en-1-yl)sulfane (2-72):** Colorless oil. **$^{1}$H NMR** (400 MHz, $CDCl_3$) δ 7.31 (d, *J* = 4.4 Hz, 4H), 7.27 – 7.19 (m, 1H), 5.46 (dddd, *J* = 13.4, 6.8, 4.9, 3.3 Hz, 1H), 5.32 (dtt, *J* = 10.9, 7.4, 1.8 Hz, 1H), 3.70 (s, 2H), 2.47 – 2.37 (m, 2H), 2.10 (q, *J* = 7.3 Hz, 2H), 1.68 – 1.52 (m, 6H) ppm. **$^{13}$C NMR** (101 MHz,

$CDCl_3$) δ 138.64, 129.48, 128.86, 128.47, 126.90, 124.75, 77.37, 77.05, 76.73, 36.28, 30.91, 29.03, 26.00, 12.81 ppm. **HRMS** (EI): calcd. for $C_{13}H_{18}S$: 206.1129. found: 206.1124. **IR** ($cm^{-1}$) 707, 1027, 1070, 1238, 1453, 1494, 1601, 1655.

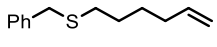

**Benzyl(hex-5-en-1-yl)sulfane (2-74):** Colorless oil. **$^1$H NMR** (400 MHz, $CDCl_3$) δ 7.31 (d, *J* = 4.4 Hz, 4H), 7.27 – 7.19 (m, 1H), 5.77 (ddt, *J* = 17.0, 10.2, 6.7 Hz, 1H), 5.05 – 4.88 (m, 2H), 3.70 (s, 2H), 2.51 – 2.31 (m, 2H), 2.11 – 1.93 (m, 2H), 1.60 – 1.52 (m, 2H), 1.44 (tt, *J* = 8.6, 6.8 Hz, 2H) ppm. **$^{13}$C NMR** (101 MHz, $CDCl_3$) δ 138.65, 138.56, 128.86, 128.48, 126.91, 114.67, 77.38, 77.07, 76.75, 36.28, 33.31, 31.17, 28.64, 28.05 ppm. **HRMS** (EI): calcd. for $C_{13}H_{18}S$: 206.1129. found: 206.1125. **IR** ($cm^{-1}$) 709, 1028, 1071, 1237, 1438, 1453, 1494, 1602, 1640.

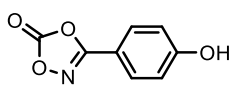

**3-(4-Hydroxyphenyl)-1,4,2-dioxazol-5-one (2-76):** White solid. $^1$H NMR (400 MHz, $CDCl_3$) δ 7.82 – 7.70 (m, 2H), 7.04 – 6.88 (m, 2H), 5.66 (s, 1H) ppm. $^{13}$C NMR (101 MHz, $CDCl_3$) δ 163.37, 160.28, 154.08, 128.90, 116.46, 112.45, 77.34, 77.02, 76.70 ppm. HRMS (ESI): calcd. for $C_7H_6NO_2^+$ (corresponds to the isocyanate from dioxazolone): 136.0399. found: 136.0392.

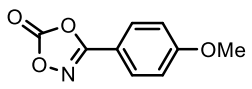

**3-(4-Methoxyphenyl)-1,4,2-dioxazol-5-one (2-77):** White solid. $^1$H NMR (400 MHz, $CDCl_3$) δ 7.82 – 7.76 (m, 2H), 7.07 – 6.99 (m, 2H), 3.89 (s, 3H) ppm. $^{13}$C NMR (101 MHz, $CDCl_3$) δ 163.88, 163.43, 154.06, 128.58, 114.89, 112.14, 55.62 ppm. HRMS (ESI): calcd. for $C_8H_8NO_2^+$ (corresponds to the isocyanate from dioxazolone): 150.0555. found: 150.0554.

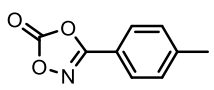

**3-(*p*-Tolyl)-1,4,2-dioxazol-5-one (2-78):** White solid. $^1$H NMR (400 MHz, $CDCl_3$) δ 7.76 – 7.69 (m, 2H), 7.34 (d, *J* = 8.1 Hz, 2H), 2.45 (s, 3H) ppm. $^{13}$C NMR (101 MHz, $CDCl_3$) δ 163.66, 153.97, 144.84, 130.09, 126.57, 117.25, 21.81 ppm. HRMS (ESI): calcd. for $C_8H_8NO^+$ (corresponds to the isocyanate from dioxazolone): 134.0606. found: 134.0603.

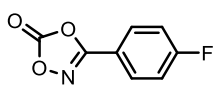

**3-(4-Fluorophenyl)-1,4,2-dioxazol-5-one (2-79):** White solid. $^{1}$H NMR (400 MHz, $CDCl_3$) δ 7.96 – 7.82 (m, 2H), 7.31 – 7.19 (m, 2H) ppm. $^{13}$C NMR (101 MHz, $CDCl_3$) δ 167.20, 164.64, 162.80, 153.68, 129.23 (d, *J* = 9.4 Hz), 117.02 (d, *J* = 22.7 Hz), 116.41 (d, *J* = 3.5 Hz) ppm. $^{19}$F NMR (377 MHz, $CDCl_3$) δ -108.59, -108.60, -108.61, -108.62, -108.62, -108.64, -108.65, -108.66 ppm. HRMS (ESI): calcd. for $C_7H_5FNO^+$ (corresponds to the isocyanate from dioxazolone): 138.0355. found: 138.0357.

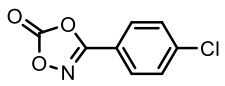

**3-(4-Chlorophenyl)-1,4,2-dioxazol-5-one (2-80):** White solid. $^{1}$H NMR (400 MHz, $CDCl_3$) δ 7.87 – 7.76 (m, 2H), 7.59 – 7.49 (m, 2H) ppm. $^{13}$C NMR (101 MHz, $CDCl_3$) δ 162.84, 153.53, 140.40, 129.91, 127.90, 118.58 ppm. HRMS (ESI): calcd. for $C_7H_5ClNO^+$ (corresponds to the isocyanate from dioxazolone): 154.0060. found: 154.0059.

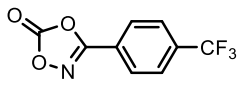

**3-(4-(Trifluoromethyl)phenyl)-1,4,2-dioxazol-5-one (2-81):** White solid. $^{1}$H NMR δ 8.01 (d, *J* = 8.2 Hz, 2H), 7.83 (d, *J* = 8.2 Hz, 2H) ppm. $^{13}$C NMR (101 MHz, $CDCl_3$) δ 162.51, 153.30, 135.57, 135.24, 127.14, 126.51 (q, *J* = 3.8 Hz), 124.51, 123.53, 121.79 ppm. $^{19}$F NMR (377 MHz, $CDCl_3$) δ -63.33 ppm. HRMS (ESI): calcd. for $C_8H_5F_3NO^+$ (corresponds to the isocyanate from dioxazolone): 188.0323. found: 188.0314.

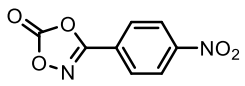

**3-(4-Nitrophenyl)-1,4,2-dioxazol-5-one (2-82):** White solid. $^{1}$H NMR (400 MHz, $CDCl_3$) δ 8.43 (d, *J* = 8.9 Hz, 2H), 8.10 (d, *J* = 8.9 Hz, 2H) ppm. $^{13}$C NMR (101 MHz, $CDCl_3$) δ 162.01, 153.00, 150.82, 127.87, 125.67, 124.66, 77.35, 77.04, 76.72 ppm. **HRMS** (ESI): dioxazolone corresponding isocyanate calcd. for $C_7H_5N_2O_3^+$: 165.0300. found: 165.0291.

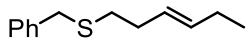

**(*Z*)-Benzyl(hex-3-en-1-yl)sulfane (2-83):** Colorless oil. **$^{1}$H NMR** (400 MHz, $CDCl_3$) δ 7.37 – 7.27 (m, 4H), 7.23 (tt, *J* = 5.1, 3.9 Hz, 1H), 5.47 – 5.38 (m, 1H), 5.36 – 5.26 (m, 1H), 3.73 (s, 2H), 2.48 – 2.36 (m, 2H), 2.29 (q, *J* = 7.3 Hz, 2H), 2.02 (pd, *J* = 7.5, 1.5 Hz, 2H), 0.95 (t, *J* = 7.5 Hz, 3H) ppm. **$^{13}$C NMR** (101

MHz, $CDCl_3$) δ 138.56, 133.25, 128.86, 128.50, 126.94, 126.83, 77.36, 77.05, 76.73, 36.35, 31.33, 27.13, 20.64, 14.28 ppm. **HRMS** (EI): calcd. for $C_{13}H_{18}S$: 206.1129. found: 206.1124. **IR** ($cm^{-1}$) 710, 1028, 1103, 1204, 1454, 1496, 1640.

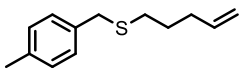

**(4-Methylbenzyl)(pent-4-en-1-yl)sulfane (2-84):** Colorless oil. $^1H$ NMR (400 MHz, $CDCl_3$) δ 7.19 (d, *J* = 8.1 Hz, 2H), 7.11 (d, *J* = 7.9 Hz, 2H), 5.76 (ddt, *J* = 17.0, 10.3, 6.7 Hz, 1H), 5.08 – 4.89 (m, 2H), 3.67 (s, 2H), 2.41 (dd, *J* = 8.2, 6.7 Hz, 2H), 2.33 (s, 3H), 2.11 (tdd, *J* = 7.9, 5.9, 1.5 Hz, 2H), 1.65 (p, *J* = 7.4 Hz, 2H) ppm. $^{13}C$ NMR (101 MHz, $CDCl_3$) δ 137.88, 136.53, 135.48, 129.16, 128.73, 115.11, 77.36, 77.04, 76.73, 35.93, 32.83, 30.71, 28.44, 21.10 ppm. HRMS (EI): calcd. for $C_{13}H_{18}S$: 206.1116 found: 206.1129.

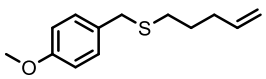

**(4-Methoxybenzyl)(pent-4-en-1-yl)sulfane (2-85):** Colorless oil. $^1H$ NMR (400 MHz, $CDCl_3$) δ 7.22 (d, *J* = 8.5 Hz, 2H), 6.88 – 6.80 (m, 2H), 5.76 (ddt, *J* = 16.9, 10.0, 6.6 Hz, 1H), 5.05 – 4.89 (m, 2H), 3.79 (s, 3H), 3.66 (s, 2H), 2.41 (t, *J* = 7.4 Hz, 2H), 2.16 – 2.06 (m, 2H), 1.65 (p, *J* = 7.4 Hz, 2H) ppm. $^{13}C$ NMR (101 MHz, $CDCl_3$) δ 158.59, 137.87, 130.56, 129.89, 115.13, 113.88, 77.36, 77.05, 76.73, 55.29, 35.61, 32.84, 30.66, 28.45 ppm.

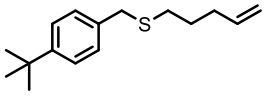

**(4-(Tert-butyl)benzyl)(pent-4-en-1-yl)sulfane (2-86):** Colorless oil. $^1H$ NMR (400 MHz, $CDCl_3$) δ 7.33 (d, J = 8.3 Hz, 2H), 7.23 (d, J = 8.2 Hz, 2H), 5.75 (ddt, J = 17.0, 10.3, 6.7 Hz, 1H), 5.04 – 4.91 (m, 2H), 3.68 (s, 2H), 2.47 – 2.40 (m, 2H), 2.12 (tdd, J = 8.0, 6.2, 1.4 Hz, 2H), 1.65 (p, J = 7.4 Hz, 2H), 1.31 (s, 10H) ppm. $^{13}C$ NMR (101 MHz, $CDCl_3$) δ 149.84, 137.89, 135.50, 128.49, 125.41, 115.11, 77.37, 77.05, 76.73, 35.86, 34.49, 32.82, 31.38, 30.86, 28.44 ppm. HRMS (EI): calcd. for $C_{16}H_{24}S$: 248.1599. found: 248.1590.

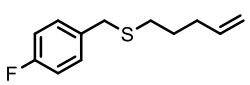

**(4-Fluorobenzyl)(pent-4-en-1-yl)sulfane (2-87):** Colorless oil. $^1H$ NMR (400 MHz, $CDCl_3$) δ 7.30 – 7.23 (m, 2H), 7.03 – 6.94 (m, 2H), 5.75 (ddt, *J* = 16.9, 10.1, 6.6 Hz, 1H), 5.07 – 4.91 (m, 2H), 3.67 (s, 2H), 2.46 – 2.37 (m, 2H), 2.12 (tdd, *J* = 8.0, 6.8, 1.4 Hz, 2H), 1.64 (p, *J* = 7.4 Hz, 2H) ppm. $^{13}C$

NMR (101 MHz, $CDCl_3$) δ 160.62, 137.74, 134.29 (d, *J* = 3.3 Hz), 130.33 (d, *J* = 8.0 Hz), 115.42, 115.22 (d, *J* = 3.7 Hz), 35.50, 32.78, 30.70, 28.35 ppm. $^{19}F$ NMR (377 MHz, $CDCl_3$) δ -121.81, -121.82, -121.83, -121.84, -121.86, -121.87, -121.88 ppm. HRMS (EI): calcd. for $C_{12}H_{15}FS$: 210.0878. found: 210.0871.

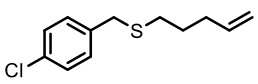


**(4-Chlorobenzyl)(pent-4-en-1-yl)sulfane (2-88):** Colorless oil. $^1H$ NMR (400 MHz, $CDCl_3$) δ 7.30 – 7.21 (m, 4H), 5.75 (ddt, *J* = 17.0, 10.2, 6.7 Hz, 1H), 5.06 – 4.92 (m, 2H), 3.66 (s, 2H), 2.46 – 2.36 (m, 2H), 2.17 – 2.07 (m, 2H), 1.64 (p, *J* = 7.4 Hz, 2H) ppm. $^{13}C$ NMR (101 MHz, $CDCl_3$) δ 137.71, 137.14, 132.67, 130.17, 128.62, 115.28, 77.36, 77.05, 76.73, 35.57, 32.76, 30.69, 28.32 ppm. HRMS (EI): calcd. for $C_{12}H_{15}ClS$: 226.0583. found: 226.0576.

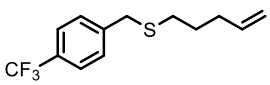


**Pent-4-en-1-yl(4-(trifluoromethyl)benzyl)sulfane (2-89):** Colorless oil. $^1H$ NMR (400 MHz, $CDCl_3$) δ 7.57 (d, *J* = 8.0 Hz, 2H), 7.43 (d, *J* = 8.0 Hz, 2H), 5.75 (ddt, *J* = 17.0, 10.1, 6.6 Hz, 1H), 5.05 – 4.92 (m, 2H), 3.73 (s, 2H), 2.42 (t, *J* = 7.4 Hz, 2H), 2.12 (q, *J* = 7.1 Hz, 2H), 1.66 (q, *J* = 7.3 Hz, 2H) ppm. $^{13}C$ NMR (101 MHz, $CDCl_3$) δ 167.32, 142.55, 134.72, 131.50, 129.16, 128.62, 126.80, 125.44 (q, *J* = 3.7 Hz), 50.74, 35.93, 34.25, 27.87, 27.85, 10.38 ppm. $^{19}F$ NMR (377 MHz, $CDCl_3$) δ -68.45 ppm. HRMS (EI): calcd. for $C_{13}H_{15}F_3S$: 260.0847. found: 260.0842.

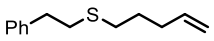


**Pent-4-en-1-yl(phenethyl)sulfane (2-90):** Colorless oil. $^1H$ NMR (400 MHz, $CDCl_3$) δ 7.29 (dd, *J* = 8.7, 6.6 Hz, 2H), 7.21 (td, *J* = 6.2, 1.8 Hz, 4H), 5.78 (ddt, *J* = 17.0, 10.2, 6.7 Hz, 1H), 5.08 – 4.95 (m, 2H), 2.88 (dd, *J* = 9.0, 5.8 Hz, 2H), 2.80 – 2.72 (m, 2H), 2.57 – 2.50 (m, 2H), 2.18 – 2.11 (m, 2H), 1.68 (p, *J* = 7.4 Hz, 2H) ppm. $^{13}C$ NMR (101 MHz, $CDCl_3$) δ 140.70, 137.85, 128.65, 128.56, 128.51, 128.50, 126.45, 126.35, 115.23, 77.40, 77.08, 76.76, 40.24, 36.43, 35.76, 33.66, 32.85, 31.66, 28.81 ppm. HRMS (EI): calcd. for $C_{13}H_{18}S$: 206.1129. found: 206.1127.

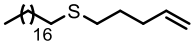


**Octadecyl(pent-4-en-1-yl)sulfane (2-91):** Colorless oil. $^1H$ NMR (400 MHz, $CDCl_3$) δ 5.79 (ddt, *J* = 17.0, 10.2, 6.7 Hz, 1H), 5.10 –

4.91 (m, 2H), 2.50 (td, *J* = 7.5, 5.6 Hz, 5H), 2.15 (q, *J* = 7.1 Hz, 2H), 1.68 (p, *J* = 7.3 Hz, 2H), 1.57 (p, *J* = 7.2 Hz, 3H), 1.26 (s, 37H), 0.88 (t, *J* = 6.7 Hz, 3H) ppm. $^{13}$C NMR (101 MHz, $CDCl_3$) δ 137.86, 115.07, 77.37, 77.05, 76.73, 32.87, 32.15, 31.95, 31.50, 29.73, 29.70, 29.68, 29.64, 29.57, 29.39, 29.29, 28.96, 28.87, 22.71, 14.11 ppm. HRMS (EI): calcd. for $C_{23}H_{46}S$: 354.3320. found: 354.3326.

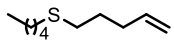

**Pent-4-en-1-yl(pentyl)sulfane (2-92):** Colorless oil. $^1$H NMR (400 MHz, $CDCl_3$) δ 5.80 (ddt, *J* = 16.9, 10.1, 6.7 Hz, 1H), 5.12 – 4.91 (m, 2H), 2.51 (td, *J* = 7.4, 5.4 Hz, 4H), 2.20 – 2.11 (m, 2H), 1.68 (p, *J* = 7.4 Hz, 2H), 1.59 (d, *J* = 7.4 Hz, 3H), 1.41 – 1.27 (m, 4H), 0.90 (t, *J* = 7.0 Hz, 3H) ppm. $^{13}$C NMR (101 MHz, $CDCl_3$) δ 137.93, 115.09, 77.34, 77.03, 76.71, 32.87, 32.13, 31.51, 31.12, 29.41, 28.87, 22.32, 13.98 ppm. HRMS (EI): calcd. for $C_{10}H_{20}S$: 172.1286. found: 172.1296.

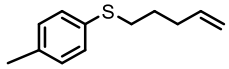

**Pent-4-en-1-yl(p-tolyl)sulfane (2-93):** Colorless oil. $^1$H NMR (400 MHz, $CDCl_3$) δ 7.25 (d, *J* = 8.3 Hz, 2H), 7.09 (d, *J* = 7.9 Hz, 2H), 5.77 (ddt, *J* = 17.0, 10.2, 6.7 Hz, 1H), 5.09 – 4.93 (m, 2H), 2.92 – 2.84 (m, 2H), 2.32 (s, 3H), 2.21 – 2.13 (m, 2H), 1.71 (p, *J* = 7.3 Hz, 2H) ppm. $^{13}$C NMR (101 MHz, $CDCl_3$) δ 137.70, 136.02, 132.81, 130.01, 129.66, 115.34, 77.36, 77.05, 76.73, 33.74, 32.70, 28.38, 21.02 ppm. HRMS (EI): calcd. for $C_{12}H_{16}S$: 192.0973. found: 192.0974. IR ($cm^{-1}$) 717, 1015, 1092, 1210, 1438, 1492, 1565, 1598 1639.

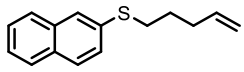

**Naphthalen-2-yl(pent-4-en-1-yl)sulfane (2-94):** Colorless oil. $^1$H NMR (400 MHz, $CDCl_3$) δ 7.79 – 7.70 (m, 4H), 7.49 – 7.37 (m, 3H), 5.79 (ddt, *J* = 16.9, 10.2, 6.6 Hz, 1H), 5.11 – 4.93 (m, 2H), 3.01 (t, *J* = 7.4 Hz, 2H), 2.21 (q, *J* = 7.1 Hz, 2H), 1.78 (p, *J* = 7.3 Hz, 2H) ppm. $^{13}$C NMR (101 MHz, $CDCl_3$) δ 137.60, 134.30, 133.83, 131.70, 128.37, 127.75, 127.35, 127.04, 126.61, 126.55, 125.57, 115.54, 77.39, 77.08, 76.76, 32.83, 32.77, 28.26 ppm. HRMS (EI): calcd. for $C_{15}H_{16}S$: 228.0973. found: 228.0970.

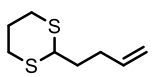

**2-(But-3-en-1-yl)-1,3-dithiane (2-95):** Colorless oil. $^1$H NMR (400 MHz, $CDCl_3$) δ 5.79 (ddt, *J* = 16.9, 10.2, 6.6 Hz, 1H), 5.14 – 4.95 (m, 2H), 4.04

(t, *J* = 7.0 Hz, 1H), 2.99 – 2.73 (m, 5H), 2.32 – 2.22 (m, 2H), 2.17 – 2.06 (m, 1H), 1.96 – 1.76 (m, 3H) ppm. $^{13}$C NMR (101 MHz, $CDCl_3$) δ 137.14, 115.65, 77.36, 77.04, 76.72, 46.72, 34.55, 30.54, 30.34, 26.03 ppm. HRMS (EI): calcd. for $C_{18}H_{14}S_2$: 174.0537. found: 174.0536.

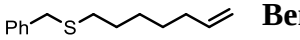

**Benzyl(hept-6-en-1-yl)sulfane (2-96):** Colorless oil. **$^1$H NMR** (400 MHz, $CDCl_3$) δ 7.30 (d, *J* = 4.3 Hz, 4H), 7.27 – 7.19 (m, 1H), 5.79 (ddt, *J* = 16.9, 10.2, 6.7 Hz, 1H), 5.05 – 4.89 (m, 2H), 3.70 (s, 2H), 2.41 (t, *J* = 7.4 Hz, 2H), 2.03 (q, *J* = 6.6 Hz, 2H), 1.55 (td, *J* = 11.2, 9.3, 4.6 Hz, 3H), 1.44 – 1.29 (m, 4H) ppm. **$^{13}$C NMR** (101 MHz, $CDCl_3$) δ 138.88, 138.68, 128.85, 128.47, 126.89, 114.41, 77.37, 77.05, 76.74, 36.32, 33.62, 31.33, 29.09, 28.49, 28.35 ppm. **HRMS** (EI): calcd. for $C_{14}H_{20}S$: 220.1286. found: 220.1288. **IR** ($cm^{-1}$) 711, 1027, 1070, 1237, 1437, 1453, 1494, 1601, 1640.

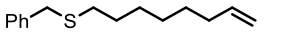

**Benzyl(oct-7-en-1-yl)sulfane (2-97):** Colorless oil. **$^1$H NMR** (400 MHz, $CDCl_3$) δ 7.31 (d, *J* = 4.4 Hz, 4H), 7.24 (dd, *J* = 8.5, 4.2 Hz, 1H), 5.79 (ddt, *J* = 17.0, 10.2, 6.7 Hz, 1H), 5.06 – 4.81 (m, 2H), 3.70 (s, 2H), 2.50 – 2.31 (m, 2H), 2.03 (q, *J* = 7.0 Hz, 2H), 1.69 – 1.48 (m, 2H), 1.43 – 1.09 (m, 6H) ppm. **$^{13}$C NMR** (101 MHz, $CDCl_3$) δ 139.07, 138.69, 128.85, 128.47, 126.89, 114.29, 77.38, 77.06, 76.74, 36.31, 33.72, 31.36, 29.16, 28.76, 28.72, 28.69 ppm. **HRMS** (EI): calcd. for $C_{15}H_{22}S$: 234.1442. found: 234.1448. **IR** ($cm^{-1}$) 709, 1027, 1070, 1237, 1437, 1453, 1494, 1602, 1640.

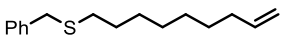

**Benzyl(non-8-en-1-yl)sulfane (2-98):** Colorless oil. **$^1$H NMR** (400 MHz, $CDCl_3$) δ 7.30 (d, *J* = 4.3 Hz, 4H), 7.23 (dd, *J* = 8.9, 4.5 Hz, 1H), 5.80 (ddt, *J* = 16.9, 10.2, 6.7 Hz, 1H), 5.08 – 4.84 (m, 2H), 3.70 (s, 2H), 2.40 (t, *J* = 7.4 Hz, 2H), 2.03 (q, *J* = 7.0 Hz, 2H), 1.61 – 1.45 (m, 3H), 1.44 – 1.08 (m, 9H) ppm. **$^{13}$C NMR** (101 MHz, $CDCl_3$) δ 139.16, 138.71, 128.85, 128.46, 126.88, 114.21, 77.37, 77.05, 76.73, 36.33, 33.78, 31.40, 29.21, 29.05, 28.97, 28.85, 28.82 ppm. **HRMS** (EI): calcd. for $C_{16}H_{24}S$: 248.1599. found: 248.1606. **IR** ($cm^{-1}$) 709, 1027, 1071, 1238, 1437, 1453, 1494, 1601, 1640.

**((Pent-4-en-1-yloxy)methyl)benzene (2-99):** Colorless oil. $^{1}$H NMR (400 MHz, $CDCl_3$) δ 7.39 – 7.32 (m, 4H), 7.29 (td, *J* = 6.6, 4.9, 3.0 Hz, 1H), 5.82 (ddtd, *J* = 16.8, 9.9, 6.6, 2.6 Hz, 1H), 5.10 – 4.91 (m, 2H), 4.51 (d, *J* = 2.2 Hz, 2H), 3.49 (td, *J* = 6.6, 2.4 Hz, 2H), 2.15 (q, *J* = 7.0 Hz, 2H), 1.72 (ddt, *J* = 13.6, 8.9, 4.8 Hz, 2H) ppm. $^{13}$C NMR (101 MHz, $CDCl_3$) δ 138.65, 138.34, 128.39, 127.66, 127.54, 114.76, 77.37, 77.05, 76.73, 72.92, 69.76, 30.38, 28.98 ppm. HRMS (EI): calcd. for $C_{12}H_{16}O$: 176.1201. found: 176.1195.

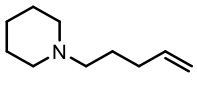

**1-(Pent-4-en-1-yl)piperidine (2-100):** Colorless oil. **$^{1}$H NMR** (400 MHz, $CDCl_3$) δ 5.81 (ddt, *J* = 16.9, 10.1, 6.6 Hz, 1H), 5.05 – 4.90 (m, 2H), 2.47 (s, 4H), 2.33 – 2.24 (m, 3H), 2.05 (q, *J* = 7.1 Hz, 2H), 1.58 (dt, *J* = 11.1, 6.1 Hz, 7H), 1.43 (p, *J* = 6.1 Hz, 2H) ppm. **$^{13}$C NMR** (101 MHz, $CDCl_3$) δ 138.61, 114.49, 77.38, 77.06, 76.74, 59.03, 54.64, 31.89, 26.11, 25.98, 24.49 ppm.

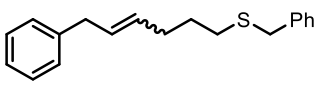

**Benzyl(6-phenylhex-4-en-1-yl)sulfane (2-102):** Colorless oil. $^{1}$H NMR (400 MHz, $CDCl_3$) δ 7.41 – 7.21 (m, 8H), 7.21 – 7.10 (m, 3H), 5.67 – 5.53 (m, 1H), 5.52 – 5.39 (m, 1H), 3.69 (d, *J* = 3.7 Hz, 2H), 3.34 (dd, *J* = 28.7, 7.0 Hz, 2H), 2.42 (dt, *J* = 13.8, 7.4 Hz, 2H), 2.22 (q, *J* = 7.3 Hz, 2H), 1.74 – 1.62 (m, 2H) ppm. $^{13}$C NMR (101 MHz, $CDCl_3$) δ 141.05, 138.64, 138.59, 130.70, 129.84, 129.65, 129.05, 128.86, 128.50, 128.48, 128.46, 128.41, 128.39, 128.35, 128.29, 126.94, 126.91, 125.95, 125.91, 77.37, 77.05, 76.73, 39.04, 36.29, 36.27, 33.51, 31.56, 31.31, 31.05, 30.91, 30.77, 29.08, 28.94, 26.38 ppm. HRMS (ESI): calcd. for $C_{19}H_{23}S^{+}$: 283.1520. found: 283.1519.

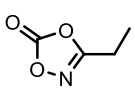

**3-Ethyl-1,4,2-dioxazol-5-one (2-103):** Colorless oil. $^{1}$H NMR (400 MHz, $CDCl_3$) δ 2.64 (q, *J* = 7.6 Hz, 2H), 1.29 (t, *J* = 7.6 Hz, 3H) ppm. $^{13}$C NMR (101 MHz, $CDCl_3$) δ 167.48, 154.22, 18.60, 8.67 ppm. HRMS (ESI): calcd. for $C_4H_6NO_3^{+}$: 116.0348. found: 116.0340.

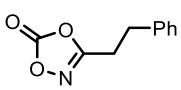

**3-Phenethyl-1,4,2-dioxazol-5-one (2-104):** Colorless oil. $^{1}$H NMR (400 MHz, $CDCl_3$) δ 7.40 – 7.12 (m, 5H), 3.07 – 2.99 (m, 2H), 2.96 –

2.88 (m, 2H) ppm. $^{13}$C NMR (101 MHz, $CDCl_3$) δ 165.87, 154.05, 138.04, 128.95, 128.21, 127.19, 30.46, 26.68 ppm. HRMS (ESI): calcd. for $C_9H_{10}NO^+$ (corresponds to the isocyanate from dioxazolone): 148.0762. found: 148.0755.

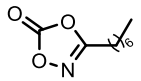

**3-Heptyl-1,4,2-dioxazol-5-one (2-105):** Colorless oil. $^1$H NMR (400 MHz, $CDCl_3$) δ 2.61 (t, *J* = 7.5 Hz, 2H), 1.71 (p, *J* = 7.5 Hz, 2H), 1.44 – 1.31 (m, 4H), 1.27 (d, *J* = 6.8 Hz, 12H), 0.88 (t, *J* = 6.8 Hz, 3H) ppm. $^{13}$C NMR (101 MHz, $CDCl_3$) δ 166.74, 31.88, 29.54, 29.50, 29.28, 28.92, 28.70, 24.74, 24.51, 22.66, 14.08 ppm. HRMS (ESI): calcd. for $C_8H_{16}NO^+$ (corresponds to the isocyanate from dioxazolone): 142.1232. found: 142.1228.

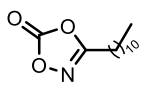

**3-Undecyl-1,4,2-dioxazol-5-one (2-106):** Colorless oil. $^1$H NMR (400 MHz, $CDCl_3$) δ 2.61 (t, *J* = 7.5 Hz, 2H), 1.71 (p, *J* = 7.4 Hz, 2H), 1.43 – 1.22 (m, 16H), 0.88 (t, *J* = 6.7 Hz, 3H) ppm. $^{13}$C NMR (101 MHz, $CDCl_3$) δ 166.76, 154.23, 31.45, 28.64, 28.57, 24.71, 24.49, 22.50, 13.96 ppm. HRMS (ESI): calcd. for $C_{12}H_{24}NO^+$ (corresponds to the isocyanate from dioxazolone): 198.1858. found: 198.1859.

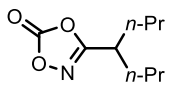

**3-(Heptan-4-yl)-1,4,2-dioxazol-5-one (2-107):** Colorless oil. $^1$H NMR (400 MHz, $CDCl_3$) δ 2.69 (tt, *J* = 8.6, 5.9 Hz, 1H), 1.66 – 1.54 (m, 4H), 1.36 – 1.27 (m, 4H), 0.90 (t, *J* = 7.3 Hz, 6H) ppm. $^{13}$C NMR (101 MHz, $CDCl_3$) δ 168.95, 36.44, 33.27, 20.13, 13.61 ppm. HRMS (ESI): calcd. for $C_8H_{16}NO^+$ (corresponds to the isocyanate from dioxazolone): 142.1232. found: 142.1227.

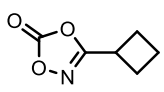

**3-Cyclobutyl-1,4,2-dioxazol-5-one (2-108):** Colorless oil. $^1$H NMR (400 MHz, $CDCl_3$) δ 3.46 (qd, *J* = 8.4, 1.1 Hz, 1H), 2.38 (td, *J* = 8.8, 7.1 Hz, 4H), 2.21 – 2.00 (m, 2H) ppm. $^{13}$C NMR (101 MHz, $CDCl_3$) δ 168.44, 154.49, 29.51, 25.18, 18.99 ppm. HRMS (ESI): calcd. for $C_6H_8NO_3^+$: 142.0504. found: 142.0499.

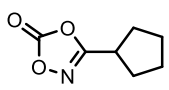

**3-Cyclopentyl-1,4,2-dioxazol-5-one (2-109):** Colorless oil. $^{1}$H NMR (400 MHz, $CDCl_3$) δ 3.06 (tt, *J* = 8.6, 7.1 Hz, 1H), 2.04 (dddd, *J* = 12.1, 9.5, 5.0, 3.2 Hz, 2H), 1.90 – 1.62 (m, 6H) ppm. $^{13}$C NMR (101 MHz, $CDCl_3$) δ 169.52, 154.44, 35.14, 29.33, 25.43 ppm. HRMS (ESI): calcd. for $C_6H_{10}NO^+$ (corresponds to the isocyanate from dioxazolone): 112.0762. found: 112.0763.

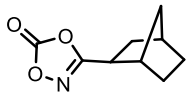

**3-(Bicyclo[2.2.1]heptan-2-yl)-1,4,2-dioxazol-5-one (2-110):** Colorless oil. $^{1}$H NMR (400 MHz, $CDCl_3$) δ 3.10 – 2.91 (m, 0.5H), 2.68 – 2.62 (m, 1H), 2.55 (d, *J* = 4.0 Hz, 0.5H), 2.41 (dt, *J* = 6.5, 4.4 Hz, 1H), 1.85 (ddt, *J* = 12.9, 6.2, 3.7 Hz, 1H), 1.50 – 1.46 (m, 2H), 1.93 – 1.25 (m, 5H) ppm. $^{13}$C NMR (101 MHz, $CDCl_3$) δ 169.10, 168.68, 154.54, 154.48, 40.44, 39.95, 39.55, 38.20, 37.28, 36.56, 36.37, 36.01, 33.10, 30.81, 29.31, 29.11, 28.36, 24.28 ppm. HRMS (ESI): calcd. for $C_8H_{12}NO^+$ (corresponds to the isocyanate from dioxazolone): 138.0919. found: 138.0916.

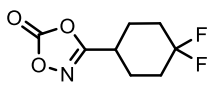

**3-(4,4-Difluorocyclohexyl)-1,4,2-dioxazol-5-one (2-111):** White solid. $^{1}$H NMR (400 MHz, $CDCl_3$) δ 2.80 (td, *J* = 9.1, 8.0, 4.6 Hz, 1H), 2.25 – 2.09 (m, 4H), 1.98 – 1.80 (m, 4H) ppm. $^{13}$C NMR (101 MHz, $CDCl_3$) δ 167.66 (d, *J* = 1.9 Hz), 153.83, 126.36 – 117.78 (m), 32.42, 32.07 (t, *J* = 25.1 Hz), 24.86 – 24.19 (m) ppm. $^{19}$F NMR (376 MHz, $CDCl_3$) δ -94.56 (d, *J* = 240.3 Hz), -100.49 (d, *J* = 240.8 Hz) ppm. HRMS (ESI): calcd. for $C_7H_{10}F_2NO^+$ (corresponds to the isocyanate from dioxazolone): 162.0730. found: 162.0734.

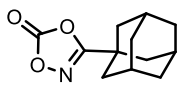

**3-(Adamantan-1-yl)-1,4,2-dioxazol-5-one (2-112):** White solid. $^{1}$H NMR (400 MHz, $CDCl_3$) δ 2.15 – 2.06 (m, 1H), 1.95 (d, *J* = 2.9 Hz, 4H), 1.88 – 1.69 (m, 4H) ppm. $^{13}$C NMR (101 MHz, $CDCl_3$) δ 171.72, 154.65, 38.08, 36.09, 34.60, 27.27 ppm. HRMS (ESI): calcd. for $C_{11}H_{16}NO^+$ (corresponds to the isocyanate from dioxazolone): 178.1232. found: 178.1230.

**Methyl-4-(5-oxo-1,4,2-dioxazol-3-yl)cubane-1-carboxylate (2-113):** White solid. $^{1}$H NMR (400 MHz, $CDCl_3$) δ 4.43 – 4.32

(m, 6H), 3.71 (s, 3H) ppm. $^{13}$C NMR (101 MHz, $CDCl_3$) δ 171.02, 164.52, 154.20, 56.03, 51.78, 47.69, 47.63, 46.82 ppm. HRMS (ESI): calcd. for $C_{11}H_{10}NO_3^+$ (corresponds to the isocyanate from dioxazolone): 204.0661. found: 204.0667.

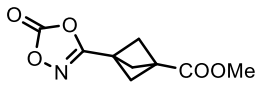

**Methyl-3-(5-oxo-1,4,2-dioxazol-3-yl)bicyclo[1.1.1]pentane-1-carboxylate (2-114):** White solid. $^1$H NMR (400 MHz, $CDCl_3$) δ 3.71 (s, 3H), 2.50 (s, 6H) ppm. $^{13}$C NMR (101 MHz, $CDCl_3$) δ 168.23, 162.89, 153.73, 53.22, 52.13, 39.87, 30.83 ppm. HRMS (ESI): calcd. for $C_8H_{10}NO_3^+$ (corresponds to the isocyanate from dioxazolone): 168.0661. found: 168.0653.

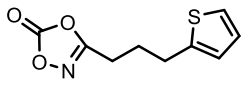

**3-(3-(Thiophen-2-yl)propyl)-1,4,2-dioxazol-5-one (2-115):** Yellow oil. $^1$H NMR (400 MHz, $CDCl_3$) δ 7.17 (dd, *J* = 5.2, 1.2 Hz, 1H), 6.94 (dd, *J* = 5.1, 3.4 Hz, 1H), 6.83 (dd, *J* = 3.4, 1.2 Hz, 1H), 2.98 (t, *J* = 7.2 Hz, 2H), 2.67 (t, *J* = 7.5 Hz, 2H), 2.11 (p, *J* = 7.3 Hz, 2H) ppm. $^{13}$C NMR (101 MHz, $CDCl_3$) δ 166.28, 154.06, 142.29, 127.03, 125.21, 123.91, 28.64, 26.25, 23.84 ppm. HRMS (ESI): calcd. for $C_8H_{10}NOS^+$ (corresponds to the isocyanate from dioxazolone): 168.0483. found: 168.0478.

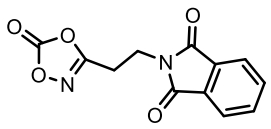

**2-(2-(5-Oxo-1,4,2-dioxazol-3-yl)ethyl)isoindoline-1,3-dione (2-116):** White solid. $^1$H NMR (400 MHz, $CDCl_3$) δ 7.92 – 7.82 (m, 2H), 7.80 – 7.68 (m, 2H), 4.08 (t, *J* = 6.4 Hz, 2H), 3.02 (t, *J* = 6.4 Hz, 2H) ppm. $^{13}$C NMR (101 MHz, $CDCl_3$) δ 167.71, 164.04, 153.65, 134.45, 131.64, 123.69, 33.20, 24.71 ppm. HRMS (ESI): calcd. for $C_{11}H_9N_2O_3^+$ (corresponds to the isocyanate from dioxazolone): 217.0613. found: 217.0618.

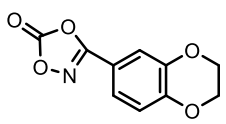

**3-(2,3-Dihydrobenzo[*b*][1,4]dioxin-6-yl)-1,4,2-dioxazol-5-one (2-117):** White solid. $^1$H NMR (400 MHz, $CDCl_3$) δ 7.36 – 7.32 (m, 2H), 7.03 – 6.94 (m, 1H), 4.39 – 4.33 (m, 2H), 4.33 – 4.27 (m, 2H) ppm. $^{13}$C NMR (101 MHz, $CDCl_3$) δ 163.24, 154.02, 148.45, 144.14, 120.44, 118.44, 115.88, 112.78, 77.37, 77.05, 76.74, 64.68, 64.16 ppm. HRMS (ESI): calcd. for

$C_9H_8NO_3^+$ (corresponds to the isocyanate from dioxazolone): 178.0504. found: 178.0502.

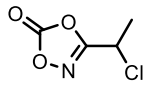

**3-(1-Chloroethyl)-1,4,2-dioxazol-5-one (2-118):** Colorless oil. $^1$H NMR (400 MHz, $CDCl_3$) δ 4.86 (q, *J* = 7.0 Hz, 1H), 1.88 (d, *J* = 7.0 Hz, 3H) ppm. $^{13}$C NMR (101 MHz, $CDCl_3$) δ 165.16, 153.04, 44.13, 20.38 ppm. HRMS (ESI): calcd. for $C_4H_5ClNO_3^+$: 149.9958. found: 149.9963.

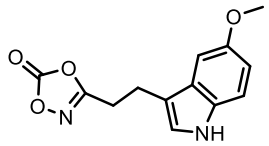

**3-(2-(5-Methoxy-1H-indol-3-yl)ethyl)-1,4,2-dioxazol-5-one (2-119):** White solid. $^1$H NMR (400 MHz, $CDCl_3$) δ 7.97 (s, 1H), 7.26 (d, *J* = 8.9 Hz, 1H), 7.00 (dd, *J* = 20.5, 2.4 Hz, 2H), 6.89 (dd, *J* = 8.8, 2.4 Hz, 1H), 3.87 (s, 3H), 3.17 (tt, *J* = 7.0, 1.0 Hz, 2H), 3.03 – 2.97 (m, 2H) ppm. $^{13}$C NMR (101 MHz, $CDCl_3$) δ 166.29, 154.29, 154.18, 131.41, 127.07, 122.64, 112.68, 112.31, 112.23, 100.03, 55.96, 25.82, 20.55 ppm. HRMS (ESI): calcd. for $C_{12}H_{13}N_2O_2^+$ (corresponds to the isocyanate from dioxazolone): 217.0977. found: 217.0984.

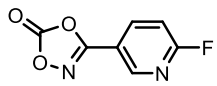

**3-(6-Fluoropyridin-3-yl)-1,4,2-dioxazol-5-one (2-120):** Brown solid. $^1$H NMR (400 MHz, $CDCl_3$) δ 8.75 (d, *J* = 2.5 Hz, 1H), 8.28 (ddd, *J* = 9.1, 7.1, 2.5 Hz, 1H), 7.17 (dd, *J* = 8.6, 3.0 Hz, 1H) ppm. $^{13}$C NMR (101 MHz, $CDCl_3$) δ 166.08 (d, *J* = 248.9 Hz), 161.15, 153.00, 147.16 (d, *J* = 16.9 Hz), 139.27 (d, *J* = 9.3 Hz), 115.25 (d, *J* = 5.0 Hz), 111.09 (d, *J* = 37.9 Hz) ppm. $^{19}$F NMR (376 MHz, $CDCl_3$) δ -58.00 ppm. HRMS (ESI): calcd. for $C_6H_4FN_2O^+$ (corresponds to the isocyanate from dioxazolone): 139.0308. found: 139.0303.

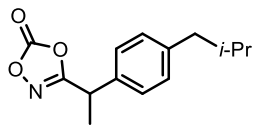

**3-(1-(4-Isobutylphenyl)ethyl)-1,4,2-dioxazol-5-one (2-121):** White solid. $^1$H NMR (400 MHz, $CDCl_3$) δ 7.18 (q, *J* = 8.3 Hz, 4H), 4.04 (q, *J* = 7.2 Hz, 1H), 2.48 (d, *J* = 7.2 Hz, 2H), 1.92 – 1.80 (m, 1H), 1.67 (d, *J* = 7.2 Hz, 3H), 0.91 (d, *J* = 6.6 Hz, 6H) ppm. $^{13}$C NMR (101 MHz, $CDCl_3$) δ 168.54, 142.11, 134.04, 129.91, 127.05, 44.97, 36.70, 30.13, 22.32,

17.19 ppm. HRMS (ESI): calcd. for $C_{13}H_{18}NO^+$ (corresponds to the isocyanate from dioxazolone): 204.1388. found: 204.1383.

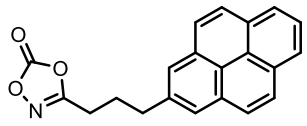

**3-(3-(Pyren-1-yl)propyl)-1,4,2-dioxazol-5-one (2-122):** White solid. $^1$H NMR (400 MHz, $CDCl_3$) δ 8.22 – 8.15 (m, 3H), 8.15 – 8.09 (m, 2H), 8.03 (d, *J* = 11.4 Hz, 3H), 7.82 (d, *J* = 7.8 Hz, 1H), 3.43 (t, *J* = 7.5 Hz, 2H), 2.66 (t, *J* = 7.4 Hz, 2H), 2.26 (p, *J* = 7.5 Hz, 2H) ppm. $^{13}$C NMR (101 MHz, $CDCl_3$) δ 166.41, 133.83, 131.41, 130.81, 130.35, 128.69, 127.83, 127.44, 127.24, 127.08, 126.06, 125.25, 125.18, 125.04, 124.93, 124.89, 122.70, 32.10, 25.97, 24.35 ppm. HRMS (ESI): calcd. for $C_{20}H_{16}NO^+$ (corresponds to the isocyanate from dioxazolone): 286.1232. found: 286.1228.

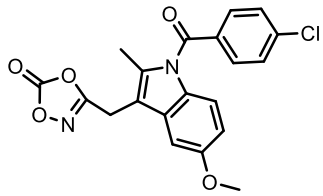

**3-((1-(4-Chlorobenzoyl)-5-methoxy-2-methyl-1H-indol-3-yl) methyl)-1,4,2-dioxazol-5-one (2-123):** White solid. $^1$H NMR (400 MHz, $CDCl_3$) δ 7.66 (d, *J* = 8.5 Hz, 2H), 7.47 (d, *J* = 8.5 Hz, 2H), 6.93 (d, *J* = 2.4 Hz, 1H), 6.83 (d, *J* = 9.0 Hz, 1H), 6.70 (dd, *J* = 9.1, 2.5 Hz, 1H), 3.99 (s, 2H), 3.83 (s, 3H), 2.44 (s, 3H) ppm. $^{13}$C NMR (101 MHz, $CDCl_3$) δ 168.16, 164.56, 156.27, 153.89, 139.74, 137.08, 133.34, 131.29, 130.75, 129.43, 129.28, 115.17, 112.24, 108.33, 100.64, 55.76, 20.43, 13.11 ppm. HRMS (ESI): calcd. for $C_{19}H_{16}ClN_2O_3^+$ (corresponds to the isocyanate from dioxazolone): 355.0849. found: 355.0848.

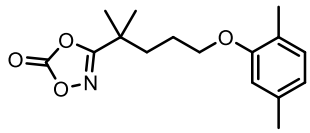

**3-(5-(2,5-Dimethylphenoxy)-2-methylpentan-2-yl)-1,4,2-dioxazol-5-one (2-124):** Colorless oil. $^1$H NMR (400 MHz, $CDCl_3$) δ 7.03 (d, *J* = 7.4 Hz, 1H), 6.75 – 6.65 (m, 1H), 6.61 (d, *J* = 1.6 Hz, 1H), 3.96 (t, *J* = 5.6 Hz, 2H), 2.33 (s, 3H), 2.19 (s, 3H), 1.90 – 1.77 (m, 4H), 1.39 (s, 6H) ppm. $^{13}$C NMR (101 MHz, $CDCl_3$) δ 171.60, 156.70, 136.55, 130.44, 123.56, 121.02, 111.95, 67.14, 36.08, 35.92, 24.62, 24.18, 21.39, 15.73 ppm. HRMS (ESI): calcd. for $C_{15}H_{22}NO_2^+$ (corresponds to the isocyanate from dioxazolone): 248.1651. found: 248.1642.

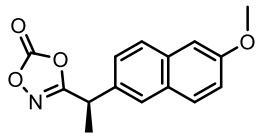

**3-(1-(6-Methoxynaphthalen-2-yl)ethyl)-1,4,2-dioxazol-5-one (2-125):** White solid. $^{1}$H NMR (400 MHz, $CDCl_3$) δ 7.74 (dd, *J* = 14.0, 8.7 Hz, 2H), 7.68 (d, *J* = 1.9 Hz, 1H), 7.35 (dd, *J* = 8.5, 1.9 Hz, 1H), 7.19 (dd, *J* = 8.9, 2.6 Hz, 1H), 7.14 (d, *J* = 2.5 Hz, 1H), 4.20 (q, *J* = 7.3 Hz, 1H), 3.93 (s, 3H), 1.75 (d, *J* = 7.2 Hz, 3H) ppm. $^{13}$C NMR (101 MHz, $CDCl_3$) δ 167.94, 153.97, 66.38, 32.10, 27.66 ppm. HRMS (ESI): calcd. for $C_{14}H_{14}NO_2^+$ (corresponds to the isocyanate from dioxazolone): 228.1025. found: 228.1030.

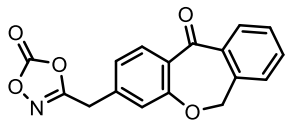

**3-((11-Oxo-6,11-dihydrodibenzo[b,e]oxepin-2-yl)methyl)-1,4,2-dioxazol-5-one (2-126):** White solid. $^{1}$H NMR (400 MHz, $CDCl_3$) δ 8.17 (d, *J* = 2.5 Hz, 1H), 7.89 (dd, *J* = 7.7, 1.4 Hz, 1H), 7.58 (td, *J* = 7.5, 1.4 Hz, 1H), 7.49 (td, *J* = 7.6, 1.3 Hz, 1H), 7.39 (ddd, *J* = 9.3, 8.0, 1.9 Hz, 2H), 7.08 (d, *J* = 8.5 Hz, 1H), 5.20 (s, 2H), 3.95 (s, 2H) ppm. $^{13}$C NMR (101 MHz, $CDCl_3$) δ 190.40, 165.10, 161.27, 153.83, 140.20, 135.48, 135.33, 133.07, 132.63, 129.56, 129.45, 127.96, 125.59, 123.98, 122.02, 73.69, 30.40 ppm. HRMS (ESI): calcd. for $C_{16}H_{12}NO_3^+$ (corresponds to the isocyanate from dioxazolone): 266.0817. found: 266.0815.

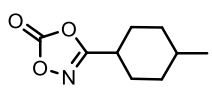

**3-(4-Methylcyclohexyl)-1,4,2-dioxazol-5-one (2-127):** white solid. $^{1}$H NMR (400 MHz, $CDCl_3$) δ 2.56 (tt, *J* = 12.3, 3.5 Hz, 1H), 2.08 – 1.98 (m, 2H), 1.89 – 1.78 (m, 2H), 1.56 – 1.35 (m, 3H), 1.01 (qd, *J* = 13.4, 3.5 Hz, 2H), 0.91 (d, *J* = 6.6 Hz, 3H) ppm. $^{13}$C NMR (101 MHz, $CDCl_3$) δ 169.44, 154.33, 34.62, 33.63, 31.67, 28.23, 22.22 ppm. HRMS (ESI): calcd. for $C_8H_{14}NO^+$ (corresponds to the isocyanate from dioxazolone): 140.1075. found: 140.1076.

## *NMR spectrum*

**2-5**

$^{1}$H NMR:

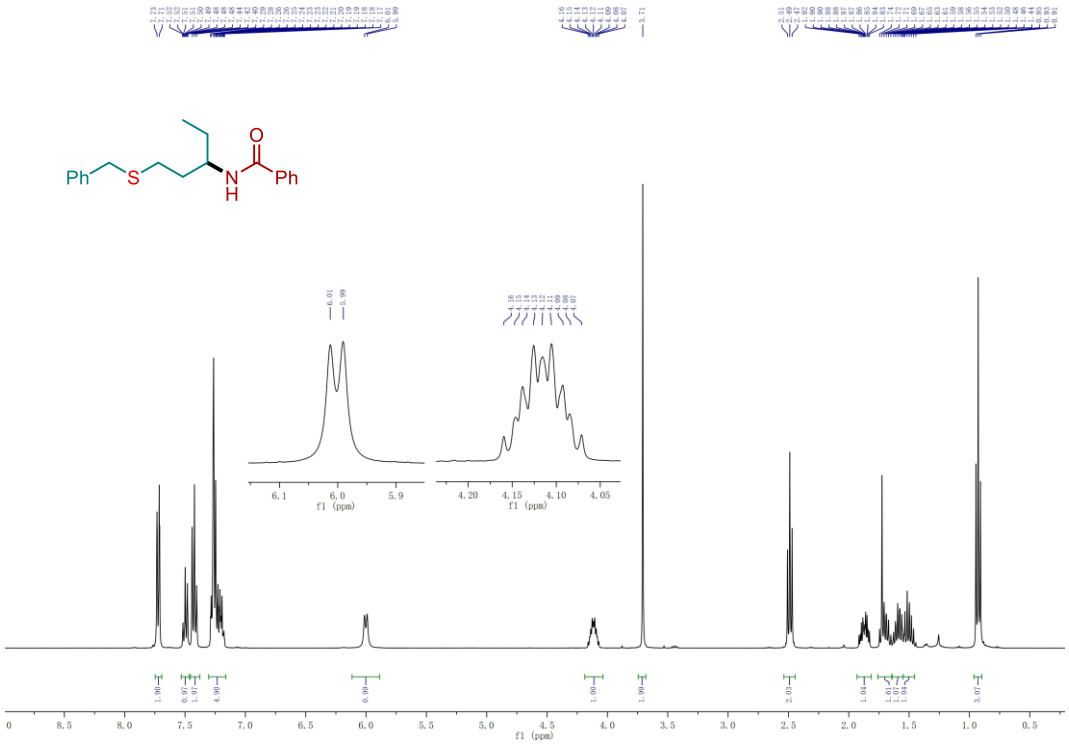


$^{13}$C NMR:

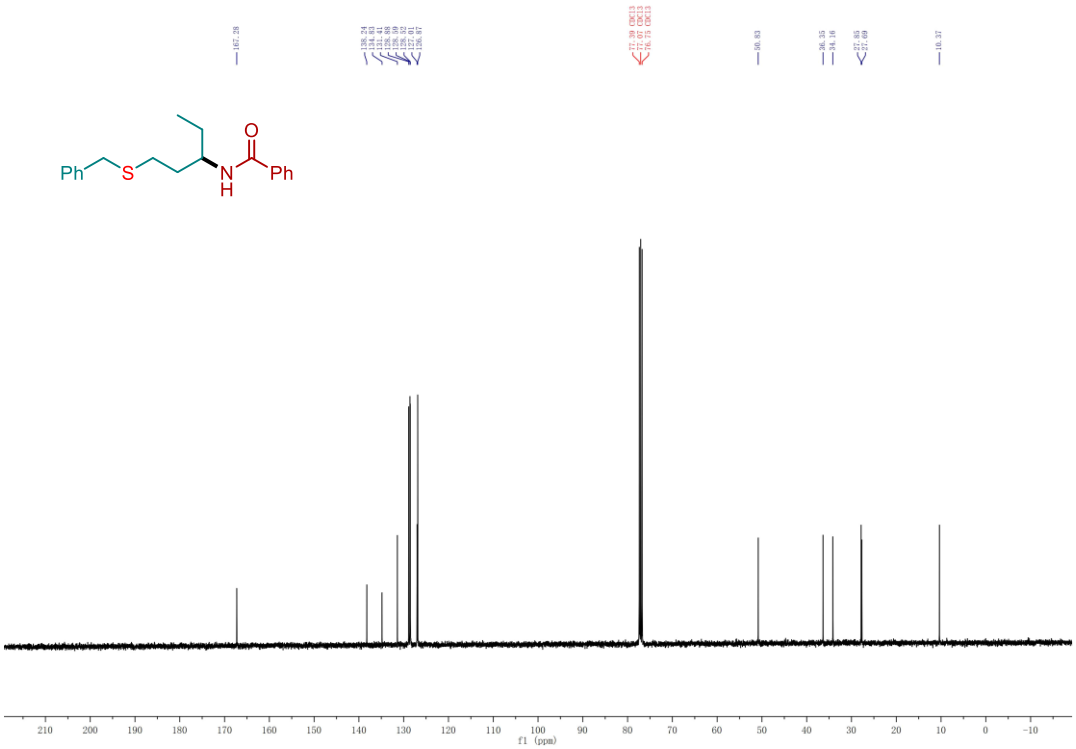

**2-6**

$^{1}$H NMR:

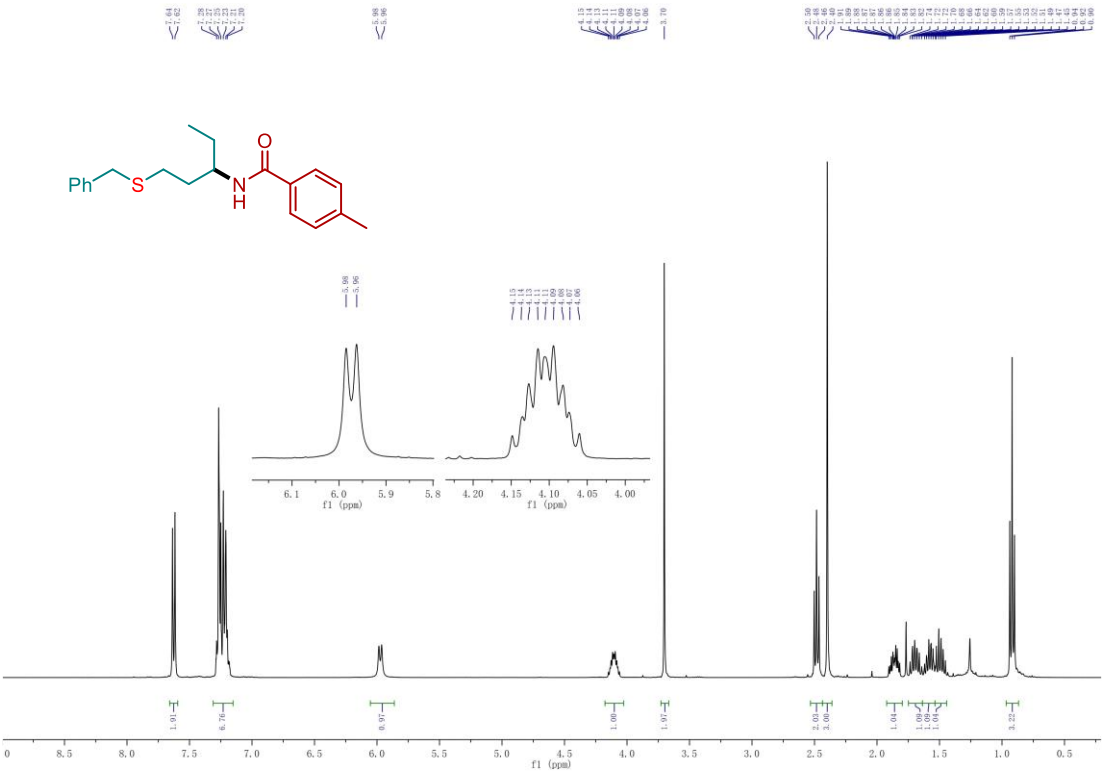


$^{13}$C NMR:

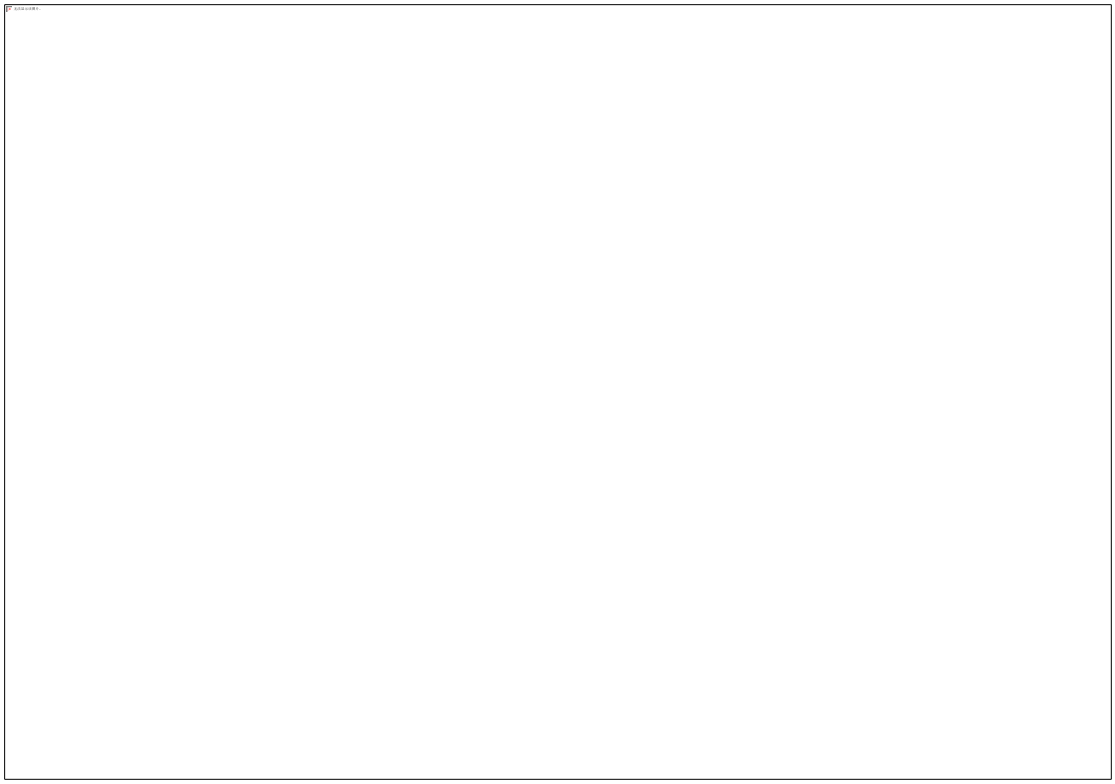

**2-7**

$^{1}$H NMR:

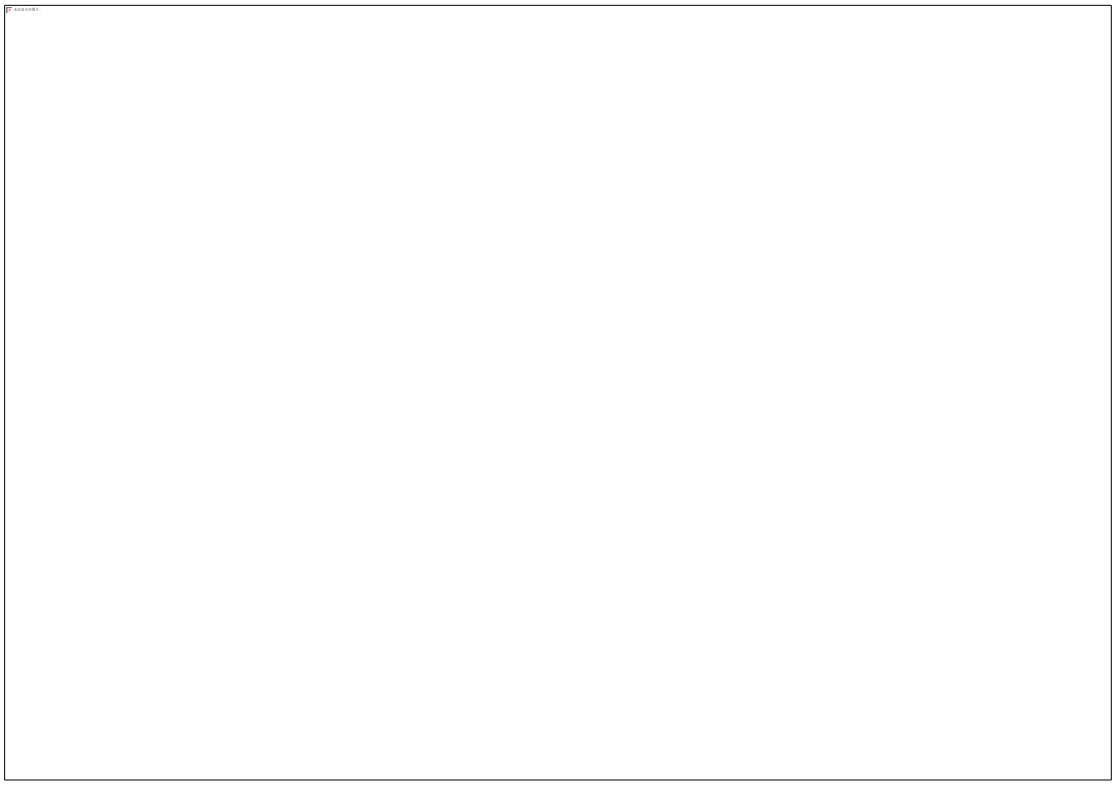

$^{13}$C NMR:

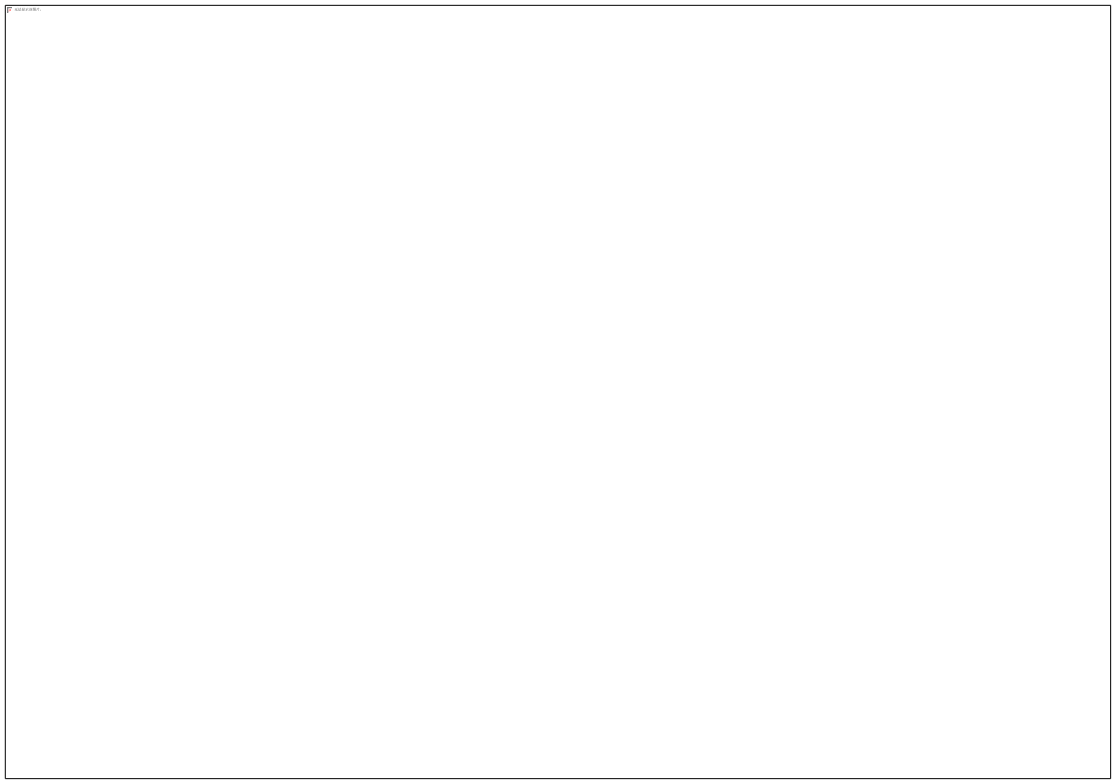

**2-8**

$^{1}$H NMR:

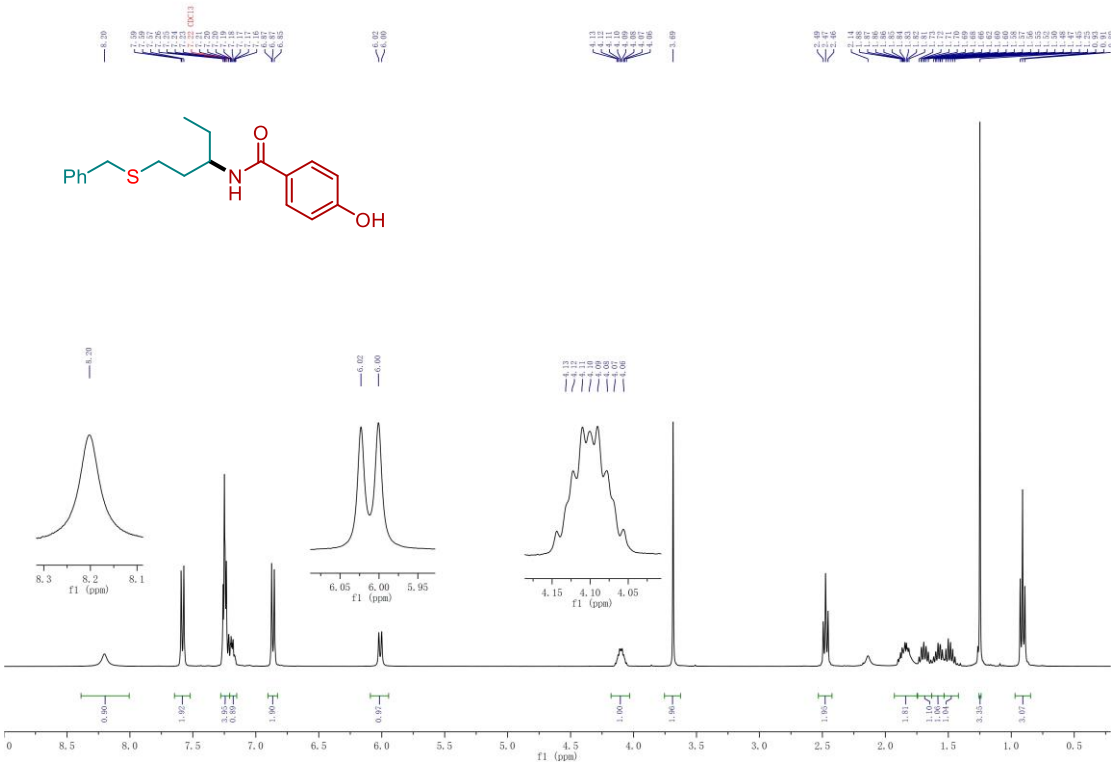


$^{13}$C NMR:

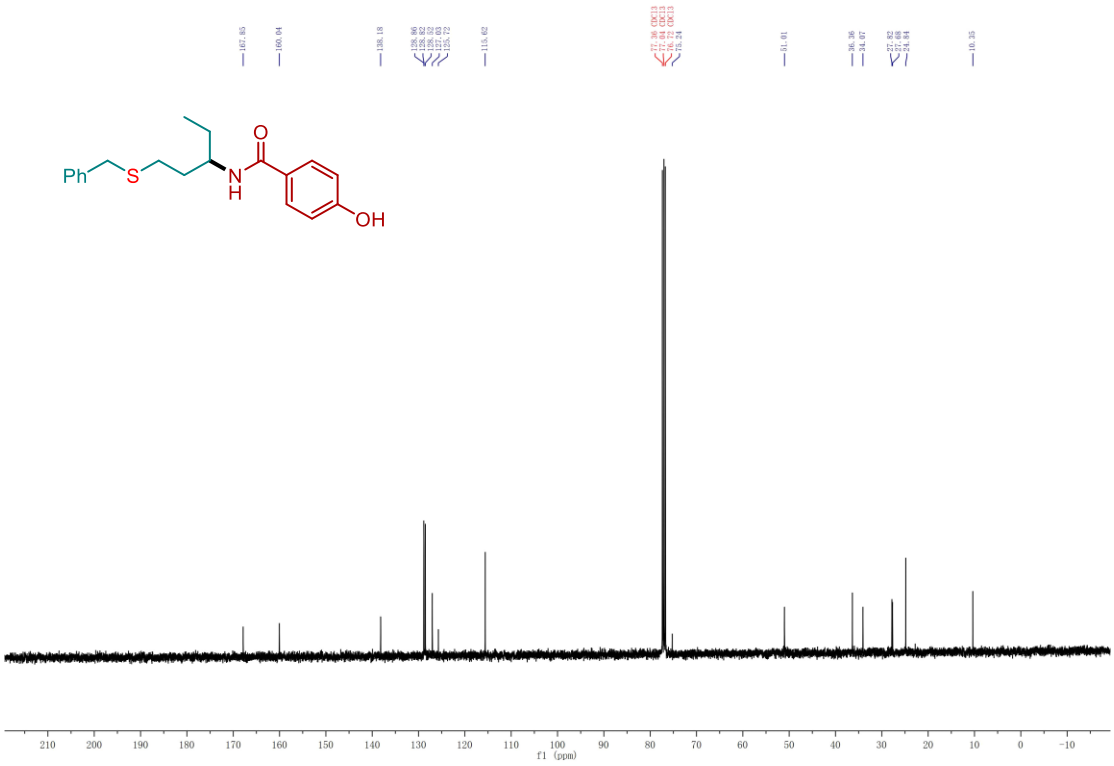

**2-9**

$^{1}$H NMR:

$^{13}$C NMR:

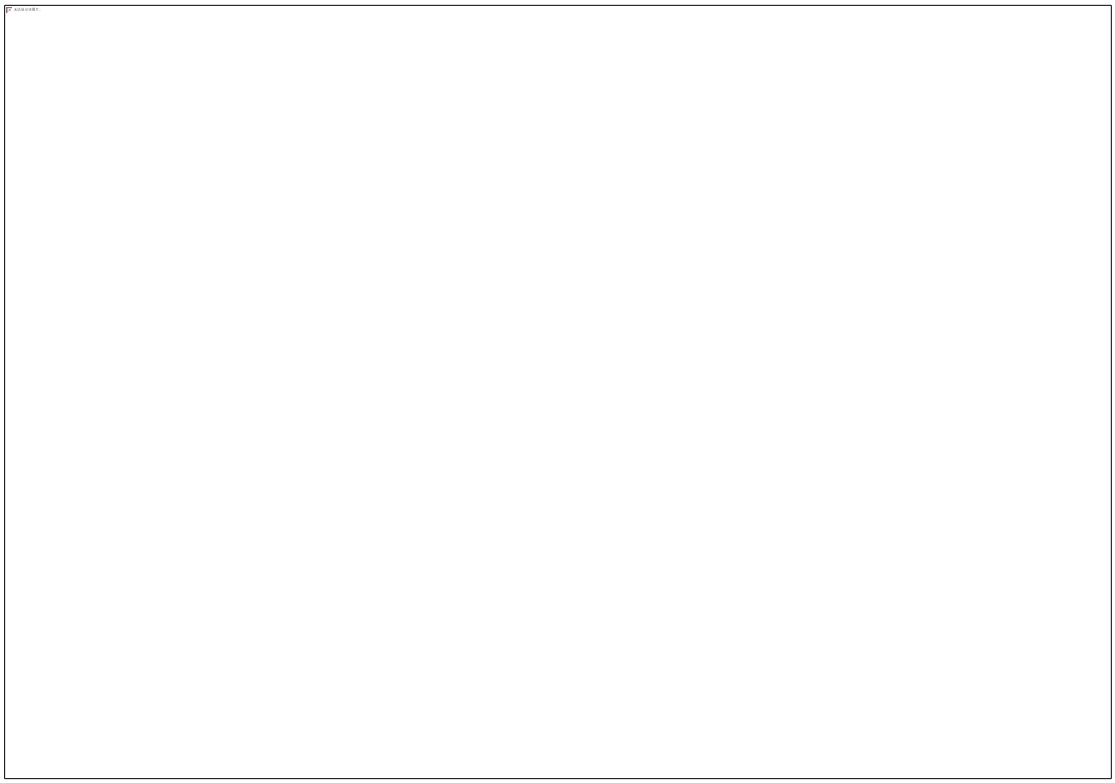

**2-9**

$^{19}$F NMR:

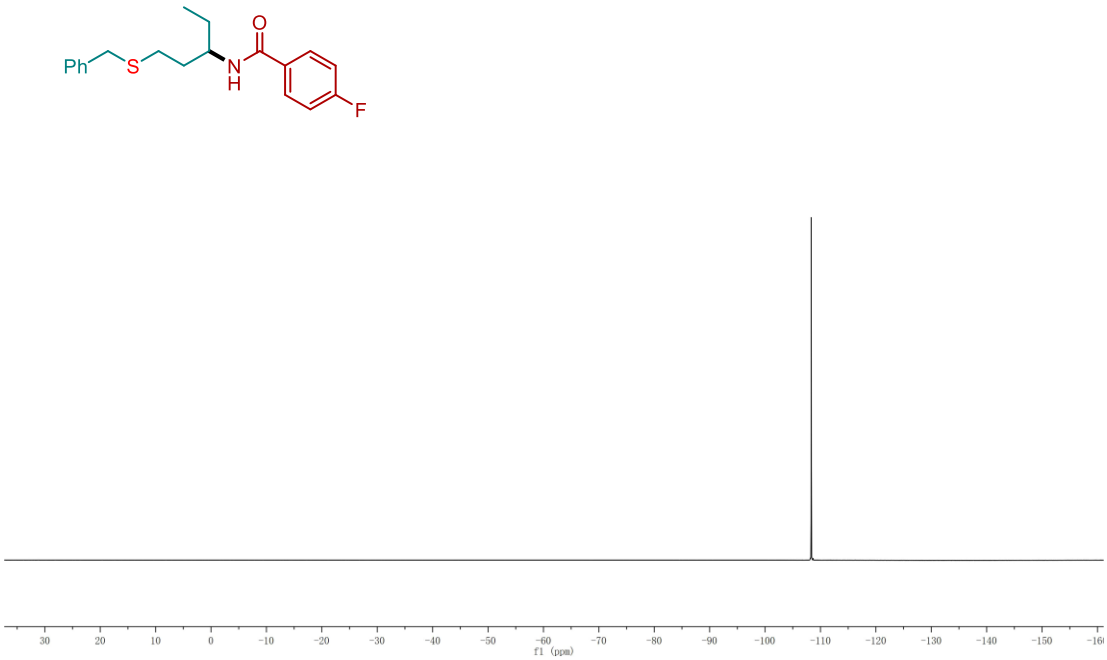
Ph
S
N
H
O
F
30
20
10
0
−10
−20
−30
−40
−50
−60
−70
−80
−90
−100
−110
−120
−130
−140
−150
f1 (ppm)

**2-10**

$^{1}$H NMR:

$^{13}$C NMR:

## 2-11

$^{1}$H NMR:

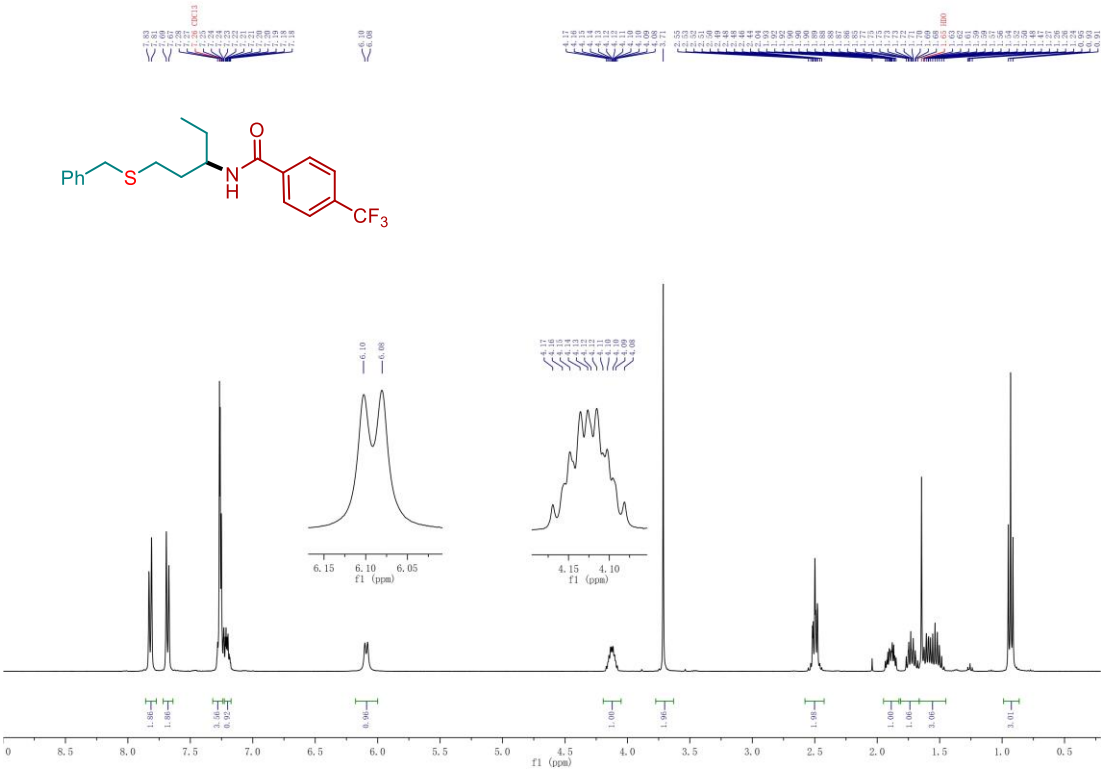


$^{13}$C NMR:

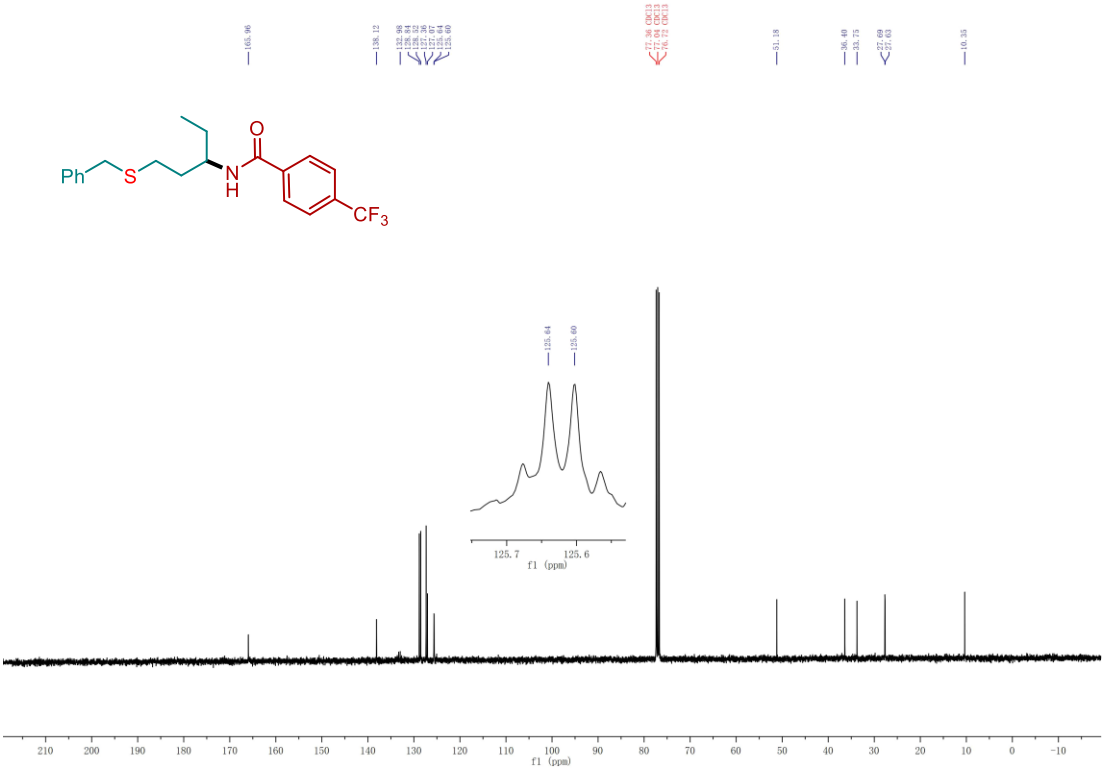

**2-11**

$^{19}$F NMR:


Ph
S
N
H
O
CF3
30
20
10
0
−10
−20
−30
−40
−50
−60
−70
−80
−90
−100
−110
−120
−130
−140
−150
f1 (ppm)

## 2-12

$^{1}$H NMR:

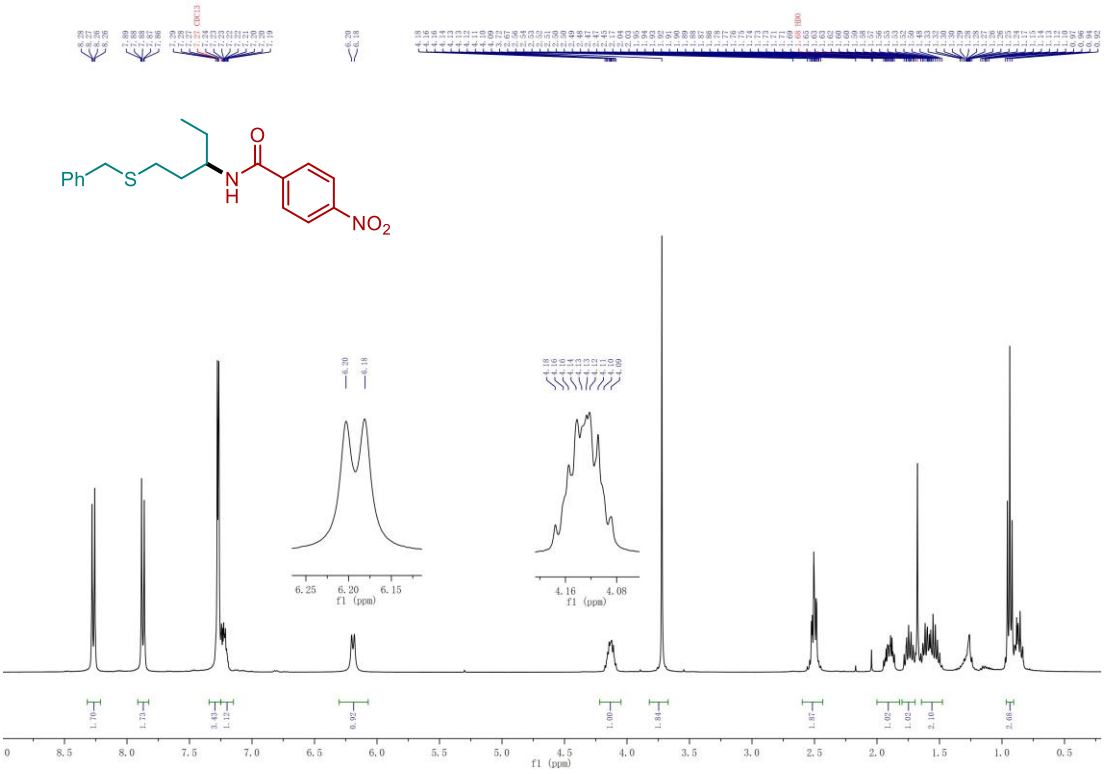


$^{13}$C NMR:

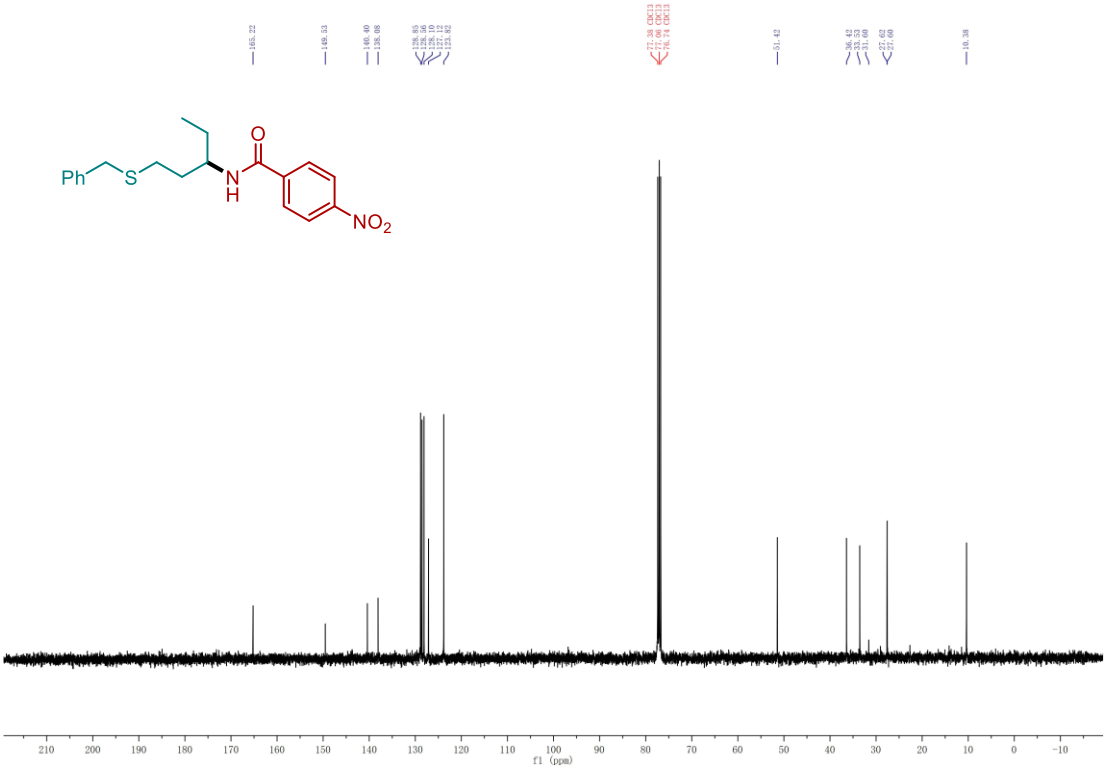

## 2-13

$^{1}$H NMR:

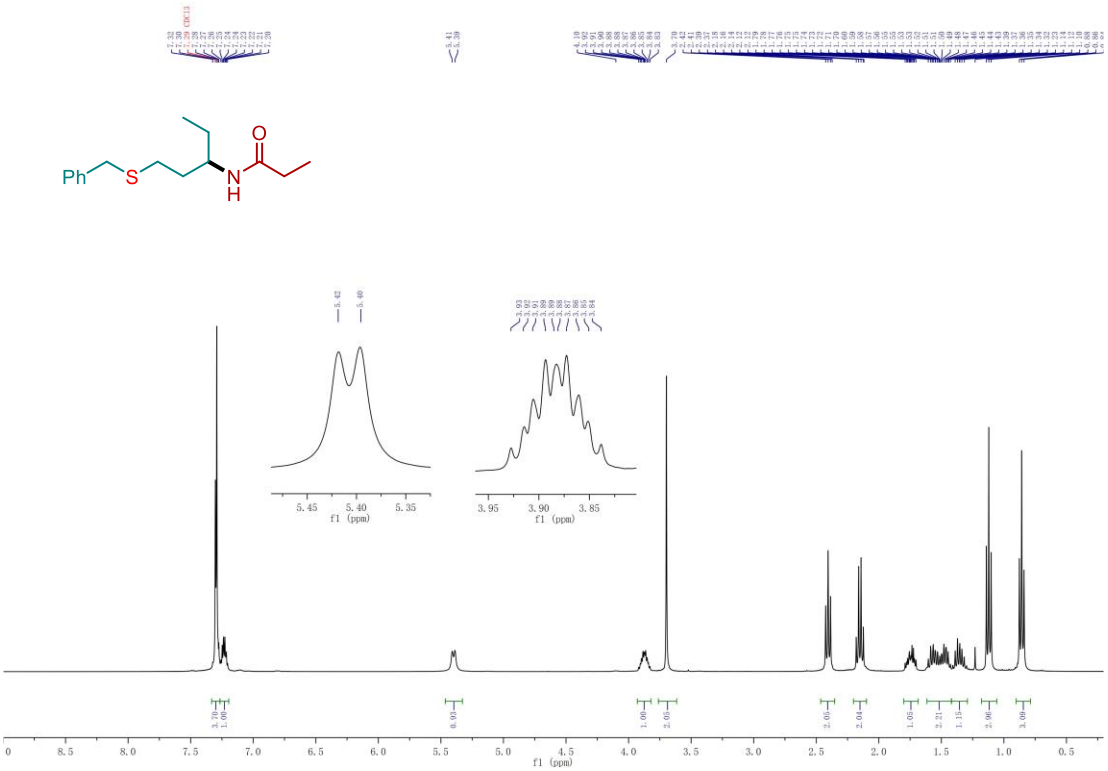


$^{13}$C NMR:

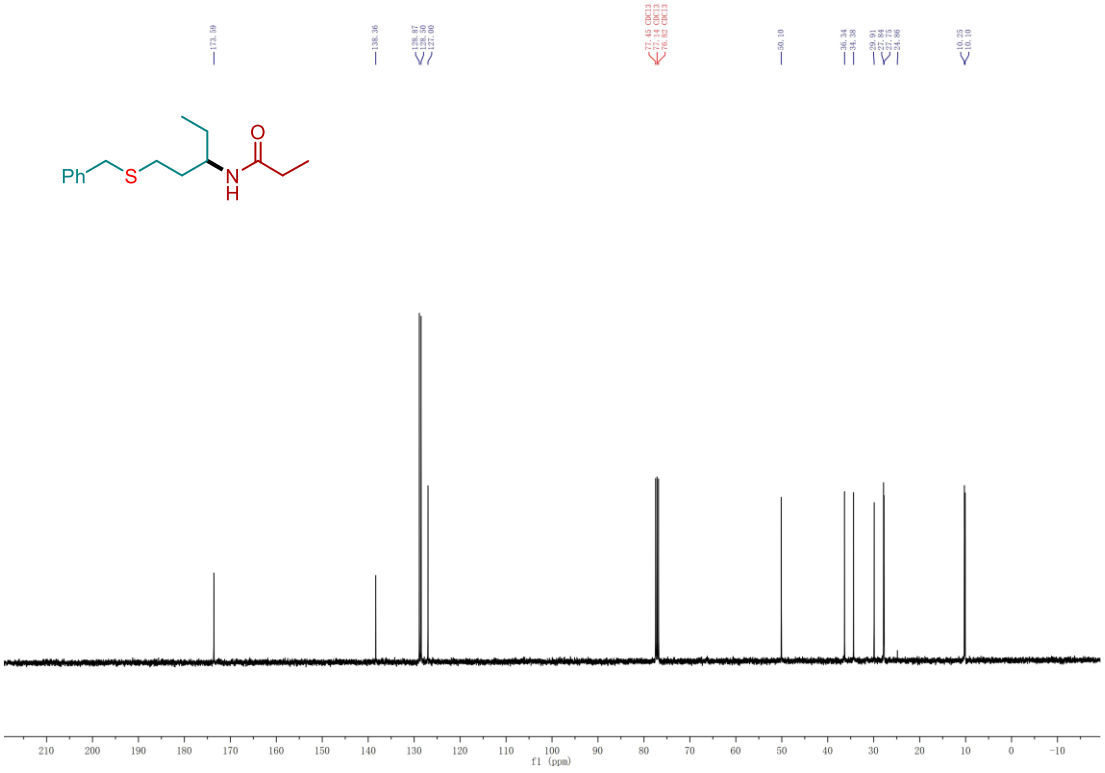

## 2-14

$^{1}$H NMR:

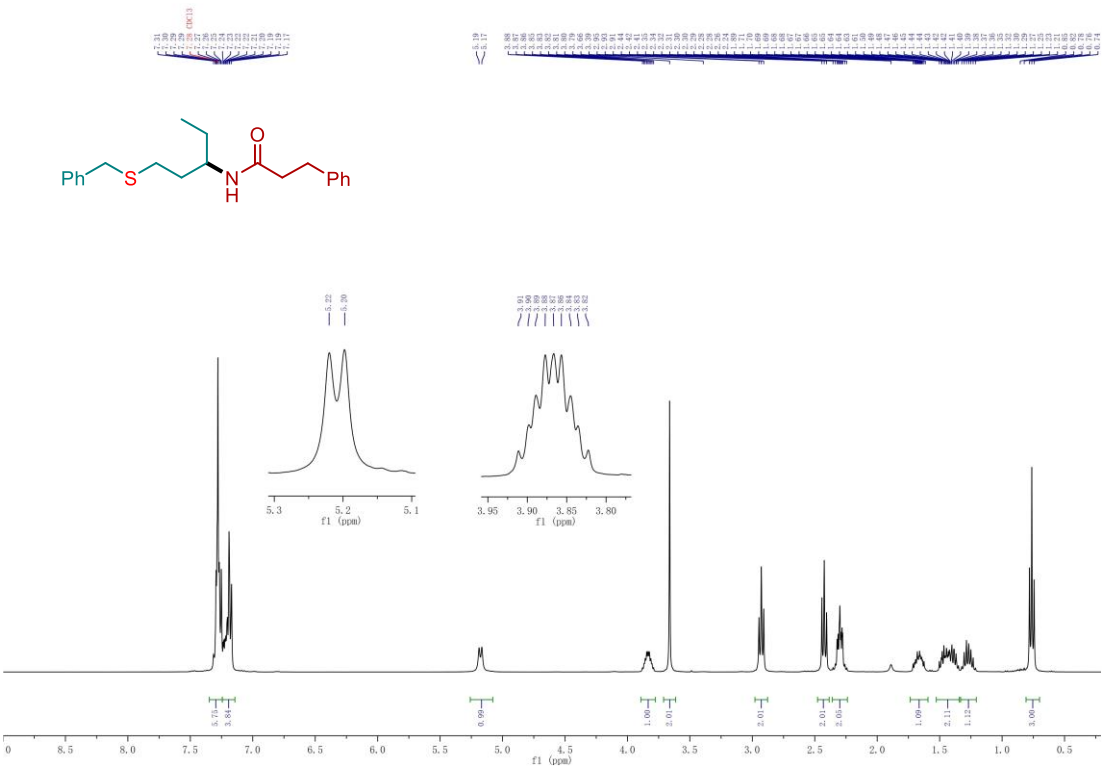


$^{13}$C NMR:

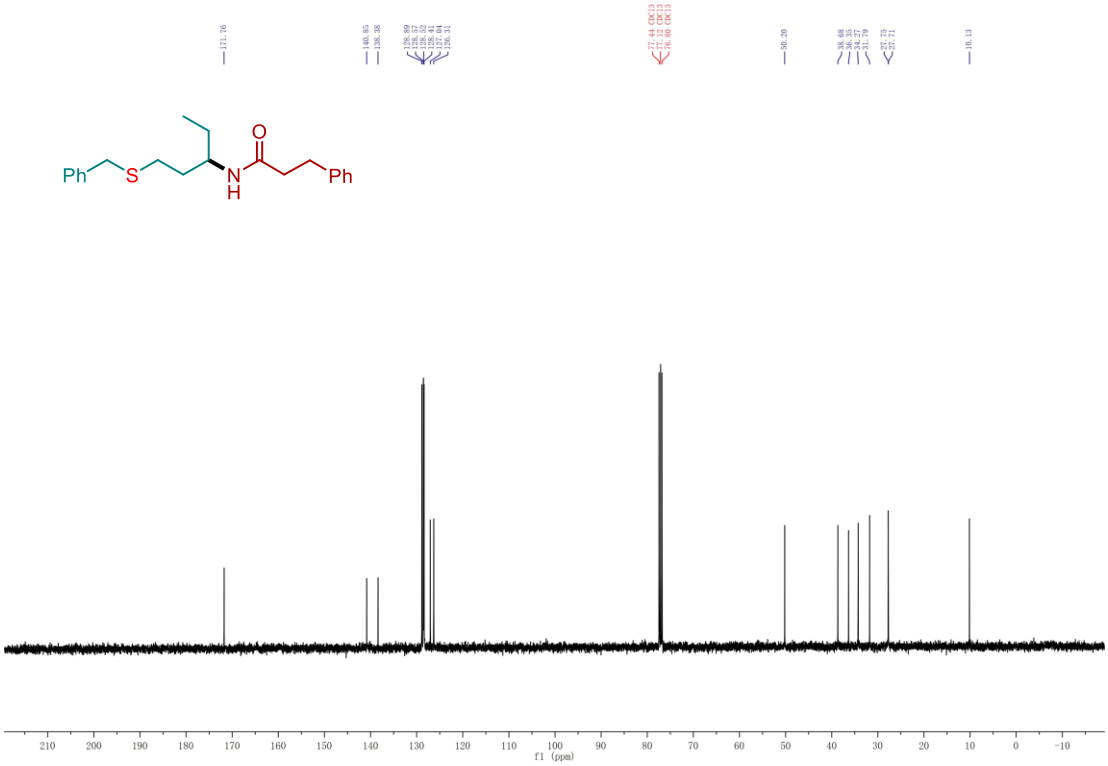

## 2-15

$^{1}$H NMR:

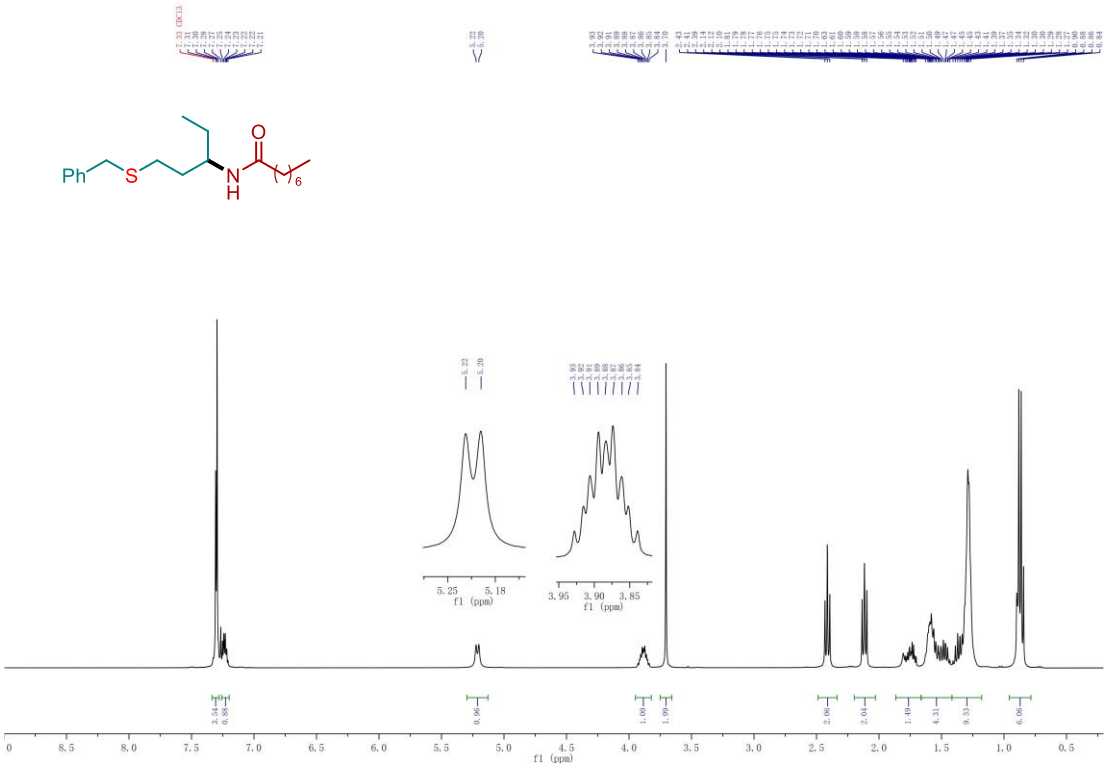


$^{13}$C NMR:

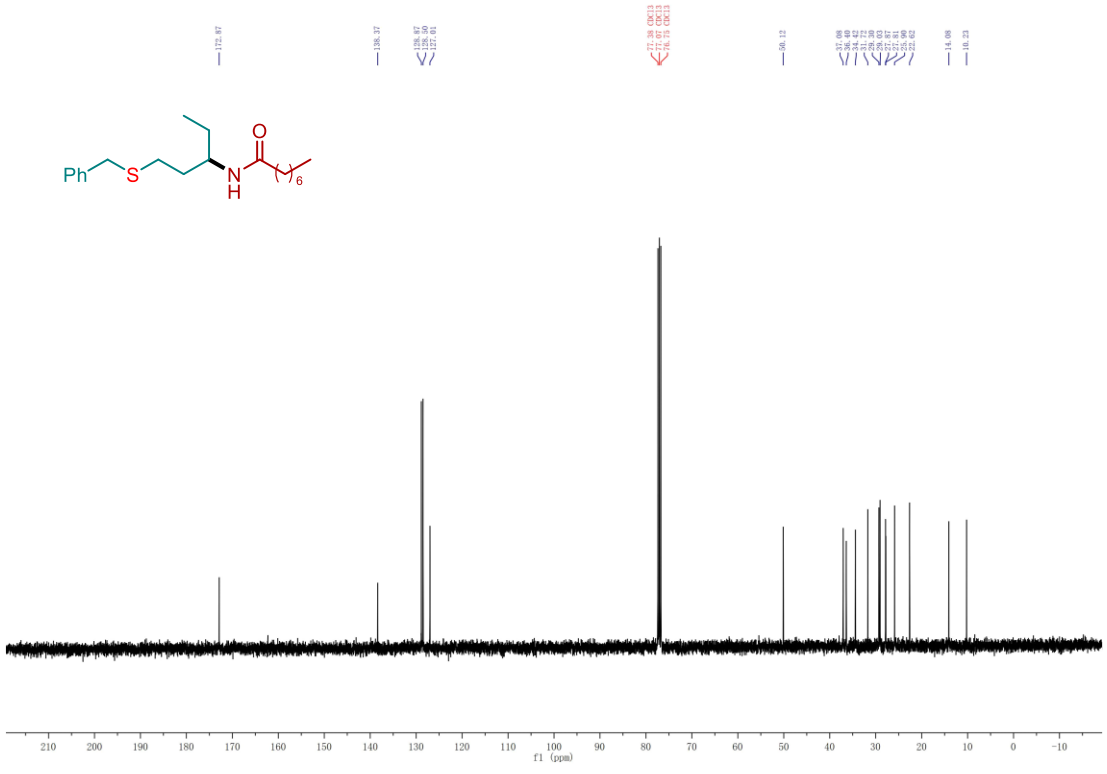

## 2-16

$^{1}$H NMR:

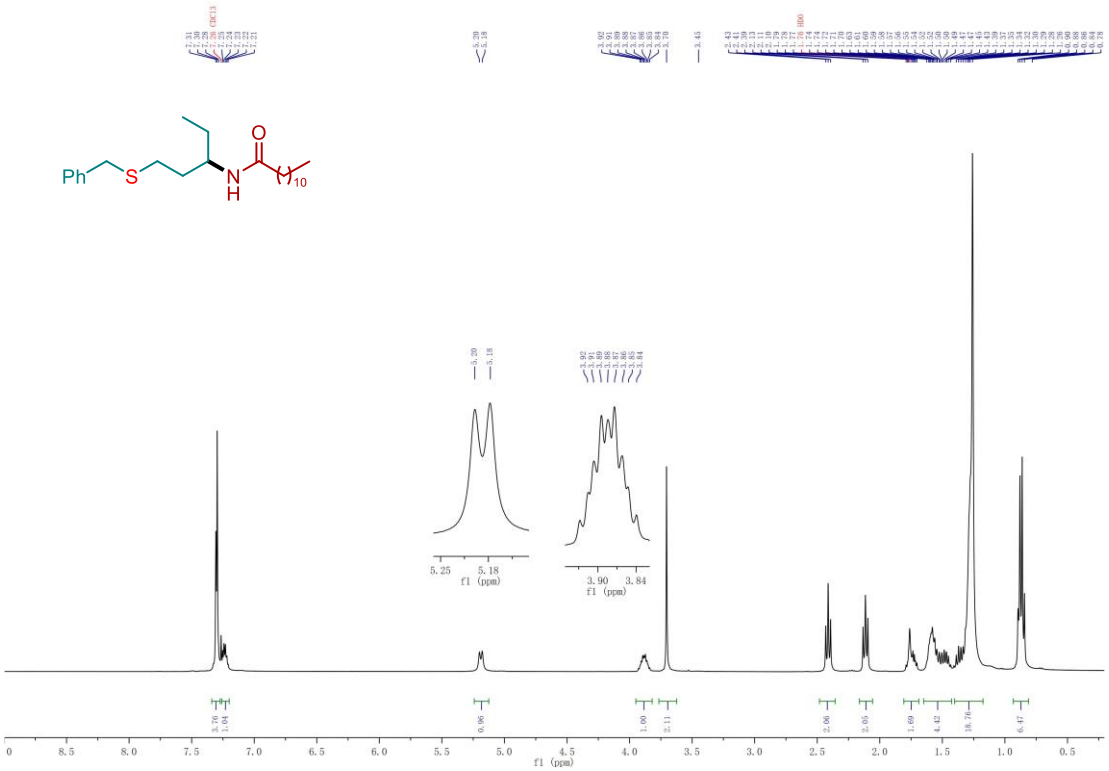


$^{13}$C NMR:

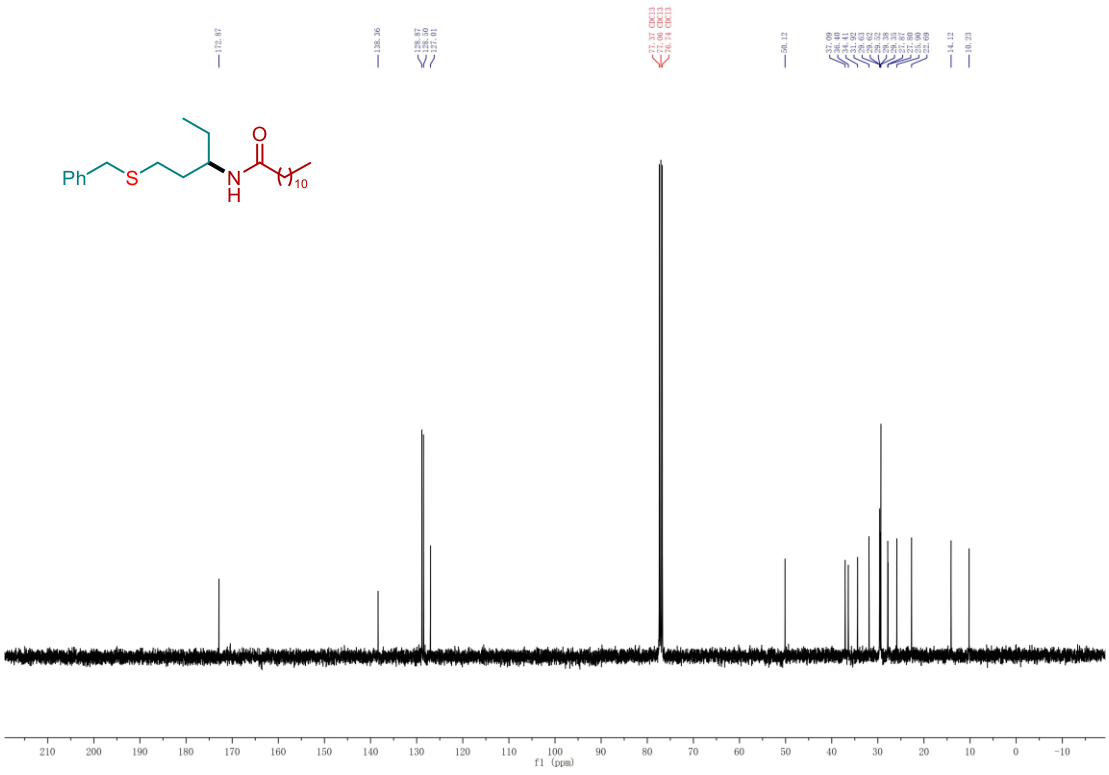

**2-17**

$^{1}$H NMR:

$^{13}$C NMR:

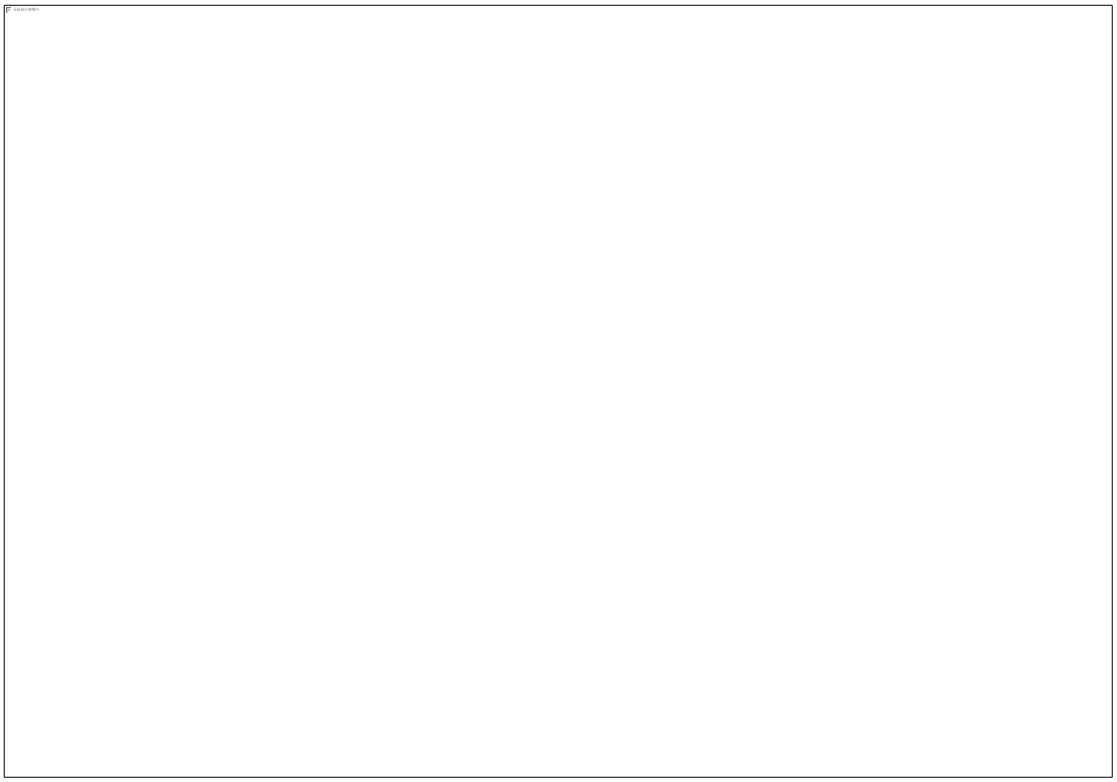

**2-18**

$^{1}$H NMR:

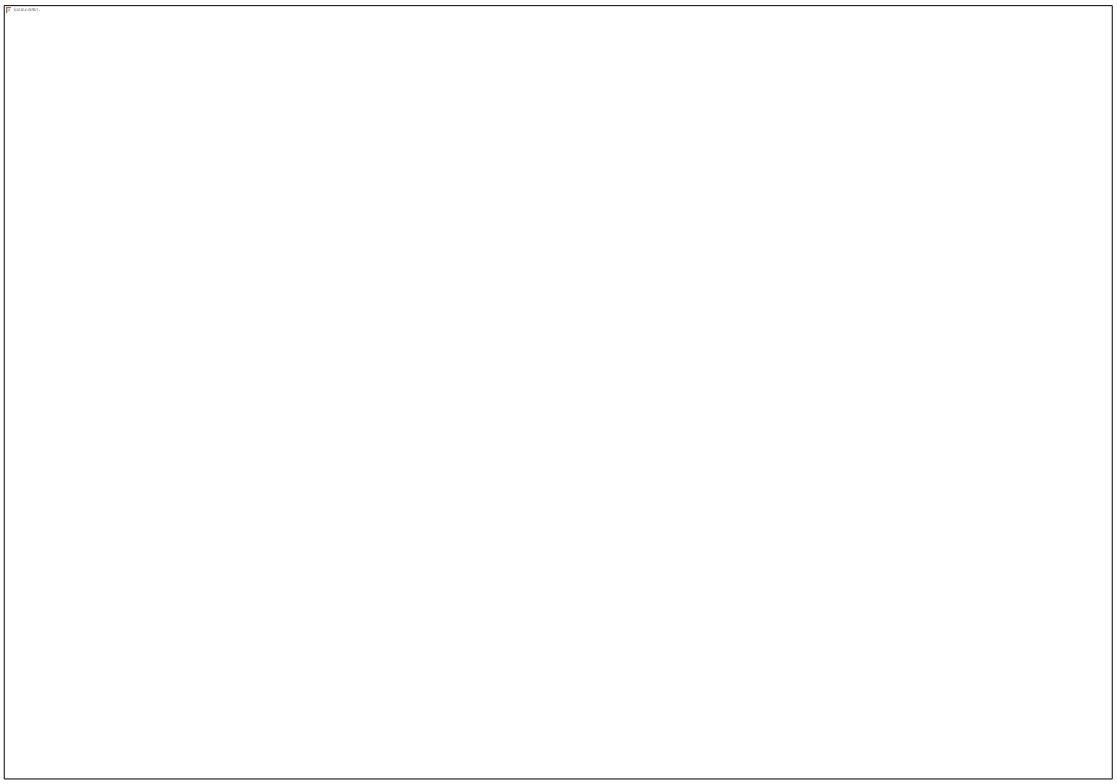

$^{13}$C NMR:

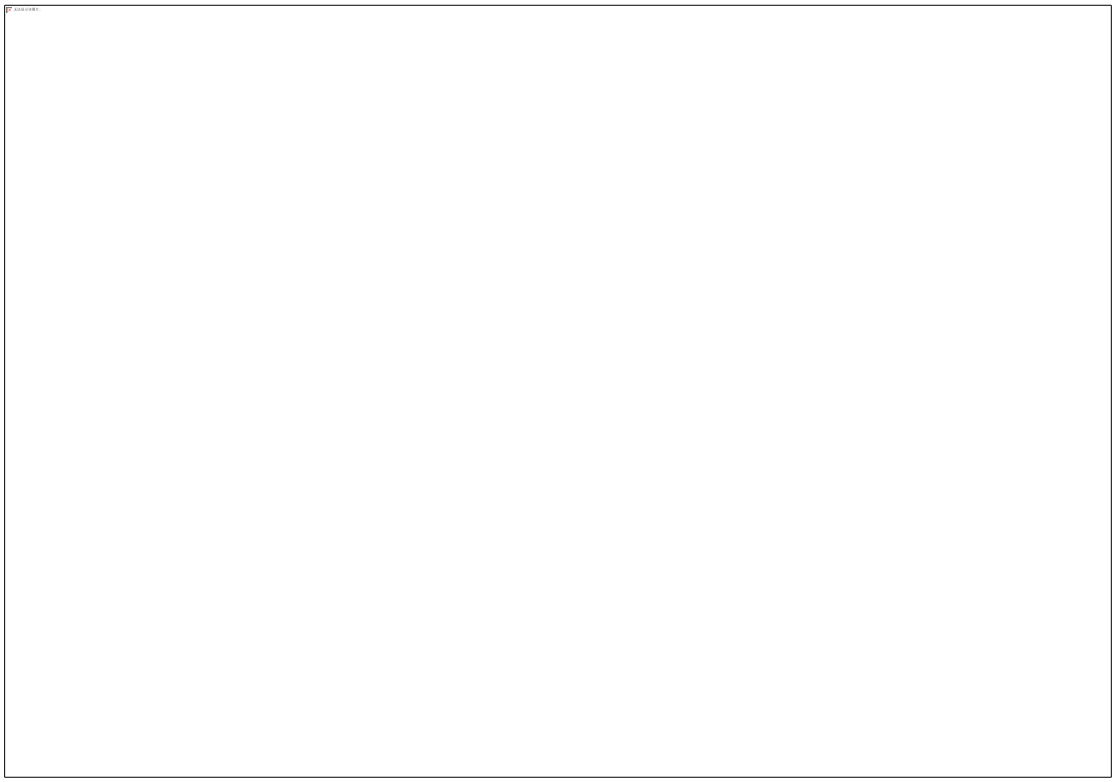

**2-19**

$^{1}$H NMR:

$^{13}$C NMR:

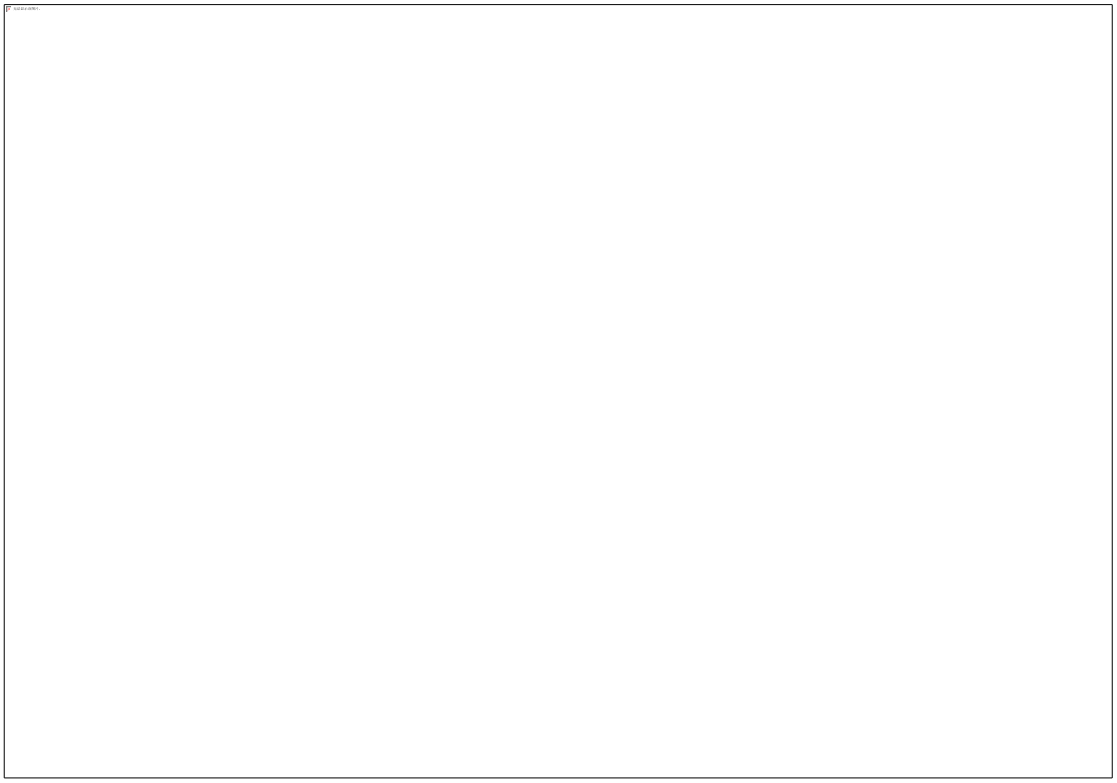

**2-20**

$^{1}$H NMR:

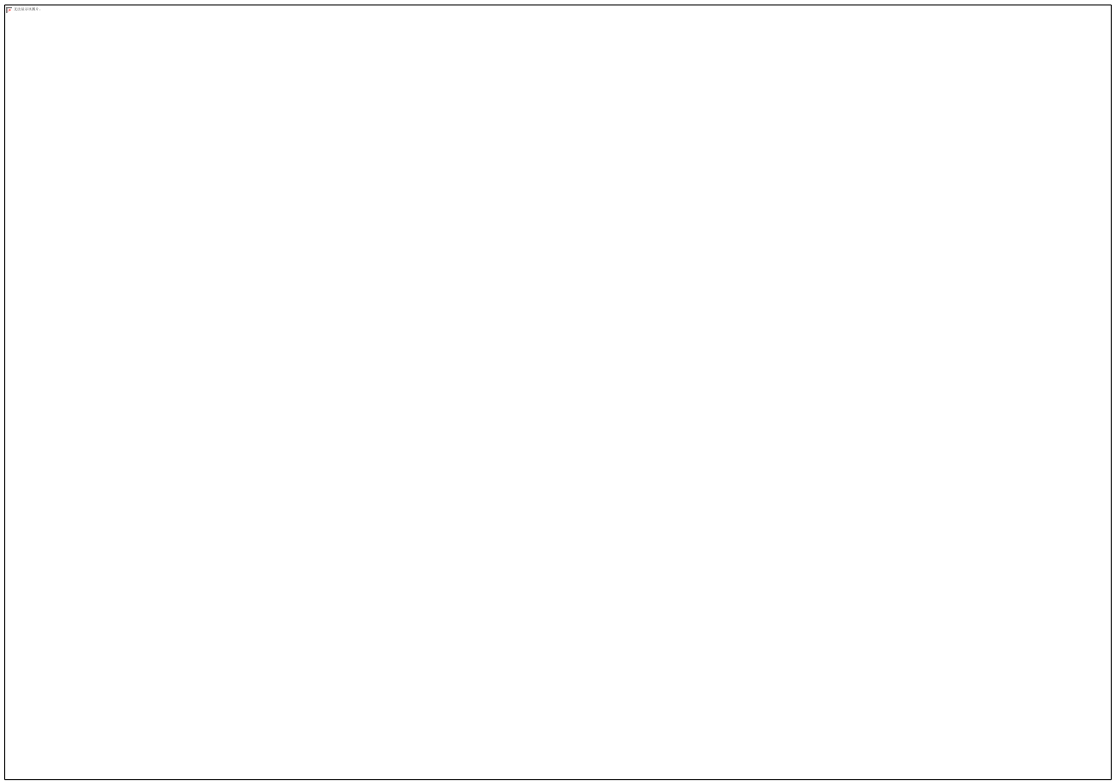

$^{13}$C NMR

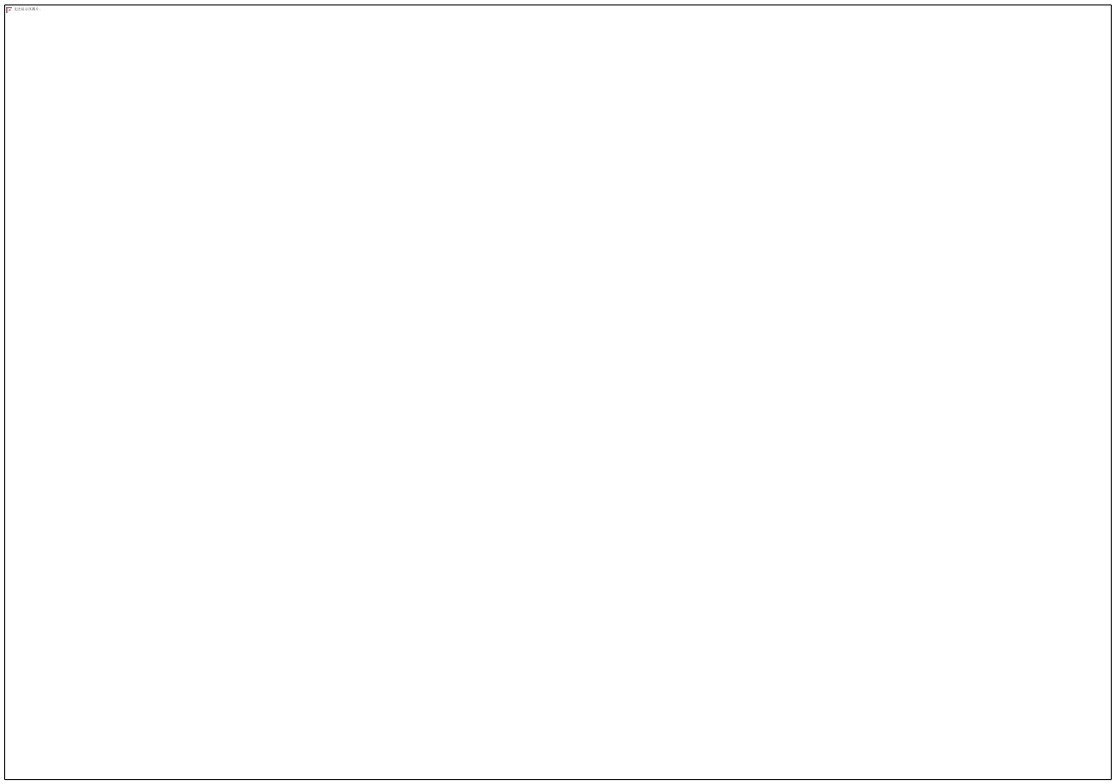

**2-21**

$^{1}$H NMR:

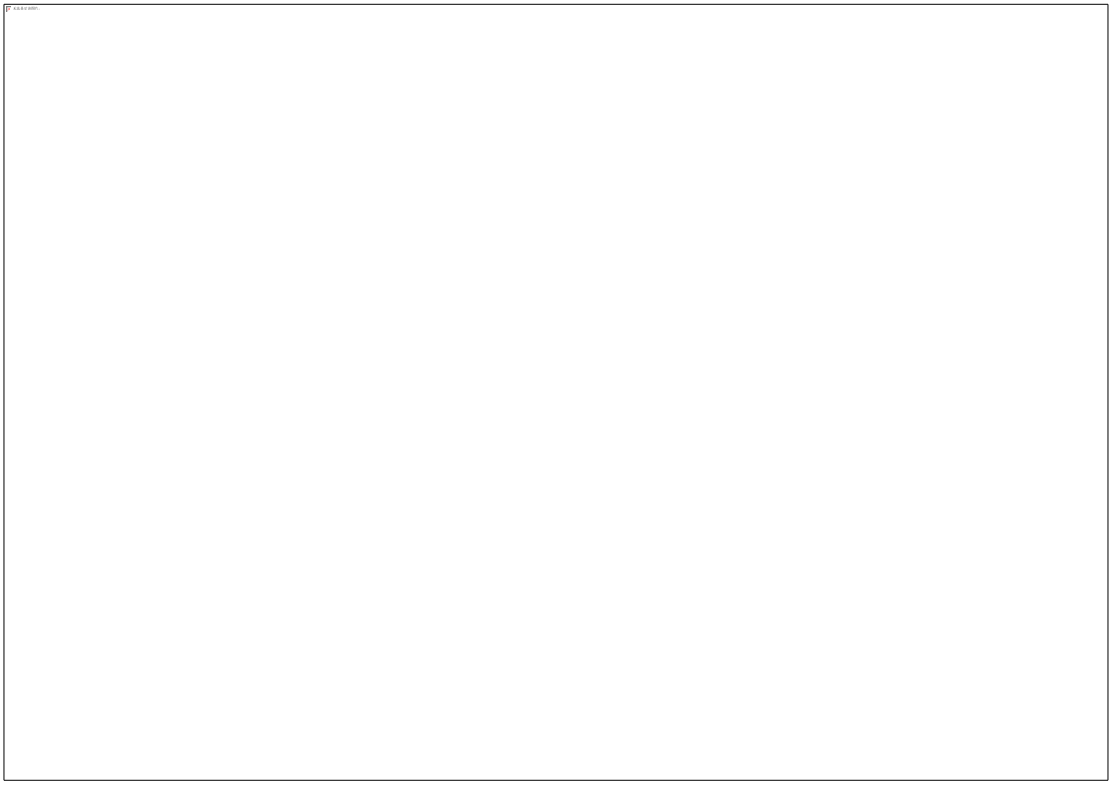

$^{13}$C NMR:

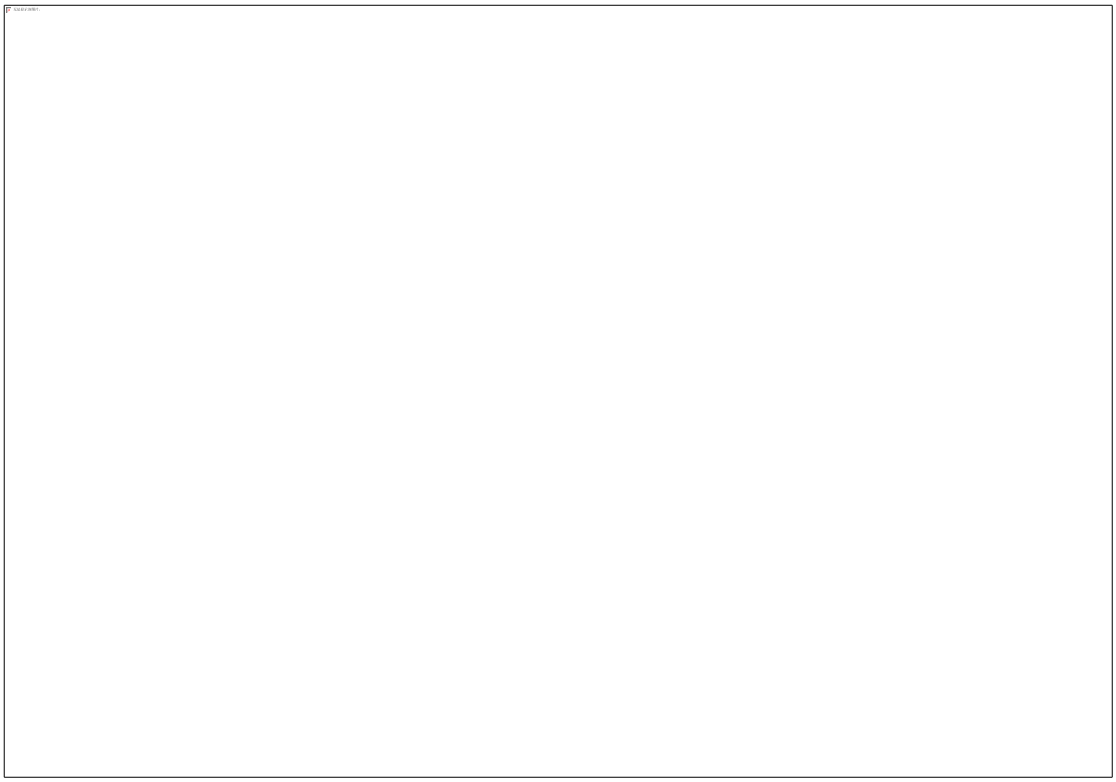

**2-21**

$^{19}$F NMR:

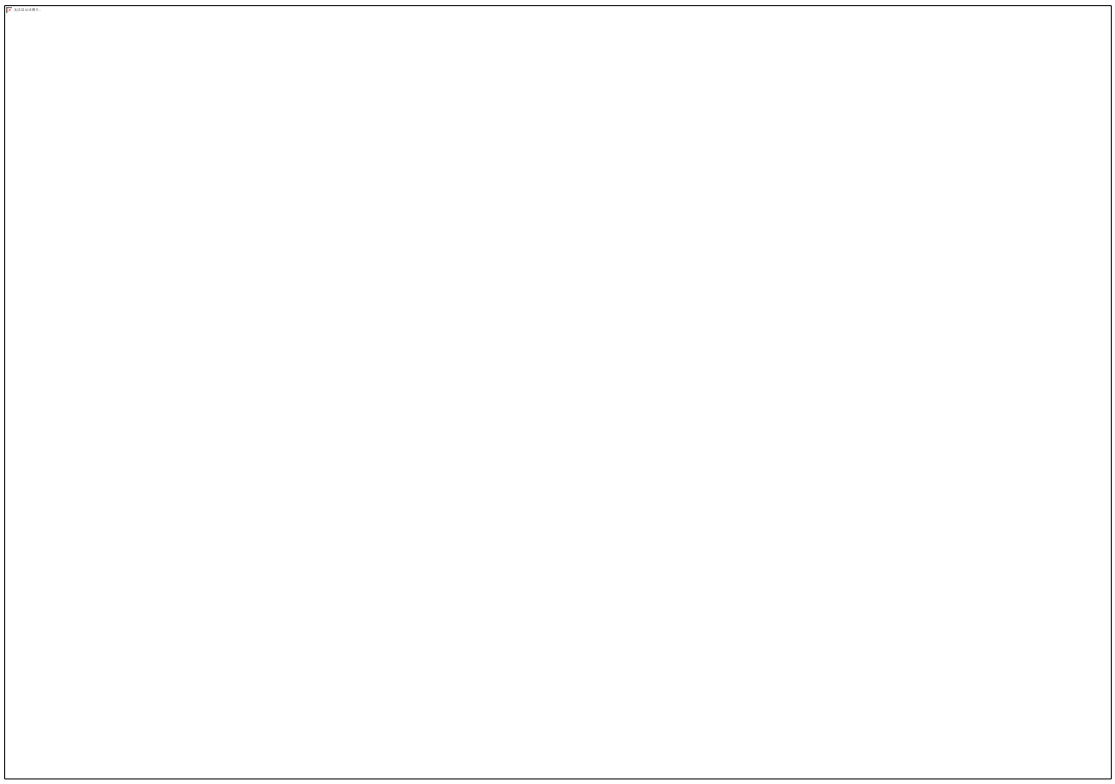

## 2-22

$^{1}$H NMR:

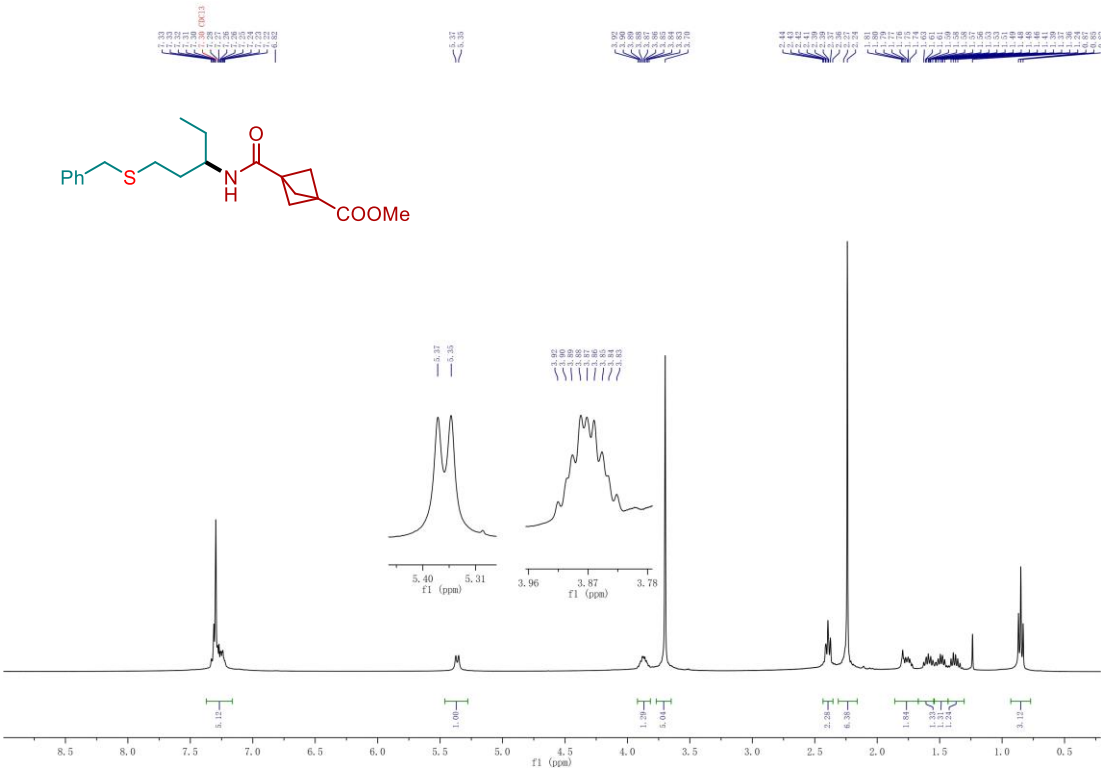


$^{13}$C NMR:

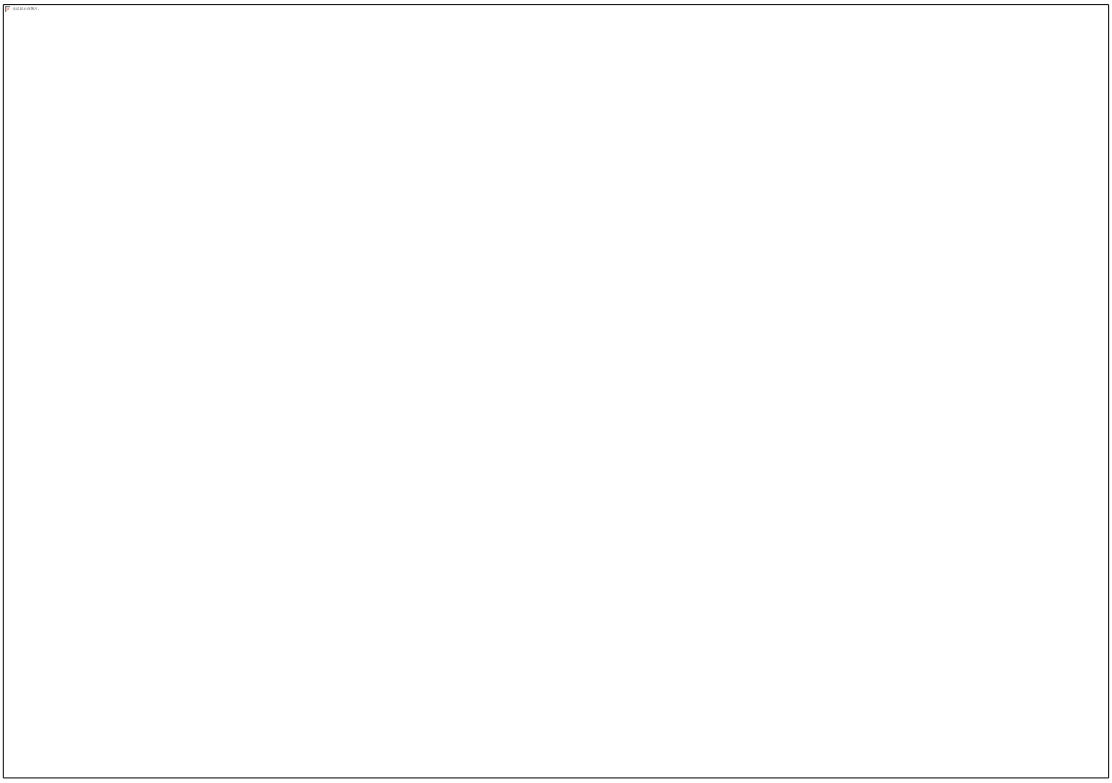

## 2-23

$^{1}$H NMR:

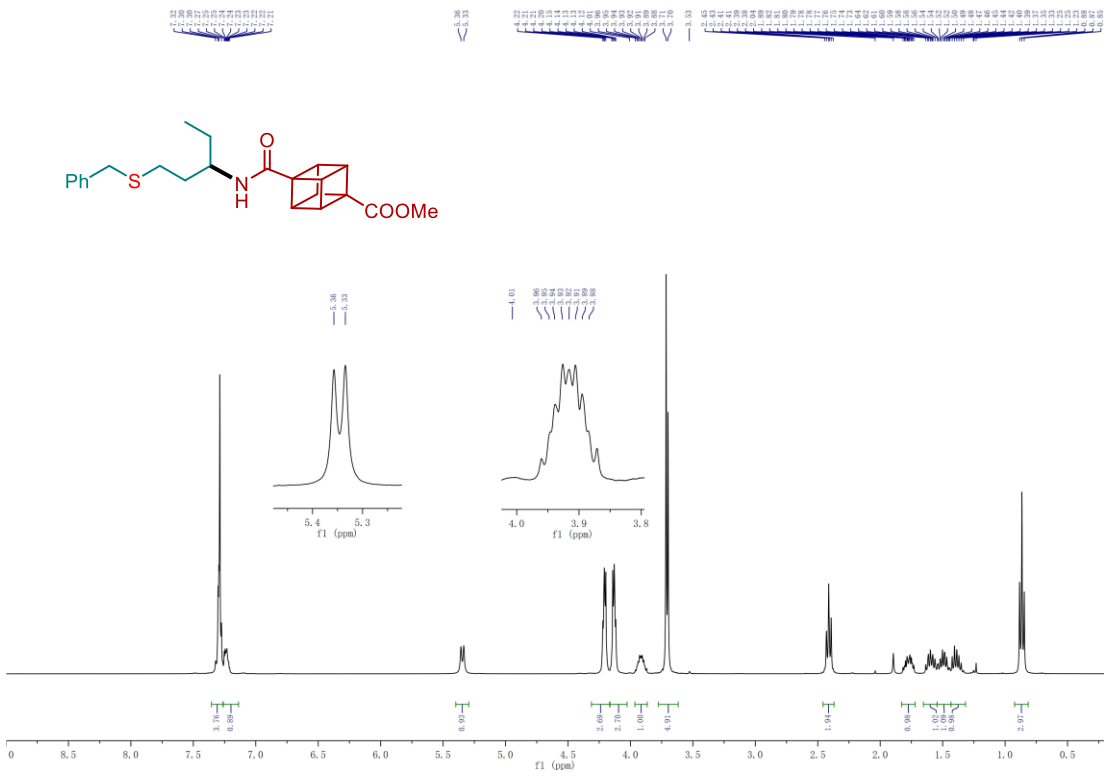


$^{13}$C NMR:

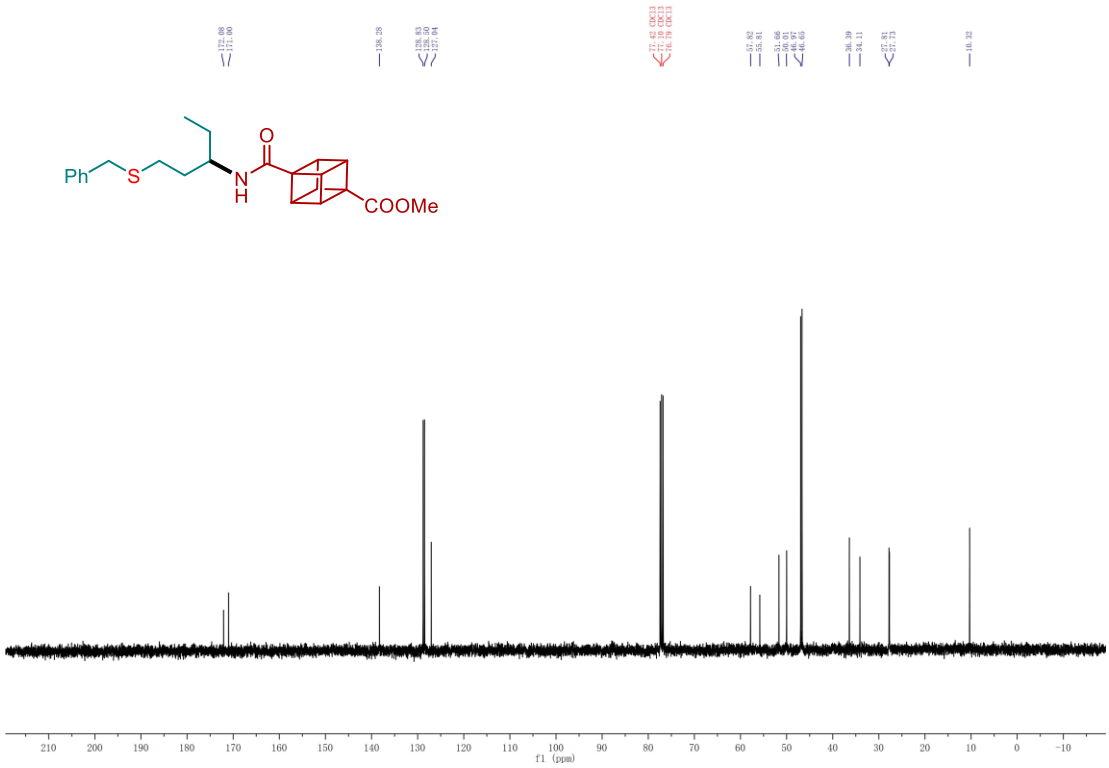

**2-24**

$^{1}$H NMR:

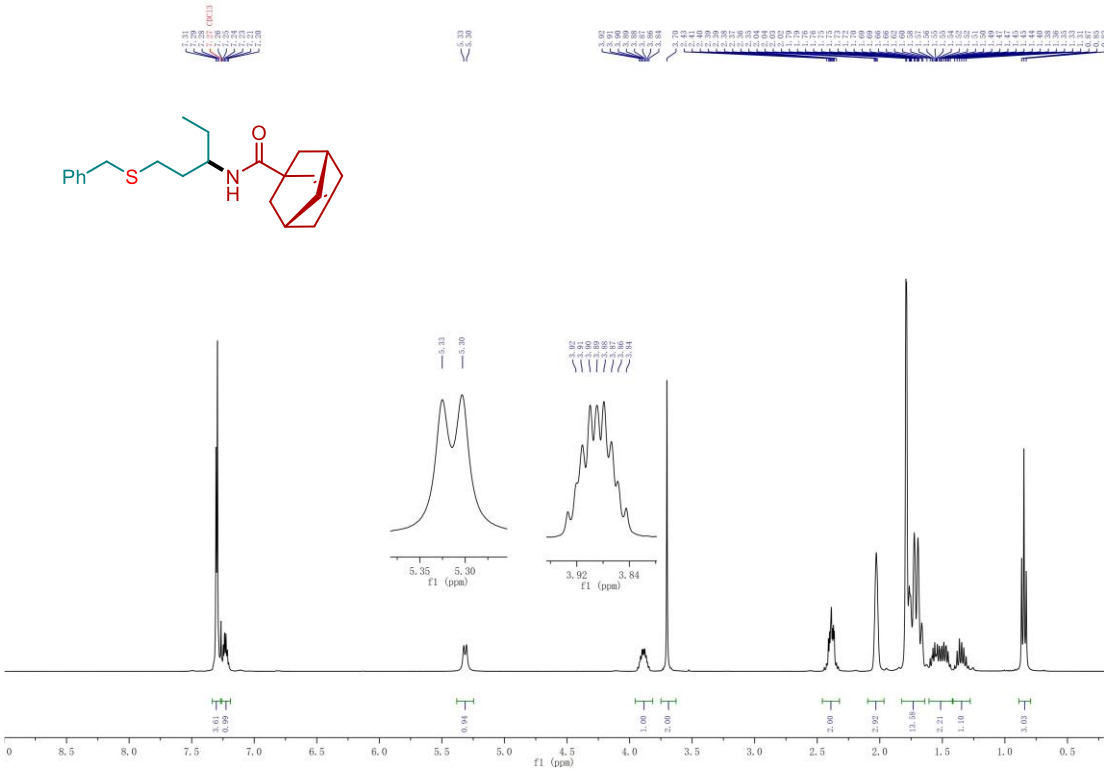


$^{13}$C NMR:

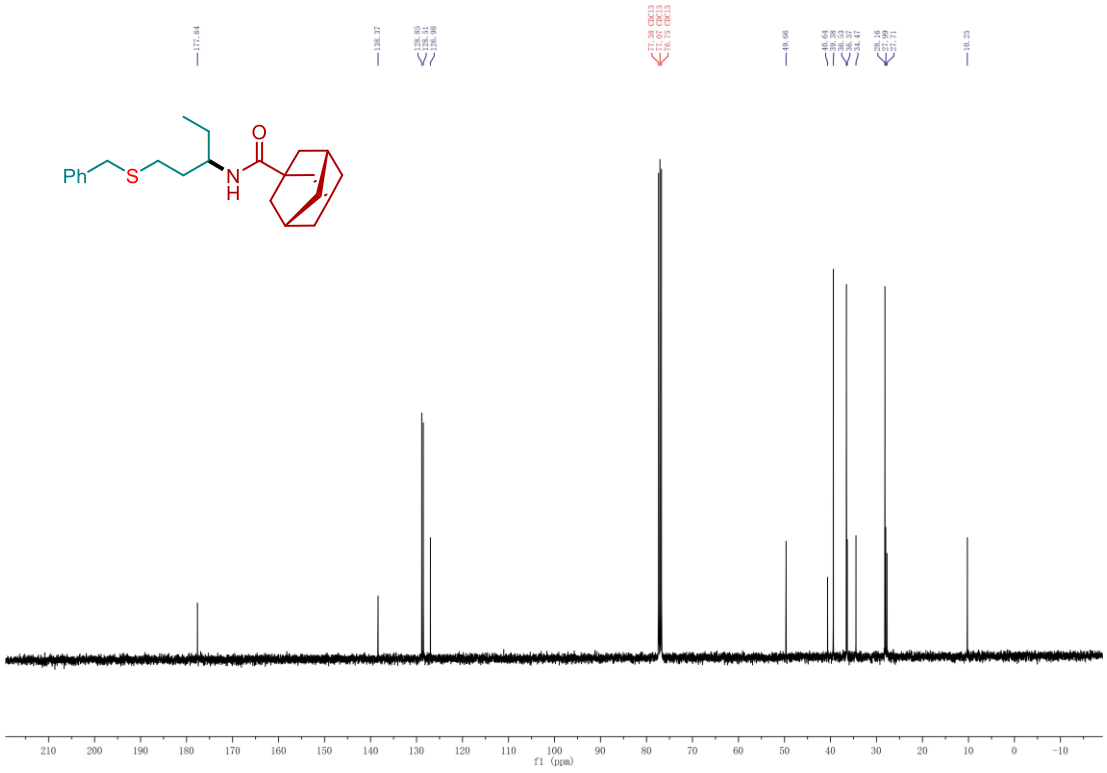

## 2-25

$^{1}$H NMR:

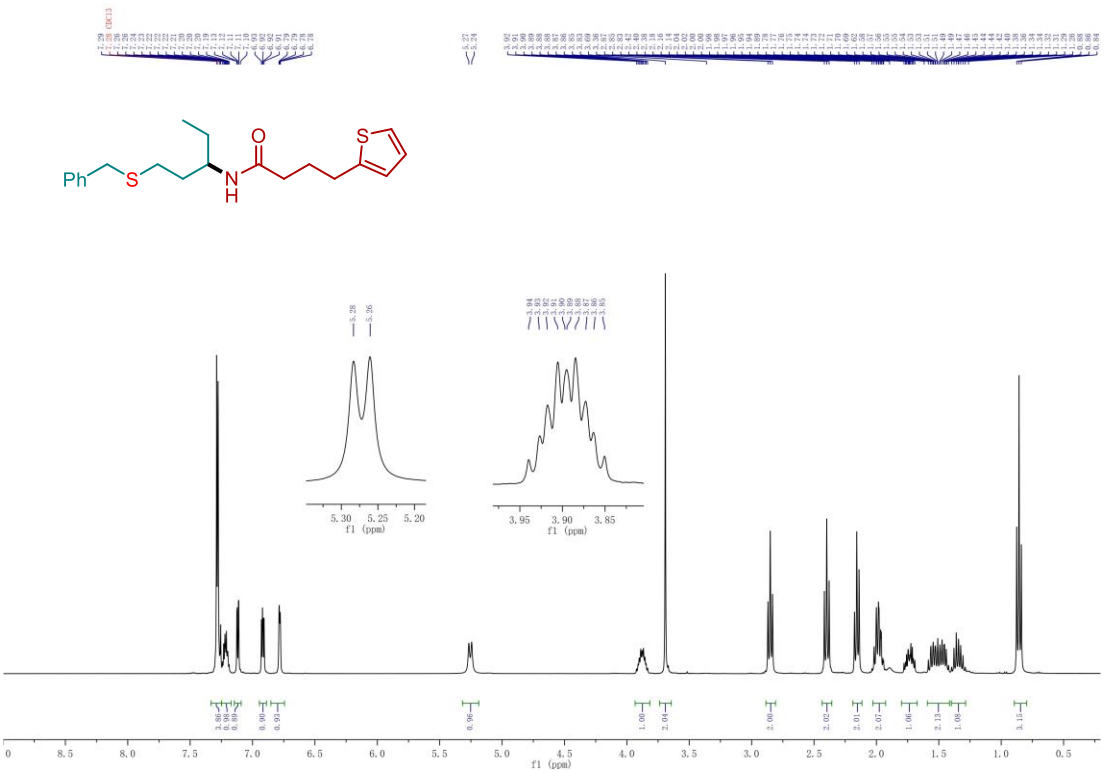


$^{13}$C NMR:

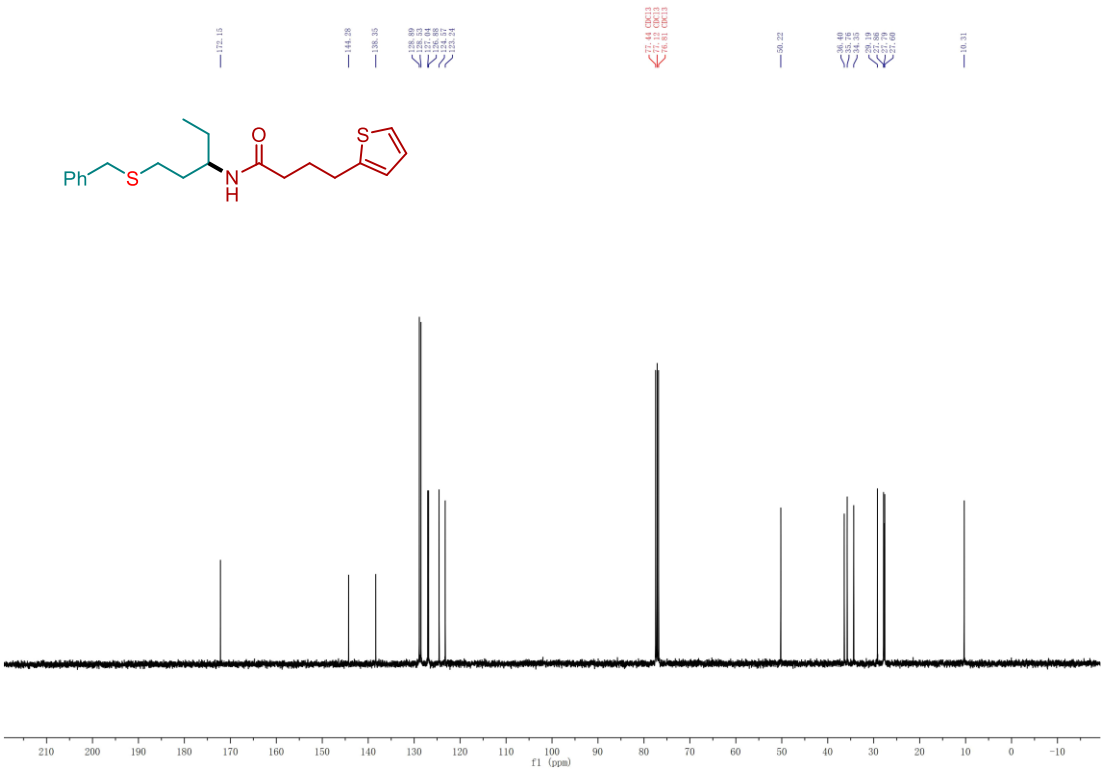

## 2-26

$^{1}$H NMR:

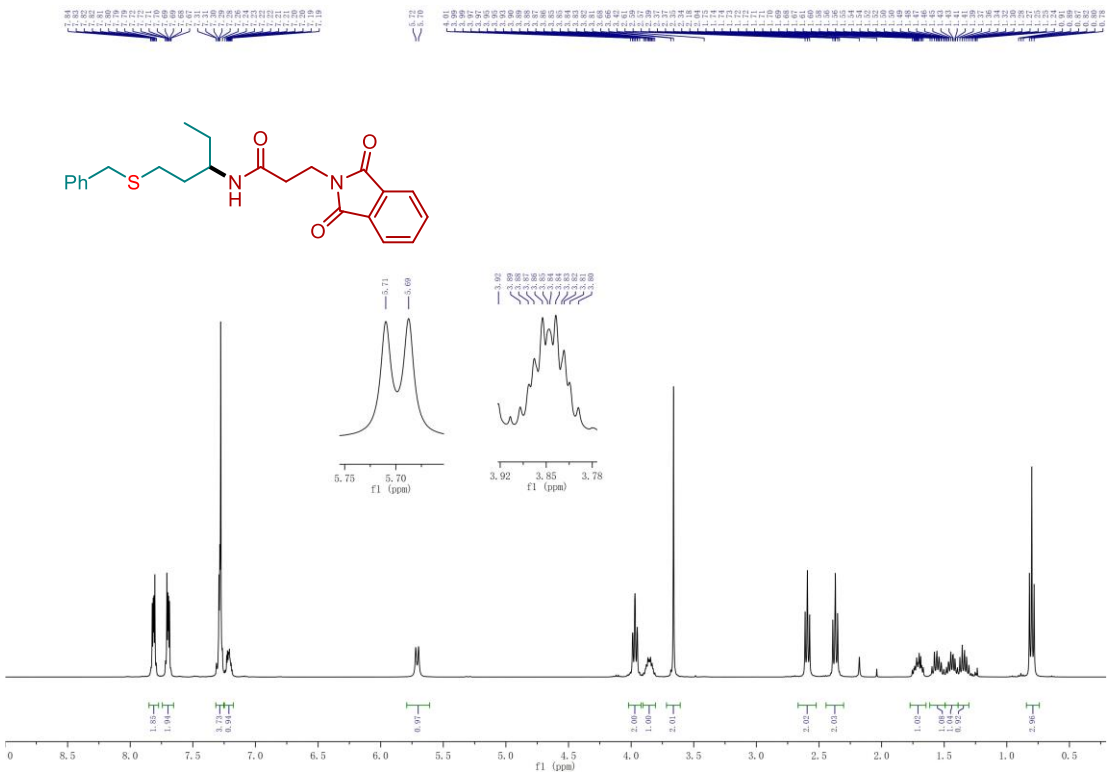


$^{13}$C NMR:

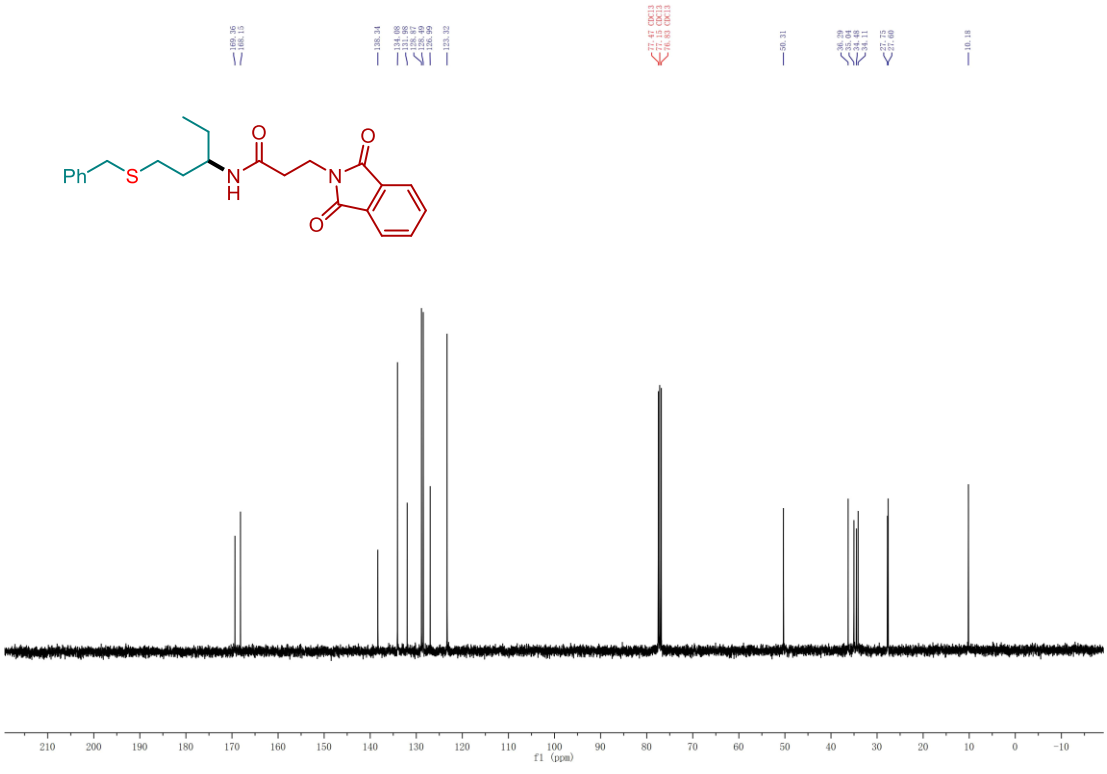

## 2-27

$^{1}$H NMR:

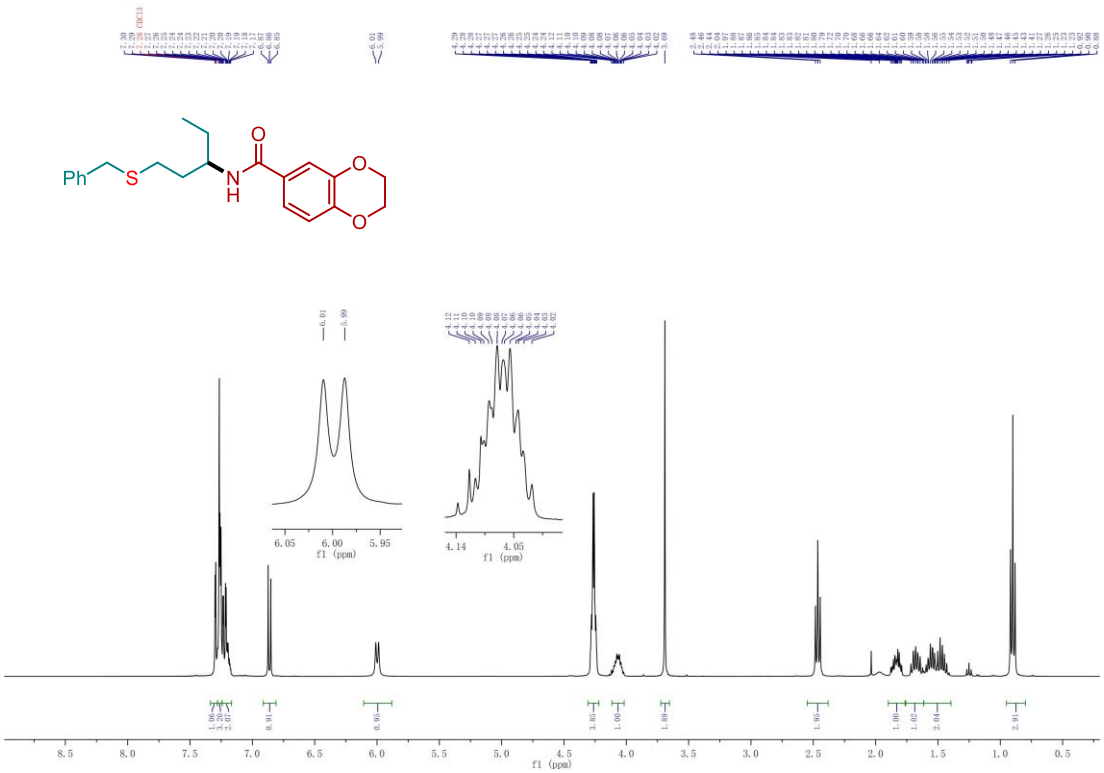


$^{13}$C NMR:

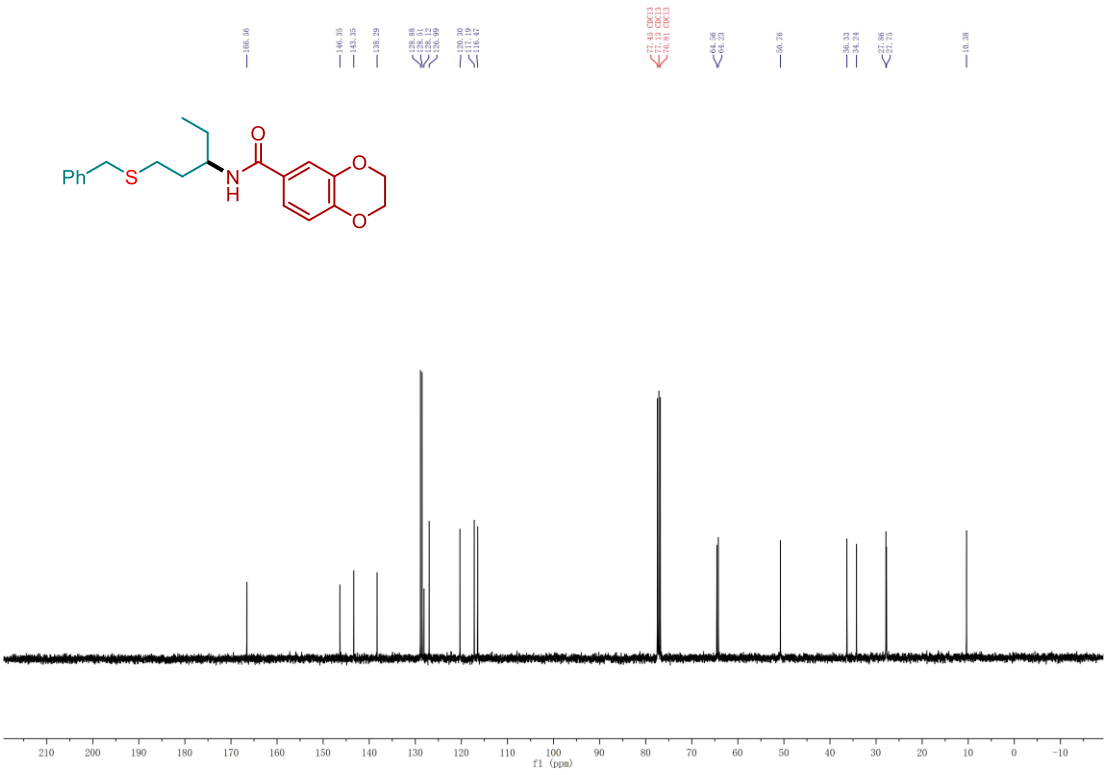

**2-28**

$^{1}$H NMR:

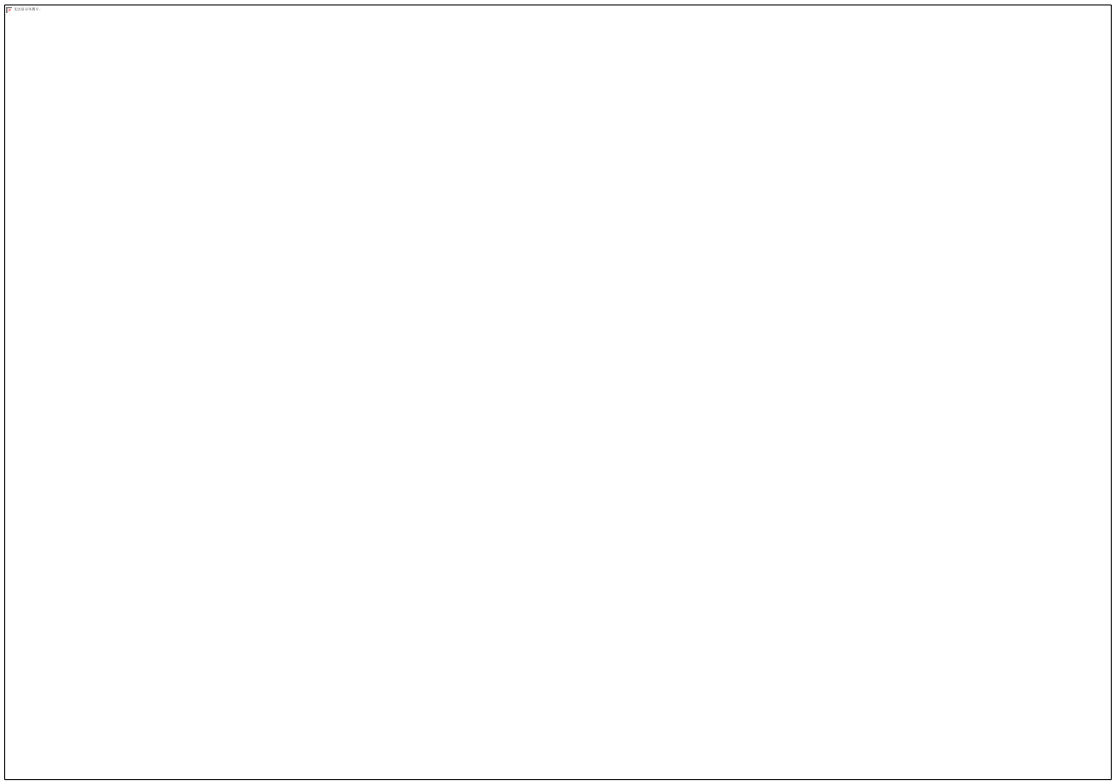

$^{13}$C NMR:

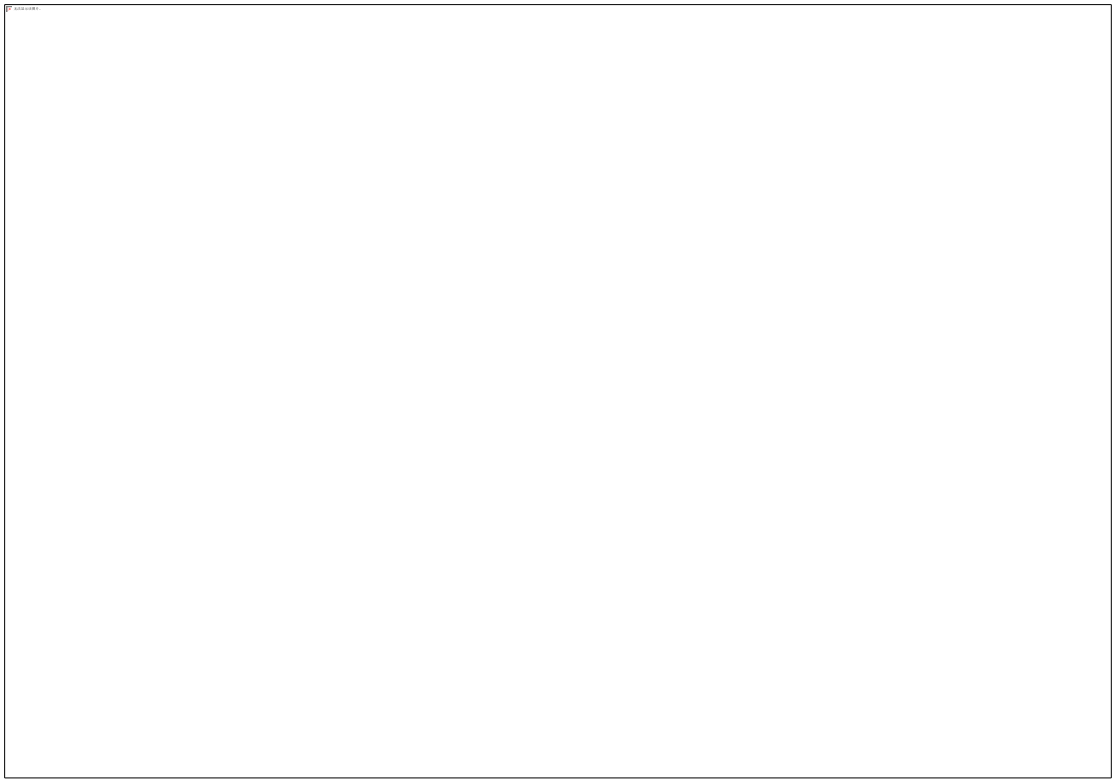

**2-29**

$^{1}$H NMR:

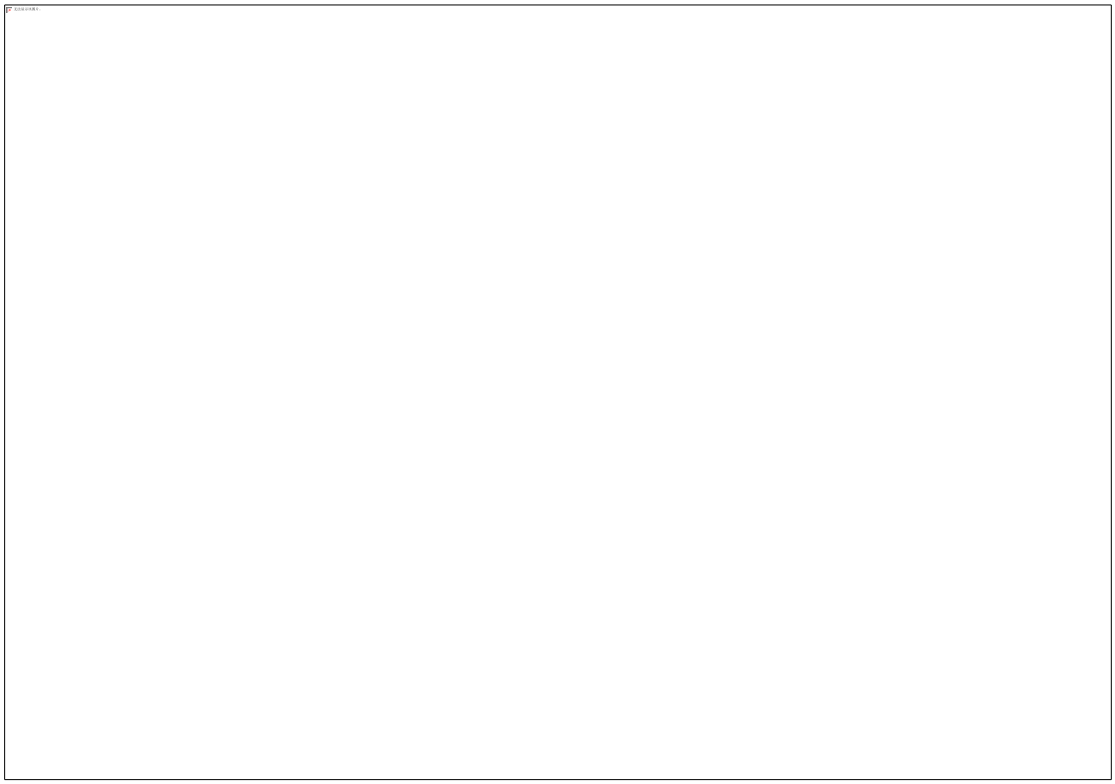

$^{13}$C NMR:

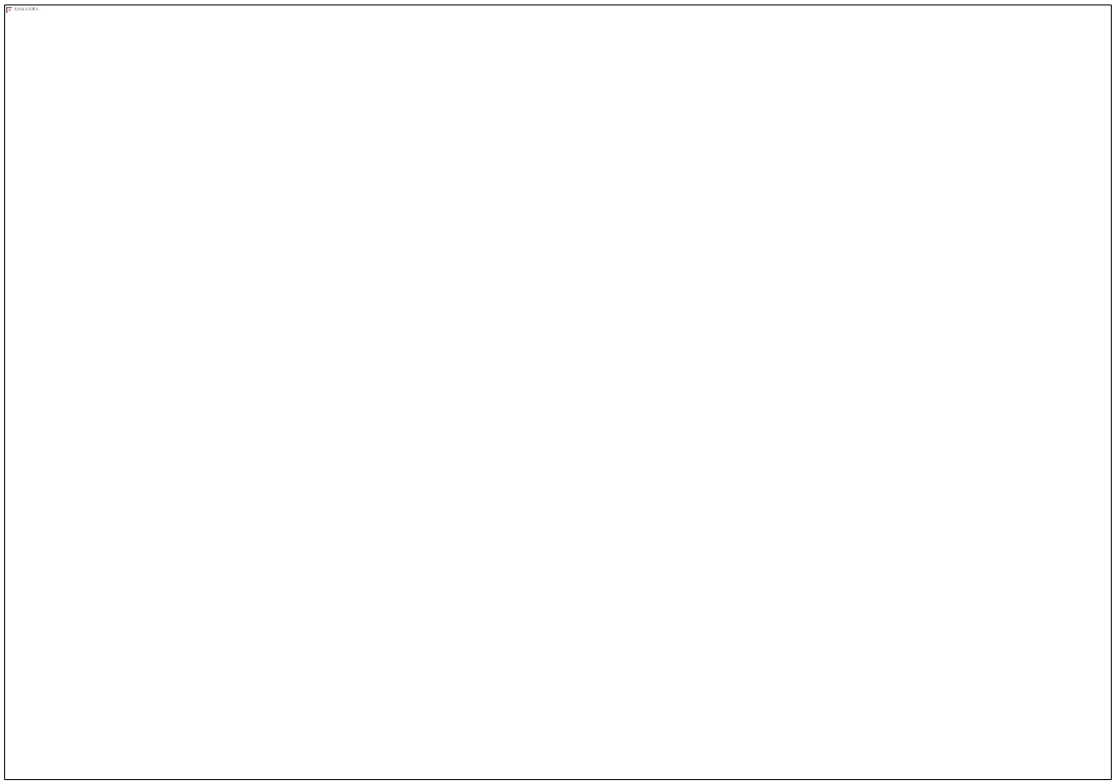

## 2-30

$^{1}$H NMR:

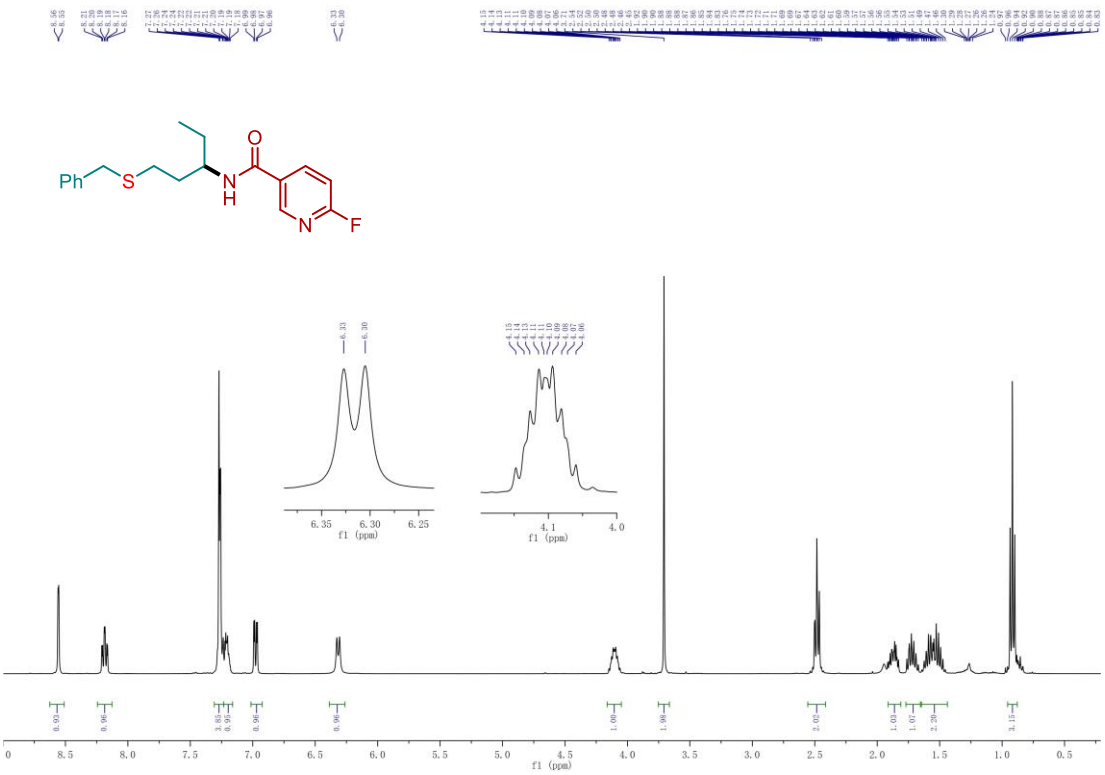


$^{13}$C NMR:

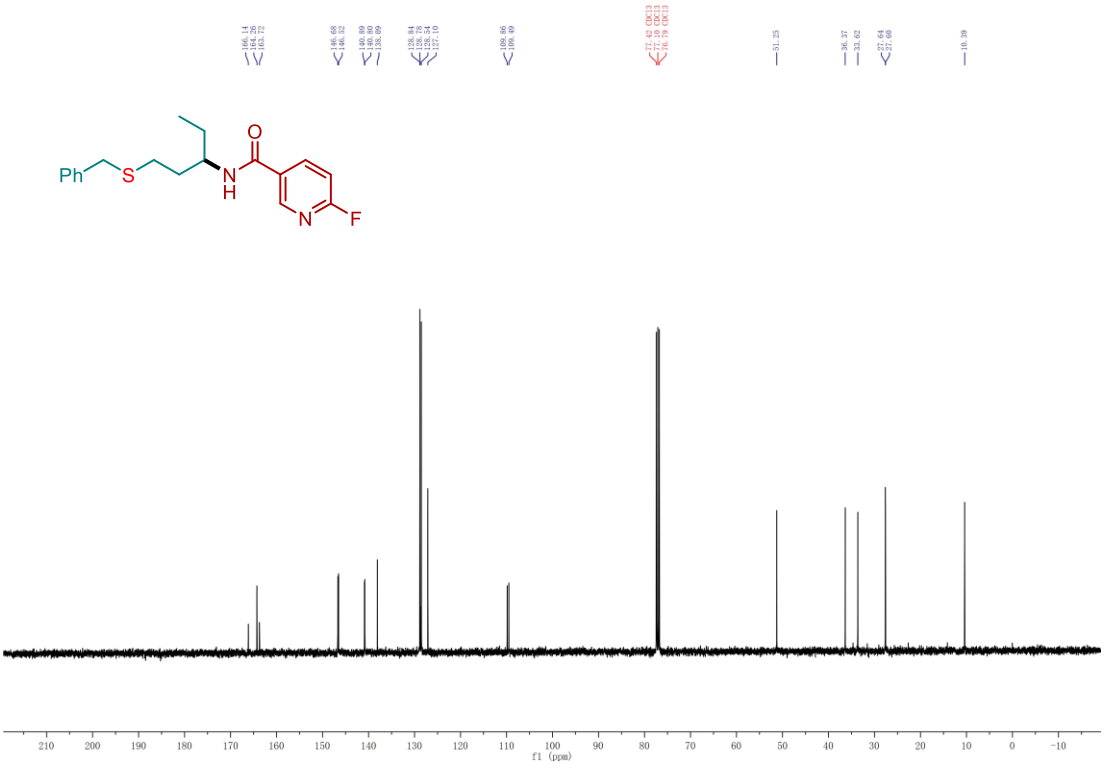

**2-30**

$^{19}$F NMR:

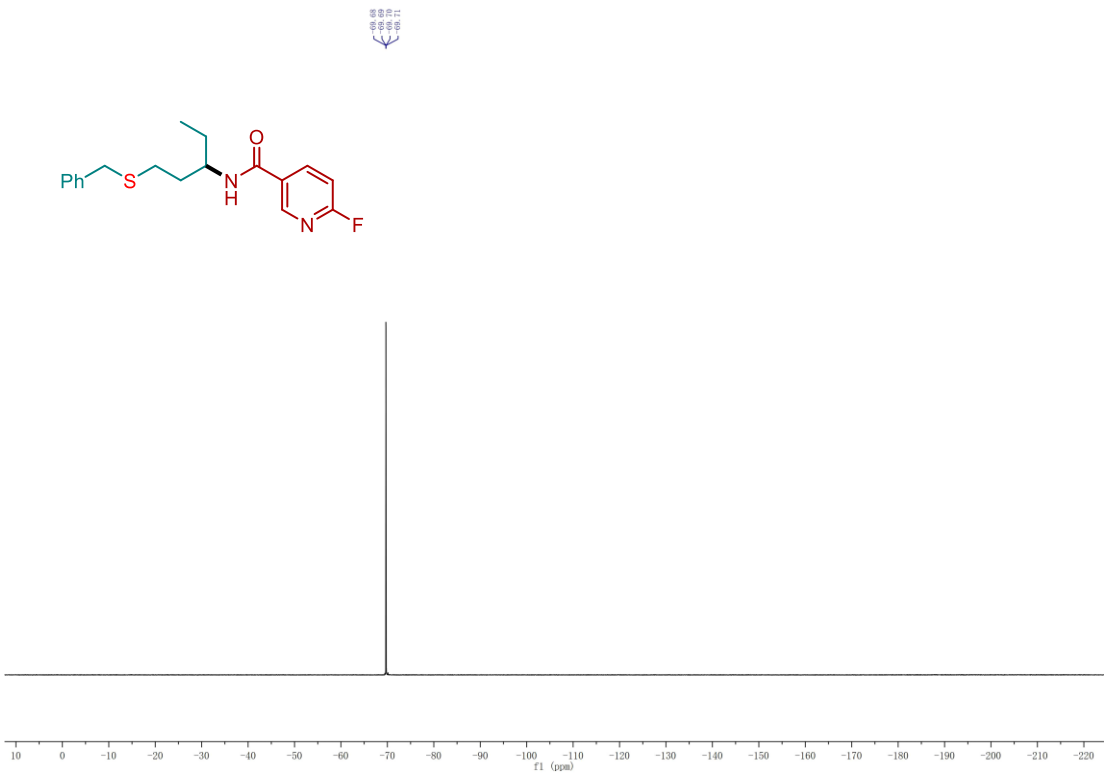
Ph
S
N
H
O
N
F
10
0
-10
-20
-30
-40
-50
-60
-70
-80
-90
-100
-110
-120
-130
-140
-150
-160
-170
-180
-190
-200
-210
-220
f1 (ppm)

**2-31**

$^{1}$H NMR:

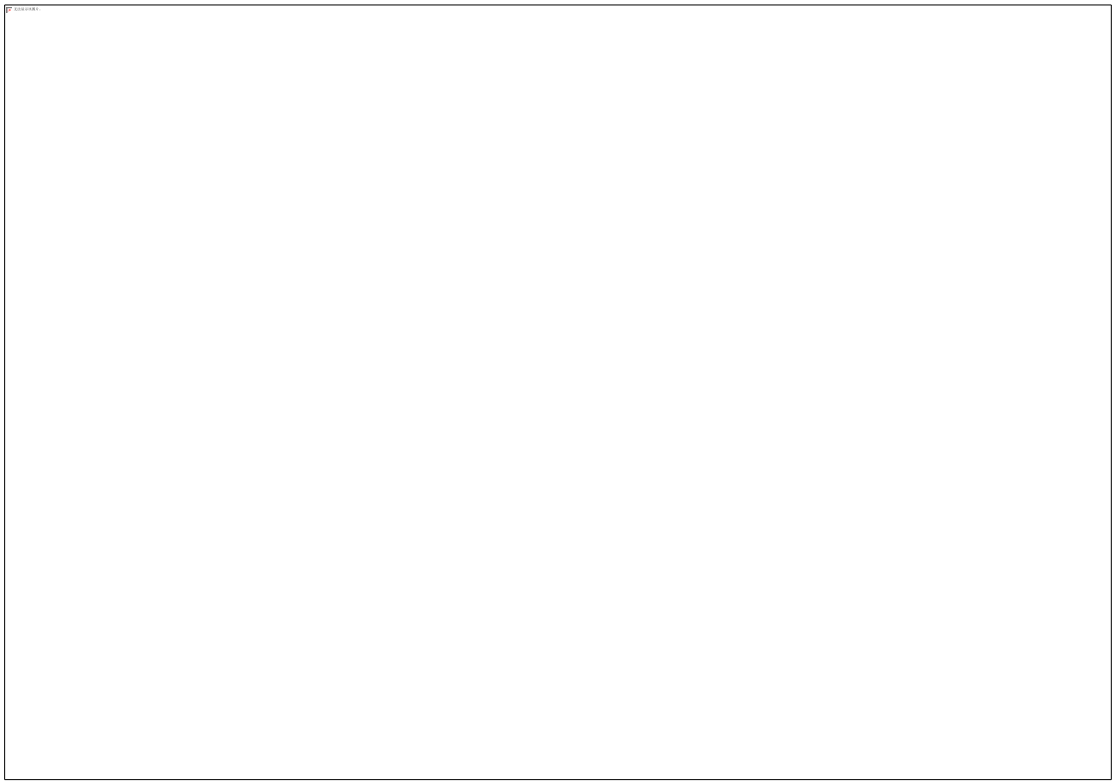

$^{13}$C NMR:

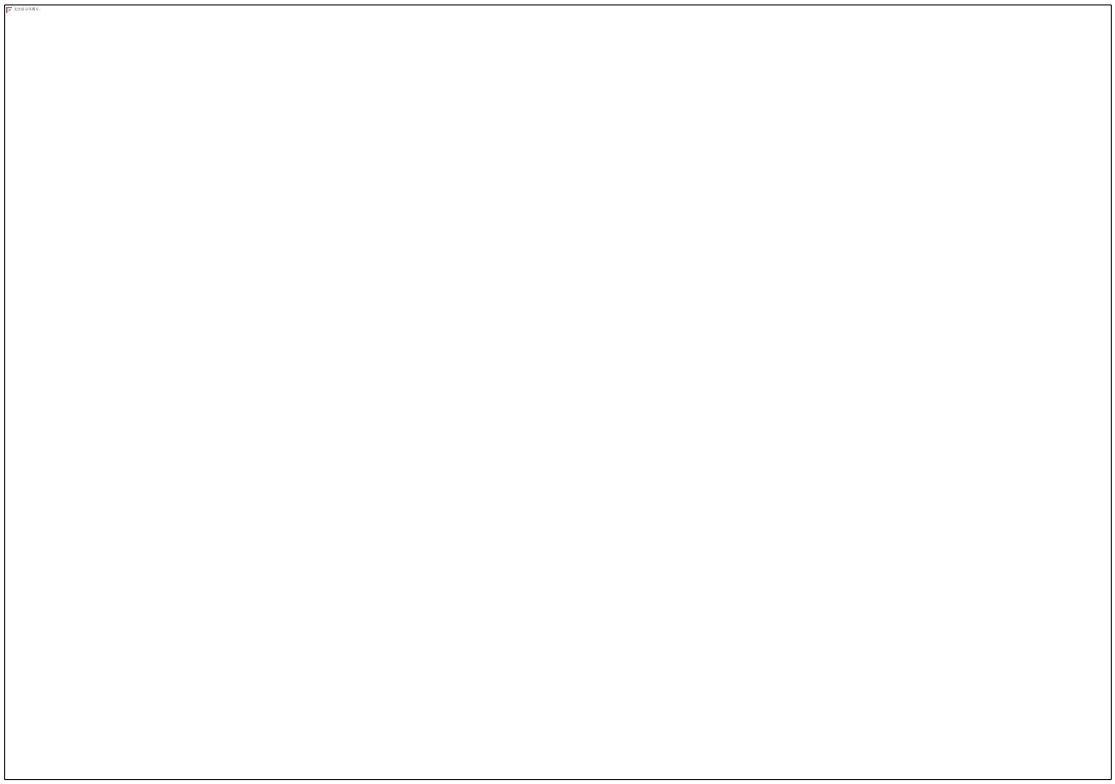

**2-32**

$^{1}$H NMR:

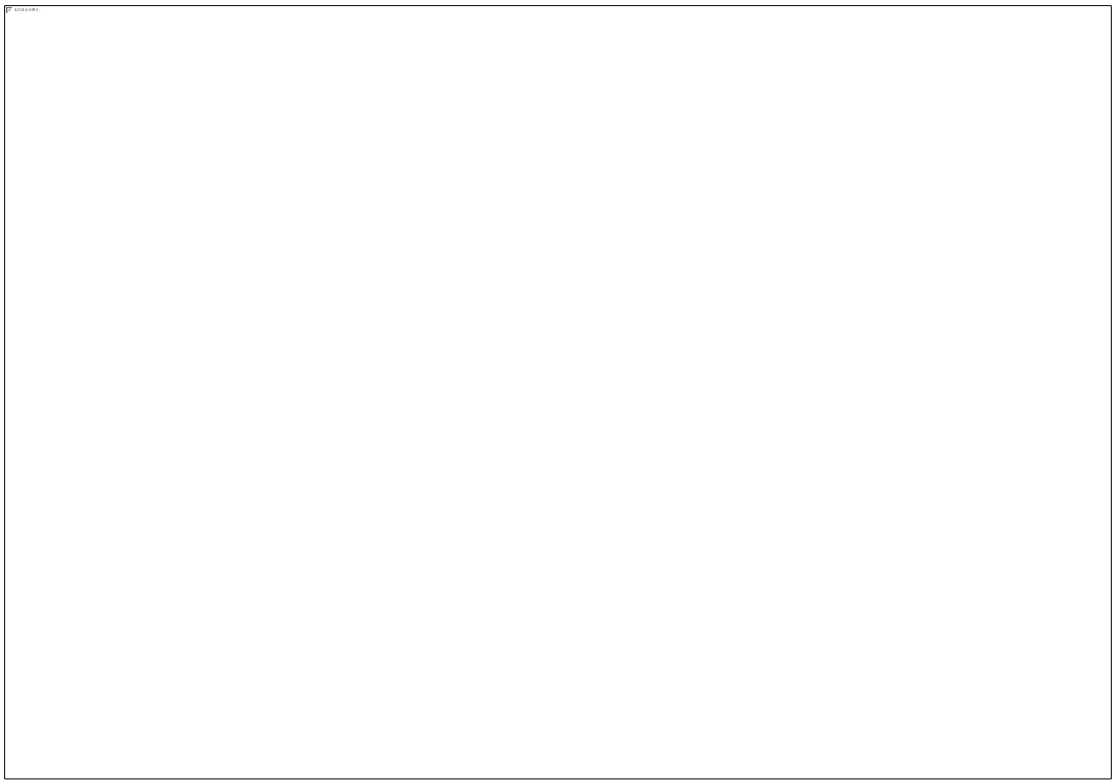

$^{13}$C NMR:

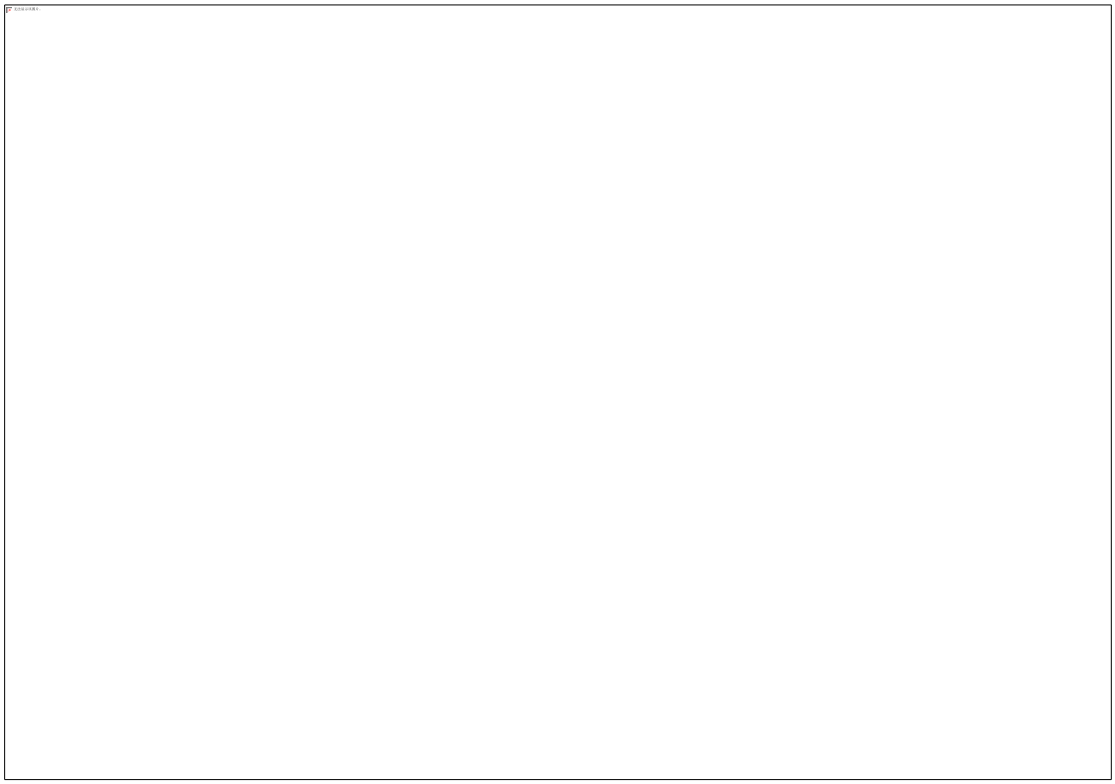

**2-33**

$^{1}$H NMR:

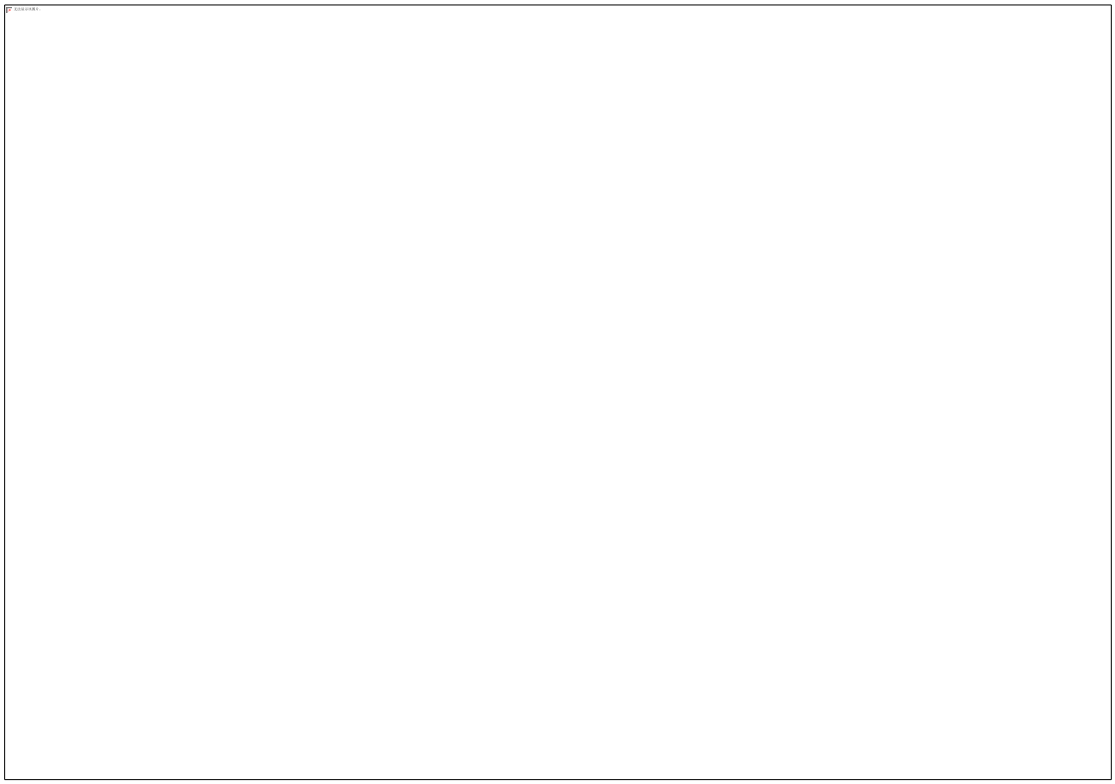

$^{13}$C NMR:

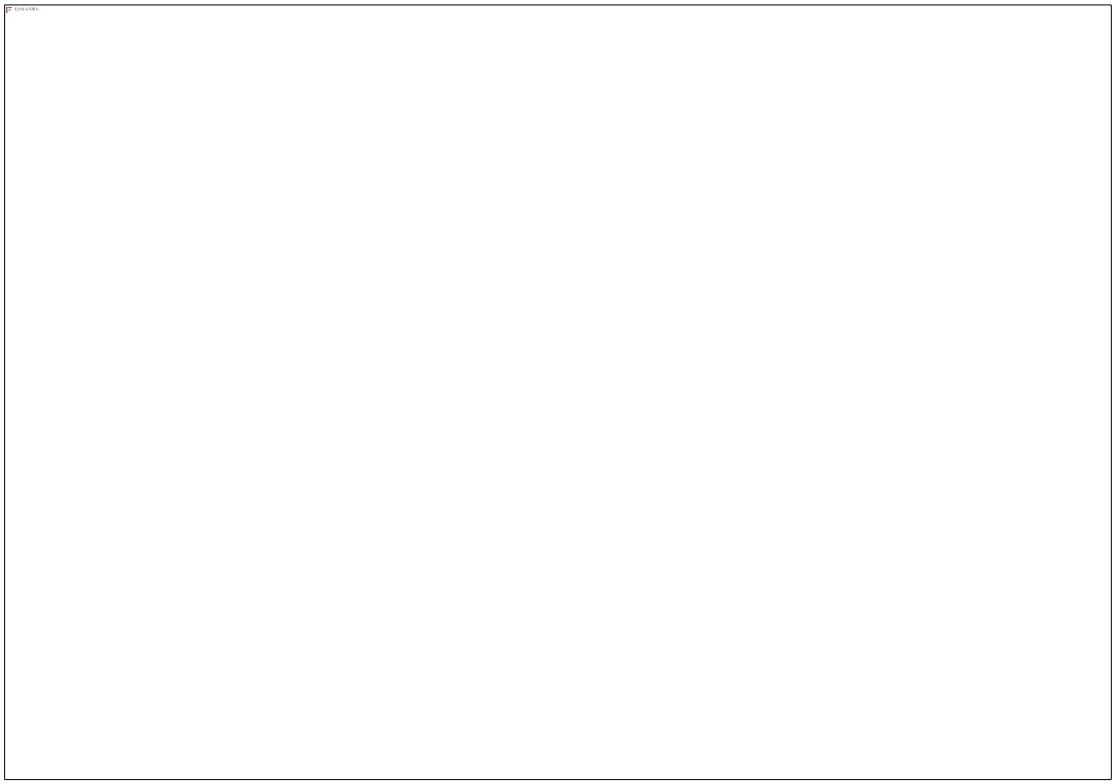

**2-34**

$^{1}$H NMR:

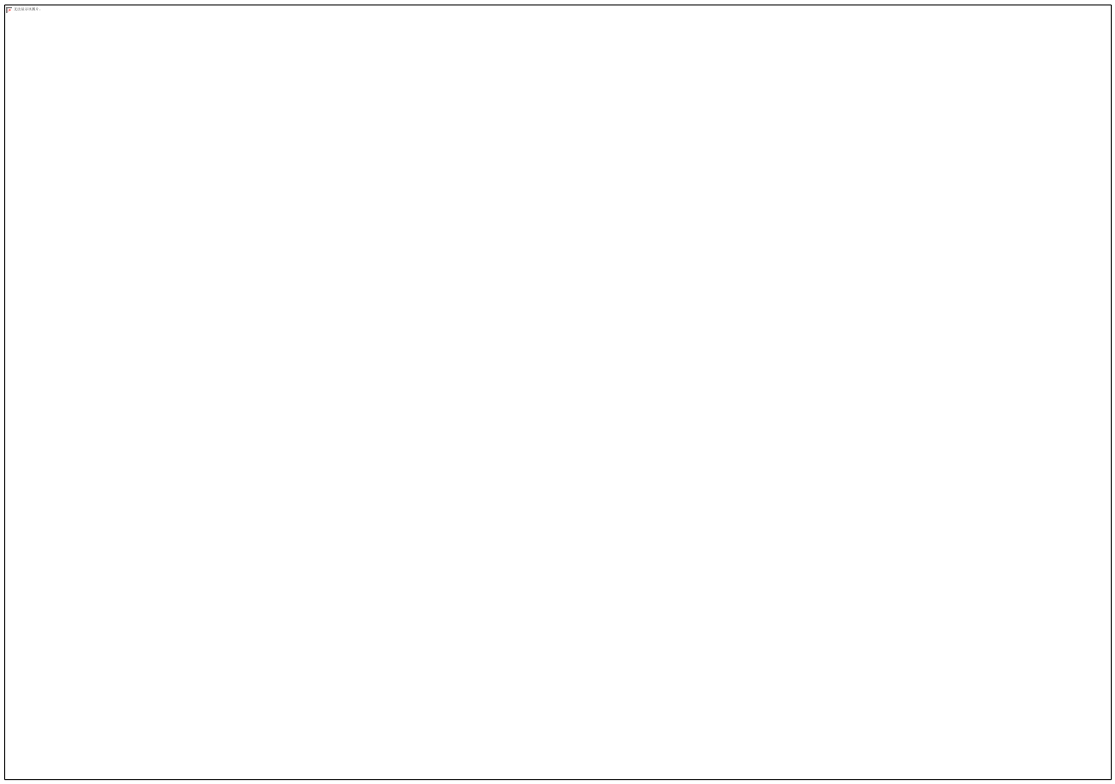

$^{13}$C NMR:

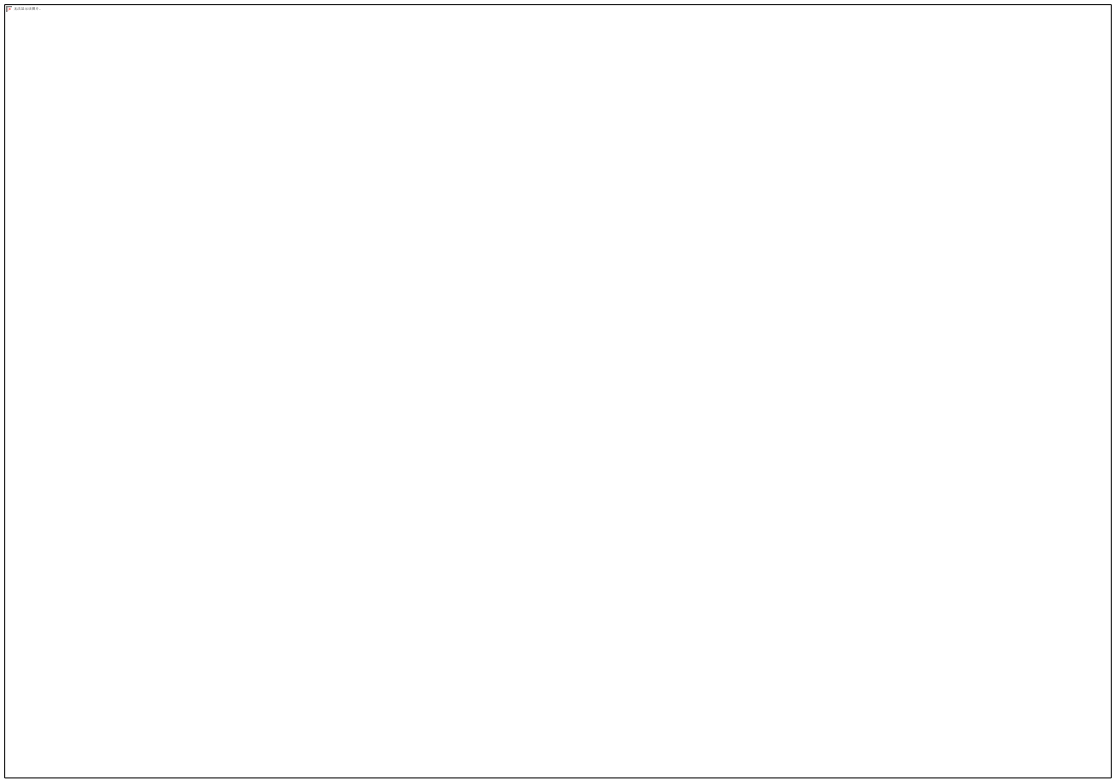

**2-35**

$^{1}$H NMR:

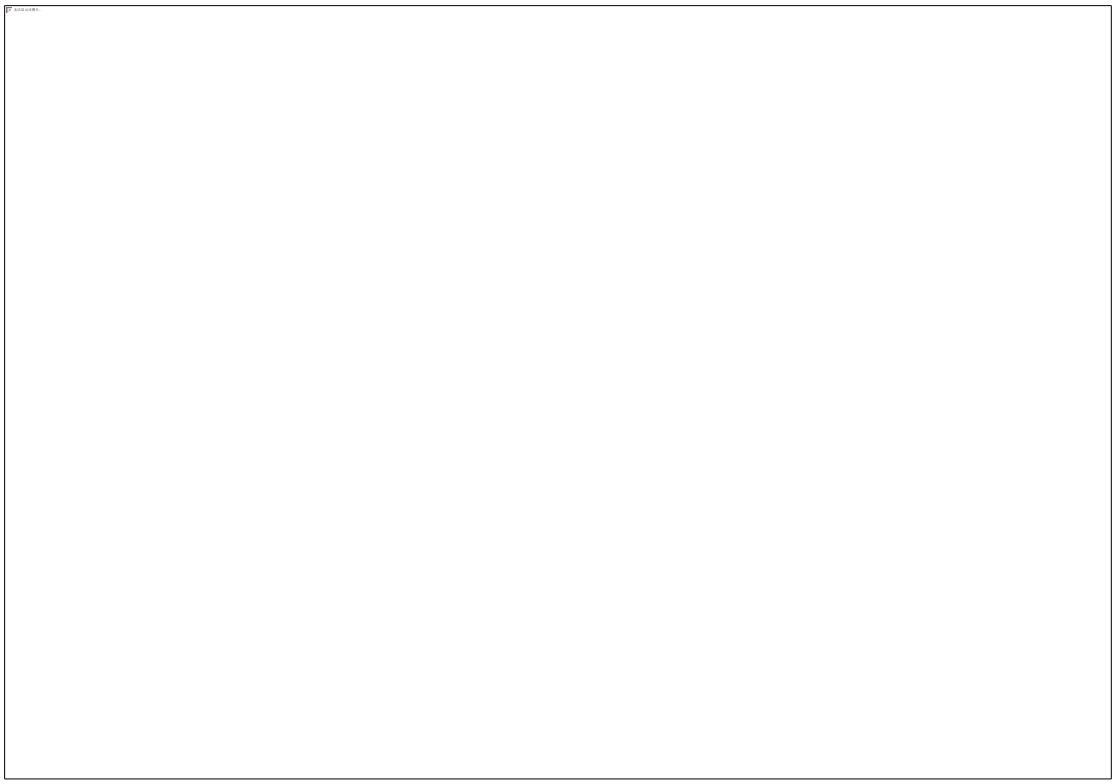

$^{13}$C NMR:

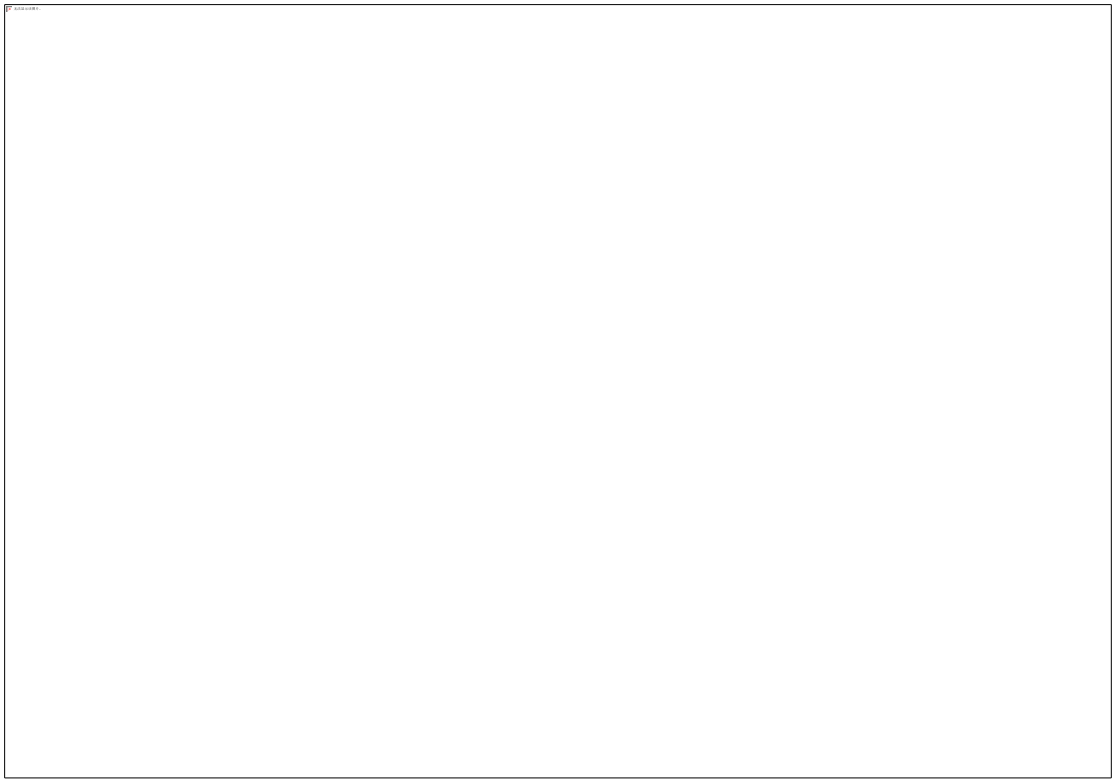

**2-36**

$^{1}$H NMR:

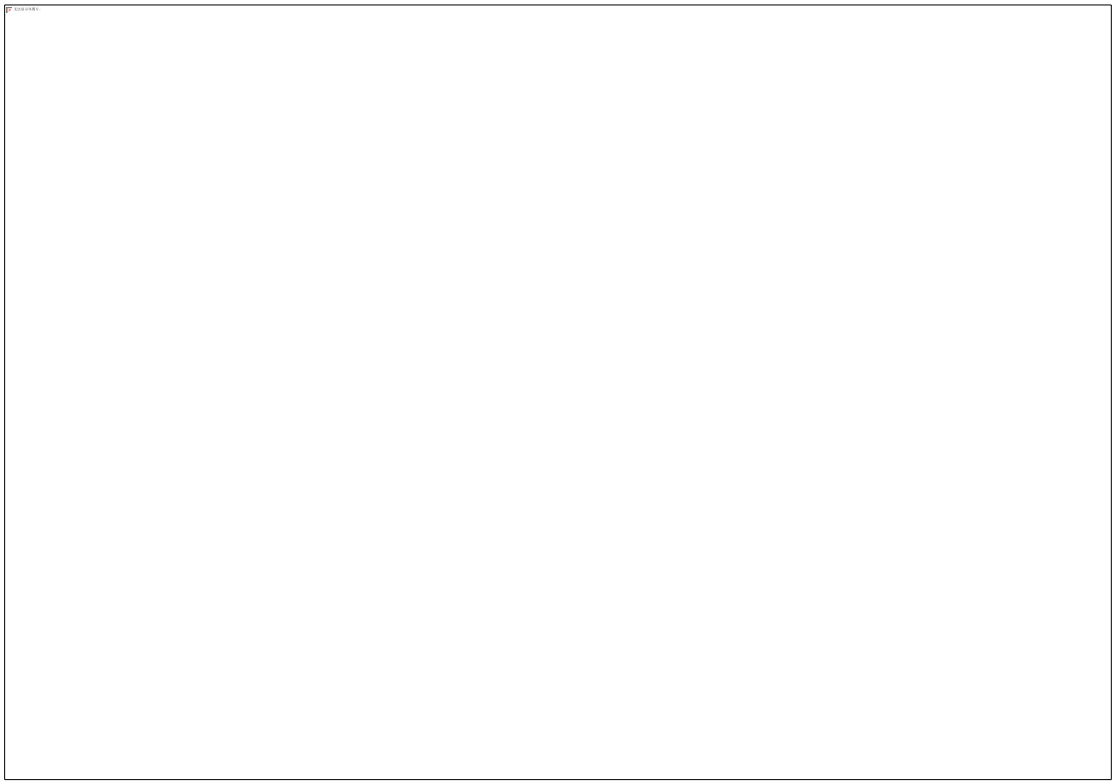

$^{13}$C NMR:

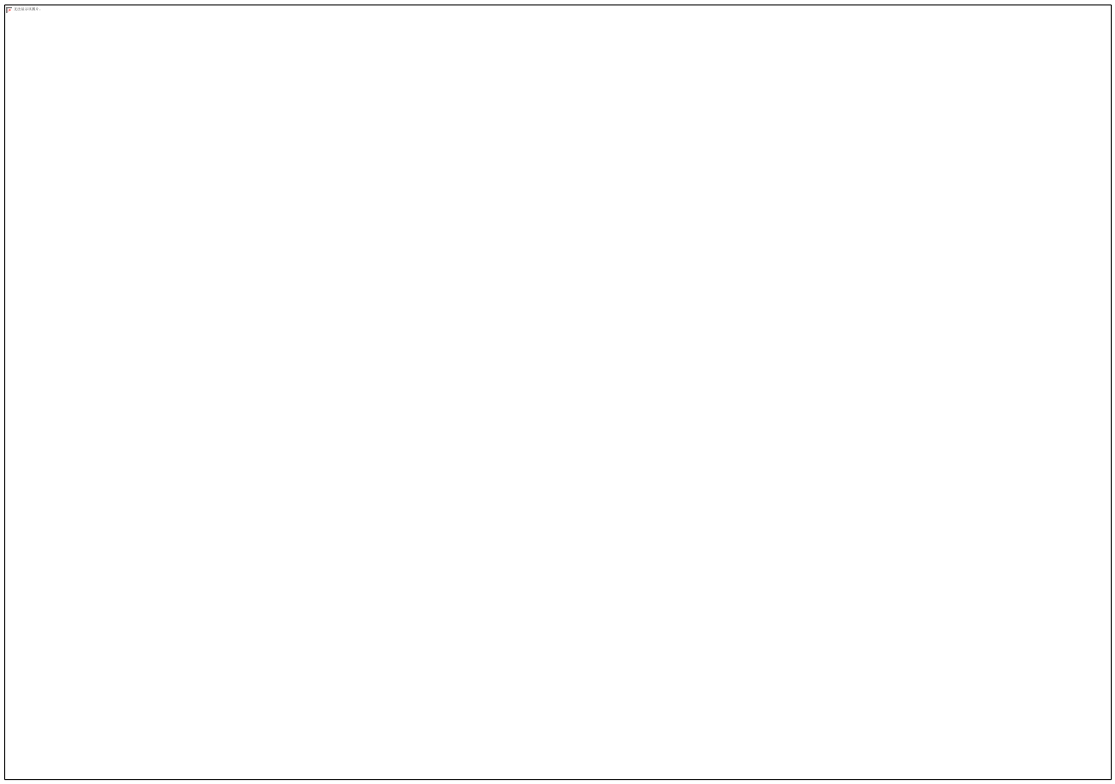

**2-37**

$^{1}$H NMR:

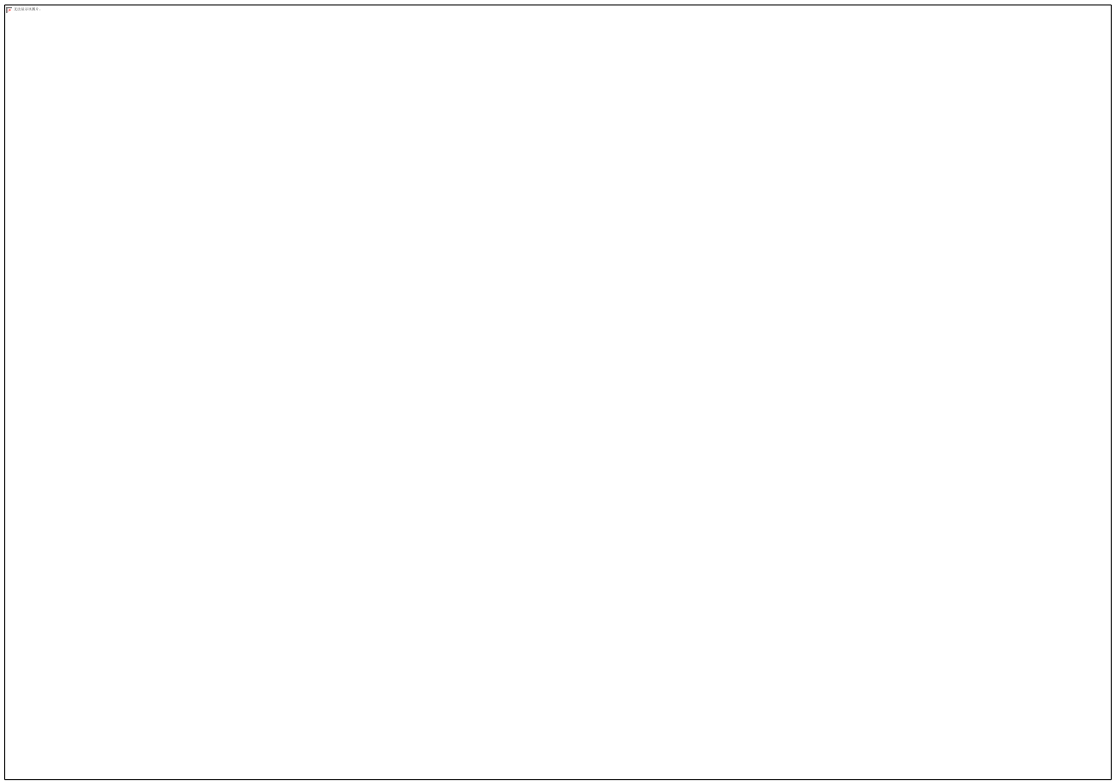

$^{13}$C NMR:

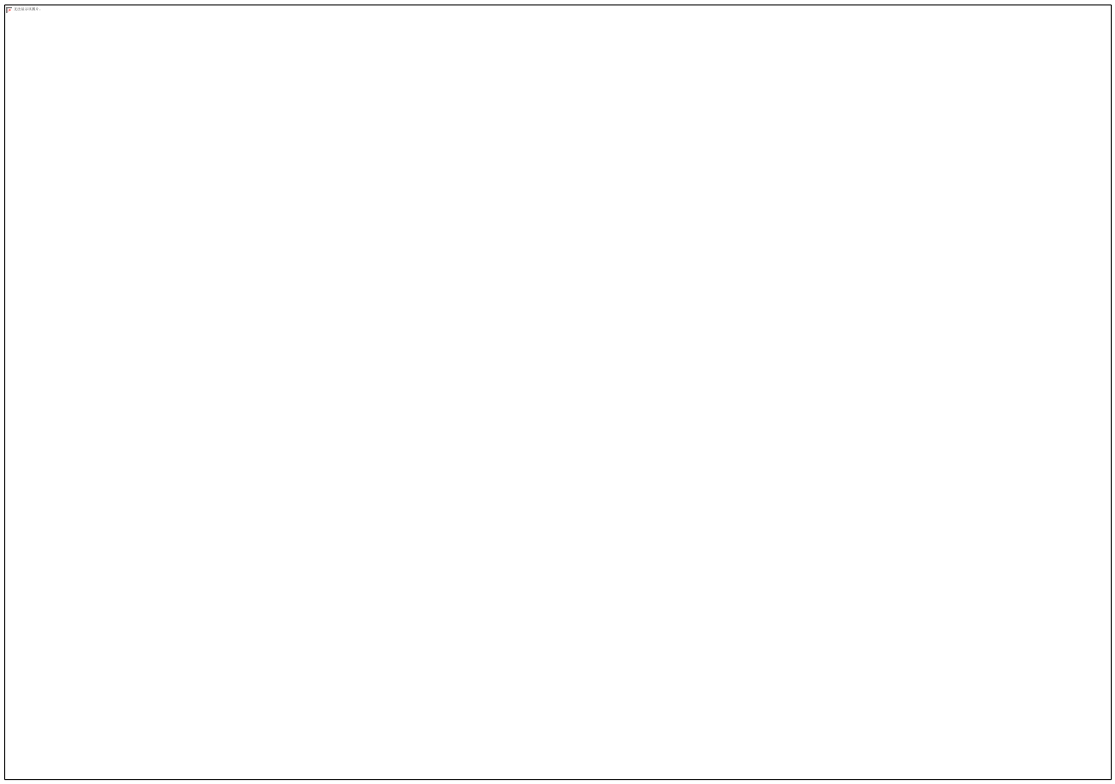

**2-38**

$^{1}$H NMR:

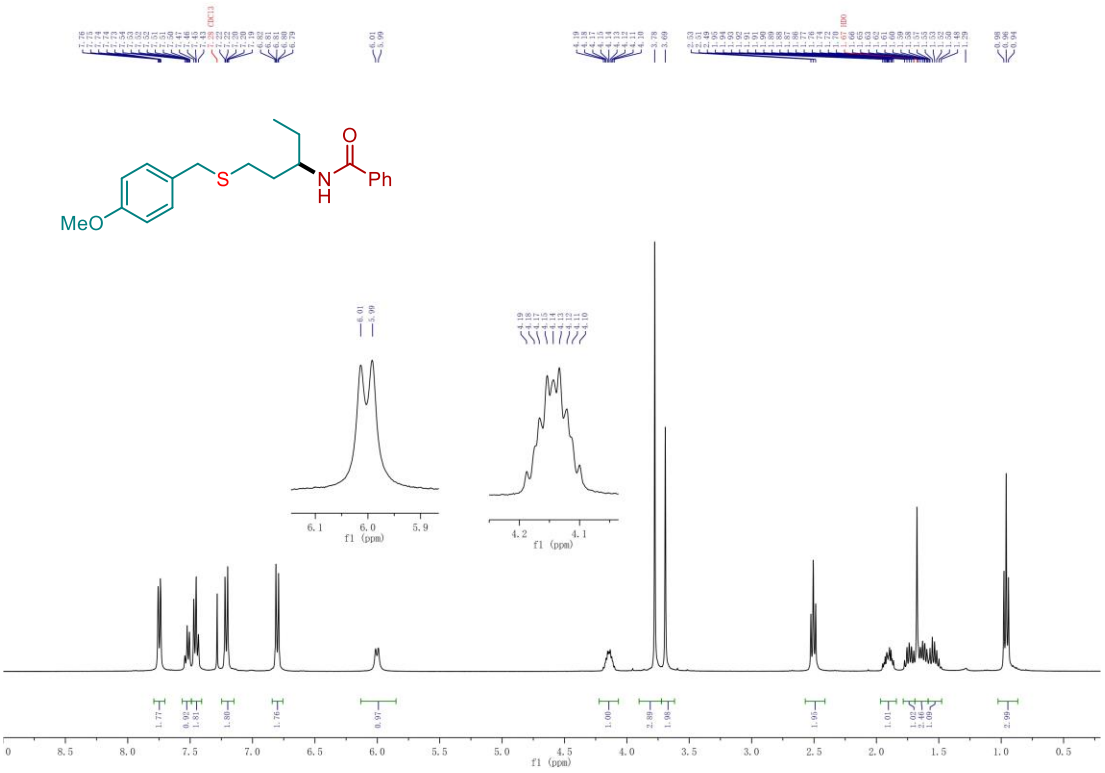


$^{13}$C NMR:

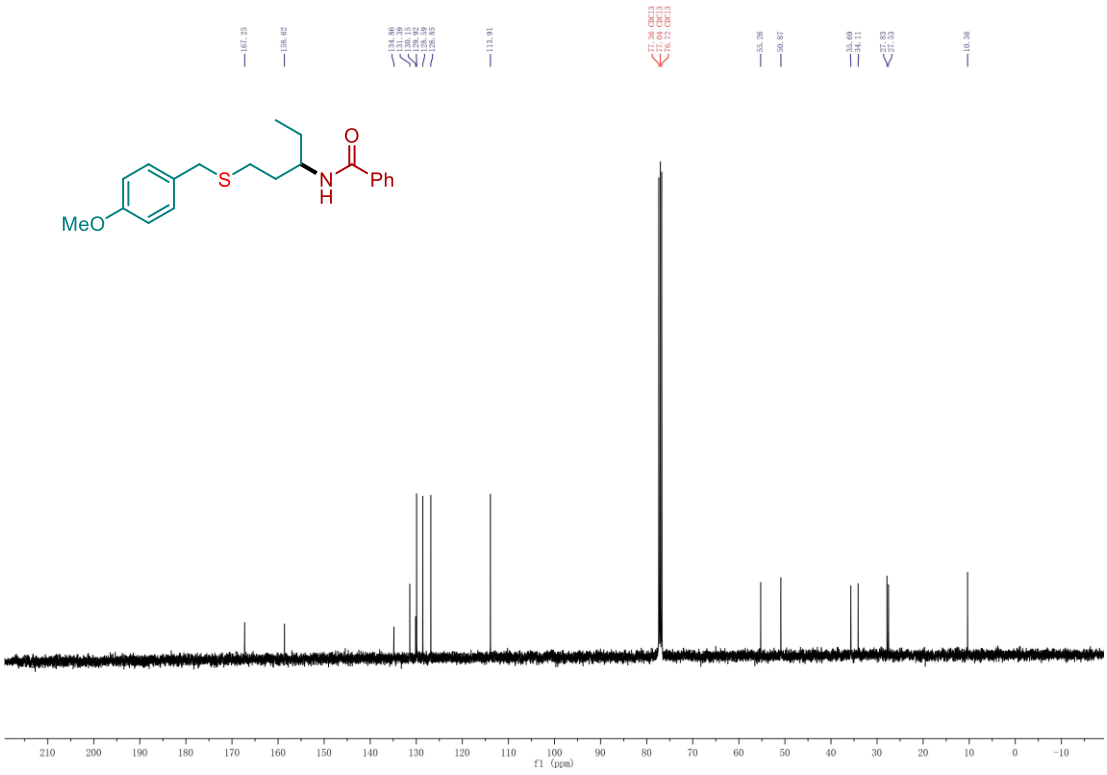

**2-39**

$^{1}$H NMR:

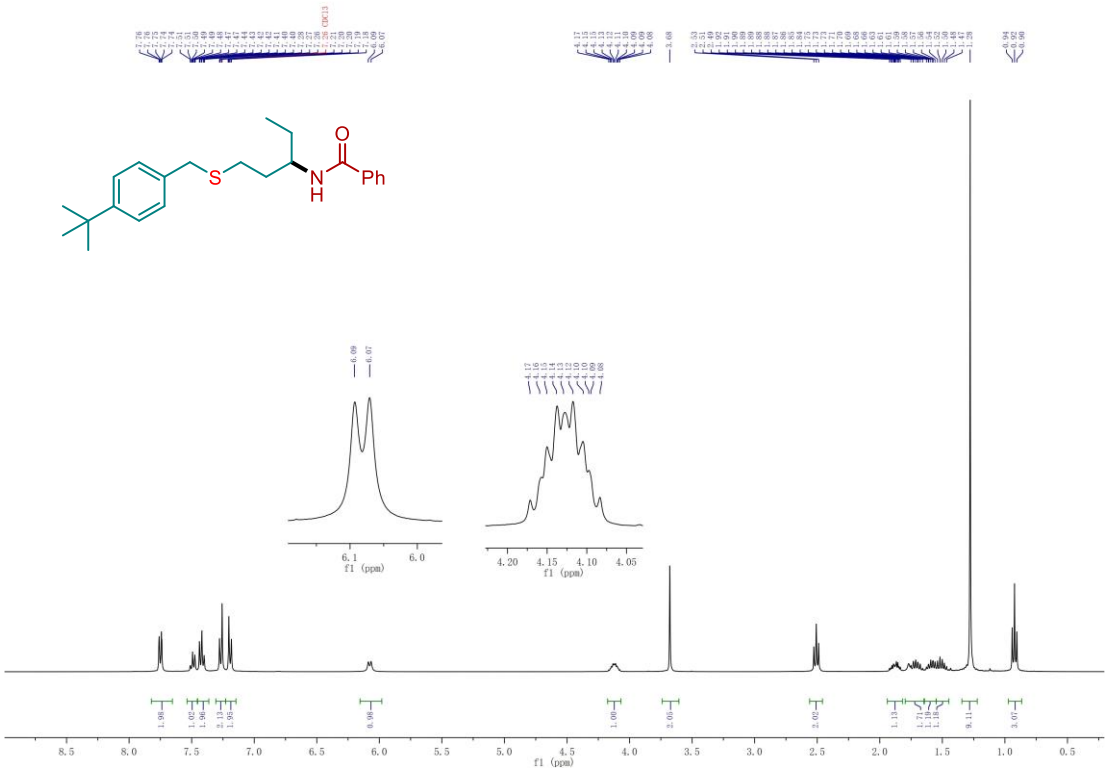


$^{13}$C NMR:

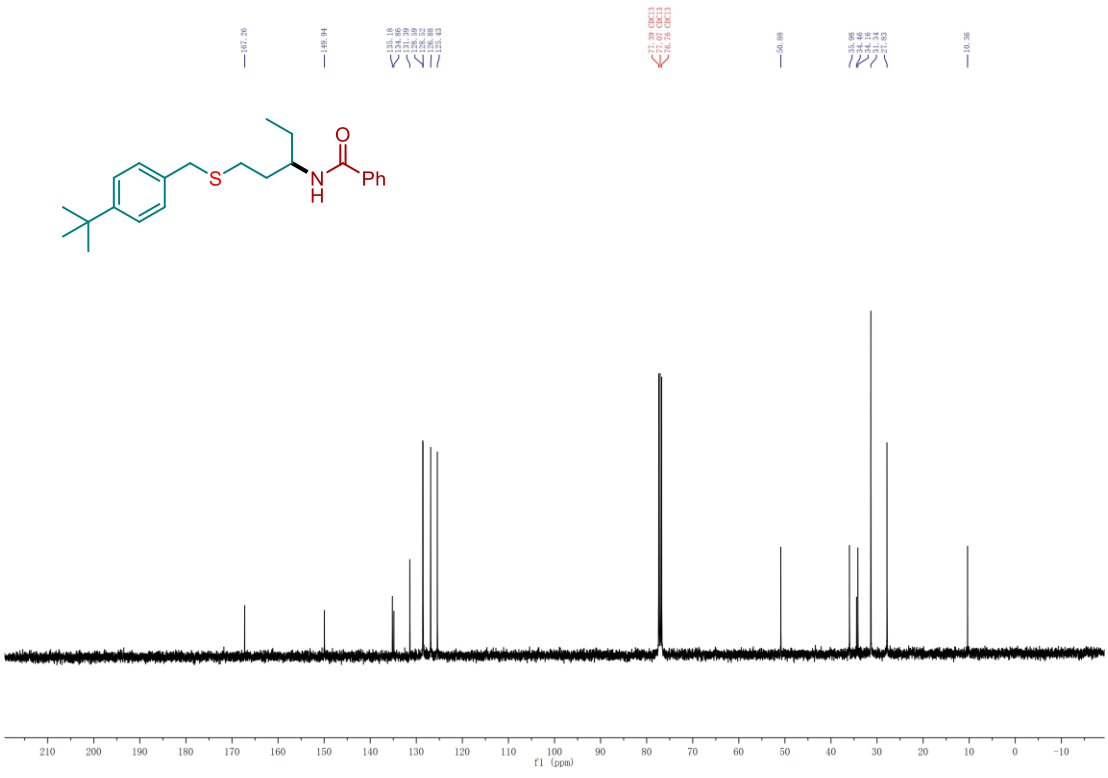

## 2-40

$^{1}$H NMR:

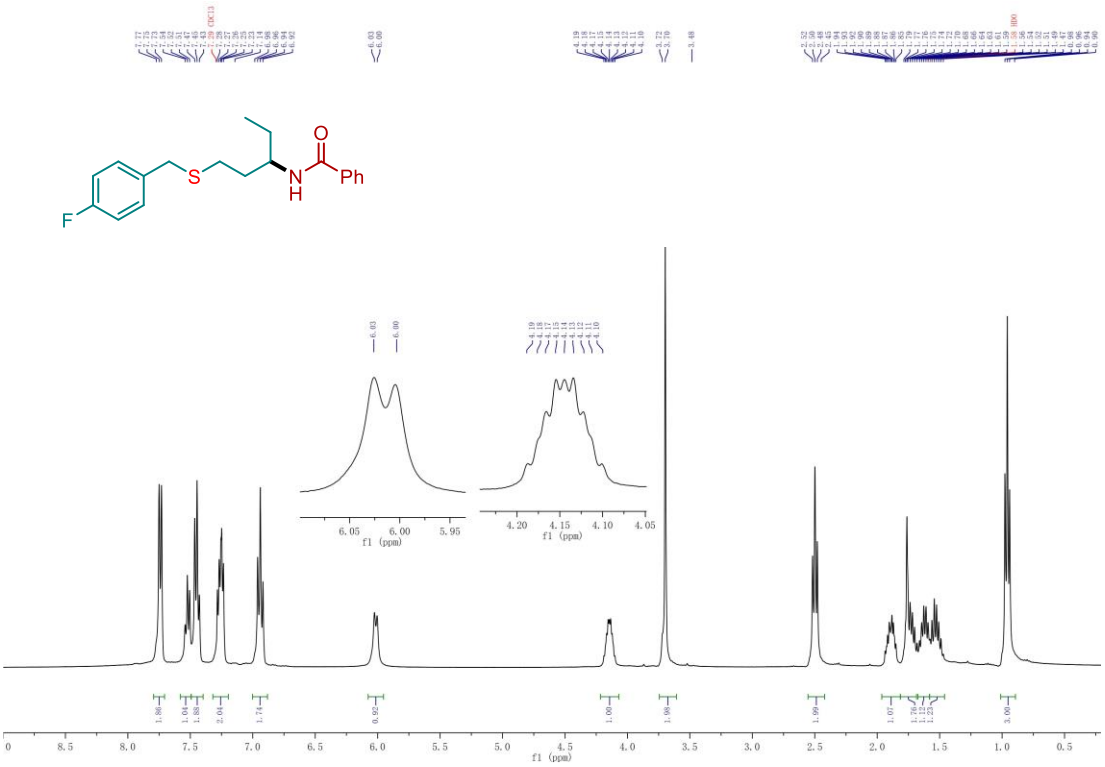


$^{13}$C NMR:

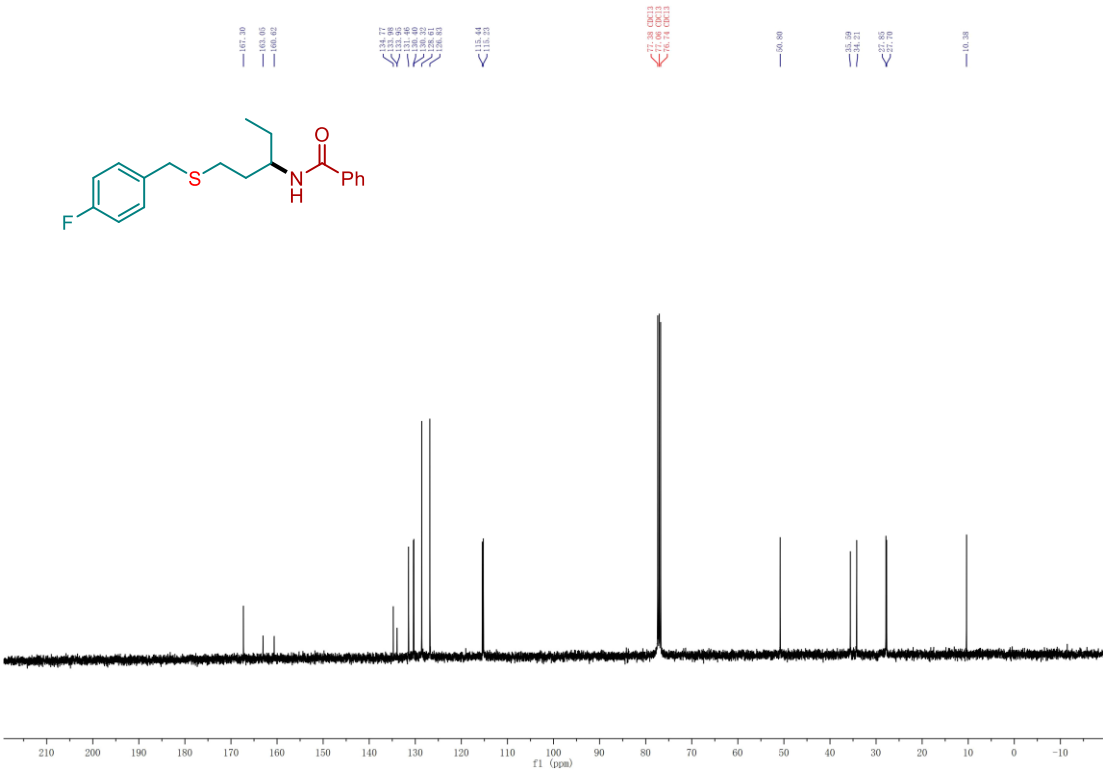

**2-40**

$^{19}$F NMR:

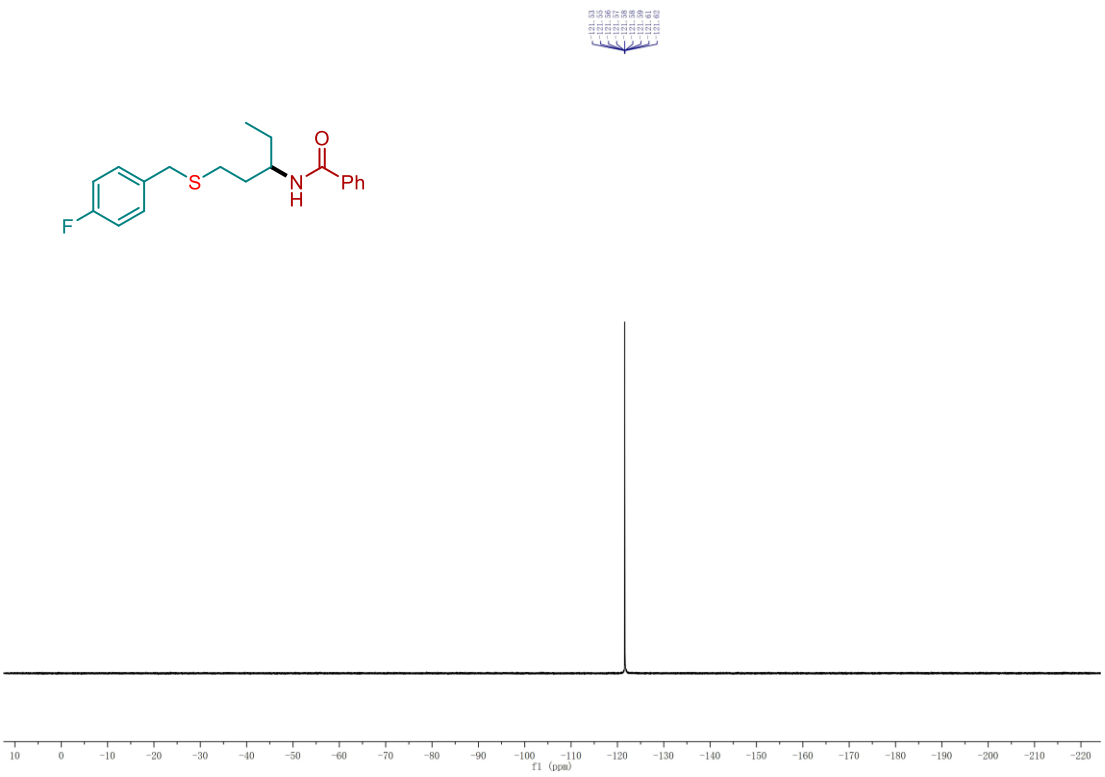
O
S
N
H
Ph
F
10
0
-10
-20
-30
-40
-50
-60
-70
-80
-90
-100
-110
-120
-130
-140
-150
-160
-170
-180
-190
-200
-210
-220
f1 (ppm)

## 2-41

$^{1}$H NMR:

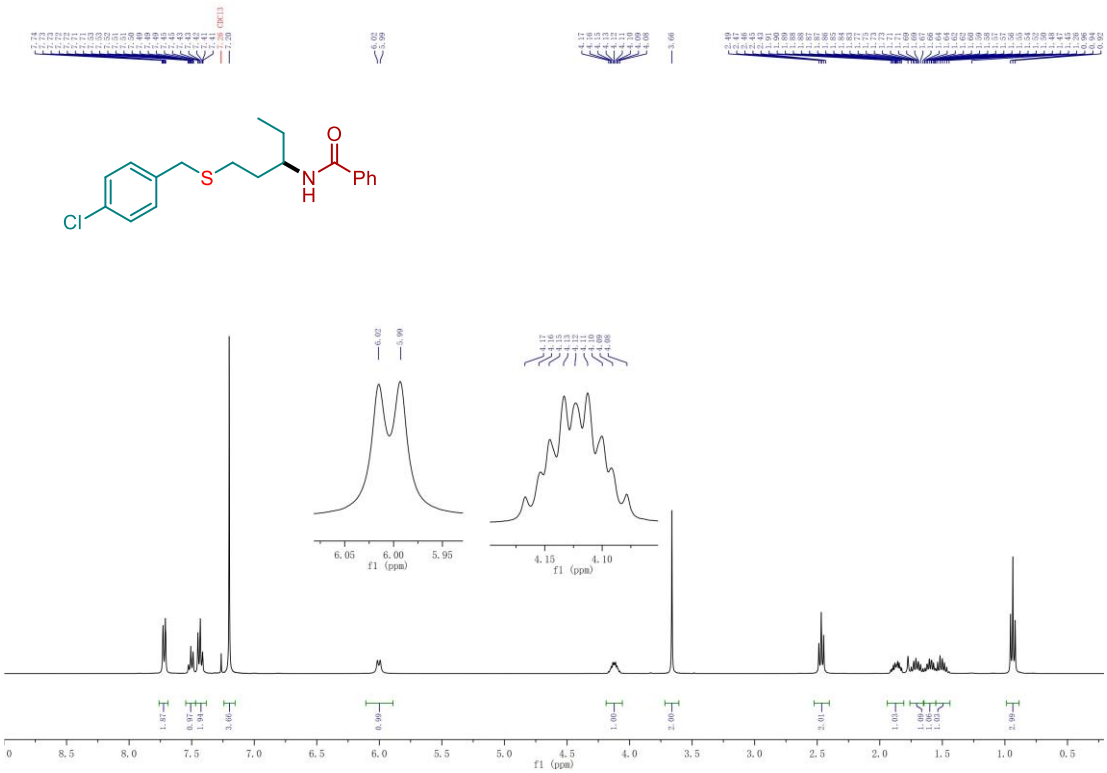


$^{13}$C NMR:

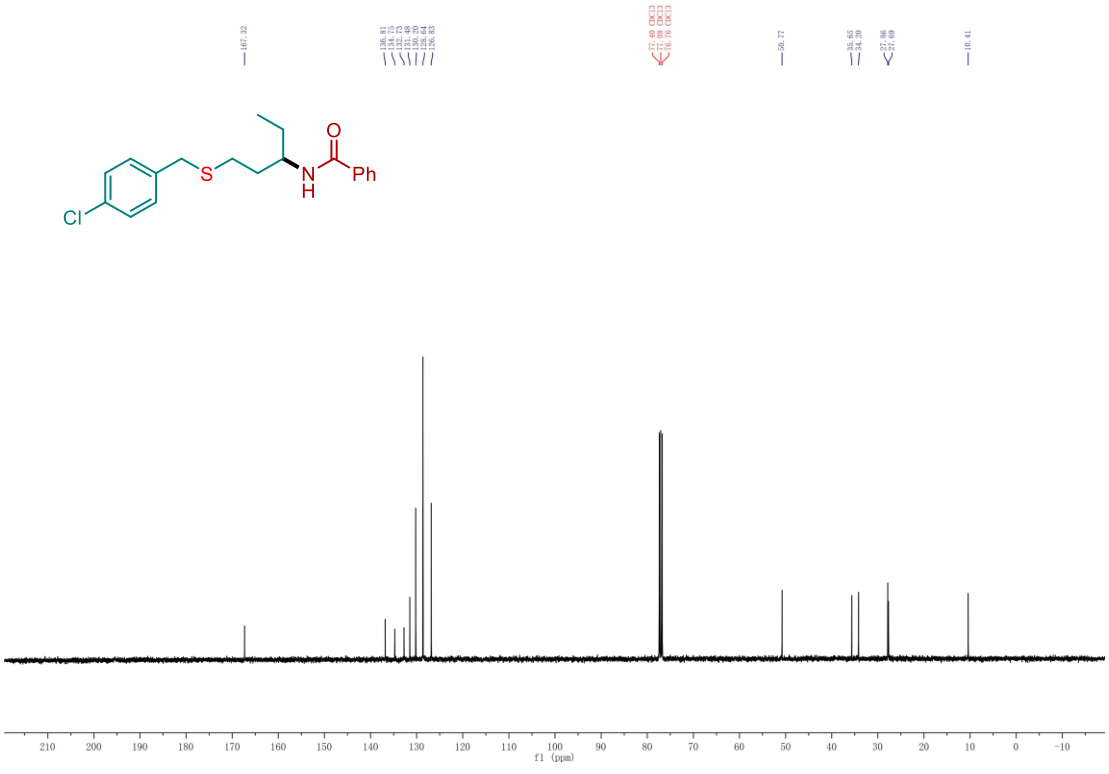

**2-42**

$^{1}$H NMR:

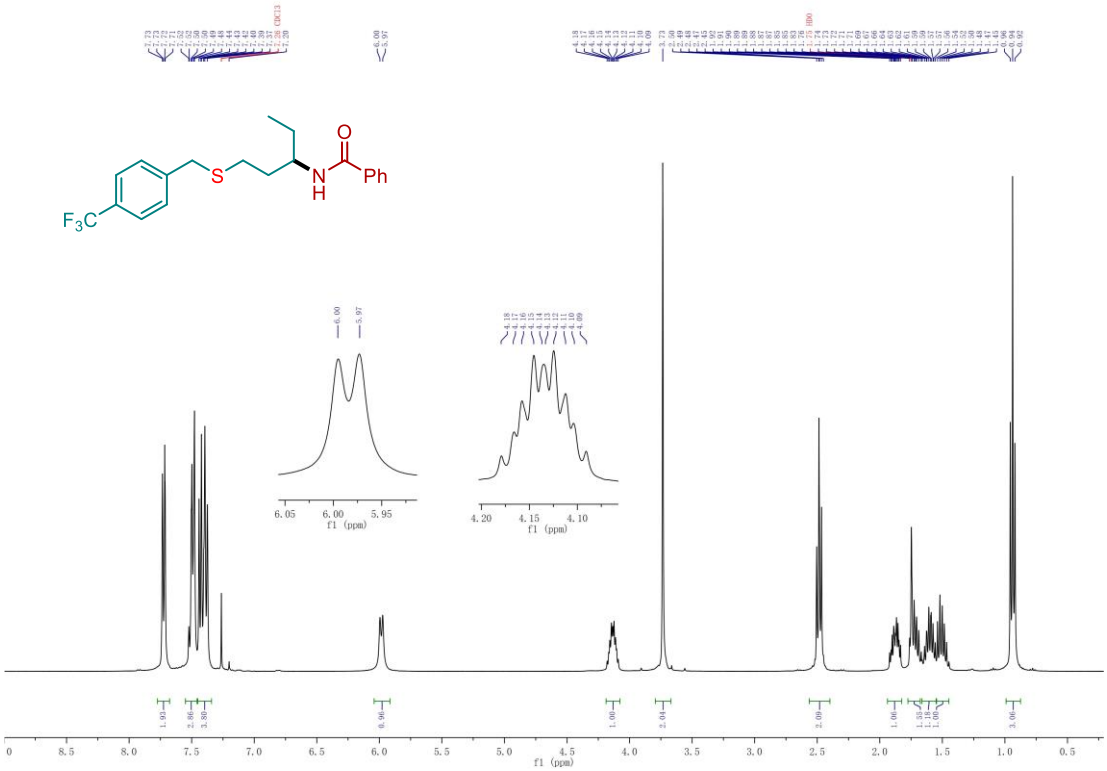


$^{13}$C NMR:

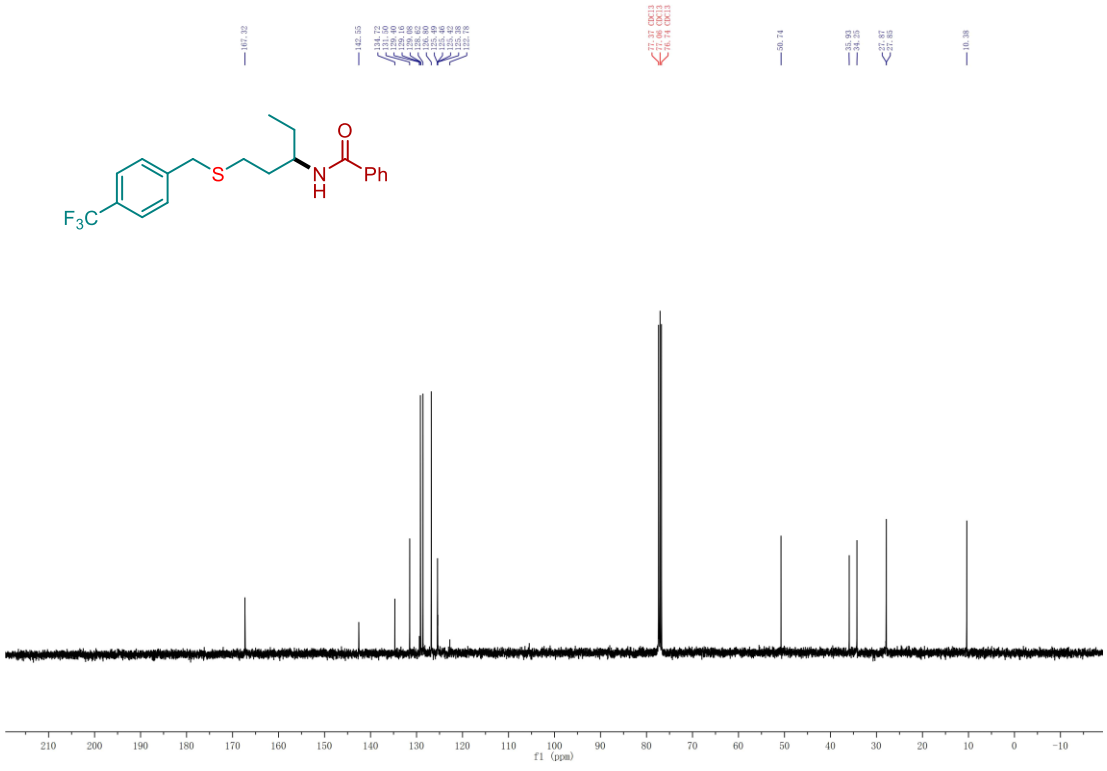

**2-42**

$^{19}$F NMR:

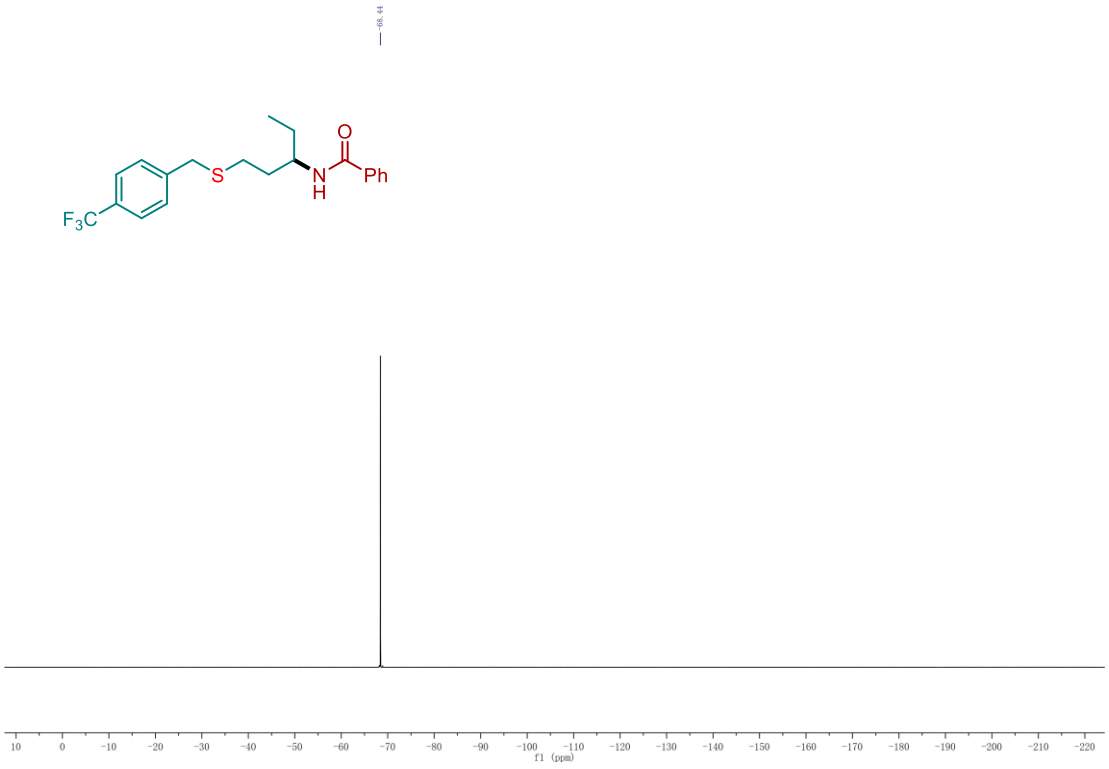
-68.44
F3C
S
N
H
O
Ph
10 0 -10 -20 -30 -40 -50 -60 -70 -80 -90 -100 -110 -120 -130 -140 -150 -160 -170 -180 -190 -200 -210 -220
f1 (ppm)

**2-43**

$^{1}$H NMR:

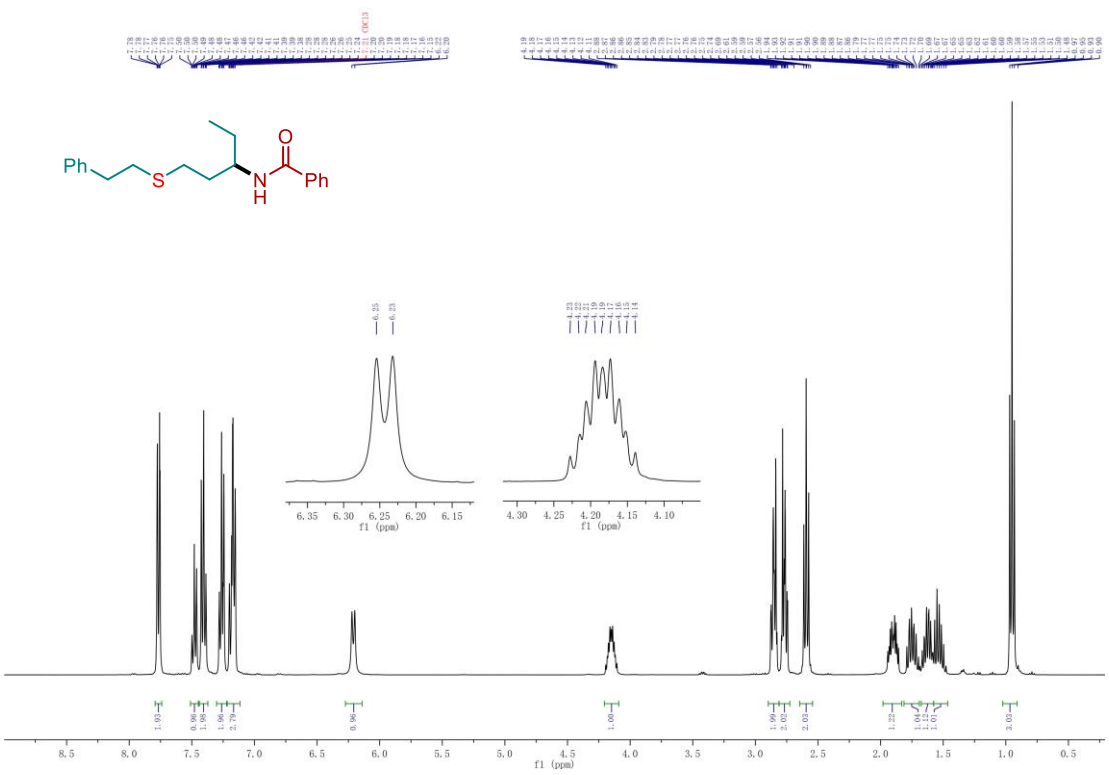


$^{13}$C NMR:

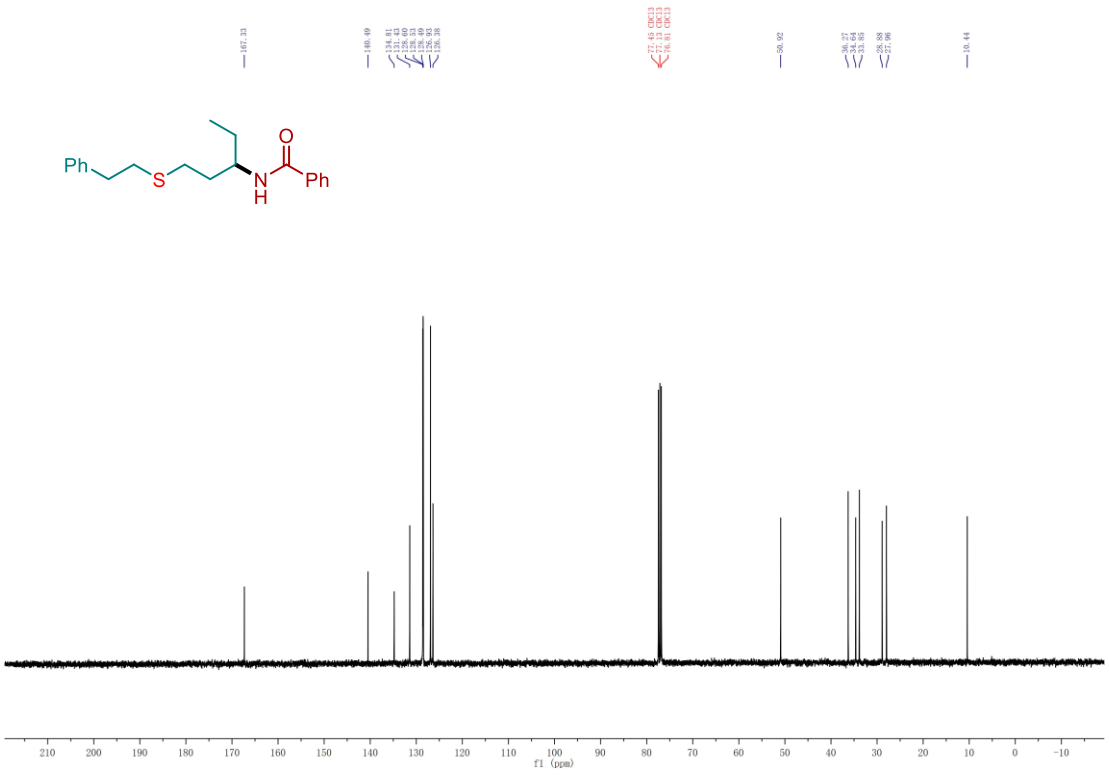

**2-44**

$^{1}$H NMR:

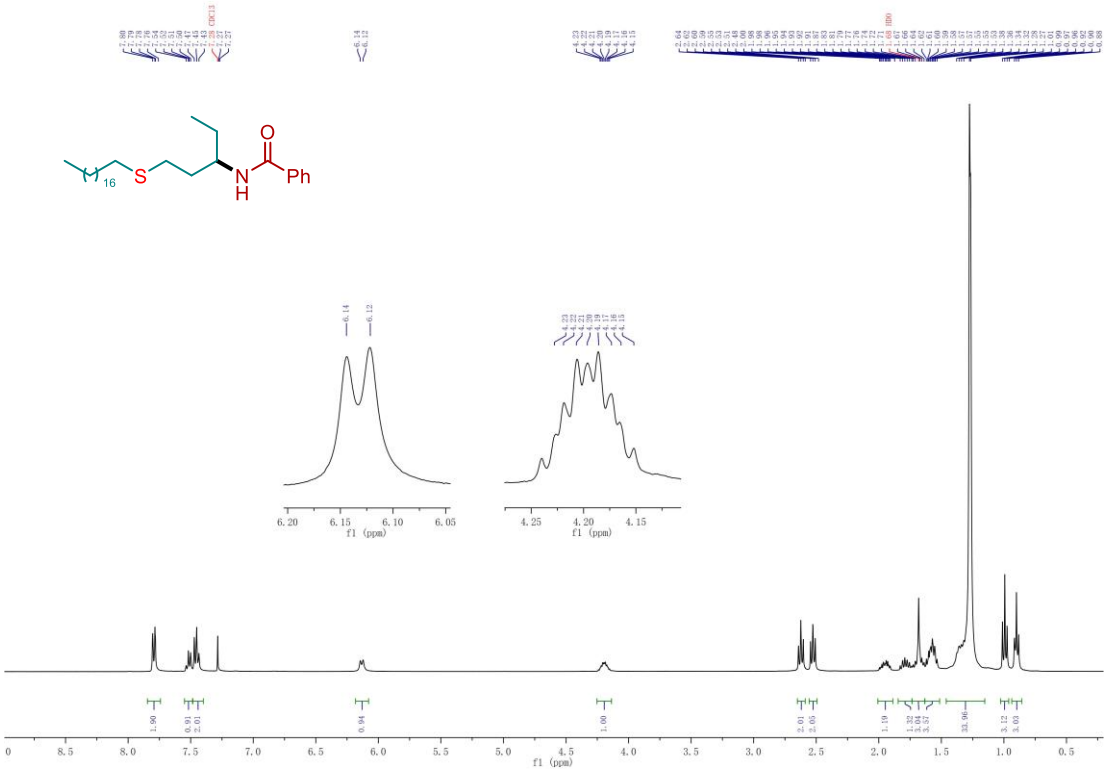


$^{13}$C NMR:

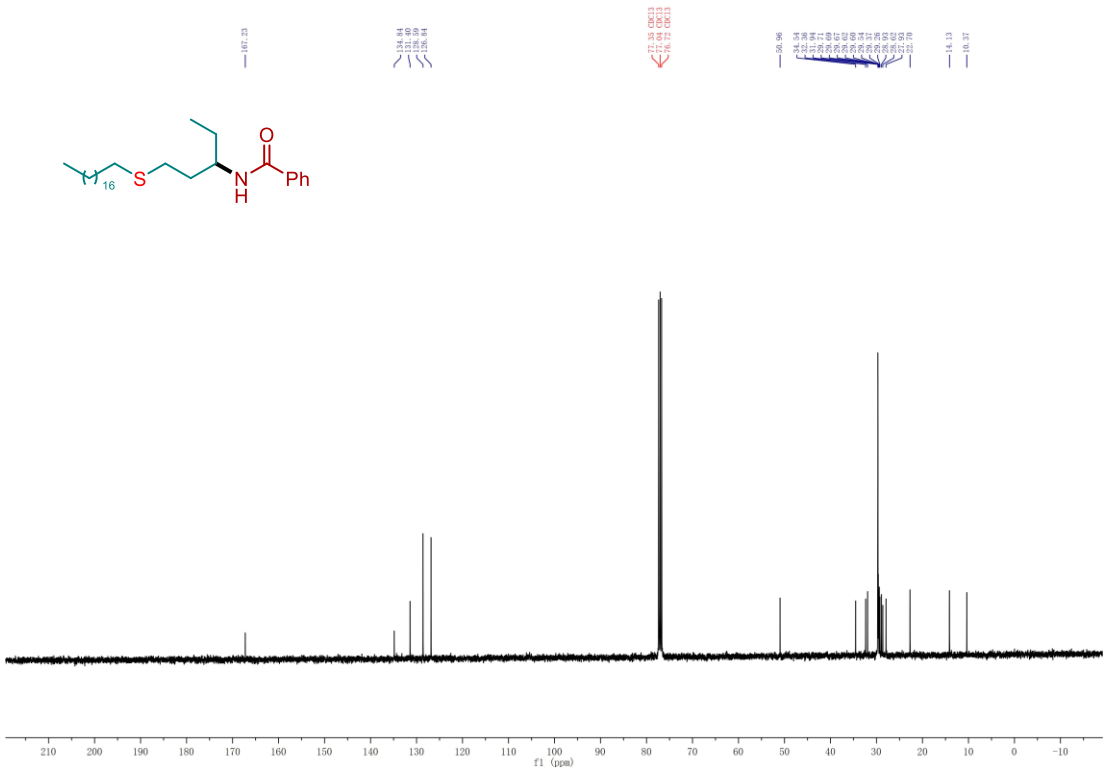

**2-45**

$^{1}$H NMR:

$^{13}$C NMR:

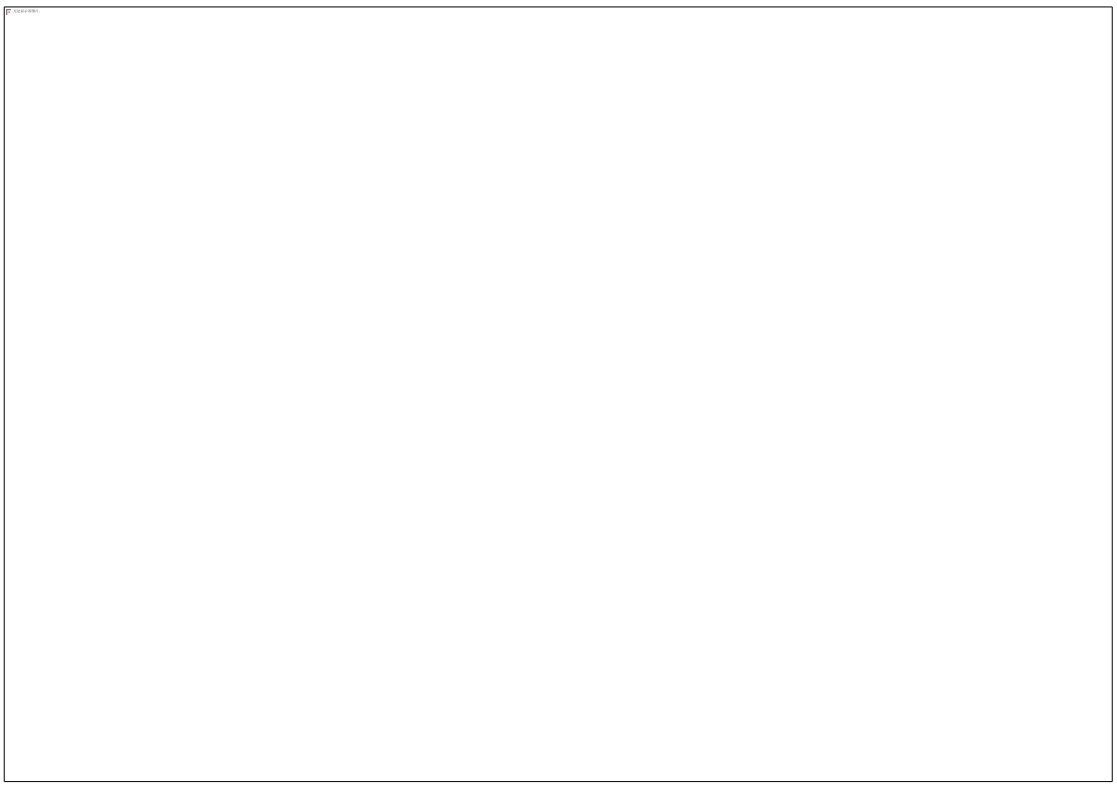

**2-46**

$^{1}$H NMR:

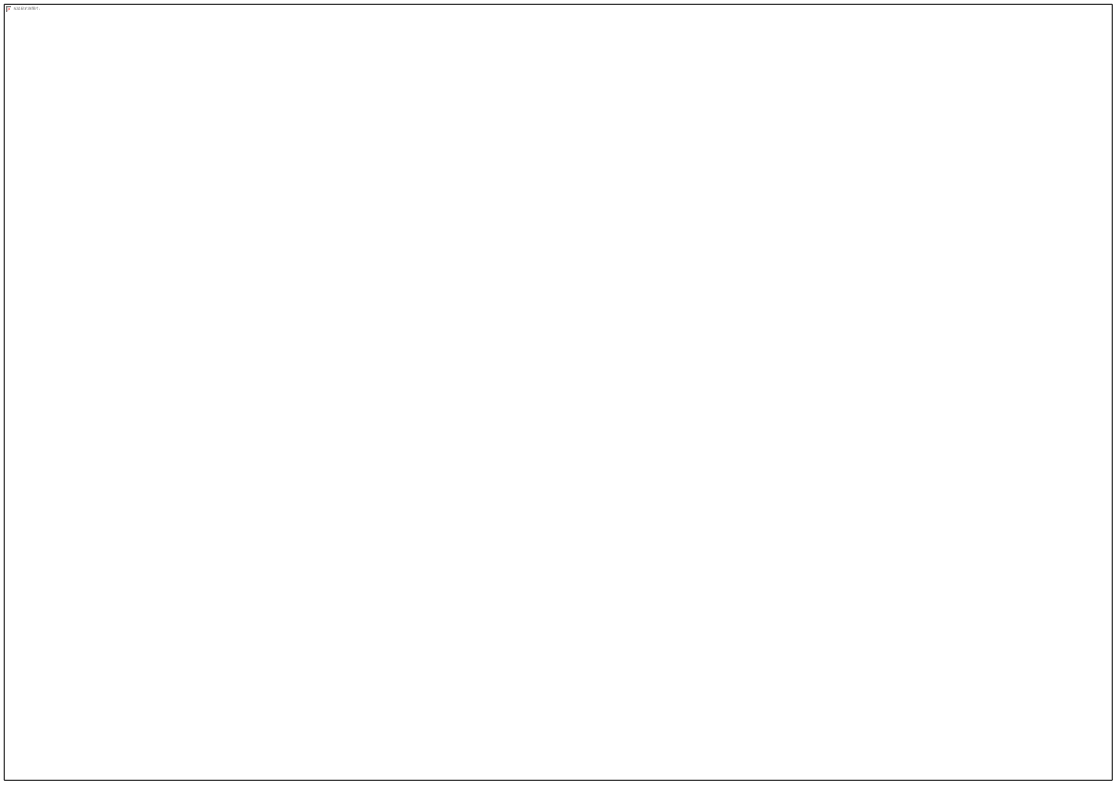

$^{13}$C NMR:

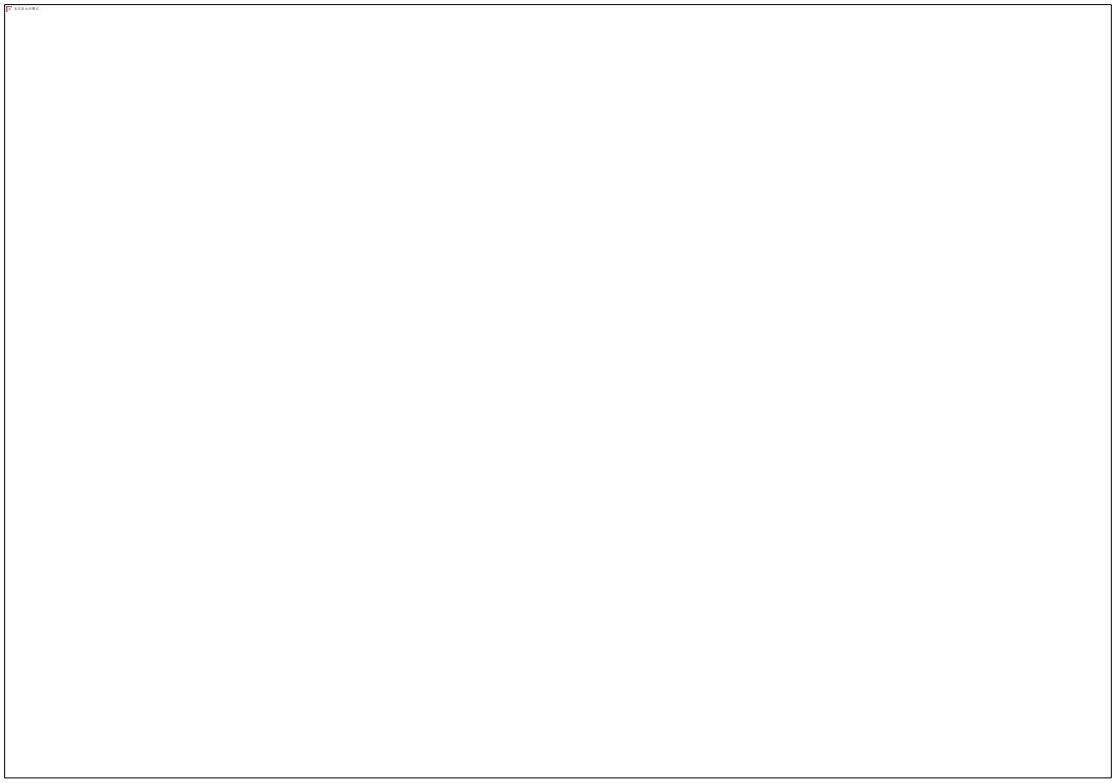

**2-47**

$^{1}$H NMR:

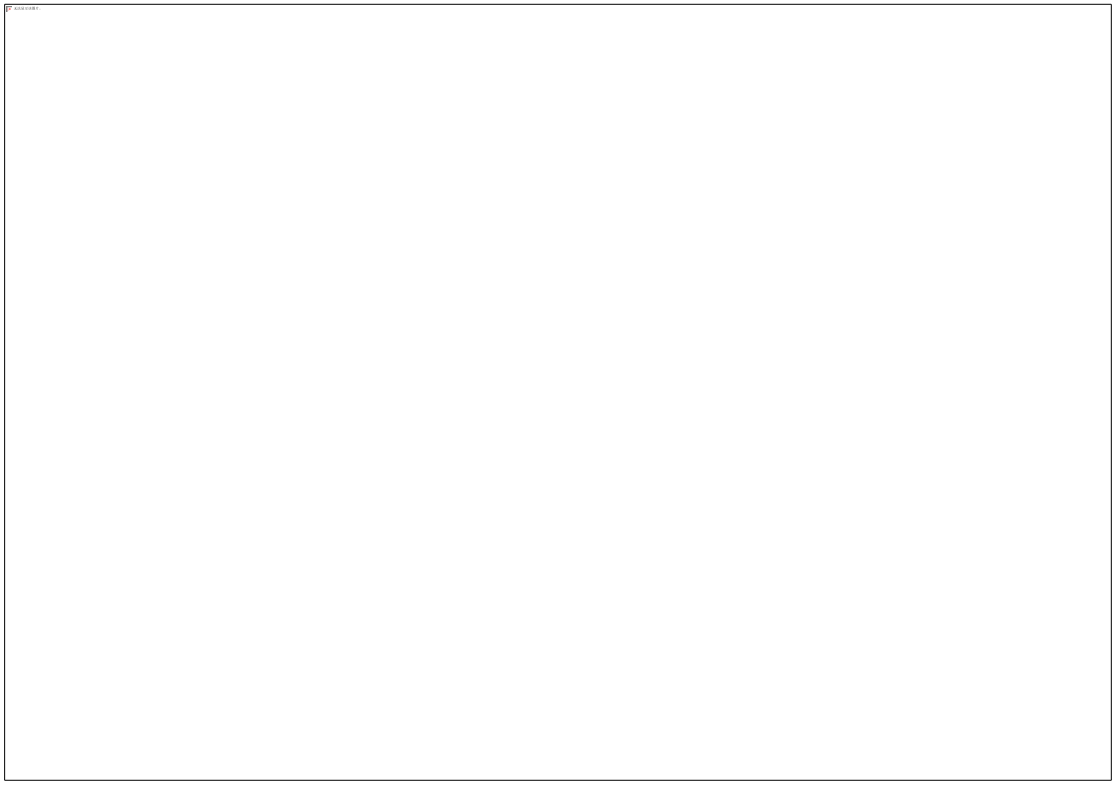

$^{13}$C NMR:

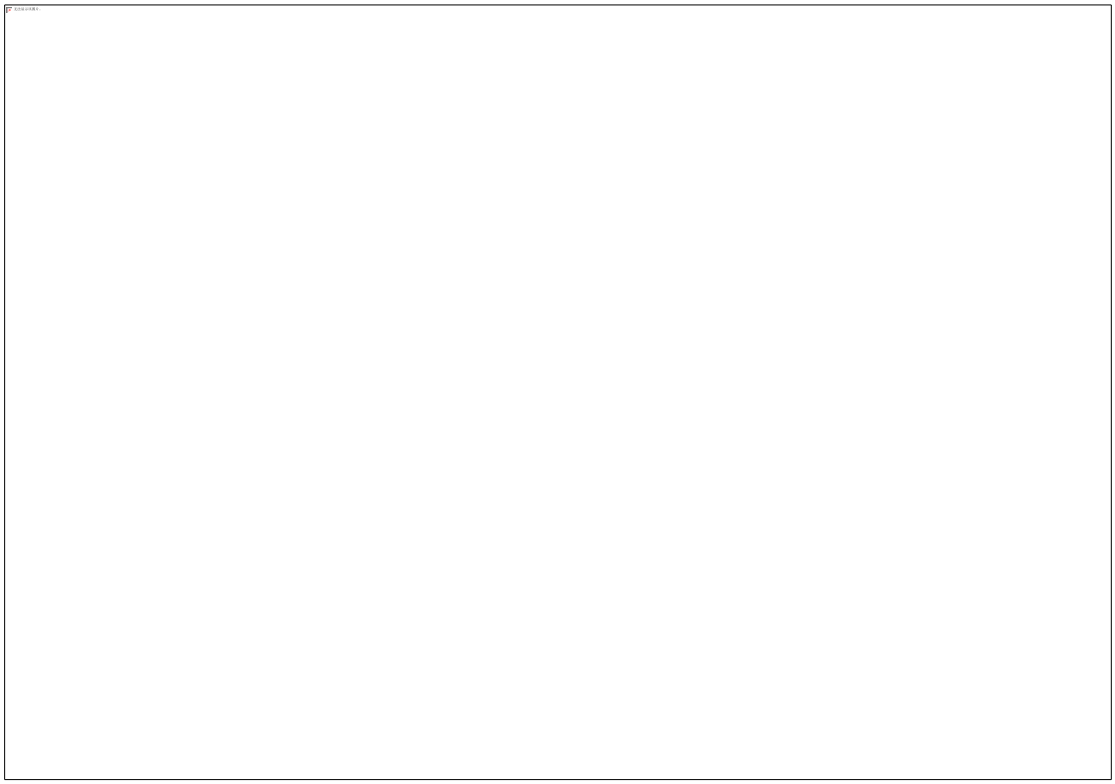

**2-48**

$^{1}$H NMR:

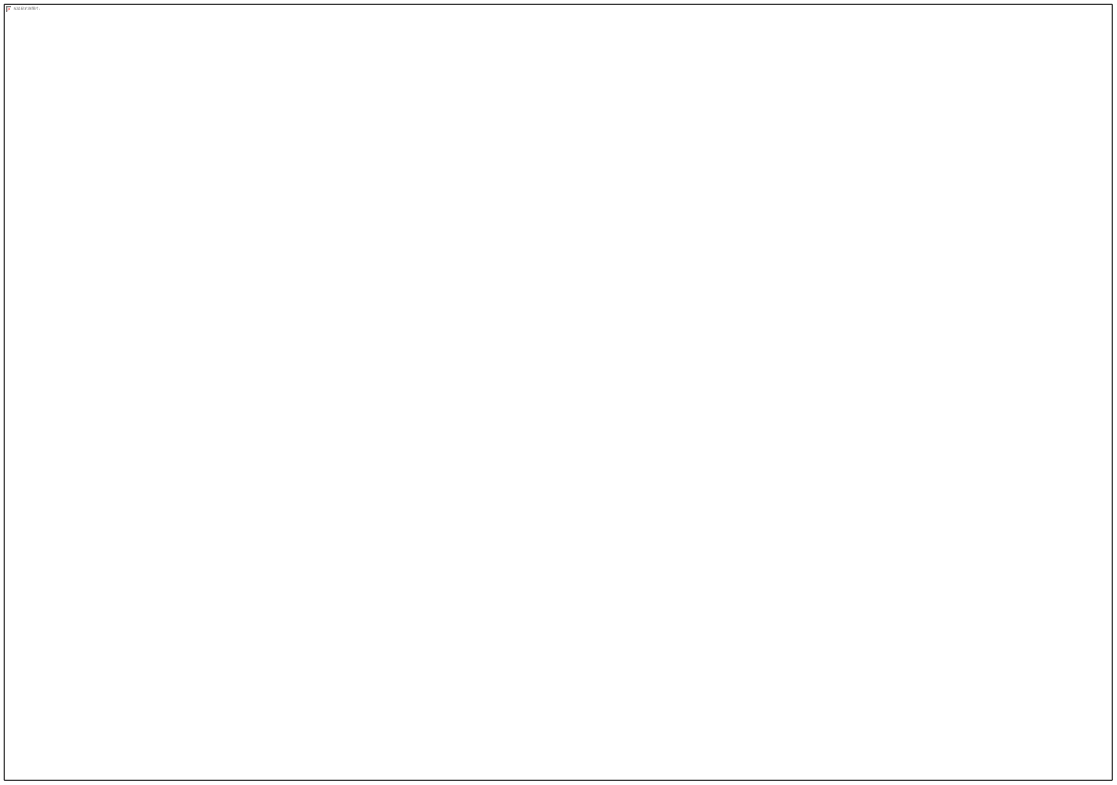

$^{13}$C NMR:

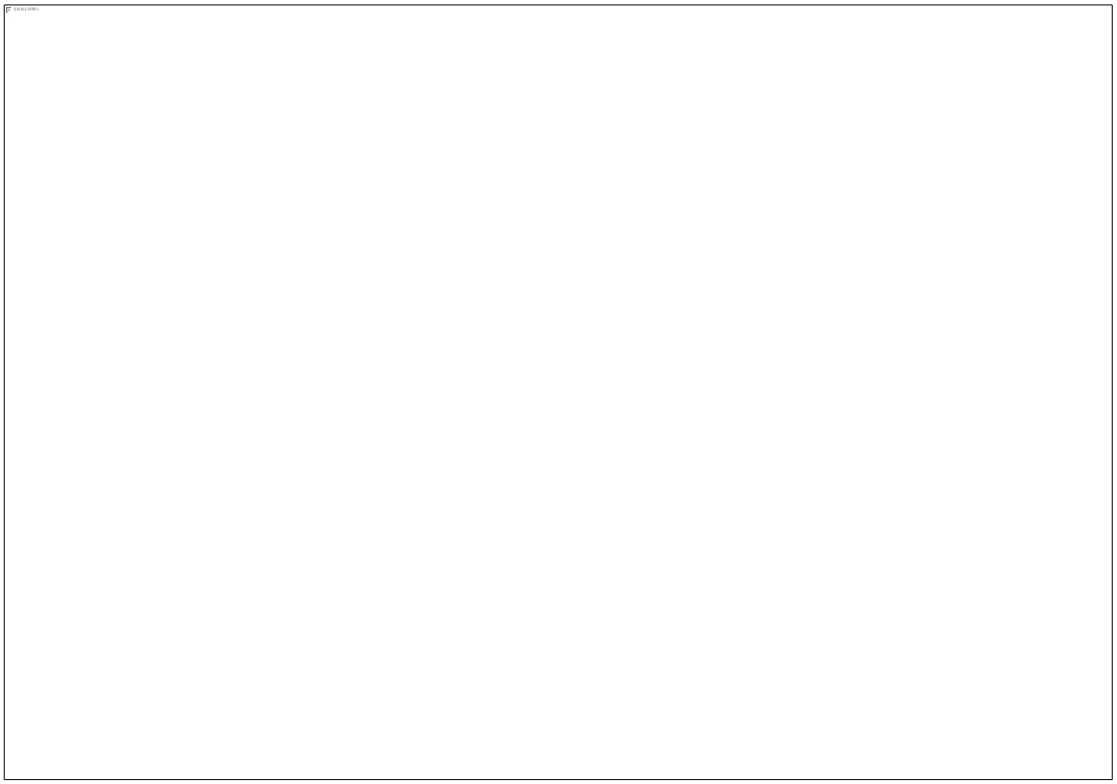

**2-49**

$^{1}$H NMR:

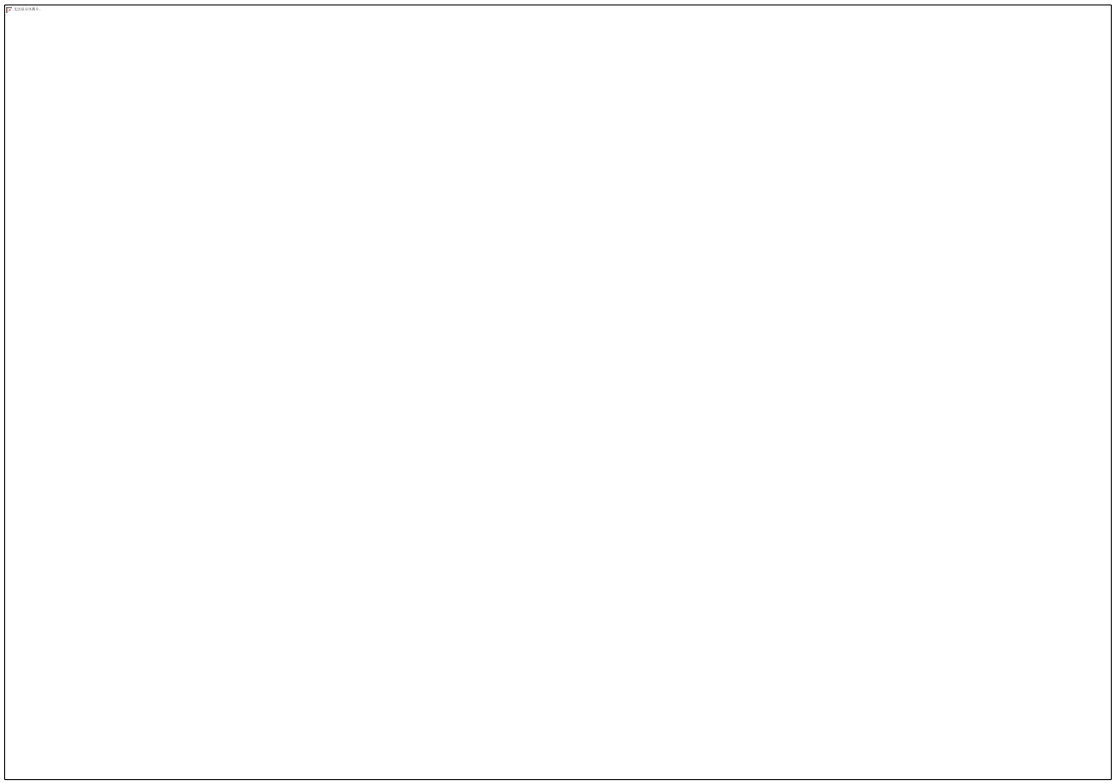

$^{13}$C NMR:

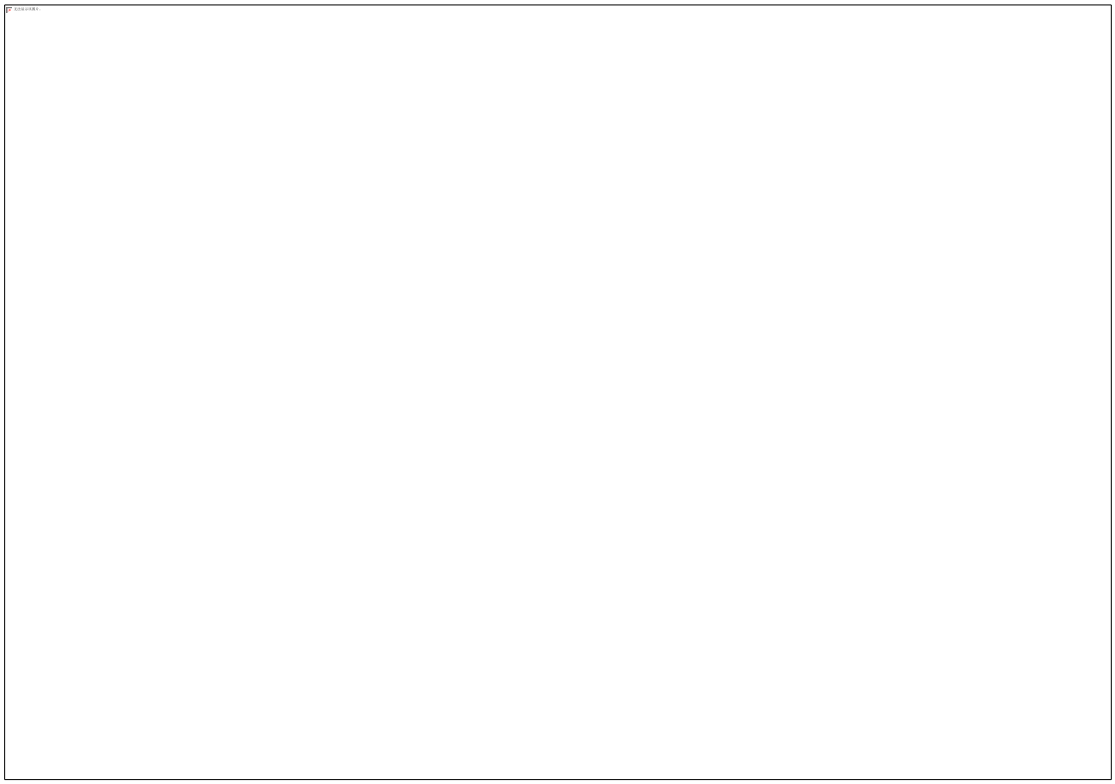

**2-50**

$^{1}$H NMR:

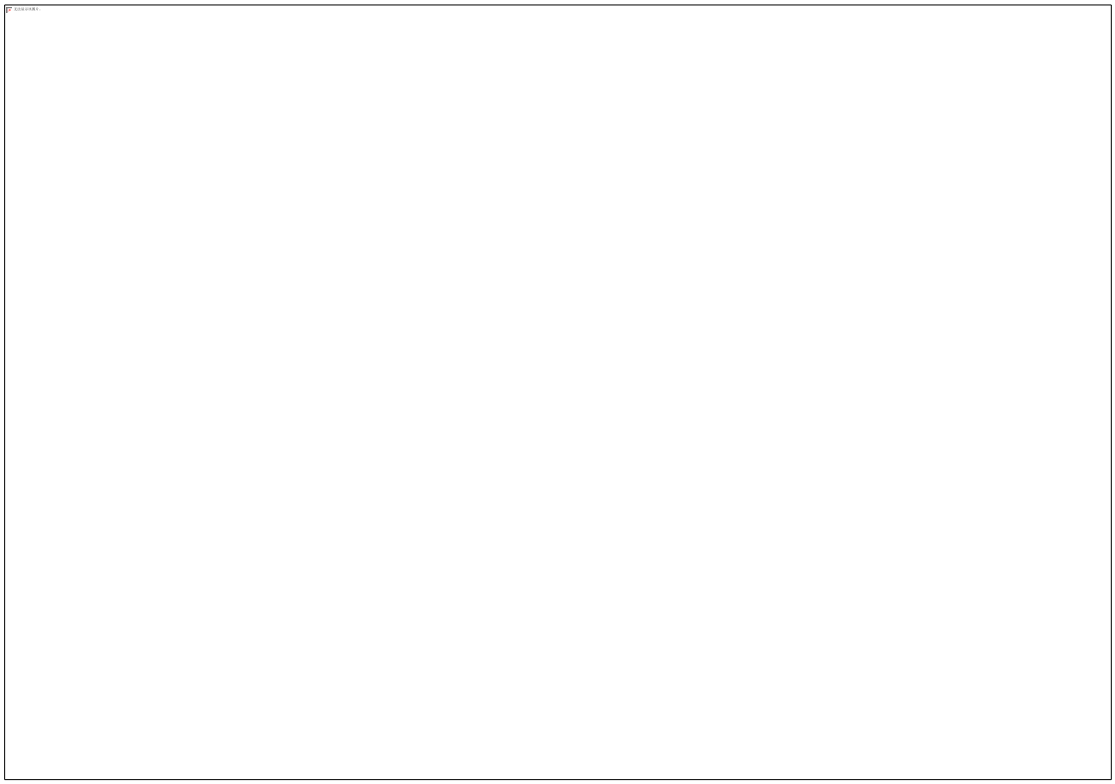

$^{13}$C NMR:

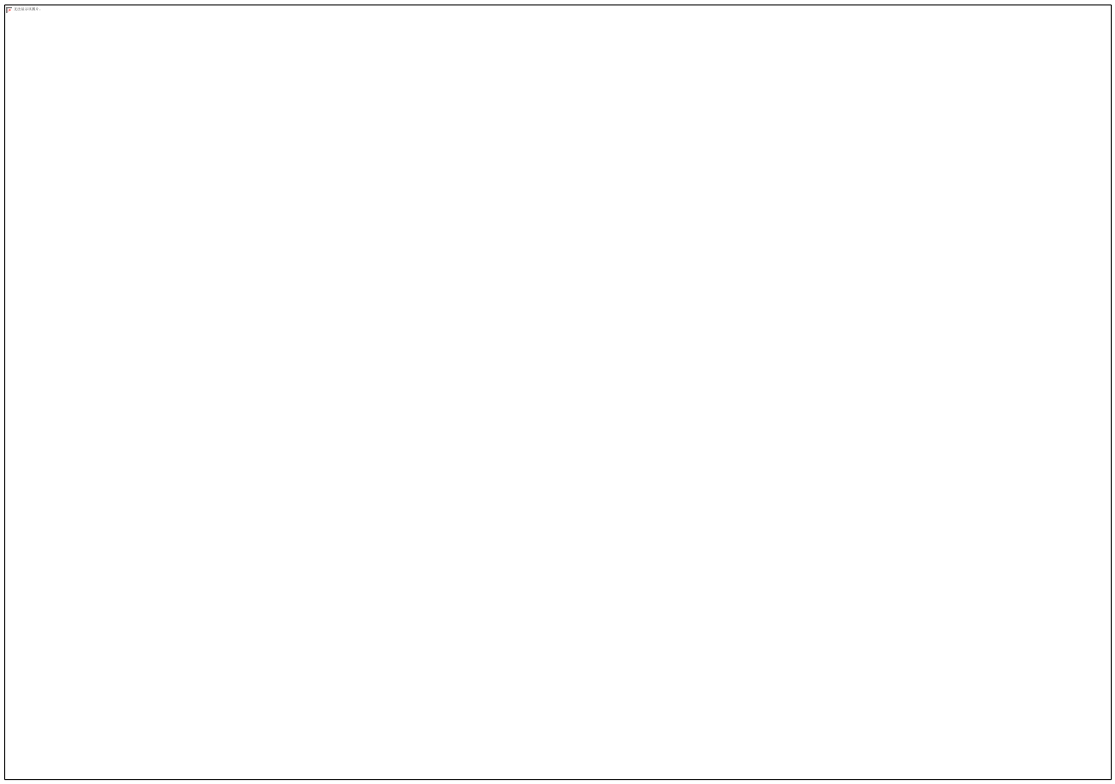

**2-51**

$^{1}$H NMR:

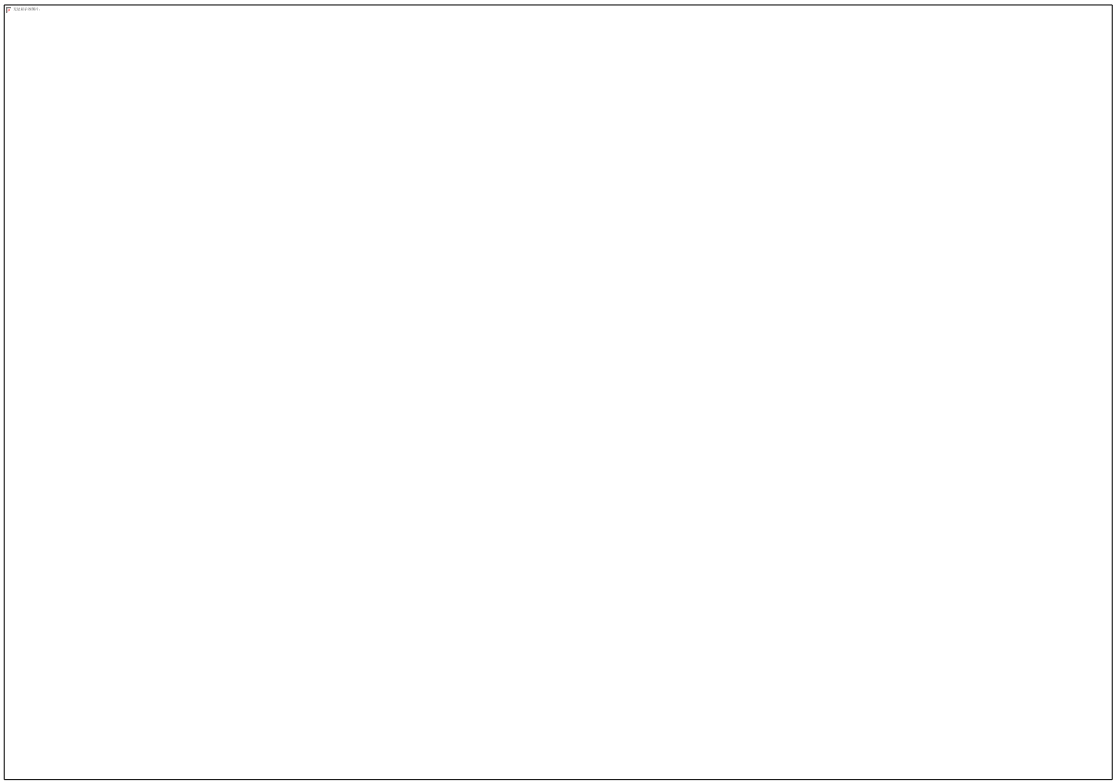

$^{13}$C NMR:

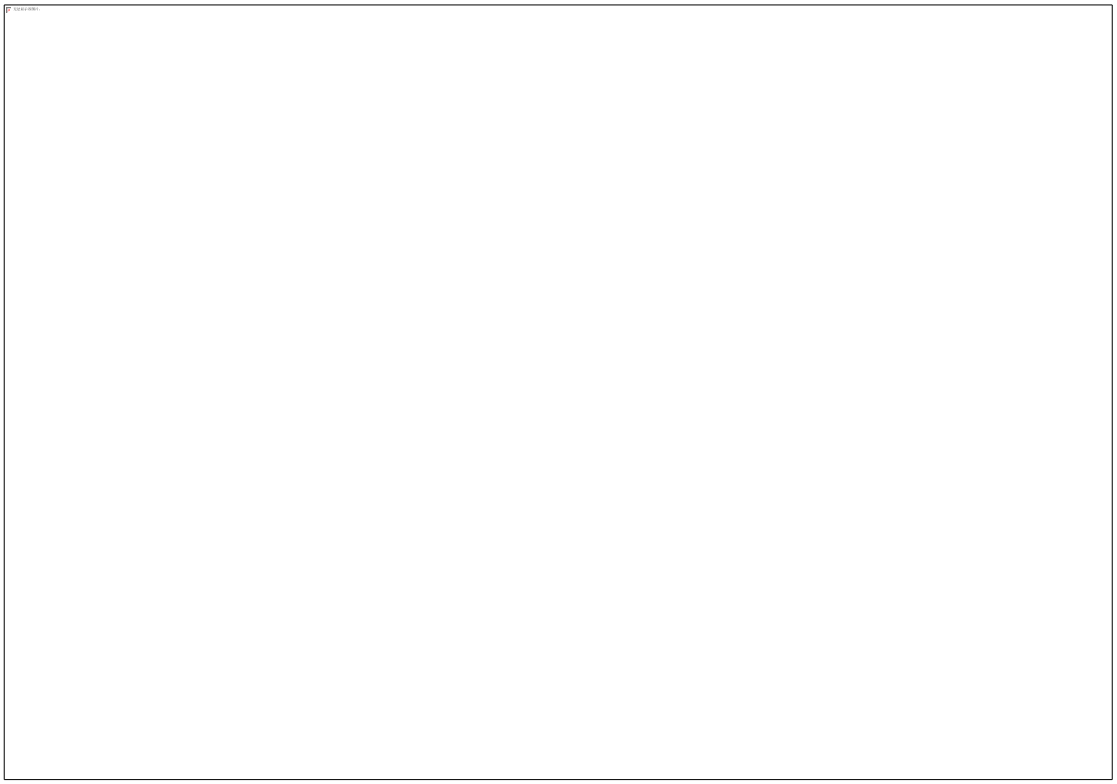

**2-52**

$^{1}$H NMR:

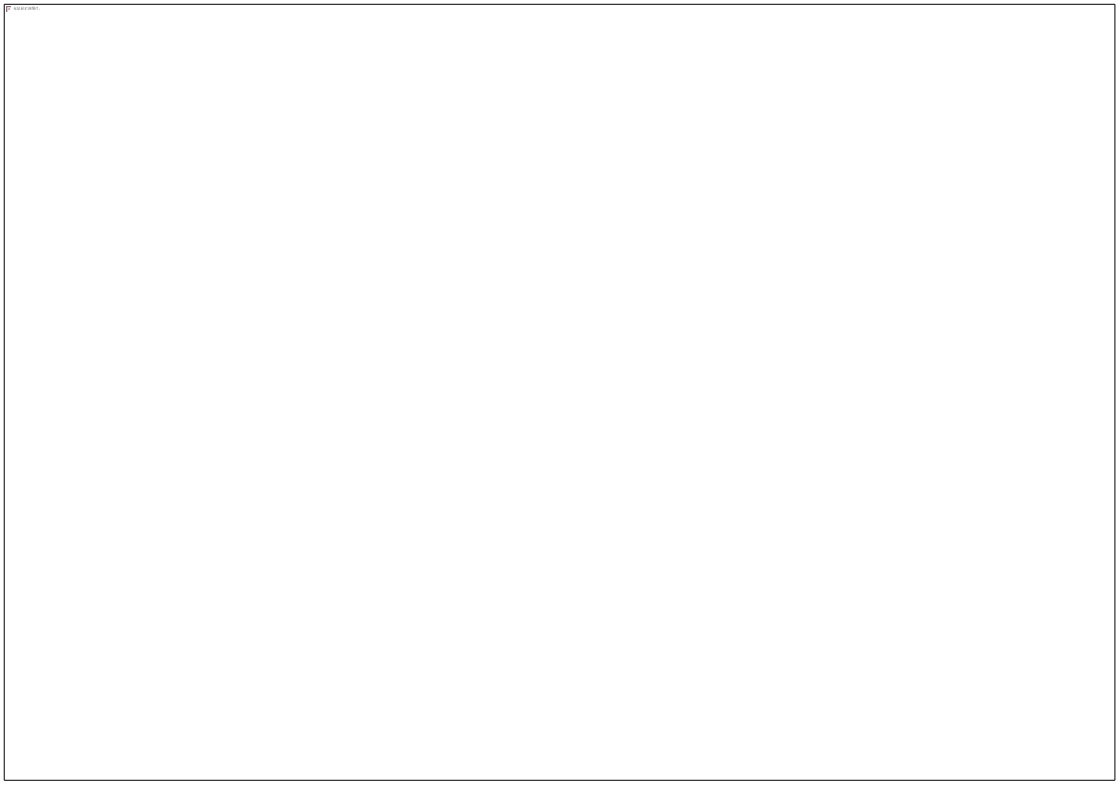

$^{13}$C NMR:

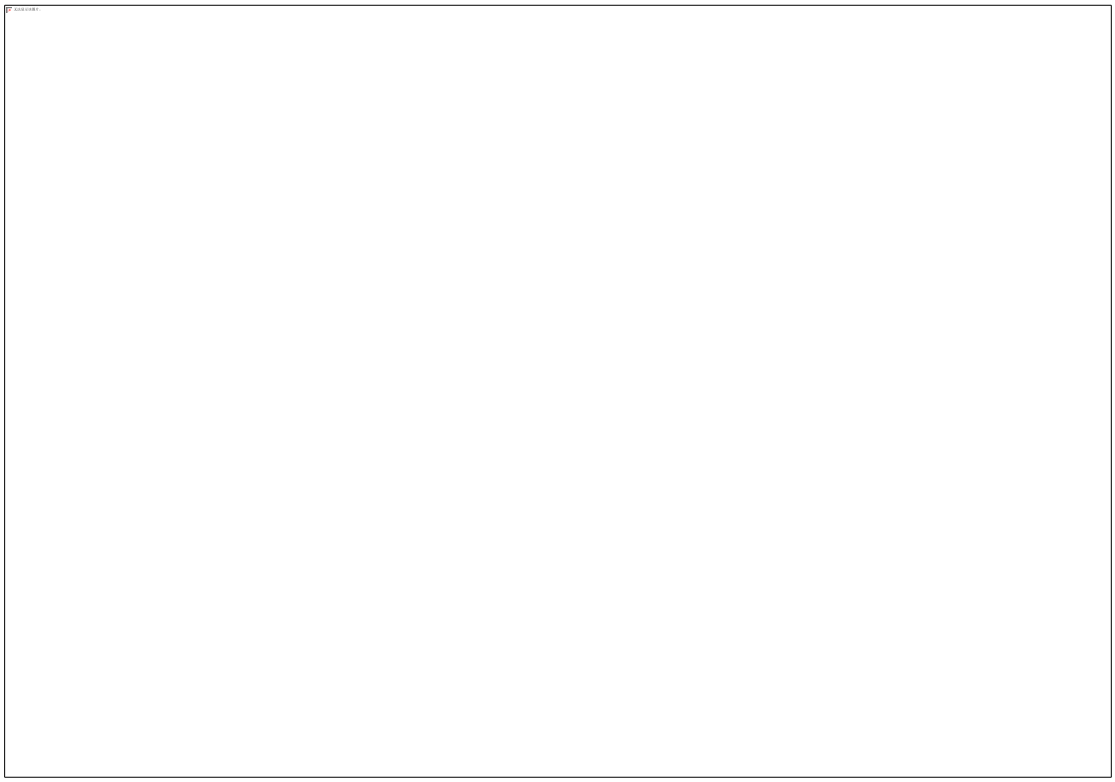

**2-53**

$^{1}$H NMR:

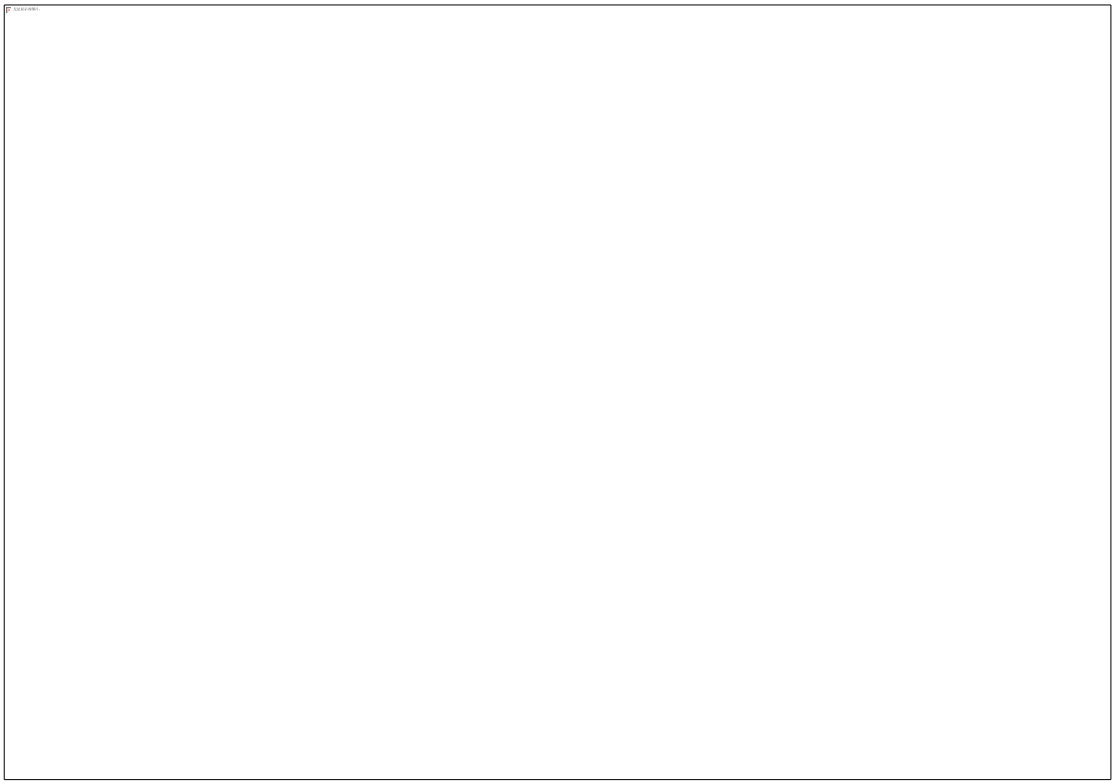

$^{13}$C NMR:

**2-54**

$^{1}$H NMR:

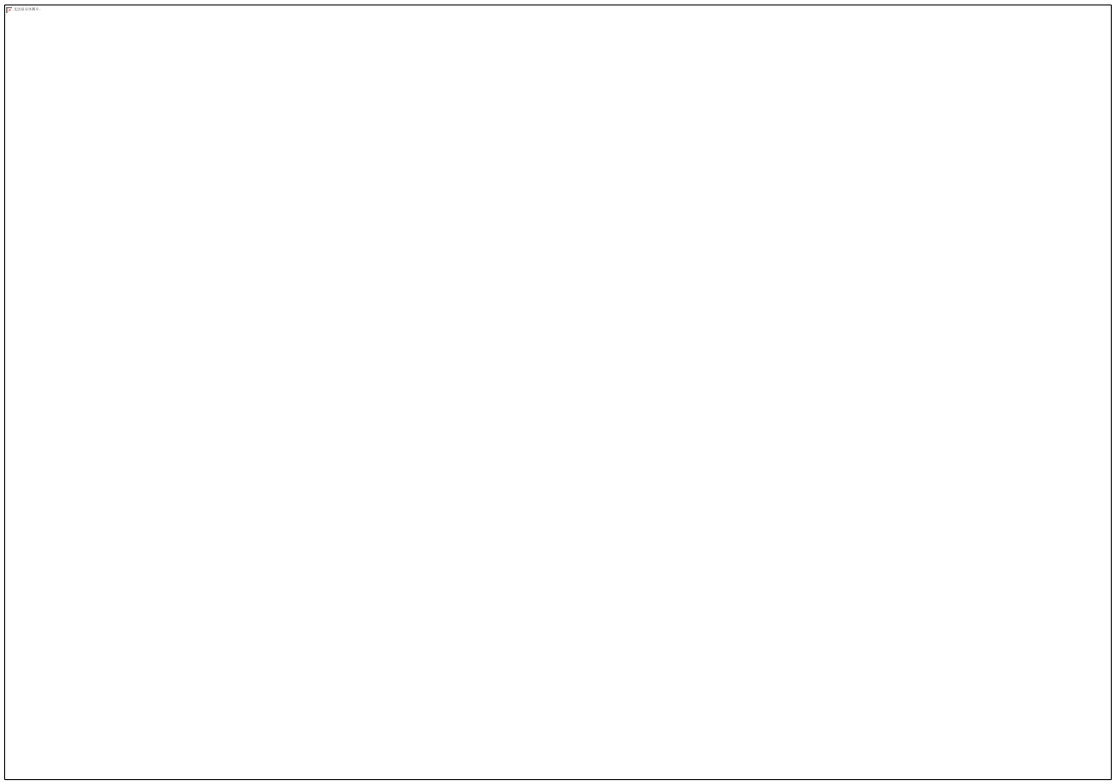

$^{13}$C NMR:

## 2-55

$^{1}$H NMR:

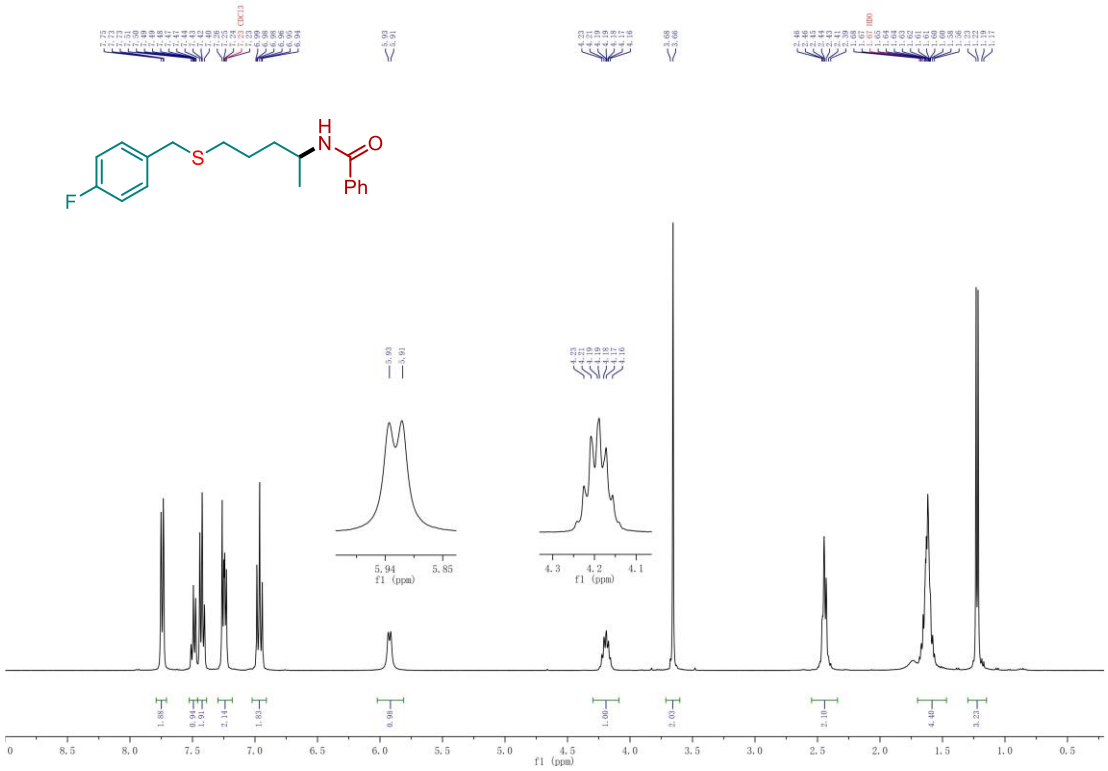


$^{13}$C NMR:

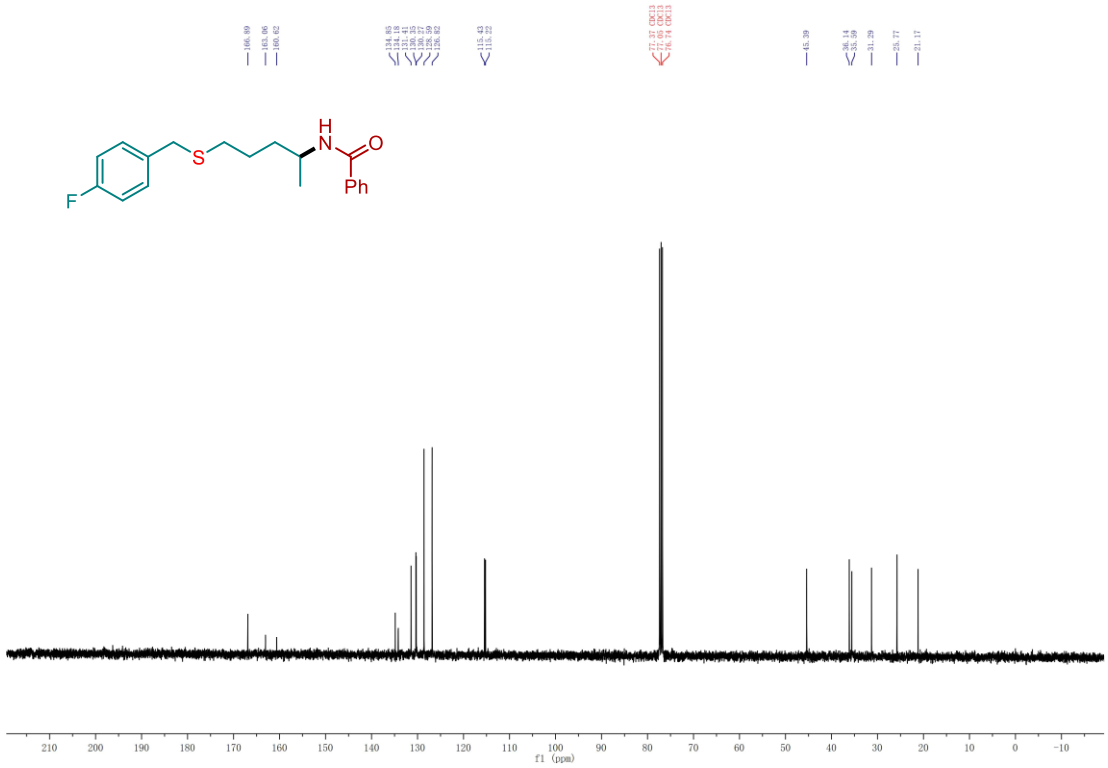

**2-55**

$^{19}$F NMR:

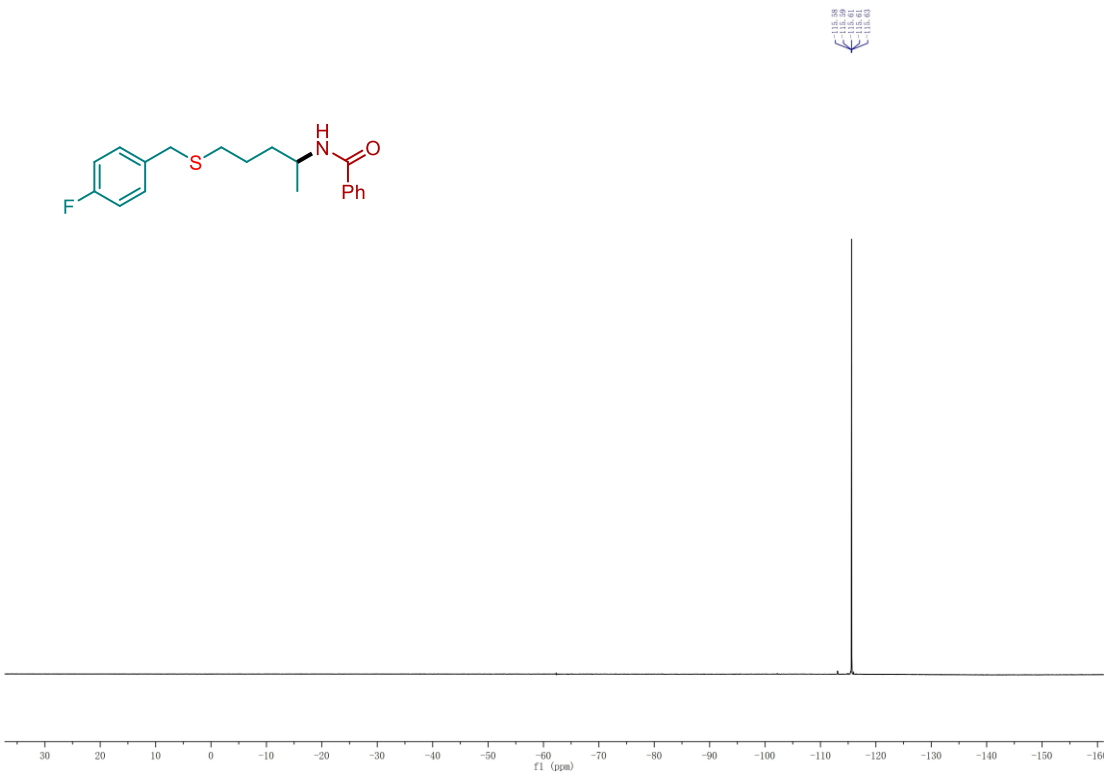
H
N
O
S
F
Ph
30
20
10
0
−10
−20
−30
−40
−50
−60
−70
−80
−90
−100
−110
−120
−130
−140
−150
f1 (ppm)

**2-56**

$^{1}$H NMR:

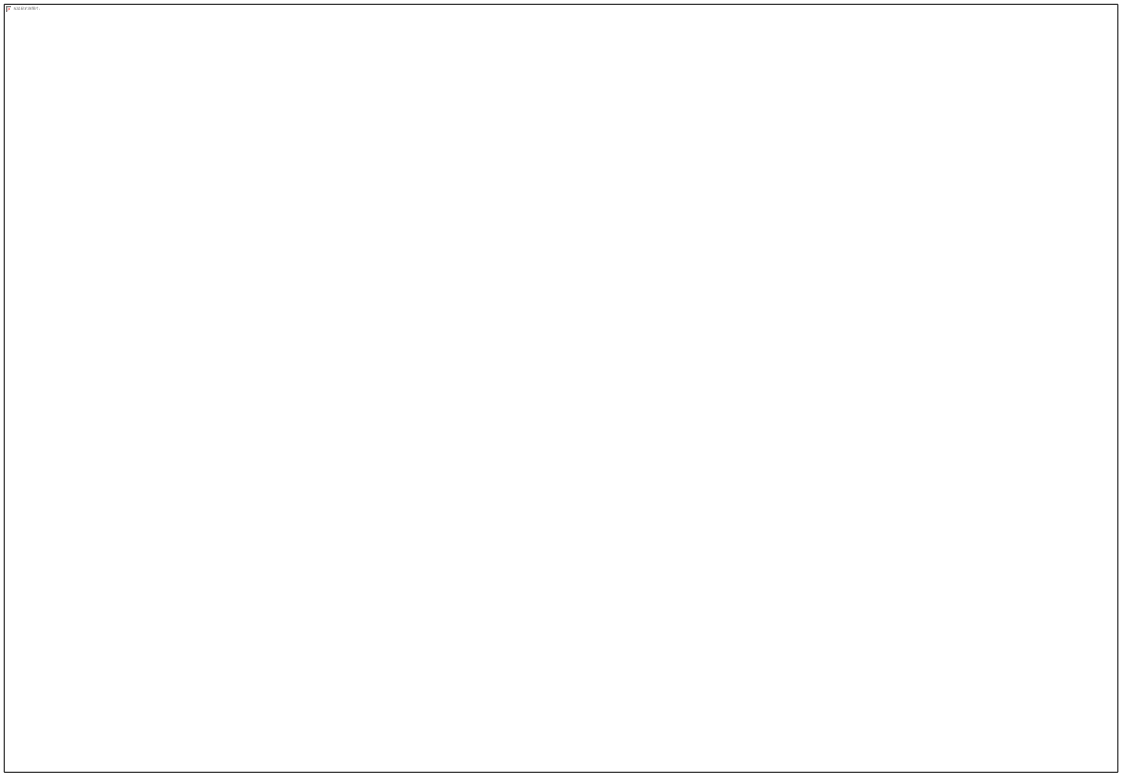

$^{13}$C NMR:

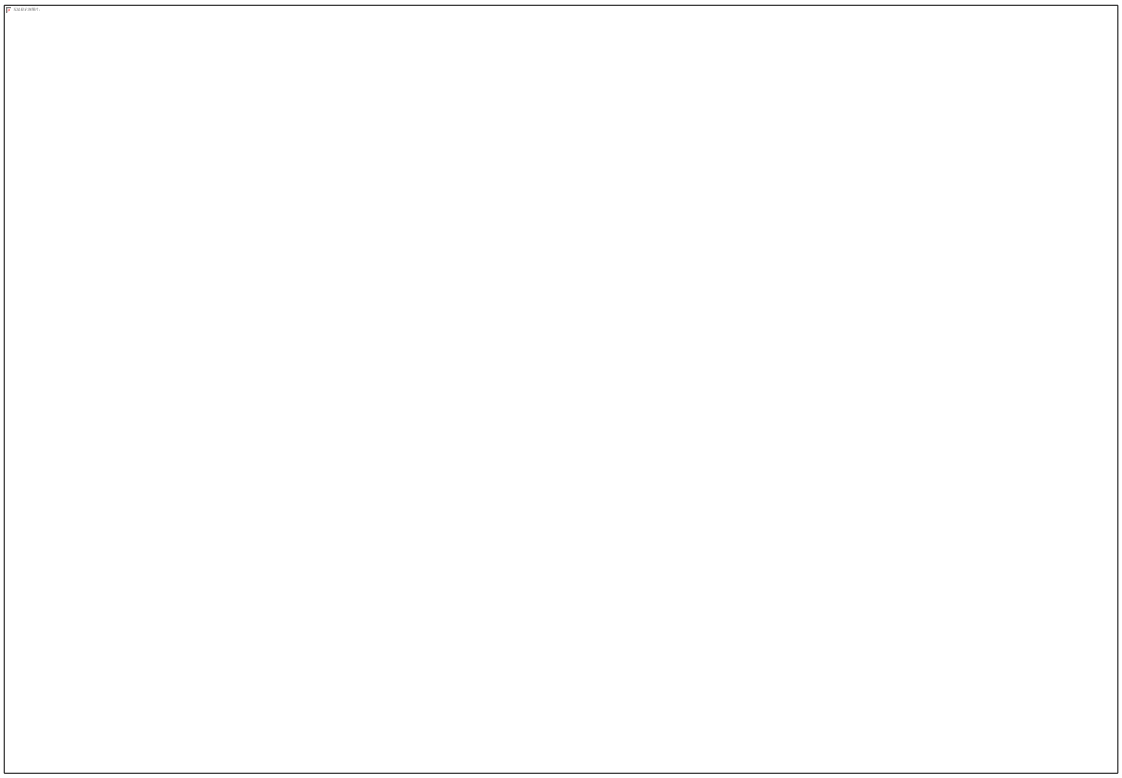

**2-57**

$^{1}$H NMR:

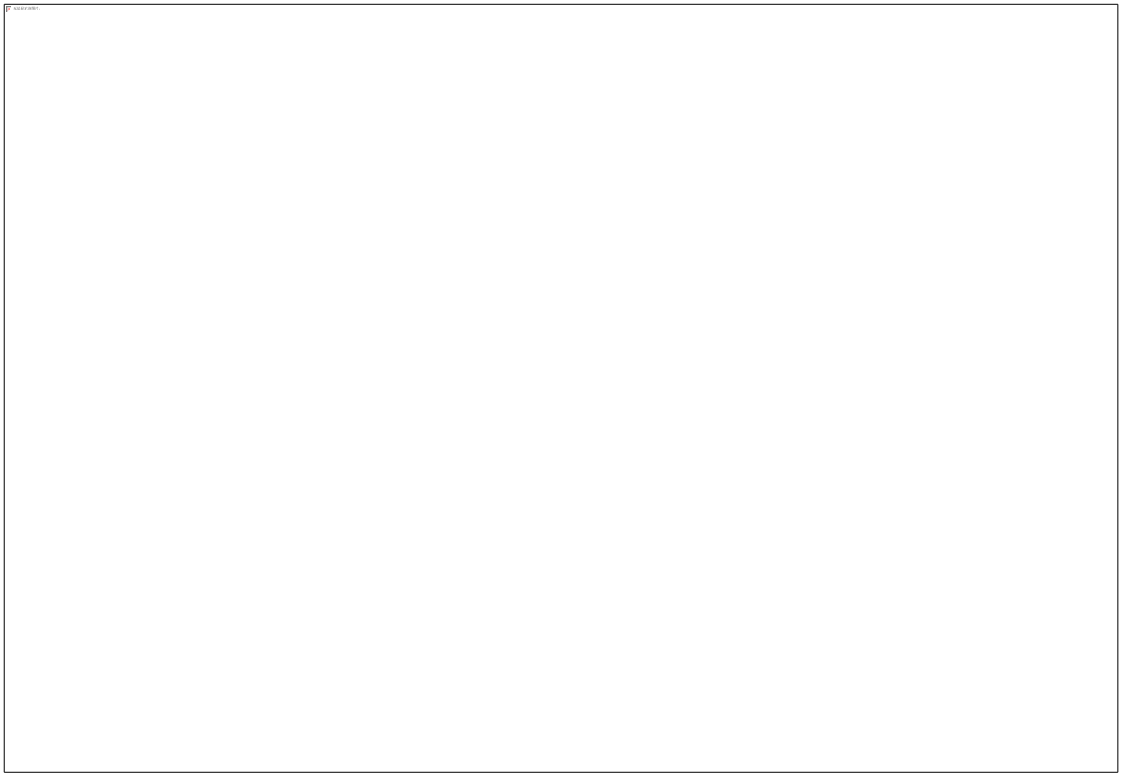

$^{13}$C NMR:

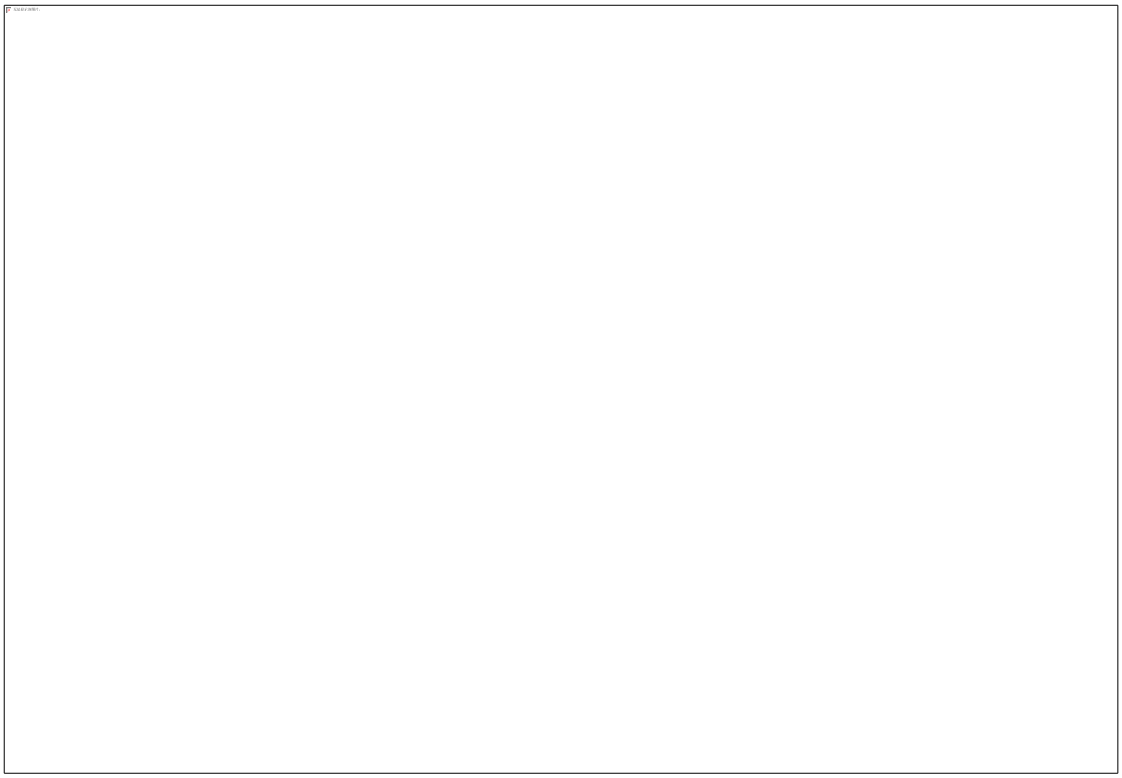

**2-57**

$^{19}$F NMR:

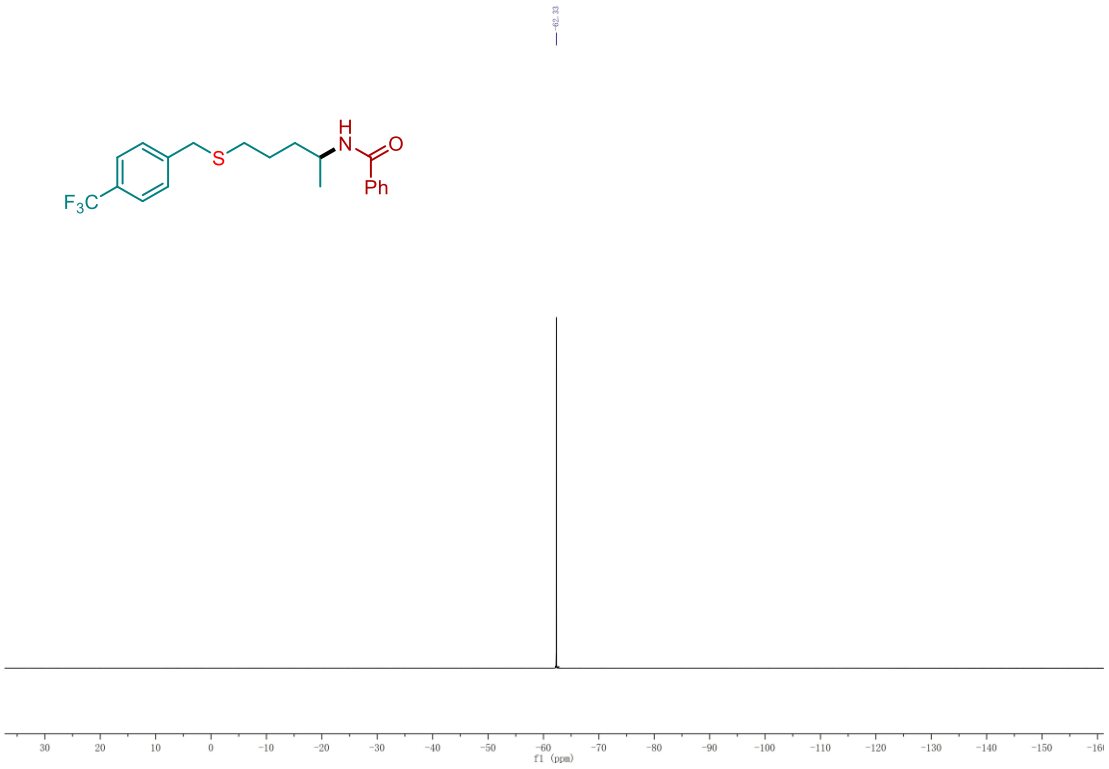
H
N
O
S
Ph
F3C
30
20
10
0
−10
−20
−30
−40
−50
−60
−70
−80
−90
−100
−110
−120
−130
−140
−150
f1 (ppm)

**2-58**

$^{1}$H NMR:

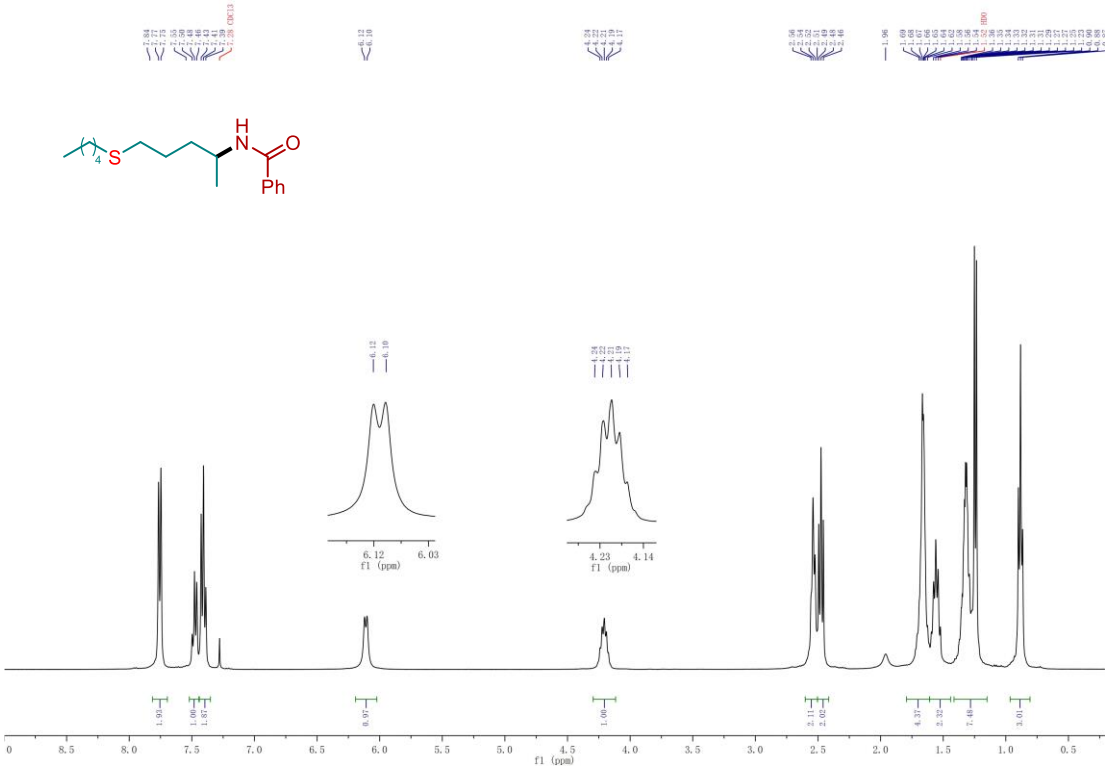


$^{13}$C NMR:

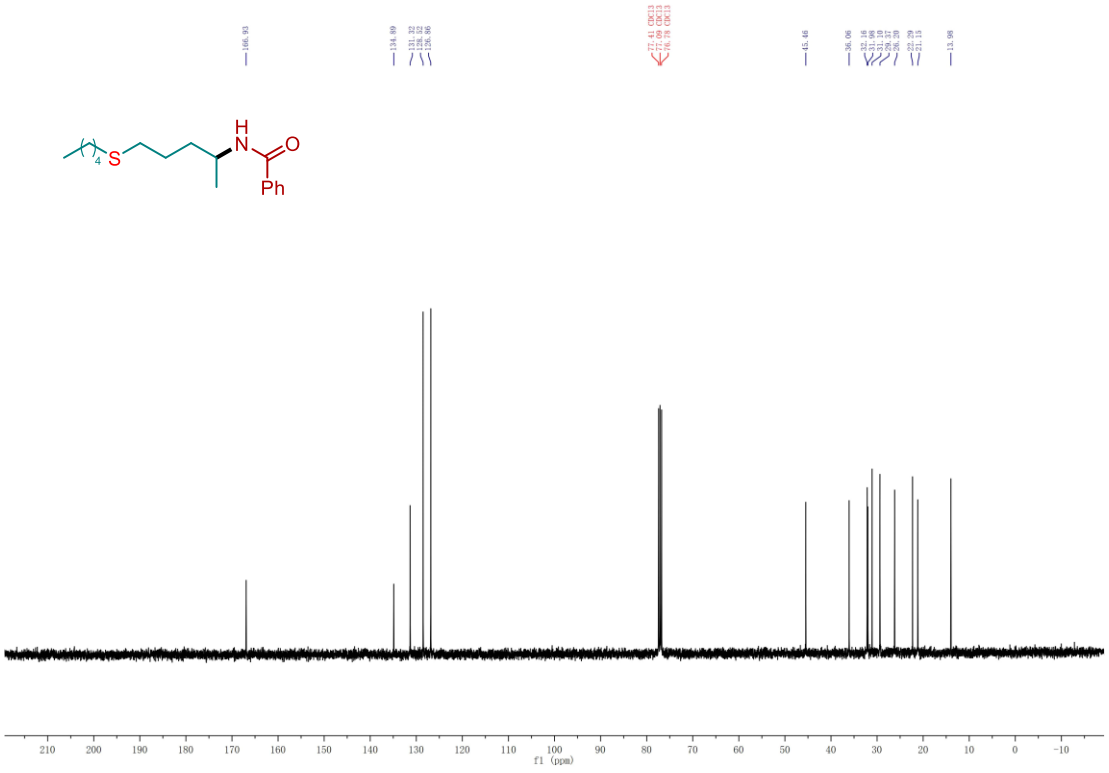

**2-59**

$^{1}$H NMR:

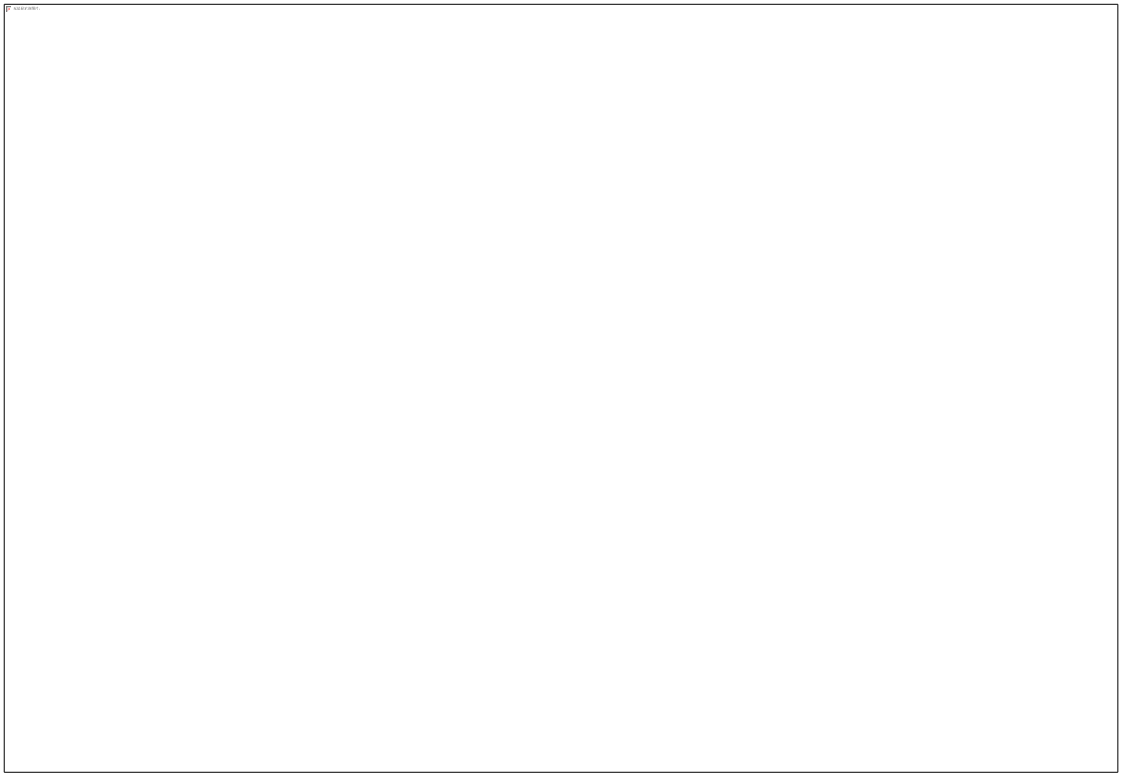

$^{13}$C NMR:

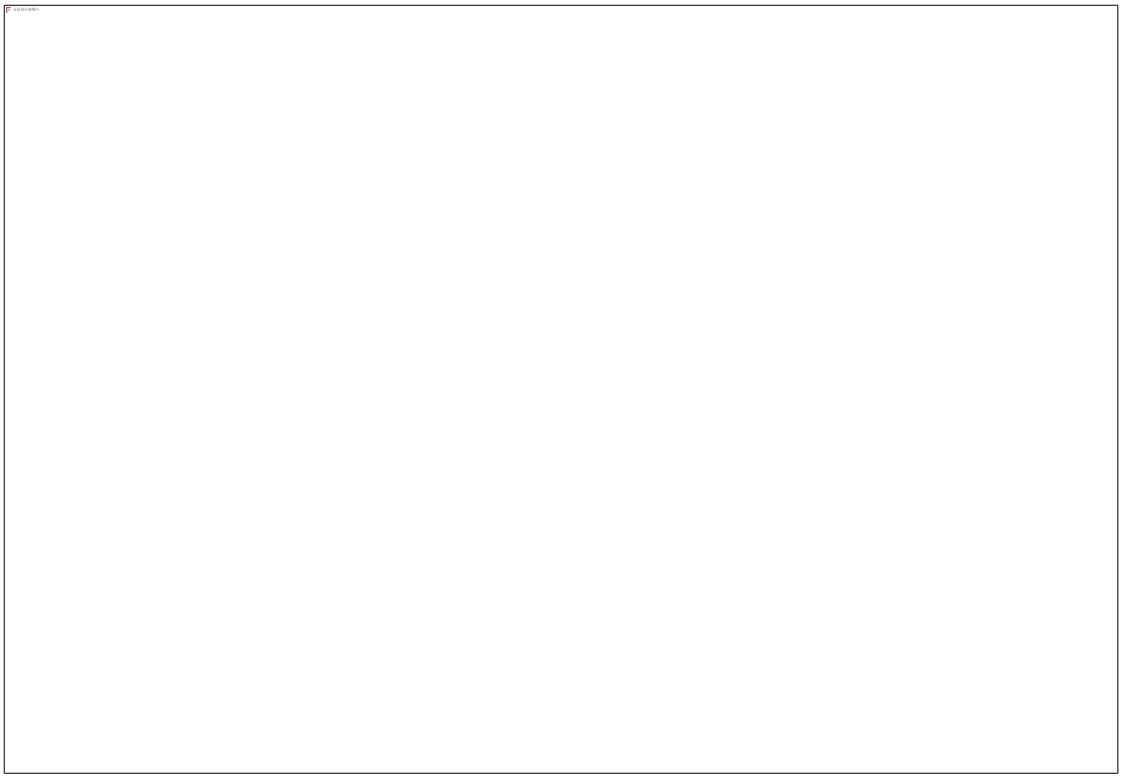

**2-60**

$^{1}$H NMR:

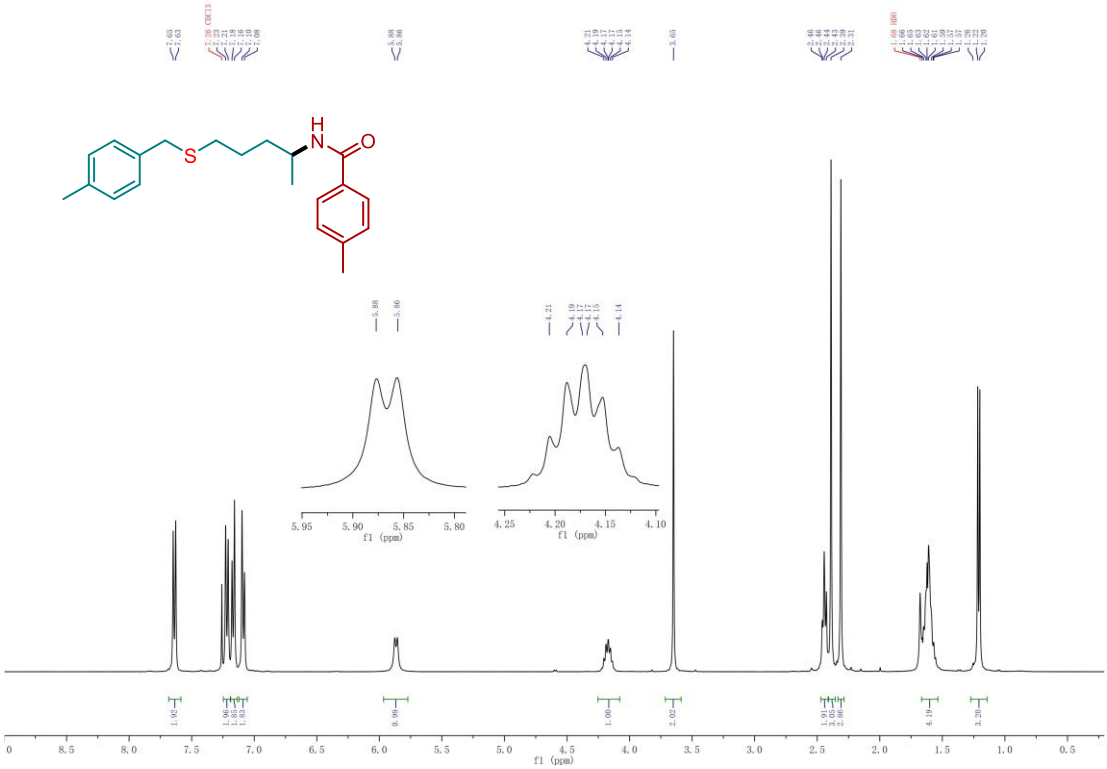

$^{13}$C NMR:

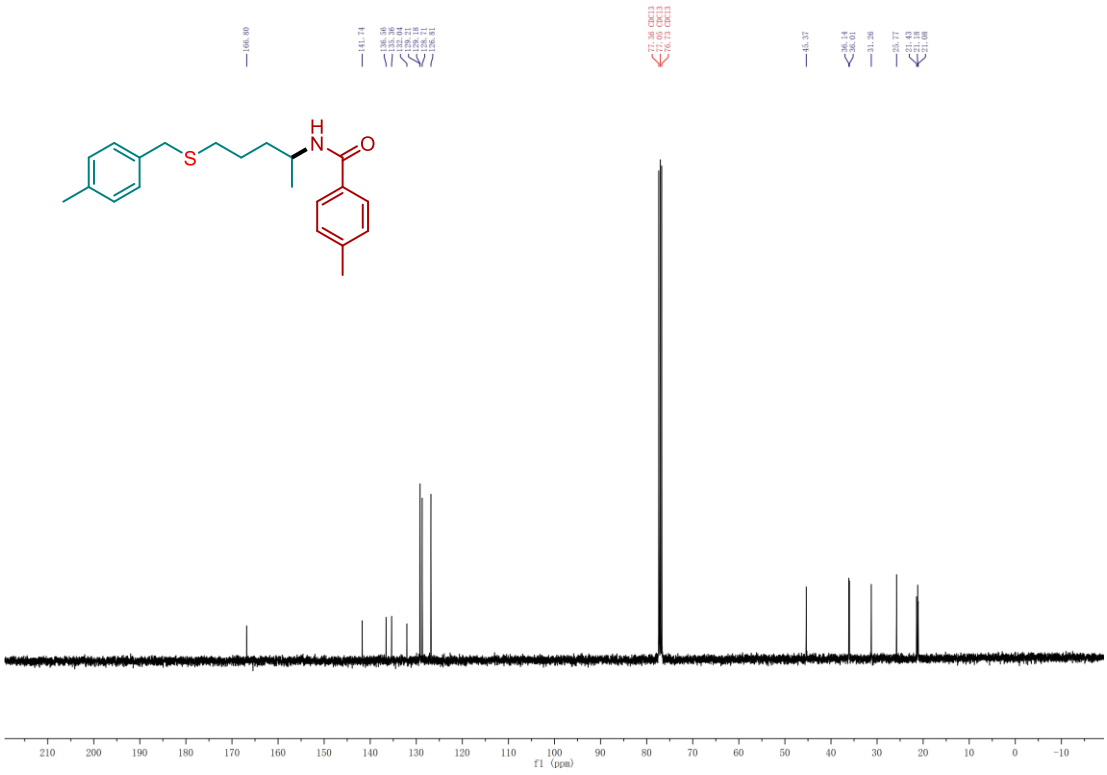

**2-61**

$^{1}$H NMR:

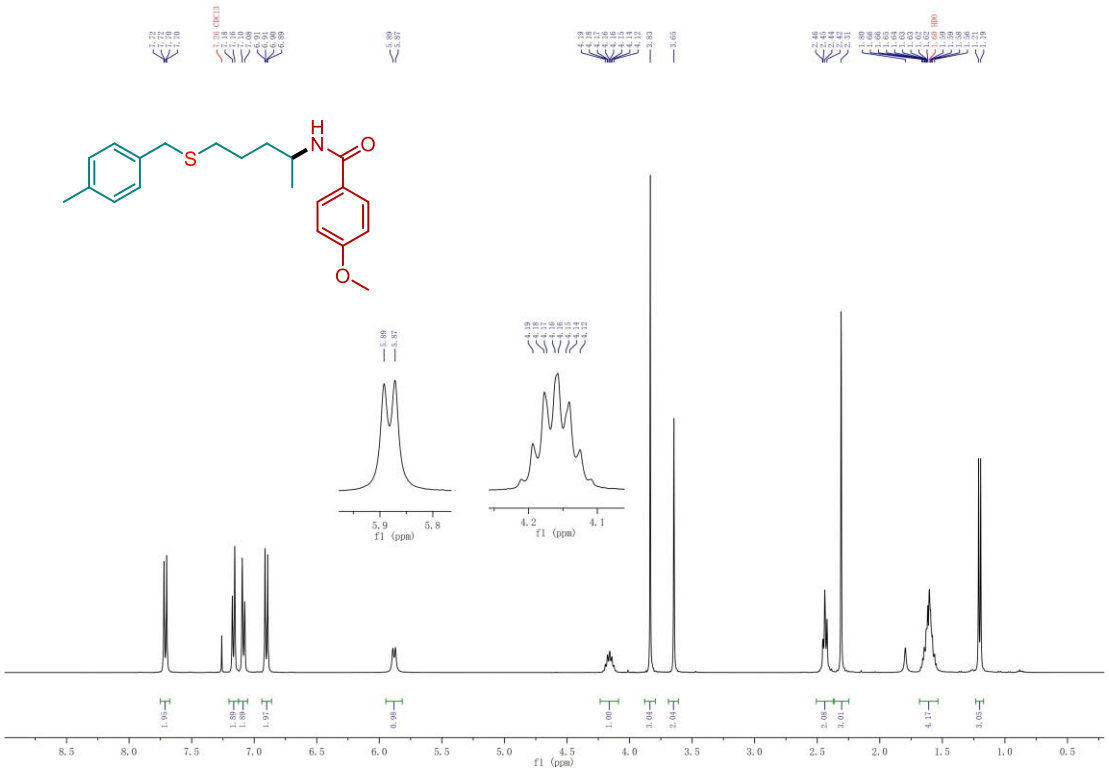

$^{13}$C NMR:

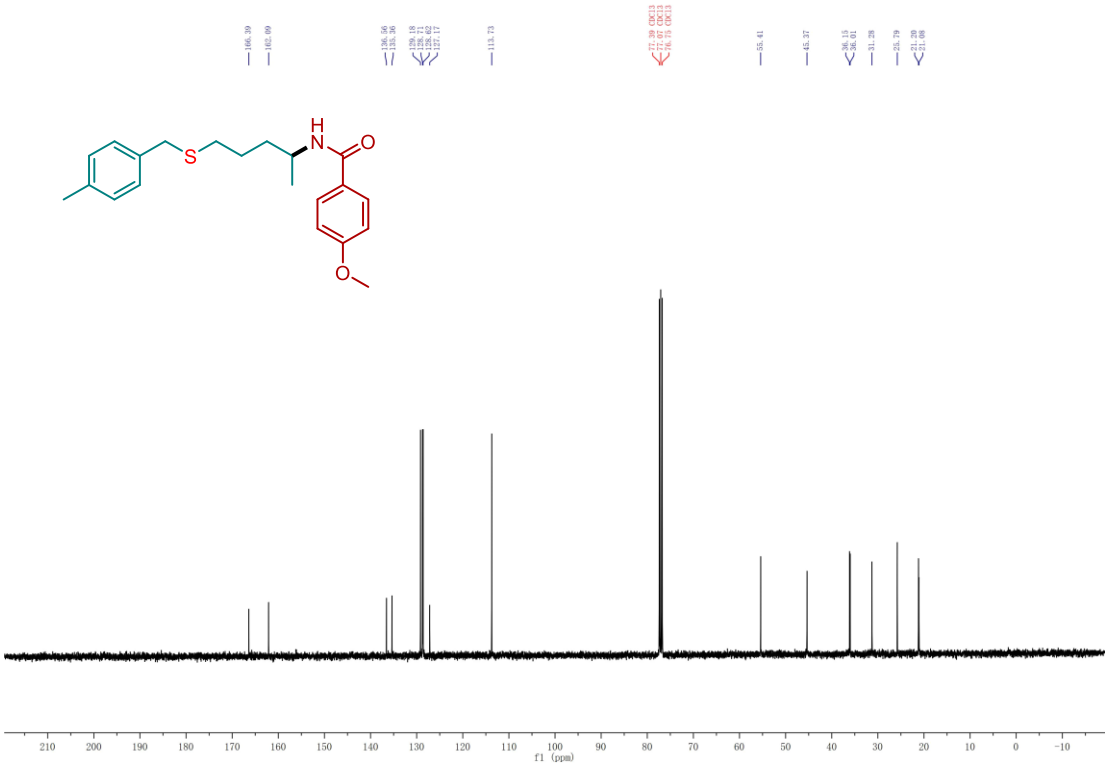

**2-62**

$^{1}$H NMR:

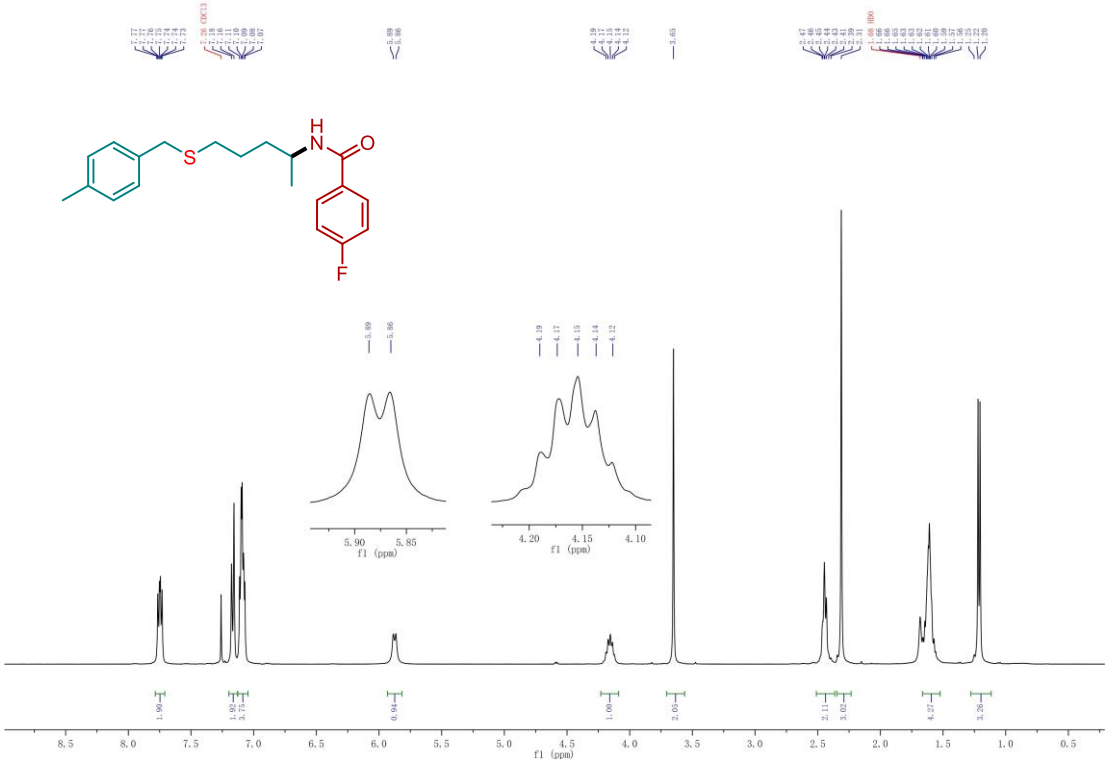


$^{13}$C NMR:

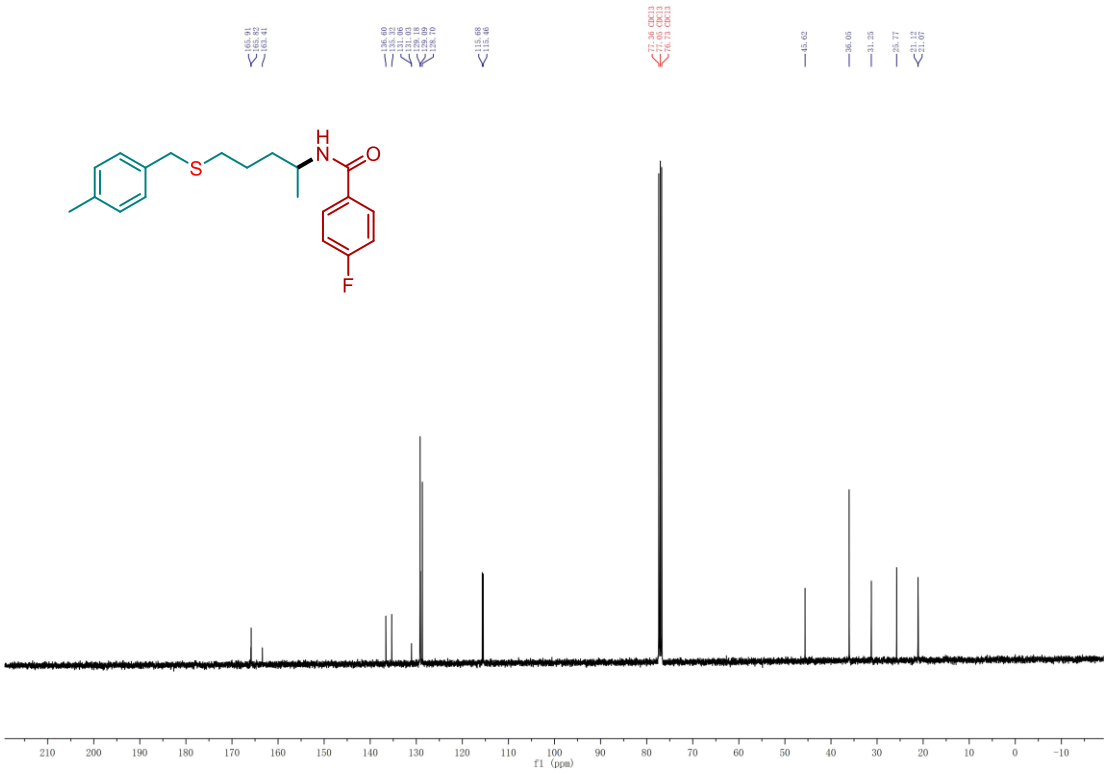

**2-62**

$^{19}$F NMR:

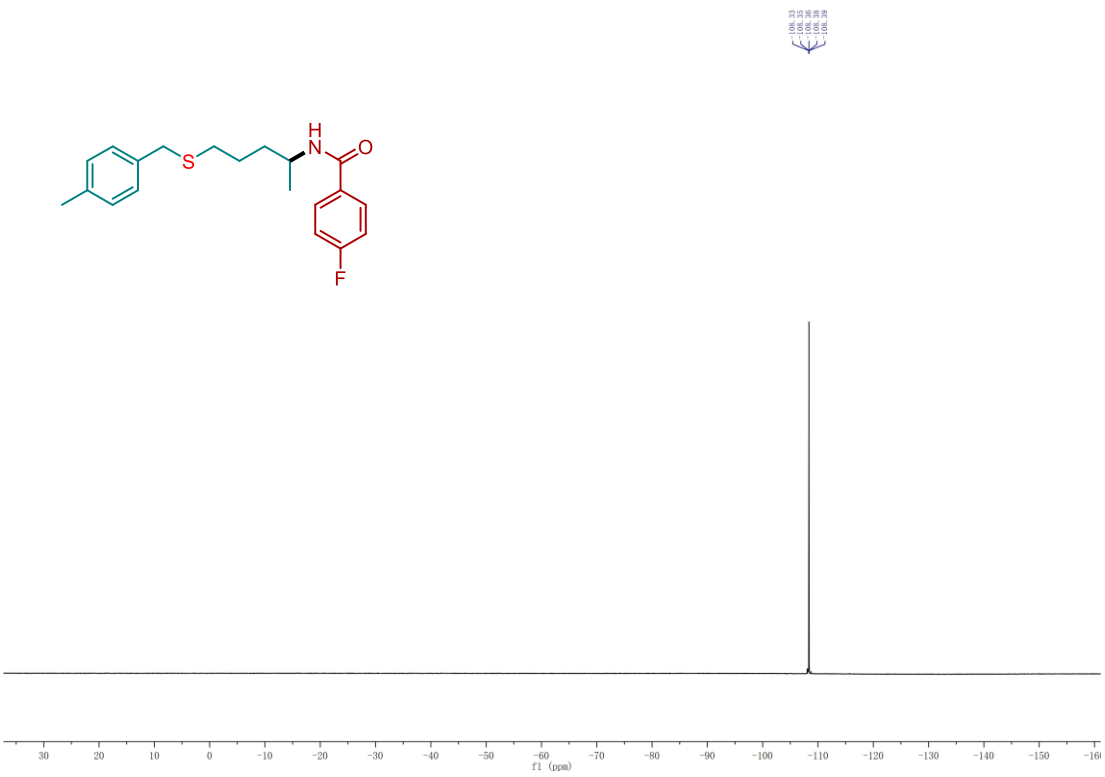
H
N
O
S
F
30
20
10
0
−10
−20
−30
−40
−50
−60
−70
−80
−90
−100
−110
−120
−130
−140
−150
f1 (ppm)

**2-63**

$^{1}$H NMR:

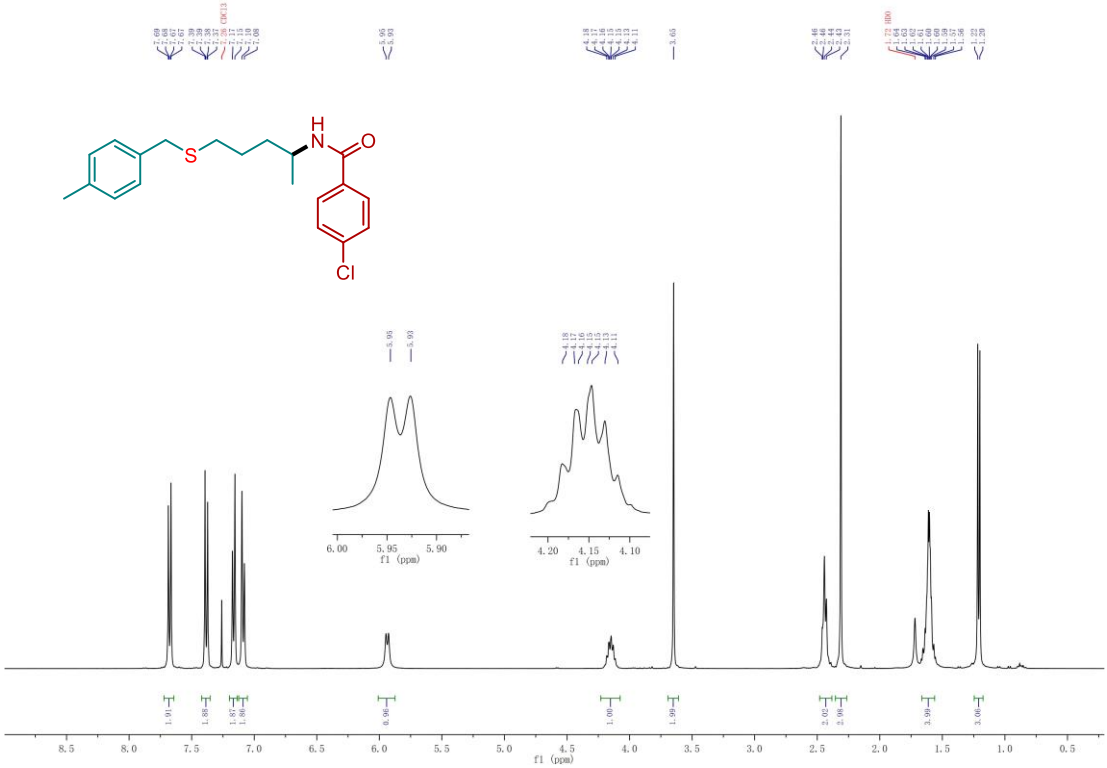

$^{13}$C NMR:

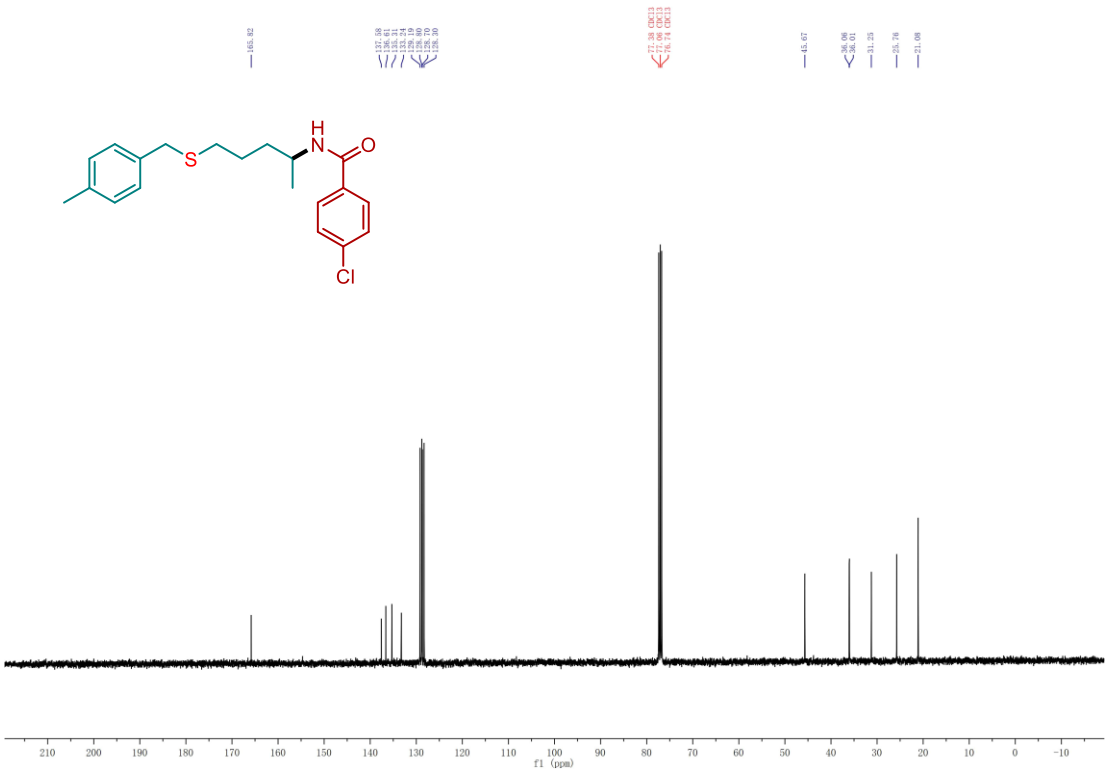

**2-64**

$^{1}$H NMR:

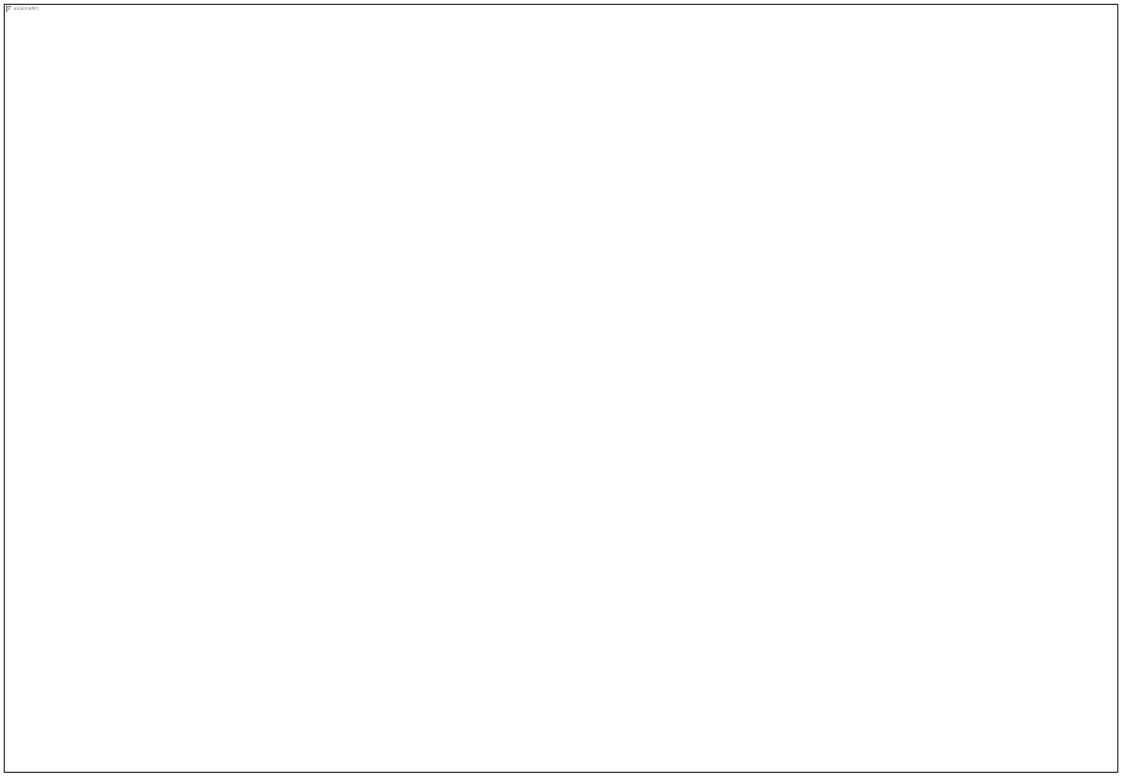

$^{13}$C NMR:

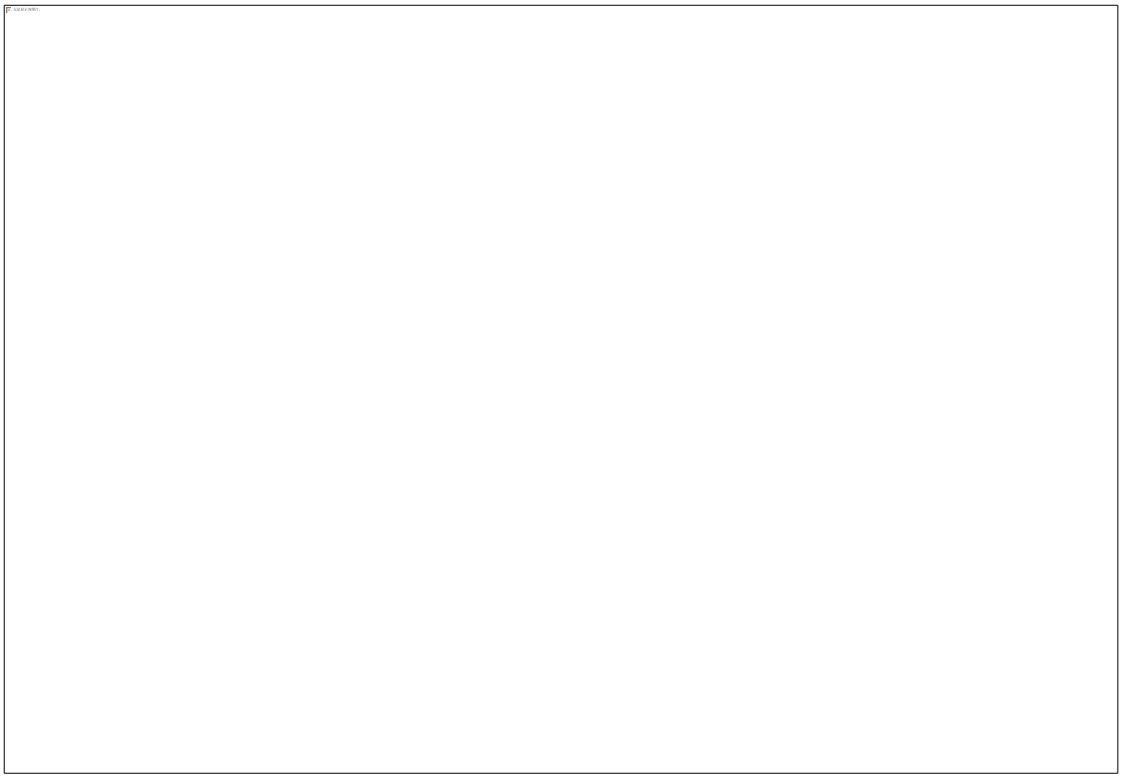

**2-64**

$^{19}$F NMR:

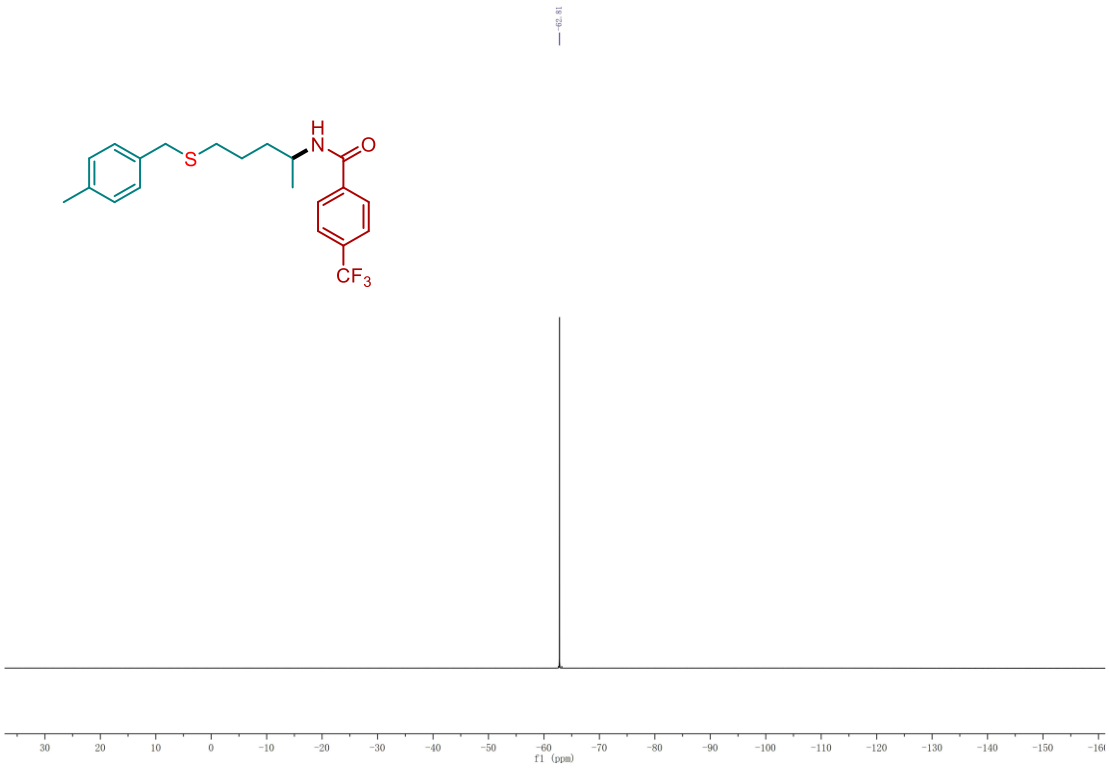
H
N
O
S
CF3
30
20
10
0
−10
−20
−30
−40
−50
−60
−70
−80
−90
−100
−110
−120
−130
−140
−150
f1 (ppm)

## 2-65

$^{1}$H NMR:

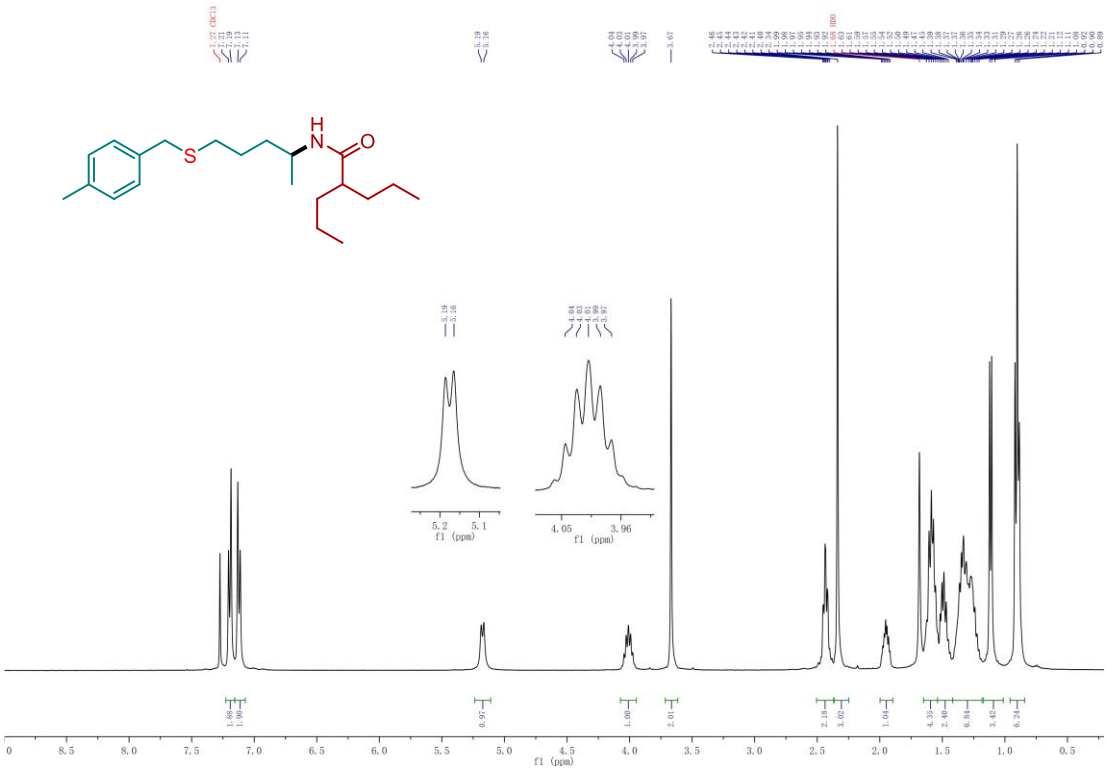

$^{13}$C NMR:

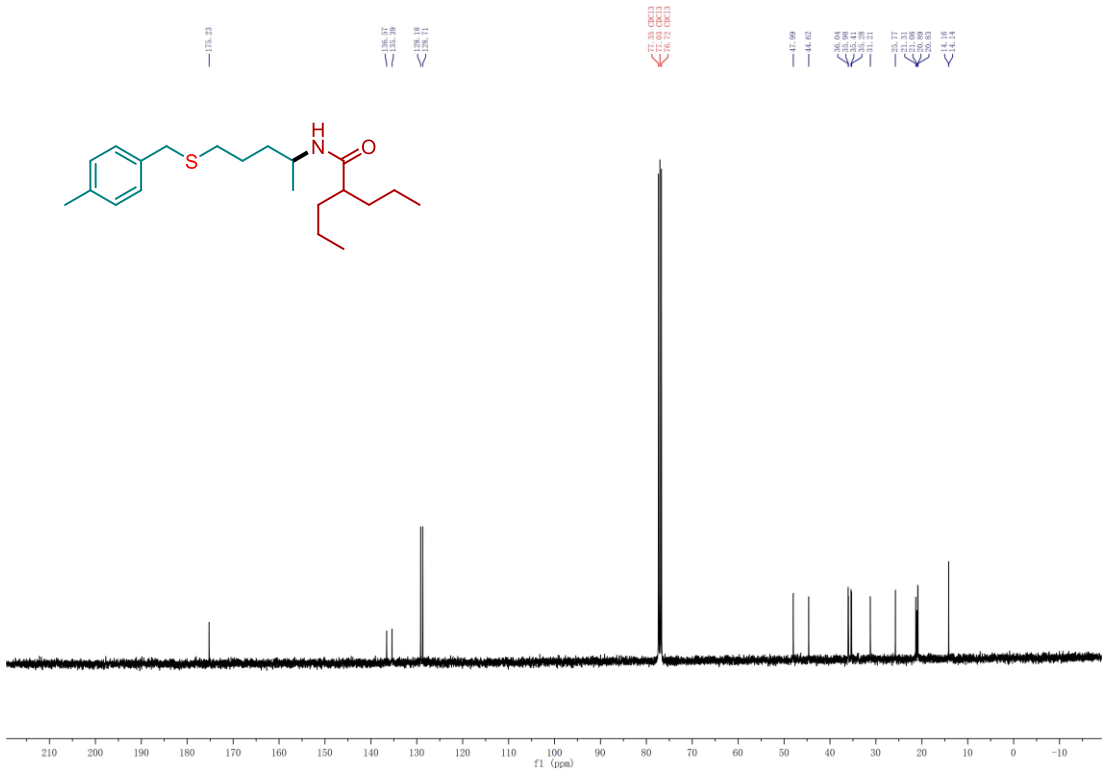

**2-66**

$^{1}$H NMR:

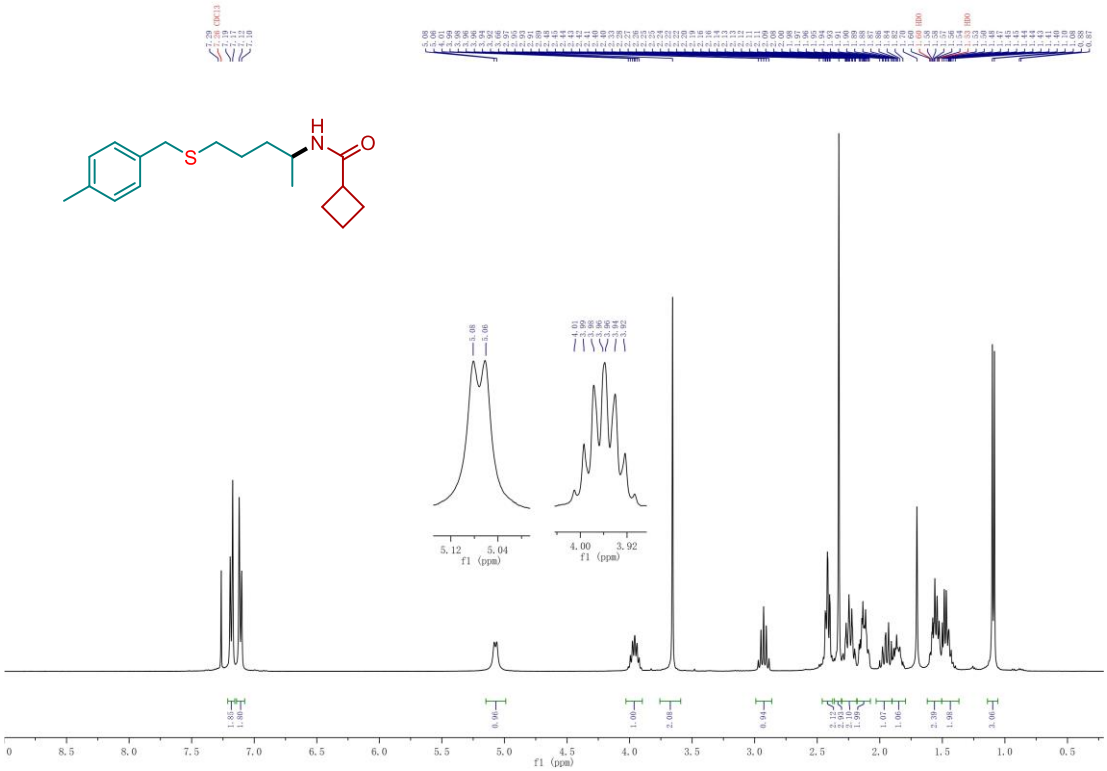

$^{13}$C NMR:

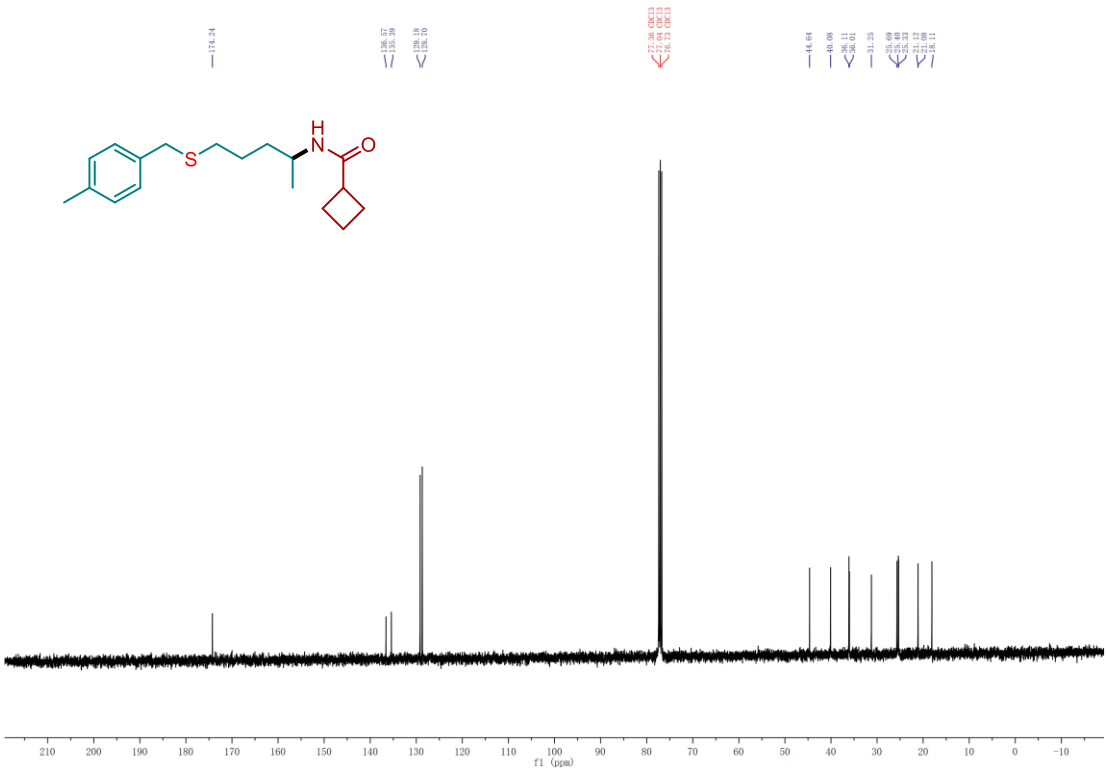

**2-67**

$^{1}$H NMR:

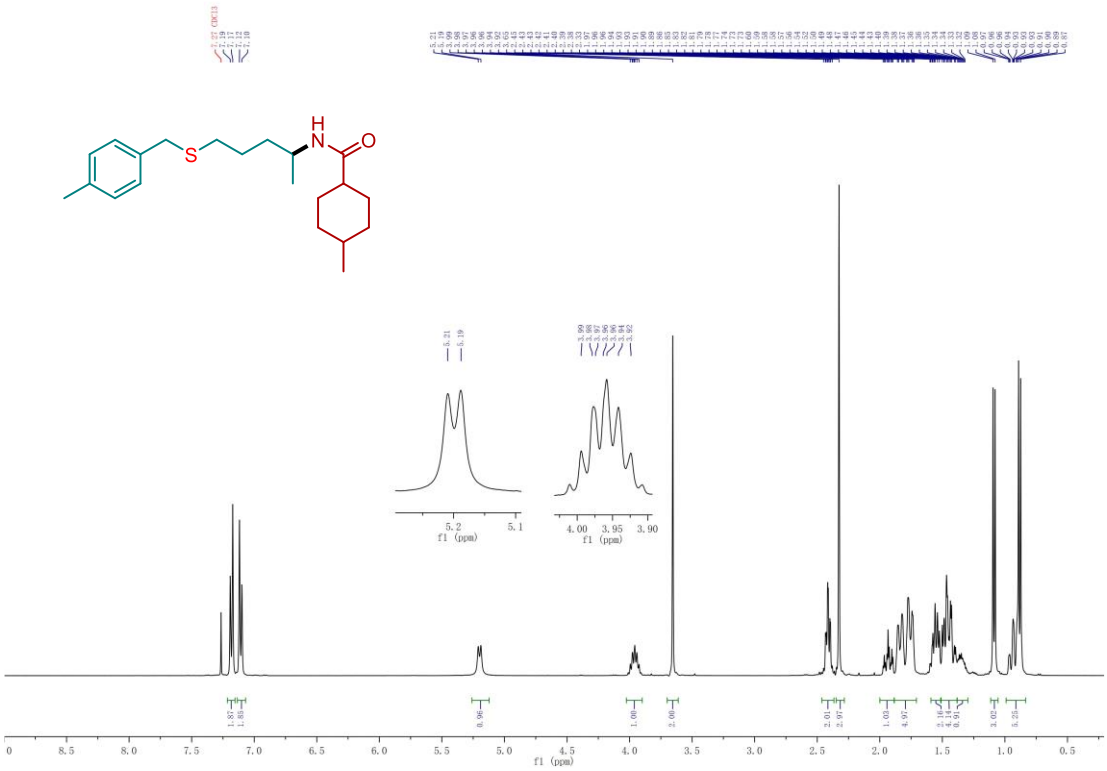

$^{13}$C NMR:

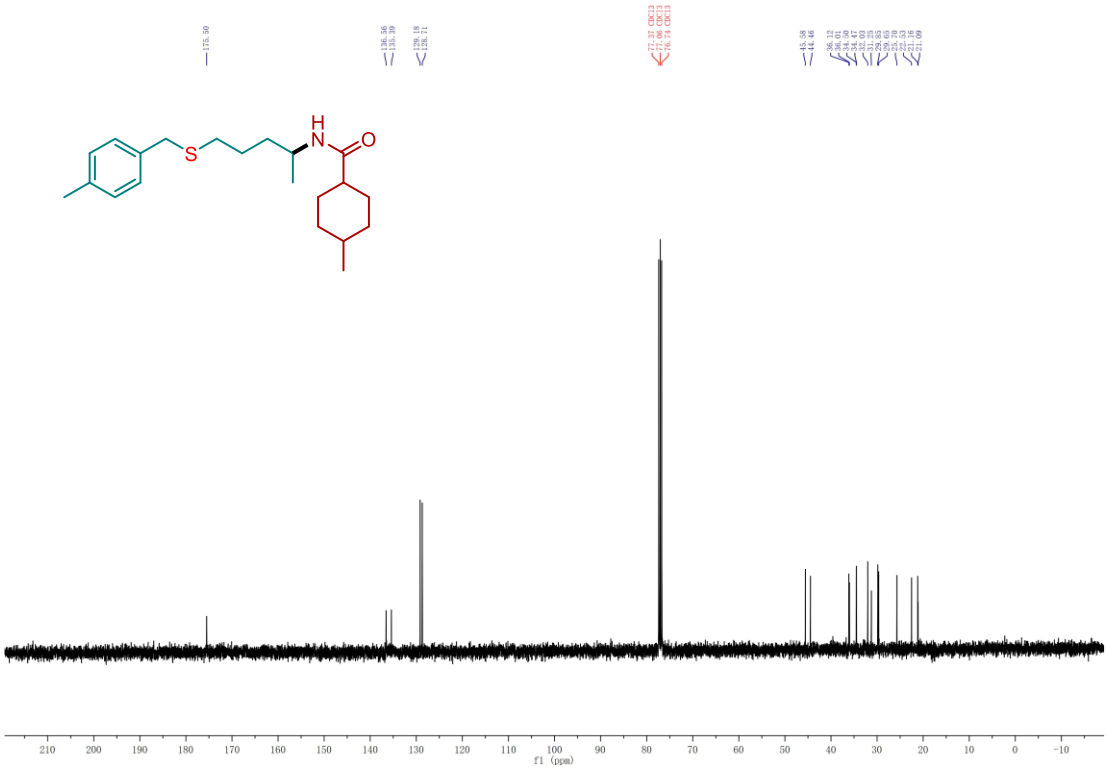

**2-70**

$^{1}$H NMR:

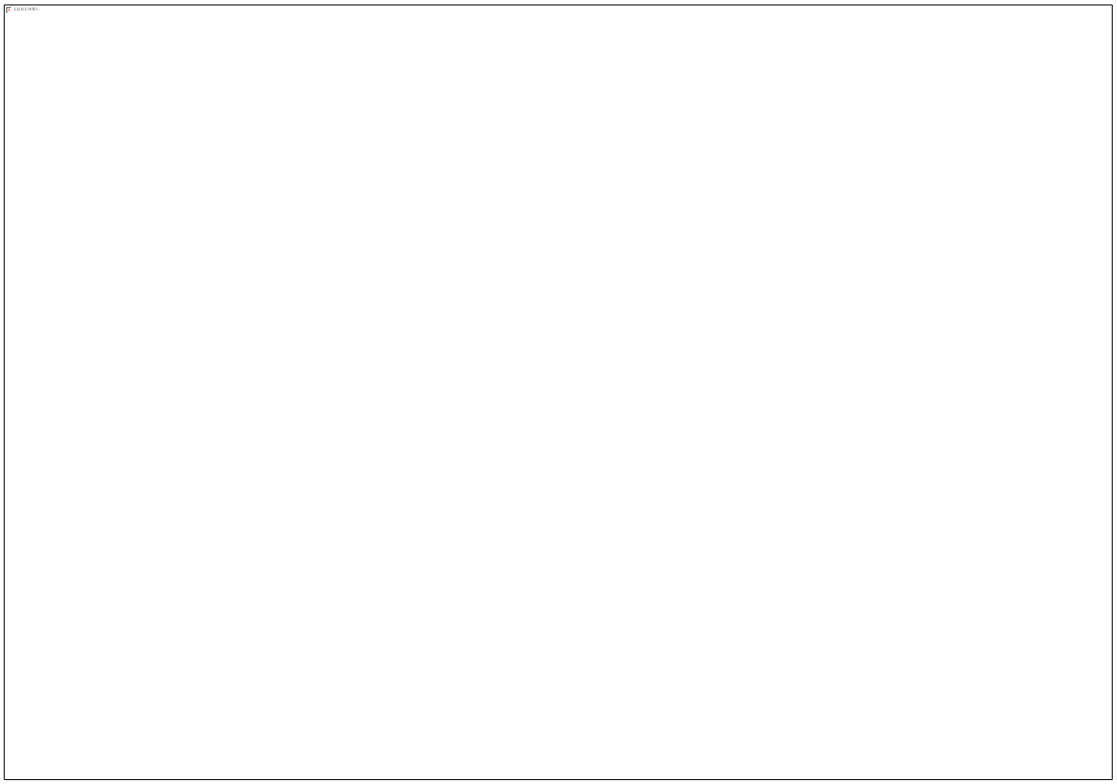

$^{13}$C NMR:

## 3-1

$^{1}$H NMR:

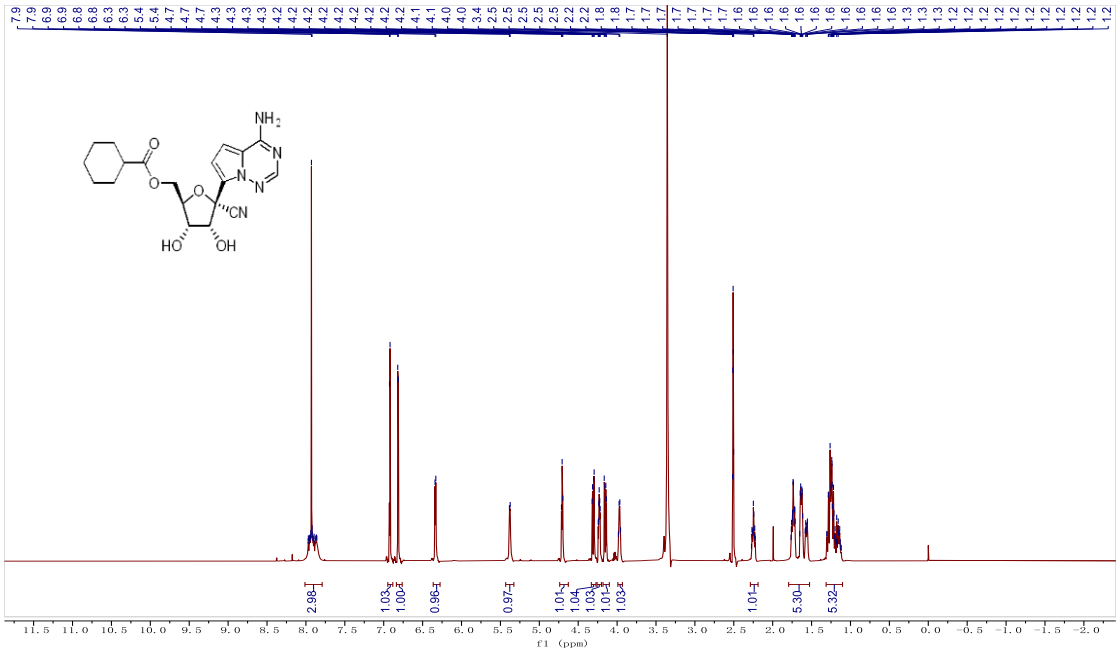


$^{13}$C NMR:

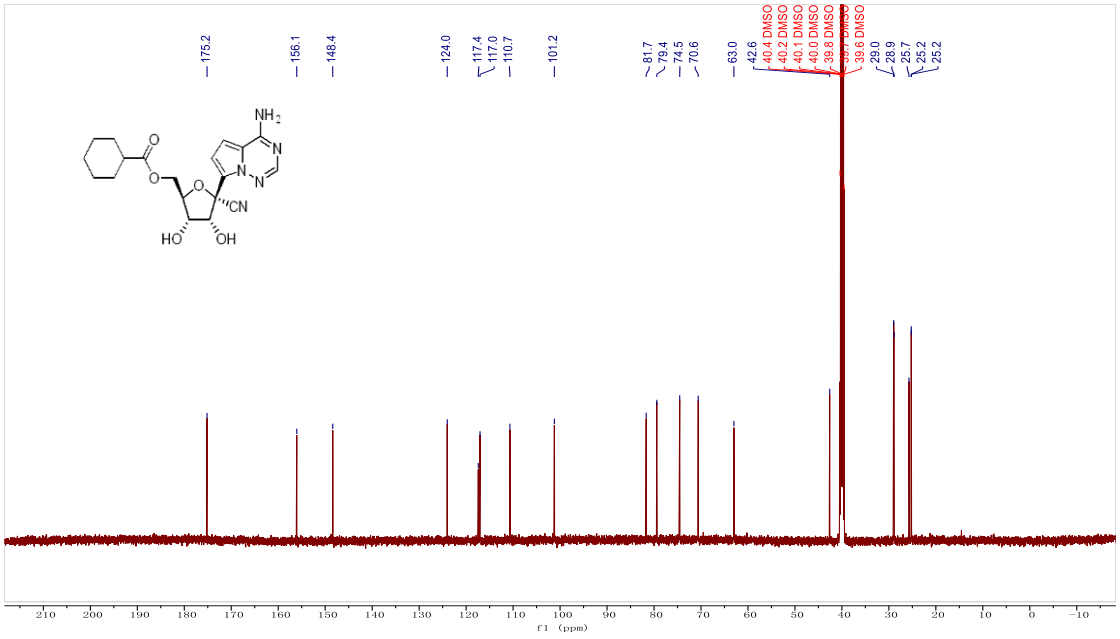

## 3-2

$^{1}$H NMR:

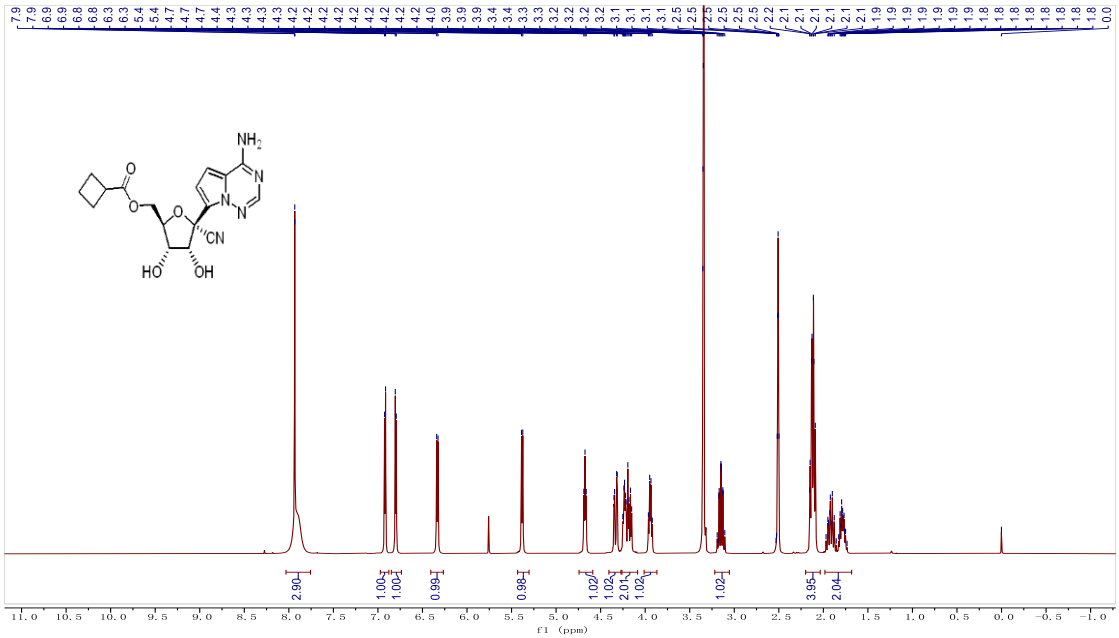


$^{13}$C NMR:

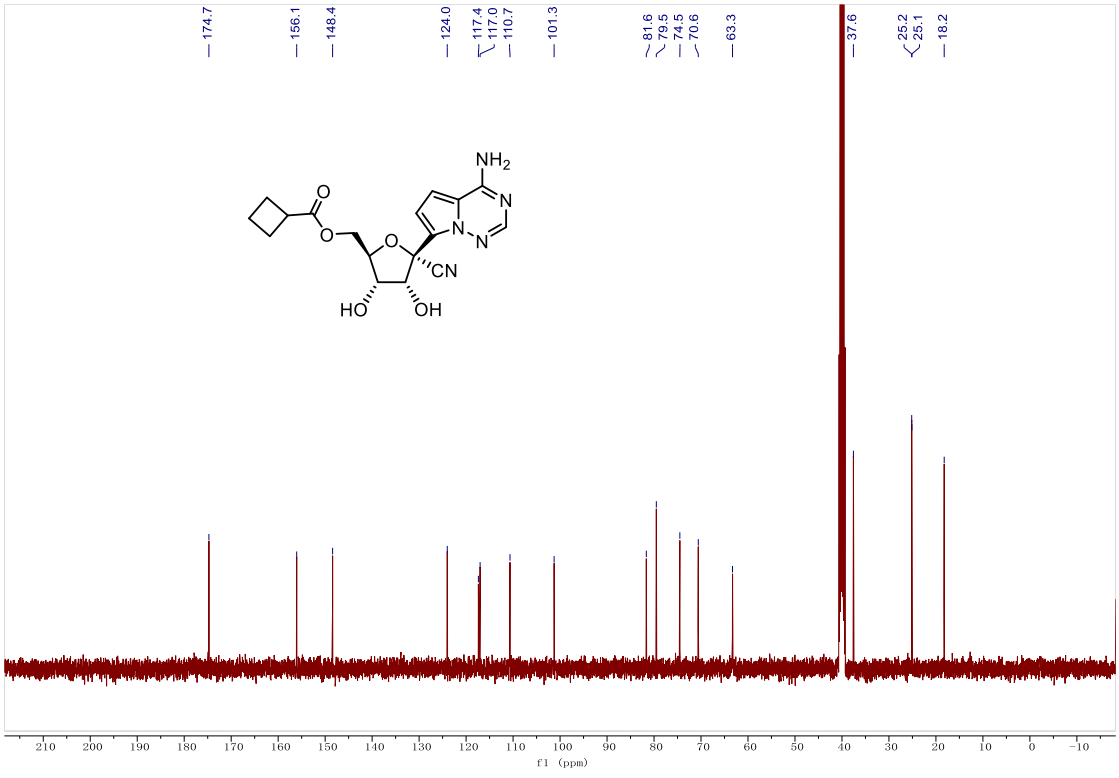

**3-3**

$^{1}$H NMR:

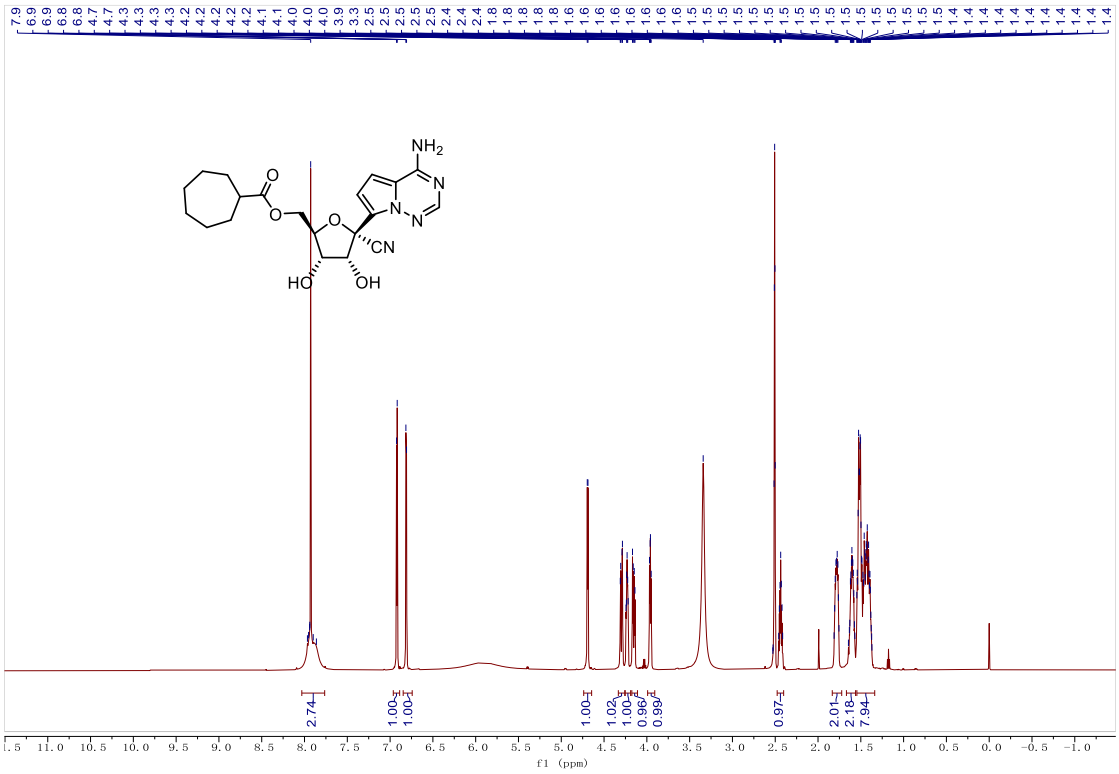


$^{13}$C NMR:

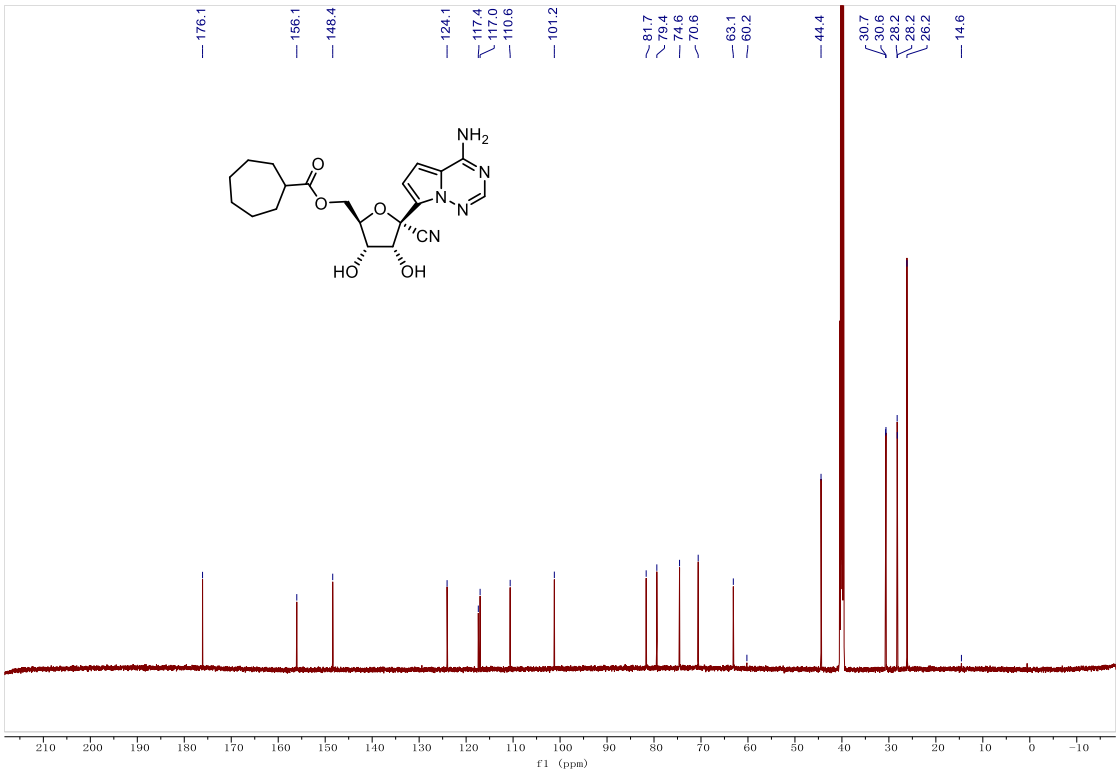

**3-4**

$^{1}$H NMR:

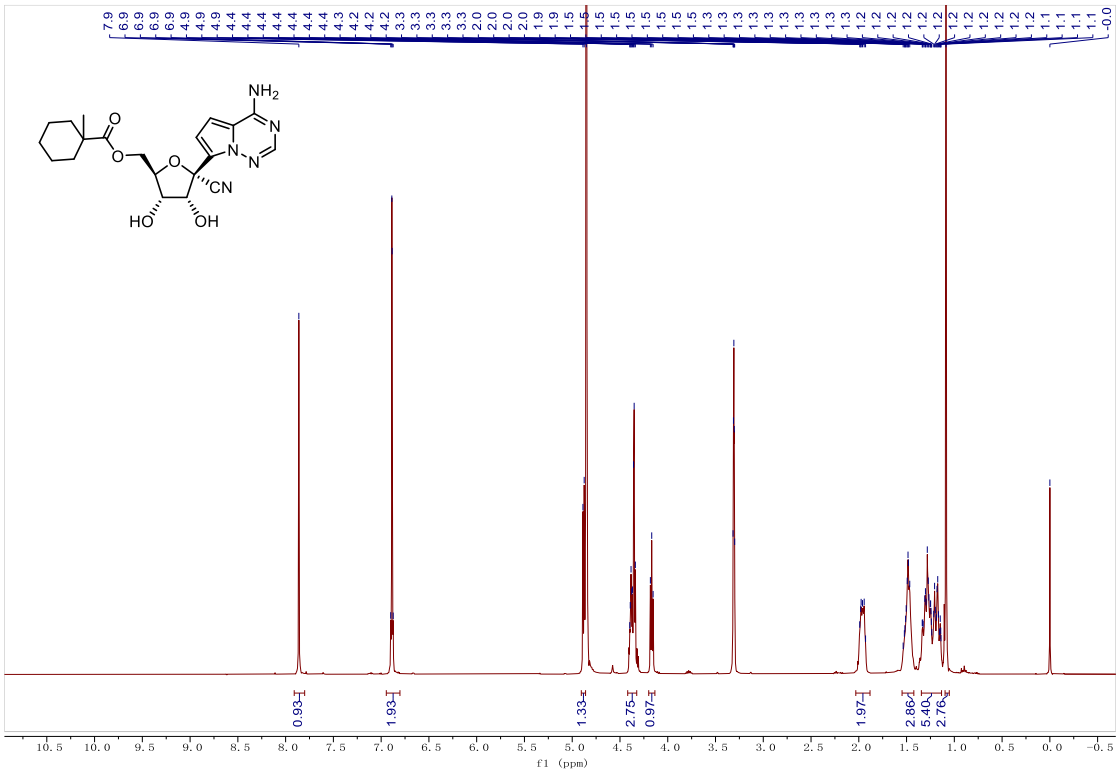


$^{13}$C NMR:

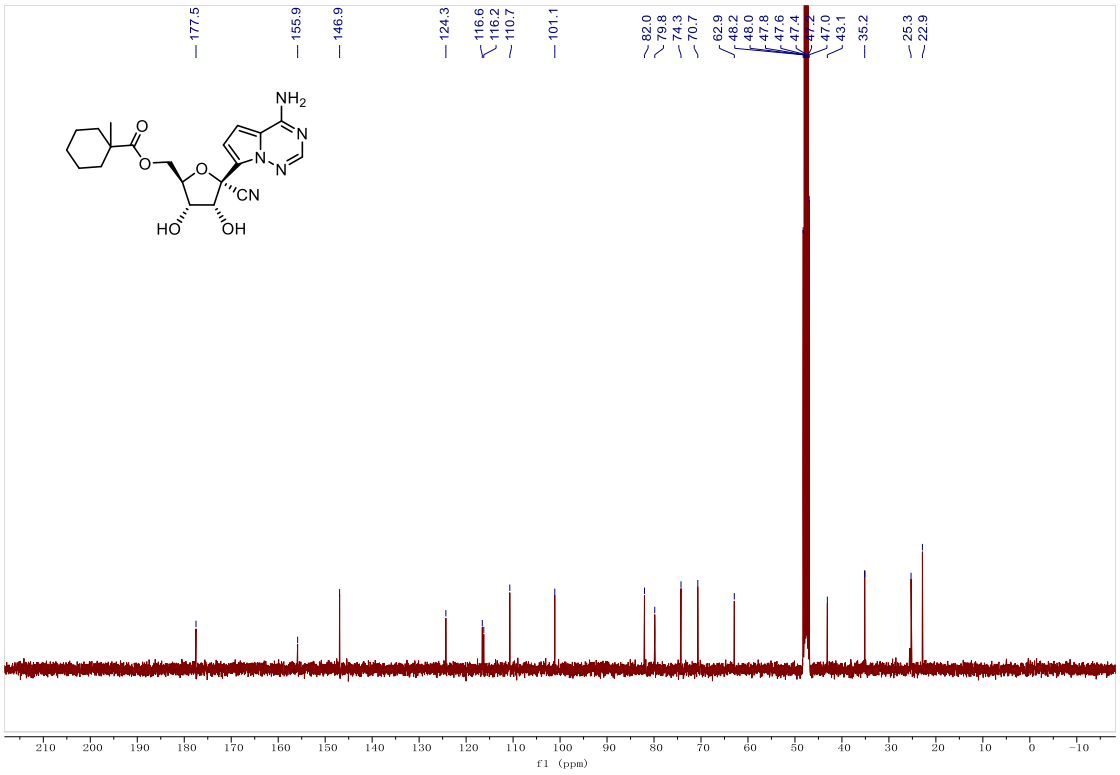

## 3-5

$^{1}$H NMR:

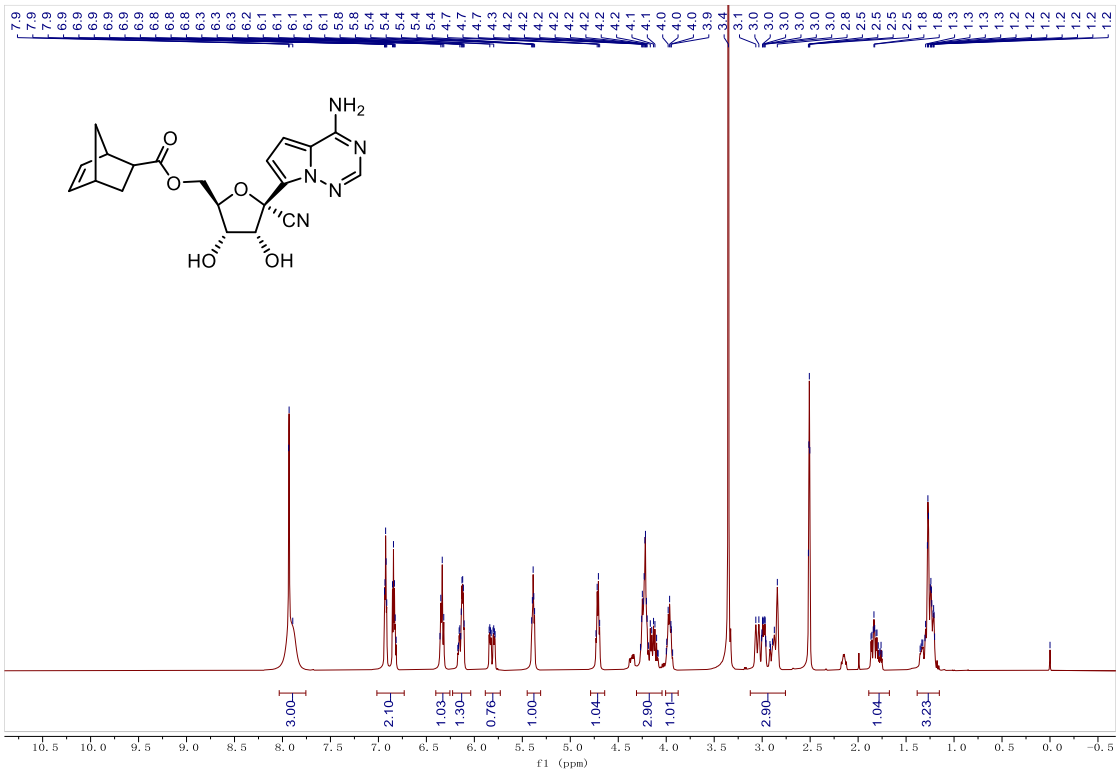


$^{13}$C NMR:

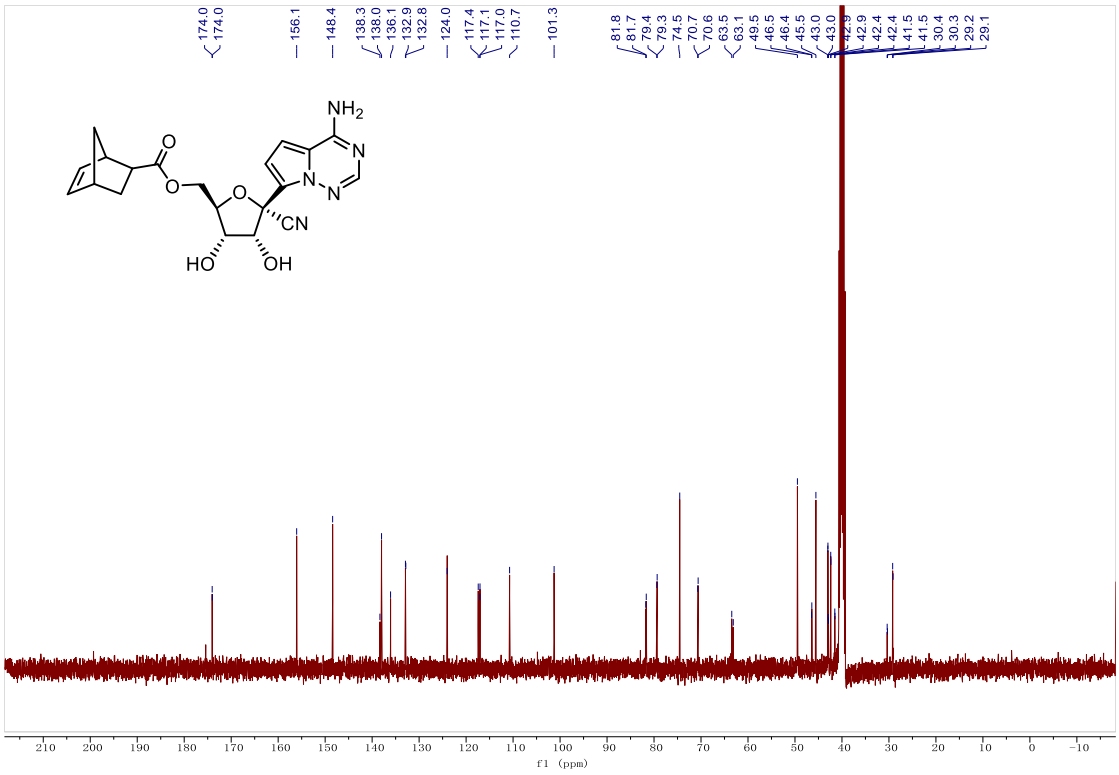

## 3-6

$^{1}$H NMR:

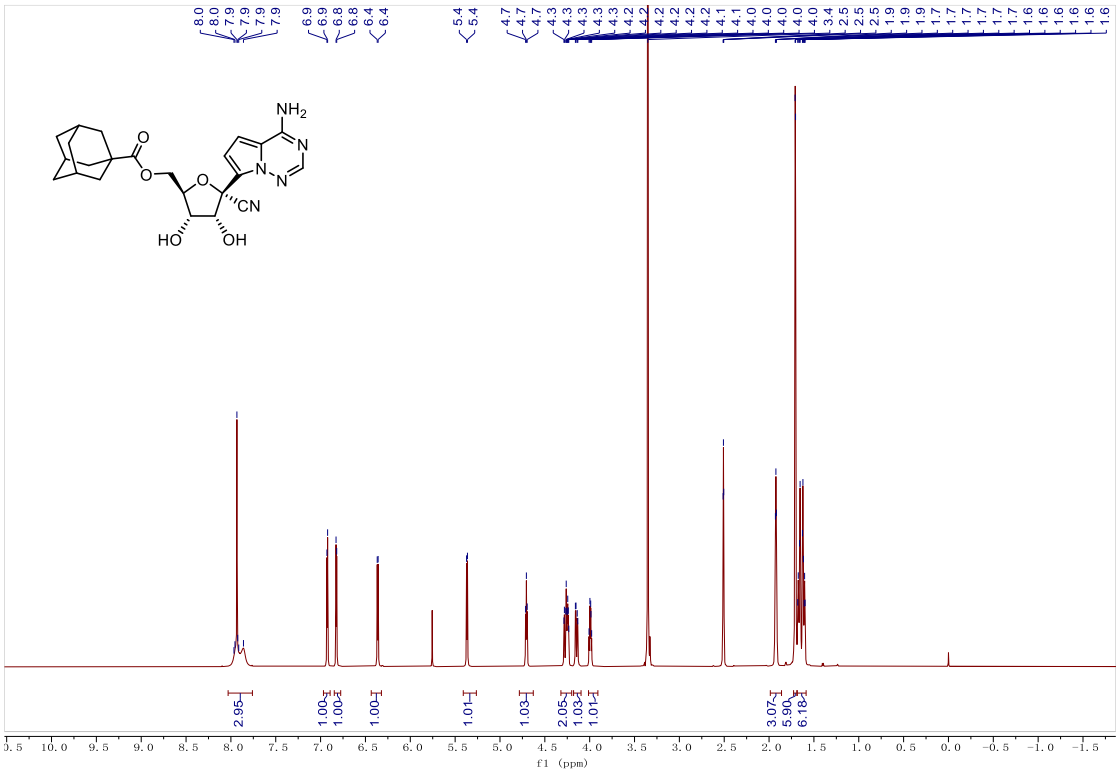


$^{13}$C NMR:

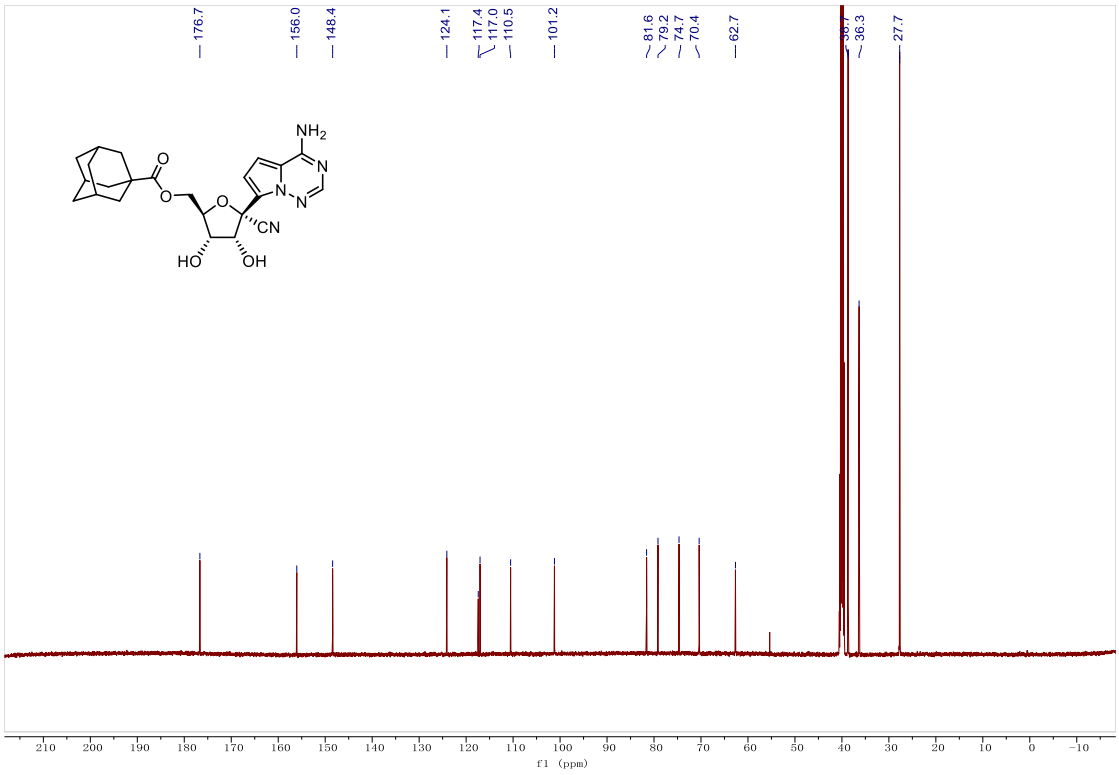

**3-7**

$^{1}$H NMR:

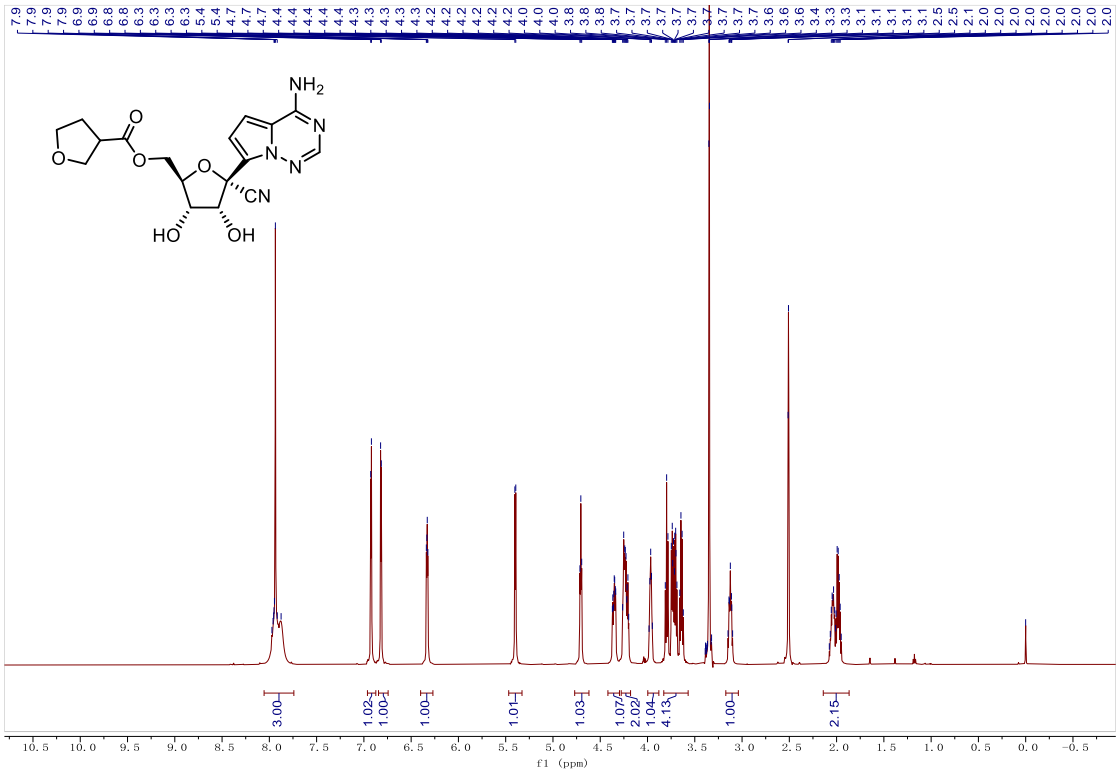


$^{13}$C NMR:

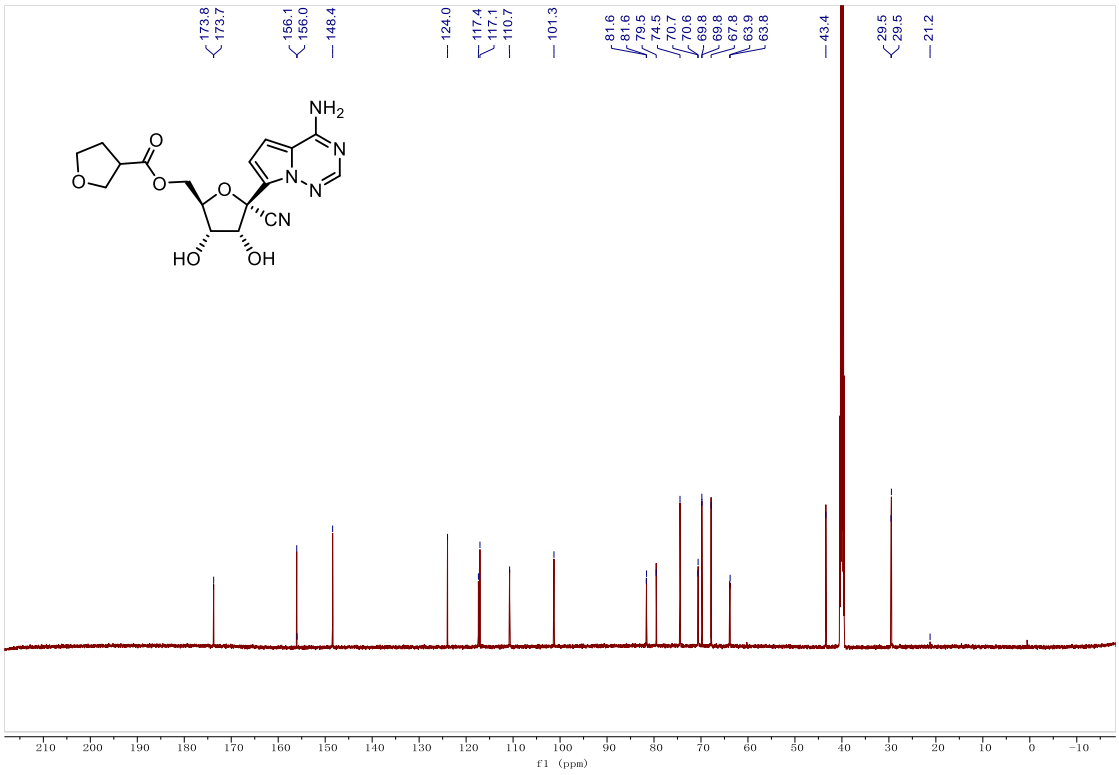

**3-8**

$^{1}$H NMR:

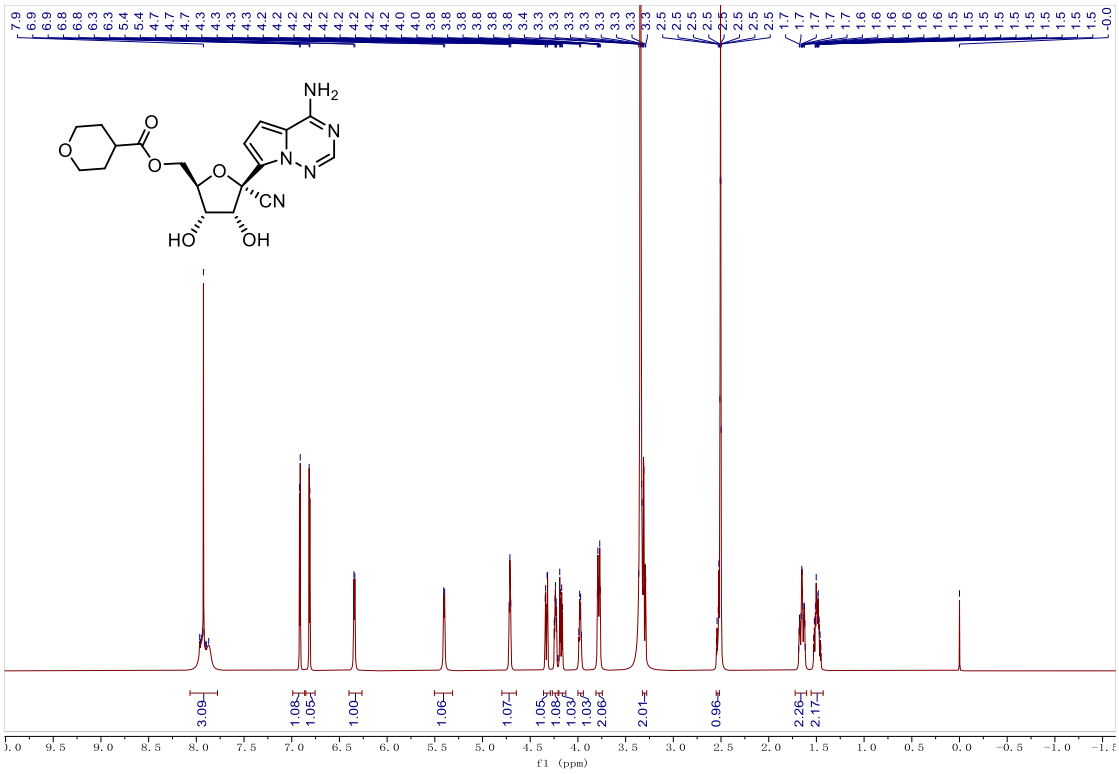


$^{13}$C NMR:

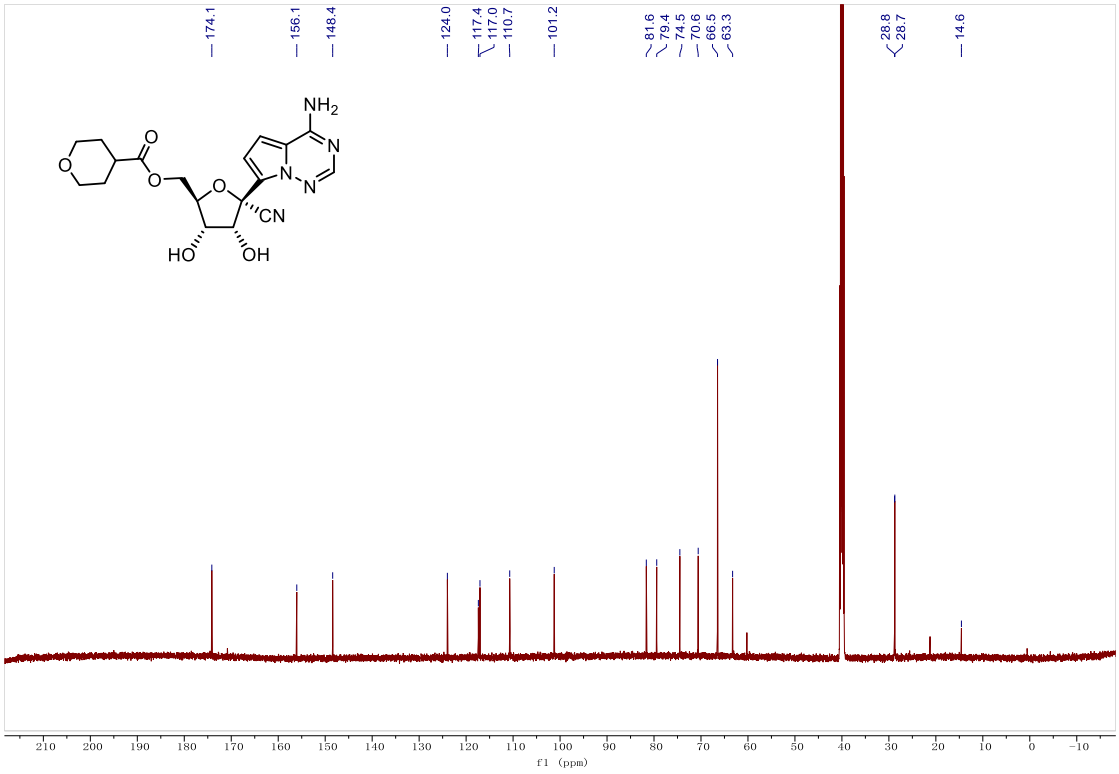

**3-9**

$^{1}$H NMR:

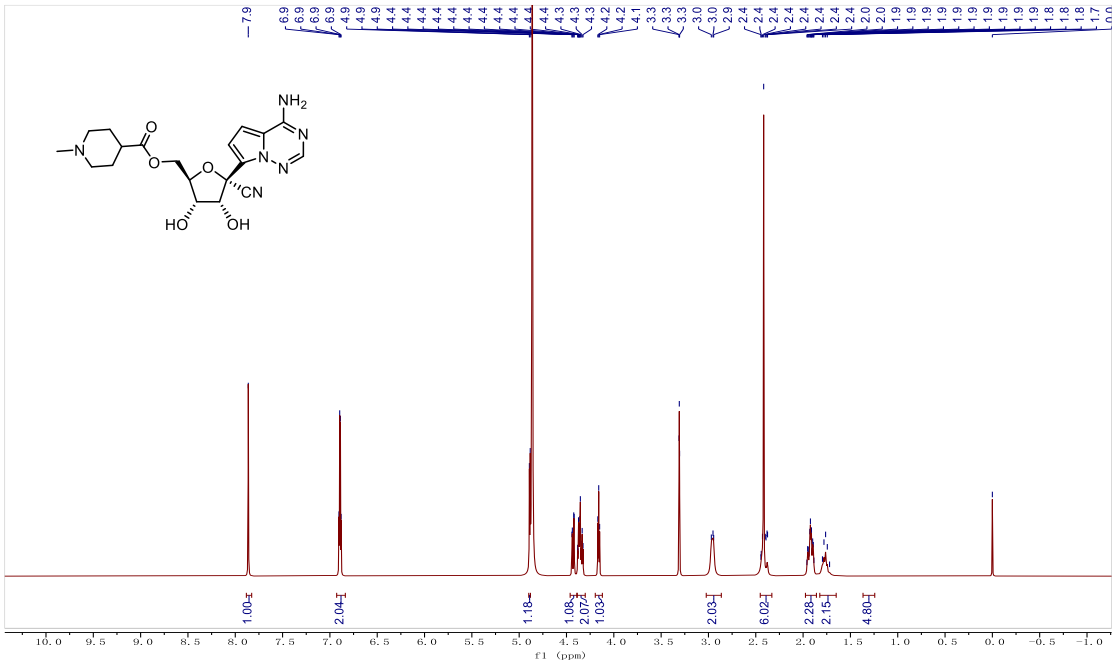


$^{13}$C NMR:

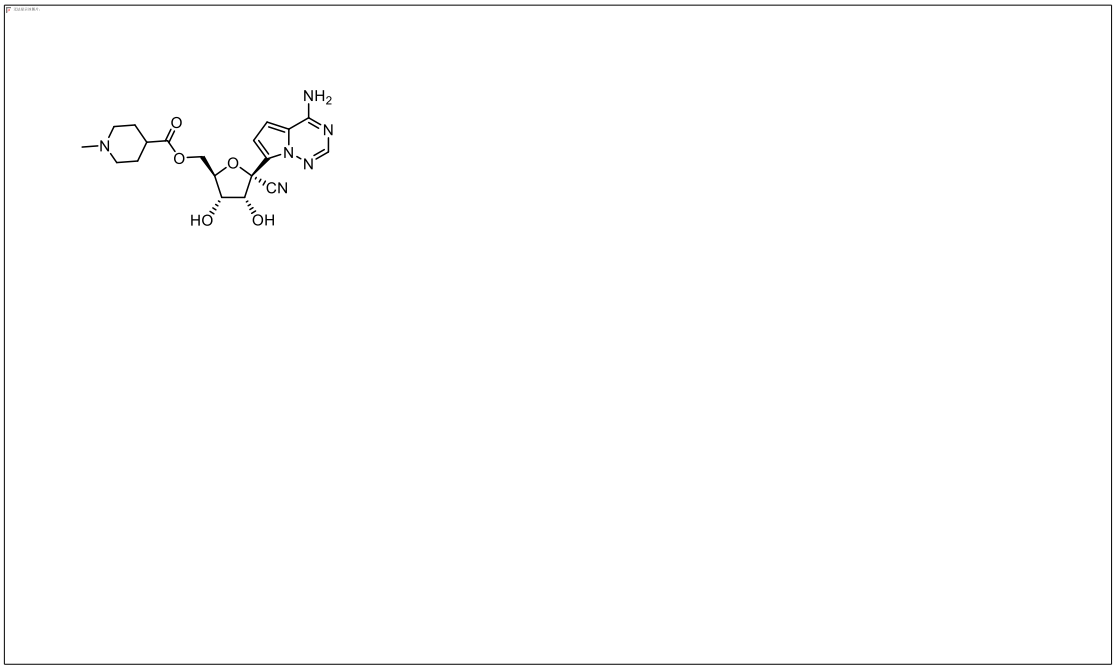

## 3-10

$^{1}$H NMR:

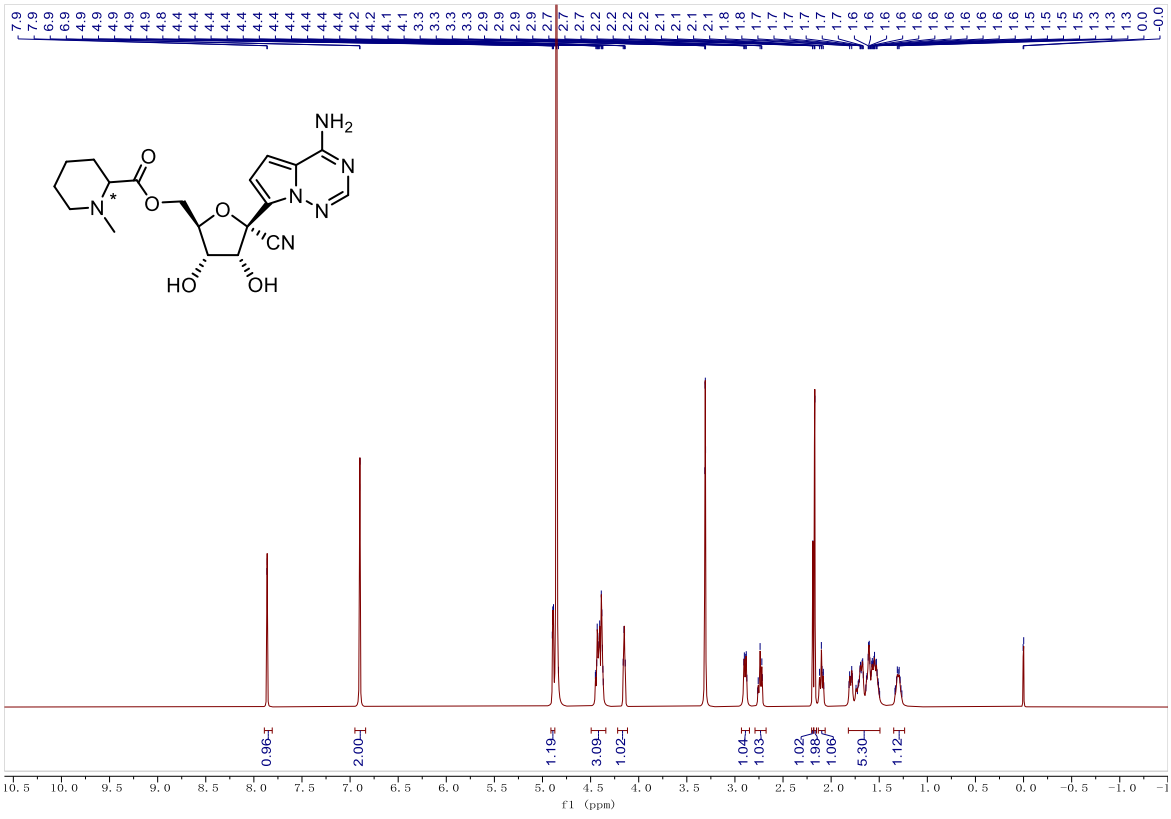


$^{13}$C NMR:

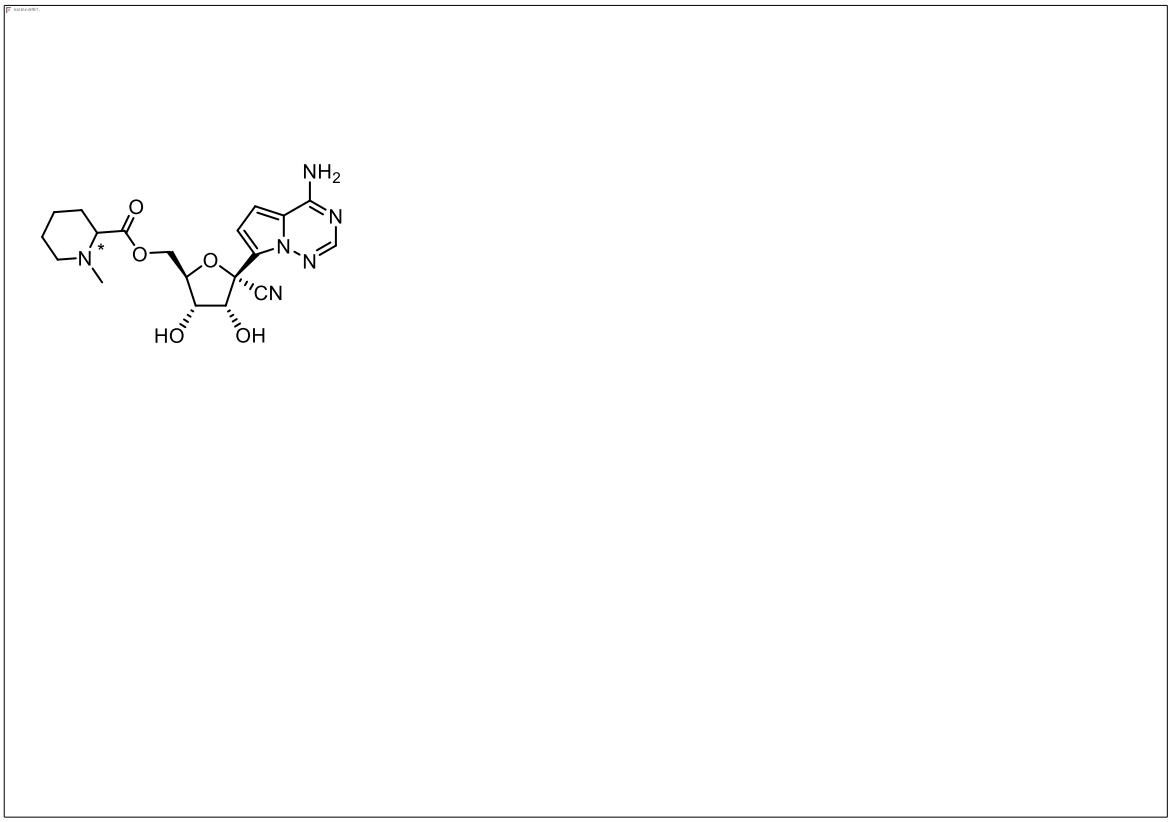

## 3-11

$^{1}$H NMR:

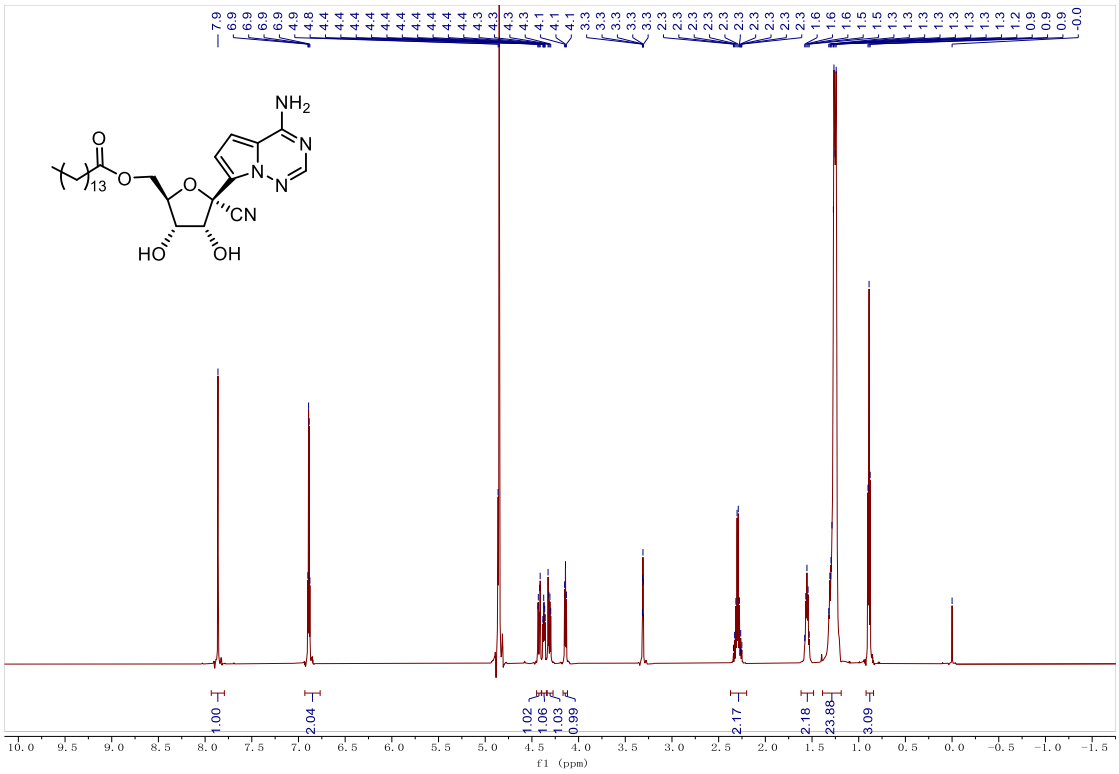


$^{13}$C NMR:

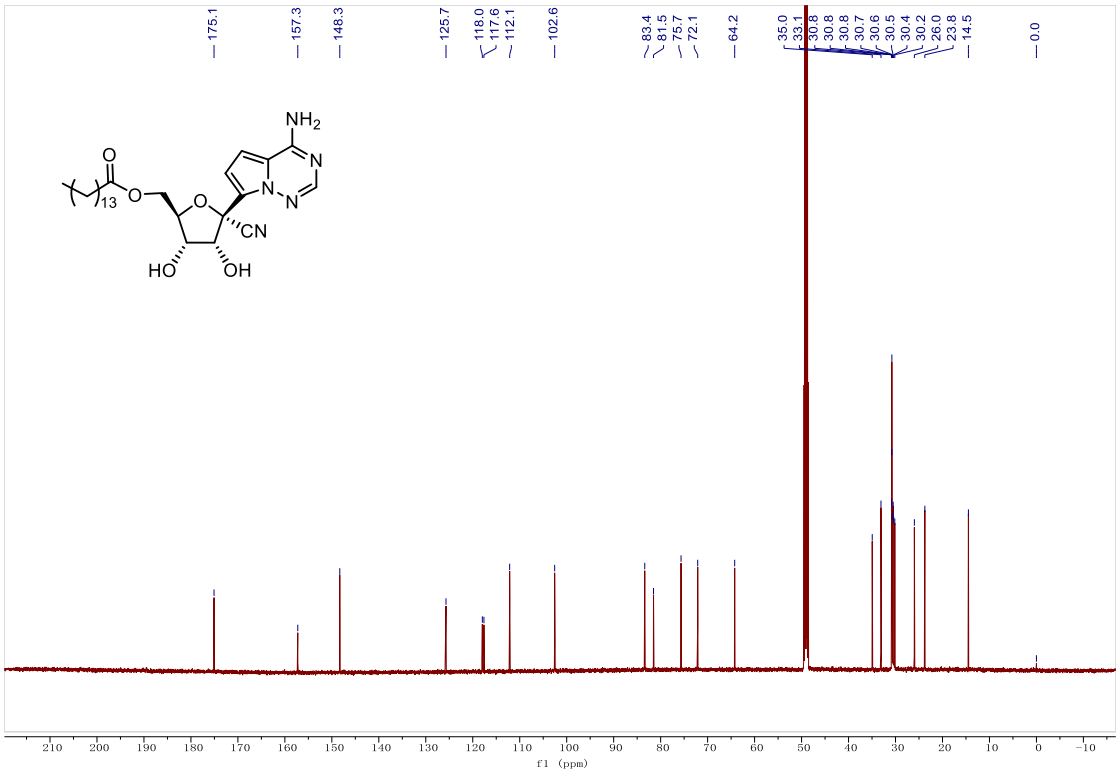

## 3-12

$^{1}$H NMR:

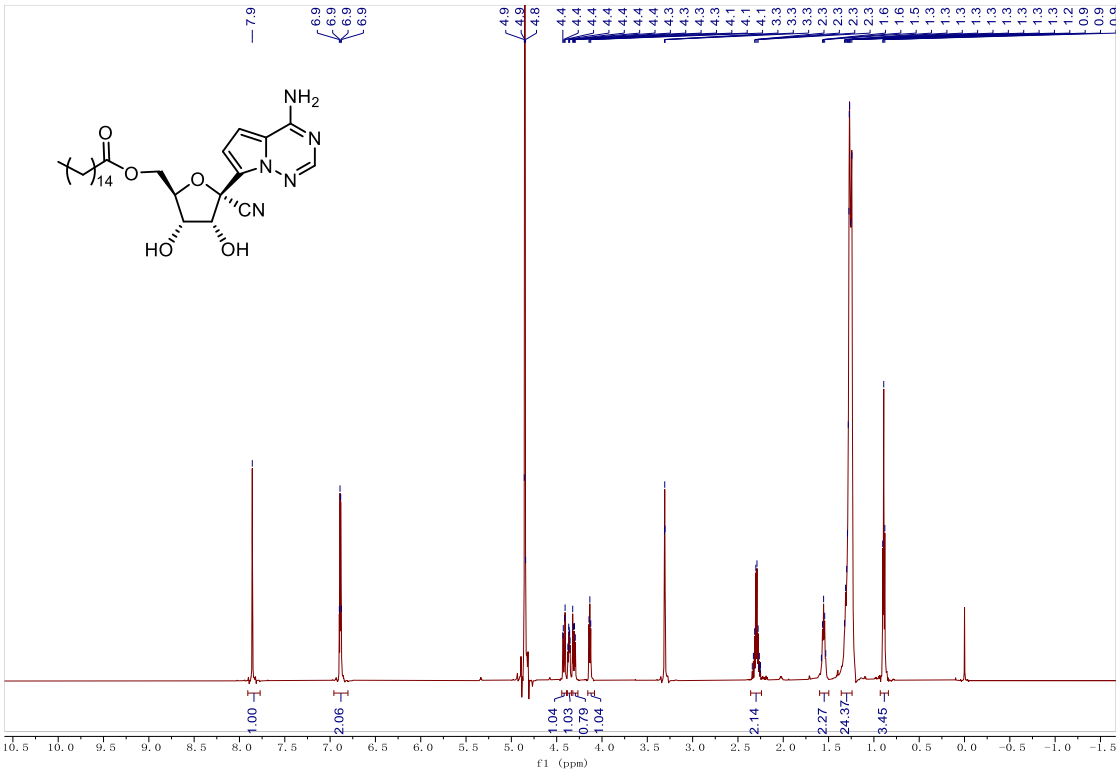


$^{13}$C NMR:

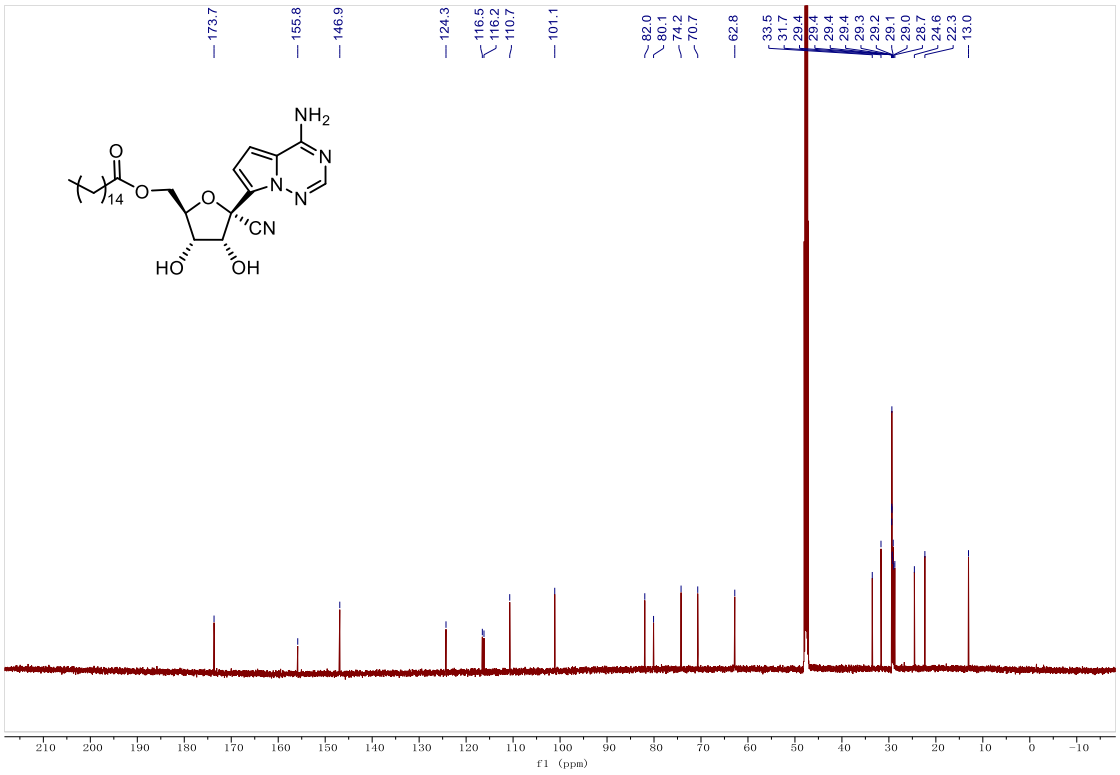

## 3-13

$^{1}$H NMR:

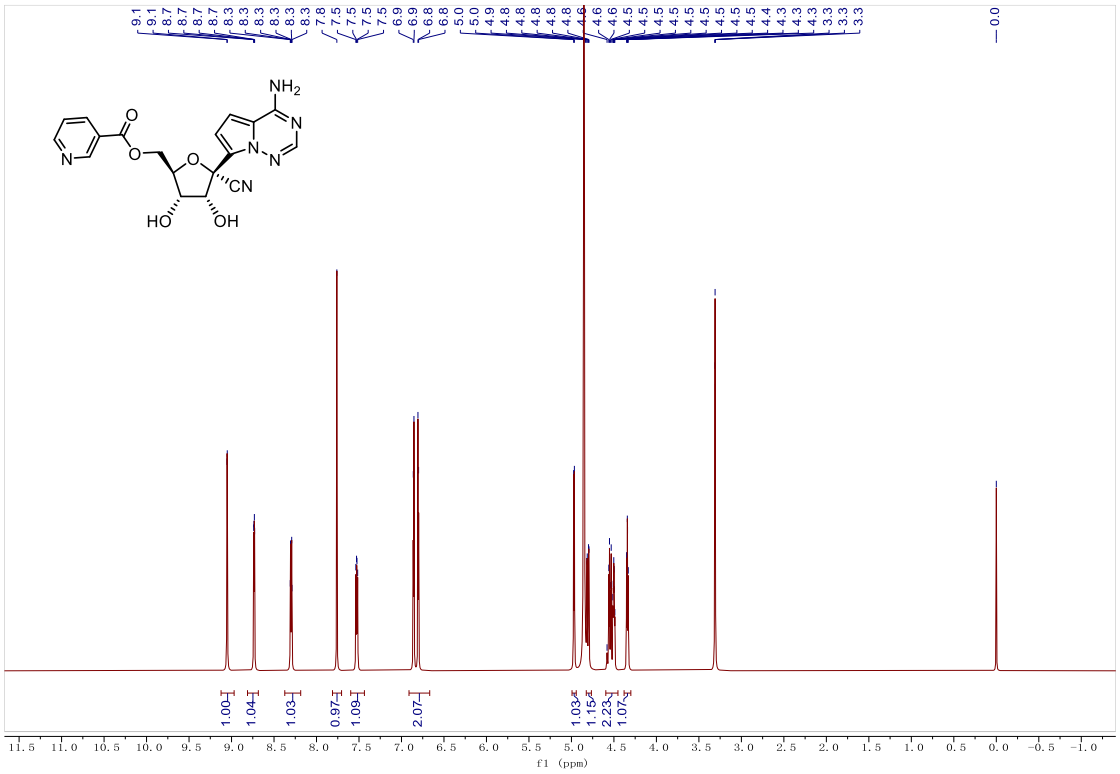


$^{13}$C NMR:

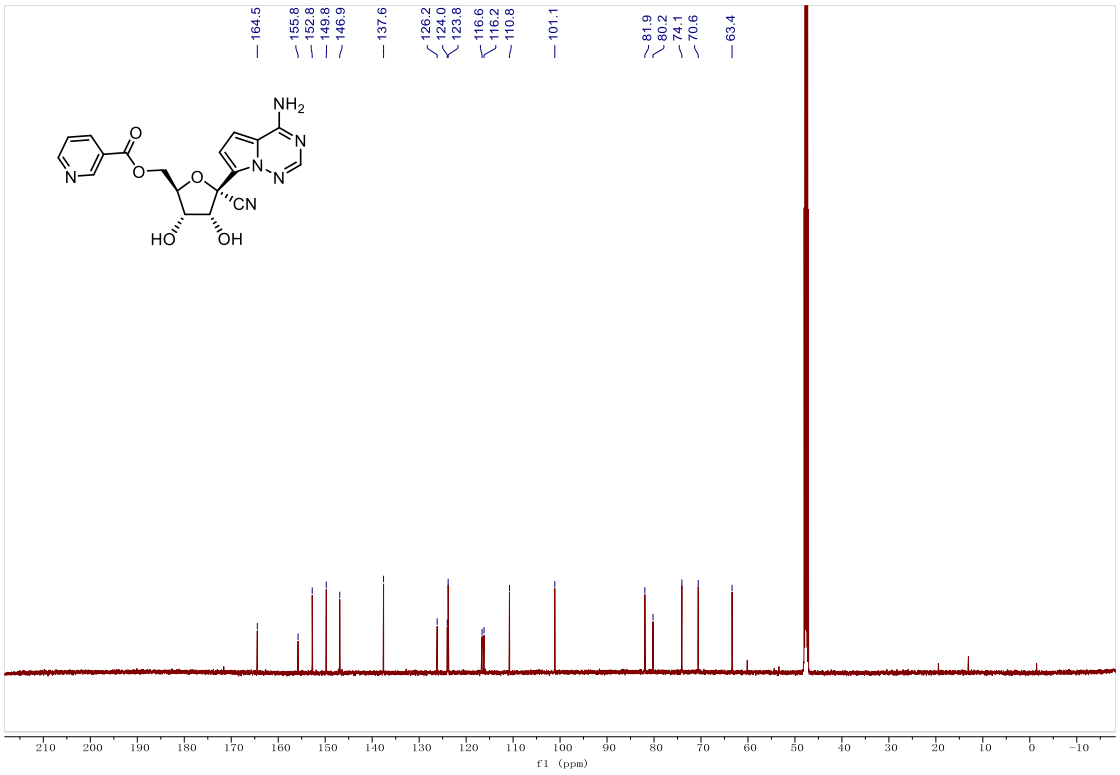

## 3-15

$^{1}$H NMR:

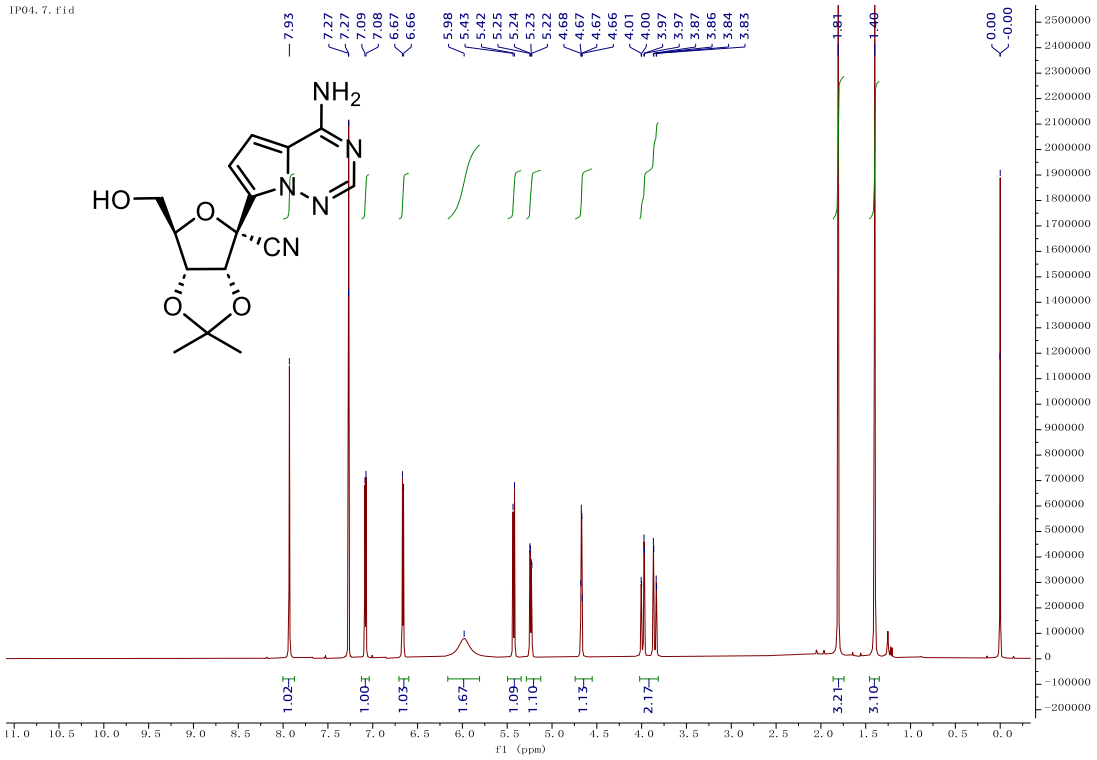


$^{13}$C NMR:

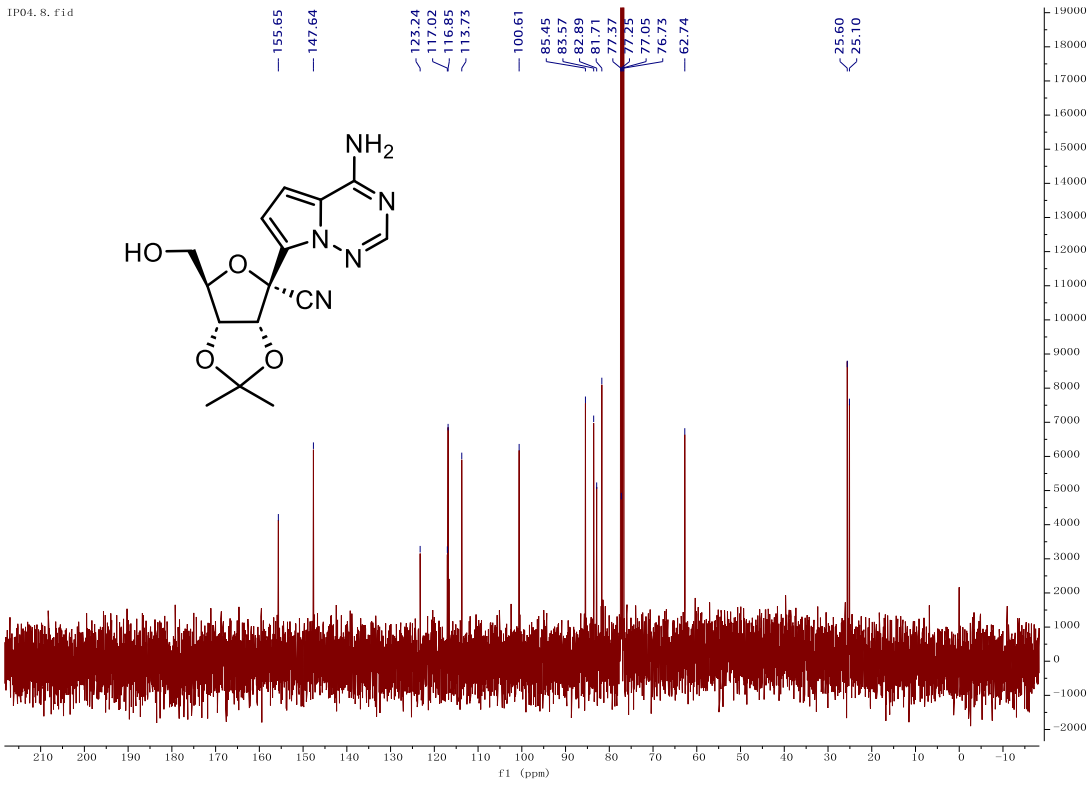

## ATV-014

$^{1}$H NMR:

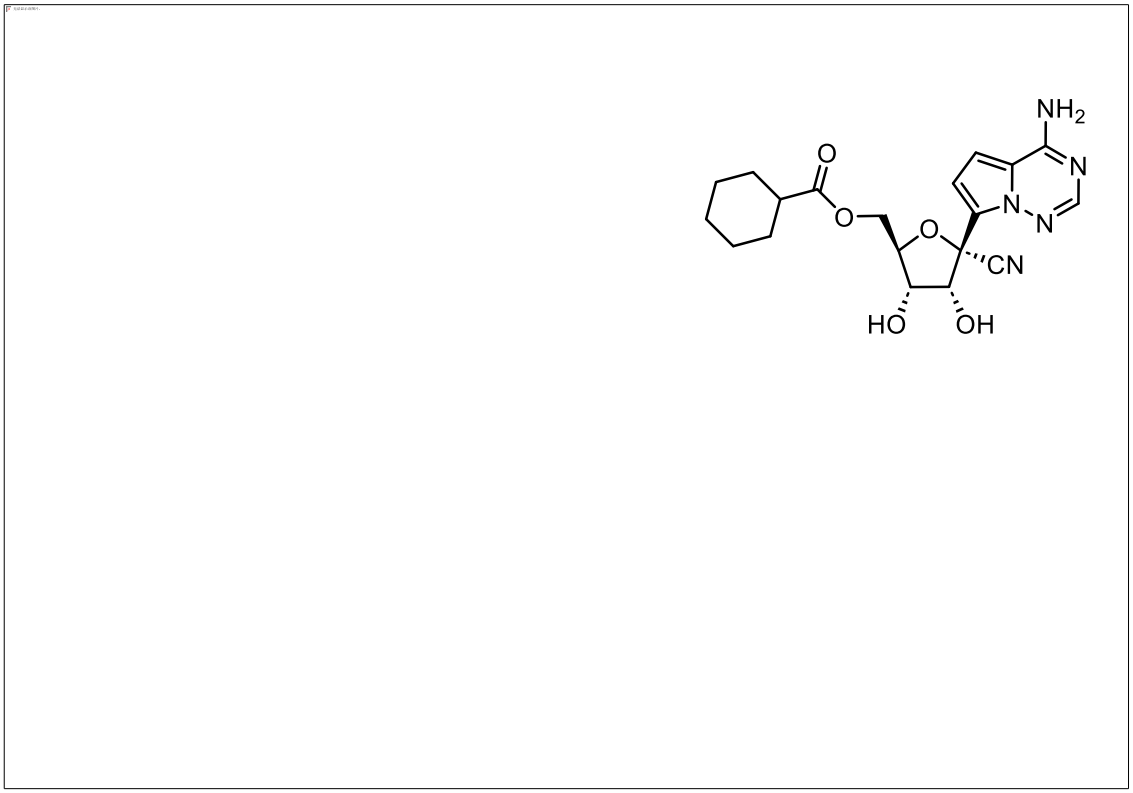


$^{13}$C NMR:

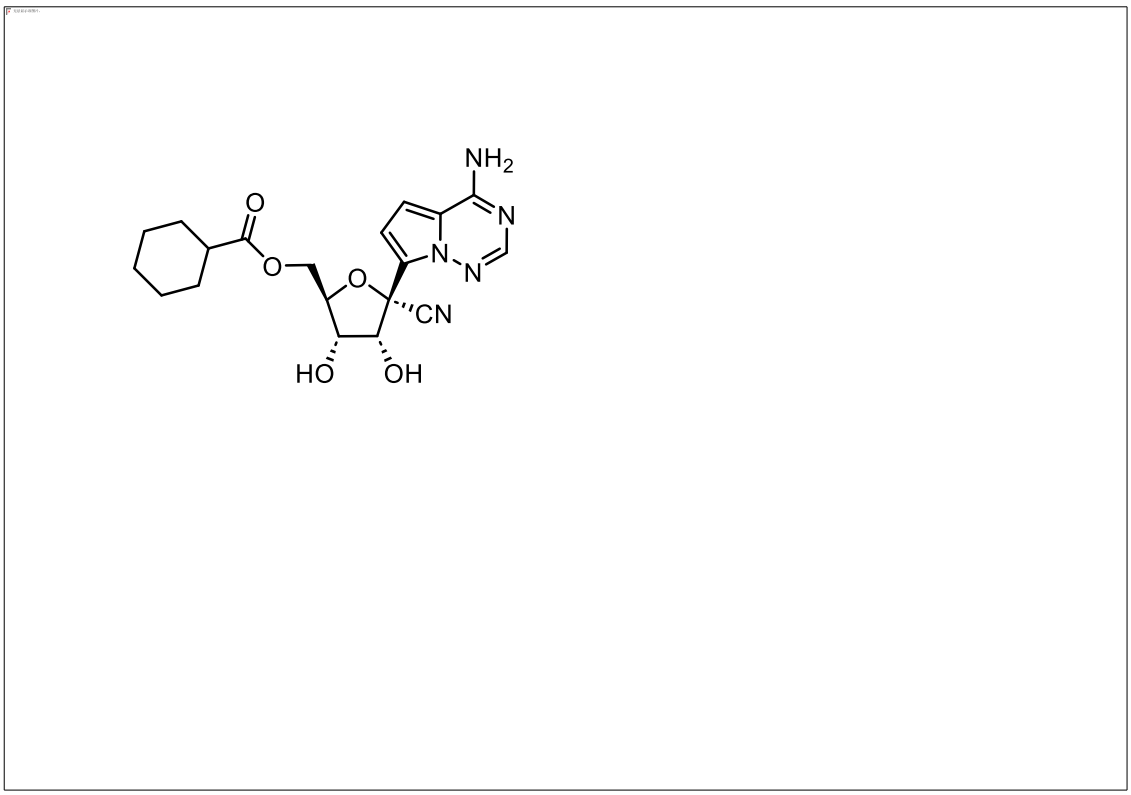

## GS-441524

$^{1}$H NMR:

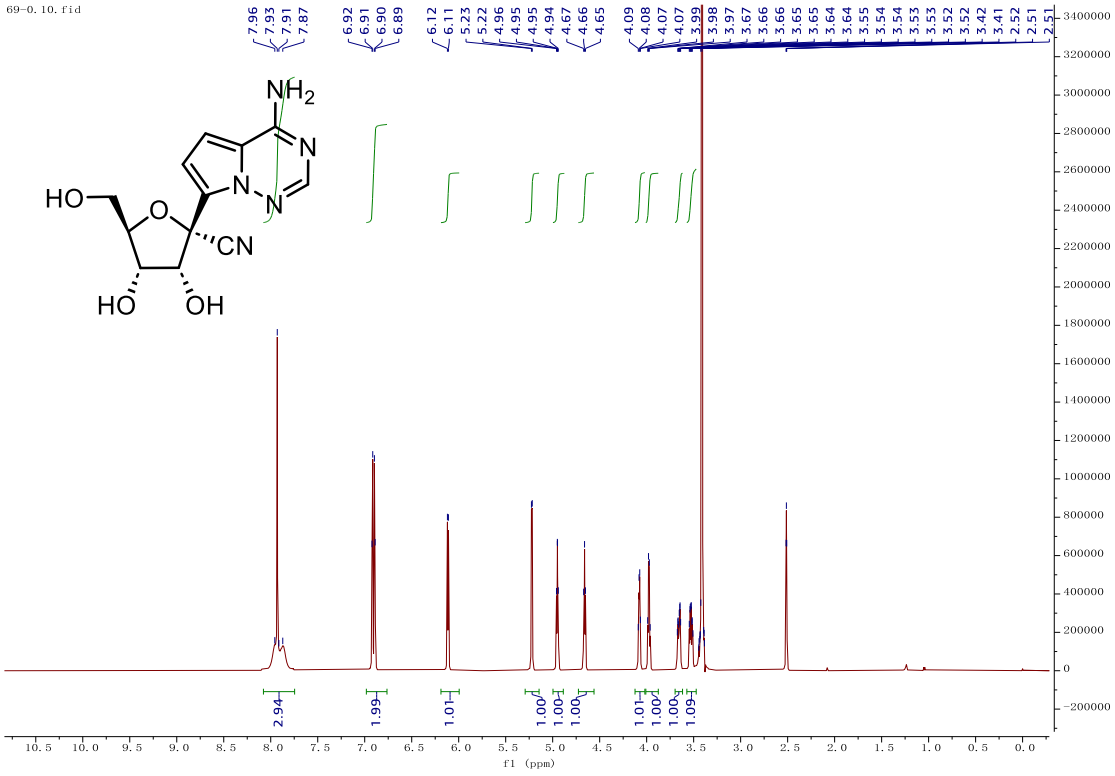


$^{13}$C NMR:

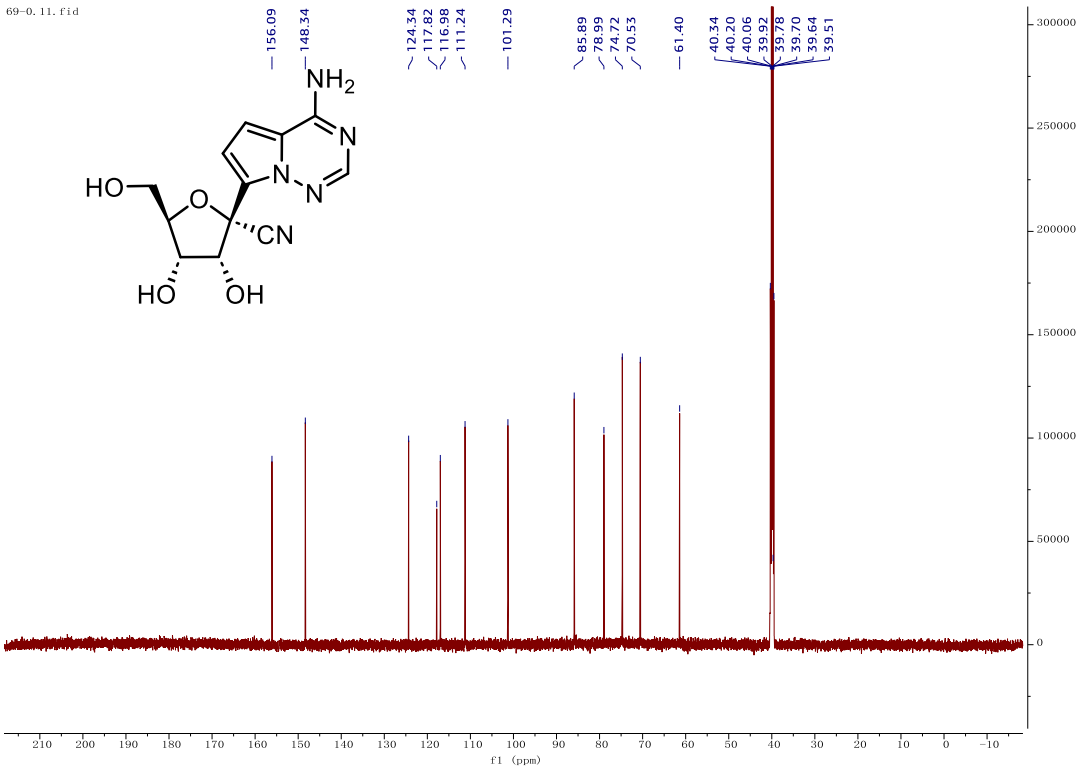

**3-17**

$^{1}$H NMR:

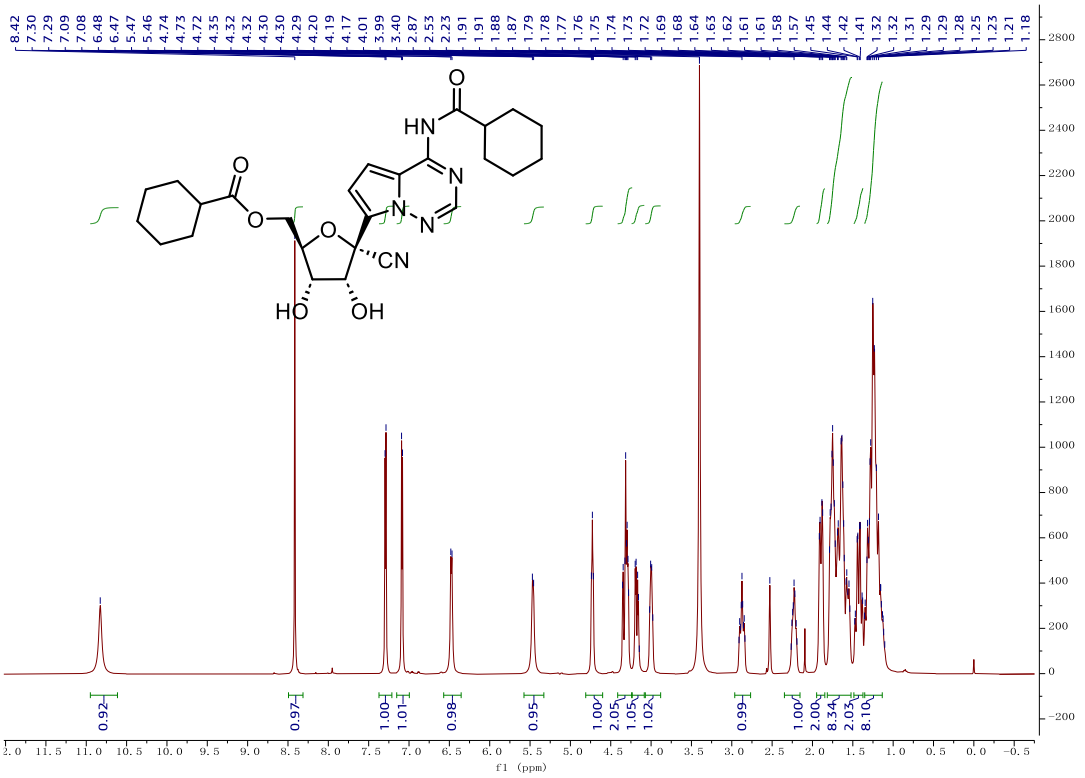


$^{13}$C NMR:

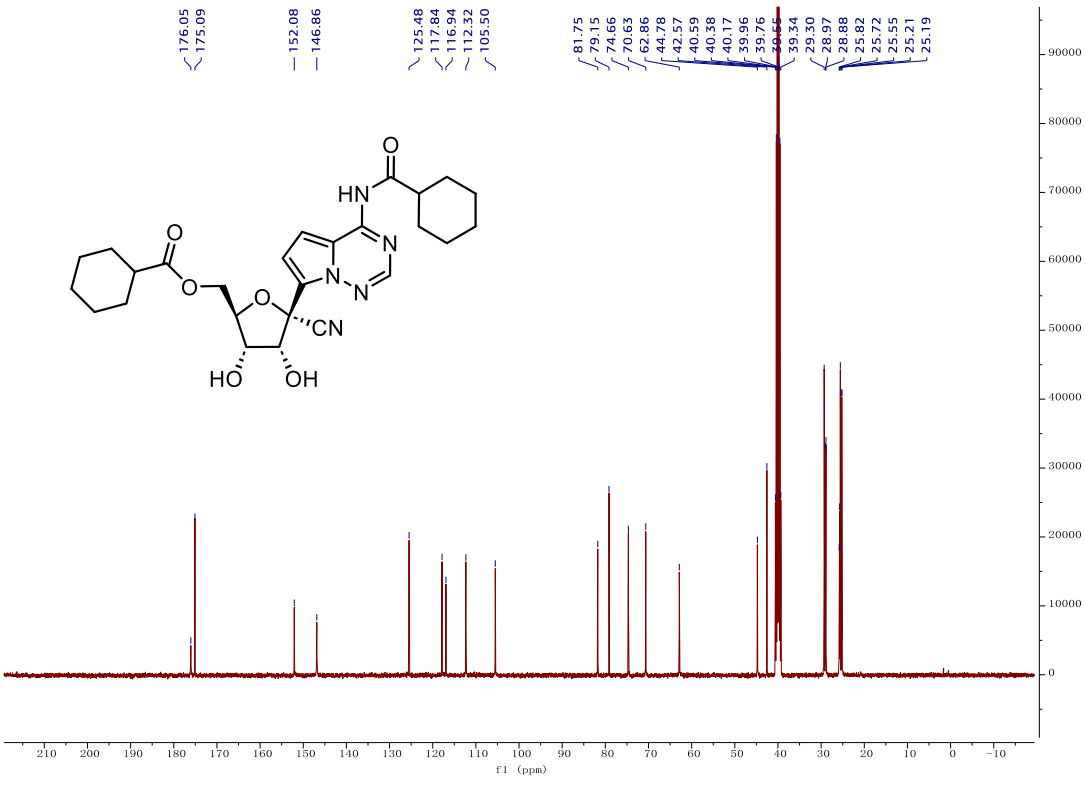

**3-19**

$^{1}$H NMR:

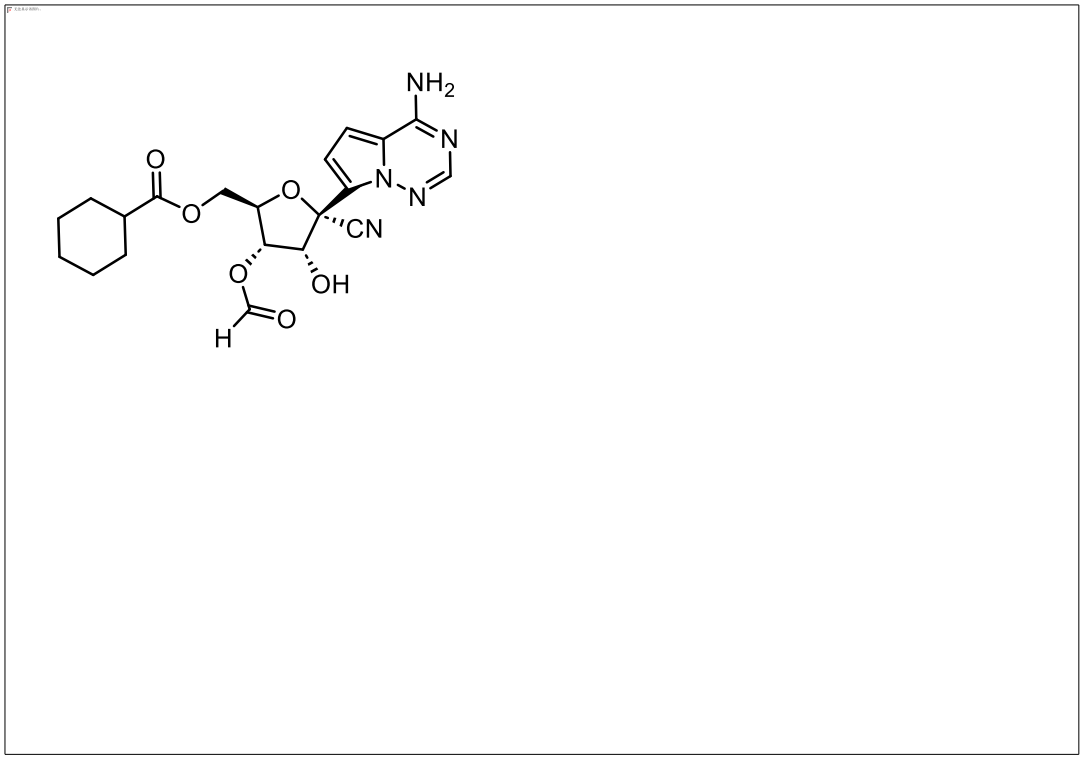


$^{13}$C NMR:

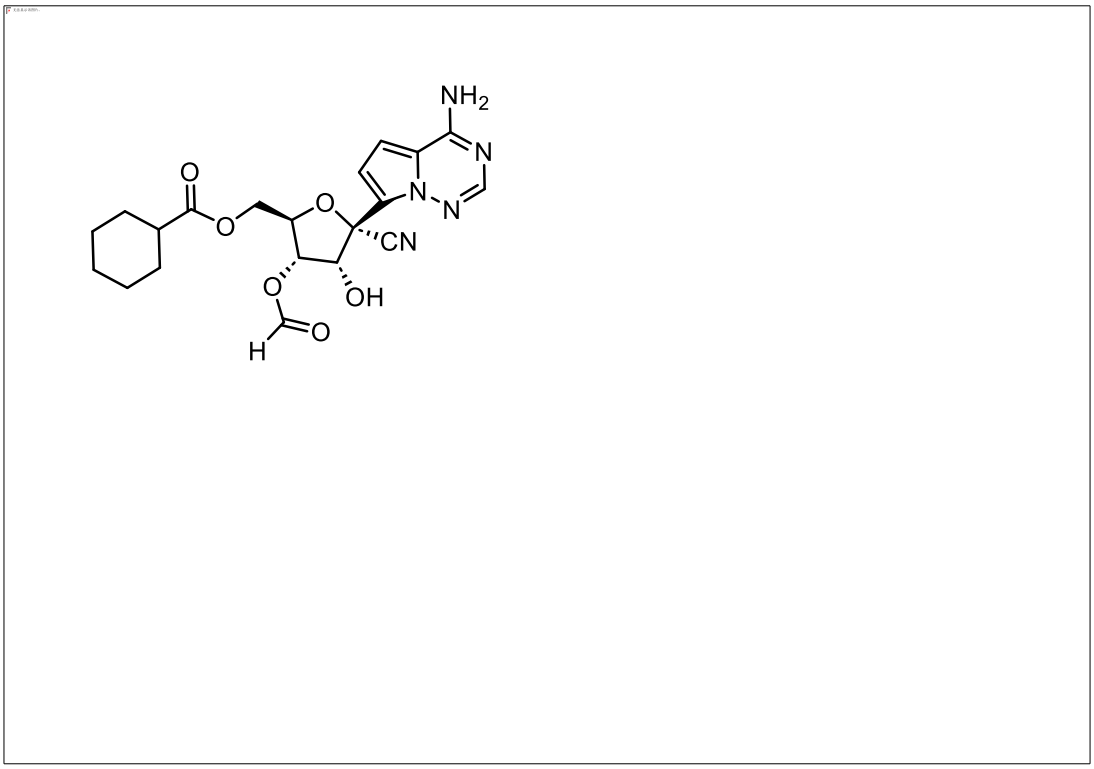

**3-20**

$^{1}$H NMR:

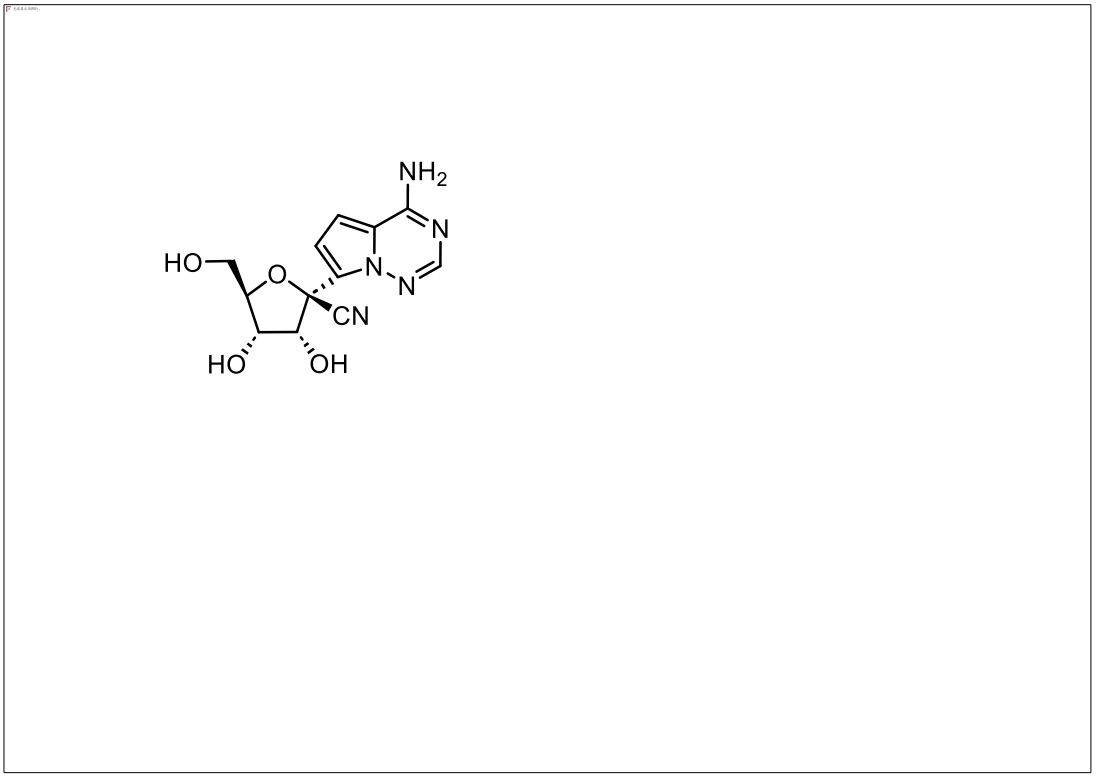

## 3-21

$^{1}$H NMR:

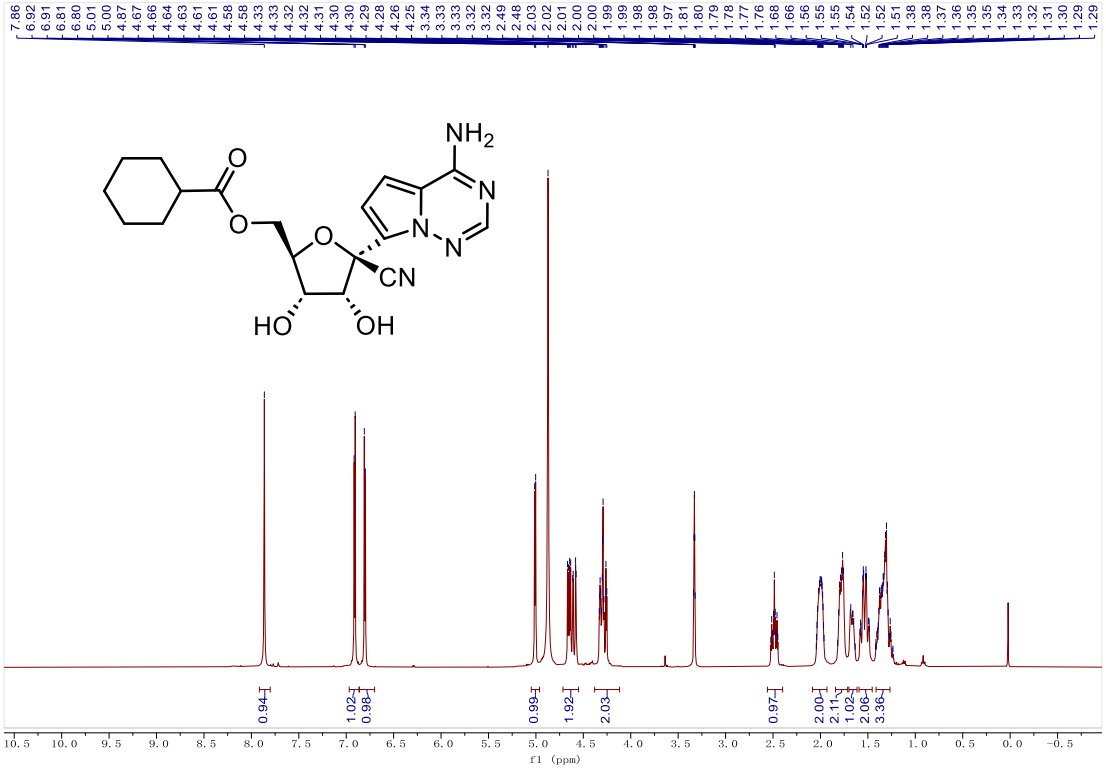

**4-1**

$^{1}$H NMR:

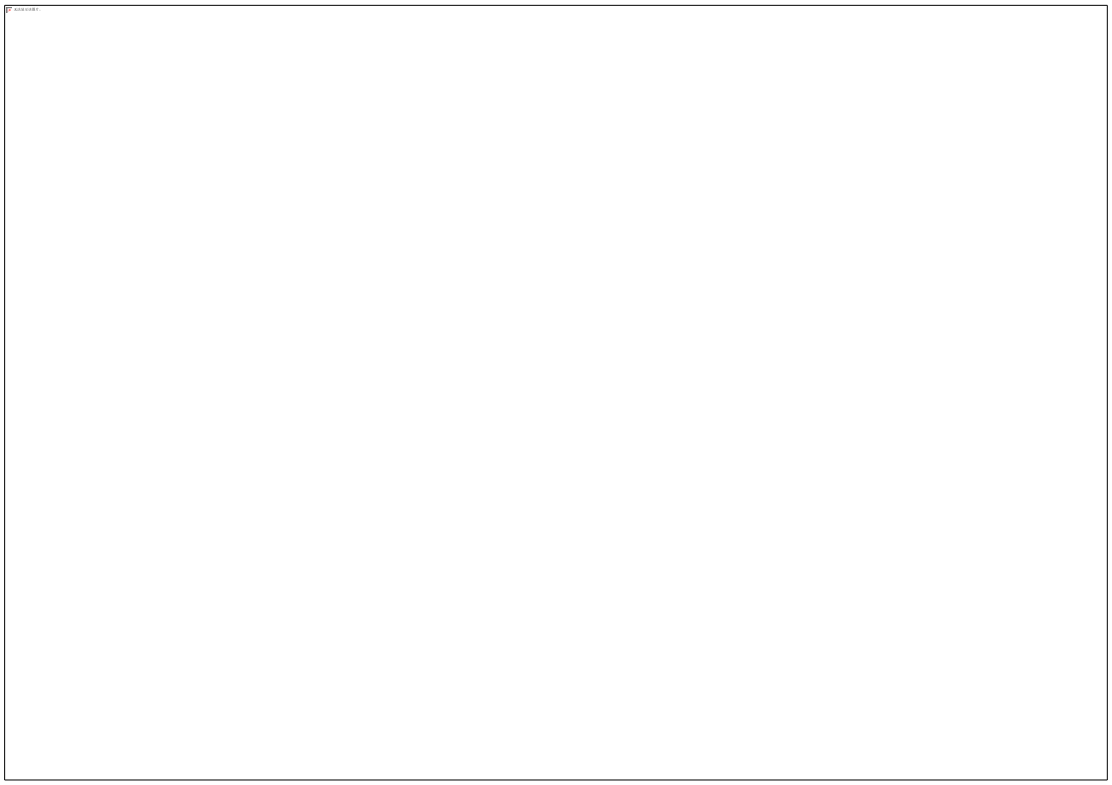

$^{13}$C NMR:

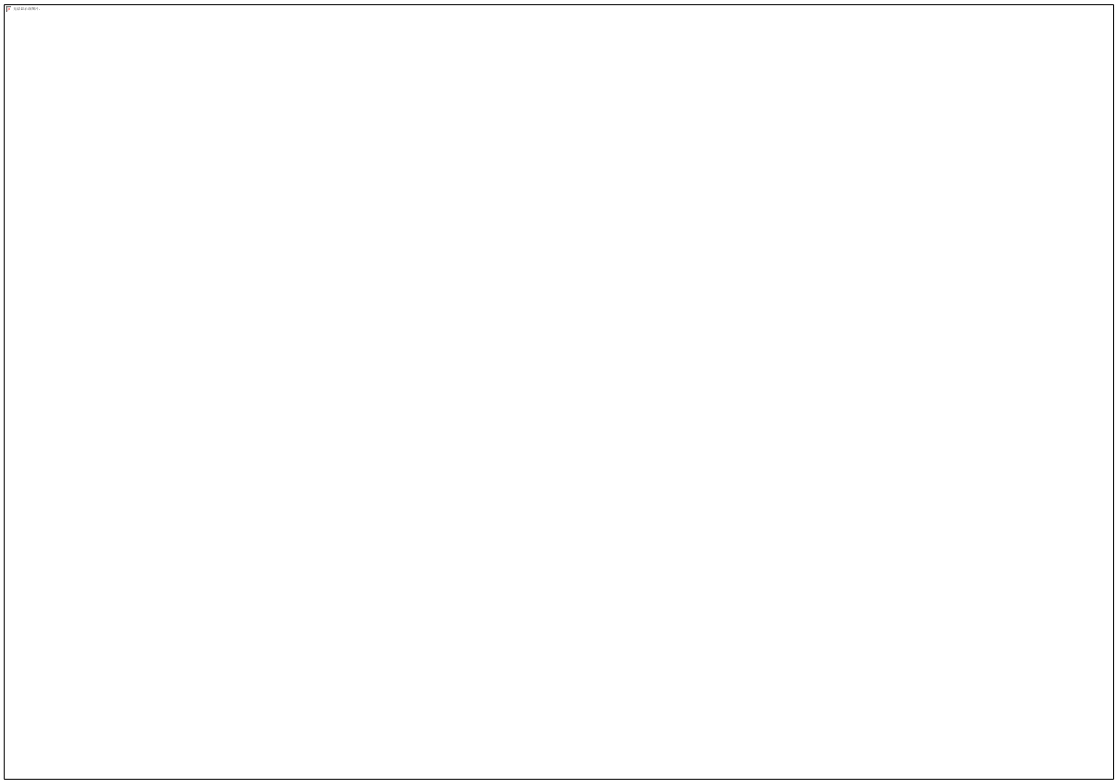

**4-2**

$^{1}$H NMR:

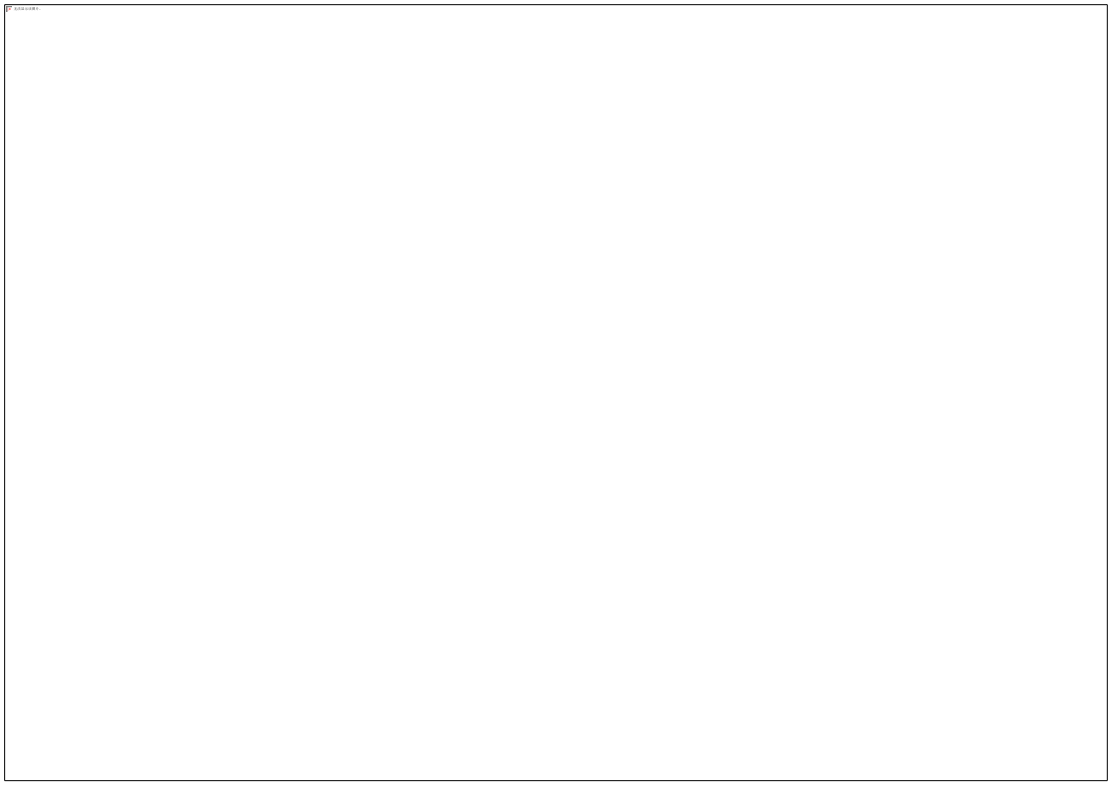

$^{13}$C NMR:

**4-3**

$^{1}$H NMR:

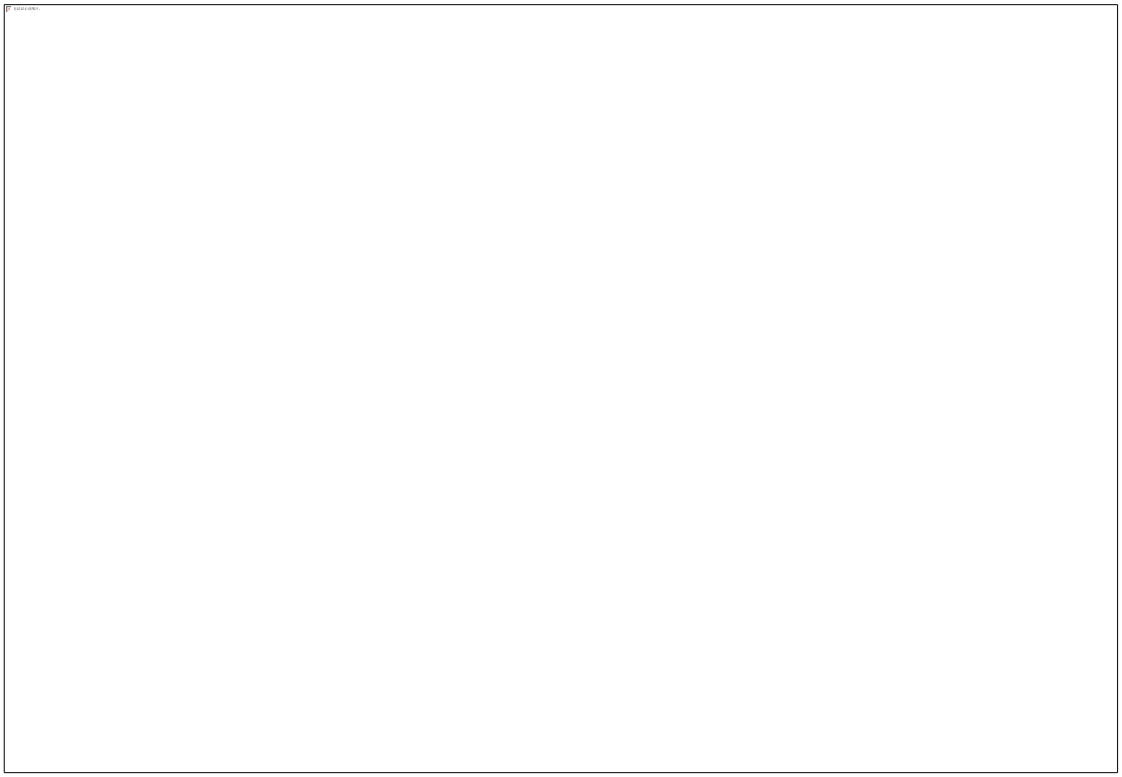

$^{13}$C NMR:

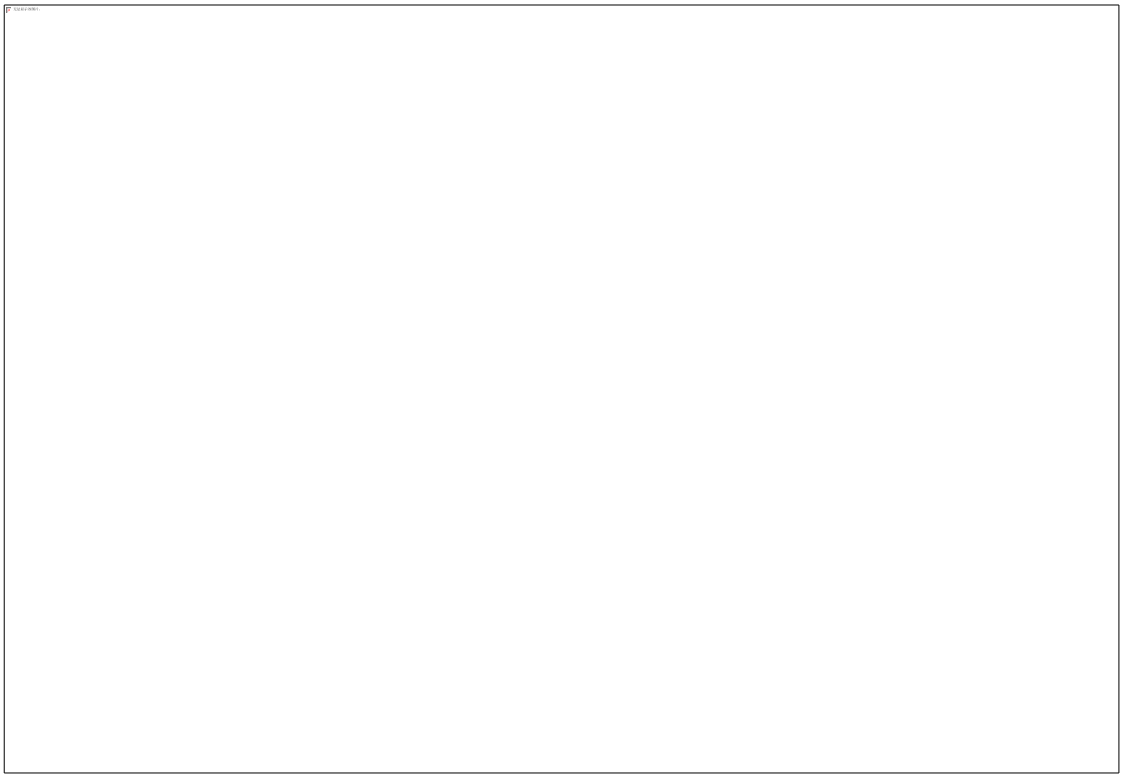

**4-4**

$^{1}$H NMR:

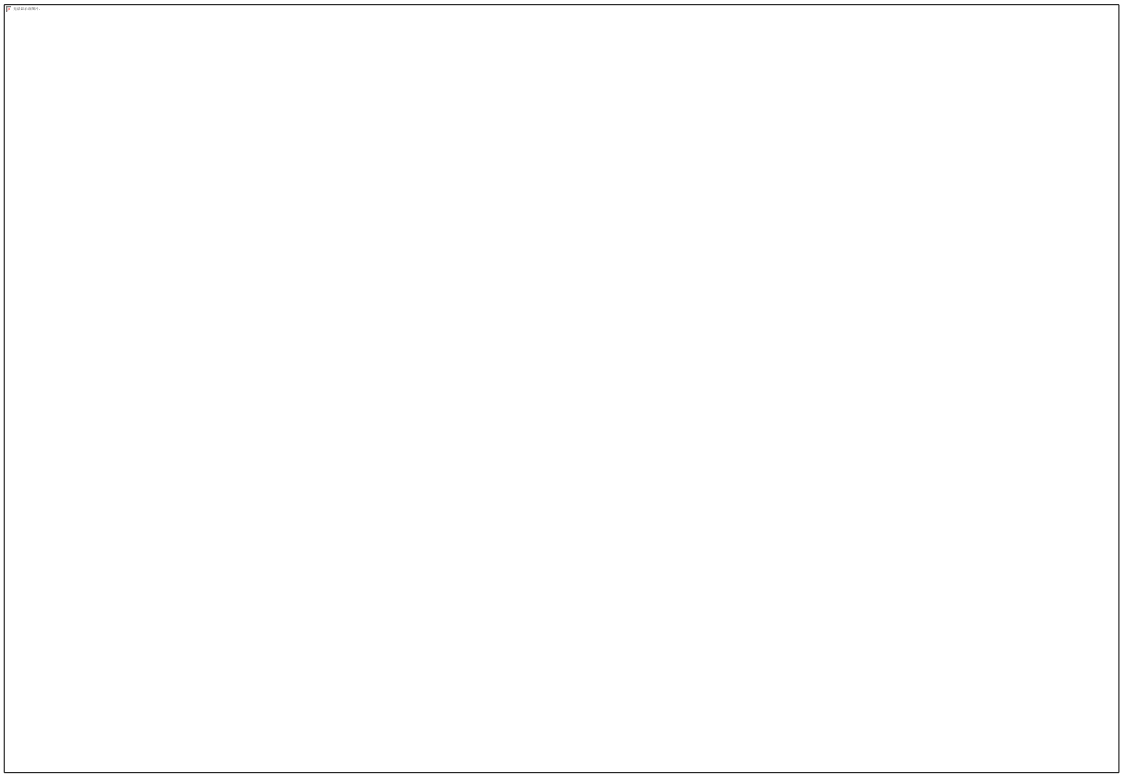

$^{13}$C NMR:

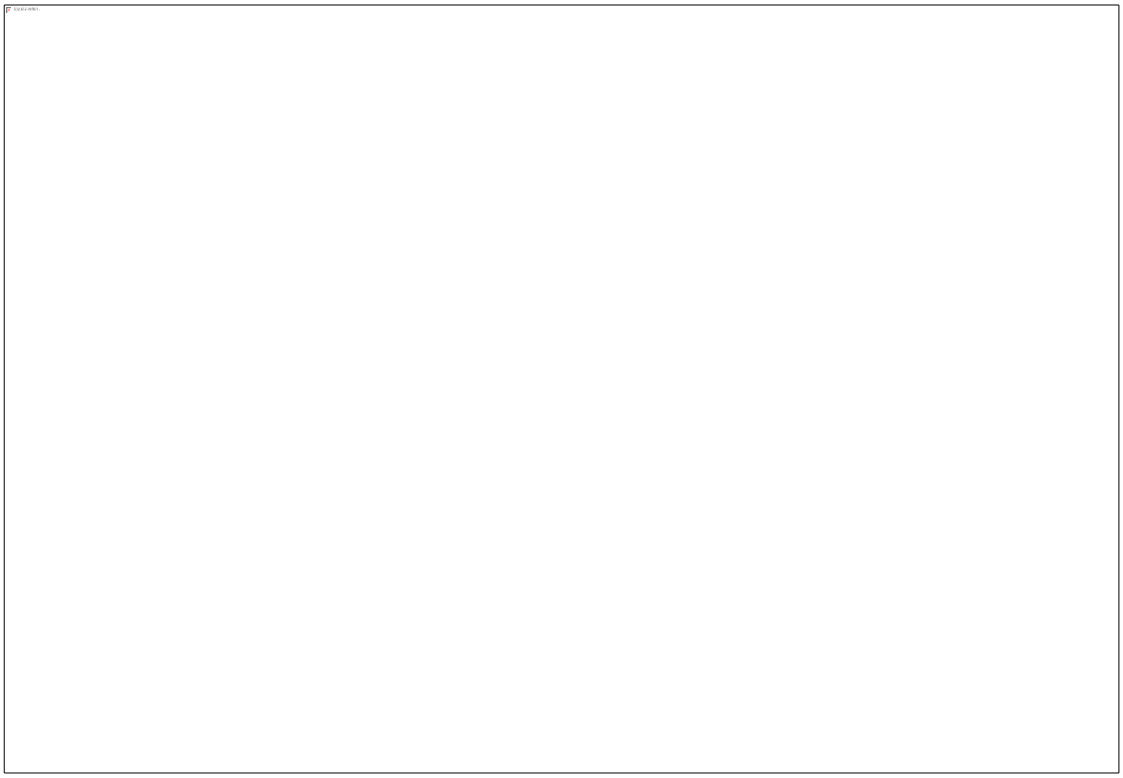

**4-5**

$^{1}$H NMR:

$^{13}$C NMR:

**4-6**

$^{1}$H NMR:

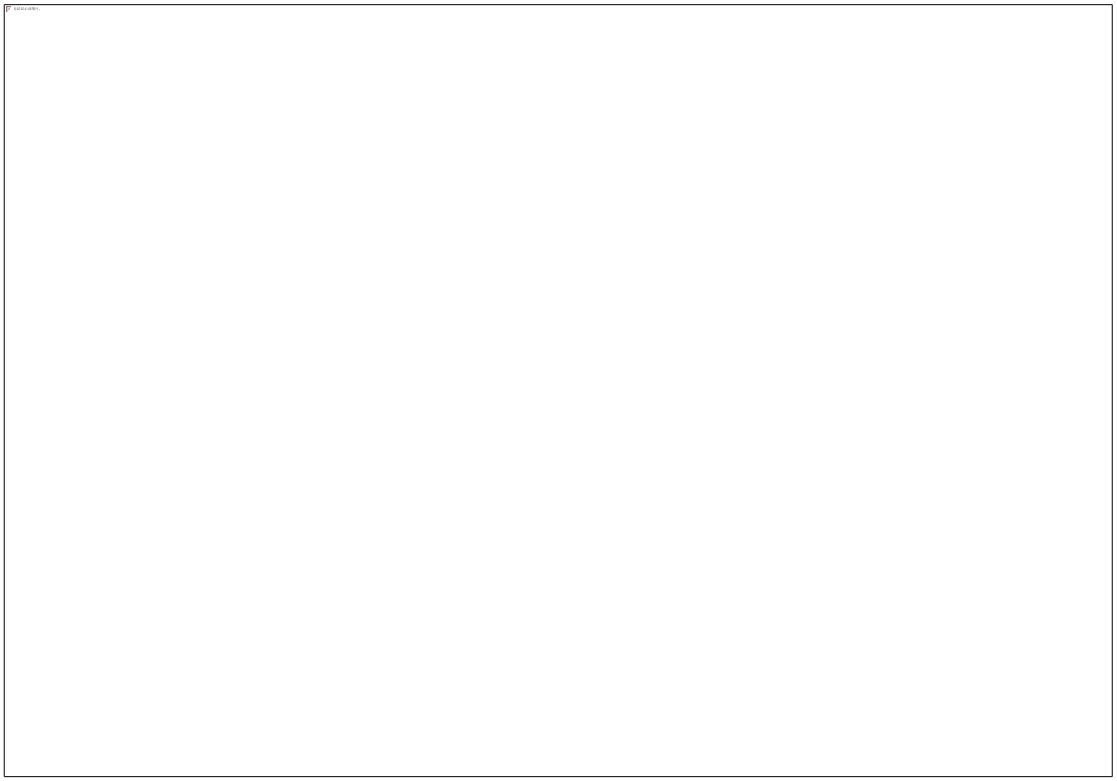

$^{13}$C NMR:

**4-7**

$^{1}$H NMR:

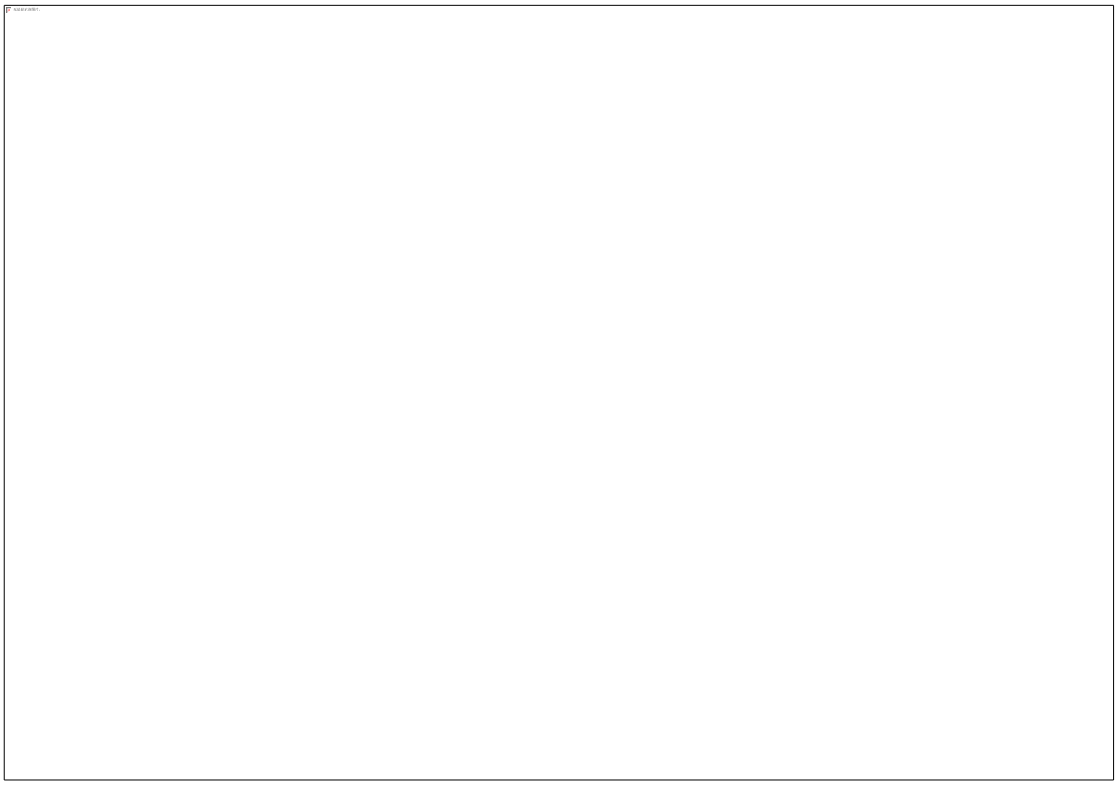

$^{13}$C NMR:

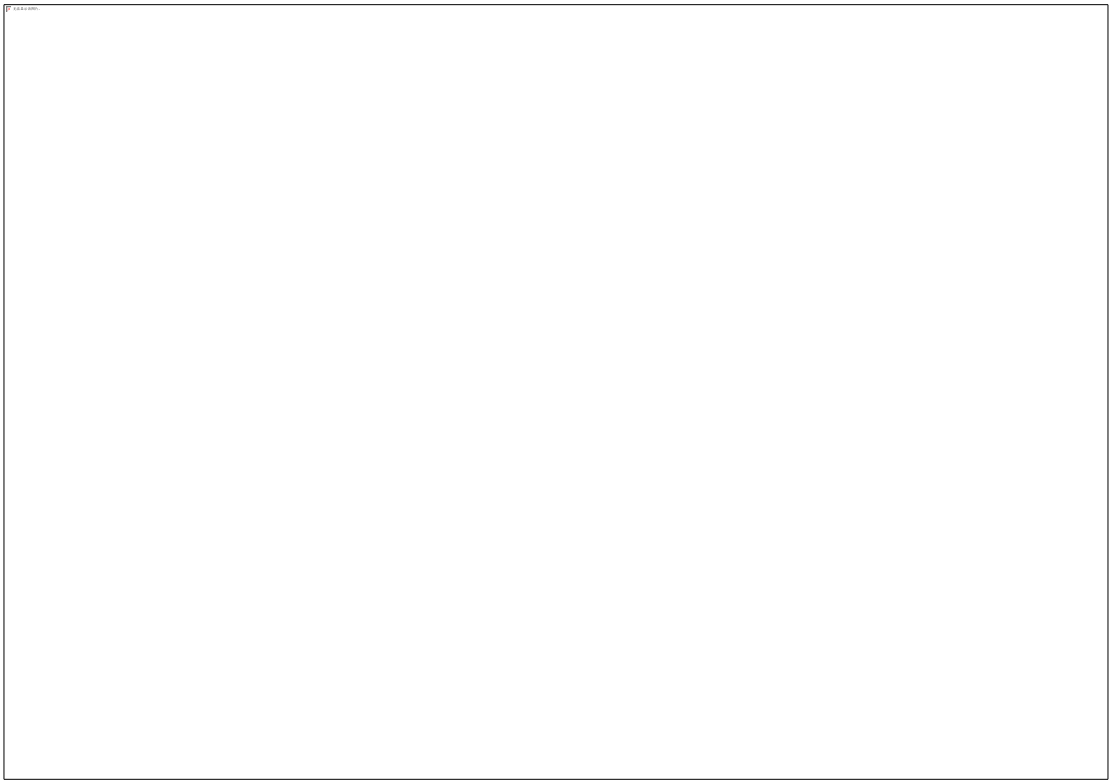

**4-8**

$^{1}$H NMR:

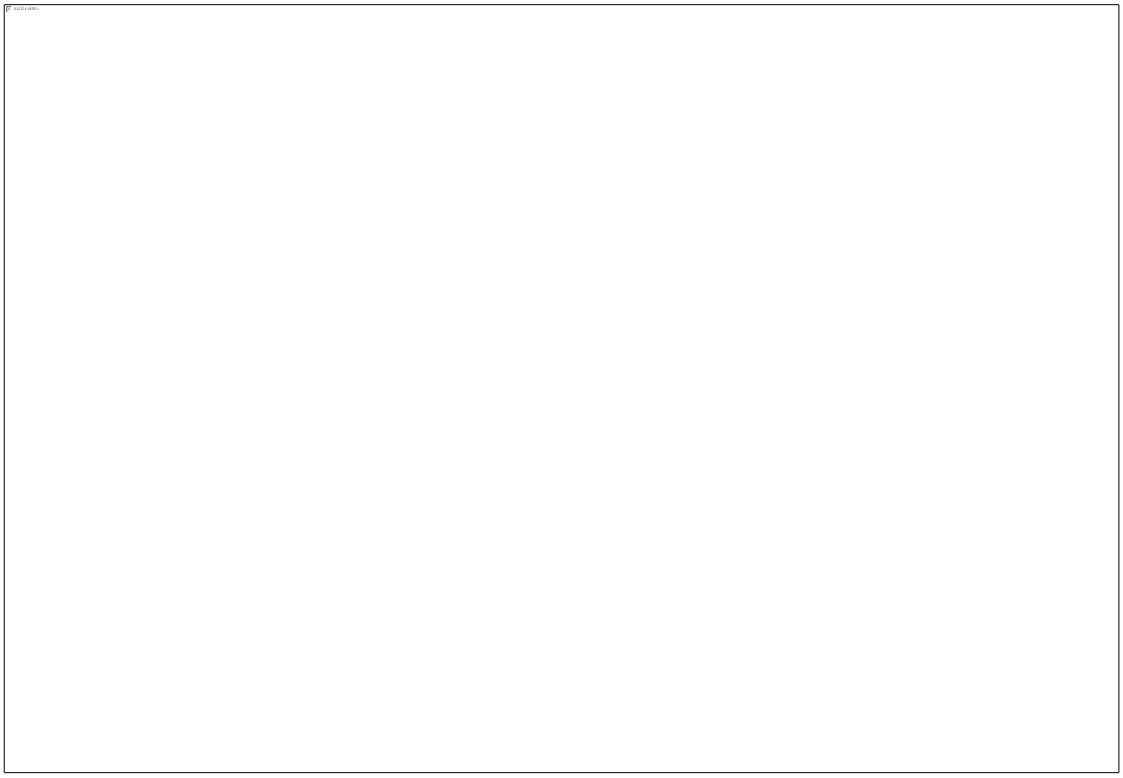

$^{13}$C NMR:

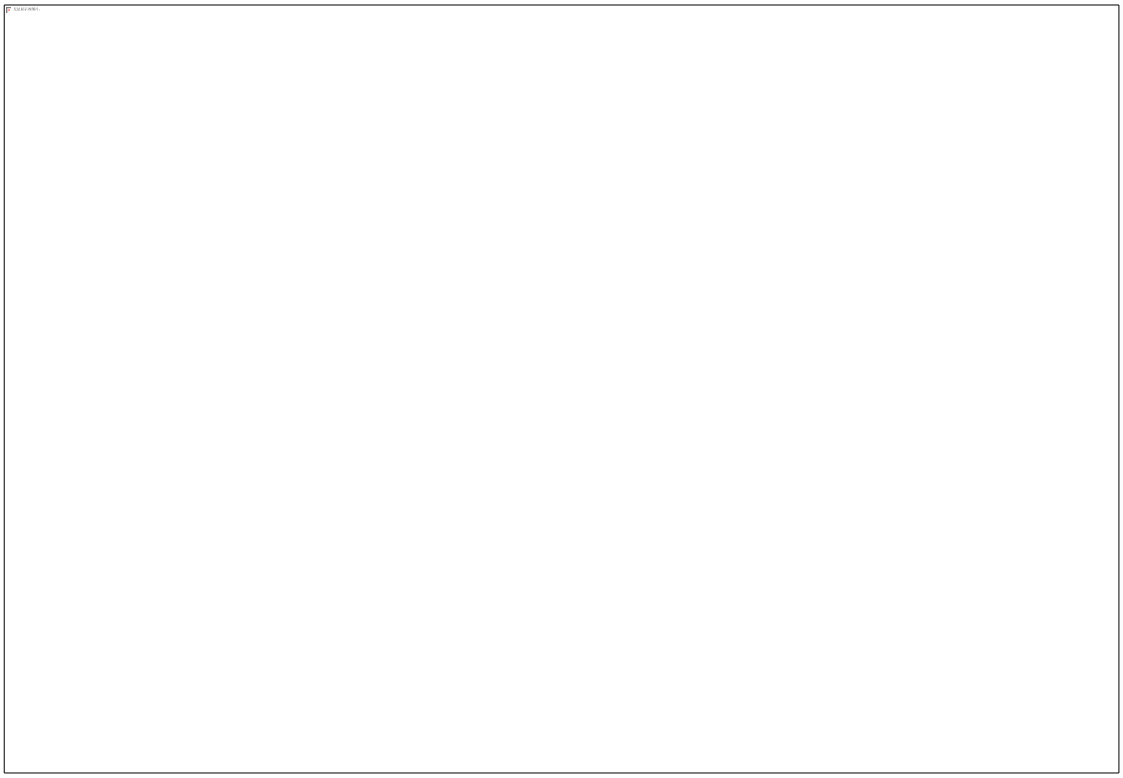

$^{19}$F NMR:

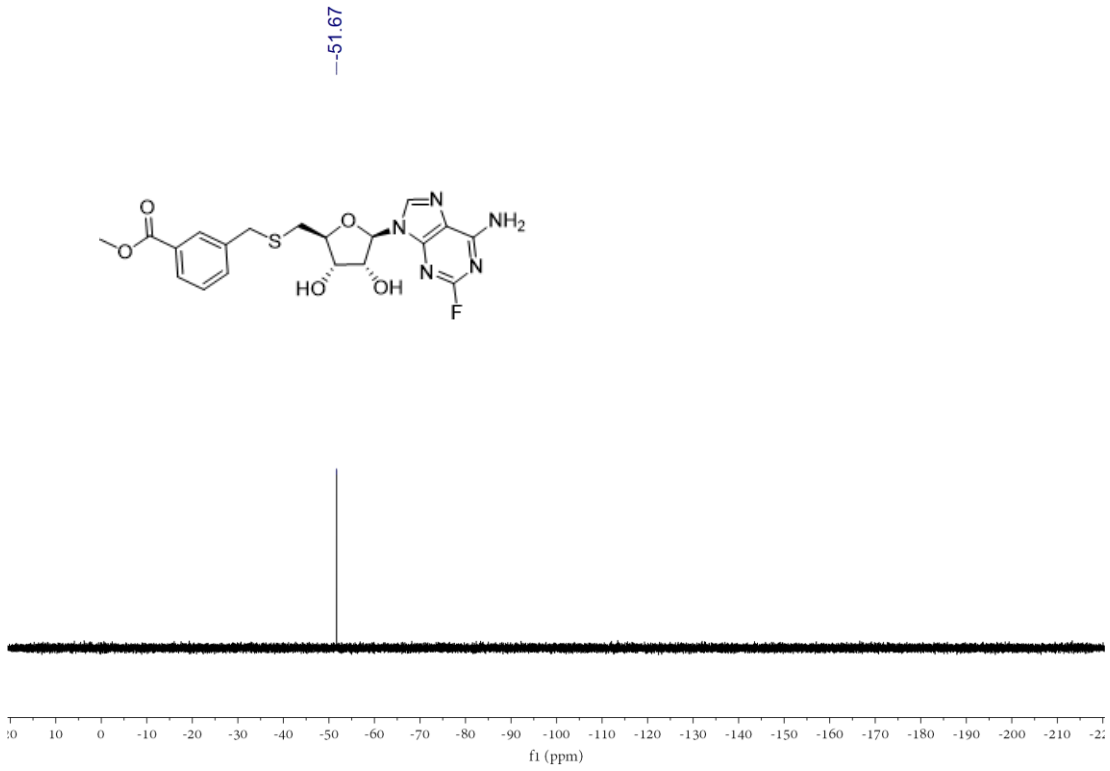
-51.67
O
O
S
O
HO
OH
N
N
N
N
NH2
F
10
0
-10
-20
-30
-40
-50
-60
-70
-80
-90
-100
-110
-120
-130
-140
-150
-160
-170
-180
-190
-200
-210
f1 (ppm)

**4-9**

$^{1}$H NMR:

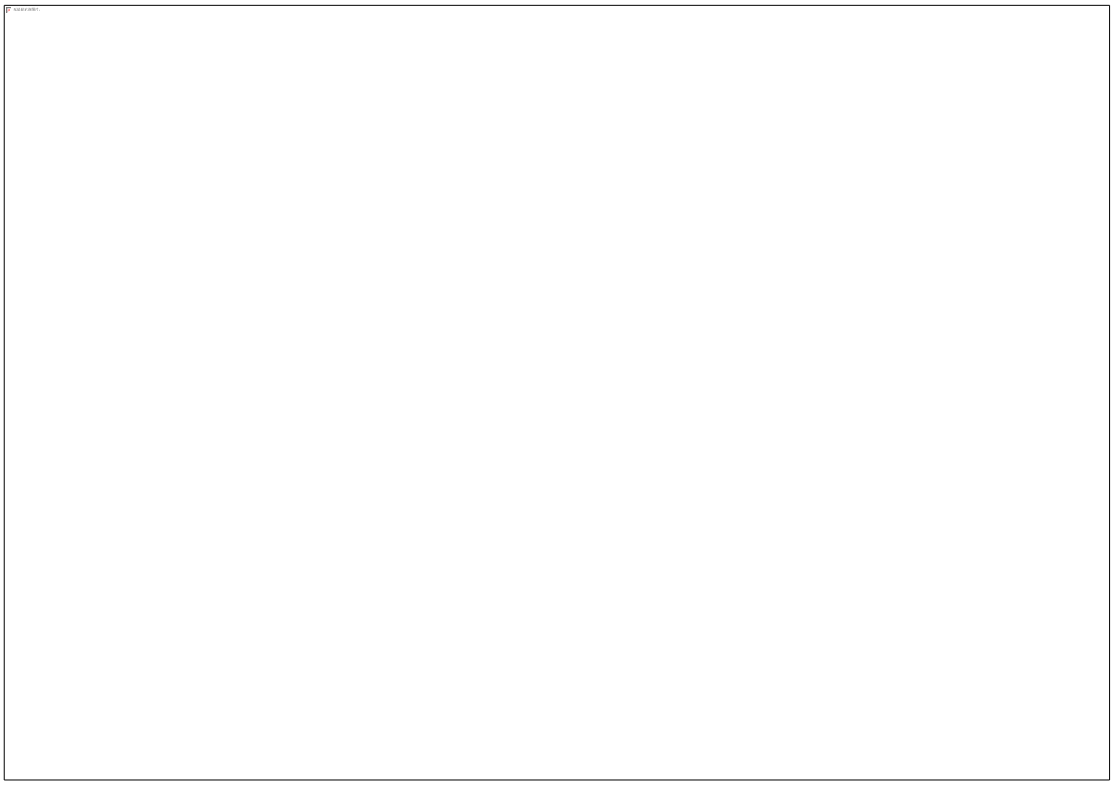

$^{13}$C NMR:

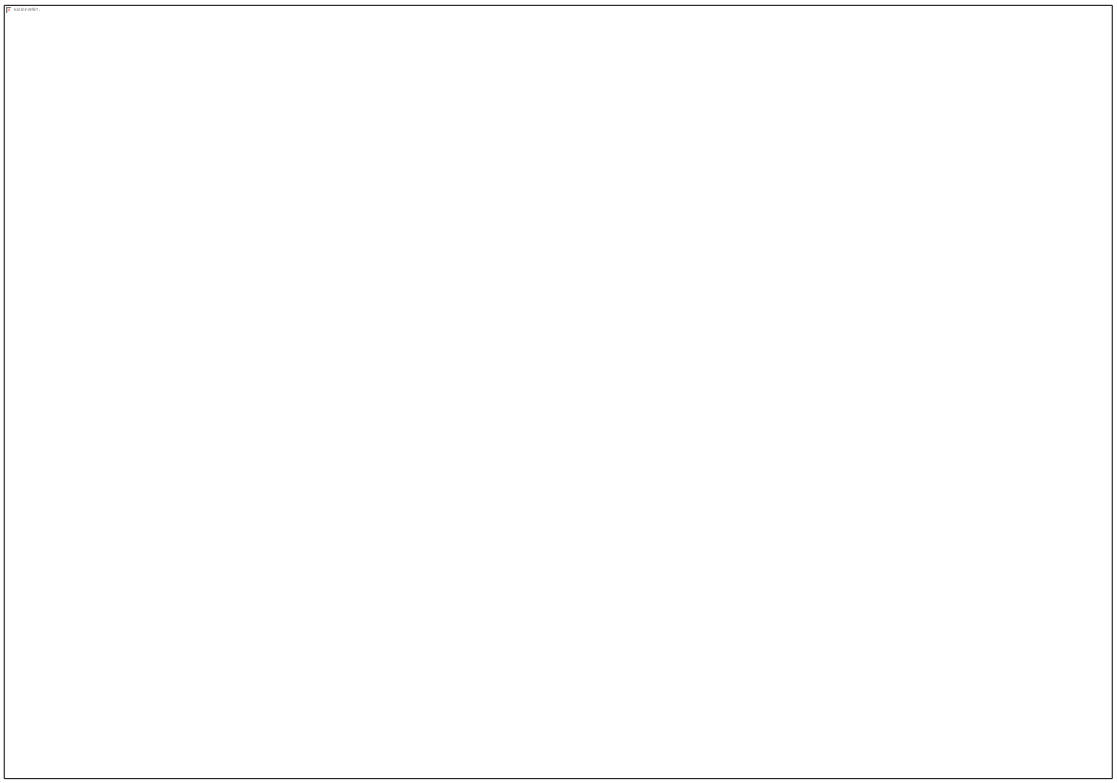

## 4-10

$^{1}$H NMR:

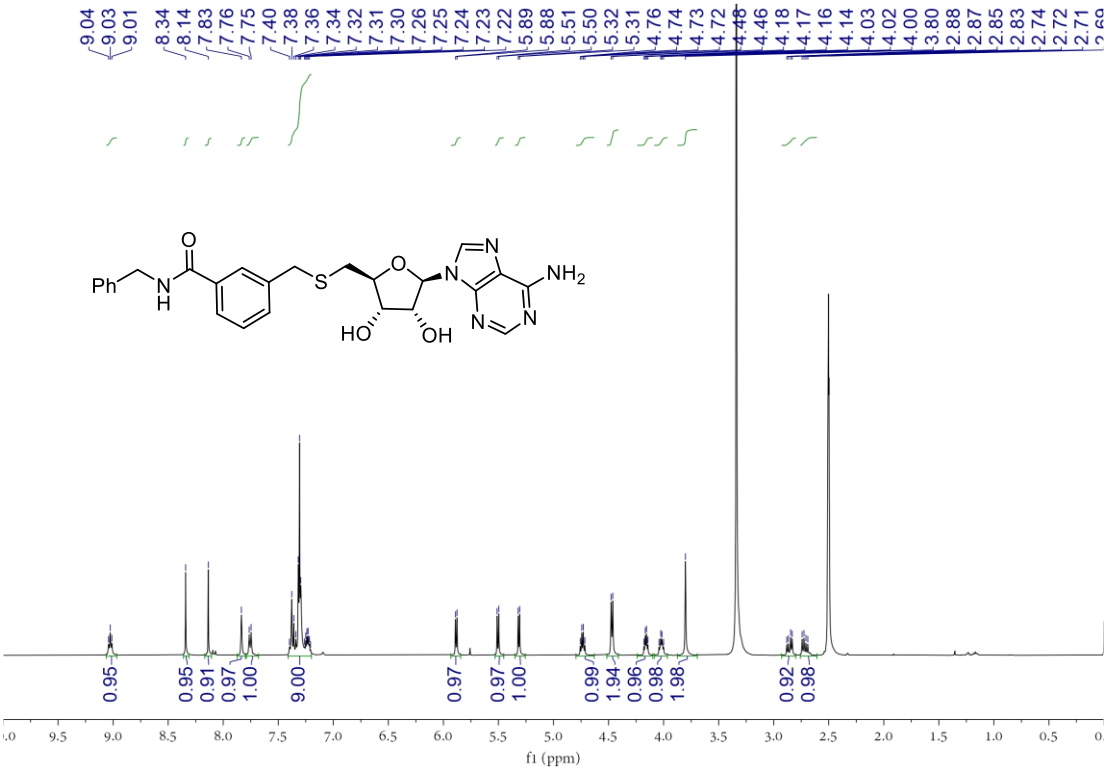


$^{13}$C NMR:

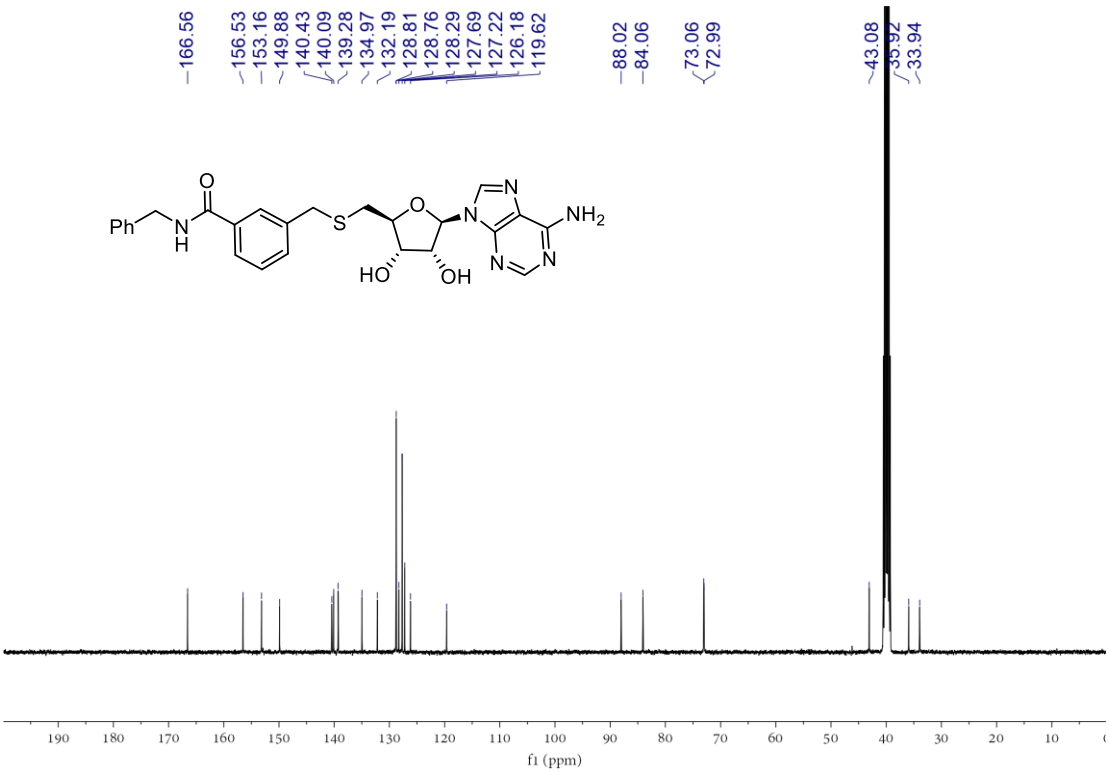

**4-11**

$^{1}$H NMR:

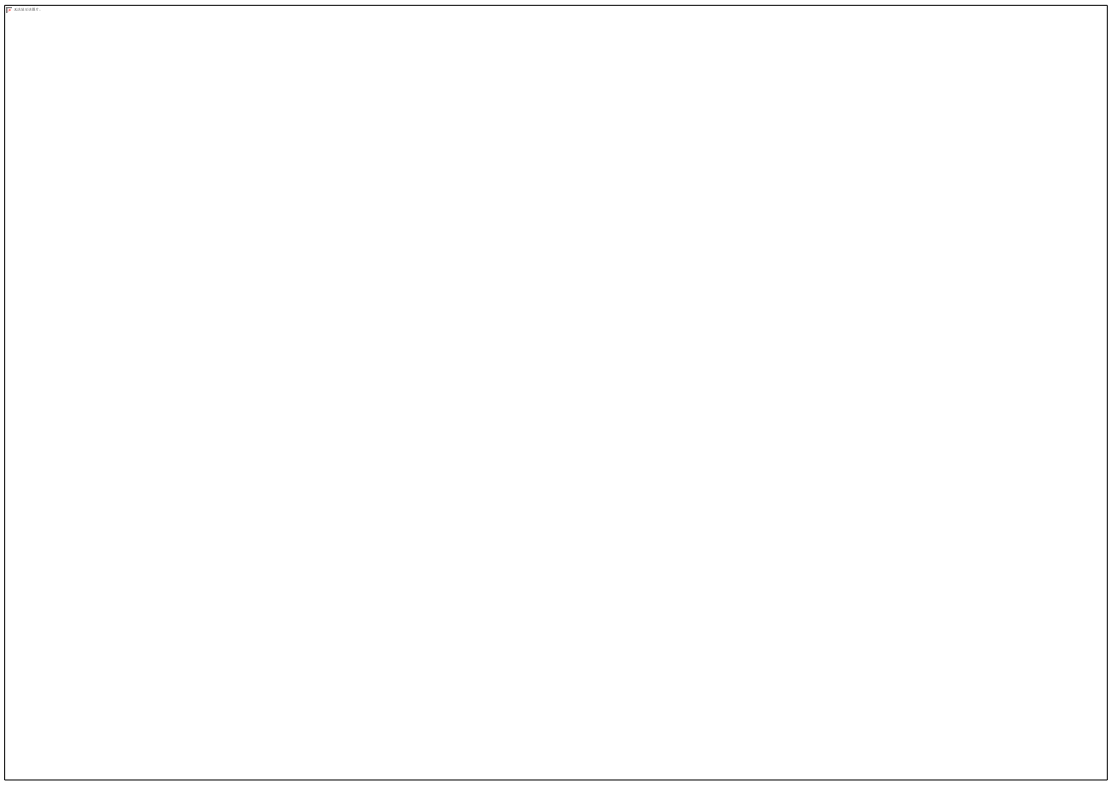

$^{13}$C NMR:

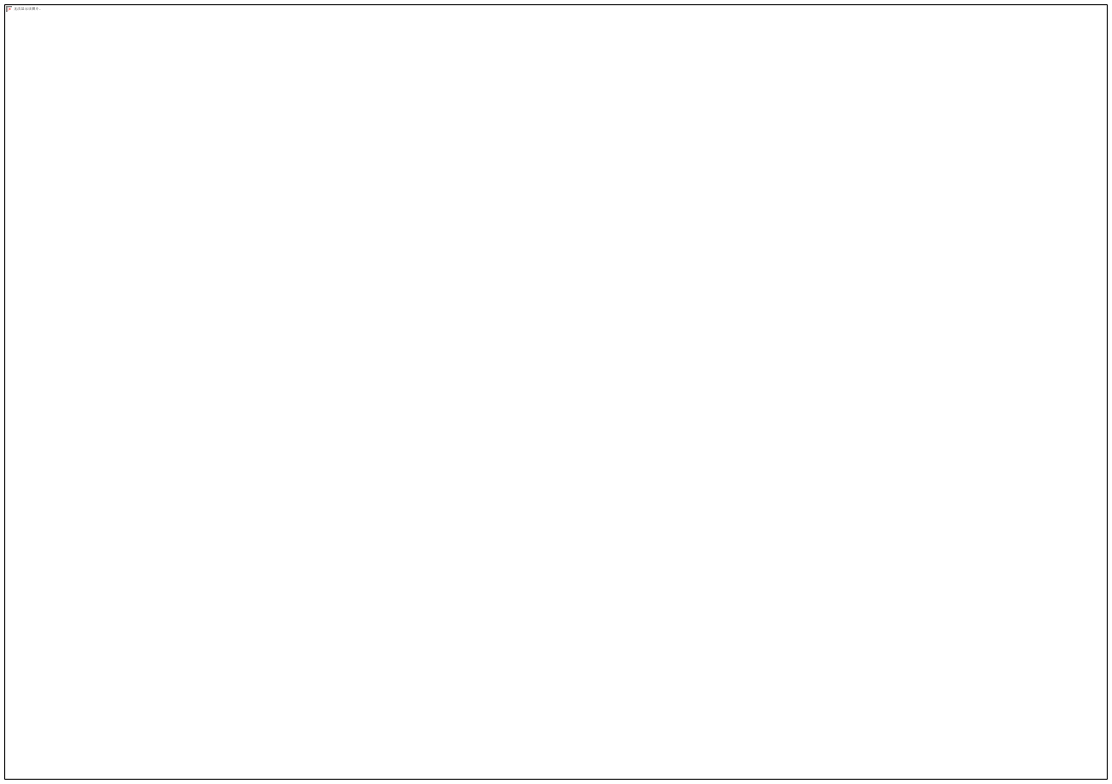

**4-12**

$^{1}$H NMR:

$^{13}$C NMR:

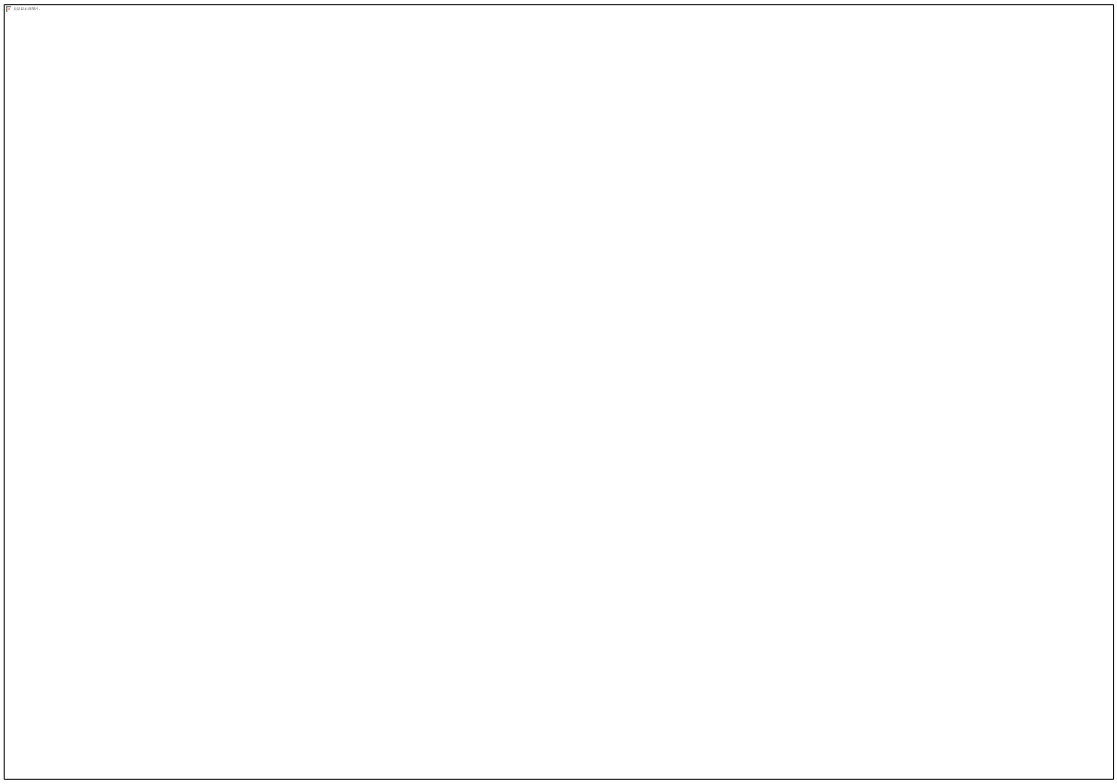

**4-13**

$^{1}$H NMR:

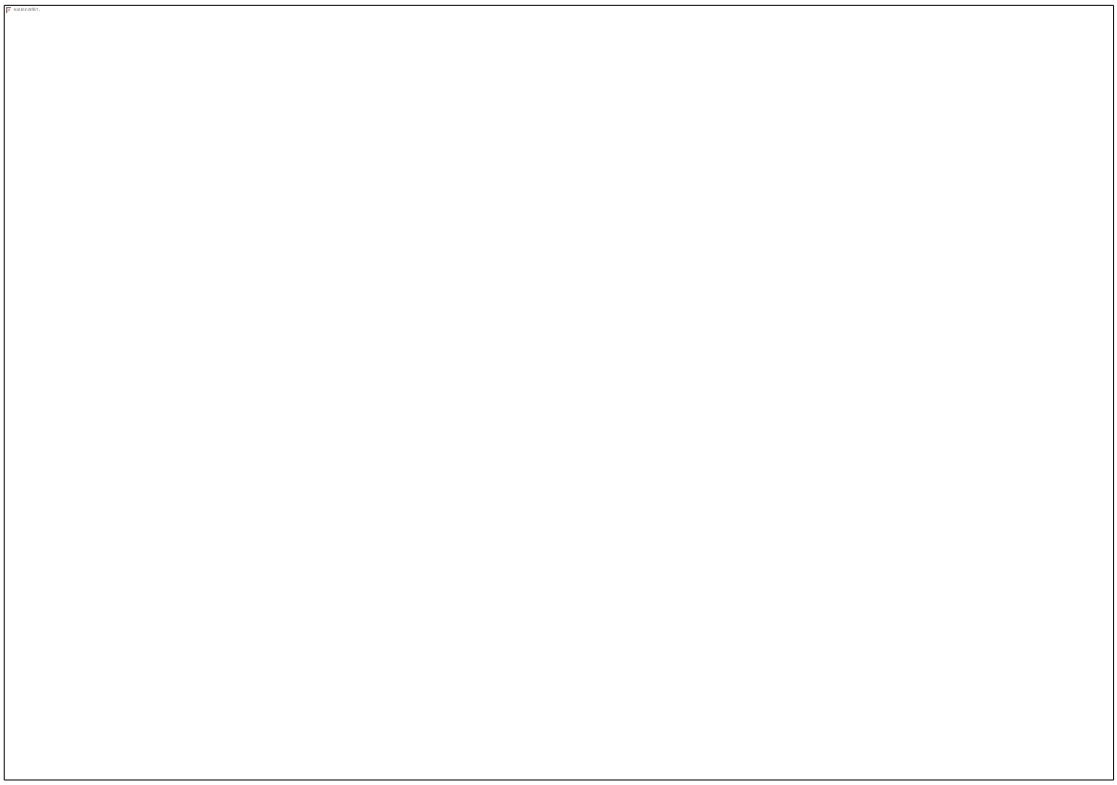

$^{13}$C NMR:

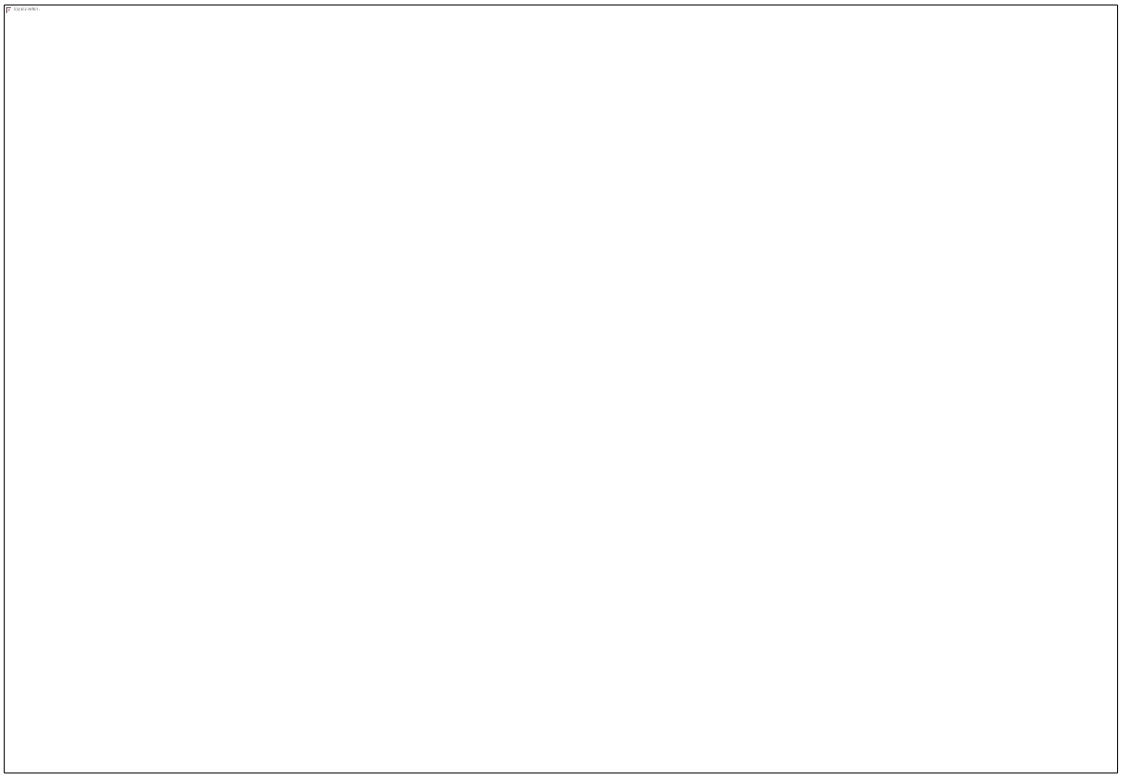

**4-14**

$^{1}$H NMR:

$^{13}$C NMR:

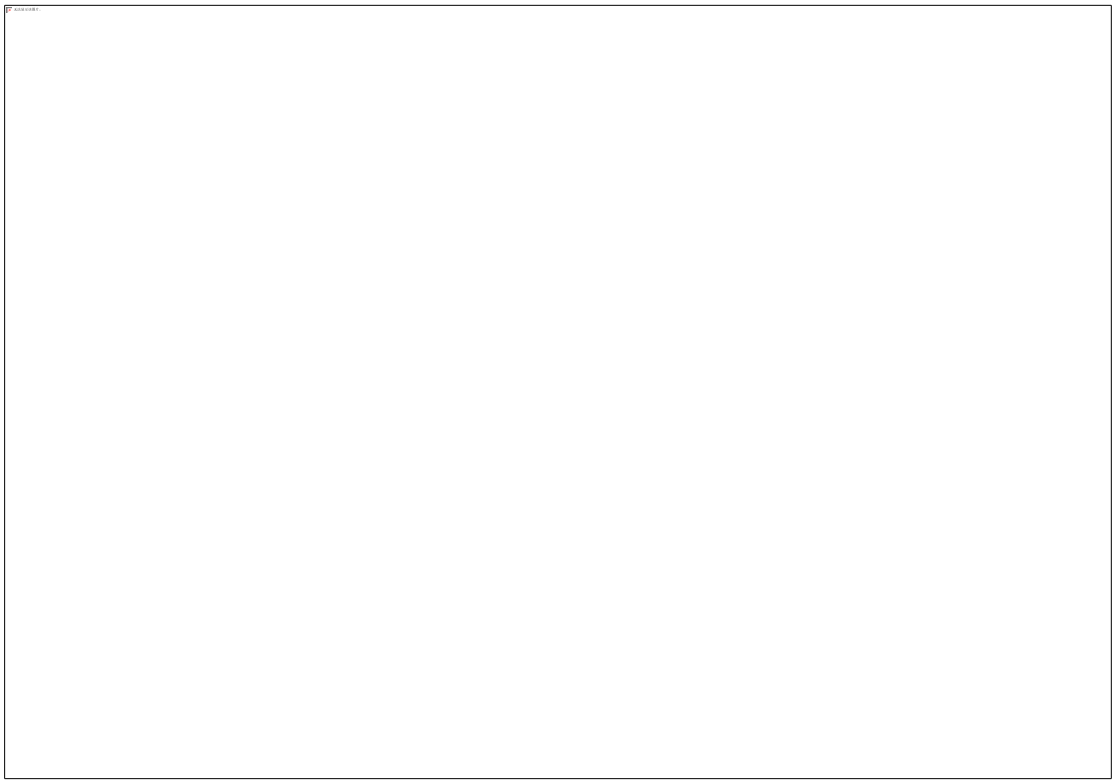

**4-15**

$^{1}$H NMR:

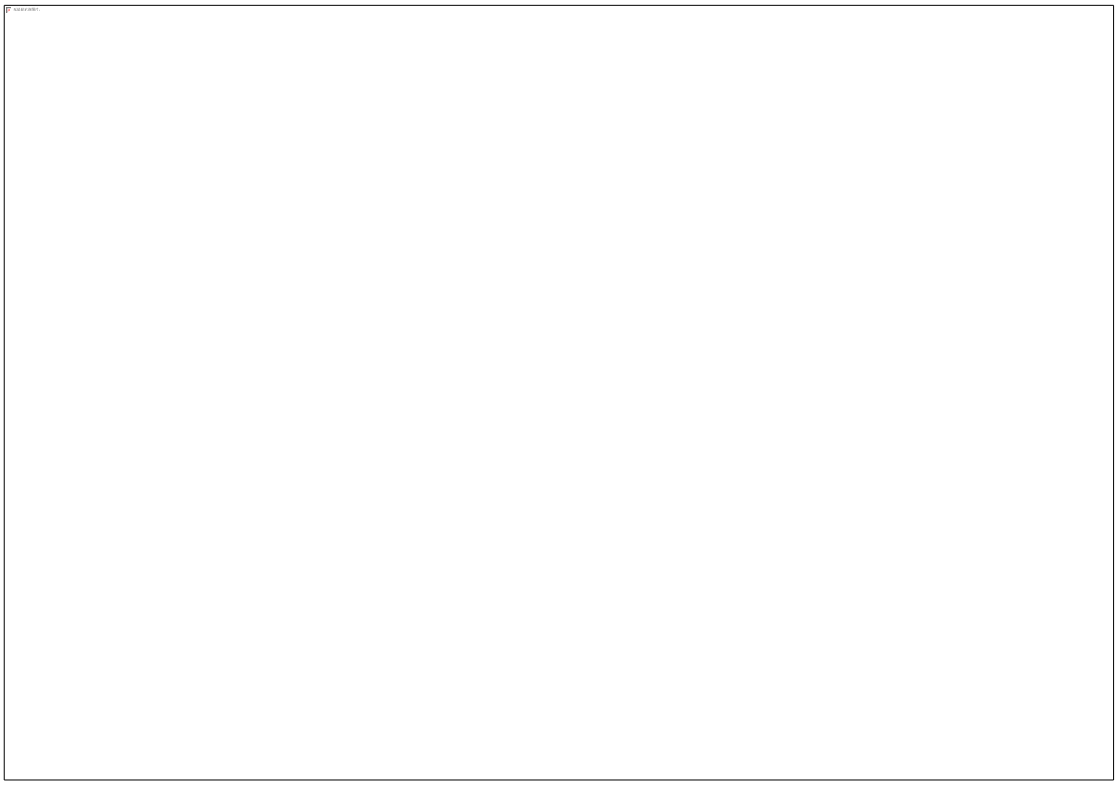

$^{13}$C NMR:

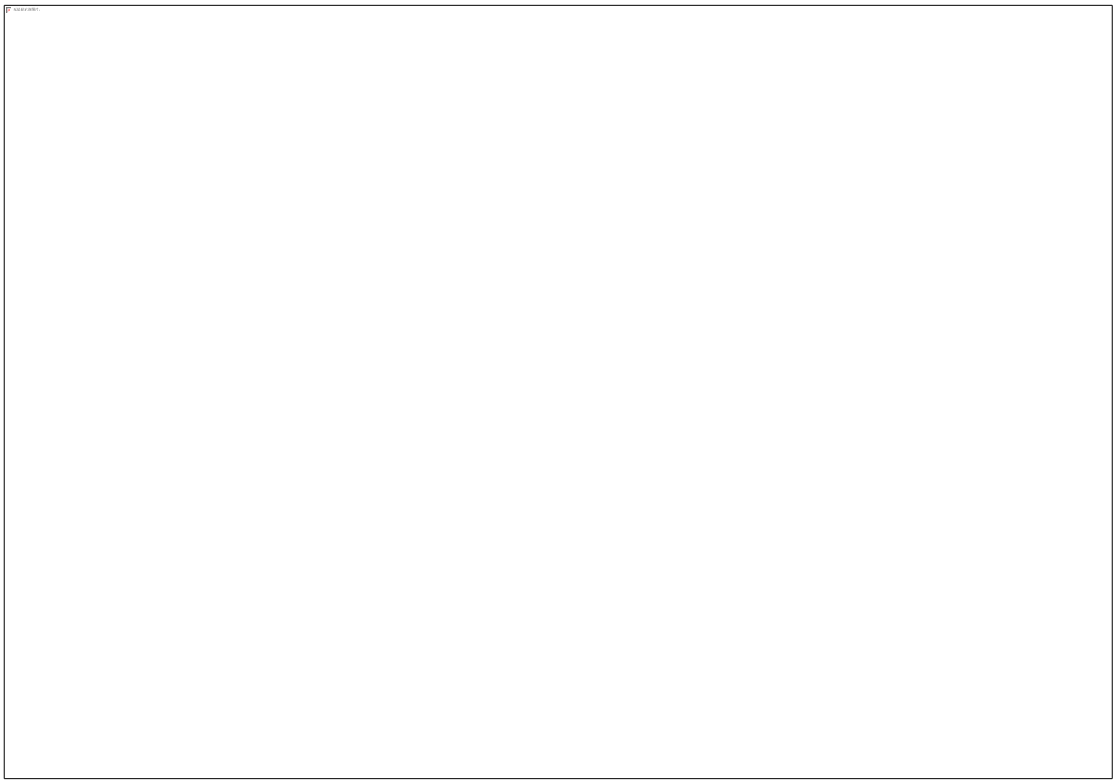

**4-16**

$^{1}$H NMR:

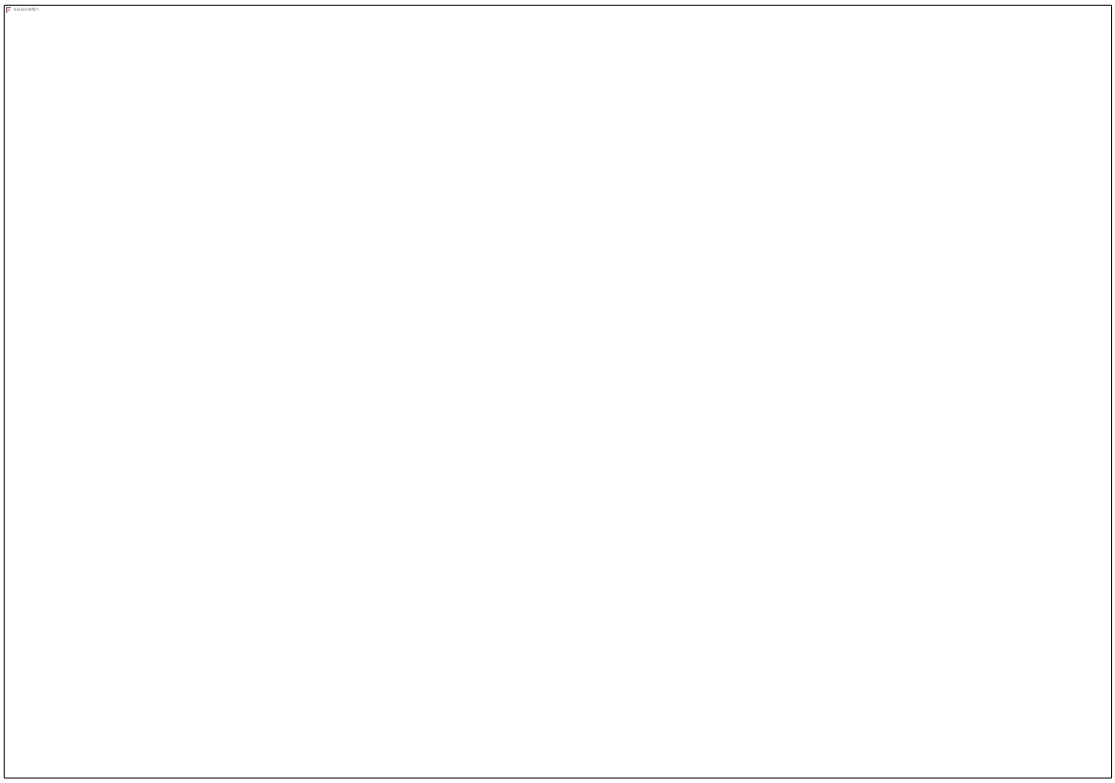

$^{13}$C NMR:

**4-17**

$^{1}$H NMR:

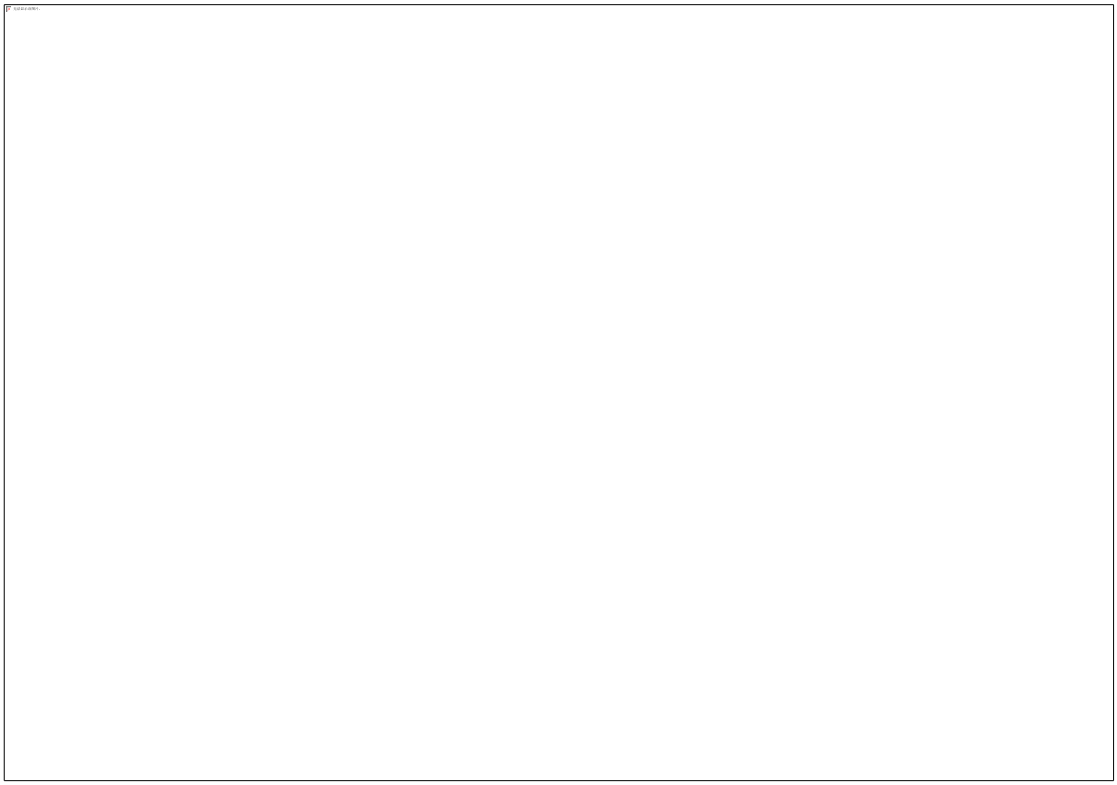

$^{13}$C NMR:

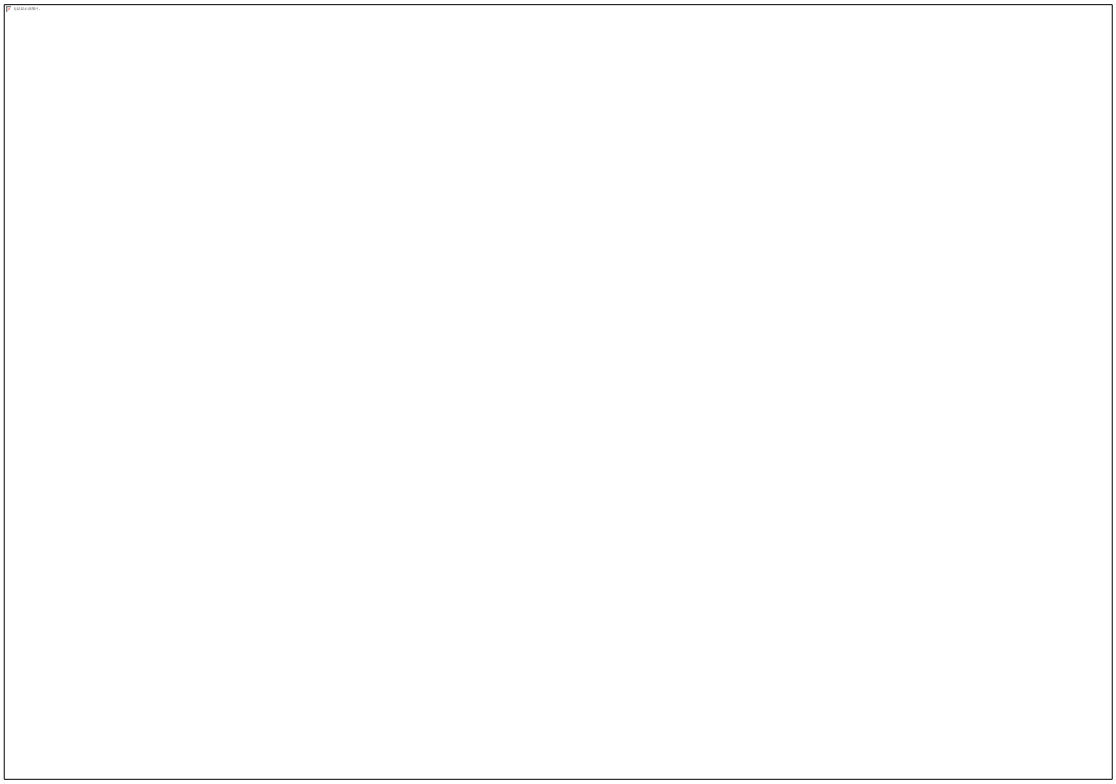

**4-18**

$^{1}$H NMR:

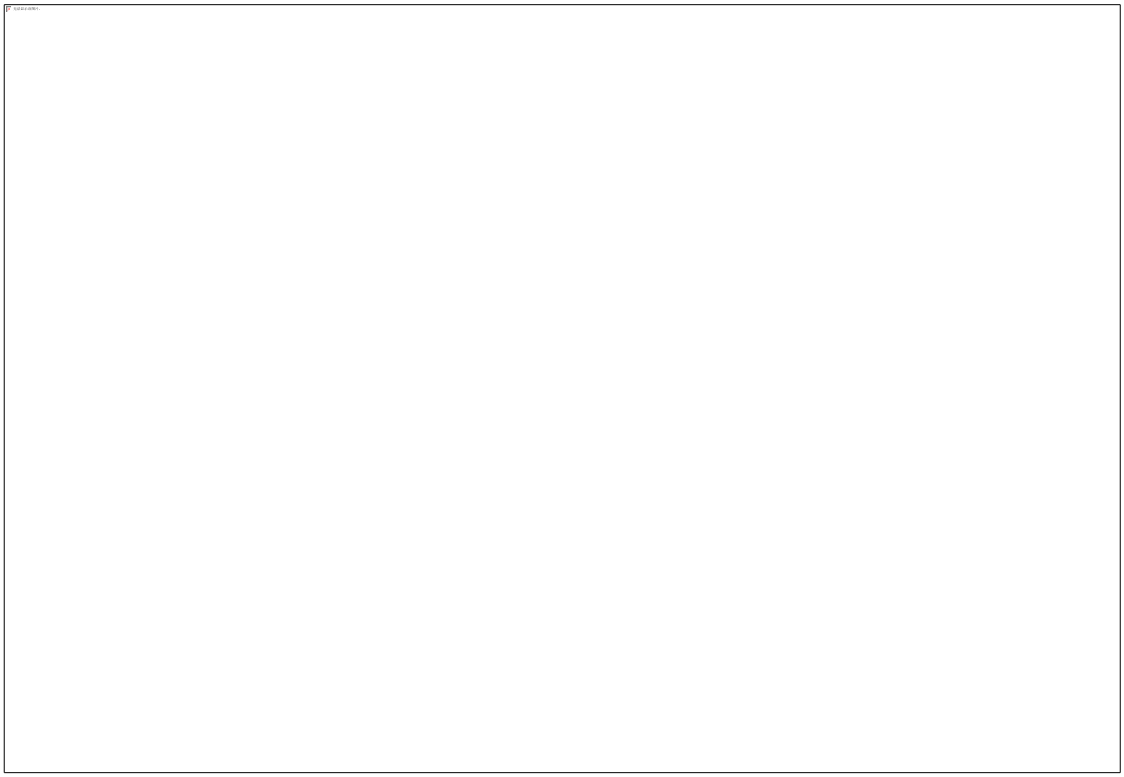

$^{13}$C NMR:

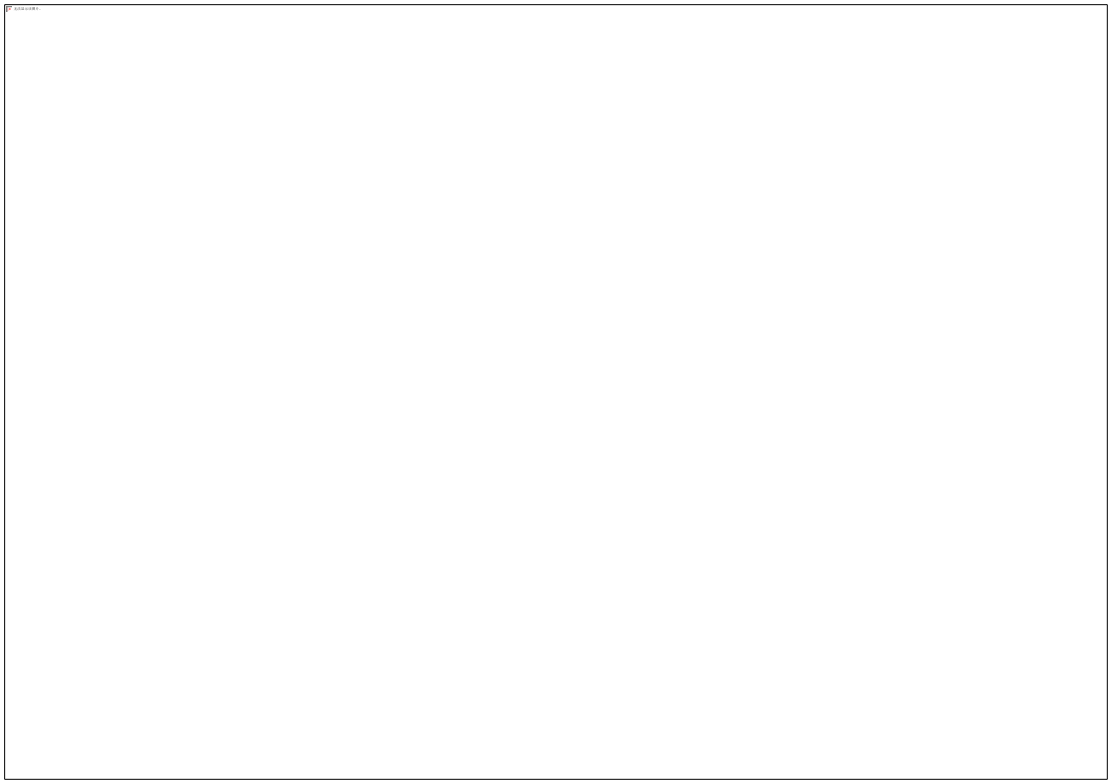

**4-19**

$^{1}$H NMR:

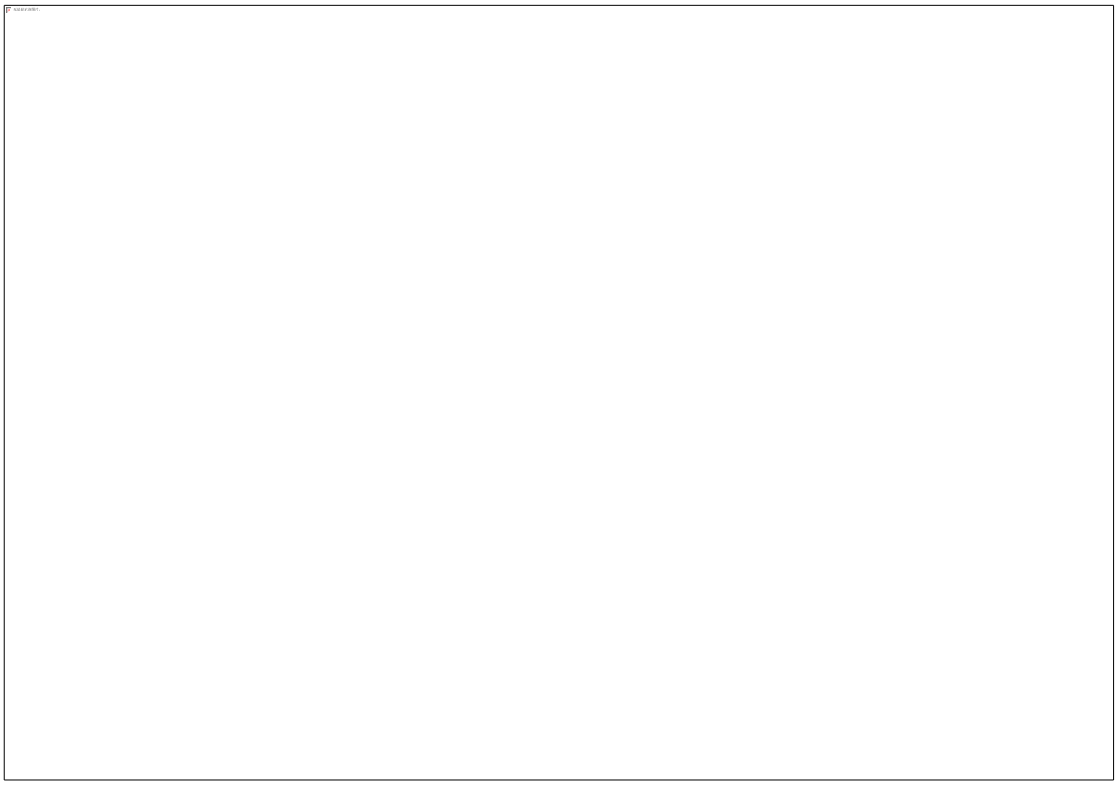

$^{13}$C NMR:

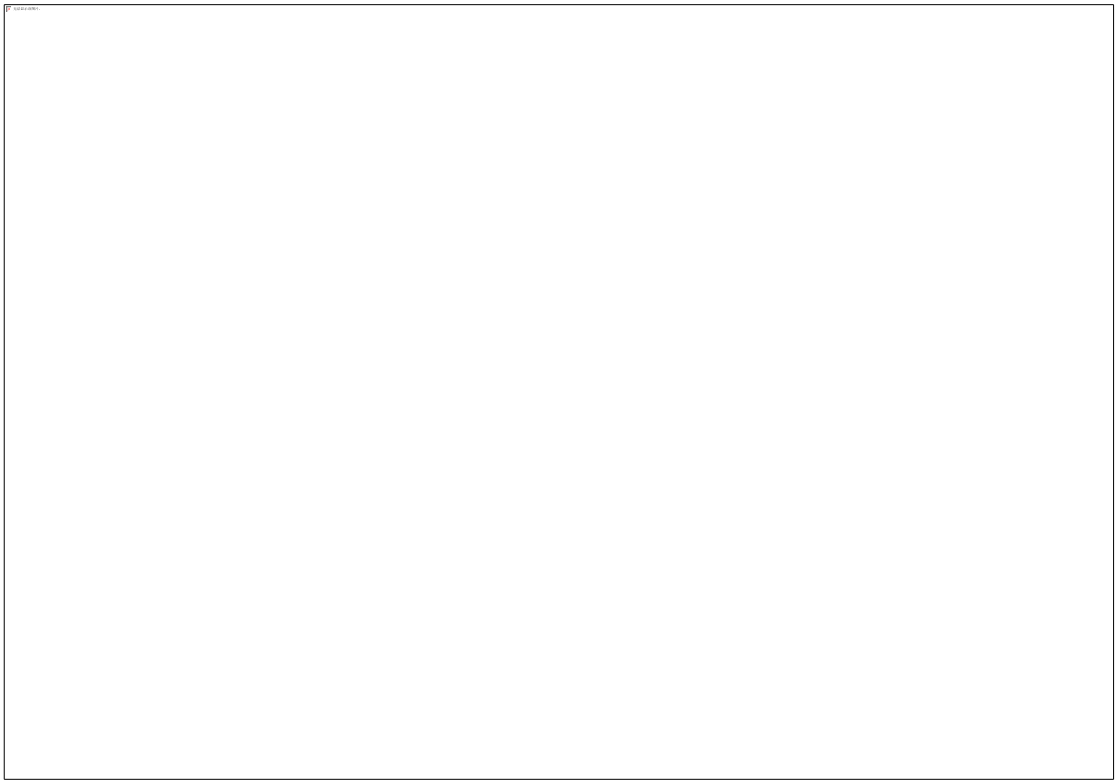

**4-20**

$^{1}$H NMR:

$^{13}$C NMR:

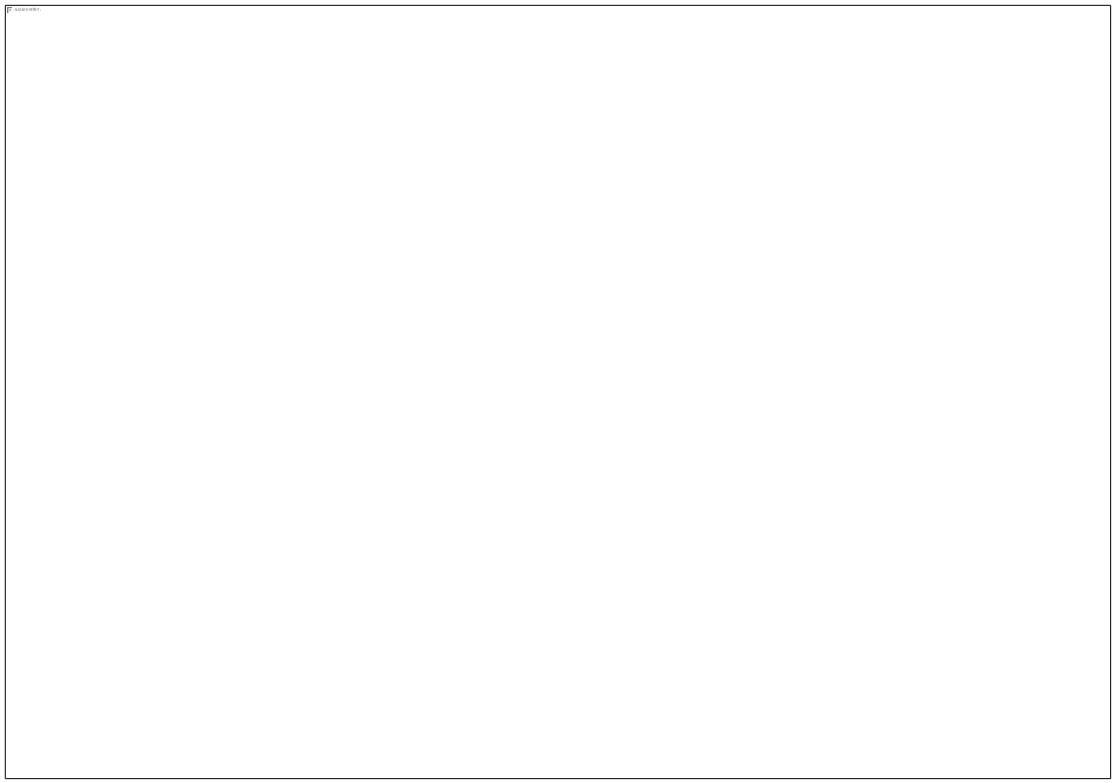

**4-21**

$^{1}$H NMR:

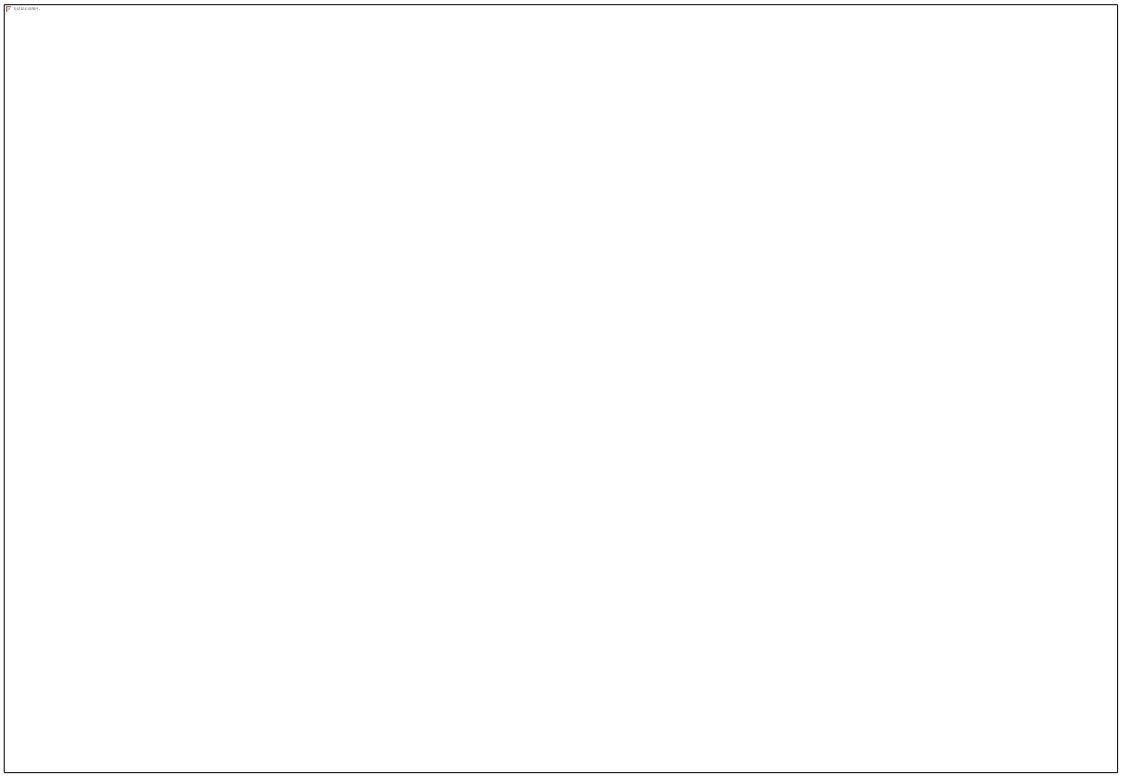

$^{13}$C NMR:

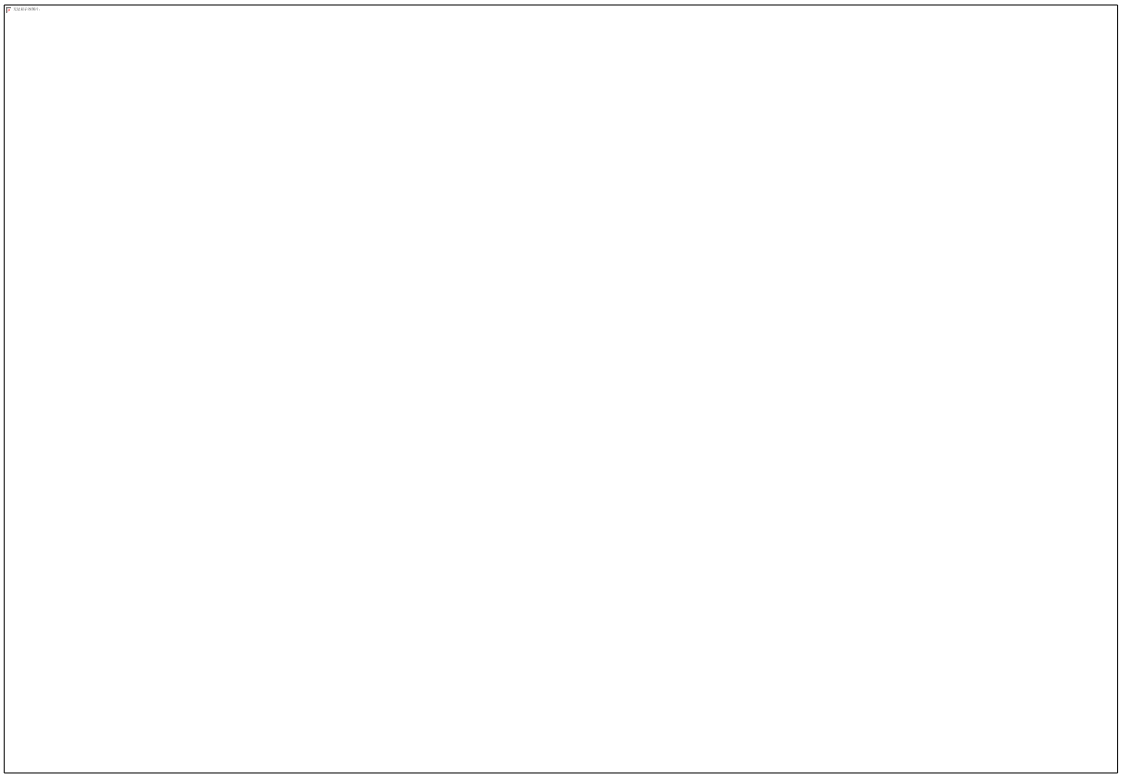

**4-28**

$^{1}$H NMR:

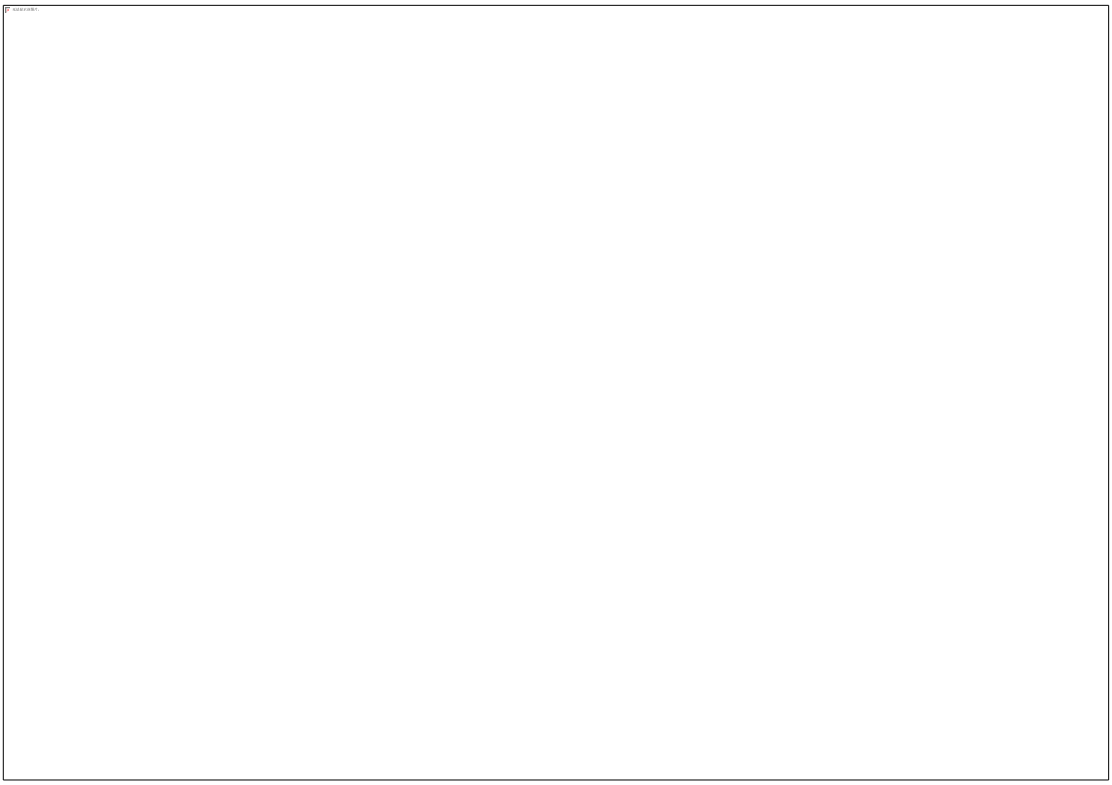

$^{13}$C NMR:

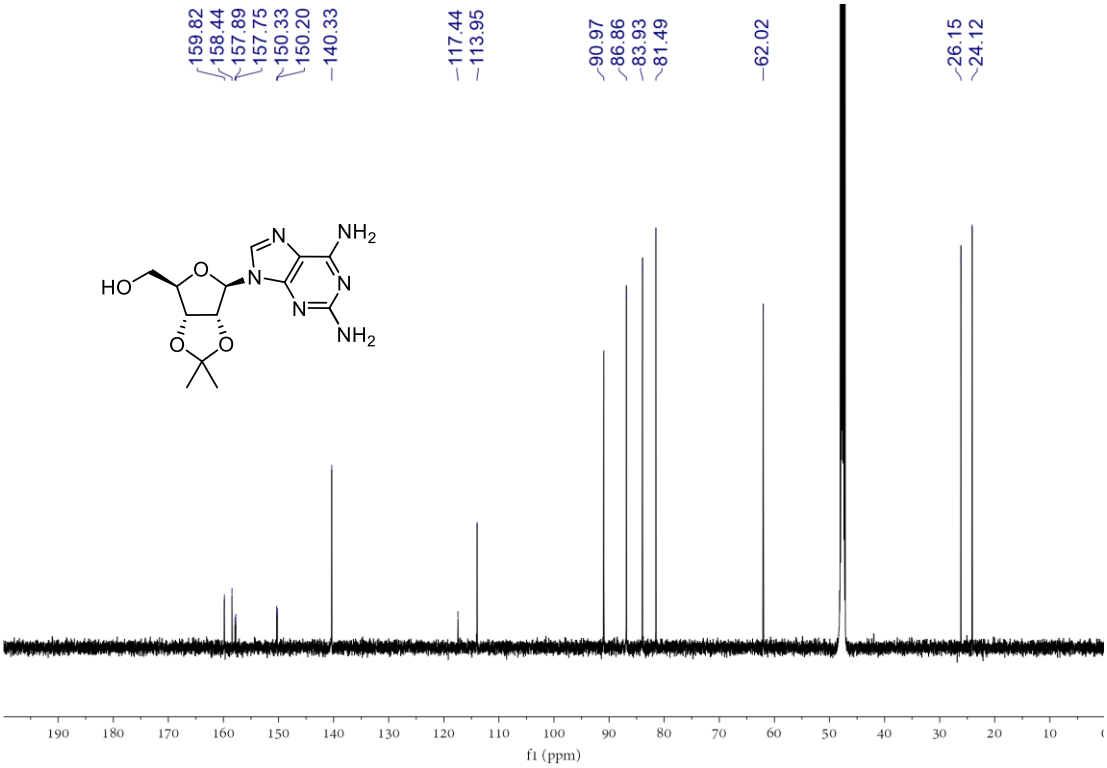

**4-35**

$^{1}$H NMR:

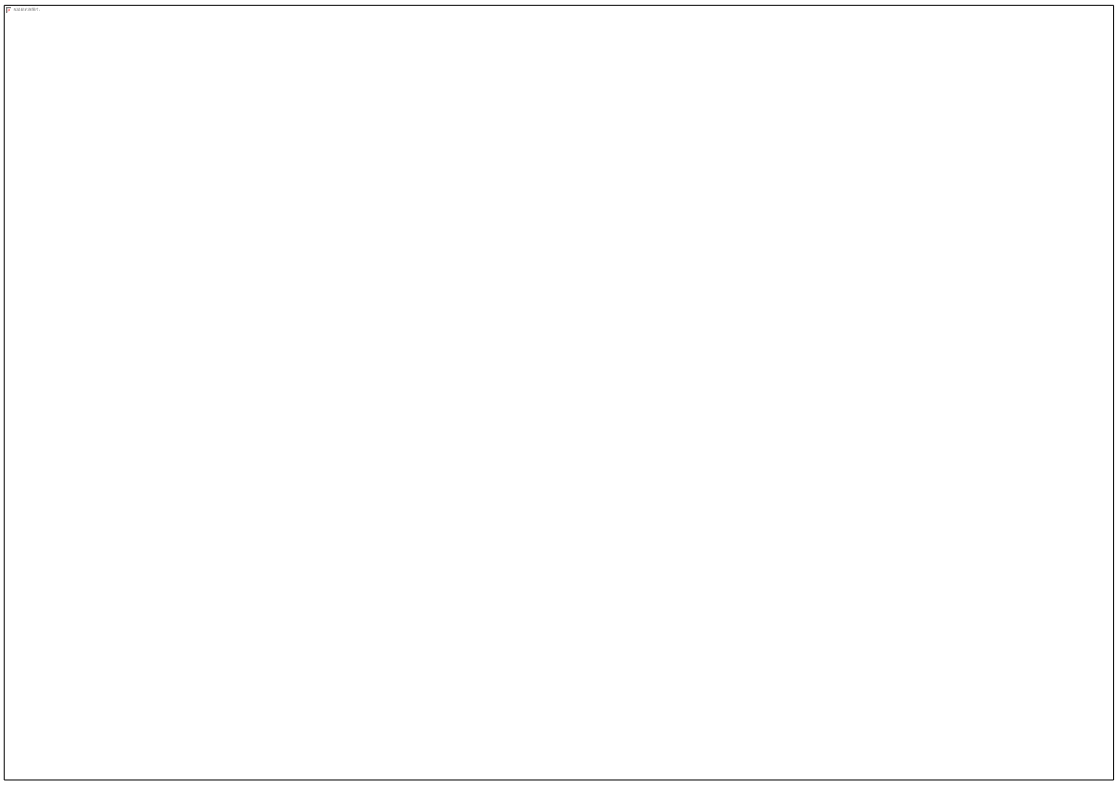

$^{13}$C NMR:

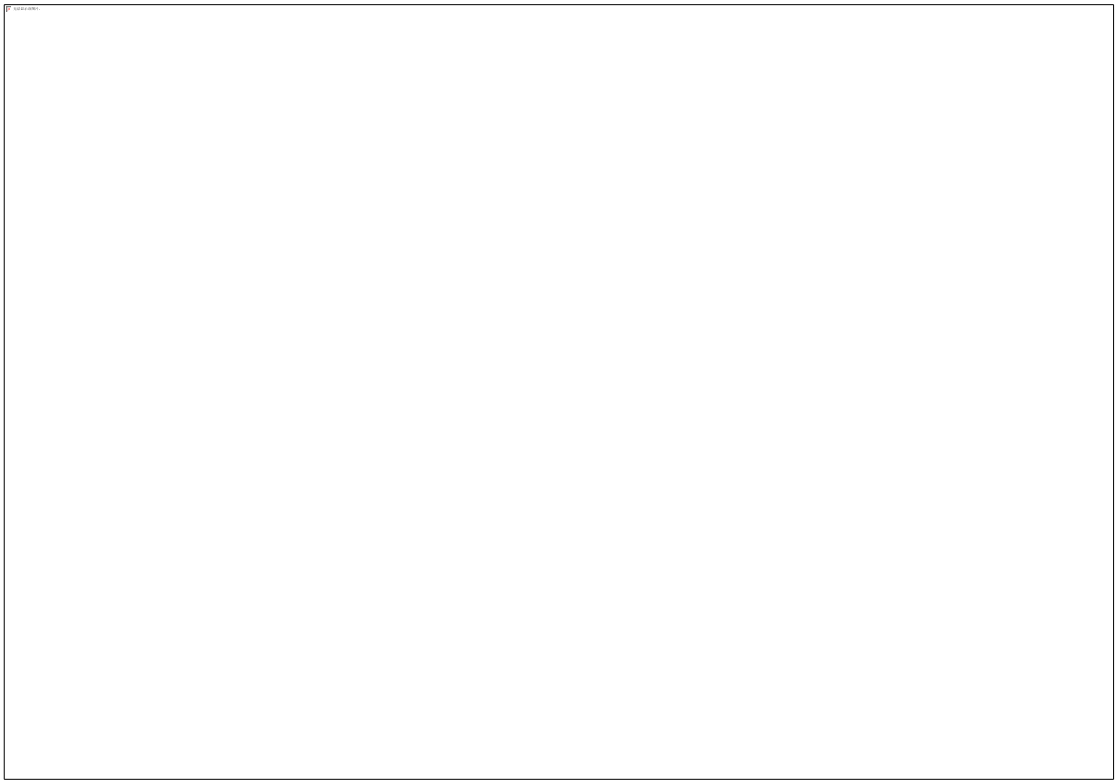

**4-37**

$^{1}$H NMR:

$^{13}$C NMR:

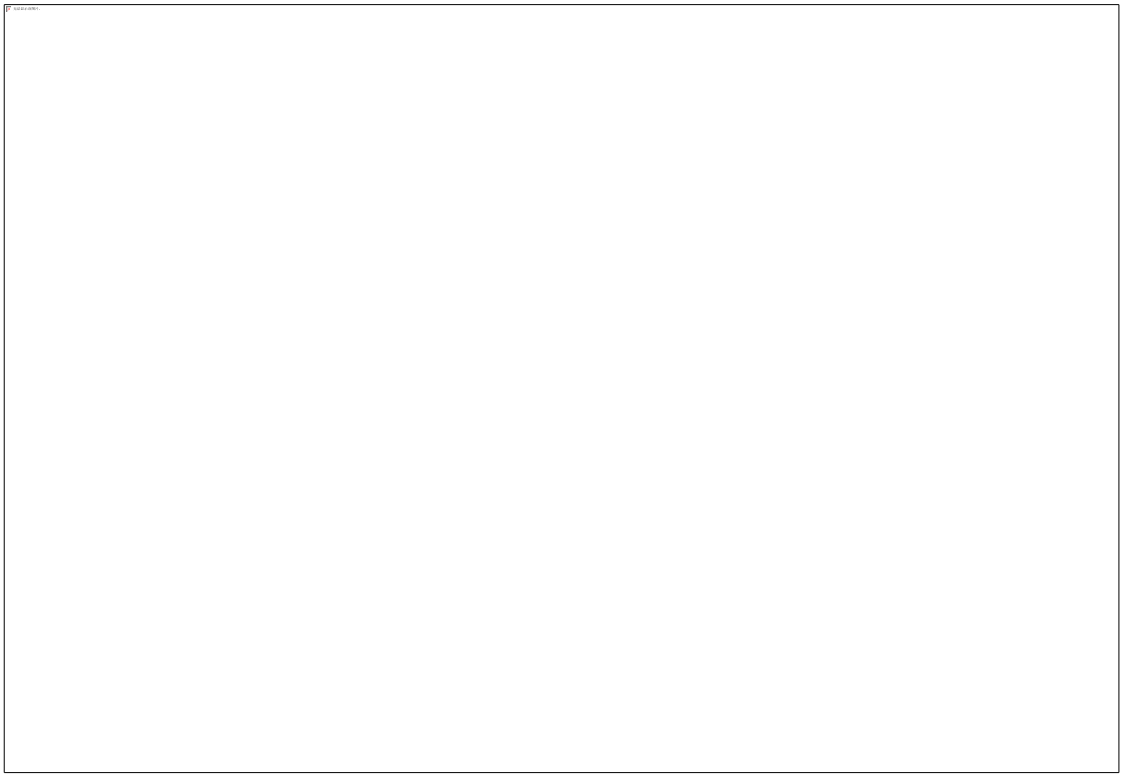

**4-50**

$^{1}$H NMR:

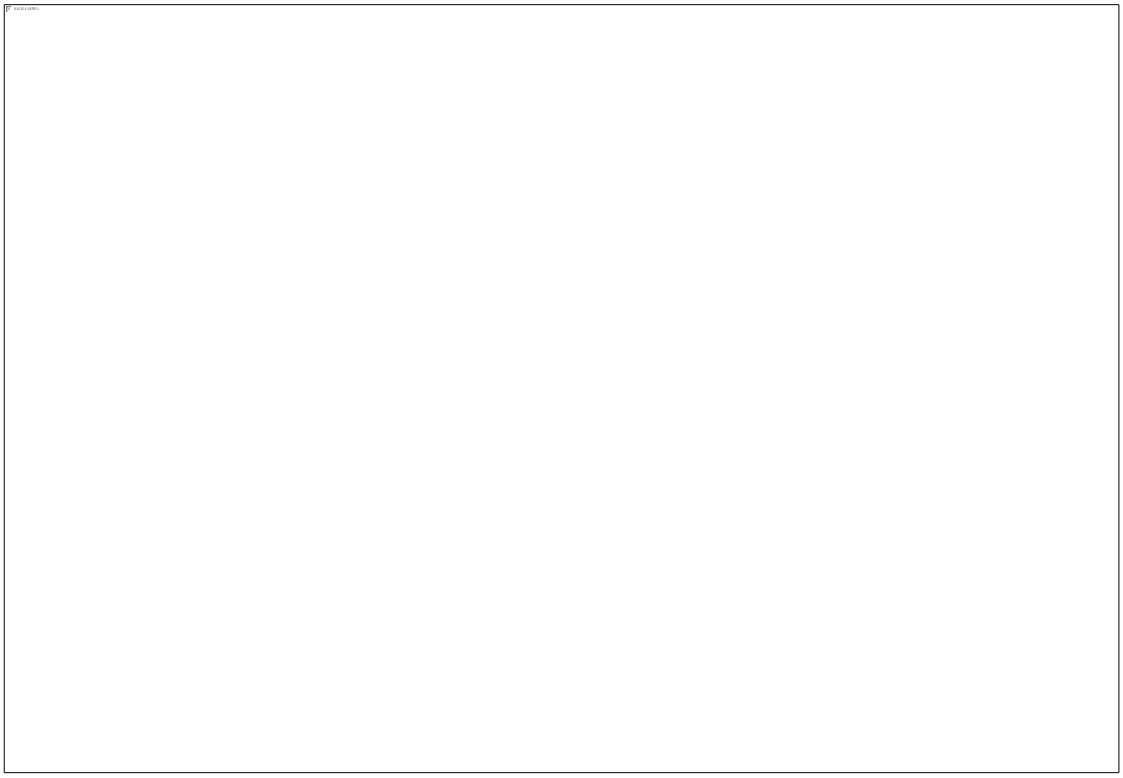

$^{13}$C NMR:

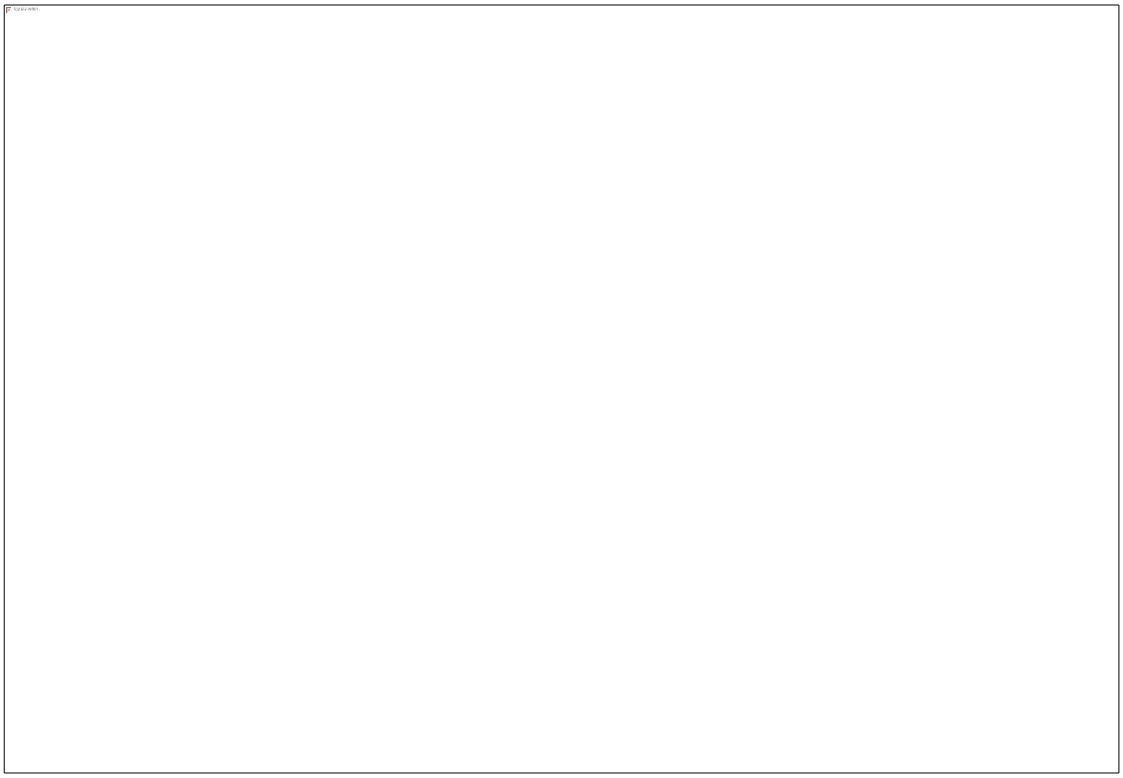

**4-51**

$^{1}$H NMR:

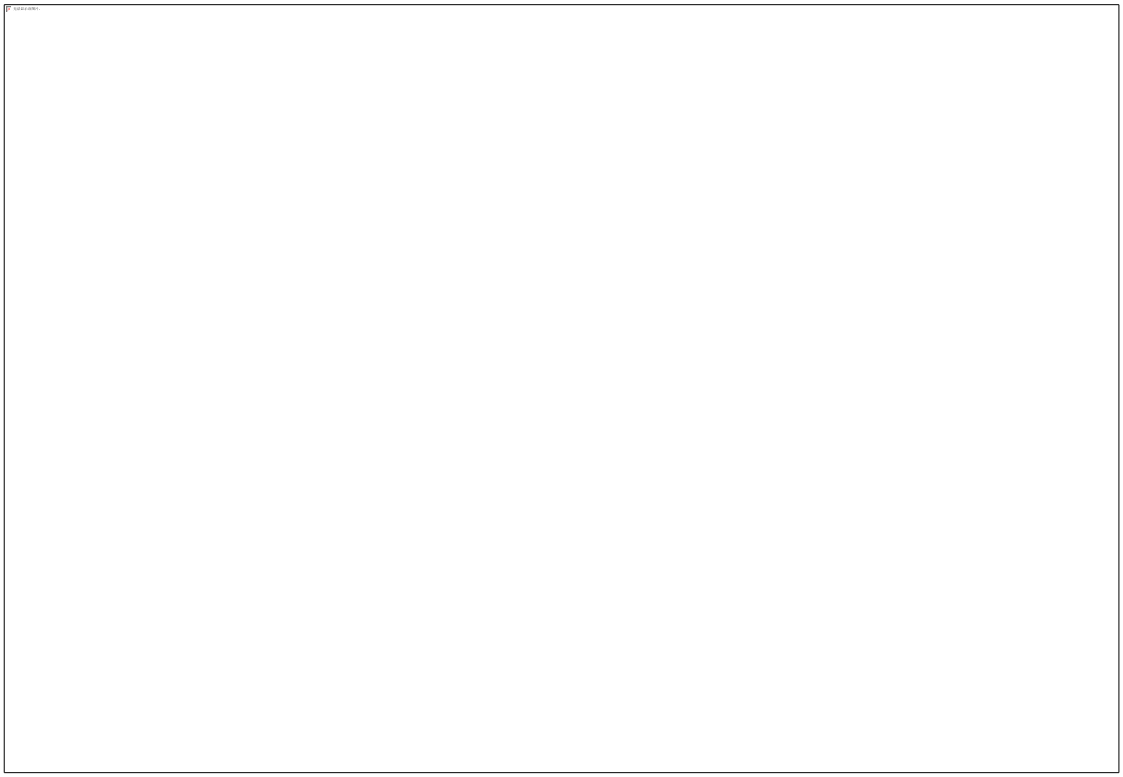

$^{13}$C NMR:

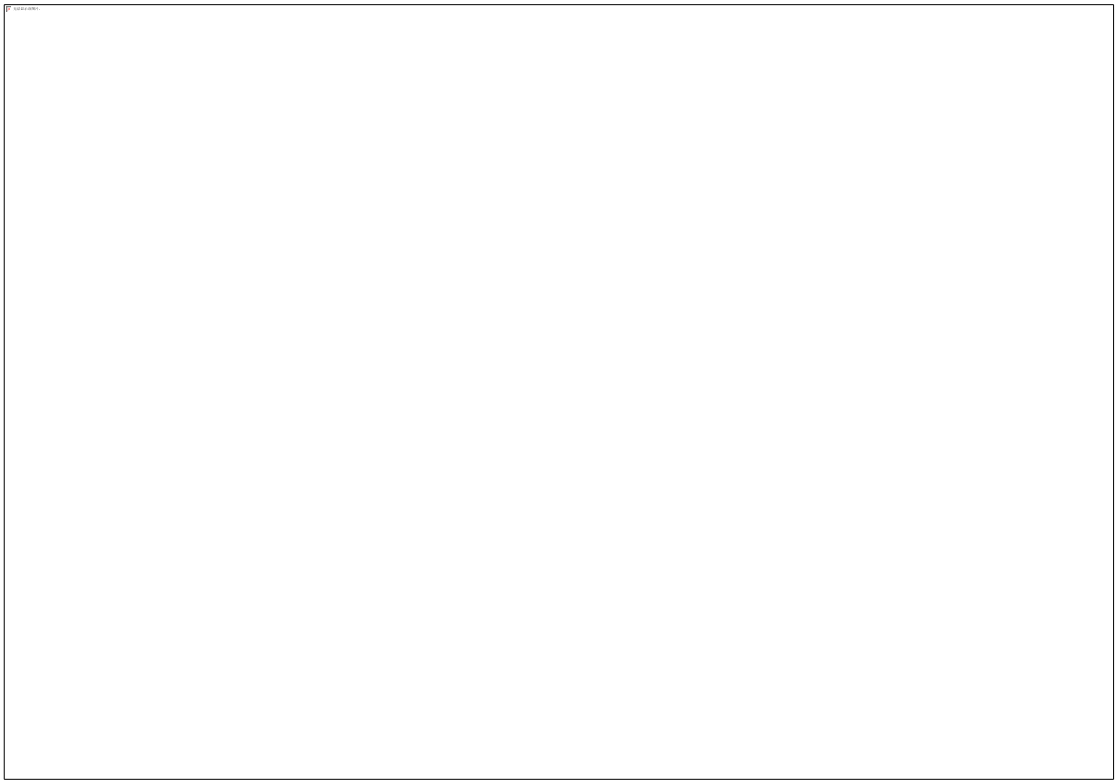

**4-54**

$^{1}$H NMR:

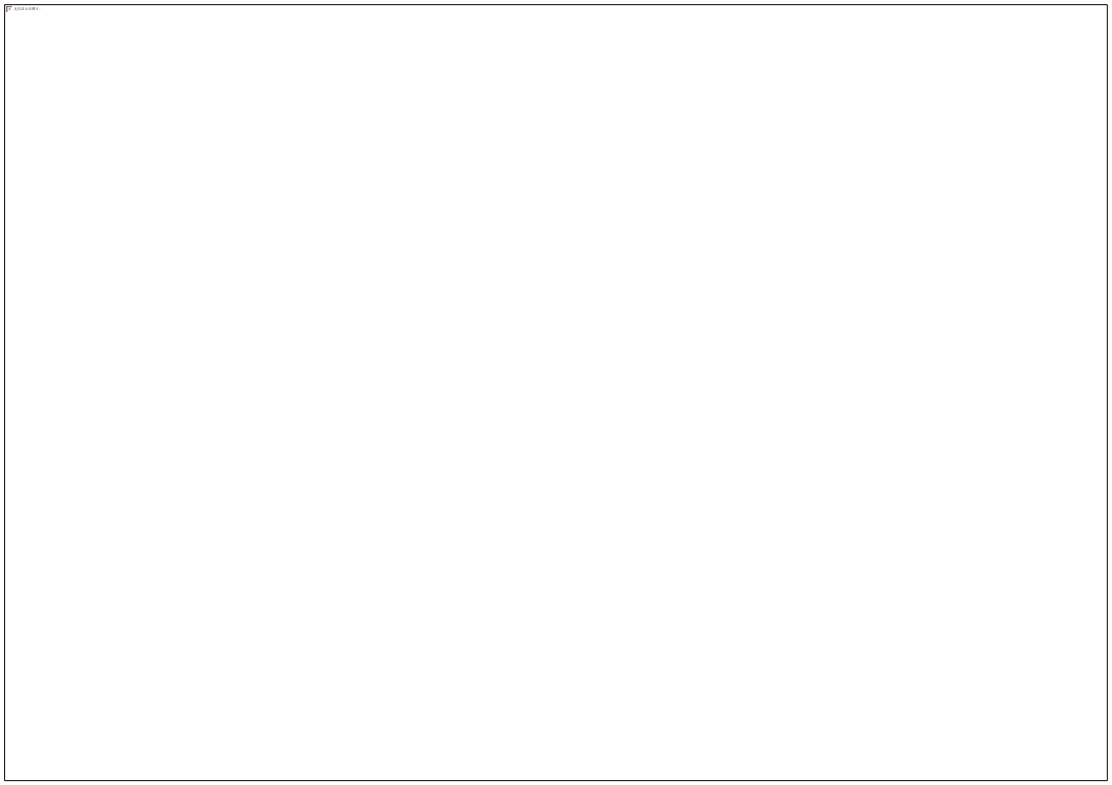

$^{13}$C NMR:

**4-66**

$^{1}$H NMR:

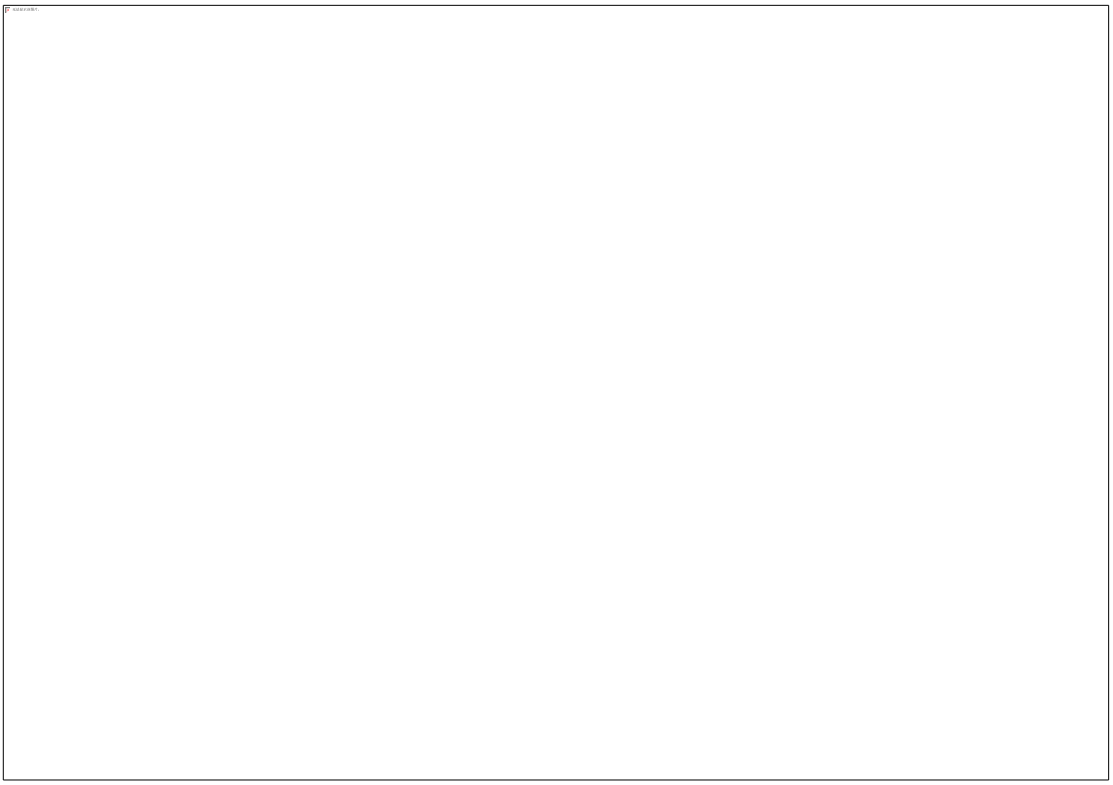

$^{13}$C NMR:

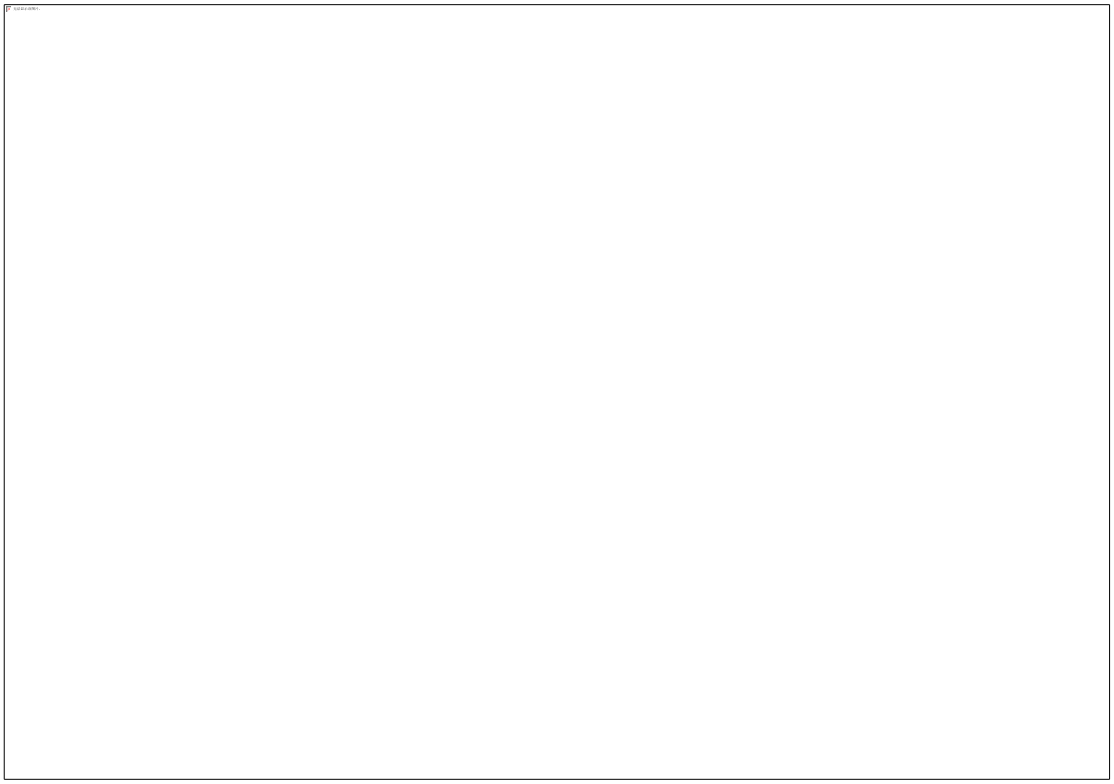

**4-67**

$^{1}$H NMR:

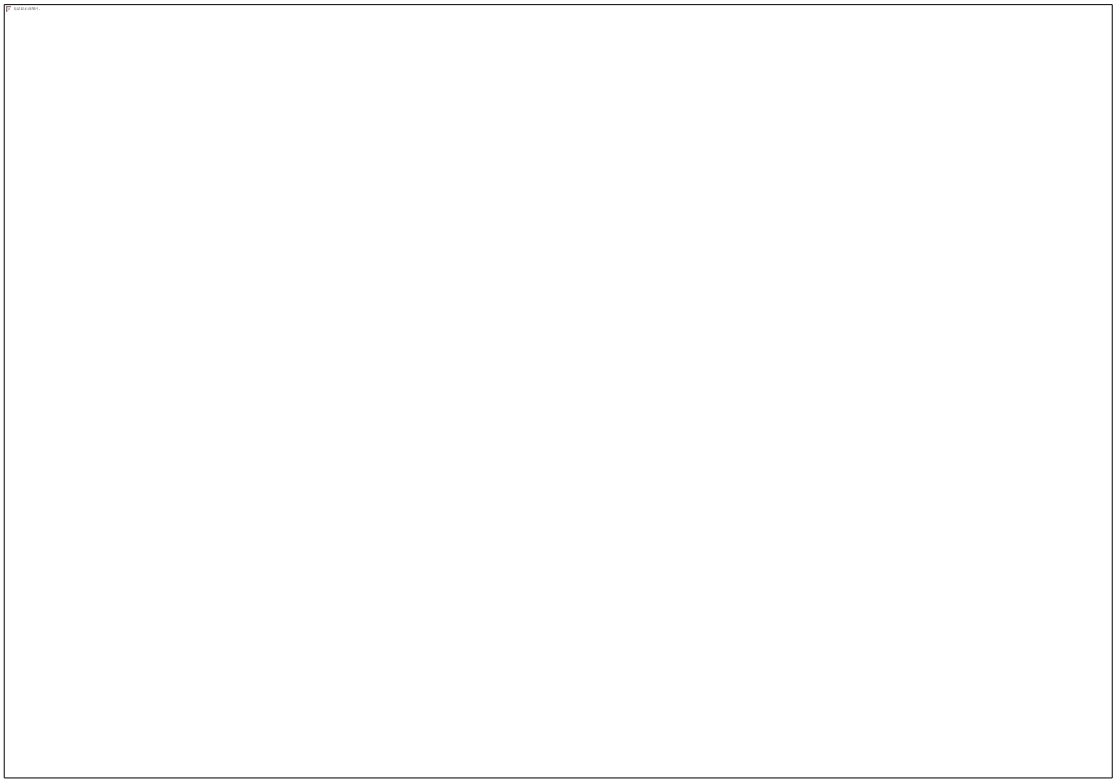

$^{13}$C NMR:

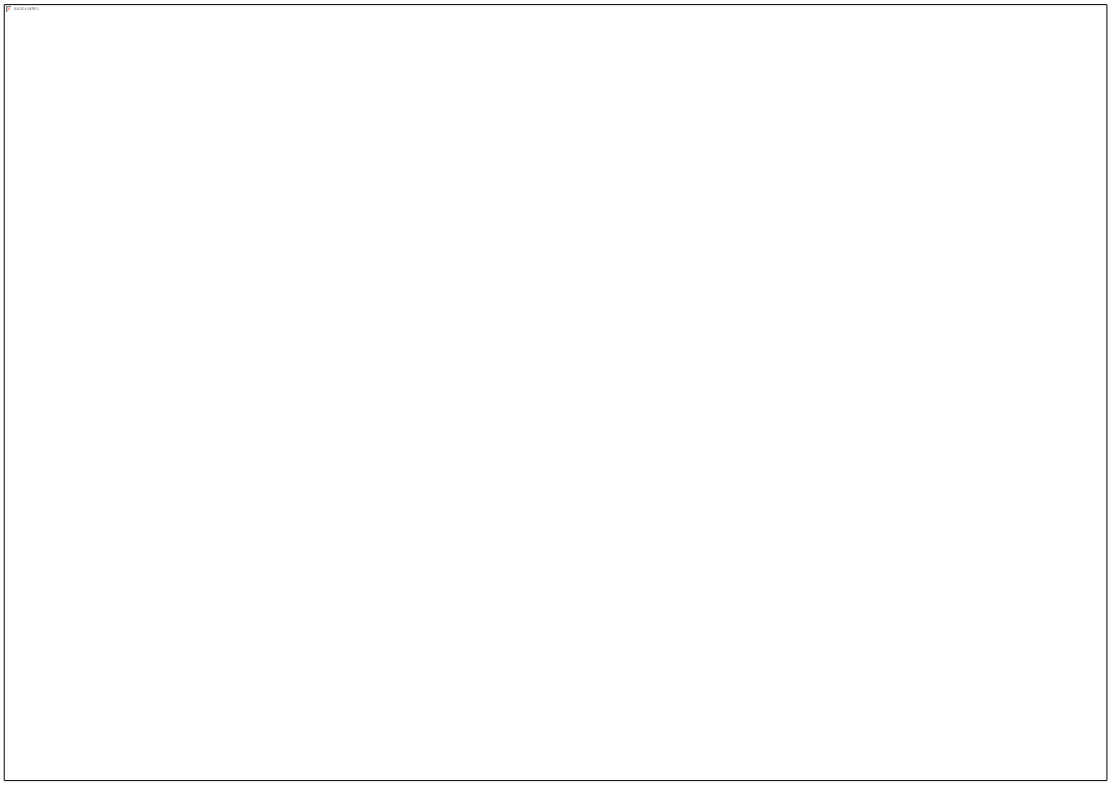

**4-68**

$^{1}$H NMR:

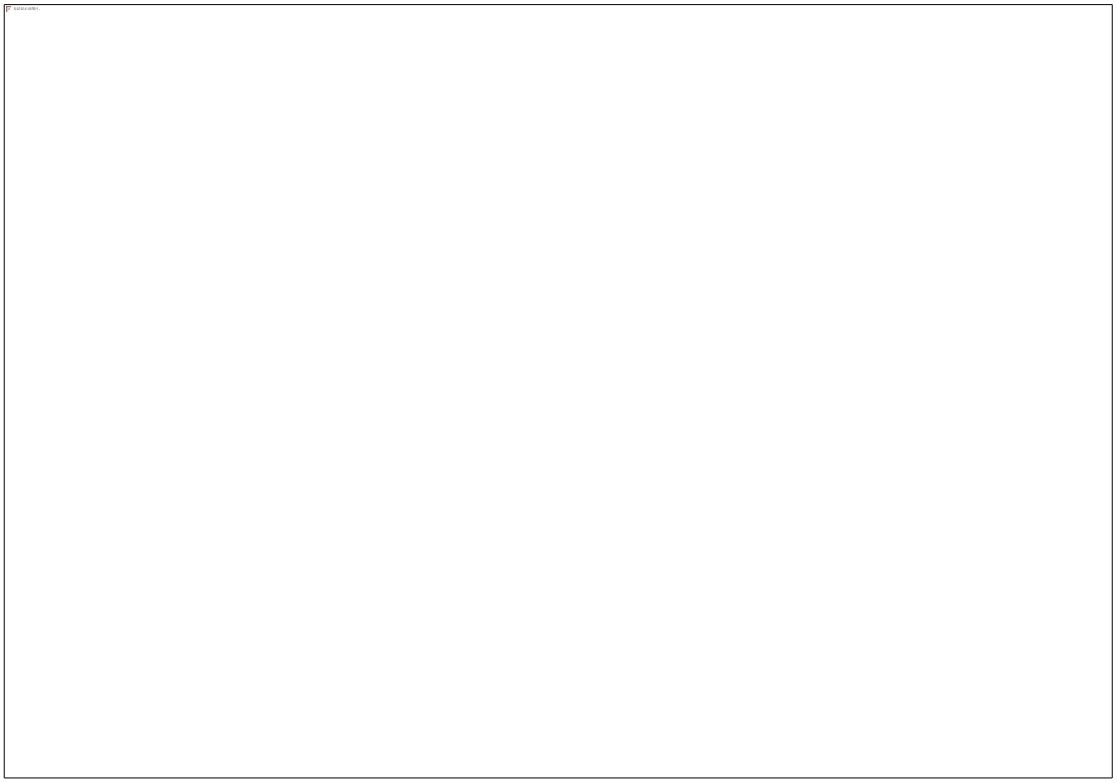

**4-69**

$^{1}$H NMR:

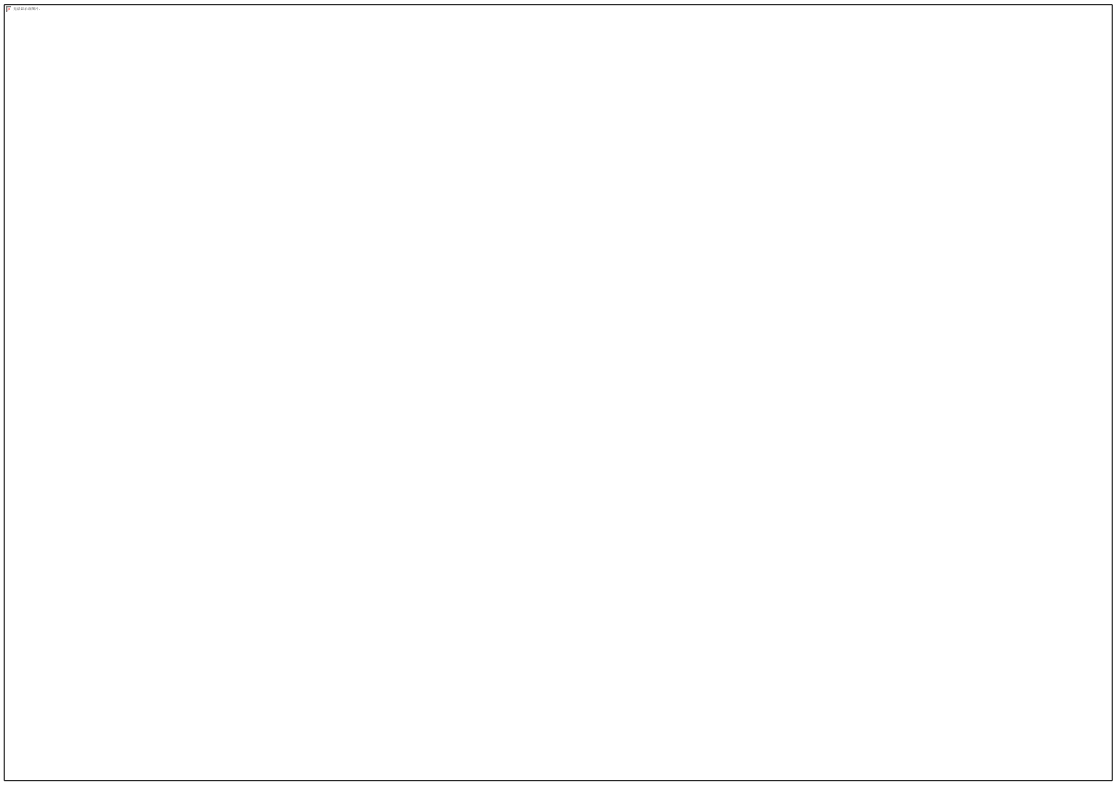

$^{13}$C NMR:

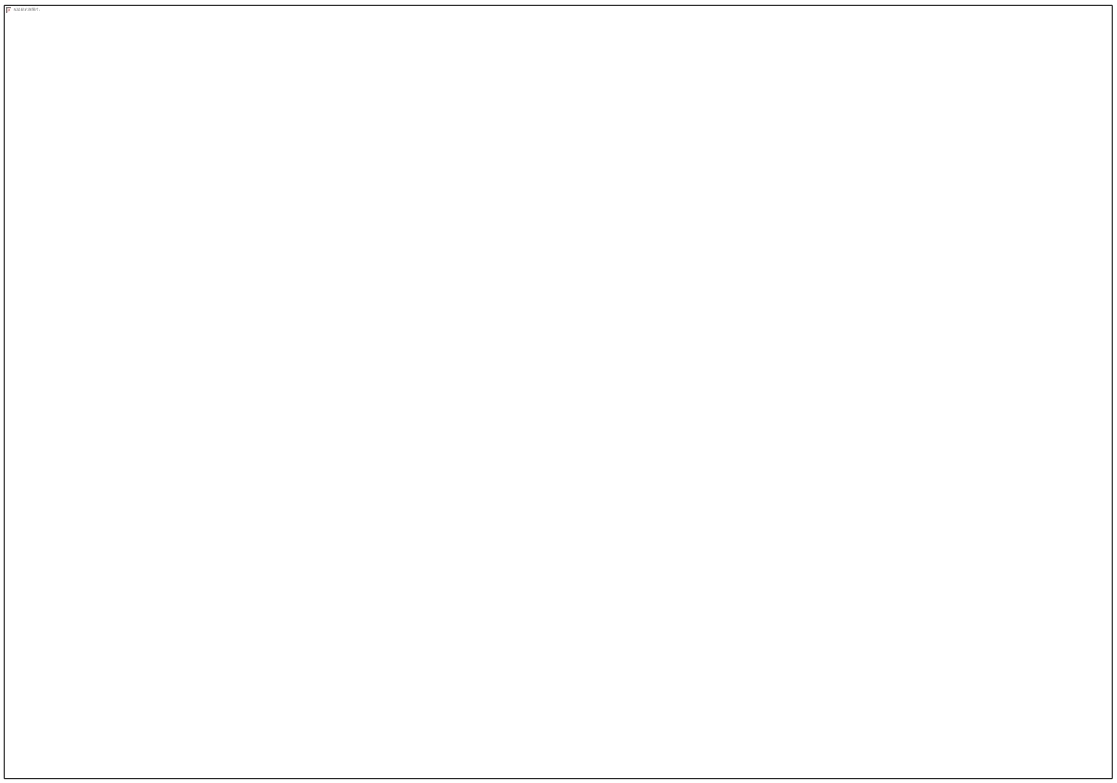

## *HPLC data in Chapter 3 (Industrial Optimization Table)*

### *Table 9. Entry 1*

### *Table 9. Entry 2*

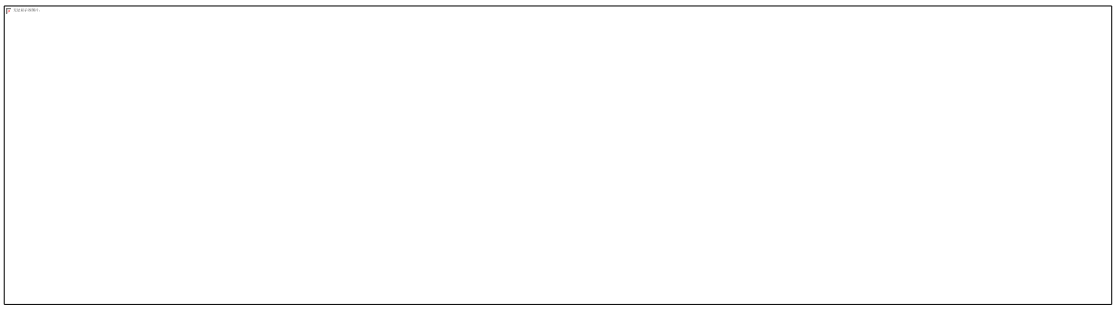

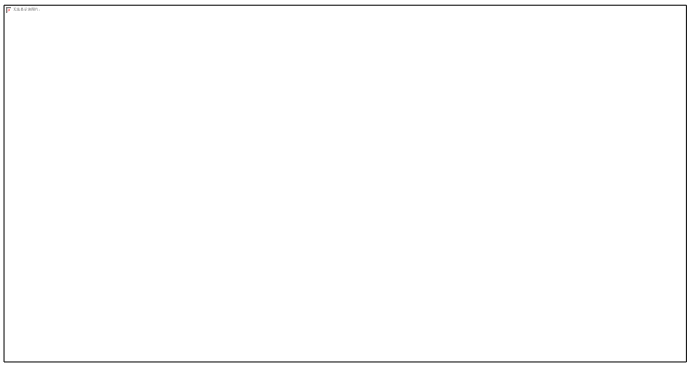

### *Table 9. Entry 3*

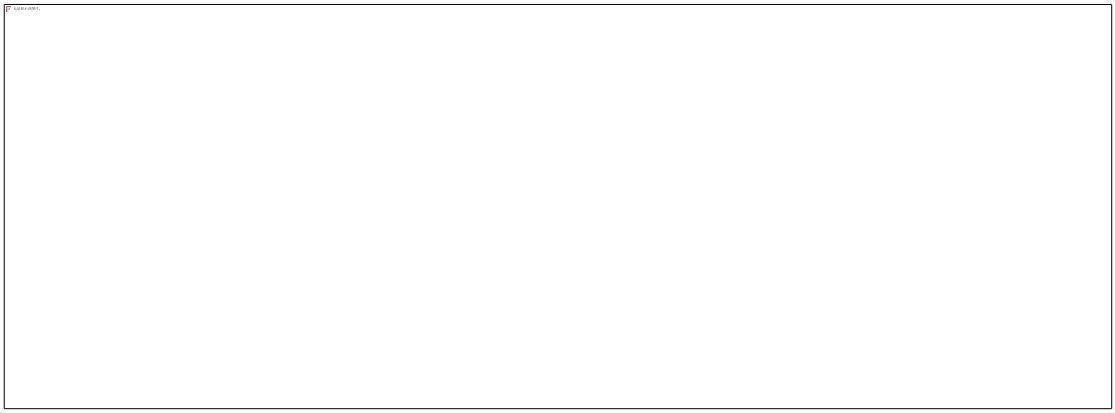

### *Table 9. Entry 4*

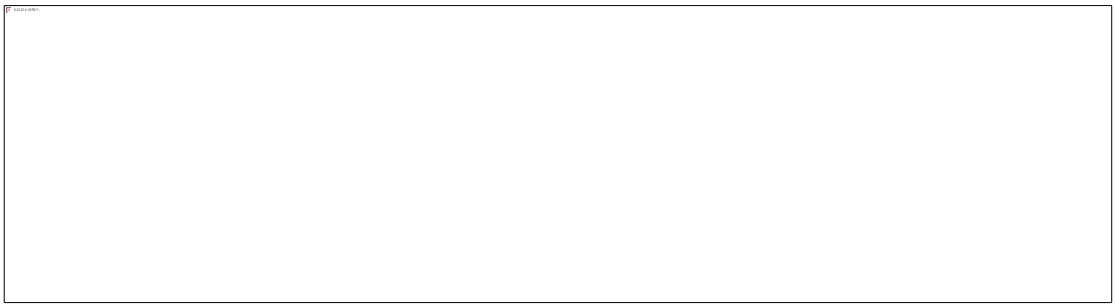

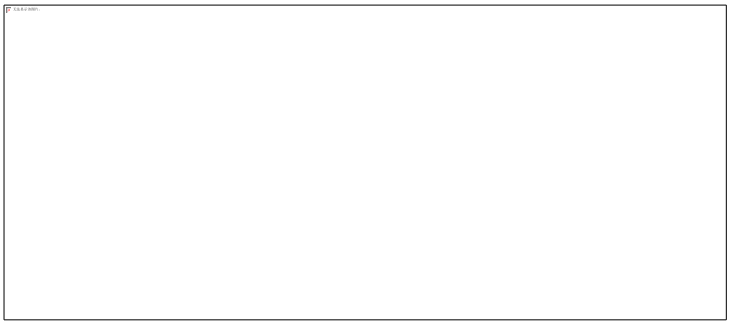

***Table 9. Entry 5***

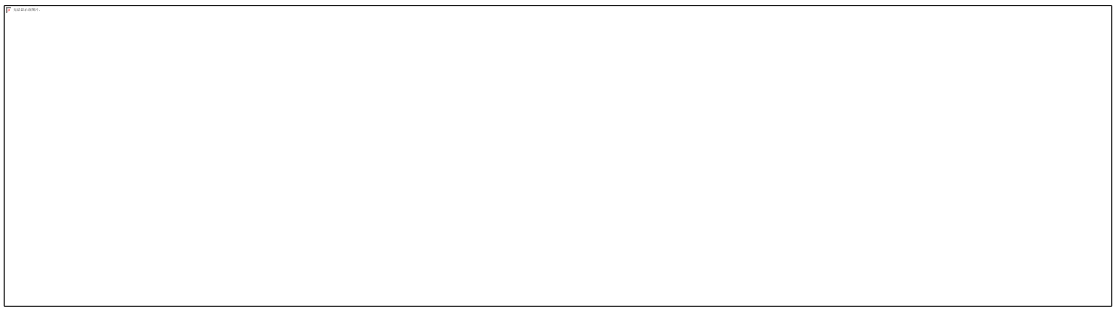

***Table 9. Entry 6***

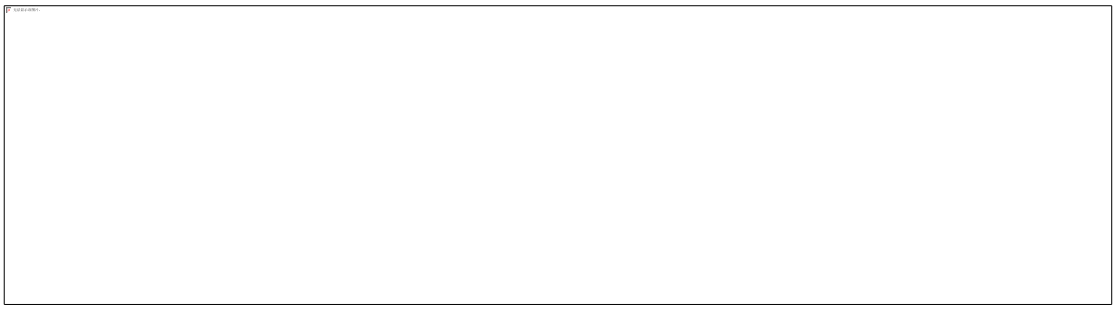

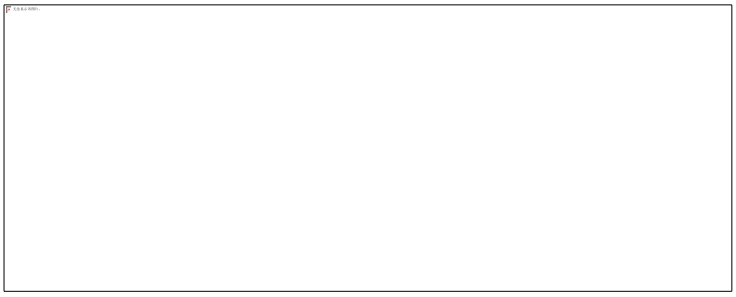

### *Table 9. Entry 7*

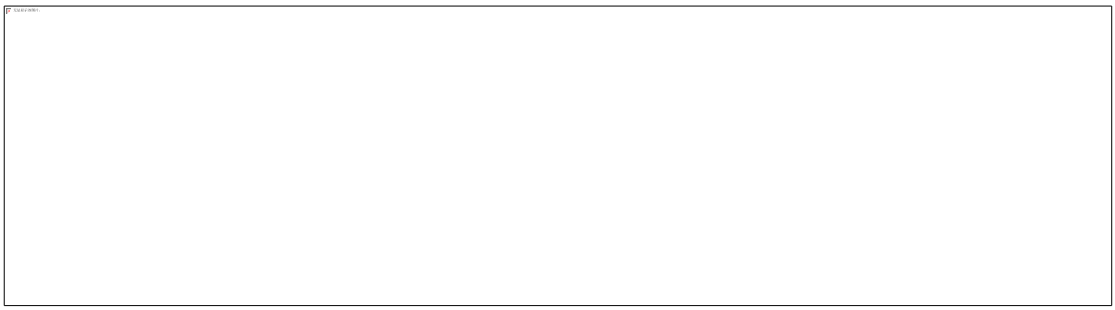

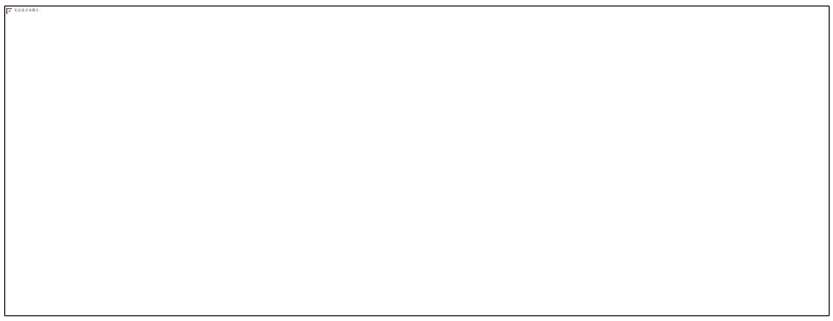

### *Table 9. Entry 8*

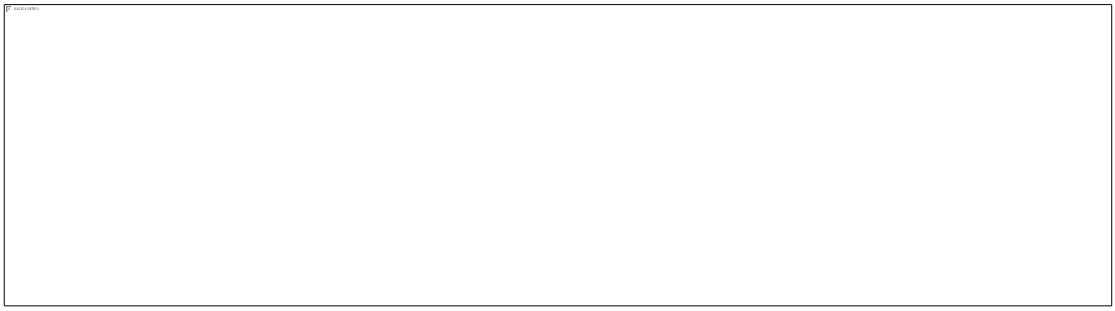

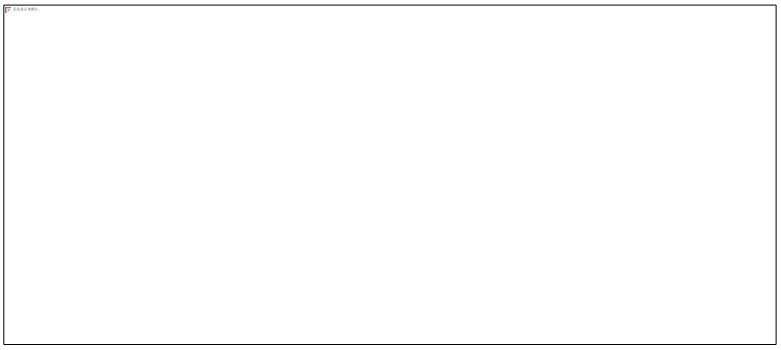

***Table 9. Entry 9***

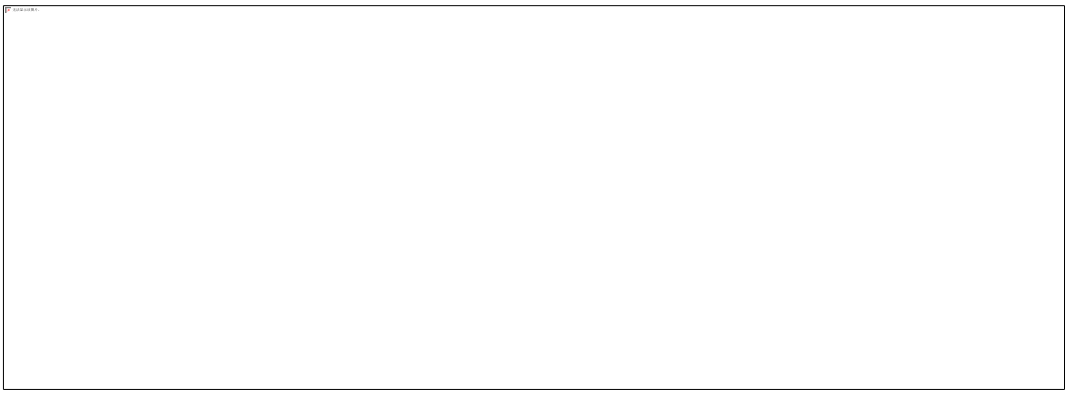

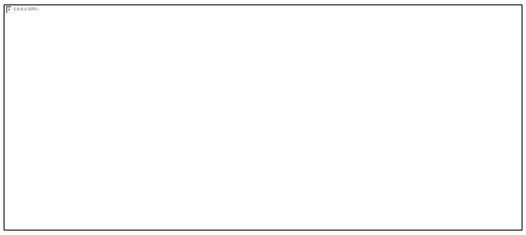

***The HPLC area of compound 1 in table 9 entry 9***

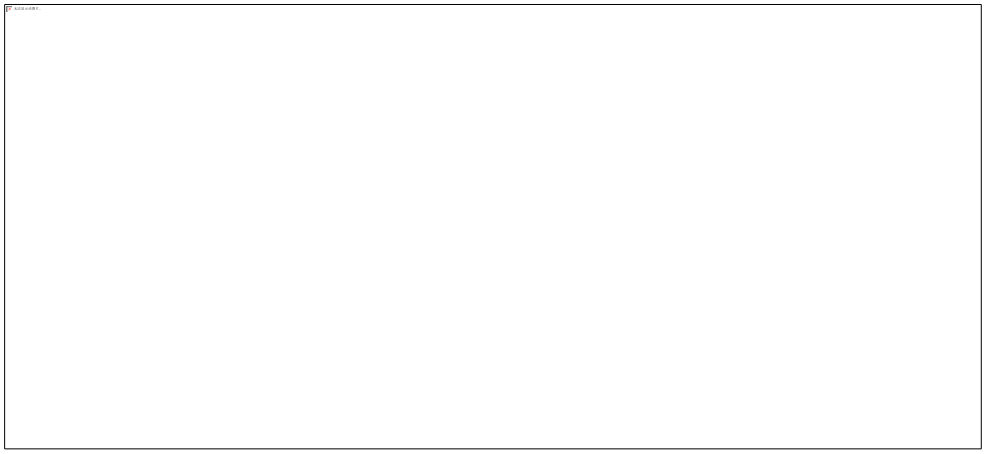

***Table 10. Entry 1***

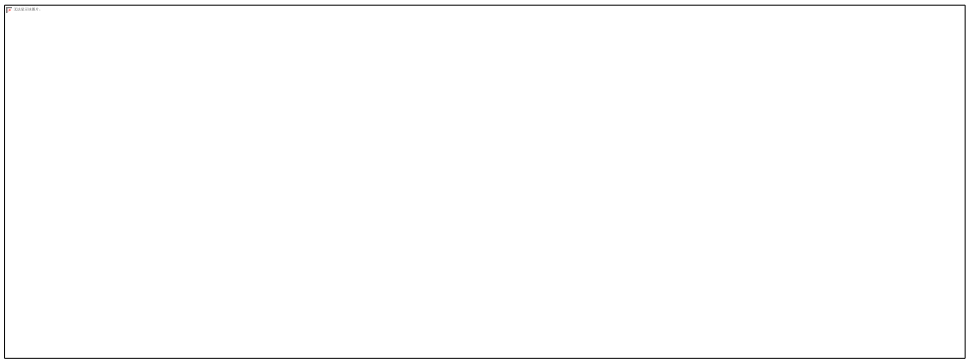

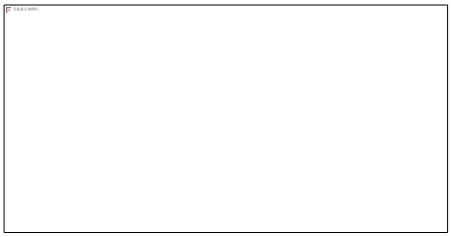

***Table 10. Entry 2***

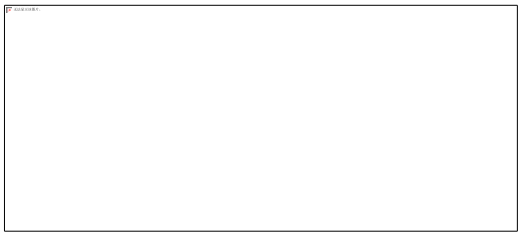

***Table 10. Entry 3***

***Table 10. Entry 4***

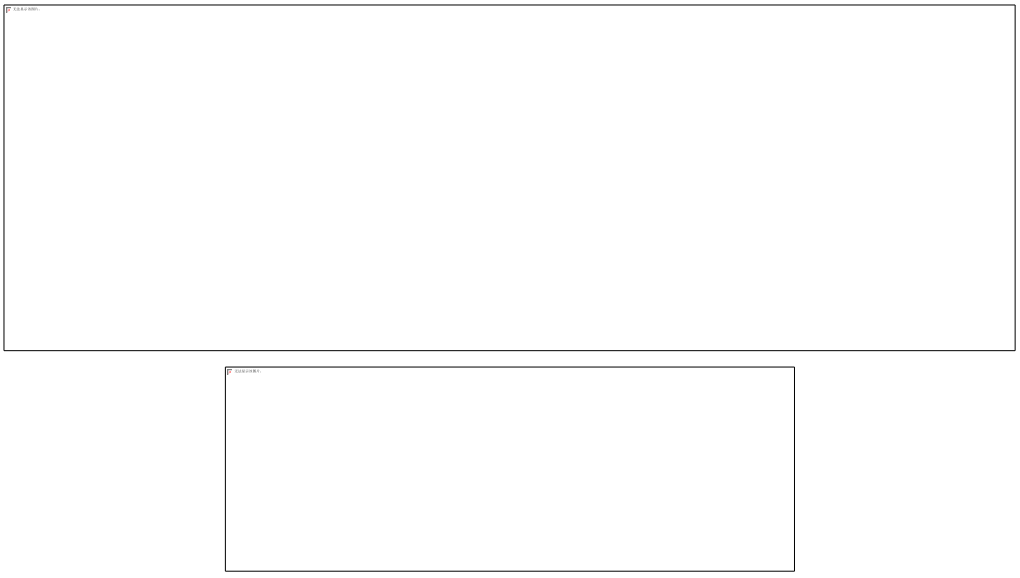

***Table 10. Entry 5***

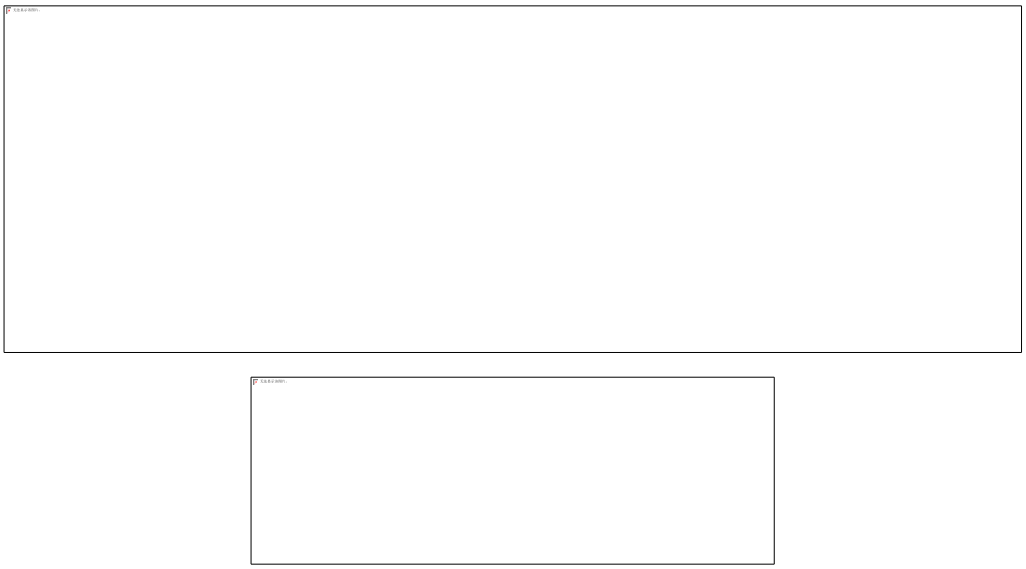



***Table 10. Entry 6***

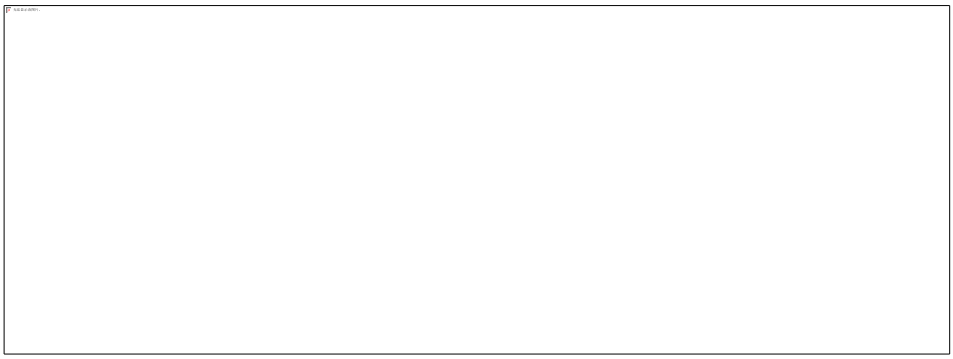

## *The HPLC area of compound 2 in table 10. entry 6*

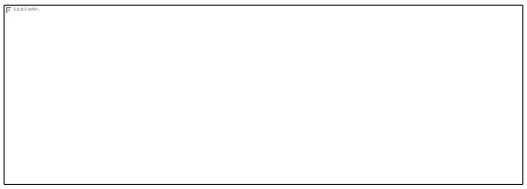

***Table 11. Entry 1***

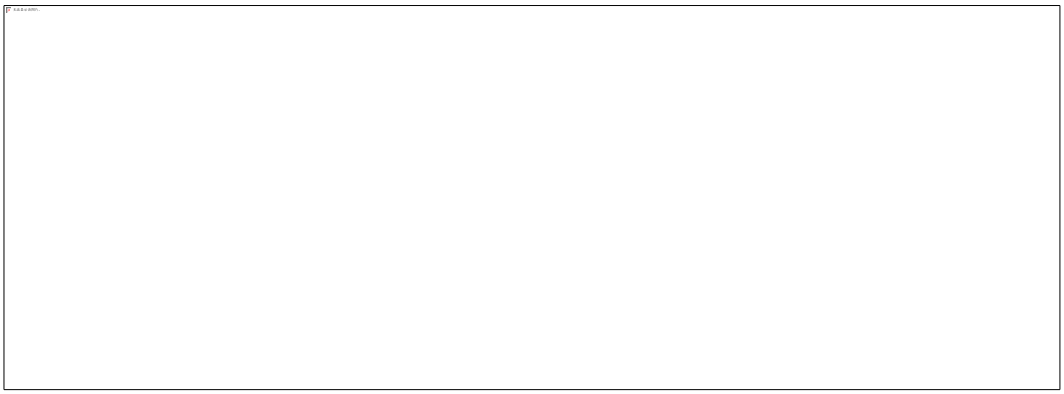

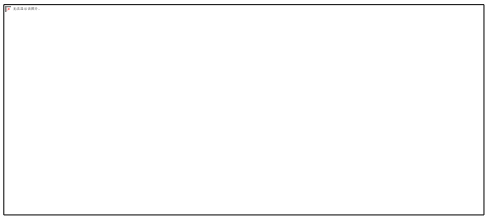

***Table 11. Entry 2***

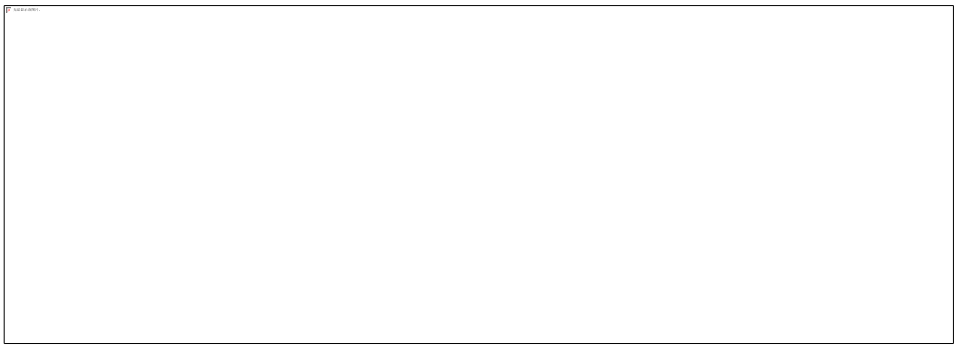

### *Table 11. Entry 3*

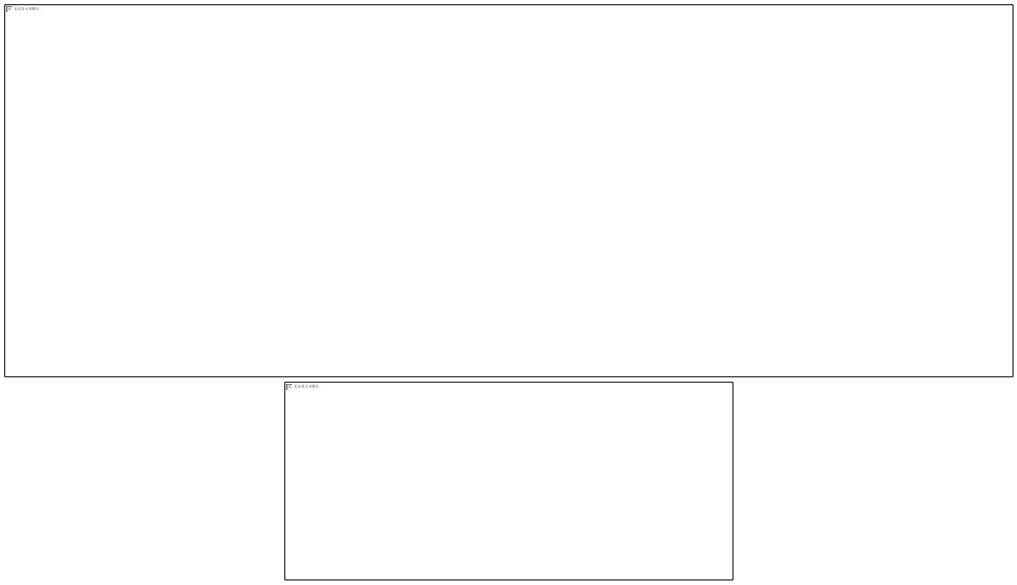

### *Table 11. Entry 4*

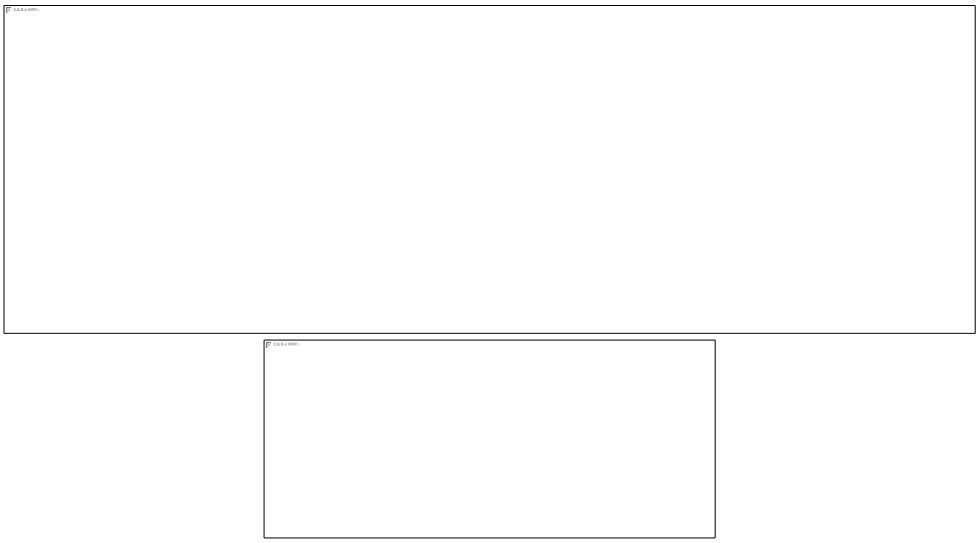

***Table 11. Entry 5***

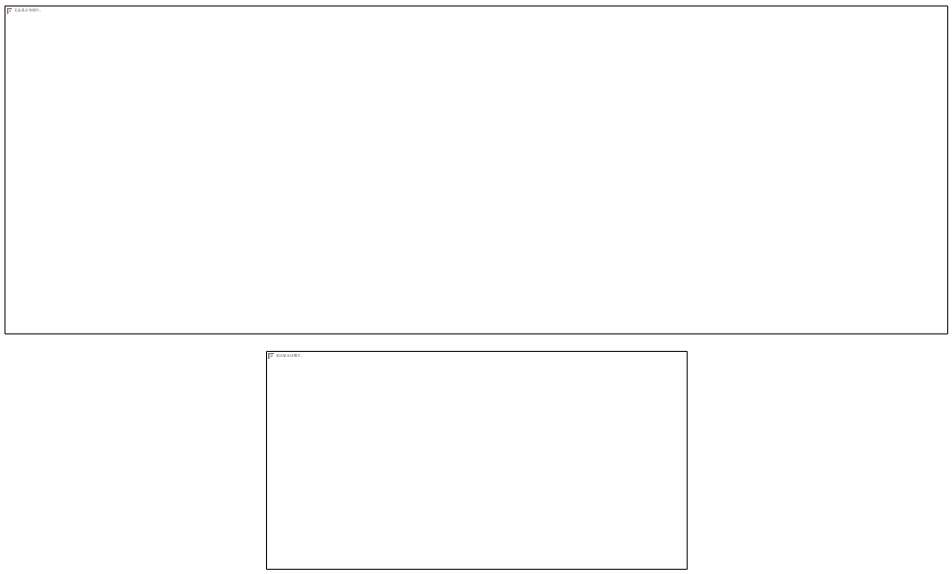



***Table 11. Entry 6***

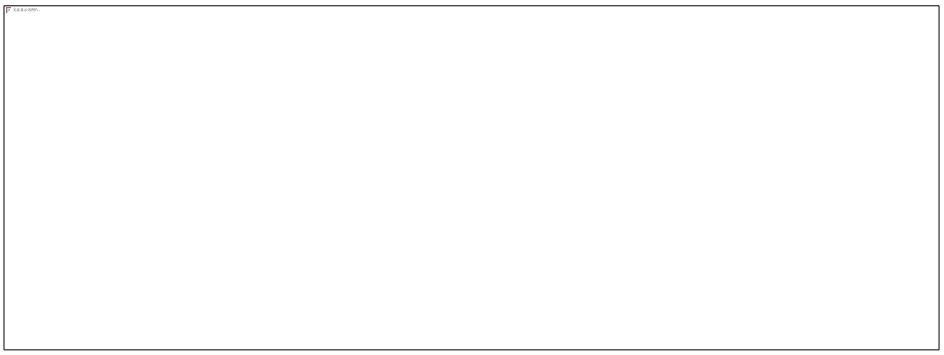

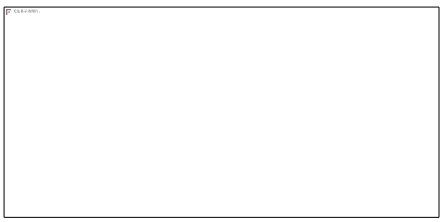

***Table 11. Entry 7***

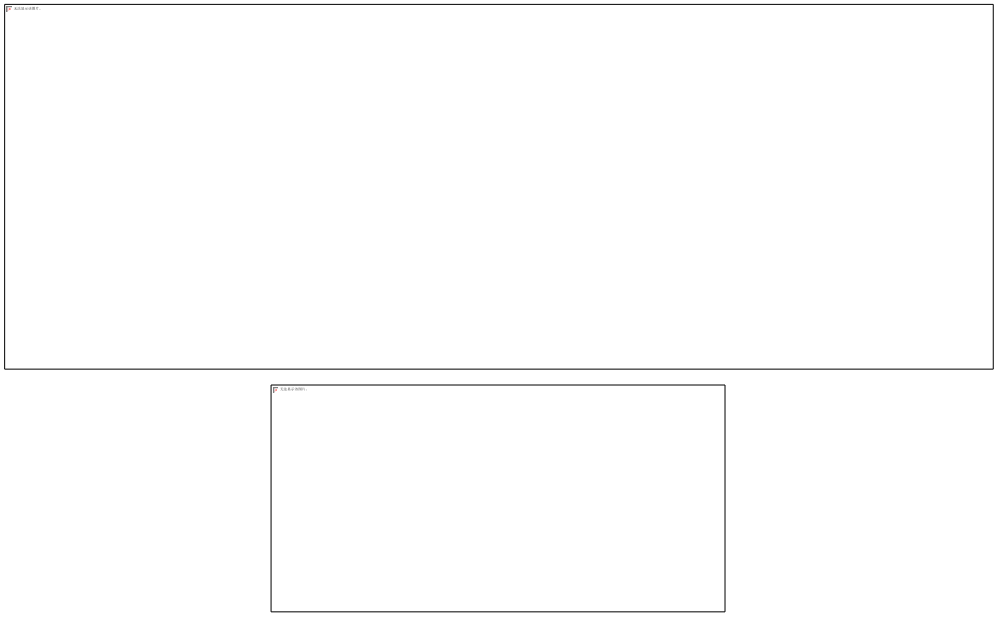

***Table 11. Entry 8***

### *Table 11. Entry 9*

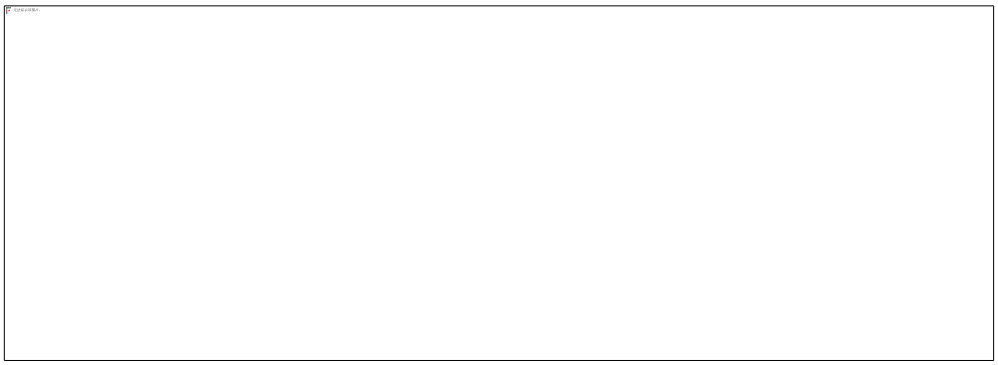

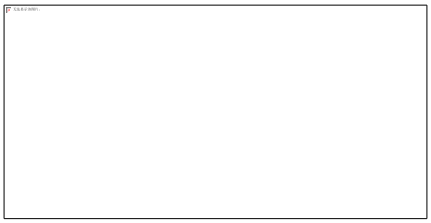

### *Table 11. Entry 9*